PALACKÝ UNIVERSITY OLOMOUC

Faculty of Science

Department of Biochemistry

Biochemical and proteomic analysis of mitogen-activated protein kinase signaling during oxidative stress

Ph.D. Thesis

Author:	**Mgr. Petr Dvořák**
Study program:	P1406 Biochemistry
Supervisor:	doc. Ing. Tomáš Takáč, Ph.D.
Form of study:	Full-time study
Submitted:	March 2021

I hereby declare that this Ph.D. thesis has been written solely by me. All the sources cited in this thesis are listed in the reference list. All published results included in this work are approved by co-authors.

In Olomouc ……

Petr Dvořák

Poděkování

Nejvíce bych chtěl poděkovat mému školiteli doc. Ing. Tomášovi Takáčovi, Ph.D. za jeho odborné vedení, rady, trpělivost a přátelský přístup po celou dobu mého studia. Dále také za časté a plodné diskuze, předané zkušenosti, uvedení do vědecké komunity a za jeho cenné připomínky a pomoc při sepisování této práce.

Dále bych rád poděkoval všem kolegům z Oddělení buněčné biologie CRH za přátelské prostředí a ochotu pomoci. Především bych rád poděkoval panu profesorovi Jozefovi Šamajovi za cenné rady, přátelský přístup, pracovní zázemí a možnost absolvování zahraniční stáže. V neposlední řadě bych rád poděkoval panu profesorovi Miroslavovi Ovečkovi za přátelský přístup, četné odborné diskuze a předané zkušenosti.

Velké díky patří taktéž panu docentovi Michaelovi Wrzaczek, u kterého jsem měl možnost absolvovat zahraniční stáž na akademické půdě University of Helsinki, a za získané zkušenosti a přátelský přístup.

Dále bych rád poděkoval rodině Brkových za poskytnutí zázemí v posledních dnech sepisování této práce a dále kamarádovi Adamovi Zeinerovi za jeho pomoc.

Na závěr bych rád poděkoval své ženě Michaele, našemu malému Tomáškovi a celé rodině za trpělivost a oporu po celou dobu mého studia, bez které bych tuto cestu nezvládl.

Tato práce byla podpořena Evropským fondem pro regionální rozvoj (ERDF), projekt č. CZ.02.1.01/0.0/0.0/16_019/0000827, „Rostliny jako prostředek udržitelného globálního rozvoje" a GAČR projektem č. 19-00598S a studentskými projekty Interní grantové agentury (IGA), IGA_PrF_2016_012, IGA_PrF_2017_026 a IGA PrF_2018_031 Přírodovědecké fakulty Univerzity Palackého v Olomouci.

Acknowledgements

I would like to thank my supervisor doc. Ing. Tomáš Takáč, Ph.D. the most for his professional guidance, advice, patience and friendly approach throughout my studies, in addition to thought provoking and prolific discussions, shared experience, introduction to the scientific community and for his valuable comments and assistance within writing this work.

I also want to thank all the colleagues from the CRH Cell Biology Department for maintaining a friendly environment and their willingness to help. In addition, I want to thank Professor Jozef Šamaj for his valuable advice, welcoming attitude, work background and the opportunity to complete an internship abroad. Last but not least, I want to thank Professor Miroslav Ovečka for his friendly guidance, numerous professional discussions and shared experience.

Many thanks also to Associate Professor Michael Wrzaczek, with whom I had the opportunity to do an internship abroad at the campus of the University of Helsinki, and for the experience gained there and his positive attitude.

Furthermore, I would also like to thank the Brkovi family for providing the supportive environment in the last days of writing this work and my friend Adam Zeiner for his help.

Finally, I want to thank my lovely wife Michaela, our little Tomáš and the whole family for their patience and support throughout my studies, without which I would not have managed this journey.

This work was supported by the European Regional Development Fund (ERDF), project No. CZ.02.1.01 / 0.0 / 0.0 / 16_019 / 0000827, "Plants as a means of sustainable global development" and GAČR project No. 19-00598S and student projects Internal grant agencies (IGA), IGA_PrF_2016_012, IGA_PrF_2017_026 and IGA PrF_2018_031 Faculty of Science, Palacky University in Olomouc.

Bibliografická identifikace

Jméno a příjmení autora:	Mgr. Petr Dvořák
Název práce:	Biochemická a proteomická analýza signalizace pomocí mitogen-aktivovaných proteinkinas při oxidativním stresu
Typ práce:	Disertační
Pracoviště:	Centrum regionu Haná pro biotechnologický a zemědělský výzkum, Oddělení buněčné biologie, Přírodovědecká fakulta, Univerzita Palackého v Olomouci
Vedoucí práce:	doc. Ing. Tomáš Takáč, Ph.D.
Rok obhajoby práce:	2021
Klíčová slova:	*Arabidopsis thaliana*, signalizace, mitogenem aktivované protein kinasy, fosforylace proteinů, reaktivní formy kyslíku, oxidační stres, antioxidační enzymy, superoxiddismutasy, FSD1, rostlinný vývoj, SQUAMOSA-PROMOTER BINDING PROTEIN-LIKE proteins, *Sinorhizobium meliloti*, nodulace, biotický stres, proteomická analýza
Počet stran:	278
Počet příloh:	4
Jazyk:	Anglický

Abstrakt

Mitogen-aktivované protein kinasové (MAPK) kaskády řadíme mezi evolučně vysoce konzervované signalizační dráhy, které hrají důležitou úlohu v řadě buněčných procesů. Jednou z jejich hlavních úloh je přenos signálu přijatého z vnějšího prostředí skrze receptory s nitro- a mezibuněčnou signalizací. Taktéž hrají nezastupitelnou signalizační roli během navazování patogenních nebo symbiotických vztahů mezi

rostlinou a mikroorganizmy. V rostlinách vystavených podmínkám působení biotického a abiotického stresu dochází ke značné akumulaci reaktivních forem kyslíku (ROS) způsobujících v buňkách oxidační stres, který v krajních případech může vést až k buněčné smrti. ROS hrají nezastupitelnou roli v buněčné signalizaci a během vývojových procesů rostlin. Zvýšená akumulace ROS aktivuje některé MAPK, které následně regulují řadu buněčných pochodů včetně modulace antioxidační obrany zahrnující superoxiddismutasy (SOD). Předchozí studie naznačují, že enzymatická aktivita a abundance některých SOD je regulována pomocí MAPK v odpovědi na různé stresové podmínky vedoucí k akumulaci ROS.

První část této práce se zabývá studiem MAPK při působení oxidačního stresu a jejich zapojením do procesu iniciace symbiotických vztahů s beneficiálními bakteriemi *Sinorhizobium meliloti* a následné nodulace u rostliny *Medicago sativa*. Biochemická, fenotypová a proteomická analýza linie *M. sativa* s cíleně sníženou abundancí MAPK kinasy (*SIMKK RNAi* linie) odkryly možné zapojení MAPK kaskád do těchto procesů. *SIMKK RNAi* linie vykazovala snížený počet nodulů v porovnání s divokým typem. Následná biochemická a proteomická analýza ukázala, že tento fenotyp může být způsoben poruchami adheze bakterií na povrch kořenů, remodelace plazmatické membrány a poruchami redox regulace včetně antioxidačních proteinů. Noduly transgenní linie vykazují postižený metabolismus dusíku a uhlíku, jak naznačuje proteomická analýza.

Cílem druhé části práce bylo popsat vývojové a lokalizační role SOD isoenzymu (FSD1) v rostlině *Arabidopsis thaliana* a navrhnout možné mechanismy jeho regulace pomocí MAPK. Zjistili jsme, že FSD1 je zapojena do vývoje laterálních kořenů a má ochrannou roli během indukovaného oxidačního a solného stresu. Pomocí mikroskopické analýzy byla definována subcelulární lokalizace FSD1 v cytoplasmě, chloroplastech a překvapivě i v buněčném jádře. FSD1 má specifickou roli při narušení epidermis během prorůstání radikuly ze semena při klíčení. FSD1 protein byl taktéž akumulován ve vyvíjející se špičce kořenového vlásku. Pomocí ko-imunoprecipitační metody v kombinaci s hmotnostní spektrometrií byli identifikováni potenciální interakční partneři FSD1 a navrženy možné úlohy FSD1. Závěr této části je věnován možnému zapojení MPK3 a MPK6 v regulaci exprese *FSD1* skrze SPL transkripční faktory.

Se zvyšujícími se potřebami lidstva a současně velmi dynamicky se měnícími environmetálními podmínkami je již v současné době konvenční zemědělství na hranici svých limitů. Pochopení mechanizmů symbiotických vztahů, a to především jeho úvodních signalizačních drah, může vést k novým biotechnologickým aplikacím spojených s možností zvýšení výnosů pícnin, jako je *Medicago sativa*. Velmi vhodnou variantou je taktéž cílená modifikace antioxidačních enzymů, která by vedla k vyšší rezistenci rostlin jak na biotický, tak především abiotický stres. Pro jejich cílenou modifikaci je však nejprve důležité pochopit veškeré jejich funkční úlohy v rostlinách. Tato práce částečně přispívá k pochopení úlohy MAPK kaskád a FSD1 proteinu v rostlinách a podporuje jejich možné zapojení do biotechnologických aplikací v zemědělství.

Bibliographical identification

Author´s first name and surname:	Mgr. Petr Dvořák
Title:	Biochemical and proteomic analysis of mitogen-activated protein kinase signaling during oxidative stress
Type of thesis:	Ph.D.
Department:	Centre of the Region Haná for Biotechnological and Agricultural Research, Department of Cell Biology, Faculty of Science, Palacký University Olomouc
Supervisor:	doc. Ing. Tomáš Takáč, Ph.D.
The year of presentation:	2021
Key words:	*Arabidopsis thaliana*, mitogen-activated protein kinase, signaling, protein phosphorylation, reactive oxygen species, oxidative stress, antioxidant enzymes, superoxide dismutase, FSD1, plant development, SQUAMOSA-PROMOTER BINDING PROTEIN-LIKE proteins, protein phosphorylation, *Sinorhizobium meliloti*, nodulation, biotic stress, proteomics
Number of pages:	278
Number of appendixes:	4
Language:	English

Abstract

Mitogen-activated protein kinase (MAPK) cascades are evolutionarily highly conserved signaling pathways that play an important role in many cellular processes. One of their main functions is to transmit the signal received from the external environment through receptors by intra- and intercellular signaling. They also play an irreplaceable signaling role during the establishment of pathogenic or symbiotic

relationships between the plants and microorganisms. Plant cells exposed to biotic and abiotic stress conditions accumulate reactive oxygen species (ROS) causing oxidative stress, which in extreme cases can lead to cell death. ROS plays a critical role in cell signaling and plant developmental processes. Increased accumulation of ROS activates MAPKs, which in turn regulate several cellular processes, including antioxidant enzymes such as superoxide dismutases (SODs).

The main aim of the first part of this thesis is to examine the role of MAPK during the initiation of symbiotic relationships of *Medicago sativa* with the beneficial bacteria *Sinorhizobium meliloti* and subsequent nodulation. Biochemical, phenotypic and proteomic analyses of the *M. sativa* transgenic *SIMKK RNAi* line with reduced expression of MAPK kinase SIMKK revealed the possible involvement of MAPK cascades in these processes. *SIMKK RNAi* line displayed a reduced number of nodules compared to the wild type. Subsequent biochemical and proteomic analysis showed that this phenotype could be caused by defects in bacterial adhesion to the root surface, plasma membrane remodeling, and redox regulation, including the abundance of antioxidant proteins. The nodules of the transgenic line show an affected nitrogen and carbon metabolism.

Within the second part, the developmental roles and localization of the SOD isoenzyme FSD1 in *Arabidopsis thaliana* were examined. Moreover, possible mechanisms of its regulation by MAPK were suggested. We found that FSD1 is involved in the development of lateral roots and it has a protective role during oxidative stress and salt stress. FSD1 localizes in the cytoplasm, chloroplasts and, surprisingly, in the nucleus, as revealed by advanced microscopy. It temporarily accumulates at the site of endosperm rupture during seed germination. With the help of co-immunoprecipitation, potential interaction partners of FSD1 were identified by mass spectrometry and possible functions of FSD1 were proposed. Finally, experiments were conducted in order to reveal the possible involvement of MPK3 and MPK6 in the regulation of *FSD1* expression through SPL transcription factors.

With the increasing demands of humanity and dynamically changing environmental conditions, conventional agriculture is nearing its limitations. The understanding of the symbiotic relationships and especially its initial signaling pathways can lead to subsequent biotechnological advances and thus increase crop

yields. A feasible alternative is also a genetic modification of antioxidant enzymes, which would lead to higher resistance of plants to both biotic and abiotic stress. However, for their targeted modification, it is important to understand their functions in plants. This work contributes to the understanding of the role of MAPK cascades and FSD1 protein in plants and supports the claim for their possible involvement in biotechnological applications in agriculture.

Content

Aim of the thesis

- Summary of current knowledge on oxidative stress in plants, mitogen-activated protein kinases (MAPKs) and their role in response to biotic and abiotic stress, superoxide dismutases (SODs), and regulation of SODs by SQUAMOSA PROMOTER-BINDING PROTEIN-LIKE proteins (SPLs), symbiotic interaction of alfalfa and the role of MAPK during nodulation.
- Proteomic analysis of the role of SIMKK during symbiotic interaction between alfalfa and rhizobia, with focus on ROS regulation.
- Developmental and biochemical characterization of FeSOD1.
- Examination of the relationship between superoxide dismutase (especially FeSOD1) and MAPK.

1 General introduction

1.1 Mitogen activated protein kinases

Due to their sessile nature, plants must cope with unfavorable environmental conditions by rapid signal perception ensuring proper physiological responses and adaptation. Thus, plants have stress responses that are coordinated via complex networks of densely interconnected signaling pathways. Phosphorylation is the key post-translational modification (PTM) of proteins allowing immediate signal transduction in response to various environmental or developmental cues (Ichimura et al., 2000). Protein phosphorylation, which is catalyzed by protein kinases, may cause enzyme activation or inactivation, a change in the substrate specificity, protein stability, protein-protein interaction and localization as well as the ability to bind protein partners (Huber, 2007; Vu et al., 2018). Around 4–5% of the *Arabidopsis* genome encodes protein kinases (Zulawski et al., 2014). Mitogen-activated protein kinases (MAPK) hold a leading position among kinases ensuring transduction of the signal generated by environmental and developmental factors (Šamajová et al., 2013; Komis et al., 2018). MAPK signaling cascades consist of MAPK kinase kinase (named also MAP3Ks, MEKKs or MAPKKKs), MAPK kinase (MAP2Ks, MEKs or MAPKK and MKKs), and MAPKs (MPKs), which are consecutively phosphorylated leading to the activation/inactivation of a wide range of target proteins including transcription factors (TFs), enzymes or other kinases (Dóczi and Bögre, 2018; Figure 1). MAPK cascades are highly conserved in eukaryotes. *Arabidopsis* genome encodes 60 putative MAP3Ks, 10 MAP2Ks, and 20 MAPKs (Rodriguez et al., 2010).

Activation of MAPK cascade is initiated by phosphorylation of MAP3K either by receptor-like kinases (RLKs), receptor-like cytoplasmic kinases (RLCK; Bi et al., 2018; Wang et al., 2020) or other protein kinases (e.g. BRASSINOSTEROID-INSENSITIVE 2; Kim et al., 2012a). Activated MAP3Ks phosphorylate MAP2Ks at a conserved S/T-$X_{3–5}$-S/T motif. Subsequently, MAPKs are double phosphorylated at a conserved TXY motif by MAP2Ks (Tanoue and Nishida, 2003). Deactivation of MAPKs is mediated by protein phosphatases (Bheri et al., 2020).

MAP3Ks are serine/threonine kinases showing a high diversity in primary structures and domain composition (Ichimura et al., 2002). They are sorted into two main subfamilies: (i) MEKK-like subfamily, which contains 10 members in *Arabidopsis* with the conserved catalytic domain, including for example, MEKK1 (Ichimura et al., 2006); and (ii) RAF-like kinase subfamily such as CONSTITUTIVE RESPONSE 1

(Zhong and Chang, 2012) or ENHANCED DISEASE RESISTANCE 1 (Frye et al., 2001).

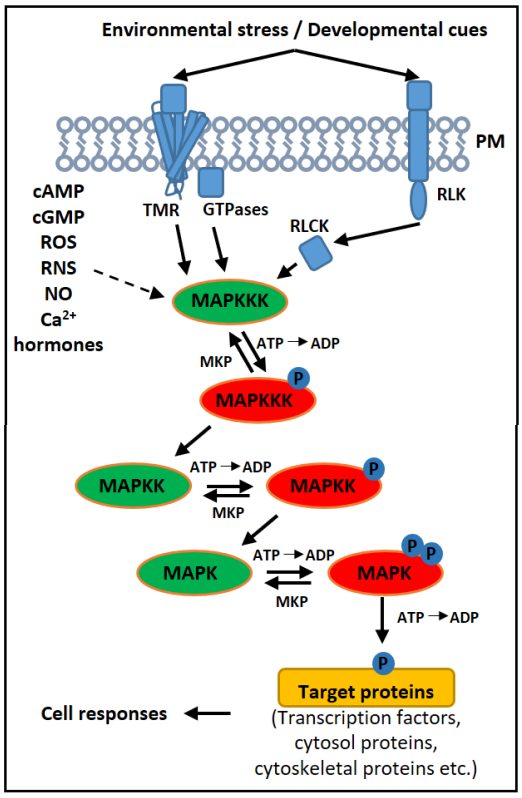

Figure 1 Schematic depiction of general MAPK cascade activation and its targets. MAPK cascades are initiated by extracellular stimuli through receptors, leading to consecutive phosphorylation of individual MAPK members. This occurs upon vital crosstalk with second messengers such as ROS. Terminal MAPK phosphorylates diverse proteins including transcription factors, enzymes, cytoskeletal proteins and others. Abbreviations: Ca^{2+} – calcium ions, cAMP – cyclic adenosine monophosphate, cGMP – cyclic guanosine monophosphate, MAPK – mitogen activated protein kinase, MAPKK – mitogen activated protein kinase kinase, MAPKKK – mitogen activated protein kinase kinase kinase, MKP – MAPK phosphatase, NO – nitric oxide, PK – protein kinase, PM – plasmatic membrane, RLCK – receptor-like cytosolic kinase, RLK – receptor-like kinase, RNS – reactive nitrogen species, ROS – reactive oxygen species, TMR – transmembrane receptor.

MAP2Ks are classified into four groups (A–D), based on differences in the primary structure and substrate specificity. MAP2Ks possess a putative MAPK-docking site composed of [K/R][K/R][K/R]X(1–5)[L/I]X[L/I] sequence in their N-terminal side. The occurrence and composition of this MAPK-docking domain, which is characterized by the presence of positively charged amino acids affects the interaction with downstream MAPK. Targeted inhibition of this domain by a specific antagonist may result in inhibition of the entire cascade (Bardwell et al., 2009).

Phylogenetically, plant MAPKs are classified into four groups (A–D) based on the structure of the kinase domain and the sequence of the activation motif. Groups A, B and C (12 members) contain TEY, and the D group (8 members) contains TDY activation motif (Ichimura et al., 2002). Most of MAPKs, especially from the groups A–C, have a specific amino acid sequence called common docking (CD) domain in their C-terminal region working as a docking site for MAPKKs, MAPK substrates and MAPK phosphatases (Ichimura et al., 2002). On the other hand, many MAPK substrates interact with MAPK CD domain via MAPK specific docking site (called D-site) in their sequence (Ichimura et al., 2002; Bardwell, 2009). Typically, D-sites are present in the N-terminal part of protein upstream (± 100 amino acid) of the MAPK specific phosphorylation site (Biondi and Nebreda, 2003). However, several other docking motifs have been reported such as FXFP (called DEF; Fernandes and Allbritton, 2009) or LXXRR motifs (Smith et al., 1999). The presence of multiple docking motifs increases the stability of MAPK-substrate interaction and enhances the effectiveness of phosphorylation (Sheridan et al., 2008).

Judging from the differences in the number of MAP3K, MAP2K and MAPK representatives, it is obvious that there is a broad crosstalk and redundancy in signaling. It means, that multiple MAP3K/MAP2Ks activate individual MAPKs in response to various stimuli. On the other hand, various MAPKs may be initiated by a single stimulus activating only a specific MAP3K/MAP2K (Smékalová et al., 2014). High variability of MAPK signaling cascades allows the generation of specific response to the perceived signal. Other mechanisms ensuring the specificity of signaling are adaptors or scaffold proteins, which provide organizing platforms for integration of kinase modules in a complex. Thus, scaffold proteins enable operative utilization of MAPK modules for various signaling outputs, and prevent crosstalking with other signaling pathways (Dhanasekaran et al., 2007; Good et al., 2011). The best-studied example in plants is the MAPK scaffolding protein named RECEPTOR FOR ACTIVATED C KINASE 1, which is responsible for scaffolding of MEKK1-MKK4/MKK5-MPK3/MPK6 module activated by the involvement of heterotrimeric GTPases in response to *P. aeruginosa* in *Arabidopsis* (Cheng et al., 2015).

1.1.1 MAPK signaling during biotic stress

Plants in their natural conditions coexist with pathogenic or beneficial microorganisms such as fungi and bacteria. The primary sensing of their presence by

plants is connected to the perception of pathogen-/microbe- and danger-associated molecular patterns (PAMPs, MAMPs and DAMPs) by cell surface-localized pattern-recognition receptors (PRRs), which transduce the signal from the apoplastic space into the cell (He et al., 2018). Stimulation of the receptors results in the onset of pathogen-triggered immunity (PTI), which is accompanied with reactive oxygen species (ROS) and Ca^{2+} accumulation (Ranf et al., 2011), stomatal closure (Melotto et al., 2017), cell wall modifications (Ellinger and Voigt, 2014), induction of ethylene, salicylic acid (SA) and jasmonic acid (JA) biosynthesis (Pieterse et al., 2012) as well as expression of defense related genes (Wani and Ashraf, 2018). The best characterized PAMP-PRR pair in *Arabidopsis* consist of FLAGELLIN SENSING 2 (FLS2) PRR which recognizes bacterial FLAGELLIN and its derived peptide elicitor flg22 (Gómez-Gómez and Boller, 2000). ELONGATION FACTOR THERMO UNSTABLE (EF-Tu) RECEPTOR (known as EFR) is a RLK binding conserved 18 amino-acid epitope (elf18) of EF-Tu (Zipfel et al., 2006). Chitin, a major component of most higher fungi and arthropods is perceived by CHITIN ELICITOR RECEPTOR KINASE 1 (CERK1; Miya et al., 2007). Other RLK representatives are WALL-ASSOCIATED KINASES 1 and 2, a DAMP-triggered receptors capable of activating MAPKs cascade (Kohorn et al., 2012). Activation of RLKs is often followed by their heterodimerization. For example, FLS2 and ETHYLENE RESPONSE FACTOR (ERF) create heterodimers with BRASSINOSTEROID INSENSITIVE 1-ASSOCIATED RECEPTOR KINASE 1 (BAK1) and interact with BAK1-LIKE1 (Roux et al., 2011).

The central consequence of plant elicitation by pathogenic or beneficial organisms is the activation of MAPK signaling (Meng and Zhang, 2013). Currently, two MAPK cascades are known to be initiated during PTI. One is composed of MEKK3/5-MKK4/5-MPK3/6 (Bi et al., 2018). Previously, MEKK1 was also suggested as an upstream activator of the MKK4/5-MPK3/6 pathway (Asai et al., 2002), however, later studies uncovered that treatment with flg22 led to the activation of MPK3 and MPK6 in *mekk1* T-DNA insertion mutants (Suarez-Rodriguez et al., 2007). The second independent cascade leads to activation of MPK4 downstream of MEKK1 and MKK1/2 (Gao et al., 2008). Based on genetic studies, MPK3 and MPK6 have a positive role on activation of plant immunity, while MPK4 is a positive and negative regulator (Kong et al., 2012; Thulasi Devendrakumar et al., 2018; Huang et al., 2020).

The regulation of pathogen defense by *Arabidopsis* MPK3 and MPK6 is multilevel and affects stomatal immunity, hormone biosynthesis and signaling as well as gene expression. MPK3 and MPK6 regulate stomatal closure, which prevents fungal invasion, by two mechanisms, either by metabolic shift of organic acids such as malate and citrate (Su et al., 2017) or by phosphorylation of nitric oxide producing enzyme NITRATE REDUCTASE 2 (Wang et al., 2010a).

MPK3 and MPK6 phosphorylate TFs belonging to the WRKY family, such as WRKY22/WRKY29 (Asai et al., 2002) or WRKY33 (Mao et al., 2011). Latter one controls the expression of defense related genes, like those involved in camalexin biosynthesis (Mao et al., 2011). ERF family of TFs are also often phosphorylated by MPK3 and MPK6 and control the expression of plant defensins (PDFs), such as *PDF1.1* and *PDF1.2* (by ERF6; Meng et al., 2013), or *PDF1.2a* and *PDF1.2b* (by ERF104; Bethke et al., 2009). MPK3 and MPK6 regulate the stability and expression of two isoforms of ethylene biosynthetic enzyme 1-AMINOCYCLOPROPANE-1-CARBOXYLIC ACID SYNTHASE 2 and 6, either by their direct phosphorylation (Liu and Zhang, 2004) or indirectly (transcriptionally) by phosphorylation of WRKY33 (Li et al., 2012a). Both MAPKs are also involved in pathogen induced ethylene and brassinosteroid signaling, through phosphorylation of ETHYLENE-INSENSITIVE 3 (Yoo et al., 2008) and BRASSINOSTEROID INSENSITIVE1-ETHYL METHANESULFONATE SUPPRESSOR 1 (Kang et al., 2015), respectively.

Similar to MPK3 and MPK6, MPK4 is involved in immune response through multiple mechanisms. MPK4 phosphorylates MPK4 SUBSTRATE 1 (MKS1; Andreasson et al., 2005), causing the release of MKS1-WRKY33 complex. This allows WRKY33 to promote the expression of *PHYTOALEXIN DEFICIENT 3*, antimicrobial camalexin biosynthetic enzyme (Qiu et al., 2008; Liu et al., 2015). A transcriptional repressor important for pathogen response ARABIDOPSIS SH4-RELATED 3 is also phosphorylated by MPK4 (Li et al., 2015a). This MAPK regulates also mRNA decay machinery during PTI responses by phosphorylation of *Arabidopsis* homolog of yeast PROTEIN ASSOCIATED WITH TOPOISOMERASE II (Roux et al., 2015). Moreover, MPK4 modulates alternative splicing of various genes in response to PAMP (Bazin et al., 2020). Activation of MPK4 promotes JA-dependent gene expression (e.g. *PDF1.2* and a pathogenesis related gene *THIONIN 2.1;* Petersen et al., 2000), while it has a negative impact on SA-dependent immune response (Kong et al., 2012).

Transcriptomic analysis of single mutants defected in the constituents of MEKK1-MKK1/2-MPK4 pathway suggested that this cascade promotes the expression of approximately 50% of flg22-responsive genes (Frei dit Frey et al., 2014). On phenotypic level, these mutants have stunted habitus, which is a consequence of an autoimmune response (Gao et al., 2008; Qiu et al., 2008). As a result, mutants show increased expression of pathogenesis-related (PR) genes as well as enhanced levels of SA (Petersen et al., 2000; Gao et al., 2008; Gawroński et al., 2014). It was found that the autoimmune response is caused by over-activation of a defense, mediated by a nucleotide-binding and leucine-rich repeat receptor protein *SUPPRESSOR OF MKK1/MKK2 2* (Zhang et al., 2012). More recent studies uncovered complex interactions behind MPK4 directed autoimmunity among *Catharanthus roseus* RECEPTOR-LIKE KINASE 1-like-LLG1 complex (Huang et al., 2020), CALMODULIN-BINDING RECEPTOR-LIKE CYTOPLASMIC KINASE 3 (Zhang et al., 2017) and malectin-like RLK LETUM 1 (Liu et al., 2020).

Within effector-triggered immunity, pathogens developed various types of effectors, which eliminate PTI by targeting the mechanisms of signal perception and transduction. Thus, *P. syringae* effectors AvrPto and AvrPtoB specifically bind and inactivate FLS2, EFR, and CERK1 receptors (Xiang et al., 2008; Zheng et al., 2012). HopF2 and HopAI1 effectors, originating from the same pathogen, specifically inactivate MKK5 (Wang et al., 2010b; Zhou et al., 2014) and MPK3/4/6 (Zhang et al., 2007; Zhang et al., 2012) respectively, by their dephosphorylation. During effector-triggered immunity, plants use resistance (R) proteins to sense the occurrence of pathogen effectors, which also occurs under the control of MAPK cascades (reviewed in Lang and Colcombet, 2020).

1.1.2 MAPK signaling during abiotic stress

Abiotic stresses such as osmotic and temperature stress, drought, heavy metals, high light or UV irradiation belong to the most important factors limiting plant growth and crop production. All of these conditions lead to the production of secondary messengers such as ROS, Ca^{2+} and phytohormones. Their crosstalk and ability to activate signaling cascades is the main driving force of plant stress adaptation (Smékalová et al., 2014).

Cold stress activates two MAPK pathways involving either MKK2 (Ichimura et al., 2000; Teige et al., 2004) or MKK4/5 as MAP2Ks (Li et al., 2017a; Zhao et al., 2017). MKK2 is phosphorylated by MEKK1 and activates MPK4 (Ichimura et al., 2000; Teige et al., 2004). MKK4/5 acting upstream of MPK3/6 negatively affect cold stress response, because phosphorylation of INDUCER OF CBF EXPRESSION 1 transcriptional activator leads to its degradation (Li et al., 2017a; Zhao et al., 2017). The MAPK regulation of cold stress response is controlled by CALCIUM/CALMODULIN-REGULATED RECEPTOR-LIKE KINASES 1 and 2, which promote the activation of MEKK1-MKK2-MPK4 (Yang et al., 2010) pathway, but suppress the activation of MKK4/5-MPK3/6 (Zhao et al., 2017).

Heat shock TFs (HSFs) are master regulators determining plant heat stress tolerance (Lämke et al., 2016). They are MAPK targets, as for example MPK6 phosphorylates HSFA2 on its Thr-249 residue, which then relocalizes from the cytoplasm to the nucleus (Evrard et al., 2013). HSFA4A is phosphorylated by MPK3, MPK4 and MPK6 on Ser-309 and promotes expression of heat shock protein (HSP) *HSP17.6A* and TFs *WRKY30* and *ZAT12* (Andrási et al., 2019). The involvement of MAPKs in heat stress tolerance is exemplified also by MPK6 directed phosphorylation of γ-VACUOLAR PROCESSING ENZYME, which plays an important role during programmed cell death (PCD) under heat stress (Li et al., 2012b). Heat stress responsive proteins HSP90s interact and activate YODA (MAP3K)-MPK3/6 cascade under heat stress. Subsequently, both MPK3/6 inhibit the activity of TF SPEECHLESS, which is responsible for stomatal development (Samakovli et al., 2020).

MAPKs are involved in drought stress responses through crosstalk with abscisic acid (ABA) as well as phosphatidic acid (PA) signaling. ABA and ROS-activated MPK9 and MPK12 act upstream of anion channels in guard cells, thus regulating a stomatal closure (Jammes et al., 2009). MPK3 was found as another principal player in guard cell signaling via ABA and H_2O_2 perception in guard cells (Gudesblat et al., 2007, Danquah et al., 2014; Sierla et al., 2016). Thus, MAPK signaling activated by ABA-induced ROS accumulation is implicated in stomatal movements. PA, a phospholipid important for ABA signaling, is binding MPK6 and stimulates its kinase activity (Yu et al., 2010). Plant drought responses are also affected by mRNA decapping that is regulated by DECAPPING 1 (DCP1), which is phosphorylated by MPK6. DCP1 is then preferentially associated with DCP5 to promote mRNA decapping

in vivo. *Arabidopsis dcp5-1* mutant and transgenic line expressing phosphomutated $DCP1^{S237A}$ were hypersensitive to drought stress in comparison with a wild type (Xu and Chua, 2012). MPK6 (downstream of MAPKKK15-MKK4) has also impact on drought responsive gene expression through phosphorylation of WRKY59, which promotes the expression of *DEHYDRATION-RESPONSIVE ELEMENT BINDING PROTEIN 2* in response to drought stress. This TF then regulates the expression of ABA-independent drought-responsive genes (Li et al., 2017b).

Osmotic stress activates MAPK signaling, particularly MPK3 and MPK6 upstream of MKK9 (Zhao and Guo, 2011) or MKKK20 (Kim et al., 2012b). It leads also to activation of MEKK1 (Su et al., 2007) and MMK2, upstream of MPK4 and MPK6 (Teige et al., 2004).

A previous study identified a lectin receptor-like kinase SALT INTOLERANCE 1 to be an upstream activator of MPK3 and MPK6 in response to salt stress. However, SALT INTOLERANCE 1-MPK3/6 complex is a negative regulator of salt stress response by affecting ROS, ethylene homeostasis and signaling (Li et al., 2014).

One of the mechanisms of how MAPKs regulate osmotic stress signaling lies in the above-mentioned positive regulation of MPK6 by PA and subsequent phosphorylation of SALT OVERLY SENSITIVE 1 Na^+/H^+ antiporter providing Na^+ efflux at the expense of cytosolic acidification (Yu et al., 2010). Interestingly, MAPKs also interact with PA-producing enzyme PHOSPHOLIPASE Dα1 (PLDα1), with an impact on ABA and osmotic stress response (Vadovič et al., 2019).

MPK3 phosphorylates AZELAIC ACID INDUCED 1, a lipid transfer protein-related hybrid proline-rich protein, conferring salt stress tolerance in *Arabidopsis* (Pitzschke et al., 2014). MICROTUBULES ASSOCIATED PROTEIN 65-1 regulates rapid depolymerization and reorganization of cortical microtubules in response to salt treatment upon phosphorylation by MPK6 (Zhou et al., 2017).

1.1.3 MAPKs in *Medicago sativa*

Medicago sativa L., also known as alfalfa or lucerne, is a perennial world's leading forage legume, with extensive green biomass production and rich root system providing beneficial impact on soil agronomical properties (Radović et al., 2009). Alfalfa is widely used as a livestock feed and as a biofuel feedstock for ethanol

production (McCoy and Bingham, 1988; Flajoulot et al., 2005). Alfalfa and other legumes are characterized by their ability to interact with nitrogen-fixing bacteria named rhizobia (e.g. *Bradyrhizobium* or *Sinorhizobium*) and their interaction can lead to a reduction of atmospheric nitrogen into ammonium in specialized organs called root nodules (Oldroyd, 2013; Wang et al., 2018a). This may contribute up to 60% of the entire nitrogen nutritional requirement of alfalfa. Thus, alfalfa provides cost-effective tool to improve nitrogen-limited soils, even under adverse environmental conditions (Radović et al., 2009; Jia et al., 2013).

The symbiotic interaction is initiated by the release of flavonoid compounds by plant roots to the rhizosphere, which are sensed by bacteria. As a response, the bacteria produce extracellular lipochitooligosaccharides, known as nodulation (Nod) factors (Figure 2; Oldroyd, 2013). Nod factors are sensed by specific receptor-like kinase complexes, which consist e.g. of NOD FACTOR RECEPTOR (LjNFR1)/LYSIN MOTIF RECEPTOR-LIKE KINASE 3 (MtLYK3) heterodimer and NOD FACTOR PERCEPTION 5 (LjNFR5/MtNFP; Roy et al., 2020). Nod factor recognition triggers specific symbiosis signaling pathways, leading to Ca^{2+} oscillations and nodule formation (Peck et al., 2006; Kosuta et al., 2008; Roy et al., 2020). Entry of bacteria into the root system is associated with curling of the root hair tip, and trapping the bacteria inside the root hair curl (Figure 2). Rhizobia are reproduced in the hair curl and penetrate to the root system through a specialized structure called infection thread (IT; Suzaki et al., 2015). Thanks to the rapidly dividing bacteria, IT elongates, allowing the bacteria to reach cortical cells and initiate nodule formation. ITs expand and branch within the cortical cells, which accelerate the bacterial colonization and development of the nodule primordium (Figure 2; Tian et al., 2012). Later, rhizobia are released from IT inside the cells of the nodule, and they differentiate to individual bacteroids, which form the basic nitrogen-fixing unit. A mature indeterminate nodule may be divided into five zones according to present biological processes: meristematic zone, infection zone, interzone, nitrogen fixing zone, and a senescent zone (Figure 2; Wang et al., 2018b). Nitrogen is assimilated from ammonia or ammonium ions by a nitrogenase enzyme complex. The effective assimilation requires nearly oxygen-free conditions, which are maintained by specialized proteins called leghemoglobins (Ott et al., 2005; Liu et al., 2018).

Since nitrogen fixation is extremely energetically expensive, alfalfa initiates symbiotic interaction only under nitrogen starvation conditions. Moreover, only a few percentage of initiated ITs lead to the formation of functional nodules (Mortier et al., 2012; Roy et al., 2020). Additionally, plants must precisely recognize a symbiotic or pathogenic organism to trigger proper signaling pathways (Soto et al., 2009; Oldroyd, 2013; Roy et al., 2020), thus, requiring complex and specific signaling cascades with strict regulation.

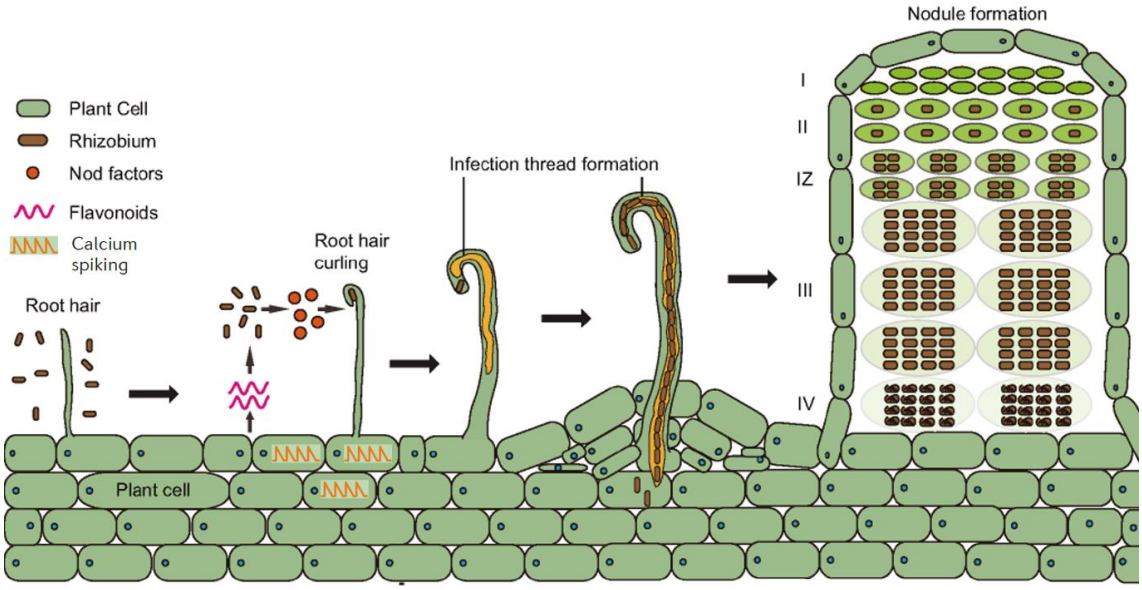

Figure 2 Process of legume-rhizobial interactions leading to nodule formation. The important steps of plant-bacteria crosstalk, initiation of infection following nodule development are showed. Plant roots cells release flavonoid compounds after recognition of rhizobia. In turn, rhizobia produce nodulation (Nod) factors that are recognized by the plant. Symbiotic signaling cascades are activated by Ca^{2+} oscillations and other compounds. Bacteria gain entry into the plant cells in structures known as root hair curl, which are trapping the bacteria. The formation of infection threads (IT) allows the entrance of rhizobia into the root tissue. Nodule formation is initiated by nodule meristem in the root cortex. Rhizobia are released from IT, captured in bacteroides and nitrogen fixation is initiated. A mature indeterminate nodule is composed from meristem zone (I), infection zone (II), interzone (IZ), nitrogen fixing zone (III), and senescent zone (IV). Adopted and modified from Wang et al. (2018b).

MAPKs plays an important role during stress signaling (Jonak et al., 1996 and 2004; Cardinale et al., 2002; Lopez-Gomez et al., 2012), development (Bögre et al., 1999; Šamaj et al., 2002; Chen et al., 2017) along with establishing a symbiotic relationship (Lee et al., 2008; Chen et al., 2012; Ryu et al., 2017; Yin et al., 2019) in *Fabaceae*. So far, four MAPKs known as SIMK (STRESS-INDUCED MAPK or MMK1), MMK2, MMK3, and SAMK (STRESS-ACTIVATED MAPK or MMK4), were identified in alfalfa (Jonak et al., 1999). SIMK is a salt and elicitor stress-induced MAPK orthologous to *Arabidopsis* MPK6 (Cardinale et al., 2002), which is activated in

response to salt stress by upstream STRESS-INDUCED MAPKK (SIMKK; Kiegerl et al., 2000). In addition to that, SIMK is localized to the nucleus and cytoplasm of the root cells, while it relocates from the nucleus to the growing tip of the developing root hairs (Šamaj et al., 2002). Activation and the subsequent sub-cellular relocation from nucleus to cytoplasmic compartments of both SIMK and its upstream SIMKK were induced by salt stress (Ovečka et al., 2014). The actin-dependent relocalization of SIMK and SIMKK to the root tip, along with their activity, is required for proper root hair formation and elongation in alfalfa (Šamaj et al, 2002). Recently, it was revealed, that their genetic modification is linked to defects in IT generation (Hrbáčková et al., 2020), which suggests the important role of the SIMKK-SIMK module in nodulation. SIMK can be activated also by upstream PATHOGEN-RESPONSIVE MAPKK (PRKK), which shares 68% identity to *Arabidopsis* MKK2, in response to Pep13 elicitor (Cardinale et al., 2002). All four alfalfa MAPKs are activated in response to excessive Cd^{2+}, Cu^{2+} concentrations and also elicitors treatment such as Pep13, chitin, ergosterol and β-glucan (Cardinale et al., 2000 and 2002). While SIMK and SAMK are activated by upstream SIMKK after Cu^{2+} treatment, this was not observed for MMK2 and MMK3 (Jonak et al., 2004). Additionally, both SAMK and SIMK are implicated in the response to abiotic stress such as wounding (Bögre et al., 1997; Bekešová et al., 2015), drought, cold (Jonak et al., 1996), and mechanical stimulation (Bögre et al., 1996). The activation of both MMK2 and MMK3 were also found after various pathogen-derived elicitor treatments (Cardinale et al., 2000), along with aminocyclopropane-1-carboxylic acid as an ethylene precursor that triggers SIMK and MMK3 (Ouaked et al., 2003). Finally, MMK3 might have a regulatory role during plant cytokinesis, while its presence and activity were observed only in actively dividing cells (Bögre et al., 1999).

Although considerable progress has been made in understanding the nodulation process and defense responses of the non-crop model *Medicago truncatula* (Ryu et al., 2017; Pfeilmeier et al., 2019), these processes and the possible involvement of MAPK signaling are much less clear in alfalfa. Further understanding of MAPK roles in both defense and symbiotic processes in alfalfa requires intensive research.

1.2 Reactive oxygen species

1.2.1 ROS and their production

The common feature of all aerobic organisms is the exploitation of O_2 in metabolism, which is powered by energy-producing reactions that lead to the generation of ROS by electron or energy leakage to O_2 (Fischer et al., 2013). ROS are defined as molecules displaying higher chemical reactivity than O_2 and about 1% of O_2 utilized by plants is turned to their production. The most important ROS in higher plants include singlet oxygen ($_1O^2$), superoxide anion ($O_2^{\cdot-}$), hydrogen peroxide (H_2O_2) and hydroxyl radical ($HO^{\cdot}$). The high reactivity of ROS may cause damaging oxidative effects on lipids, nucleic acids, and proteins eventually resulting in cell death. Individual ROS are characterized by different reactivity, which is closely related to the time of their existence (Table 1; Mittler, 2017; Waszczak et al., 2018). The most reactive and damaging ROS is $HO^{\cdot}$ with the shortest half lifetime. Based on the high stability and relatively low reactivity, H_2O_2 has many additional functions and is unique among ROS (Mattila et al., 2015). Moreover, H_2O_2 could be transported by membrane-localized aquaporins and cause rapid and reversible oxidation of redox-sensitive proteins (Miller et al., 2010; Mittler, 2017). All these features make H_2O_2 a suitable candidate for signaling roles under both optimal and adverse environmental conditions (Apel and Hirt, 2004; Waszczak et al., 2018).

Table 1 Characterization of major reactive oxygen species. Asterisks indicate the degree of reactivity. Adopted and modified from Mittler (2017).

Name	Symbol	Diffusion range (nm)	Half life (µs)	Reactivity	Reactive specificity
Singlet oxygen	$^1O_2$	30	1–4	***	Lipids and proteins oxidation (Cys, His, Trp, Tyr residues)
Superoxide	$O_2^{\bullet-}$	30	1–4	**	Reacts with Fe-S proteins
Hydrogen peroxide	H_2O_2	> 1000	> 1000	*	Reacts with DNA, proteins (Cys, Met residues)
Hydroxyl radical	$OH^{\bullet}$	1	< 1	****	DNA, RNA, lipids, proteins

Chloroplasts are the main ROS producers in photosynthesizing organisms. Production of ROS in chloroplasts is connected to the light-dependent photosynthetic electron transport chain. The formation of $_1O^2$ is attributed to the excited triplet state of chlorophyll pigments in the antenna at photosystem II (PSII) and its reaction centers (Triantaphylidès and Havaux, 2009). $O_2^{\cdot-}$ is produced in both photosystems, however,

PSI is reported as a predominant site, where $O_2^{\cdot-}$ is generated by Mehler reaction in conditions of low $NADP^+$ concentrations and in the presence of reduced thioredoxin, ferredoxin and iron-sulfur proteins (Mattila et al., 2015). Dismutation of $O_2^{\cdot-}$ leads to production of H_2O_2, which could be reduced to $HO^{\cdot}$ by the non-hem iron, within Fenton reaction (Pospíšil, 2016; Takagi et al., 2016).

The contribution of mitochondria to ROS production is relatively small in photosynthetic tissues in comparison with chloroplasts. Anyway, the imbalance in mitochondrial ROS production is an indicator of stress and it very often follows altered ROS homeostasis in chloroplast (Zhao et al., 2020). As in chloroplast, the production of ROS in mitochondria is mainly connected to electron transport chain (ETC), which takes place in the inner mitochondrial membrane. All three mitochondrial complexes (I, II, and III) are suggested as sources of $O_2^{\cdot-}$ generation. While complexes I and II produce $O_2^{\cdot-}$ on the matrix side of the inner mitochondrial membrane, complex III releases $O_2^{\cdot-}$ on both sides of the inner mitochondrial membrane (Bleier and Dröse, 2013; Huang et al., 2016). The production of mitochondrial ROS can be prevented by bypassing the complexes III and IV by alternative oxidases. These enzymes, acting upstream of complex III, contribute to mitochondrial redox balance maintenance during various stresses (Giraud et al., 2008; Vanlerberghe, 2013). Besides, mitochondrial redox homeostasis is also maintained by *Arabidopsis* UNCOUPLING PROTEIN 1 by uncoupling the electrochemical gradient (Barreto et al., 2014 and 2017).

Peroxisomes are the place of various metabolic processes resulting in ROS production including photorespiration, ureides metabolism, xenobiotics detoxifications and β-oxidation (Pan et al., 2020). Decreased availability of CO_2, high temperature and irradiation result in a higher rate of photorespiration, where RuBisCO catalyzes oxygenation rather than carboxylation of ribulose-1,5-bisphosphate. This reaction leads to the accumulation of 2-phosphoglycolate, which is metabolized to glycolate and after its relocalization into peroxisomes it is metabolized in glycolate oxidase-dependent oxidation producing glyoxylate and H_2O_2 (Noctor et al., 1999; Flügel et al., 2017). In addition, peroxisomal membrane contains an electron transport chain involving NADH:ferricyanide reductase and cytochrome b, which produces $O_2^{\cdot-}$ into the cytosol (Bowditch and Donaldson, 1990). Production of $O_2^{\cdot-}$ is described also for peroxisomal xanthine oxidase as a part of purine catabolism (López-Huertas et al., 1999; Del Río and Lopez-Huertas, 2016). ROS are produced also in the endoplasmic reticulum and it is

connected particularly with ETC located in endoplasmic reticulum membranes. The ROS production is linked with enzymes such as NADPH OXIDASE 4 and NADPH-P450 REDUCTASE (Zeeshan et al., 2016).

The cytosolic pool of ROS is formed mainly by H_2O_2 transported across the membranes from the above mentioned organelles. In addition, aldehyde oxidase (AO), involved in phytohormone biosynthesis and purine metabolism, is proposed to generate ROS in the cytosol (Yesbergenova et al., 2005).

Extracellular space, including cell wall, defines the integrity of plant cell and allows regulated material exchange with the surrounding environment. Apoplast is also a place of ROS production during stress response or developmental processes. Moreover, it represents the first layer of plant interaction with beneficial or pathogenic organisms (Keegstra, 2010; Qi et al., 2017; Soukup and Tylová, 2018). Therefore, it is not surprising that several ROS-producing enzymes were identified in extracellular space. The large group of extracellular class III heme peroxidases is potent producers of a significant amount of apoplastic ROS (Daudi et al., 2012). The key producer of ROS, specifically $O_2^{\cdot-}$, into the apoplast are NADPH oxidases, in plants encoded by *RBOH* (*RESPIRATORY BURST OXIDASE HOMOLOGUES)* genes. Polyamine oxidases, which catalyze the aerobic degradation of polyamines as spermidine and spermine, are important producers of H_2O_2. Other enzymes potent to produce ROS into the apoplast and cell wall space are oxalate oxidases (Berna and Bernier, 1999; Li et al., 2016), quinone reductases (Schopfer et al., 2008), and lipoxygenases (Podgórska et al., 2017; Prasad et al., 2017).

Currently, ROS are recognized as universal signaling metabolites playing an important role during stress responses (Noctor et al., 2017) and development (Mhamdi and Van Breusegem, 2018). This idea is supported by the presence of ROS within almost all cell compartments as is described above. Roles of ROS during signaling and development are discussed in the following chapters.

1.2.2 Signaling roles of ROS

The production of ROS is strictly regulated by a complex antioxidant system, which is keeping ROS in physiological concentrations. Depending on the generated ROS concentration, severity of stress, antioxidant capacity, and cellular energetic status, different cellular and physiological outcomes may be obtained. In higher concentrations,

ROS shift the compartmental redox balance toward an oxidized state and this change can be sensed by various compartment-specific systems (Noctor et al., 2017). The key consequence of ROS accumulation is the modification of signaling targets (e.g. kinases, TFs, stress response proteins) by their oxidizing properties (Waszczak et al., 2014). ROS can modulate signaling through their capability to affect protein redox status via oxidation of methionine residues and thiol groups of cysteines. This leads to activation, inactivation, or alters the structure and function of the target proteins (Waszczak et al., 2015). These modifications are strictly regulated by redox-sensitive proteins such as thioredoxins, peroxiredoxins and glutaredoxins, which can undergo reversible oxidation/reduction and are activated/inactivated in the response to the cellular redox state (Waszczak et al., 2015 and 2018). The oxidation of Cys-residue as a regulatory mechanism is employed also for sensing of extracellular H_2O_2 (Wu et al., 2020). HYDROGEN-PEROXIDE-INDUCED Ca^{2+} INCREASES 1 (HPCA1) is a membrane-spanning enzyme belonging to a protein family of leucine-rich repeat receptor kinases, which senses apoplastic H_2O_2 in stomatal guard cells via the oxidation of two special pairs of cysteine amino-acid residues in its extracellular domain, leading to its autophosphorylation. This promotes the acceleration of Ca^{2+} influx through Ca^{2+}-channels and subsequent stomata closure (Wu et al., 2020).

Redox perturbations driven by ROS production in chloroplasts and mitochondria are transduced by metabolic signals to the nucleus in order to activate rapid adaptive mechanisms within retrograde signaling (Chan et al., 2016; Cui et al., 2019). These metabolites may include 3'-phosphoadenosine 5'-phosphate, methylerythritol cyclodiphosphate, and β-carotene or their oxidative derivatives (Estavillo et al., 2011; Waszczak et al., 2018). Moreover, chloroplastic H_2O_2 itself is transported to the nucleus by stromules in order to activate the expression of defense genes (Erickson et al., 2017; Hanson and Conklin, 2020).

Mitochondrial ROS play an important role during various processes as hormone (He et al., 2012; Zhang et al., 2014), redox and retrograde signaling (Rhoads and Subbaiah, 2007), PCD (Van Aken and Van Breusegem, 2015) or defense against pathogens (Colombatti et al., 2014). Peroxisomal ROS are also involved in signaling because peroxisomal glycolate oxidase produces almost half of the cellular H_2O_2 pool under normal conditions (Foyer and Noctor, 2003). Increased production of peroxisomal ROS leads to a change of redox status from reduced to oxidized state

leading to fast reprogramming of gene expression (Sandalio and Romero-Puertas, 2015; Kerchev et al., 2016).

The perception of the apoplastic ROS is a crucial source of the signaling information for plants. Apoplastic ROS are involved in stress responses (Chaouch et al., 2012; Qi et al., 2017), long-distance signaling (Gilroy et al., 2016; Fichman and Mittler, 2020), various developmental processes (Orman-Ligeza et al., 2016; Mhamdi and Van Breusegem, 2018; Choudhary et al., 2019), and induction of cell death (Van Breusegem and Dat, 2006). They are sensed either by their recognition by above mentioned membrane receptors (Wu et al., 2020), or by recognition of oxidized apoplastic peptides, ligands and metabolites (Tavormina et al., 2015; Kimura et al., 2017; Waszczak et al., 2018). Alternatively ROS are sensed by oxidative PTMs of intracellular signaling proteins (Waszczak et al., 2015).

RBOHs are encoded by ten genes in *Arabidopsis* genome (Torres and Dangl, 2005). These enzymes contain six transmembrane domains with evolutionary conserved C-terminal region carrying FAD- and NADPH-binding domains crucial for transferring electrons to generate $O_2^{\cdot-}$ and an N-terminal region with Ca^{2+} binding motifs (Sumimoto et al., 2008). Activation of RBOH enzymes requires binding of Ca^{2+} ions and phosphorylation, which is provided by various calcium-dependent protein kinases (CDPK; Ogasawara et al., 2008; Kimura et al., 2012; Asai et al., 2013). The small GTPase called Rho of Plants 6 (ROP6) interacts with RBOHD and RBOHF and this complex, which is clustering in specific nanodomains preconditions ROS formation upon osmotic stimulation (Smokvarska et al., 2020). RBOHs are also activated by PA binding in order to regulate ABA-induced stomatal closure (Zhang et al., 2009).

ROS exhibit also vital crosstalk with second messengers, such as Ca^{2+} and reactive nitrogen species (RNS). The interplay between Ca^{2+} and ROS is mutual, because the cytosolic Ca^{2+} content is regulated by ROS, and *vice versa*, Ca^{2+} is crucial for ROS production (Choi et al., 2014; Gaupels et al., 2017). Therefore, Ca^{2+}-dependent ROS signaling through RBOHs as key signaling hubs and ROS-dependent Ca^{2+} signaling through the direct regulation of Ca^{2+} channels and sensors, amplify each other (Marcec et al., 2019).

ROS interact with one of the key ubiquitous secondary messengers, nitric oxide, involved in plant development, metabolism, (a)biotic stress responses, stomatal closure,

and other processes (Piterková et al., 2015; Farnese et al., 2016; Niu and Liao, 2016). The first evidence of nitric oxide and H_2O_2 interplay was related to its cytotoxic effects during the hypersensitive response (Delledonne et al., 2001). Generally, ROS and RNS crosstalk is Janus-like, since it has concentration-dependent, organelle-specific, beneficial, and deleterious effects in the plant cell (Kohli et al., 2019).

ROS can cause carbonylation, which is a type of protein oxidation, where the carbonyl groups (aldehydes and ketones) are produced on protein side chains (Pro, Arg, Lys, and Thr). Carbonylation alters protein stability and might increase the susceptibility to proteolysis (Dalle-Donne et al., 2003; Suzuki et al., 2010; Ciacka et al., 2020).

Signal perceived by organ, tissue or single cell is spread to distal parts of the plant (so called systemic tissue) by mobile systemic signals transduced by different chemical compounds, by ROS-, Ca^{2+}- and hydraulic waves, electric and redox signals as well as phytohormones (Mittler and Blumwald, 2015; Gilroy et al., 2016; Fichman and Mittler, 2020). This leads to the initiation of acclimation and defense mechanisms (Suzuki et al., 2013; Mittler and Blumwald, 2015; Kollist et al., 2019). This process is called either systemic acquired acclimation (SAA) for abiotic stresses such as high light, cold, heat, osmotic stress, and salinity or systemic acquired resistance (SAR) for biotic stresses (Alvarez et al., 1998; Karpinski et al., 1999). SAA and SAR involve a reprogramming of gene expression, aiming to increase the plant tolerance (Rejeb et al., 2014; Chen and Yang, 2020).

As mentioned above, a systemic signal may be transduced by ROS wave, a process of cell-to-cell signaling occurring in terms of seconds and minutes (Miller et al., 2009; Fichman and Mittler, 2020). The auto-propagating ROS wave is driven by Ca^{2+}-dependent RBOHD and is directly linked to the Ca^{2+} (Gilroy et al., 2016). This fast long-distance ROS signaling requires activation of RBOHD, which generates $O_2^{\cdot-}$ to the apoplast followed by its dismutation to H_2O_2. H_2O_2 enters the neighboring cells and activates plasma membrane-located Ca^{2+} channels, leading to increased intracellular accumulation of Ca^{2+} and subsequent activation of RBHOD via CDPK (Miller et al., 2009; Gilroy et al., 2016; Fichman et al., 2019; Hu et al., 2020). Systemic acclimation is ROS wave dependent, which highlights the importance of ROS during stress signaling (Suzuki et al., 2013; Zandalinas et al., 2019). A simplified schematic overview of ROS

networks controlling abiotic and biotic stress responses locally and systemically is presented in Figure 3.

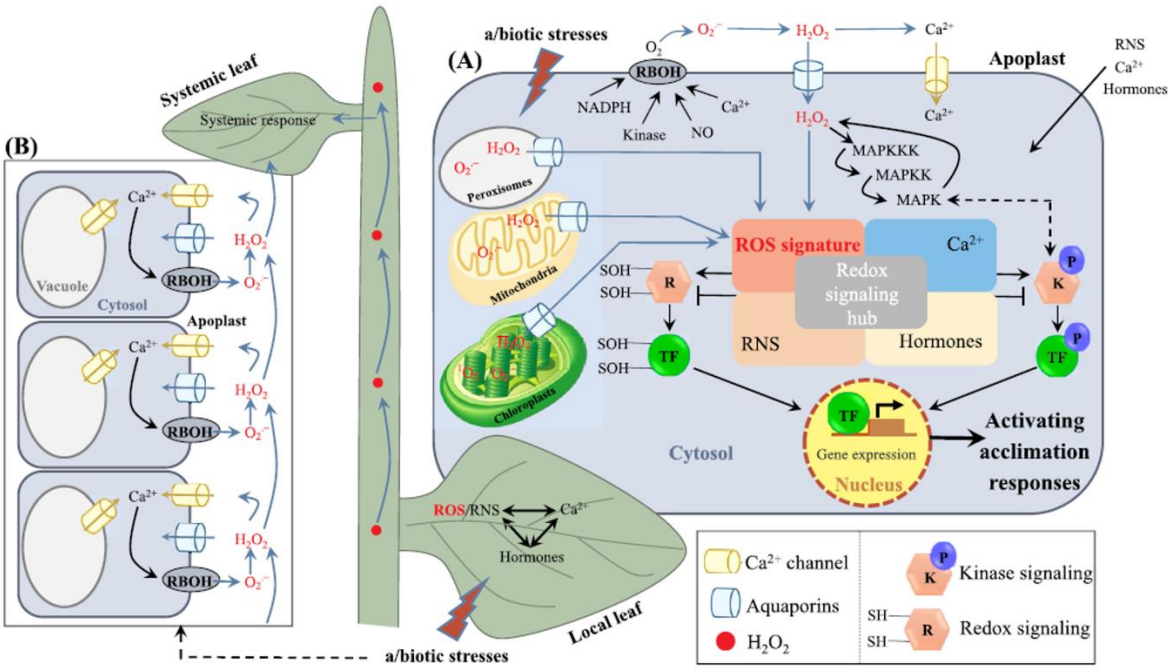

Figure 3 Schematic model of simplified cellular ROS networks orchestrating (a)biotic stress responses locally and systemically. (A) The cellular networks activated by or involved in ROS signal perception during (a)biotic stresses with the potential to spread to the whole plant. (B) Representative scheme of simplified cell-to-cell auto-propagating (called ROS-waves) communication initiated by various stimuli. Abbreviations: RBOH – respiratory burst oxidase homolog, ROS – reactive oxygen species, RNS – reactive nitrogen species, TF – transcription factor, MAPKKK – mitogen activated protein kinase kinase kinase, MAPKK – mitogen activated protein kinase kinase, MAPK – mitogen activated protein kinase. Adopted from Farooq et al. (2019).

1.2.2.1 ROS-induced MAPK signaling pathways

It is well-known that MAPK signaling pathways are activated by ROS accumulated during plant responses to either abiotic stresses or biotic interactions. So far, two MAP3Ks were identified to be activated by ROS, namely ARABIDOPSIS HOMOLOGUES OF NUCLEUS AND PHRAGMOPLAST LOCALIZED KINASES (ANPs), and MAPKKK1 (or MEKK1). ANPs are required for the plant immune response (Kovtun et al., 2000; Savatin et al., 2014), while the ROS-triggered signal is further transduced via MPK3 and MPK6 (Kovtun et al., 2000; Nakagami et al., 2006). The full activation of MPK3 and MPK6 is preconditioned by the presence of OXIDATIVE SIGNAL INDUCIBLE 1 kinase, which is an essential component of this signal transduction pathway (Rentel et al., 2004).

Another ROS-activated MAPK cascade consists of MEKK1, MKK1/2, and MPK4 (Nakagami et al., 2006; Pitzschke et al., 2009). This pathway is also important for basal plant defense against a pathogen attack (Zhang et al., 2012). Moreover, a pathogen-induced oxidative burst activates the MPK7 downstream of MKK3 (MAP2K), thus triggering the expression of *PR* genes, independently of flagellin receptor FLS2 (Dóczi et al., 2007).

Furthermore, MPK1 and MPK2 are activated by oxidative stress, as well as by JA, ABA, and wounding (Ortiz-Masia et al., 2007). In turn, ABA and ROS-activated MPK9 and MPK12 act upstream of anion channels in guard cells, thus regulating stomatal closure (Jammes et al., 2009). MPK3 was found as another principal player in guard cell signaling via ABA and H_2O_2 perception in guard cells, which leads to stomatal closure (Gudesblat et al., 2007). Thus, MAPK signaling activated by ABA-induced ROS accumulation is generally implicated in stomatal movements (Danquah et al., 2014; Sierla et al., 2016).

MAPKs also respond to ROS produced in chloroplasts and mitochondria. In this respect, MPK6 is implicated in chloroplast to nucleus-directed retrograde signaling upon intense light exposure. The activation of MPK6 under such conditions is preceded by the export of a Calvin-Benson cycle intermediate dihydroxyacetone phosphate from chloroplasts to the cytosol. These events lead to the rapid (within several minutes) expression of *APETALA2/ETHYLENE-RESPONSIVE ELEMENT BINDING FACTOR* TFs and other downstream genes, such as *CHLOROPLAST PROTEIN KINASE like*, *CHITINASE FAMILY PROTEIN*, *HSP20-like*, and *PR1* (Vogel et al., 2014). Similarly, MPK4 orchestrates plastid retrograde signaling in a SA-dependent manner (Gawroński et al., 2014). Mitochondrial ROS production induced by oxygen deprivation activates MPK6 and subsequent retrograde signaling toward the nucleus, leading to transcriptional reprogramming and triggering plant defense mechanisms (Chang et al., 2012).

Several studies report on the regulation of MAPKs by direct interactions with ROS. Waszczak et al. (2014) identified MPK2, MPK4, and MPK7 as capable of being sulfenylated in an H_2O_2-dependent manner. Another example pertains to *Brassica napus* BnMPK4, an ortholog of *Arabidopsis* MPK4, which is activated by H_2O_2 and undergoes aggregation upon the H_2O_2-dependent oxidation of the Cys-232 residue (Zhang et al.,

2015). Thus, it is obvious that MAPKs could be modified on Cys-residues by direct oxidation, which can affect their stability, aggregation, and probably protein-protein interactions. It is noteworthy that the redox regulation of MAPKs may lead either to their activation or inactivation and that the oxidation of kinase amino acid residues was reported to interfere with ATP binding and cause inactivation (Diao et al., 2010), but at the same time it may also lead to their super-activation state (Corcoran and Cotter, 2013).

1.2.3 Developmental roles of ROS

ROS are widely involved in plant growth and developmental processes (Xia et al., 2015; Mhamdi and Van Breusegem, 2018; Considine and Foyer, 2020). Proper plant growth in both normal and stress conditions is ensured by precise regulation of cell cycle, proliferation, and expansion, which are affected by ROS or redox-dependent mechanisms (Tsukagoshi, 2012; Diaz-Vivancos et al., 2015; De Simone et al., 2017). The cell cycle is regulated by interaction of cyclins and cyclin-dependent kinases, which are, in addition to other mechanisms, controlled by redox perturbations (Féher et al., 2008; Verbon et al., 2012; Yi et al., 2014). ROS produced by RBOHC control cell proliferation by affecting assembly/disassembly of mitotic microtubule structures (Livanos et al., 2012). ROS, especially $HO^{\cdot}$, have direct impact on cell wall rigidity and relaxation thus influencing cell expansion (Schopfer et al., 2002; Kärkönen and Kuchitsu, 2015; Schmidt et al., 2016). ROS-orchestrated PCD plays an important role in the development of various tissues and organs, such as the tapetum, seed coat, lateral root cap and endosperm (Daneva et al., 2016).

Initial stages of seed germination are accompanied with the accumulation of ROS after water imbibition, which is important for proficient germination and radicle protrusion (Bailly et al., 2008; Müller et al., 2009; Singh et al., 2016). The level of seed dormancy depends on the homeostasis between ROS and antioxidants (Leymarie et al., 2012). Various studies showed the influence of ROS during primary root, lateral root and root hair growth (Foreman et al., 2003; Li et al., 2015b; Tsukagoshi, 2016). RBOH-mediated ROS production promotes lateral root primordia (LRP) formation by inducing cell wall remodeling of overlying parental tissues and via crosstalk between ROS and auxin signaling pathways. Genetic manipulation of RBOHD showed an increased number of LRP in overexpressing lines and decreased in knockout (KO) mutant lines (Orman-Ligeza et al., 2016). Root hair elongation is promoted by ROS produced by

RBOH (specifically by RBOHC) in root hair tip. This was confirmed in *rhd2* mutants deficient in *RBOHC* (identical to RHD2; ROOT HAIR DEFECTIVE 2), which does not accumulate ROS in the tip of bulged root hair leading to short root hairs (Foreman et al., 2003). In addition, a fine-tuned equivalence within H_2O_2 and $O_2^{\cdot -}$ levels serves as a signal defining root hair cell differentiation (Sundaravelpandian et al., 2013). ROS can also participate in the regulation of root elongation (Schopfer et al., 2002), gravitropism (Joo et al., 2001 and 2005) as well as embryogenesis (Rodríguez-Serrano et al., 2012), trichome development (Hülskamp, 2004), pollen tube elongation (Duan et al., 2014; Lassig et al., 2014), flower and gametophyte development (Mhamdi and van Breusegem, 2018), and various types of senescence (Allu et al., 2014; Rogers and Munné-Bosch, 2016).

Moreover, ROS regulate these processes in the close interplay with plant phytohormones, such as auxin and cytokinins (Xia et al., 2015; Zwack et al., 2016). Phytohormones auxin and ABA are capable to promote ROS production by activating NADPH oxidase (Joo et al., 2001; Schopfer et al., 2002; Pasternak et al., 2007). Oppositely, ROS may induce perturbations in the auxin levels (Takáč et al., 2016a) and auxin homeostasis leading to altered shoot branching and leaf rosette shape (Tognetti et al., 2010).

1.3 Antioxidant defense in plants with focus on superoxide dismutases

Generally, enzymatic antioxidant capacity inevitably contributes to plant survival in adverse conditions, especially when the stress pressure exceeds the mechanisms preventing ROS over-accumulation. The significance of antioxidant enzymes has been documented by genetic studies reporting on the positive correlation between their expression and plant stress tolerance. By contrast, the downregulation of these enzymes is connected with plant hypersensitivity to stress and PCD (De Pinto et al., 2012).

ROS scavenging is performed via enzymatic or non-enzymatic antioxidant defense pathways, which control the regulation of ROS levels through strict compartmentalization (Mignolet-Spruyt et al., 2016; Foyer and Noctor, 2020). Non-enzymatic antioxidant defense is mainly mediated by low molecular-weight metabolites such as ascorbate, glutathione, α-tocopherol, carotenoids, and flavonoids. (Locato et al., 2017; Zechmann, 2018; Muñoz and Munné-Bosch, 2019; Foyer and Noctor, 2020).

1.3.1 H_2O_2 decomposing enzymes

Catalases (CATs), ascorbate peroxidases (APXs), dehydroascorbate reductases (DHARs), monodehydroascorbate reductases (MDHARs), and glutathione reductases (GRs) are among the main antioxidant enzyme classes. Furthermore, glutathione peroxidases, peroxidases, and thio-, gluta-, and peroxiredoxins are potent ROS scavengers as well (Dietz, 2011; Kang et al., 2019; Foyer and Noctor, 2020).

CATs are responsible for the detoxification of the overproduced H_2O_2, which occurs owing to their kinetic properties (Tuzet et al., 2019). As iron-containing homotetrameric proteins, CATs catalyze the decomposition of H_2O_2 to H_2O and O_2, predominantly produced during photorespiration. Three genes (*CAT1*, *CAT2,* and *CAT3*) encoding CATs have been found in the *Arabidopsis* genome. CAT isozymes are localized in peroxisomes (Frugoli et al., 1996; Du et al., 2008) and play important roles under unfavorable conditions for plants. Various PTM, such as phosphorylation, glycation, acetylation, S-nitrosation, were found to have a regulatory effect on the activity of CATs (Zou, et al., 2015; Zhou et al., 2018; Rodríguez-Ruiz et al., 2019; Zhang et al., 2020). Moreover, circadian regulation was described for *CAT3* and *CAT2* with opposite diurnal peaks of expression (Zhong et al., 1996 and 1997). Taken together, CATs are admitted as a key antioxidant enzymes with an irreplaceable role during plant development, and stress responses (Su et al., 2018; Palma et al., 2020).

Balance in cellular H_2O_2 levels is also maintained by enzymes of the ascorbate-glutathione cycle, such as APXs, MDHARs, DHARs, and GRs. APXs, as heme-containing peroxidases, detoxify H_2O_2 via the electron transfer from ascorbate to form monodehydroascorbate (MDHA) and H_2O. The presence of nine putative *APX* genes has been described in the *Arabidopsis* genome, nevertheless, the *APX4* gene product is lacking H_2O_2 decomposing activity and *APX7* is annotated as a pseudogene (Granlund et al., 2009). Cytosolic (APX1, APX2 and APX6), stromal APX and thylakoid APX, peroxisomal (APX3 and APX5), and mitochondrial (stromal APX with dual localization) APXs have been recognized in *Arabidopsis* (Maruta et al., 2016). Chloroplastic APX isozymes are involved in the water-water cycle, which decomposes H_2O_2 generated by $O_2^{\cdot -}$ dismutation (Huang et al., 2019). They are therefore crucial for photoprotection (Murgia et al., 2004; Kangasjärvi et al., 2008; Maruta et al., 2010). Remarkably, the chloroplastic H_2O_2 detoxification turns out to be inactive in plants depleted of cytosolic APX1 (Pnueli et al., 2003; Davletova et al., 2005). Activity of

APXs as extremely redox sensitive proteins could be modulated by several PTMs in response to oxidative stress (Aroca et al., 2015; Yang et al., 2015; Begara-Morales et al., 2016).

The reverse reduction of MDHA to ascorbate, catalyzed by MDHAR, occurs in the presence of NAD(P)H as a reductant (Foyer and Noctor, 2011). Overall, five *Arabidopsis* genes encode six functional proteins of MDHARs (Obara et al., 2002). Cytosolic localization is confirmed for MDHAR2 and 3, whereas MDHAR1 has been found also in peroxisomes. MDHAR4 is located in peroxisomal membrane (Lisenbee et al., 2005; Eubel et al., 2008; Kaur and Hu, 2011). The *MDHAR6* gene is expressed in two splicing variants, producing two protein products localized either in mitochondria (MDHAR5) or chloroplasts (MDHAR6; Obara et al., 2002). The overexpression of *Arabidopsis MDHAR1* in tobacco leads to an increased tolerance to ozone, salt, and osmotic stresses (Eltayeb et al., 2007). The overexpression of cytosolic *Acanthus ebracteatus* MDHAR in rice leads to an increased resistance to salt stress and higher germination rate and grain weight (Sultana et al., 2012). A study exploiting the genetic manipulation of *MDHAR4* suggests that it is implicated in plant germination, post-germination growth, and possibly in senescence (Eastmond, 2007). MDHAR2 and MDHAR5 play important roles during the interaction of *Arabidopsis* with plant growth-promoting endophyte *Piriformospora indica* (Vadassery et al., 2009). Moreover, MDHAR was suggested to be affected by PTMs with impact on their regulation (Hu et al., 2015; Begara-Morales et al., 2016).

Dehydroascorbate is enzymatically reduced by DHAR by using glutathione as an electron donor, which is oxidized to glutathione disulfide. DHARs are soluble monomeric enzymes and their thiol group participates in the catalyzed reaction. Three functional genes are present in the *Arabidopsis* genome. Their protein products are localized either in the cytosol (DHAR1, DHAR2) or chloroplasts (DHAR3; Rahantaniaina et al., 2017). Recently, their role in the regulation of ascorbate and glutathione homeostasis was described during plant developmental processes (Ding et al., 2020). The overexpression of *DHAR1* protects *Arabidopsis* from methyl viologen (MV)-induced oxidative, high temperature, and high light stresses (Ushimaru et al., 2006; Wang et al., 2010c; Noshi et al., 2017). DHAR2 has an antioxidant role in plant responses to ozone (Yoshida et al., 2006), drought, salt, and polyethylene glycol (Yin et

al., 2010; Eltayeb et al., 2011), while DHAR3 is involved in the high light response (Noshi et al., 2016).

The pool of reduced glutathione consumed by DHAR activity is recovered by GR in a NADPH dependent reaction, which is essential for glutathione homeostasis. Structurally, the GR protein contains a FAD-binding domain, a dimerization domain, and a NADPH-binding domain, which are crucial for proper enzymatic activity (Berkholz et al., 2008). Two isozymes were described in *Arabidopsis*, showing dual localization in the cytosol and peroxisomes for GR1 and in chloroplasts and mitochondria for GR2 (Kataya and Reumann, 2010; Marty et al., 2019). GR1 is involved in the tolerance of *Arabidopsis* to high light (Müller-Schüssele et al., 2020), heavy metals (Guo et al., 2016; Yin et al., 2017), and salt stress (Csiszár et al., 2018). GR2 is involved in MV-induced oxidative stress (Wang et al., 2019), chilling stress (Kornyeyev et al., 2003), and high light stress (Karpinski et al., 1997), but also in developmental processes such as root growth, root apical meristem maintenance (Yu et al., 2013), embryo development (Marty et al., 2019), and seed germination (Sumugat et al., 2010). In addition, the knock-out mutation of *GR3* confers salt stress sensitivity in rice (Wu et al., 2015).

1.3.2 Superoxide dismutases

SODs (EC 1.15.1.1) are antioxidant metalloenzymes expressed in all living organisms (McCord et al., 1971; Fridovich, 1978; Foyer and Noctor, 2005). SODs catalyze the dismutation of $O_2^{\cdot-}$ to molecular oxygen and less toxic H_2O_2 ($2O_2^{\cdot-} + 2H^+ \leftrightarrow H_2O_2 + O_2$). The enzymatic dismutation of $O_2^{\cdot-}$ by SODs is an extremely effective reaction, occurring at the almost diffusion-limited rate of $\approx 10^9$ $M^{-1} \cdot s^{-1}$ (Sheng et al., 2014). $O_2^{\cdot-}$ can be also spontaneously dismutated to H_2O_2. However, this reaction is 10^4 times slower in comparison with the catalyzed reaction and the rate is highly dependent on the concentration of $O_2^{\cdot-}$ (Murphy, 2009; Sheng et al., 2014). The comparison of catalyzed and spontaneous $O_2^{\cdot-}$ dismutation upon different substrate and enzyme concentrations is showed in Table 2. It should be also noted that SODs are not the only enzymes catalyzing the transformation of $O_2^{\cdot-}$ to H_2O_2. This activity was also found for superoxide reductases, which are present in anaerobic archaea, bacteria (Nivière and Fontecave, 2004) and unicellular eukaryotes (Testa et al., 2011), with different enzymatic mechanisms of reaction ($2O_2^{\cdot-} + 2H^+ + e^- \rightarrow H_2O_2$) requiring reactivation of enzyme by its reduction (Sheng et al., 2014).

Table 2 Comparison of catalyzed and spontaneous $O_2^{\cdot-}$ dismutation at different concentrations of substrate and SOD. Adopted from Sheng et al. (2014).

Concentration		Half life	Acceleration factor
$O_2^{\bullet-}$	SOD		
10^{-6}	None	3000 ms	
10^{-6}	10^{-9}	175 ms	20x
10^{-9}	None	Hours	
10^{-9}	10^{-9}	175 ms	10 000x
10^{-9}	10^{-6}	0.175 ms	10 000 000x

Based on the presence of metal cofactors in their active site, four different SODs exist in living organisms, namely NiSOD, FeSOD, MnSOD, and Cu/ZnSOD. Except for green algae *Ostreococcus tauri* no evidence for NiSODs in eukaryotes has been described (Schmidt et al., 2009) and therefore NiSOD is not discussed in this work.

Fe/MnSOD family is on an evolutionary scale the most ancient and it has been found in archaea, bacteria, and eukaryotes. During evolution it was separated into two individual FeSOD and MnSOD subfamilies in higher eukaryotes. The presence of FeSOD is restricted to photosynthesizing organisms (Case, 2017; Dreyer and Schippers, 2019). Both MnSOD and FeSOD share more than 50% sequence homology with almost an identical active site (Vance and Miller, 1998 and 2001), and both have the cambialistic ability to use Fe^{2+} or Mn^{2+} in their active site depending on ion availability (Meier et al., 1982; Case, 2017). All available information suggests, that FeSOD and MnSOD evolved in primitive lifeforms in the conditions rich for both metals. On the contrary, the evolutionary youngest Cu/ZnSODs have no structural similarity with other SOD isoforms and evolved independently (Bowler et al., 1994). The Cu/ZnSOD have been detected ubiquitously in eukaryotes, but they are also present in bacteria. However, they have been not detected in archaea or algae (Banci et al., 2005; Case, 2017), confirming the idea of evolutionary younger origin compared to FeSOD or MnSOD. Possible physiological explanation of Cu/ZnSOD evolution might be the increase of oxygen in the biosphere, which led to a reduction in Fe^{2+} availability, and the conversion of the insoluble Cu^{1+} into soluble Cu^{2+} (Bannister et al., 1991; Saito et al., 2003). Presence of individual SODs families within the life kingdom species is showed in Figure 4.

Plant SODs compartmentalize into the main compartments of $O_2^{\cdot-}$ production: chloroplast and plastids, cytosol, mitochondria, peroxisome, and apoplast (Kliebenstein

et al., 1998). In the genome of *Arabidopsis*, three *FeSOD* (*FSD1*, *FSD2*, and *FSD3*), one *MnSOD* (*MSD1*), and three *Cu/ZnSOD* (*CSD1*, *CSD2*, and *CSD3*; Kliebenstein et al., 1998; Pilon et al., 2011) gene isoforms have been identified. Mitochondrial $O_2^{\cdot-}$ is eliminated by MSD1 (Morgan et al., 2008), peroxisomes contain CSD3 (Kliebenstein et al., 1998) and cytosolic $O_2^{\cdot-}$ is decomposed by CSD1 and FSD1 (Kliebenstein et al., 1998, Myouga et al., 2008). Photosynthetic $O_2^{\cdot-}$ is decomposed by FSD1 in the chloroplast stroma (Kuo et al., 2013), and by CSD2, FSD2, and FSD3 in thylakoids (Kliebenstein et al., 1998; Myouga et al., 2008).

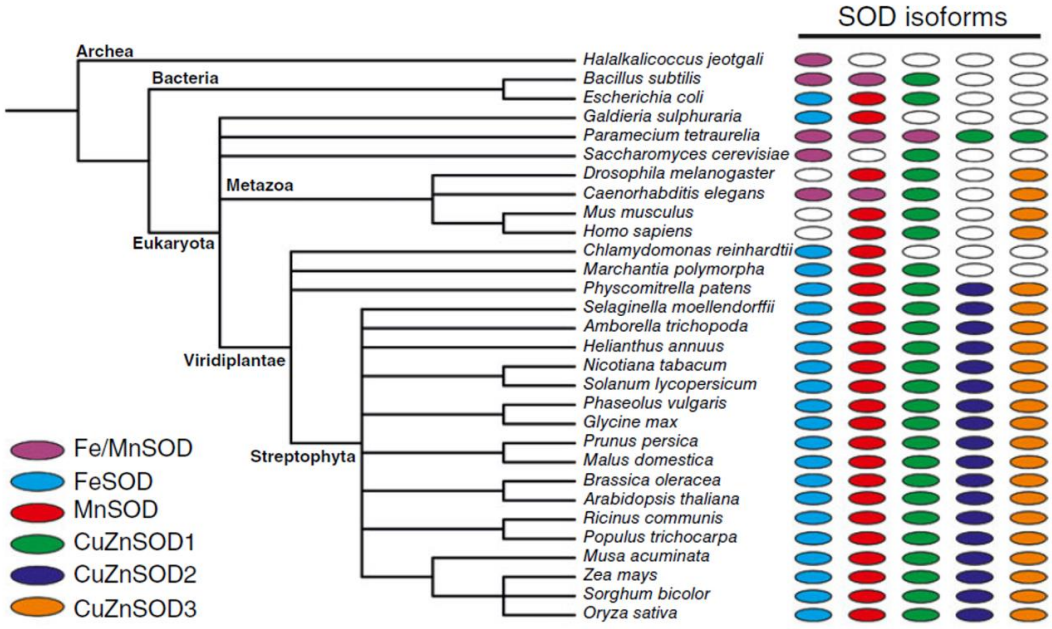

Figure 4 The overview of SOD proteins occurrence within various evolutionary lineages. Adopted from Dreyer and Schippers (2019).

Expression of plant *SODs* is developmentally regulated. This is evident in the case of *Arabidopsis FSD1*, *CSD1* and *CSD2*, while other *Arabidopsis SOD* isoforms show relatively stable expression (Figure 5; Pilon et al., 2011). *MSD1*, *FSD1*, *CSD1*, and *CSD2* are expressed at a significantly higher level in comparison with other *Arabidopsis* SOD isoforms. Interestingly, *FSD1* has an opposite expression pattern during the course of plant growth compared to *CSD1* and *CSD2*. While *FSD1* shows the highest expression at earlier developmental stages, the expression of *CSD1* and *CSD2* is the highest during later stages of rosette development (Figure 5; Pilon et al., 2011). SODs are subjects of various PTMs such as phosphorylation, tyrosine nitration, glutathionylation, and glycation, with impact on their activity, stability or localization (Yamakura and Kawasaki, 2010; Banks and Andersen, 2019). The effect of

S-nitrosylation and tyrosine nitration was examined on recombinant *Arabidopsis* SODs, by treatment with S-nitrosoglutathione and peroxynitrite. No significant effect of S-nitrosylation on activities of recombinant enzymes was detected, but tyrosine nitration of MSD1 led to a drastic reduction (90%) of its activity. In addition, CSD3 and FSD3 showed also slight reduction (30%) of activities in response to tyrosine nitration (Holzmeister et al., 2015). Similar effect of strong inhibition of activity by tyrosine nitration (at Tyr-34) was observed for mammalian MnSOD (Yamakura et al., 1998).

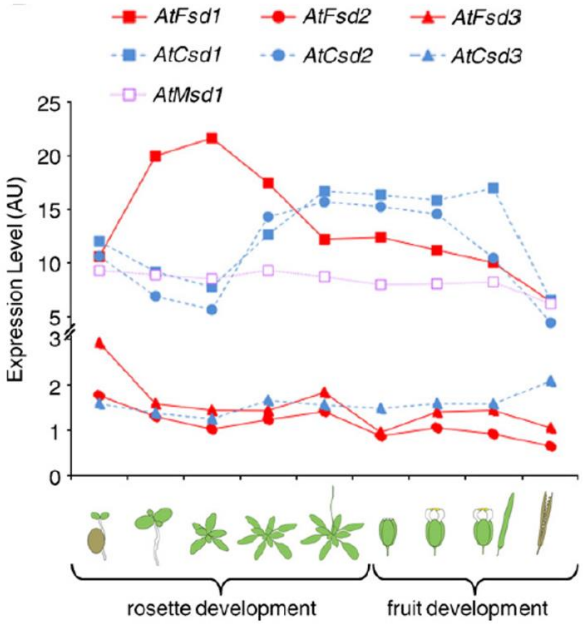

Figure 5 Comparison of expression of *Arabidopsis SOD*s during rosette and fruit development. Data were obtained from Genevestigator. mRNA expression levels are presented in arbitrary units (AU). Adopted from Pilon et al. (2011).

1.3.2.1 FSDs

Interestingly, all *Arabidopsis* FSD isoforms are localized in chloroplast while FSD1 has dual localization in the cytosol and chloroplast as shown in *Arabidopsis* protoplasts (Kuo et al., 2013) and tobacco leaves transiently transformed by particle bombardment (Myouga et al., 2008).

Although FSD1 is the most abundant SOD in *Arabidopsis* with more than 10 times higher expression than *FSD2* and *FSD3*, *fsd1* T-DNA mutants do not exhibit obvious phenotypic defects. Contrariwise, the leaves of *fsd2* and *fsd3* mutants are pale-green in color, with abnormalities in chloroplast development and impaired growth (Myouga et al., 2008). The phenotype of *fsd2*/*fsd3* double mutant is even more pronounced, suggesting that FSD2 and FSD3 have complementary functions. Both

FSD2 and FSD3 are tightly attached to the stromal side of the thylakoid membranes and they form heterocomplexes in chloroplast nucleoids. Here, they possibly prevent DNA damage caused by $O_2^{\cdot-}$ as indicated by the physical interaction of FSD3 with a plastid nucleoid protein called PLASTID ENVELOPE DNA BINDING PROTEIN (Myouga et al., 2008). Both *fsd2* and *fsd3* mutants show a higher accumulation of $O_2^{\cdot-}$ in normal conditions and high sensitivity to high light, while *fsd1* has a similar response as wild type. Additionally, *fsd2* mutant displays decreased chlorophyll concentrations, decreased PSII efficiency followed by reduced rate of CO_2 assimilation under normal conditions. On the other hand, *FSD2* and *FSD3* overexpression confer on increased oxidative tolerance induced by MV (Myouga et al., 2008; Gallie and Chen, 2019). These mentioned reverse genetic studies have questioned the role of FSD1 in oxidative stress tolerance. Interestingly, heterologous overexpression of *Arabidopsis FSD1* in tobacco and maize led to an increased tolerance against MV and in maize also to increased growth rates (Van Camp et al., 1996; Van Breusegem et al., 1999).

The precise mechanism of FSDs activation is still quite unclear (Burkhead et al., 2009; Dreyer and Schippers, 2019). It is known that FSD1 activity is stimulated by the interaction of FSD1 with chloroplast localized CHAPERONIN 20 (CPN20; Kuo et al., 2013).

The main factors affecting *FSD1* expression and activity are the availability of Fe^{2+} (Waters et al., 2012), Cu^{2+} (Cohu et al., 2009; Yamasaki et al., 2009), nitrogen (Mermod et al., 2019), and sucrose (Dugas and Bartel, 2008). FSD1 expression/abundance increases upon low Cu^{2+} availability, in parallel with the drop of expression of *CSD1* and *CSD2* and Cu^{2+} is redirected into housekeeping proteins and compounds as plastocyanin and cytochrome-c oxidase (Burkhead et al., 2009; Cohu et al., 2009; Pilon, 2017). By contrast, in conditions of Cu^{2+} sufficiency, CSD1 and CSD2 abundance rises and FSD1 abundance drops to minimal levels (Cohu et al., 2009; Yamasaki et al., 2009). The expression of *FSD1* and both *CSD1* and *CSD2* is also similarly affected by sucrose (Dugas and Bartel, 2008) and nitrogen availability (Mermod et al., 2019). The expression of *FSD2* and *FSD3*, but not *FSD1* is sensitive to stress conditions as high light and oxidative stress (Kliebenstein et al., 1998; Myouga et al., 2008), heavy metals (Abdel-Ghany et al., 2005; Abercrombie et al., 2008), ozone (Kliebenstein et al., 1998) and cold (Soitamo et al., 2008).

1.3.2.2 CSDs

CSDs are activated by *Arabidopsis* COPPER CHAPERONE FOR SUPEROXIDE DISMUTASE 1 (CCS1; Rae et al., 1999; Abdel-Ghany et al., 2005), which delivers Cu^{2+} to their active site. CCS1 occurs in three splicing variants in *Arabidopsis*, out of which CCS320 (contains N-terminal plastid transit peptide) provides specific activation of CSD2, while CSD1 and CSD3 are activated by CCS184 and CCS229. Additionally, an unknown CCS-independent activation pathway is suggested for CSD1 and CSD3, since the activity of both enzymes but not CSD2 was detected in the *ccs* mutant (Huang et al., 2012). CCS seems to be an evolutionarily conserved protein because *Arabidopsis*, *S. cerevisiae* and *H. sapiens* CSSs share high homology in amino acid sequence and protein domain composition (Abdel-Ghany et al., 2005; Dreyer and Schippers, 2019).

Individual CSDs are positively responding to salinity (Shafi et al., 2015), heavy metals (Abercrombie et al., 2008; Kawachi et al., 2009), high light irradiation, MV (Kliebenstein et al., 1999; Sunkar et al., 2006) and treatment with SA (Kliebenstein et al., 1999).

There are not many studies exploiting genetically modified CSDs in plants. One of them, using *csd2* T-DNA insertion mutant known as KD-SOD, showed suppressed growth, rate of photosynthesis, reduced chlorophyll content and light hypersensitivity (Rizhsky et al., 2003). Later, it was found that this T-DNA mutation in the *CSD2* promoter does not disrupt CSD2 protein production, and KD-SOD plants contain additional unidentified insertions that are likely responsible for the plant phenotype (Cohu et al., 2009). On the other hand, the RNAi mediated downregulation of CSD2 leads to phenotypes very similar to those presented for KD-SOD (Xing et al., 2013). Studies employing homologous or heterologous overexpression of *Arabidopsis CSDs* showed increased tolerance to the various stressors such as MV, chilling temperatures, highlight (Gupta et al., 1993), ozone (Pitcher and Zilinskas, 1996), salt stress (Guan et al., 2017) and heavy metals (Li et al., 2017c).

The abundances of CSDs are primarily regulated by TF SQUAMOSA PROMOTER BINDING PROTEIN-LIKE 7 (SPL7) through the expression of *miRNA398*, which upon low Cu^{2+} concentrations specifically block translation of CSDs, but also CCS and the mitochondrial cytochrome c oxidase subunit (Cohu et al., 2009). miRNA398-directed regulation of CSD abundance depends also on sucrose availability

(Sunkar et al., 2006; Dugas and Bartel, 2008). Further, *CSD1* and *CSD2* expression is also regulated by miRNA408 (Ma et al., 2015), illustrating that the post-transcriptional control of SOD expression is quite complex.

The activation of CSD1 might be also mediated by its interaction with a protein with potential antioxidant function called DJ-1a, which also occurs in Cu^{2+} dependent fashion (Xu et al., 2010).

1.3.2.3 MSD1

MSD1 is important for mitochondrial functions and it is implicated in root development, because *Arabidopsis* MSD1 RNAi line showed retardation in root growth and defects in mitochondrial redox balance. RNAi lines also showed an inhibition of tricarboxylic acid cycle enzymes as aconitase and isocitrate dehydrogenase and a repression of tricarboxylic acid cycle flux in isolated mitochondria (Morgan et al., 2008). MSD1 is highly expressed during development of female reproductive organs and correlates with the pattern of mitochondrial $O_2^{\cdot -}$ (Martin et al., 2013). Overexpressing lines suggest also a protective role of MnSOD in various plants such as tobacco (Slooten et al., 1995), alfalfa (Samis et al., 2002) and *Arabidopsis* (Wang et al., 2004). Moreover, a direct targeting of an overexpressed MSD1 into the chloroplast confers increased resistance to MV (Slooten et al., 1995; Samis et al., 2002).

Taken together, SODs are antioxidant enzymes that constitute the first line of cellular defense against ROS produced in response to various stress stimuli and are an important part of the ROS signaling pathways, at least partially ensuring the pool of H_2O_2.

1.3.3 Regulation of SODs by MAPK signaling

MAPKs appear as crucial regulators of antioxidant defenses, since their genetic modification alters the expression of many antioxidant enzymes in diverse environmental conditions. Among others, also SODs falls under the regulation of MAPKs.

Under high light (Xing et al., 2013) and salinity (Xing et al., 2015), the expression of *Arabidopsis SODs* is regulated by MKK5. *CSD1* and *CSD2* expression is known to be elevated in conditions of high light irradiance (Xing et al., 2013). Interestingly, the transcript levels of both *CSD* genes remained unchanged under these conditions in

a transgenic *Arabidopsis* line with a downregulated MKK5, which is hypersensitive to high light. In contrast, a transgenic *Arabidopsis* line overexpressing MKK5 was resistant to high light stress and showed increased activity of both CSDs (Xing et al., 2013). Moreover, downregulation of MKK5 negatively affected the activation of MPK3 and MPK6 in high light condition, which suggest these MAPKs to be downstream of MKK5 (Xing et al., 2013). Interestingly, MKK5, downstream of MEKK1 and upstream of MPK6 is essential also for the expression of chloroplastic *FSD2* and *FSD3* during salt stress (Xing et al., 2015). MKK1 mediates also the activation of *CAT1* expression (but not *CAT2* and *CAT3*) during salt stress, drought and ABA (Xing et al., 2007). CAT1 was shown to be important for the regulation of ABA-mediated H_2O_2 production. Here, *CAT1* expression is activated by MPK6, acting downstream of MKK1 (Xing et al., 2008).

Further MAPK cascade activated by ROS consists of ANPs (MAP3K) phosphorylating MKK4/MKK5, which leads to the subsequent phosphorylation of MPK3 and MPK6 (Kovtun et al., 2000). Shot-gun proteomic analysis of *Arabidopsis anp2/anp3* double mutants found, that this exhibits over-abundances of several proteins important for anti-oxidative defenses. FSD1, MSD1 and enzymes of the ascorbate-glutathione cycle including APX and DHAR showed higher abundances and activities (Takáč et al., 2014). Finally, the double mutant shows enhanced resistance to the oxidative stress, caused by MV. It might be therefore concluded, that ANPs are activated and negatively regulate tolerance of *Arabidopsis* to oxidative stress (Takáč et al., 2014). It is likely that ANPs might represent a master regulators of antioxidant defense. On the other hand, the same MAPKs confer resistance of *Arabidopsis* to *Botrytis cinerea* (Savatin et al., 2014), which is a clear sign of functional divergence of ANPs in *Arabidopsis*.

1.3.4 Phosphorylation of SODs

PTMs of proteins represent versatile, dynamic, and flexible regulatory mechanisms for the reprogramming of a wide range of cellular functions. For example, these processes ensure the fast and targeted activation of plant immune responses upon pathogen attacks. Generally, PTMs affect enzymatic activities, subcellular localization, protein interactions, and stability (reviewed in Vu et al., 2018; Ruiz-May et al., 2019). Among PTMs, the reversible phosphorylation of proteins represents a driving force of signaling processes during plant development and stress challenges (Arsova et al.,

2018). Several antioxidant proteins are modified by direct phosphorylation, as found mainly by proteomic approaches (Table S1).

Although the phosphorylation of SODs has been documented for human SOD1 (Fay et al., 2016; Tsang et al., 2018) and SOD2 (Candas et al., 2013; Jin et al., 2015), mouse SOD2 (Candas et al., 2013), or yeast SOD1 (Leitch et al., 2012; Tsang et al., 2014), the phosphorylation of SOD isoforms in plants has not been approved by genetic means so far. Mammalian SOD1 is phosphorylated at Thr-2 (Fay et al., 2016) and Thr-40 (Tsang et al., 2018), having a pronounced impact on its activity. For example, the MAMMALIAN TARGET OF RAPAMYCIN COMPLEX 1 (mTORC1) is a negative regulator of SOD1 activity under nutrient rich conditions by reversible phosphorylation at Thr-40 (Tsang et al., 2018). Yeast SOD1 is phosphorylated at Ser-38 under low oxygen conditions, which allows its interaction with Cu^{2+} chaperone CCS, and, consequently proper folding and activation (Leitch et al., 2012). Contrarily, the double phosphorylation of yeast SOD1 at Ser-60 and Ser-99 by a DNA damage checkpoint kinase Dun1 during oxidative stress leads to the translocation of this SOD to the nucleus, where it binds to the promoters and activates ROS-responsive and DNA repair genes (Tsang et al., 2014). Rarely, phosphoproteomic studies have reported on the detection of phosphorylated amino acid residues in plant SODs. A gel-based study on mitochondrial phosphoproteomes identified phosphorylated MSD1 (Bykova et al., 2003). In addition, CSD2 and CSD3 were found to be phosphorylated in response to auxin and isoxaben, respectively (Zhang et al., 2013). Multiple phosphorylation sites were also detected in FSD2 after an ABA treatment (Wang et al., 2013). These findings demonstrate that the phosphorylation of plant SODs may have some important functions which need to be elucidated in future studies.

1.4 SQUAMOSA-PROMOTER BINDING PROTEIN-LIKE proteins

A characteristic feature of SPLs protein family is the presence of the SQUAMOSA PROMOTER BINDING PROTEIN (SBP) domain, which consists of a highly conserved region of 76 amino acids. This domain is responsible for nuclear import and binding to the specific promoter regions by two unconventional zinc fingers formed of eight conserved histidine and cysteine residues (Yamasaki et al., 2004; Birkenbihl et al., 2005; Guo et al., 2008). The structural motif recognized in the promoter sequence is known as TNCGTACAA *cis*-element (Cardon et al., 1999; Yamasaki et al., 2004), nevertheless, the sequence GTAC is the essential core

indispensable for binding SPLs (Birkenbihl et al., 2005; Kropat et al., 2005). The size, structure, and presence of other structural domains may vary significantly among SPLs.

SPL genes are expressed in green plants, green algae and mosses (Preston and Hileman, 2013). *Arabidopsis* genome encodes 17 *SPL* genes, however, *SPL13A* and *SPL13B* emerged as a tandem duplication (Yang et al., 2008). The number of *SPL* genes varies depending on the plant species: 18 genes were identified in *Betula luminifera* (Li et al., 2018), 17 in *Hordeum vulgare* (Tripathi et al., 2018), 18 in *Oryza sativa* (Xie et al., 2006), and 31 in *Zea mays* (Hultquist and Dorweiler, 2008) with a high degree of functional homology across the species (Zhang et al., 2014; Liu et al., 2016; Si et al., 2016; Chao et al., 2017). SPLs show high variability in length of their amino acid sequence, which range in *Arabidopsis* from 131 (SPL3) to 1037 (SPL14) amino acids. Depending on protein domain composition (e.g. the presence of transmembrane domain and ankyrine repetition), SPLs are subclassified into structurally more complex large SPLs (SPL1/7/12/14/16), and small SPLs. Small SPLs are post-transcriptionally regulated by miRNA, except SPL8, because of an absence of miRNA responsive element in its mRNA sequence (Rhoades et al., 2002; Schwab et al., 2005; Garcia-Molina et al., 2014).

SPLs are involved in root and rosette development (Yang et al., 2008), generative growth (Schmid et al., 2003), flower formation (Salinas et al., 2012; Jorgensen and Preston, 2014), embryo development and seed germination (Nodine and Bartel, 2010). They contribute to plant responses to abiotic and biotic stresses (Stief et al., 2014; Chao et al., 2017; Cai et al., 2018) along with heteroblasty (Usami et al., 2009).

1.4.1 SPL7

Expression of *SPL7* is gradually increasing during the ontogenesis peaking prior to flowering (Yamasaki et al., 2009; Garcia-Molina et al., 2014; Jorgensen and Preston, 2014). SPL7 is localized in the nucleus, in the plasma membrane vicinity, and attached to the endoplasmic reticulum (Garcia-Molina et al., 2014). SPL7 together with Cu-DEFICIENCY INDUCED TRANSCRIPTION FACTOR 1 are the master regulators of Cu^{2+} homeostasis (Yamasaki et al., 2009; Yan et al., 2017a) and regulators of JA biosynthetic genes under Cu^{2+} deficiency (Yan et al., 2017a). Besides *miRNA389* and *FSD1* promoters, SPL7 targets also *FERRIC REDUCTASE OXIDASES* (Jain et al.,

2014), *COPPER TRANSPORTERS FAMILY* (Jung et al., 2012; Gayomba et al., 2013), *Cu-RESPONSIVE miRNAs*, and others (Yamasaki et al., 2009; Yan et al., 2017a).

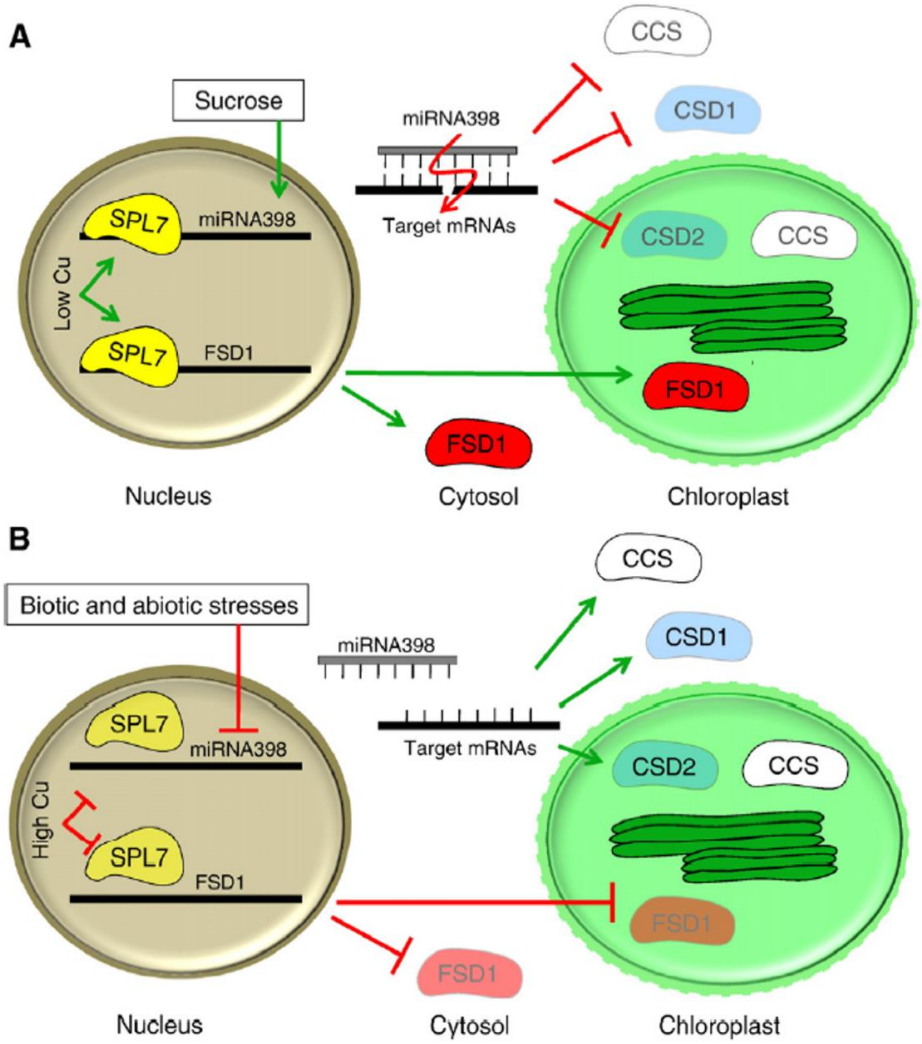

Figure 6 Scheme showing the regulation of *FSD1* and *CSDs* orchestrated by SPL7 in response to different Cu^{2+} concentrations. (A) At low Cu^{2+} levels, SPL7 triggers the transcription of *FSD1* and *miRNA398*, the latter downregulating *CCS*, *CSD1* and *CSD2*. miRNA398 is also regulated in response to sucrose. (B) At high concentration of Cu^{2+} inhibits the expression of *FSD1* and miRNA398 by blocking the binding of SPL7 to its promoter sequence and CSDs are expressed. Abbreviations: CCS – Cu^{2+} chaperone for superoxide dismutase, CSD1 – cytosolic Cu/ZnSOD; CSD2 – chloroplastic Cu/ZnSOD; FSD1 – FeSOD1, SPL7 – SQUAMOSA PROMOTER BINDING PROTEIN-LIKE 7. Adopted from Pilon et al. (2011).

As mentioned before, *FSD1*, *CSD1* and *CSD2* are transcriptionally and post-transcriptionally regulated by SPL7 in a Cu-dependent manner (Yamasaki et al., 2007 and 2009; Garcia-Molina et al., 2014). Under Cu^{2+} deficiency, SPL7 binds to Cu^{2+} responsive (CuRE) promoter sequence and induces the expression of *FSD1*, leading to increased abundance and activity of the FSD1 enzyme. At the same time, *CSD1*, *CSD2*, and *CCS* are post-transcriptionally downregulated by miRNA398, which is induced by

the SPL7-positive regulation in the promoter sequence (Cohu et al., 2009; Yamasaki et al., 2009). Therefore, SPL7 is an important modulator of Cu^{2+} balance via Cu^{2+}-responsive proteins and miRNAs (Burkhead et al., 2009; Araki et al., 2018). Of note, miRNA398 levels are downregulated during oxidative stress in order to allow the post-transcriptional *CSD1* and *CSD2* mRNA accumulation and elevate (oxidative) stress tolerance (Sunkar et al., 2006; Li et al., 2020). The schematic depiction of SODs regulation in response to various Cu^{2+} concentrations via SPL7 activity is illustrated in Figure 6. All of these important roles are supported by studies employing *spl7* mutant, which accumulates less Cu^{2+} and it has developmental defects unless higher Cu^{2+} concentration is added in the growth medium (Yamasaki et al., 2009; Gayomba et al., 2013; Schulten et al., 2019). Recently, it has been shown that *SPL7* expression depends also on nitrogen concentration in the media (Mermod et al., 2019). SPL7 is also implicated in the circadian regulation of *FSD1* expression, since changes in amplitude of a FSD1 classical clock output were found in *spl7* mutants (Perea-García et al., 2016).

1.4.2 SPL1 and SPL12

SPL1 and SPL12 show a high level of homology (up to 72% at protein sequence level), which is due to the duplication and translocation of the ancestral gene (Cardon et al., 1999; Chao et al., 2017). This also explains the partial functional redundancy (Cardon et al., 1999; Schulten et al., 2019) and similar level of expression with a constitutive pattern, which has been observed within tissues with a higher ratio in generative than in vegetative organs (Jorgensen and Preston, 2014; Chao et al., 2017). *SPL1* shows higher expression compared to *SPL12*, suggesting more dominant roles for *SPL1* (Cardon et al., 1999). Differences in their functions are expected also due to their distinct tissue-specific expression (Jorgensen and Preston, 2014).

Neither *Arabidopsis* single T-DNA insertion mutants in *SPL1* and *SPL12*, nor *spl1/spl12* double mutant show obvious phenotypic defects under optimal growth conditions (Chao et al., 2017). Nevertheless, the double mutation was associated with reduced fertility owing to defective flower development, and reduced amounts of siliques and seeds (Chao et al., 2017; Schulten et al., 2019). The double mutant *spl1/spl12* inflorescences are hypersensitive to heat stress, while overexpression of *SPL1* or *SPL12* improved the thermotolerance. Additionally, transcriptomic analysis of double mutant exposed to heat stress suggests a heat-triggered transcriptional reprogramming in the inflorescence and indicated the impact of SPL1 and SPL12 in

ABA signaling via modulating of ABA-responsive genes (Chao et al., 2017). Interestingly, higher temperatures lead to a decrease in SOD activities in double mutant, and increase in ROS concentrations resulting in cell death (Chao et al., 2017). This observation can suggest the impact of both SPL1 and SPL12 on the role of SODs during stress conditions.

2 MAPK activation and function in response to elicitation and symbiotic bacteria

2.1 Material and Methods

2.1.1 Biological material and growth conditions

Transgenic *SIMKK RNAi* line (SIMKKi) was obtained by stable transformation of *Medicago sativa cv.* Regen-SY (RSY) leaves by *A. tumefaciens* GV3101::pMP90 carrying *pHellsgate12-SIMKKi* expression plasmid as described in Bekešová et al. (2015). Induction of callogenesis from leaf explants, production of somatic embryos from calli, development of shoots and their rooting were performed under selective conditions on the appropriate media (Gamborg medium for cocultivation, callus initiation and embryo formation and MMS media for plant rooting, development and maintenance). Transgenic plantlets were transferred to either to MS medium or Fåhreus medium without nitrogen (Fåhreus, 1957) both solidified with 0.5% (w/v) gellan gum.

Alfalfa plants were grown vertically at 21°C, 16/8 h (light/dark) photoperiod with intensity of illumination 150 $\mu mol \cdot m^{-2} \cdot s^{-1}$ in phytotron (Weiss Technik, USA) for 10–30 days prior to treatments.

2.1.2 Specification of flg22 and *Sinorhizobium meliloti* treatments

For comparison of proteomes of alfalfa wild type and SIMKKi plants, roots of 15-days-old plants were harvested. Roots of three plants were pooled in one biological replicate and the analysis was performed in three biological replicates.

For flg22-induced MAPK activation analyses, 15-days-old plants of alfalfa wild type and SIMKKi line grown on MS medium were surface treated by 200 nM flg22 (CRB Discovery) diluted in MS liquid medium for different time periods (from 5 min to 6 h) by keeping them horizontally at the same cultivation conditions as before. To avoid hypoxia, plants were treated upon continuous slow shaking on a rocker. As controls, we used either untreated (designated as „dry“) or mock (liquid MS) treated plants. Roots were excised by razor blade and immediately frozen in liquid nitrogen.

For inoculation, roots of 15-days-old plants (MAPKs activation) of alfalfa, ecotype RSY and SIMKKi were surface treated with 3 ml culture of *Sinorhizobium meliloti* SM2011 (OD_{600} 0.5) in Fåhreus medium. For MAPK activation assay, roots were harvested after different time periods ranging from 10 min to 24 h and subsequently frozen in liquid nitrogen. For proteomic analysis, roots were harvested 6 h after the treatment. In both cases, three plants were used for one biological replicate,

performing three biological replicates in total. For evaluation of nodule generation, inoculated plants were grown for additional 20 days. Plants were documented 20 days after inoculation using stereo microscope (Axio Zoom.V16; Carl Zeiss, Germany) and scanner (ImageScanner III, GE Healthcare, Little Chalfont, UK) for nodule number and root length estimation, respectively. The root length was measured using ImageJ software (http://rsbweb.nih.gov/ij/). Roots and nodules from 10 plants were considered as 1 biological replicate by performing 3 biological replicates in total. Mature non-senescent nodules were harvested 20 days after inoculation from both lines in three replicates (at least 20 nodules from 10 plants per one repetition).

2.1.3 Immunoblotting and SOD activity analysis

Material was homogenized into fine powder in a mortar with liquid nitrogen. Proteins were extracted in E-buffer (50 mM HEPES, pH 7.5, 75 mM NaCl, 1 mM EGTA, 1 mM $MgCl_2$, 1 mM NaF, 10% (v/v) glycerol, PhosSTOP™ phosphatase inhibitor cocktail and Complete™ EDTA-free protease inhibitor (Roche)) and the extract was centrifuged 15 min at 13 000 g at 4°C. Protein concentrations were measured using the Bradford assay (Bio-Rad). Equal amounts of proteins were mixed with 4x concentrated Laemmli Sample Buffer (Bio-Rad) and boiled at 95°C for 5 min. Denatured protein extracts were separated by sodium dodecyl sulphate-polyacrylamide gel electrophoresis (SDS-PAGE) on 10% TGX Stain-Free™ Fast-Cast™ gels (Bio-Rad). Separated proteins were transferred to a polyvinylidene difluoride (PVDF) membrane (GE Healthcare) using a wet tank unit (Bio-Rad) with Tris/glycine/methanol transfer buffer at 24 V and 4°C overnight. Nonspecific epitopes were blocked by overnight incubation of the membrane either in 5% (w/v) bovine serum albumin (BSA; for detection of anti-phospho ERK Ab (pERK)), or in 4% (w/v) BSA and 4% (w/v) low-fat dry milk (for detection of HSP70 Ab), or in 5% (w/v) low-fat dry milk (for detection of MMK3 Ab, MnSOD1 Ab, CAT Ab), in Tris-buffered-saline with Tween 20 (TBS-T, 100 mM Tris-HCl; 150 mM NaCl; 0.1% (v/v) Tween 20; pH 7.4). Subsequently, the membranes were incubated with anti-pERK (1:1000; Cell signaling), anti-MMK3 (1:3000; GenScript), anti-MnSOD (1:3000; Agrisera), anti-HSP70 (1:5000; Sigma) and anti-CAT (1:1000; Agrisera) primary antibodies in TBS-T (TBS; 0.1% (v/v) Tween 20) containing 1% (w/v) BSA at 4°C overnight. Following repeated washing in TBS-T, membranes were incubated with a secondary antibody diluted in TBS-T containing 1% (w/v) BSA for 1.5 h. Horseradish peroxidase-conjugated goat anti-rabbit

and anti-mouse IgG secondary antibodies (both diluted 1:5000; Thermo Scientific) were used for the detection. The signal was developed after five washing steps in TBS-T using the Clarity Western ECL (Enhanced chemiluminescence) substrate (Bio-Rad) and documented using the Chemidoc MP system (Bio-Rad).

For the analysis of SOD isoenzymes activities, roots (non-treated and *S. meliloti* treated alfalfa) were homogenized in liquid nitrogen and subjected to protein extraction using 50 mM sodium phosphate buffer (pH 7.8), 1 mM ascorbate, 1 mM EDTA and 10% (v/v) glycerol. The extract was cleaned by centrifugation at 13 000 g at 4°C for 15 min, followed by measurement of the protein concentration. Samples of equal protein content were loaded on a 10% native PAGE gel and separated at constant 20 mA/gel for 2 h. Gels were preincubated in 50 mM sodium phosphate buffer, pH 7.8 for 10 min after separation. SOD isoform activities and their specific inhibition were visualized as described by Takáč et al. (2014).

Both immunoblotting and enzyme activity analyses were performed in three biological replicates and the statistical significance was evaluated using one-way ANOVA test.

2.1.4 Proteomic analysis

The protein extraction and the preparation of peptide mixture were performed according to Takáč et al. (2017) with slight modification. Fresh material from 1g of roots and 500 mg of nodules was homogenized in liquid nitrogen with 1 ml of cold extraction medium (0.9 M sucrose, 0.1 M Tris-HCl (pH 8.8), 10 mM EDTA, 100 mM KCl, and 0.4% (v/v) 2-mercaptoethanol) and an equal amount of Tris-HCl-buffered phenol (pH 8.1). The following steps were carried out as described in Takáč et al. (2017).

The nano-liquid chromatography followed by tandem mass spectrometry analysis (nLC-MS/MS) was performed in the laboratory of Dr. Tibor Pechan (Mississippi University, Starkville) as a service. Two micrograms of protein tryptic digest were subjected to nLC-MS/MS analysis as published previously (Takáč et al., 2016b). Briefly, peptides were separated using reversed phase C18 75 μm x 150 mm column and Ultimate 3000 high-performance liquid chromatography (HPLC) system (both Thermo Fisher Scientific) via nonlinear, 170 min long, constant flow (0.3 $\mu l \cdot min^{-1}$)

gradient of acetonitrile (in 0.1% formic acid) as follows: 2%–55% for 125 min, 95% for 20 min, 2% for 25 min.

Mass spectra were collected by nano-electro spray ionization LTQ-Orbitrap Velos mass spectrometer (Thermo Fisher Scientific) directly linked to the nLC system. The mass spectrometer operated in the result dependent acquisition (RDA) mode of 18 scan events: one MS scan (m/z range: 300–1700) followed by 17 MS/MS scans for the 17 most intense ions detected in MS scan, with dynamics exclusion allowed.

For protein identification, the raw data files were searched using the SEQUEST algorithm of the Proteome Discoverer software version 2.1 (Thermo Fisher Scientific), as described previously (Takáč et al., 2017). Variable modifications were considered for: cysteine carbamidomethylation (+57.021), methionine oxidation (+15.995), and methionine dioxidation (+31.990). *Medicago truncatula* NCBI protein database (as of August 2019, with 25 395 entries) served as the target database, while its reversed copy (created automatically by the software) served as a decoy database. Only high confidence protein identifications (FDR < 1%) were further considered. The proteins without functional annotations were searched against the UniProt SwissProt database (release 07/2019) using BLAST+. The function of the best blast hit was used to annotate the protein.

Proteins showing different abundance between samples were classified using Gene Ontology (GO) annotation analysis, KEGG pathways analysis and by Interpro protein family distribution analysis using OmicsBox software (BioBam Bioinformatics, Valencia, Spain). Blast was made against *Medicago truncatula* NCBI database permitting
3 BLAST Hits. Following parameters were used for annotation: E value hit filter$1.0E^{-6}$; annotation cutoff: 55; Gene Ontology weight: 5, GO Slim.

2.2 Results

2.2.1 MAPK activation in SIMKKi line in response to elicitation and *Sinorhizobium meliloti*

Within the following experiments, we aimed to monitor the abundance and activation of SIMK, a MAPK acting downstream of SIMKK, in response to flg22 elicitation, and in response to *S. meliloti* inoculation. Afterward, we attempted to uncover proteins, metabolic processes or signaling events occurring downstream of SIMKK in response to symbiotic bacteria *S. meliloti* by comparative shot-gun proteomic analysis.

Flg22 treatment lead to appearance of two bands with 46 kDa and 40 kDa on immunoblots prepared using pERK antibody in wild type roots (Figure 7). The alignment of anti-MPK6 immunoreactive band with those recognized by pERK antibody helped to define the upper band (46 kDa) as SIMK (Figure S1; note, that SIMK is a MAPK with high homology to *Arabidopsis* MPK6). Time course observation of MAPK activation showed that the intensity of both bands peaked after 20 min of flg22 treatment, followed by continuous decrease (deactivation). SIMK activation showed a steeper rise compared to the 40 kDa band. Immunoblotting analysis indicated that SIMK abundance did not change after 20 min flg22 treatment (Figure 8). Very similar results were obtained upon inoculation of wild type plants with *S. meliloti* suspension culture (Figure 9), thus confirming the common initial signaling events for pathogenic and symbiotic plant-bacteria interactions.

As expected from the previously published results (Bekešová et al., 2015), only one band (with 40 kDa) was resolved on immunoblots prepared from SIMKKi line (Figure 7). The band corresponding to SIMK was not present in SIMKKi line, owing to its strong downregulation (Figure 8; Bekešová et al., 2015). To compare the rate of activation of MAPK with 40 kDa in wild type and SIMKKi line, both samples were loaded on one gel keeping equal protein loading. This experiment showed that the examined MAPK was over-activated in SIMKKi line (Figure 7E, F) suggesting possible a compensatory mechanism.

Next, we wanted to elucidate the impact of SIMKK downregulation on nodule formation. The quantitative phenotypic analysis showed that the SIMKKi line formed

roughly half of the nodules as compared to wild type (Figure 10), suggesting that SIMKK and SIMK are involved in nodulation evoked by *S. meliloti*.

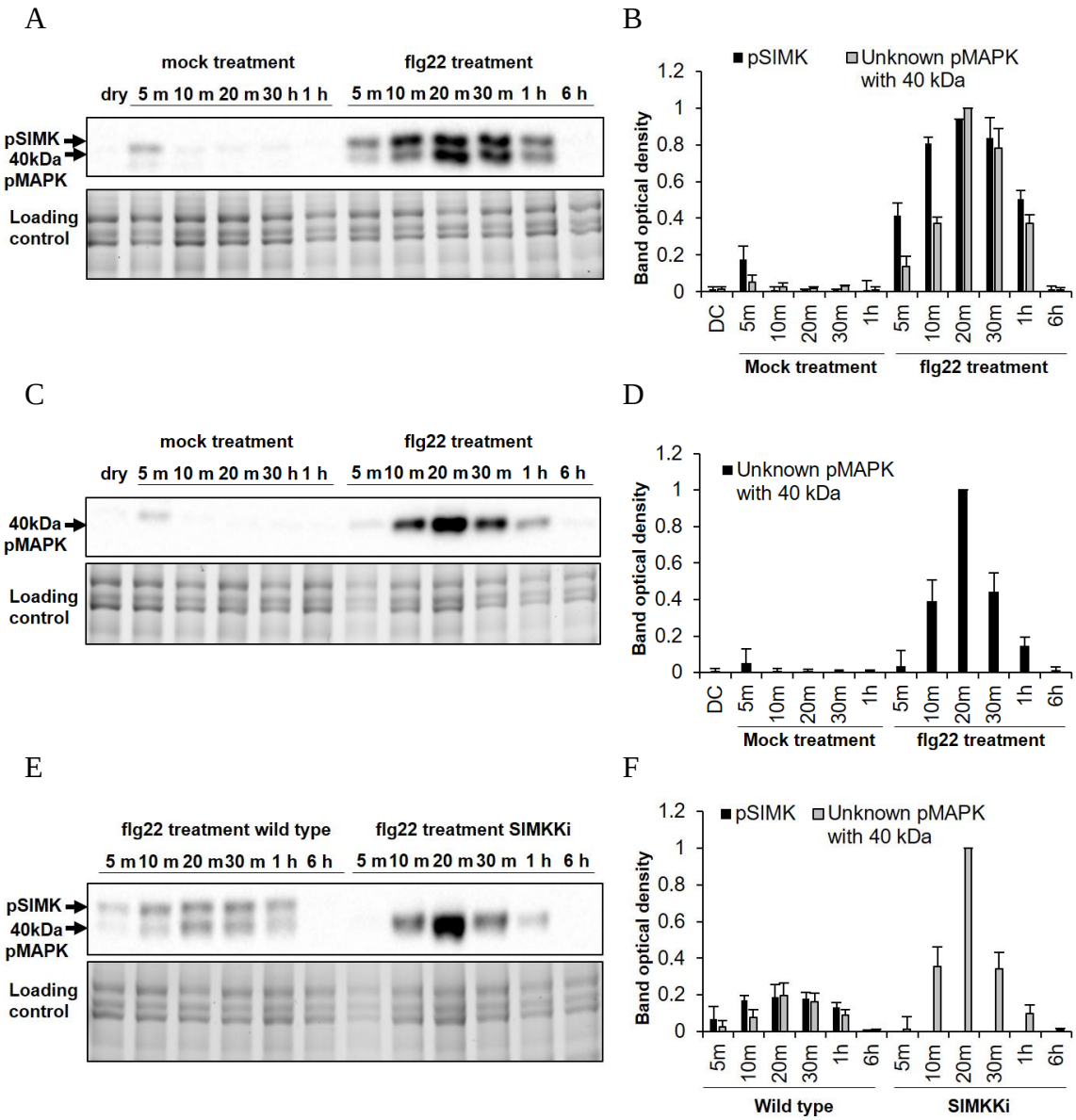

Figure 7 Effect of flg22 on activation of MAPKs in roots of alfalfa wild type and SIMKKi line. Fifteen-days-old wild type (RSY) and SIMKKi plants were treated by 200 nM flg22 for different time periods. (A, C, E) Immunoblot analysis of MAPK activation by using phosphospecific anti-pERK antibody on root protein extracts. (A) Treatment of wild type with mock treatment and flg22. (C) Treatment of SIMKKi line with mock treatment and flg22. (E) Comparison of wild type and SIMKKi line after flg22. (B, D, F) Quantification of band optical densities of phosphorylated MAPKs. All densities are expressed as relative to the highest value. Error bars represent standard deviation.

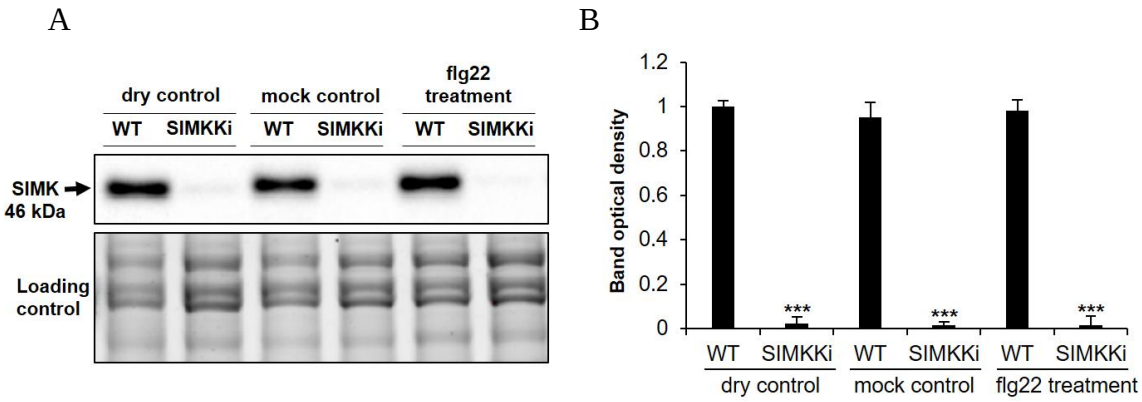

Figure 8 Effect of flg22 on SIMK abundance in roots of alfalfa wild type and SIMKKi line. Fifteen-days-old wild type (RSY) and SIMKKi line plants were treated by 200 nM flg22 or MS medium for 20 min. (A) Immunoblot analysis of SIMK abundance by using anti-MPK6 antibody in root protein extracts. (B) Quantification of band optical densities. All densities are expressed as relative to the highest value. Error bars represent standard deviation. Stars indicate statistically significant difference (one-way ANOVA, ***p < 0.001).

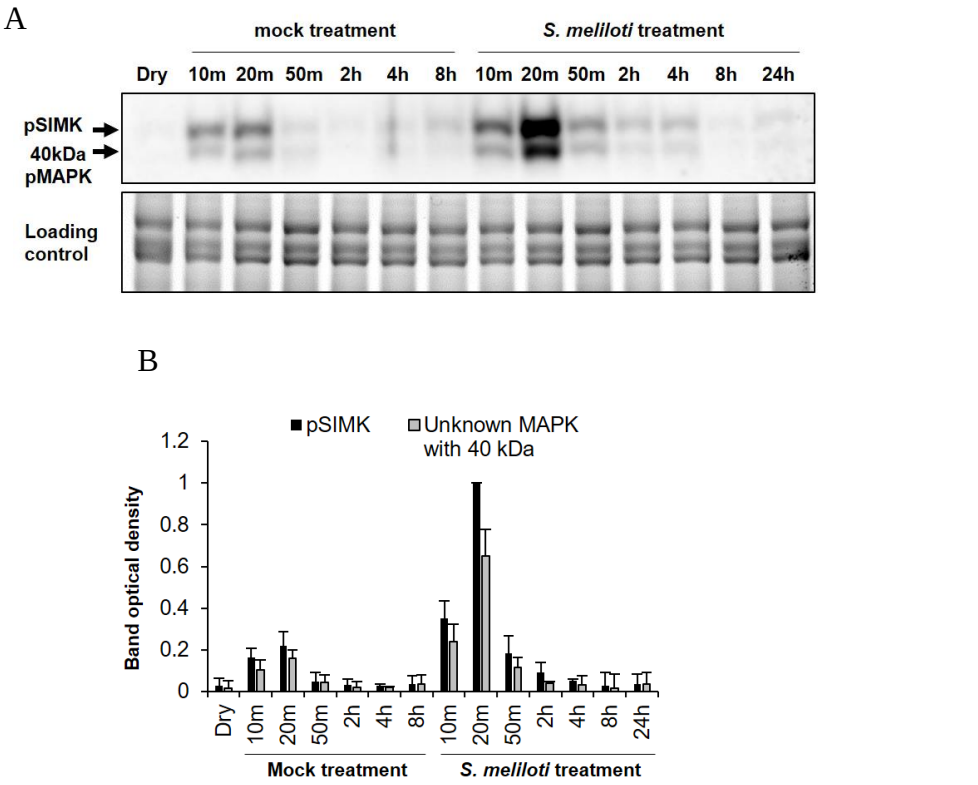

Figure 9 Activation of MAPKs after *S. meliloti* treatment in roots of alfalfa wild type. Fifteen-days-old plants were treated by *S. meliloti* for different time periods. (A) Immunoblot analysis of MAPK activation by using phosphospecific anti-pERK antibody in root protein extracts. (B) Quantification of band optical densities of phosphorylated MAPKs. All densities are expressed as relative to the highest value. Error bars represent standard deviation

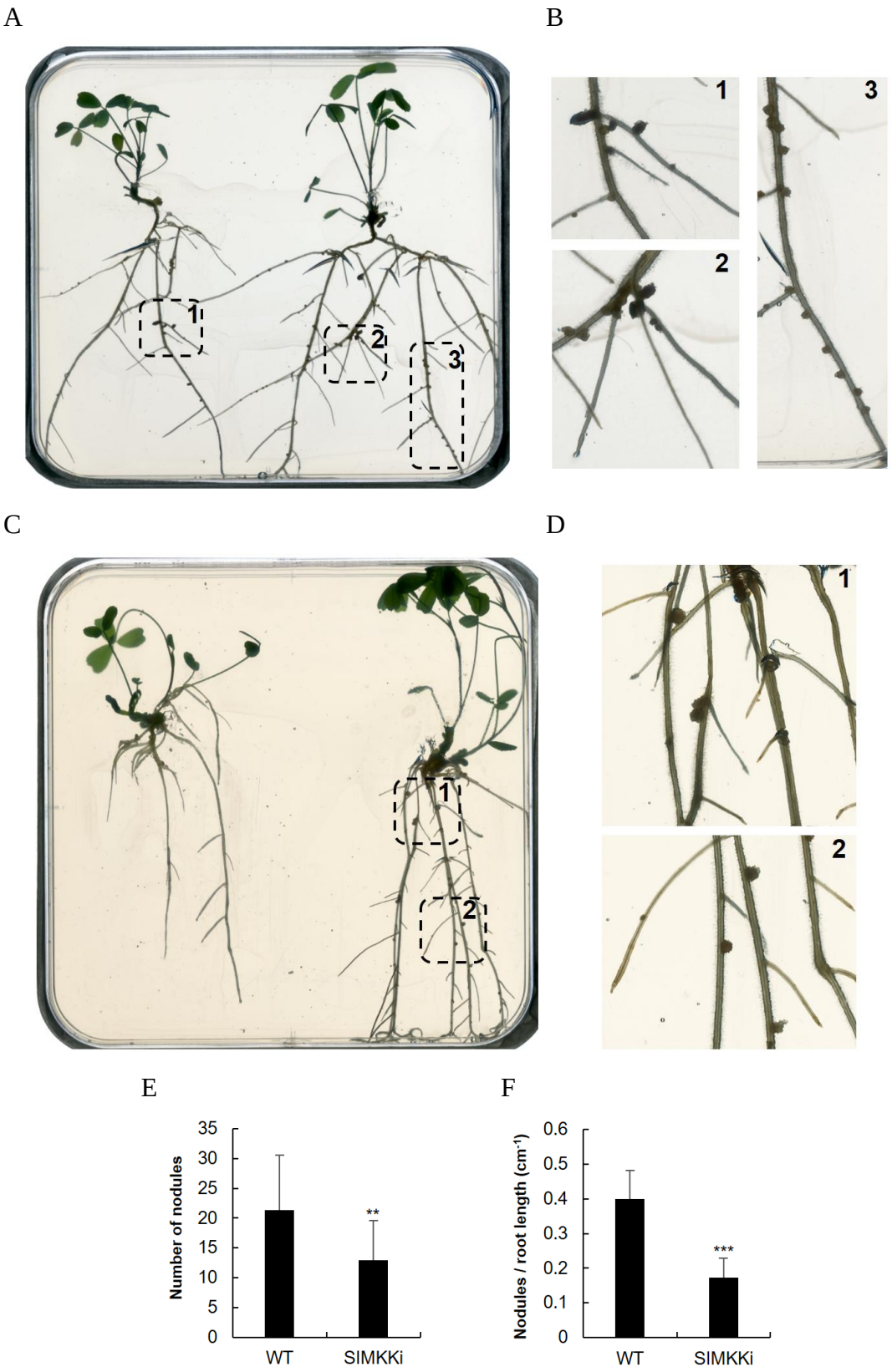

Figure 10 Nodule formation in roots of alfalfa wild type and SIMKKi seedlings inoculated with *S. meliloti*. (A-D) Representative images of root nodules formed in respective alfalfa lines, (A) wild type, (C) SIMKKi. (B) are close-ups from (A), and (D) are close-ups from (C). Quantification of the number of nodules (E), and number of nodules per root length (F; cm^{-1}) at 20 days after inoculation. Phenotypic analysis was performed in three repetitions (n = 30). Error bars represent standard deviation. Stars indicate statistically significant difference (one-way ANOVA, **p < 0.01; ***p < 0.001).

2.2.2 Proteome-wide examination of processes regulated by SIMKK

Within the following experiments, comparative shotgun proteomic analyses were employed to gain more insights into the processes regulated by SIMKK in alfalfa.

First, we compared root proteomes of wild type with SIMKKi line, and the differential proteome was evaluated using bioinformatics. Prior to proteomic analysis, we successfully proved the SIMK downregulation in SIMKKi plants using immunoblotting (Figure 11).

Together 129 differentially abundant proteins (DAPs) were identified and evaluated. Among them, 49 proteins were more abundant and 36 were less abundant in SIMKKi line. Twelve proteins were unique for SIMKKi line, while 32 proteins were found solely in the wild type. DAPs are mostly assigned to metabolic GO annotations, while catabolic and biosynthetic processes appeared as balanced (Figure 12A). Substantial number of DAPs are involved in response to stimulus, stress as well as chemical. Fourteen proteins belong to GO annotation called establishment of localization and 13 to transport. In terms of cellular compartment, DAPs were mostly localized in cytoplasm, but we detected also membranous, plastidic, nucleolar and extracellular proteins. Remarkably, SIMKK downregulation may lead to the disturbance of protein complexes (Figure 12B).

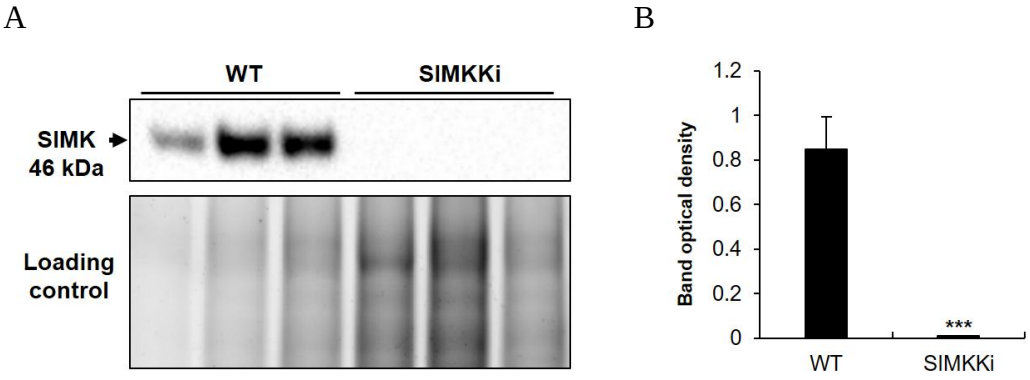

Figure 11 Analysis of SIMK abundance in *S. meliloti*-treated wild type and SIMKKi line in roots. (A) Immunoblot analysis by using anti-MPK6 antibody on three replicates of wild type and SIMKKi line. The anti-MPK6 antibody specifically recognizes SIMK. (B) Quantification of band optical densities. Densities are expressed as relative to the highest value and normalized according to loading control differences. Error bars represent standard deviation. Stars indicate statistically significant difference (one-way ANOVA, ***$p < 0.001$).

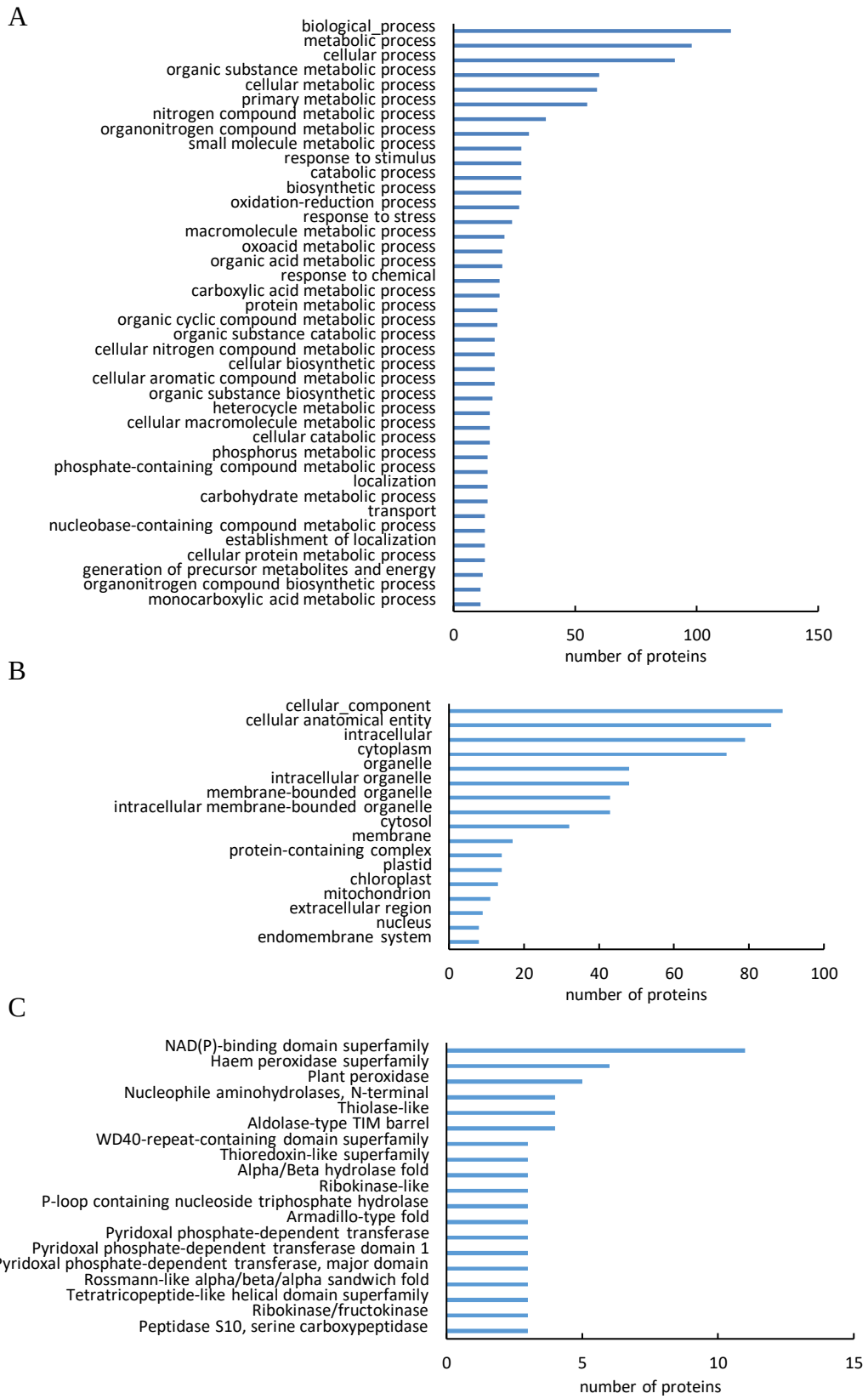

Figure 12 Classification of differentially abundant proteins (DAPs) detected in roots of SIMKKi line as compared to the wild type into Gene ontology annotations according to biological process (A) and cellular compartment (B). (C) Distribution of DAPs into protein families.

Eleven DAPs belong to NAD(P)-binding domain superfamily, indicating that processes connected to redox homeostasis might be affected in the transgenic line. Haem peroxidases, thiolases and aldolase type TIM barrel family of proteins were also abundant within the DAPs (Figure 12C). KEGG pathway analysis allows acquiring insight into the status of metabolic processes in the studied material. SIMKK downregulation negatively affected the starch and glucose metabolism as well as glycolysis/gluconeogenesis. In addition, carbon fixation, amino acid metabolism, galactose pyruvate and glyoxylate and dicarboxylate metabolism were affected as well. SIMKKi line show also downregulation of proteins involved in nitrogen metabolism, such as two isoforms of glutamate dehydrogenase, CARBONIC ANHYDRASE 2 ISOFORM X1 and FERREDOXIN-DEPENDENT GLUTAMATE SYNTHASE (Figure 13).

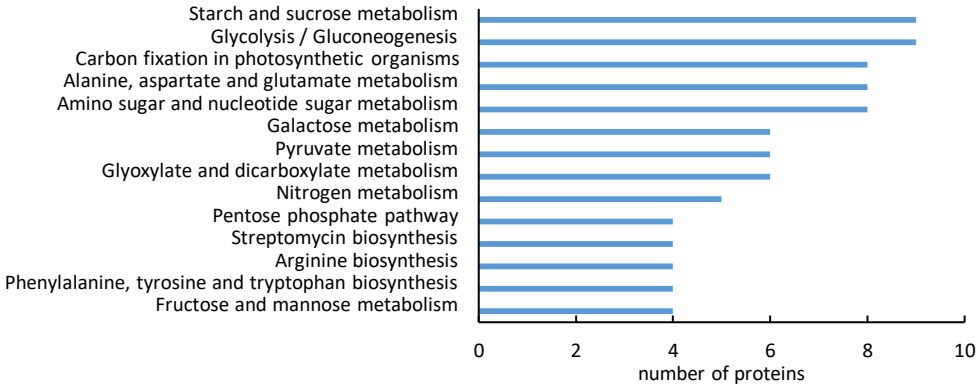

Figure 13 Classification of differentially abundant proteins (DAPs) detected in roots of SIMKKi line as compared to the wild type into KEGG annotations.

Closer inspection of stress related proteins (Table S2) showed that some important proteins involved in redox homeostasis and oxidative stress were upregulated including 4 peroxidase isoforms, two peroxiredoxin isoforms and MnSOD in SIMKKi line. On the other hand, CATALASE 4, PEROXIDASE 3 and L-ASCORBATE OXIDASE HOMOLOG were downregulated. This data indicates the involvement of SIMKK in redox homeostasis regulation.

Other remarkable findings are the downregulation of RHICADHESIN RECEPTOR, SUCROSE SYNTHASE and upregulation of NODULIN RELATED PROTEIN 1, all participating in the symbiotic interaction. Membrane transport is apparently deregulated in SIMKKi, as proposed by the downregulation of the seven proteins (for example CLATHRIN HEAVY CHAIN 1, V-TYPE PROTON ATPASE

SUBUNIT C, RAS-RELATED PROTEIN RAB 7, COATOMER SUBUNIT GAMMA) involved in this process. Interestingly, the SIMKK downregulation had an impact on the differential abundance of HEAT SHOCK FACTOR-BINDING PROTEIN 1, HEAT SHOCK COGNATE 70kDa PROTEIN 2, HSP70-HSP90 ORGANIZING PROTEIN 3 indicating the involvement of SIMKK in heat stress response. In order to validate the proteomic data, immunoblotting analysis using specific primary antibodies against HSP70, catalase and MnSOD was carried out. The obtained differences in protein abundance were in agreement with the proteomic data (Figure 14A-D and 15A, B). We also tested whether increased abundance of MnSOD will be reflected in the level of MnSOD activity in the SIMKKi line using SOD activity staining on native PAGE gels. This analysis confirmed the significantly increased MnSOD activity in the transgenic line (Figure 15C, D). Other SODs isoforms did not show significant difference in activity.

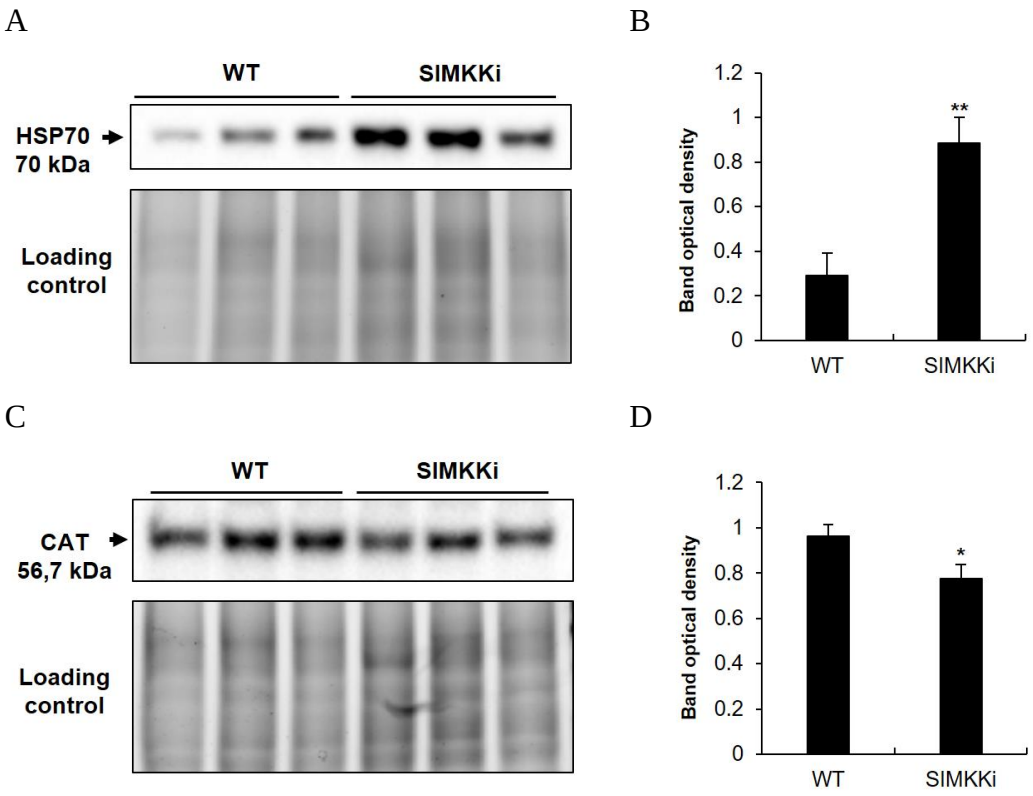

Figure 14 Analysis of HSP70 and catalase abundances in non-treated alfalfa wild type and SIMKKi line roots. (A, C) Immunoblot analysis by using anti-HSP70 antibody (A) and anti-CAT antibody (C) on three replicates of wild type and SIMKKi line. (B) Quantification of band optical densities in (A). (D) Quantification of band optical densities in (C). Densities are expressed as relative to the highest value. Error bars represent standard deviation. Stars indicate statistically significant difference (one-way ANOVA, *$p < 0.05$, **$p < 0.01$).

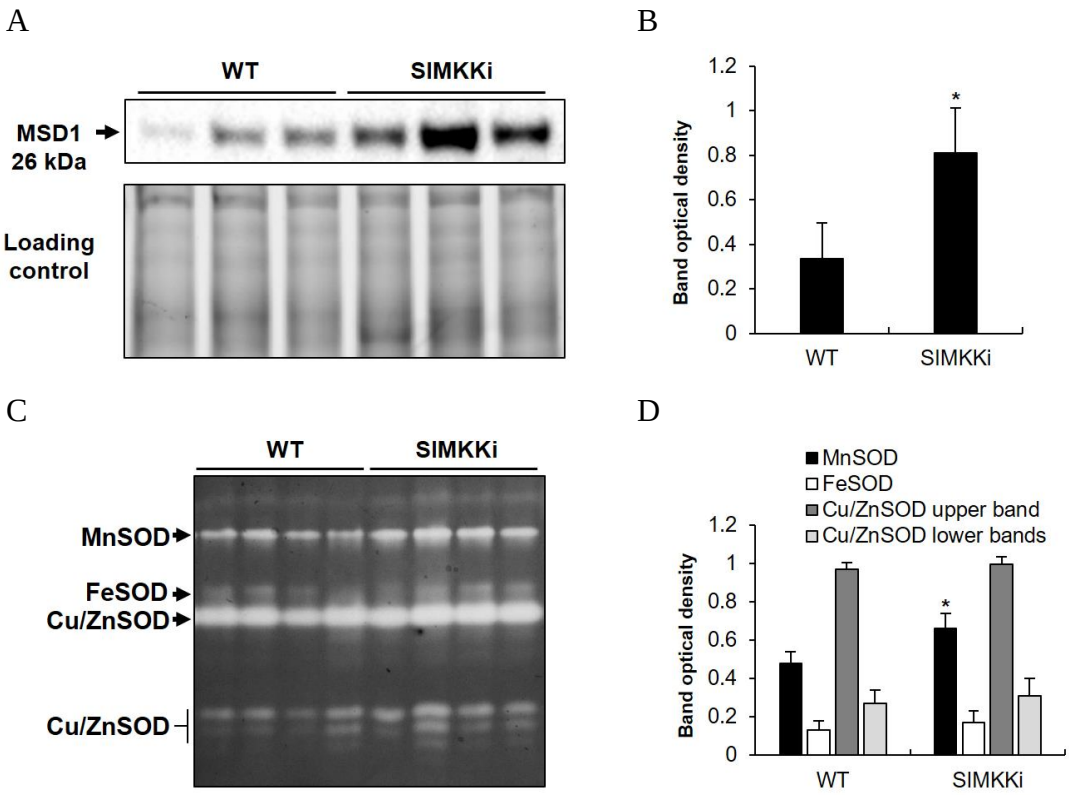

Figure 15 Analysis of MnSOD abundance and SOD isoenzymes activities in non-treated alfalfa wild type and SIMKKi line roots. (A) Immunoblot analysis by using anti-MnSOD antibody on three replicates of wild type and SIMKKi line. (B) Quantification of band optical densities in (A). (C) Visualization of SOD isoenzymes activities on native polyacrylamide gels by specific staining. (D) Quantification of band optical densities in (C). Densities are expressed as relative to the highest value. Error bars represent standard deviation. Stars indicate statistically significant difference in individual isoforms between SIMKKi and wild type (one-way ANOVA, *$p < 0.05$).

Our results show, that SIMKK downregulation leads to disturbance in homeostasis of proteins involved in metabolism, redox regulation, abiotic and biotic stress response as well as membrane transport. The functional links of these proteins to SIMKK signaling and phenotypes of SIMKKi line are discussed in the Discussion section.

Within the next experiment, we compared the responses of both lines to 6 h long *S. meliloti* inoculation to monitor the impact of SIMKK downregulation on the initial events undergoing upon alfalfa-rhizobia interaction. *S. meliloti* treatment did not affect SIMK abundance in SIMKKi line and it remained substantially downregulated (Figure 16A, B). We have identified 70 and 92 differentially abundant proteins in wild type and SIMKKi line, respectively. Similar to the previous experiment, we adopted GO annotation and compared the differential proteomes of both lines. The *S. meliloti* inoculation led to differential regulation of metabolic proteins, mainly in favor of

biosynthetic, compared to catabolic processes in both lines. Proteins involved in response to stress, gene expression, translation and transport were substantially affected as well (Figure 17A). In terms of cellular compartment, the differential proteome consisted mainly from cytoplasmic, membranous, nuclear, mitochondrial proteins as well as proteins in protein complexes (Figure 17B). Most striking differences between the examined lines were observed in GO annotations named cellular nitrogen compound metabolic process, organic cyclic compound metabolic process and response to stress, all being prevalently abundant in wild type. Proteins localized in mitochondria and the endomembrane system were more affected in wild type (Figure 17B). Concerning protein families, *S. meliloti* treatment affected 7 proteins belonging to NAD(P) binding domain superfamily, while just one was found in wild type. Oppositely, 4 and 1 protein belonging to START-like domain superfamily were found in wild type and SIMKKi, respectively. Transgenic line exhibited also more proteins from thioredoxin superfamily, RNA binding domain superfamily or pyridoxal phosphate dependent transferase domain family (Figure 17C).

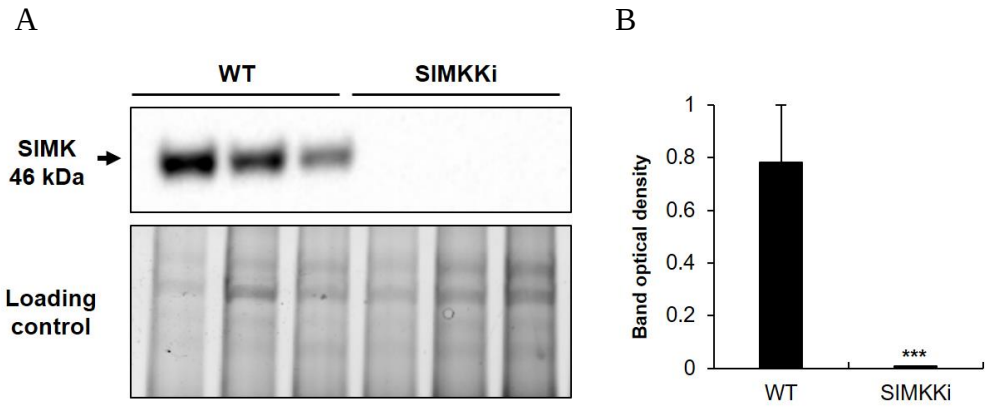

Figure 16 Analysis of SIMK abundance of *S. meliloti*-treated wild type and SIMKKi line in roots. (A) Immunoblot analysis was prepared by using anti-MPK6 antibody on three replicates of wild type and SIMKKi line. The anti-MPK6 antibody specifically recognizes SIMK. (B) Quantification of band optical densities. Densities are expressed as relative to the highest value. Error bars represent standard deviation. Stars indicate statistically significant difference (one-way ANOVA, ***$p < 0.001$).

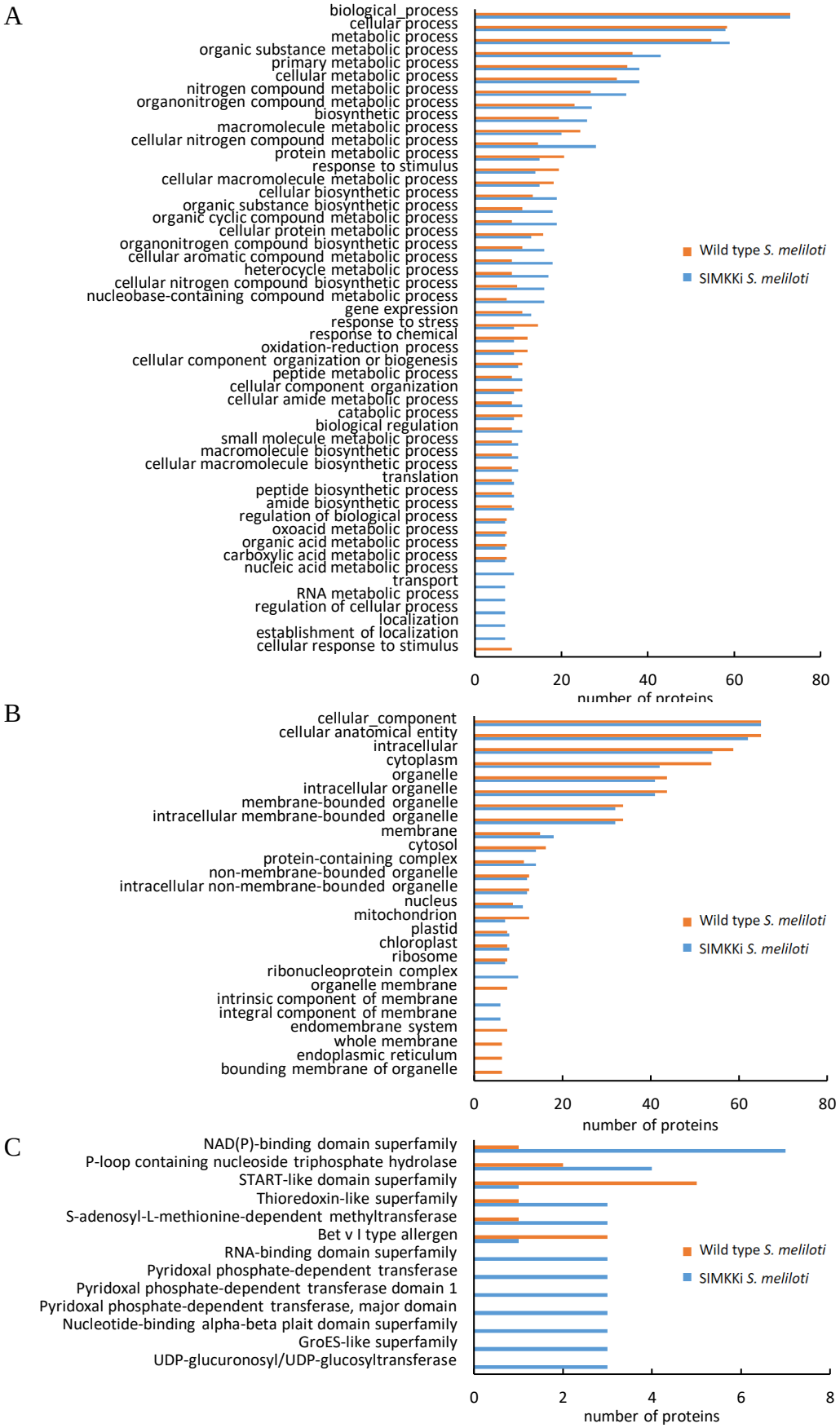

Figure 17 Comparison of classification of differential proteomes found in SIMKKi and wild type seedlings after 6 h long *S. meliloti* treatment. (A, B) GO annotation analysis according to biological process (A) and cellular compartments (B). Distribution of differentially abundant proteins into protein families (C).

Detailed views on the differential proteomes (Tables S3 and S4) showed that wild type responded to *S. meliloti* by upregulation of antioxidant defense, as exemplified by increased abundance of Cu/Zn SUPEROXIDASE DISMUTASE, L-ASCORBATE PEROXIDASE 3 and PEROXIDASE A2. This is confirmed also by the staining of SOD specific activity on native gels indicating dramatically increased activities of Cu/ZnSODs in the 6 h after inoculation by *S. meliloti* in wild type plants, which is not observed in SIMKKi line (Figure 18A, B). These antioxidant enzymes were not detected as significantly affected in SIMKKi. Nevertheless, signs of favorable redox regulation are present also in SIMKKi differential proteome by increased abundance of THIOREDOXIN H TYPE. The abundance of two glutathione S-transferases had opposing abundances in SIMKKi line. These data may indicate that different from SIMKKi, wild type plants effectively responded to ROS generated by *S. meliloti* inoculation by upregulation of ROS scavenging mechanism.

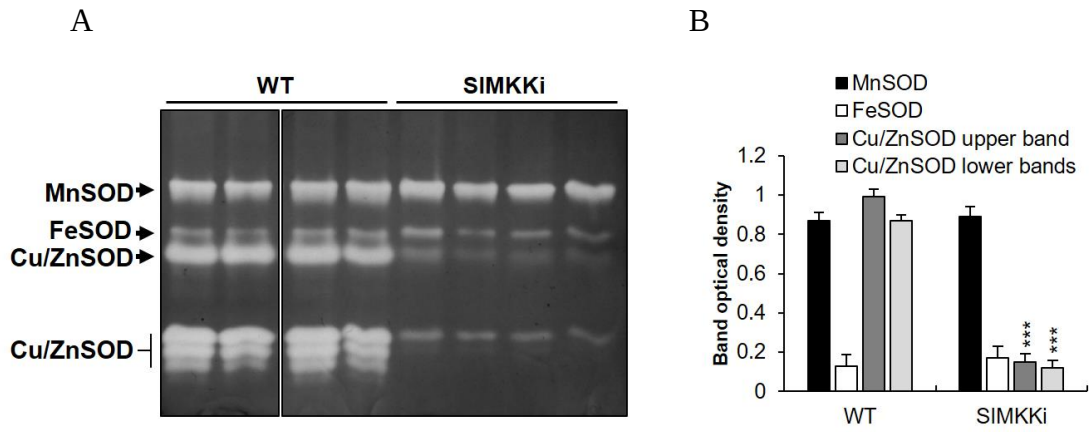

Figure 18 Comparison of individual SODs activity in *S. meliloti* treated wild type and SIMKKi line alfalfa roots. Treatment of indicated plants was performed with *S. meliloti* for 6 h. (A) Visualization of SODs isoforms activities on native polyacrylamide gels in indicated plant lines by specific staining. (B) Quantification of optical densities of bands in (A). The optical densities are displayed as relative to the highest value. Error bars represent standard deviation. Stars indicate statistically significant difference of in individual isoforms between SIMKKi and wild type (one-way ANOVA, ***$p < 0.001$).

We also found several defense related proteins to be upregulated in wild type. These include protein EXORDIUM-like 2, POLYGALACTURONASE INHIBITOR 1-LIKE, GLUCAN ENDO-1,3-BETA-GLUCOSIDASE BASIC ISOFORM ISOFORM X 1, UDP-GLUCURONIC ACID DECARBOXYLASE 6, THAUMATIN-LIKE PROTEIN 1. This upregulation was not so evident in SIMKKi line possessing rather downregulation of majority of defense related proteins. Differently to SIMKKi line,

S. meliloti treatment disturbed the sterol homeostasis in wild type as shown by 4 sterol or steroid binding proteins.

The interrogation of nodule proteomes of wild type and SIMKKi may shed light on SIMKK regulated biochemical processes undergoing in nodules. We again examined the abundance of SIMK in nodules of wild type and SIMKKi showing downregulation in SIMKKi nodules (Figure 19A, B).

Similar to the previous experiments, the differential proteome of SIMKKi nodules also included mostly proteins involved in metabolic processes, including nitrogen compound, oxoacid, lipid, protein and carbohydrates (Figure 20A). More of the DAPs were involved in catabolic processes compared to biosynthetic ones. Proteins involved in response to stimulus, stress and chemical were affected as well (Figure 20A; Table S5). Proteins localized to compartments such as cytosol, membrane, extracellular space, nucleus and mitochondrion were the most abundant (Figure 20B). The peroxidase protein family was the most affected among the DAPs. Remarkably, all peroxidases were downregulated in the transgenic line (Figure 20C).

The central enzyme of nitrogen assimilation, CYTOSOLIC GLUTAMINE SYNTHETASE shows increased abundance in the mutant. Interestingly, SIMKK downregulation leads to deregulation of endoplasmic reticulum proteins involved in protein folding. This may indicate the onset of endoplasmic reticulum stress in the SIMKKi line (Figure 20C).

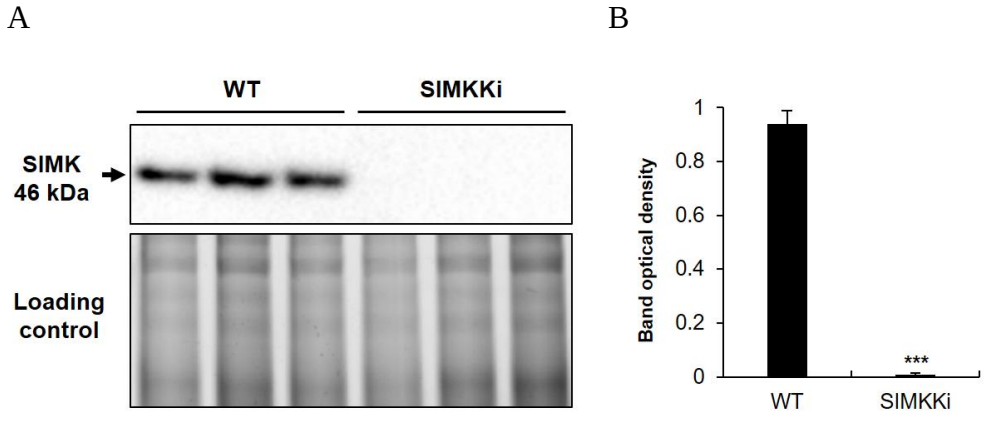

Figure 19 Analysis of SIMK abundance in nodules of wild type and SIMKKi line. (A) Immunoblot analysis by using anti-MPK6 antibody in three replicates of wild type and SIMKKi line. The anti-MPK6 antibody specifically recognizes SIMK. (B) Quantification of band optical densities. Densities are expressed as relative to the highest value. Error bars represent standard deviation. Stars indicate statistically significant difference (one-way ANOVA, ***$p < 0.001$).

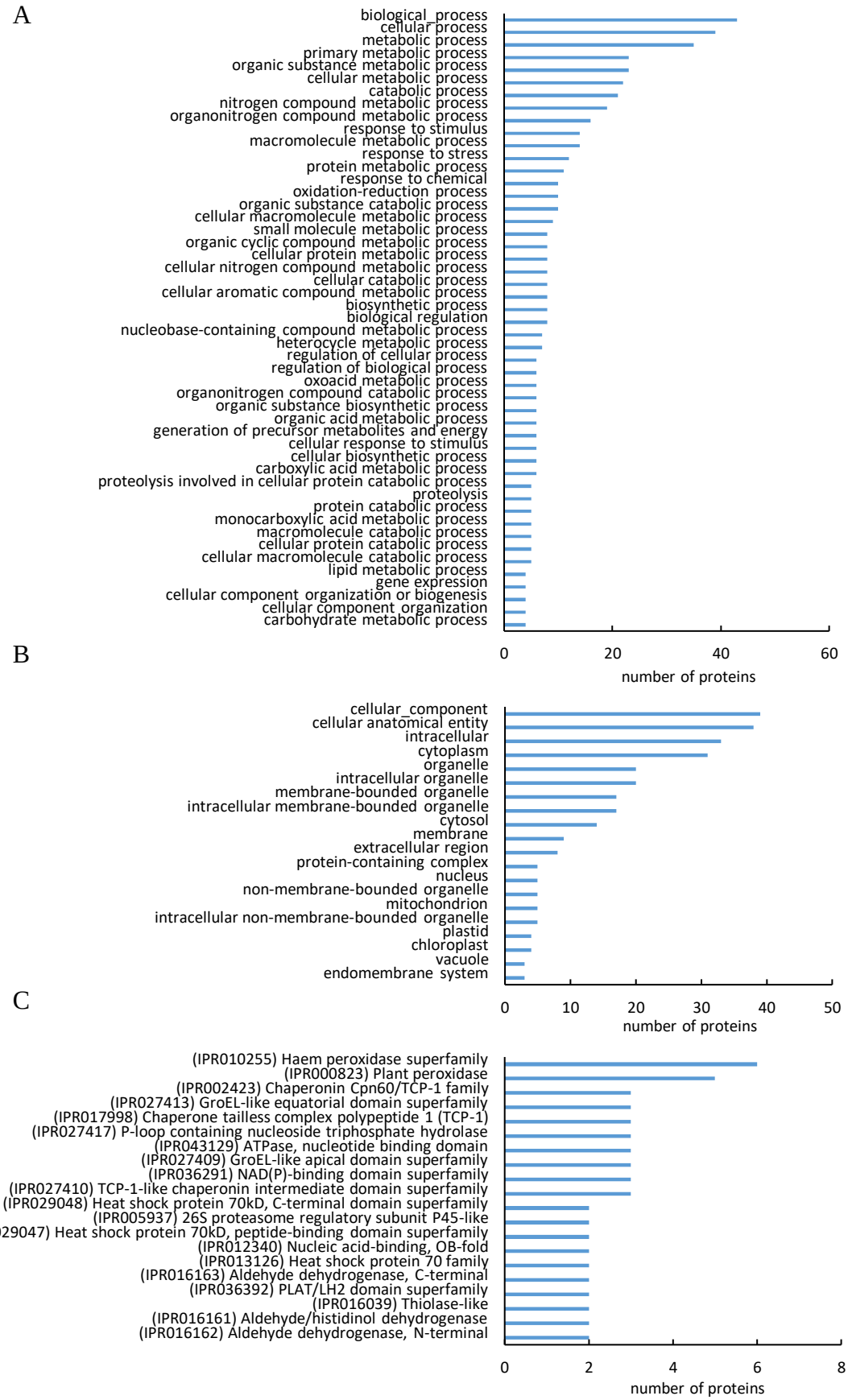

Figure 20 Classification of differentially abundant proteins (DAPs) detected in nodules of SIMKKi line as compared to the wild type into Gene ontology annotations according to biological process (A) and cellular compartment (B). (C) Distribution of DAPs into protein families.

KEGG pathway analysis showed that SIMKK downregulation in nodules affected processes connected with carbon processing and assimilation such as glycolysis/gluconeogenesis, carbon fixation, pentose phosphate pathway, and pyruvate, glyoxylate and dicarboxylate metabolism. SIMKKi line show also downregulation of proteins involved in nitrogen metabolism (Figure 21).

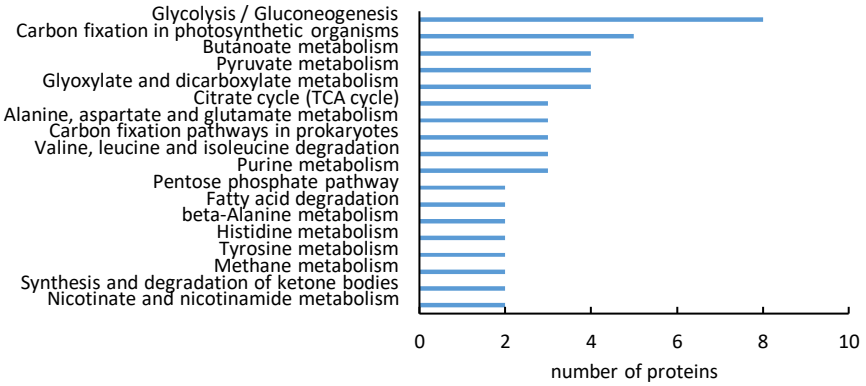

Figure 21 Classification of differentially abundant proteins (DAPs) detected in nodules of SIMKKi line as compared to the wild type into KEGG annotations.

2.3 Discussion

SIMKK is a stress induced alfalfa MAPKK acting upstream of SIMK (Kiegerl et al., 2000). Interestingly, SIMKK downregulation leads to almost complete silencing of SIMK in SIMKKi plants (Bekešová et al., 2015; Hrbáčková et al., 2020, our study). SIMK is activated by bacterial elicitation (Cardinale et al., 2000) or salt stress (Ovečka et al., 2014). Its heterologous overexpression in *Arabidopsis* leads to hypersensitivity to salt stress, which was consistent with the constitutive proteome of the SIMKK-YFP (yellow fluorescent protein) overexpressing *Arabidopsis* plants (Ovečka et al., 2014).

MAPK mutants often possess altered expression and abundances of stress related proteins and this may be explained by their essential role in regulation of stress responses (Frei dit Frey et al., 2014; Takáč and Šamaj, 2015). Our results show upregulation of enzymes involved in antioxidant defense in SIMKKi line, including four isoforms of secretory peroxidases, MnSOD, PEROXIREDOXIN-2E and 2-Cys PEROXIREDOXIN BAS 1, thus underlining the SIMKK and SIMK mediated regulation of antioxidant defense in alfalfa. This might indicate that SIMKK negatively regulates the expression of *MnSOD*, *PEROXIREDOXIN-2E* and *2-Cys PEROXIREDOXIN BAS1*. So far, evidence exists about the MPK6 mediated control of *FSD2*, *FSD3* (Xing et al., 2015) and *CSD1*, *CSD2* expression (Xing et al., 2013) which are located in cytosol (CSD1), and plastids (FSD2, FSD3, CSD2). The possible link between MAPKs and mitochondrial MSD1 was not reported yet. We hypothesize, that SIMK regulates *MnSOD* on expression level via mitochondrial retrograde signaling. Mitochondrial proteins represented a substantial portion of the differential proteome of SIMKKi line. Furthermore, SIMK ortholog MPK6 was shown to transduce the mitochondria generated retrograde signal in *Arabidopsis* (Chang et al., 2012).

This elevated antioxidant defense, in hand with the hypersensitivity of the SIMKK-YFP overexpressing *Arabidopsis* (Ovečka et al., 2014), may suggest better survival of SIMKKi transgenes under abiotic stress. Anticipating from our differential proteome, heat stress is another promising candidate, because SIMKKi line show elevated levels of HEAT SHOCK FACTOR-BINDING PROTEIN 1, HEAT SHOCK COGNATE 70 kDa PROTEIN 2 and HSP70-HSP90 ORGANIZING PROTEIN 3, all implicated in heat stress response (Hsu et al., 2010). In this case, alfalfa SIMKK-SIMK signaling module may have roles resembling *Arabidopsis* MPK6, which phosphorylates heat stress factor HSFA2 during heat stress response (Evrard et al., 2013).

Secretory peroxidases are ubiquitous enzymes with multiple functions. Except for their antioxidant roles, they have also an ability to generate H_2O_2, thus contributing to cell wall loosening in order to promote cell elongation (Passardi et al., 2006; Almagro et al., 2009). This function of peroxidases is connected to MAPKs, as MPK6 can control the expression of *PEROXIDASE 34* to regulate *Arabidopsis* root elongation (Han et al., 2015). This again supports the close similarity of *Arabidopsis* MPK6 and SIMK.

MAPK signaling cascades were earlier showed to be activated upon plant infection with symbiotic rhizobia (Lopez-Gomez et al., 2012). A well-described example is MAPKK SIP2 form *Lotus japonicus,* which interacts with SYMBIOSIS RECEPTOR-LIKE KINASE SymRK (Chen et al., 2012). Moreover, SIP2 is an upstream activator of LjMPK6 and the SymRK-SIP2-MPK6 cascade is an important signaling transduction module during nodulation in *L. japonicus* (Yin et al., 2019). Additionally, MKK4 from *Medicago truncatula* is an orthologue of SIP2 and it is important for root nodule formation. MMK4 interacts with MtMPK3 and MtMPK6 (Chen et al., 2017). Alfalfa SIMKK showed 88% amino acid identity with LjSIP2 (Chen et al., 2012), and shares a high amino acid similarity with MtMKK4 (Chen et al., 2017). SIMKK and SIMK regulate root hair growth (Šamaj et al., 2002, Hrbáčková et al., 2020), formation of infection threads as well as nodules (Hrbáčková et al., 2020). MKK5 from *M. truncatula,* which interacts with both MtMPK3 and MtMPK6 acts as negative player in the symbiotic nodule formation (Ryu et al., 2017).

Multiple molecular processes determine the successful establishment of plant-rhizobia interaction, including the attraction of bacteria by plant derived flavonoids, and attachment of bacteria on root hairs followed by root hair curling and subsequent signaling events (Oldroyd, 2013). The bacteria attachment is mainly facilitated by specific plant cell wall components such as lectins, arabinogalactan like proteins, but also bacterial surface components such as adhesins, glucomannans and lipopolysacharides (Downie, 2010; Janczarek et al., 2015). Ricadhesin was previously identified as a bacterial surface polysaccharide present in one of the bacterial poles with a role in rhizobacteria attachment (Smit et al., 1991). Moreover, a glycoprotein with putative rhicadhesin receptor activity was identified in pea (Swart et al, 1994). A protein named RHICADHESIN RECEPTOR was substantially downregulated in SIMKKi line, indicating the possible defects in rhizobia attachment on the surface of its root hairs. The possible defects in bacterial adhesion in SIMKKi line are also supported by

decreased abundance of PUTATIVE BARK AGGLUTININ LECRP A 3, bearing a legume lectin beta domain. Proteins with legume lectin domain bind to rhizobia and contribute to the bacteria attachment (Lagarda-Diaz et al., 2017). Furthermore, SIMKKi line specific deregulation of lectins is observable also after *S. meliloti* inoculation, as shown by downregulation of EPIDERMIS-SPECIFIC SECRETED GLYCOPROTEIN EP 1, a protein with bulb-type lectin domain. Altered ability for bacterial attachment likely contributes to the reduced nodulation in SIMKKi line.

The ROS signaling plays also important role during the establishment of symbiotic relationship between rhizobia and plants (Roy et al., 2020). Nod factor triggers ROS production in plant roots by induction of the nodulin gene RHIZOBIUM INDUCED PEROXIDASE1 in *M. truncatula* (Ramu et al., 2002). ROS production is also connected with activation of NADPH oxidase genes, which are required for early symbiotic signalization (Lohar et al., 2007) and nitrogen fixation in nodules (Marino et al., 2011). Differential regulation of SODs after *S. meliloti* treatment may be connected to the altered initial ROS signaling in SIMKKi line, which likely caused the decreased number of IT formation (Hrbačková et al., 2021). This may be also linked to induction of expression SYMBIOTIC PROTEIN KINASE1, which is induced by both Nod factor and H_2O_2, primarily in infected root hair cells and the infection zones of nodules (Andrio et al., 2013).

SIMKK and SIMK are implicated in root hair growth and development (Šamaj et al., 2002; Hrbáčková et al., 2020). SIMK is relocalizing from nucleus to the cytoplasmic vesicles, which accumulate in tips of growing root hairs in actin dependent manner (Ovečka et al., 2014). Cytoskeletal inhibitor mediated modifications of actin disturb the SIMK distribution in the root hairs and negatively affect the root hair development (Šamaj et al., 2002). VILLIN 4, actin-binding protein highly homologous to *Arabidopsis* VILLIN 4, is considerably upregulated in SIMKKi line compared to wild type. *Arabidopsis* VILLIN 4 is involved in root elongation and root hair development by regulation of actin organization in Ca^{2+} dependent manner (Zhang et al., 2011). Furthermore, VILLIN 4 was substantially downregulated in SIMKKi line after *S. meliloti* treatment, but not in wild type. These data indicate the close link between SIMKK and VILLIN 4 in alfalfa. Villins were also identified as MAPK phosphorylation targets (Rayapuram et al., 2018), further supporting the hypothesis about the villin-mediated defects of root hair development in SIMKKi plants.

The dynamicity of membrane transport is crucially dependent on proper functioning of actin cytoskeleton (Wang et al., 2017). Therefore, actin disturbances, as those caused by villin modifications have obvious effect on membrane trafficking (Zou et al., 2019). It is reasonable to claim that SIMKK-mediated VILLIN 4 disturbances are connected to robust changes in membrane transport associated proteins, which also might participate on root hair defects in SIMKKi line. Root hair formation and elongation is tightly connected also to structural sterols, which accumulate in trichoblasts during the prebulging and bulge stages and show a polar accumulation in the tip during root hair elongation (Ovečka et al., 2010). Notably, *S. meliloti* treatment caused changes in abundances of MEMBRANE STEROID-BINDING PROTEIN 1, OXYSTEROL-BINDING PROTEIN-RELATED PROTEIN 3 A and PROBABLE STEROID-BINDING PROTEIN 3 in wild type, while sterol metabolism was less affected in SIMKKi line. The altered homeostasis of plasma membrane sterol composition alters the protein clustering into microdomains (Gao et al., 2015) a site of localization of LYK3 an entry receptor for alfalfa infection by rhizobia (Smit et al., 2007). Our results imply plasma membrane sterol content rearrangements in wild type. This is in agreement with changes in LYK3 localization in response to bacterial inoculation (Haney et al., 2011), in a time scale comparable to the length of treatment in our experiment. It was suggested that LYK3 undergoes endocytosis similar to other receptors, such as FLS2 (Ott, 2017). Our data suggest possible differences in sterol rearrangements upon *S. meliloti* inoculation between SIMKKi and wild type line with possible impact on nodule formation.

Proteomic analyses is a powerful tool to uncover processes undergoing in nodules including nitrogen and carbohydrate metabolism as well as redox homeostasis (Larrainzar et al., 2007). Nitrogen fixation requires a constant supply of energy, which is provided by high metabolic rate (Becana et al., 2010). This leads to increased production of ROS leading to protein oxidative modifications (Matamoros et al., 2018). To avoid the negative effects of ROS, nodules are equipped with a broad battery of antioxidants (Becana et al., 2010). We have found that SIMKKi directed downregulation increased the abundance of PEROXIREDOXIN-2B, a redox buffering protein positively contributing to redox homeostasis (Dietz, 2011) indicating the suppressed regulation redox homeostasis in SIMKKi nodules. An intriguing finding is the downregulation of 5 secretory peroxidases in SIMKKi nodules. As noted above,

they may contribute to apoplastic ROS production and thus affect cell wall modifications and defense responses (Fernández-Pérez et al., 2015). These results suggest that SIMKK downregulation substantially affects secretory peroxidases in nodules. Further investigation is necessary to explain this downregulation.

SIMKKi possesses elevated abundance of CYTOSOLIC GLUTAMINE SYNTHETASE, a master enzyme involved in nitrogen assimilation (Kaur et al., 2019), indicating possible increased efficiency of N assimilation. The concept of elevated N assimilation may be also substantiated by increased cysteine biosynthesis in the SIMKKi line. This increased amino acid production requires an elevated supply of carbon assimilates. PHOSPHOENOLPYRUVATE CARBOXYLASE, which provides a substantial portion of carbon required for nitrogenase activity and ammonia assimilation (Pathirana et al., 1992) is downregulated in the transgenic line. Moreover, energy-providing glycolysis shows also disturbances, since glycolytic enzymes such as FRUCTOSE-BISPHOSPHATE ALDOLASE, PHOSPHOGLYCERATE KINASE, both cytosolic, show altered abundances. Taken together, except for reduced nodule formation, SIMKKi nodules exhibit apparent disturbances in N assimilation and carbon supply.

In conclusion, SIMKK may contribute to multiple events connected to *S. meliloti* – alfalfa interactions, including bacteria attachment, root hair development or plasma membrane remodeling.

3 FSD1 is a plastidial, cytosolic and nuclear enzyme and plays a role in *Arabidopsis* root development and stress tolerance

3.1 Material and Methods

3.1.1 Plant material and growth conditions

Seeds of *Arabidopsis thaliana* (L.) Heynh of the wild-type Columbia (Col-0) and *fsd1-1*, *fsd1-2*, *fsd1-3* and other lines (all in the Col-0 background) were surface-sterilized by ethanol sterilization and placed on a 1/2 MS medium solidified with 0.5% (w/v) gellan gum, enriched with 1% (w/v) sucrose and stratified at 4°C for 1–2 days. Media with different concentrations of Cu^{2+} (0–2 μM), were prepared by adjustments of $CuSO_4 \cdot 5H_2O$. Seedlings were grown vertically at 21°C, 16/8 h (light/dark) photoperiod with an illumination intensity of 150 $\mu mol \cdot m^{-2} \cdot s^{-1}$ in a phytochamber (Weiss Technik). Etiolated plants were prepared by covering of Petri dishes by aluminium foil. *Arabidopsis FSD1* T-DNA insertion mutants *fsd1-1* (SALK_029455), *fsd1-2* (GABI_740E11) and *fsd1-3* (SALK_036006) were obtained from the European Arabidopsis Stock Centre (http://arabidopsis.info/BasicForm).

Apart from the above mentioned lines, a stably transformed *A. thaliana* transgenic line carrying *35S::sGFP* construct cloned using pMAT037 plasmid (Matsuoka and Nakamura, 1991; Mano et al., 1999) was used as a positive control for GFP detection in immunoblotting, microscopic and FRAP analyses.

3.1.2 Selection of *FSD1* mutants by genotyping

Twelve-days-old seedlings of *fsd1-1*, *fsd1-2* and *fsd1-3* mutants grown on 1/2 MS medium were utilized for genotyping analysis. Phire Plant Direct PCR Kit (Thermos Fisher Scientific) was used for isolation of genomic DNA according to manufacture's protocol. Subsequently, homozygous individuals were detected by PCR using primers (Table 3). Wild-type (Col-0) plants were used as a positive and negative control.

Table 3 List of primers used for the genotyping of *fsd1* mutants.

Name	Sequence
LBb1.3	5'-ATTTTGCCGATTTCGGAAC-3'
SALK_029455_RP	5'-GTTGAAAGCAGGGAGGAGATC-3'
SALK_029455_LP	5'-TTTGTTTGGTCTCCCAACAAC-3'
SALK_036006_RP	5'-AAAACAAAATGACATTTGCCG-3'
SALK_036006_LP	5'-TTGGCATATGGTTTACCCATC-3'
GABI_740E11_RP	5'-AGTTTGTTTGCTCATATGCGG-3'
GABI_740E11_LP	5'-AAACACACAGATTCCACTGGC -3'

3.1.3 Isolation of genomic DNA and Southern blot analysis

About 300–600 mg of fresh leaf tissue was homogenized in liquid nitrogen from both *fsd1-1* and *fsd1-3* mutant plants. The isolation of gDNA was performed according to protocol of Pallotta et al. (2000). Subsequently, gDNA samples were separately digested with EcoRI, SacI and HindIII restriction enzymes and separated by electrophoresis on gel containing 0.8% (w/v) agarose in 0.5x TBE buffer (5x TBE: 54 g Tris base, 27.5 g boric acid and 20 ml 0.5 M EDTA with pH 8.0). Gel was depurinated, then denaturated, washed and neutralized. Subsequently, it was washed in 20x saline-sodium citrate buffer (SSC; 175.2 $g \cdot 1^{-1}$ NaCl, 100.5 g sodium citrate dihydrate, pH 7) and blotted onto nylon membranes in 20x SSC. DNA fragments were cross-linked to the membrane by UV for 3 min. Prepared membrane was prehybridized in digoxigenin (DIG)-easy prehybridization mix (Roche Diagnostics) at 55°C for 3.5 h and then hybridized overnight at 50°C in PCR-amplified DIG-probe (Roche Diagnostics) specific to kanamycin resistance in T-DNA mutants. DIG-probe was amplified by PCR reaction (primers are present in Table 4). After the hybridization, membranes were incubated three-times in 2x SSC with 1% (w/v) SDS for 10 min at RT, three-times in 0.5x SSC with 1% (w/v) SDS for 8 min at RT and also three-times in 0.1x SSC with 1% (w/v) SDS for 20 min at 65°C. The signal from DIG was exposed using a commercially available kit (Roche Diagnostics).

Table 4 List of primers used for amplification kanamycin probe.

Name	Sequence
Fwd - Kan	5′-AAAAGCGGCCATTTTCCACC-3′
Rev - Kan	5′-GATGGATTGCACGCAGGTTC-3′

3.1.4 Immunoblotting and SOD activity analysis

Immunoblotting was performed as described in section 2.1.3 with slight modifications. For immunoblotting, seedlings of each line (15 seedlings per one replicate) were homogenized into fine powder in a mortar with liquid nitrogen. Nonspecific epitopes were blocked by overnight incubation of the membrane either in 5% (w/v) low-fat dry milk (for the detection of FSD1 and CSDs) or in 4% (w/v) low-fat dry milk and 4% (w/v) BSA (for detection of GFP), in TBS-T. The membranes were incubated with anti-FSD or anti-CSDs primary antibodies (both Agrisera, dilution 1:3000 in TBS-T with 3% (w/v) low-fat dry milk) or anti-GFP (Sigma-Aldrich, dilution 1:1000 in TBS-T with 3% BSA) primary antibody at 4°C overnight. Following repeated

washing in TBS-T, membranes were incubated with a secondary antibody diluted in TBS-T containing 1% (w/v) BSA for 1.5 h. Horseradish peroxidase-conjugated goat anti-rabbit or anti-mouse IgG secondary antibodies (Thermo Scientific, both diluted 1:5000) were used for the detection of FSD1, CSDs and GFP.

SOD isoenzymatic activities on native PAGE gels were carried out as in section 2.1.3, analyzing 15 seedlings per one biological replicate.

Both analyses were performed in three biological replicates and the statistical significance was evaluated using one-way ANOVA test.

3.1.5 Phenotypic analysis

For the detailed root phenotyping, seedlings were recorded daily and documented using a scanner (ImageScanner TM III, Little Chalfont, UK) and ZOOM microscope (Leica MZ FLIII 165FC, Mannheim, Germany) for two weeks. The primary root lengths of 7- and 10- day-old seedlings were measured from the individual scans using ImageJ. Lateral root number was counted on the 7^{th} and 10^{th} day after germination and it was standardized to the primary root length. Fresh weight of 14-day-old seedlings was measured from 30 plants in three independent repetitions for each plant line.

3.1.6 Cloning of GFP-tagged *FSD1* gene under native promoter

Both C- and N-terminal fusion constructs of *eGFP* with genomic DNA of FSD1 (*pFSD1-gFSD1::GFP:3ˈUTR-FSD1* (GFP-FSD1) and *pFSD1::GFP:gFSD1-3ˈUTR-FSD1* (FSD1-GFP)) were cloned under its native promoter from *Arabidopsis* wild type (Col-0). The sequence of the native promoter was taken 1270 bp upstream of the start codon and for 3ˈUTR 1070 bp downstream of the stop codon. MultiSite Gateway® Three-Fragment Vector Construction (Thermo Fisher Scientific) was used as the cloning method for the preparation of these constructs. Amplified sequences of the promoter, genomic DNA and 3ˈUTR (primers are listed in Table 5) were recombined into pDONR™P4-P1R and pDONR™P2R-P3 donor vectors, where plasmids pEN-L1-F-L2 with and without stop-codon were used as B fragment for the subsequent three-fragment vectors LR recombination into the destination vector pB7m34GW. Sequencing-validated cloning products were transformed into *Agrobacterium tumefaciens* GW3101, and used further for floral dip stable transformation of *fsd1-1* and *fsd1-2* mutants. Several transgenic lines possessing intense fluorescent signals have

been selected from the T1 generation. Selected lines with one insertion were propagated into T3 homozygous generation and used in further experiments.

Table 5 List of used primers for *pFSD1-gFSD1::GFP:3'UTR-FSD1* and *pFSD1::GFP:gFSD1-3'UTR-FSD1* MultiSite Gateway cloning.

Oligo name	Sequence 5' - 3'
C-terminal fusion: Promoter + gene_FWD	GGGGACAACTTTGTATAGAAAAGTTGCG GGCATTTGCTGTATATGAGAAGCC
C-terminal fusion: Promoter + gene_REV	GGGGACTGCTTTTTTGTACAAACTTGG AGCAGAAGCAGCCTTGGC
C-terminal fusion: 3′UTR_FWD	GGGGACAGCTTTCTTGTACAAAGTGGTC GCAAATTTCTGAACAATTTGAC
C-terminal fusion: 3′UTR_REV	GGGGACAACTTTGTATAATAAAGTTGG TTACTTCAAAGCTCACTCTCTGC
N-terminal fusion: Promoter_FWD	GGGGACAACTTTGTATAGAAAAGTTGGC GCTGTATATGAGAAGCCCTTC
N-terminal fusion: Promoter_REV	GGGGACTGCTTTTTTGTACAAACTTGG TCTTTGTAATTGAAGCTGCAC
N-terminal fusion: Gene + 3′UTR_FWD	GGGGACAGCTTTCTTGTACAAAGTGGGA ATGGCTGCTTCAAGTGCTG
N-terminal fusion: Gene + 3′UTR_REV	GGGGACAACTTTGTATAATAAAGTTGC CTCACTCTCTGCATTGGTTCGTC

3.1.7 Transient transformation of *Nicotiana benthamiana* leaves

The inoculums with *Agrobacterium tumefaciens* GV3101 bearing FSD1-GFP and FSD1-GFP constructs were prepared in 10 ml of YEB medium with SPE antibiotic (50 μg·ml^{-1}). Culture grown at 28 °C, 200 rpm to OD_{600} 0.6 was centrifuged at 2500 g, 4°C for 15 min. Harvested cells were resuspended in 5 ml buffer with added 10 mM $MgCl_2$, 10 mM MES (pH 5,6), and 150 μM acetosyringon. The prepared solutions were incubated at room temperature for 2 h. Both bacterial cultures were infiltrated into 7 weeks old *Nicotiana benthamiana* leaves using the syringe. Infiltrated plants were covered by plastic bags and kept overnight in the dark overnight. Plants were uncovered and put in the phytotron for the next 24 h. After 48 h, representative parts of transformed epidermal cells were used for microscopic observation.

3.1.8 Stable transformation of *Arabidopsis* plants

Transformed *Agrobacterium tumefaciens* bearing FSD1-GFP and GFP-FSD1 constructs were used for the transformation of *Arabidopsis fsd1-1* and *fsd1-2* mutant plants according to the optimized protocol (Clough and Bent, 1998; Davis et al., 2009). Obtained seeds were planted on hygromycin B (10 μg·ml^{-1}) selection medium and led grown to identify T1 transgenic plants. Surviving plants were tested for the presence of GFP signal by using stereomicroscope (Axio Zoom.V16; Carl Zeiss, Germany).

Seedlings with the presence of GFP signal were propagated into T3 generation, which has all progeny with the presence of GFP signal.

3.1.9 Co-imunoprecipitation with anti-GFP beads with mass spectrometry detection

For co-immunoprecipitation, 14-day-old *fsd1-1* lines complemented by either FSD1-GFP or GFP-FSD1 constructs (both in four repetitions) were ground by liquid nitrogen in a mortar. Three grams of whole seedlings material in fresh weight was used. Proteins were extracted using extraction buffer (50 mM Tris-HCl (pH 7.5), 150 mM NaCl, 1% (v/v) Nonidet P-40 (NP40), protease inhibitors mix cocktail (Roche, 1 tablet per 50 ml)) for 30 min. Subsequently, supernatant was collected after centrifugation (14 000 g, 20 min at 4°C). The co-immunoprecipitation (by using anti-GDF beads; Miltenyi Biotec) and the preparation of protein digest was performed according to Hunter et al. (2019).

The mass spectrometry analysis and the protein identification was performed as a commercial service at University of Turku. Briefly, the LC-ESI-MS/MS analysis was performed on a nanoflow HPLC system (Easy-nLC1200, Thermo Fisher Scientific) coupled to the Q Exactive HF mass spectrometer (Thermo Fisher Scientific, Bremen, Germany) equipped with a nano-electrospray ionization source. Peptides were first loaded on a trapping column and subsequently separated inline on a 15 cm C18 column (75 μm x 15 cm, ReproSil-Pur 5 μm 200 Å C18-AQ, Dr. Maisch HPLC GmbH, Ammerbuch-Entringen, Germany). The mobile phase consisted of water with 0.1% formic acid (solvent A) or acetonitrile/water (80:20 (v/v)) with 0.1% formic acid (solvent B). A 60 min gradient (from 8% to 43% solvent B, followed by wash stage at 100% solvent B) was used to elute peptides. MS data was acquired automatically by using Thermo Xcalibur 4.1 software (Thermo Fisher Scientific). An information dependent acquisition method consisted of an Orbitrap MS survey scan of mass range 300–2000 m/z followed by higher-energy collisional dissociation fragmentation for 10 most intense peptide ions. Data files were searched for protein identification using Proteome Discoverer 2.3 software (Thermo Fisher Scientific) connected to an in-house server running the Mascot 2.6.1 software (Matrix Science). Data was searched against a SwissProt database (version 2019_09).

STRING (Szklarczyk et al., 2015) application was used for projection of protein interaction network applying minimum required interaction score 0.55.

3.1.10 Whole mount immunofluorescence labeling

Arabidopsis Col-0 and *fsd1* mutants grown on 1/2 MS medium were used at 3rd day after germination (DAG) for immunofluorescence labelling of the root tips according to the protocol established by Šamajová et al. (2014) with minor modifications. Samples were incubated with rat anti-FSD (Agrisera) primary antibody diluted at 1:250, in phosphate-buffered saline (PBS) containing 3% (w/v) BSA at 4°C overnight. In the next step, samples were incubated with Alexa-Fluor 488 conjugated goat anti-rat secondary antibody diluted at 1:500 in PBS with 3% (w/v) BSA at room temperature for 3 h. DNA was counterstained with 250 $\mu g \cdot ml^{-1}$ 4,6-diamidino-2-phenylindole (DAPI, Sigma-Aldrich) in PBS for 10 min. After a final wash in PBS, the specimens were mounted in an antifade solution (0.5% (w/v) p-phenylenediamine in 90% (v/v) glycerol in PBS or 1 M Tris-HCl, pH 8.0) or in the commercial antifade VectashieldTM (Vector Laboratories).

3.1.11 Salt sensitivity assay and plasmolysis

Germination analysis of Col-0, both *fsd1* mutants and *fsd1-1* complemented lines (GFP-FSD1 and FSD1-GFP) was performed on 1/2 MS medium with and without 150 mM NaCl. Plates with seeds were kept at 4°C for 2 days and incubated as mentioned above. Percentage of germinated seeds (with visible radicle) was counted under stereomicroscope after 24, 48, and 78 h. Measurements were performed in four repetitions (total examined seeds 120) and statistical significance was tested by one-way ANOVA test.

For salt stress sensitivity determination, 4-day-old seedlings of Col-0, *fsd1* mutants and *fsd1-1* complemented lines (GFP-FSD1 and FSD1-GFP) growing on 1/2 MS medium were transferred to 1/2 MS medium containing 150 mM NaCl. The ratio of bleached seedlings was counted at the 5th day after transfer. Measurements were performed in four repetitions (total examined seedlings 120) and the statistical significance was evaluated by one-way ANOVA test.

For plasmolysis induction, 4-day-old seedlings of *fsd1-1* complemented lines (FSD1-GFP and GFP-FSD1) and *Arabidopsis* transgenic line expressing *35S::eGFP* were mounted between glass slide and coverslip in liquid 1/2 MS media. Plasmolysis

was induced with 500 mM NaCl (hypocotyls) or 250 mM NaCl (roots) in liquid 1/2 MS media applied by perfusion. Plasmolysed cells were observed 5–30 min after the perfusion by confocal laser scanning microscopy (CLSM) 880 equipped with an Airyscan detector (ACLSM, Carl Zeiss, Germany) and a spinning disk microscope (Cell Observer, SD, Carl Zeiss, Germany).

3.1.12 Analysis of oxidative stress tolerance

To determine the sensitivity of examined lines to oxidative stress, 4-day-old seedlings of Col-0, *fsd1* mutants and *fsd1-1* complemented lines (GFP-FSD1 and FSD1-GFP) growing on 1/2 MS medium were transferred to 1/2 MS medium containing 2 μM MV. The ratio of seedlings with fully green cotyledons was counted at the 5th day after transfer. Measurements were performed in four repetitions (total examined seedlings 160) and the statistical significance was evaluated by one-way ANOVA test.

The relative amount of chlorophyll a and b was measured from 30 seedlings of each line according to Barnes et al. (1992). The measurement correlated to the weight of examined seedlings was performed in three repetitions (total examined seedlings 90) and the statistical significance was evaluated by one-way ANOVA test.

3.1.13 Fluorescent detection of ROS

ROS in plasmolysed roots were visualized by incubation in 30 μM CellROX® Deep Red Reagent (Thermo Fisher Scientific), diluted in 1/2 MS with or without 250 mM NaCl for 15 min in darkness. The emitted signal (excited at 633 nm) was recorded at 652–713 nm using CLSM 720 (Carl Zeiss, Germany). The signal was quantified using ImageJ software. Images were transformed into 8-bit grayscale format and the mean density of the signal was quantified in 6 cells in each of 3 plants per line.

3.1.14 Confocal laser scanning microscopy

Three and 8-day-old seedlings of *fsd1-1* mutants carrying recombinant GFP-fused FSD1 were used for microscopy. Imaging of living or fixed samples was performed using a confocal laser scanning microscope LSM710 (Carl Zeiss, Germany), ACLSM (Carl Zeiss, Germany) and a spinning disk microscope (Cell Observer, SD, Carl Zeiss, Germany). Image acquisition was done with 20× (0.8 numerical aperture (NA)) dry Plan-Apochromat, 40× (1.4 NA) and 63× (1.4 NA) Plan-Apochromat oil-immersion objectives. Samples were imaged with a 488 nm excitation laser using emission filters

BP420–480+BP495–550 for eGFP detection and BP 420–480 + LP 605 for chlorophyll a detection. Laser excitation intensity did not exceed 2% of the available laser intensity range. Immunolabelled samples were imaged using the excitation laser line 488 nm and emission spectrum 493–630 nm for Alexa-Fluor 488 fluorescence detection, and excitation laser line 405 nm and emission spectrum 410–495 nm for DAPI. Images were processed as single plane maximum intensity projections of Z-stacks in Zen Blue 2012 software (Carl Zeiss, Jena, Germany), assembled and finalized in Microsoft PowerPoint to final figures.

3.1.15 Fluorescence recovery after photobleaching

Fluorescence recovery after photobleaching (FRAP) analysis of FSD1-GFP and GFP alone in *Arabidopsis* transgenic line expressing *35S::eGFP* was performed in nuclei (selected as regions of interest, ROI) of hypocotyl epidermal cells using confocal laser scanning microscope LSM710 (Carl Zeiss, Germany). Argon laser line of 488 nm at 2% laser intensity was used for pre-bleach scans, which was followed by scanning at 100% laser intensity for photobleaching of GPF. Selected regions were scanned each 5 s in total 4 min, where first three scans were pre-bleach scans (0–10 s). Each time point was scanned with 112.5 x 62.5 μm image size and with scaling of 0.21 μm pixel size. Speed of the scanning was 2.41 μs pixel dwell and 3.69 s scan time with 4 time averaging at depth of 16 bit for pre-bleach and post-bleach scanning, and scanning speed of 11.91 μs pixel dwell for bleaching. Quantitative analysis of FRAP experiments was done in ZEN 2011 software (black edition; Carl Zeiss, Germany). Briefly, regions of interest for bleaching, reference and background were selected and these areas were scanned. Bleaching was done with full laser power (100%). To keep physiological conditions for examined cells, bleaching was stopped after reaching of 40–45% of the original pre-bleached fluorescence signal intensity. Values of fluorescence intensity were measured in arbitrary units using ZEN 2011 software and they were used for calculations of corresponding half-time of signal recovery and mobile-to-immobile fraction ratios directly in ZEN 2011 software. Data from in total 49 regions of interest were exported to the Microsoft Excel software and normalized to absolute fluorescence intensities, where the highest intensity (before bleaching) was 1 and the lowest intensity (immediately after bleaching) was 0. FRAP measurement was performed in three biological replicates (5 seedlings per one repetition).

3.1.16 Light-sheet fluorescence microscopy

Seeds of *fsd1-1* mutant expressing FSD1-GFP were surface-sterilized and placed on 1/2 MS medium solidified with 0.5% (w/v) gellan gum and stratified at 4°C for 1–2 days. Subsequently, seeds were transferred to horizontally-oriented plates with the same culture medium and a height of at least 15 mm. Horizontal cultivation allowed seeds to germinate and roots to grow inside of a solidified medium. Seedlings were inserted into fluorinated ethylene propylene (FEP) tubes with an inner diameter of 2.8 mm and wall thickness of 0.2 mm (Wolf-Technik, Germany), in which roots grew in the block of the culture medium inside the FEP tube, while the upper green part of the seedling developed in an open space of the FEP tube with access to the air (Ovečka et al., 2015). The FEP tube with seedling was inserted into a sample holder and placed into the observation chamber of the light-sheet Z.1 fluorescence microscope (Carl Zeiss, Germany). Before insertion of the sample into the microscope, plants were ejected slightly out of the FEP tube allowing for imaging of the root in the block of the solidified culture medium, but without the FEP tube. The sample chamber of the microscope was filled with sterile 1/2 MS medium and tempered to 21°C using the peltier heating/cooling system. Developmental live cell imaging was done with dual-side light-sheet illumination using two light sheet fluorescence microscopy 10× (0.2 NA) illumination objectives (Carl Zeiss, Germany) with excitation laser line 488 nm, beam splitter LP 560 and with emission filter BP505–545. Image acquisition was done with a W Plan-Apochromat 20× (1.0 NA) objective (Carl Zeiss, Germany) and images were recorded with the PCO. Edge sCMOS camera (PCO AG, Germany) with an exposure time of 100 ms and imaging frequency of every 2 min in the Z-stack mode for 2–20 h.

3.1.17 Image processing

The post-processing, default deconvolution and profile measurement of all fluorescence images in this study, including 3D reconstruction or maximum intensity projection from individual Z-stacks and creating subsets was done using ZEN 2010 software. All images exported from ZEN 2010 software were assembled and captioned in Microsoft PowerPoint to final pictures.

3.1.18 Bioinformatics predictions

AthaMap (Hehl et al., 2016) was used to predict possible TFs binding to *cis*-elements present in promoter sequence of *FSD1*. We analyzed 1000 bp upstream of start codon with following parameters: Downstream region: 50, % Restriction to highly conserved TF binding sites: 0, Select ALL. Identified putative TFs were analyzed with GPS 3.0 (Species Specific, All kinases; Xue et al., 2005) and annotated by PhosPhAt 4.0 (Zulawski et al., 2013) to obtain information about possible and experimentally confirmed phosphorylation and presence of phosphopeptides. TFs without predicted phosphorylation for MAPK (CMGC/MAPK) were excluded. The presence of MAPK-specific docking sequence in TFs protein sequences (retrieved from Araport11; Cheng et al., 2017) was evaluated by ELM (Cell compartment: not specified, Taxonomic Context: *Arabidopsis thaliana*; Kumar et al., 2020). Coexpression of identified TFs with *FSD1* and *MPK3*, *MPK4*, and/or *MPK6* was inspected by ATTED-II (CoExSearch; Obayashi et al., 2018).

3.1.19 Preparation of recombinant proteins and *in vitro* kinase assay

Constructs for GST-SPL1 (Glutathione S-transferase tag), MBP-SPL1 (Maltose-binding protein tag), MBP-SPL7 and MBP-FSD1 recombinant proteins were generated using double restriction and ligation into pGEX-6P-1 (Sigma-Aldrich) and pMAL-p2 (NEB) vectors, respectively. The cDNA of individual genes was amplified by PCR (primers are listed in table 6). PCR products were digested and ligated into the destination vectors. Prepared constructs were validated by restriction analysis and by sequencing. Final product was transformed into *E. coli* BL21 Star (DE3). Constructs of GST-MPK3 and GST-MPK6 were kindly provided by Michael Wrzaczek (Helsinki University). The protein expression, purification and *in vitro* kinase assay were performed according to Hunter et al., (2019). Myelin basic protein (MyBP; Sigma-Aldrich) was used as an artificial substrate for *in vitro* kinase assay.

Table 6 List of primers used for amplification of *SPL1*, *SPL7* and *FSD1* cDNA for molecular cloning.

Name	Sequence
Fwd - pGEX-SPL1	5'-CGCGGATCCATGGAAGCTAGAATTGATGAAG-3'
Rev - pGEX-SPL1	5'-CCGCTCGAGTCAGCTTGTTCCATAGTCC-3'
Fwd - pMAL-SPL1	5'-CGCGGATCCATGGAAGCTAGAATTGATGAAG-3'
Rev - pMAL-SPL1	5'-ACGCGTCGACTCAGCTTGTTCCATAGTCC-3'
Fwd - pMAL-SPL7	5'-GCTCTAGAATGTCTTCTCTGTCGCAATC-3'
Rev - pMAL-SPL7	5'-CCCAAGCTTTCATATCCTGTCTCTTTCTGAAG-3'
Fwd - pMAL-FSD1	5'-CCGGAATTCATGGCTGCTTCAAGTGCT-3'
Rev - pMAL-FSD1	5'-CGCGGATCCTTAAGCAGAAGCAGCCTTG-3'

3.2 Results

3.2.1 Selection and verification of *fsd1* mutants

Seedlings of homozygous individuals of three *fsd1* mutants, namely *fsd1-1* (SALK_029455), *fsd1-2* (GABI_740E11) and *fsd1-3* (SALK_036006) were selected for this study. They were thoroughly genotyped (Figure S2), verified by immunoblotting with specific anti-FSD antibody (Figure S3A), and by SOD activity analyses (Figure S3B), showing absence of FSD1 protein and activity. One T-DNA insertion was found in the *fsd1-1* mutant, while *fsd1-3* contained more than one insertion (Figure S4). For this reason, *fsd1-3* was excluded from further studies.

3.2.2 Cloning of GFP-fused FSD1 driven under native promoter, *Arabidopsis* stable transformation

The GFP-fused FSD1 constructs *pFSD1-gFSD1::GFP:3'UTR-FSD1* (*FSD1-GFP*) and *pFSD1::GFP:gFSD1-3'UTR-FSD1* (*FSD1-GFP*) were prepared with 1270 bp long promoter sequence upstream from the start codon and 1070 bp long 3'UTR sequence downstream from stop codon by using MultiSite Gateway® cloning technology (Figures S5-7). Transient transformation of tobacco leaves were employed to confirm the functionality of prepared constructs in tobacco leaf epidermal cells (Figures S8, S9).

For the elucidation of *FSD1* expression and localization *in vivo*, we generated stably transformed *fsd1* mutants carrying *FSD1* under its own native promoter and fused with GFP to both N- and C-terminus. All lines with one insertion were propagated into the T3 homozygous generation.

The presence of FSD1 protein and its GFP-fused variants were examined in wild type and transgenic lines by immunoblotting with anti-FSD (Figure 22A, B) and anti-GFP (Figure S10) antibodies and by analysis of SOD isoforms activities on the native PAGE gel (Figure 22C, D). Both immunoblotting analyses showed the presence of FSD1-GFP and GFP-FSD1 proteins in transgenic lines. While FSD1 protein levels were comparable in wild type and FSD1-GFP line, GFP-FSD1 line showed significantly lower FSD1 abundance (Figure 22A, B). Quantitatively, a decrease of abundance in GFP-FSD1 protein was approximately 70% in comparison with wild type and FSD1-GFP by using the anti-FSD antibody and 56% in comparison with FSD1-GFP by using the anti-GFP antibody. This trend was also observed at the level of FSD1 activity as

examined by specific activity staining on native gels (Figure 22 C, D). The identity of bands corresponding to GFP-fused FSD1 proteins in both lines was confirmed by preincubation of gels in inhibitors (Figure S11). The functionality of the GFP-fused proteins in the transgenic lines was proved by their response to different Cu^{2+} concentrations using immunoblotting as well as enzymatic activity analysis (Figure 23A-D).

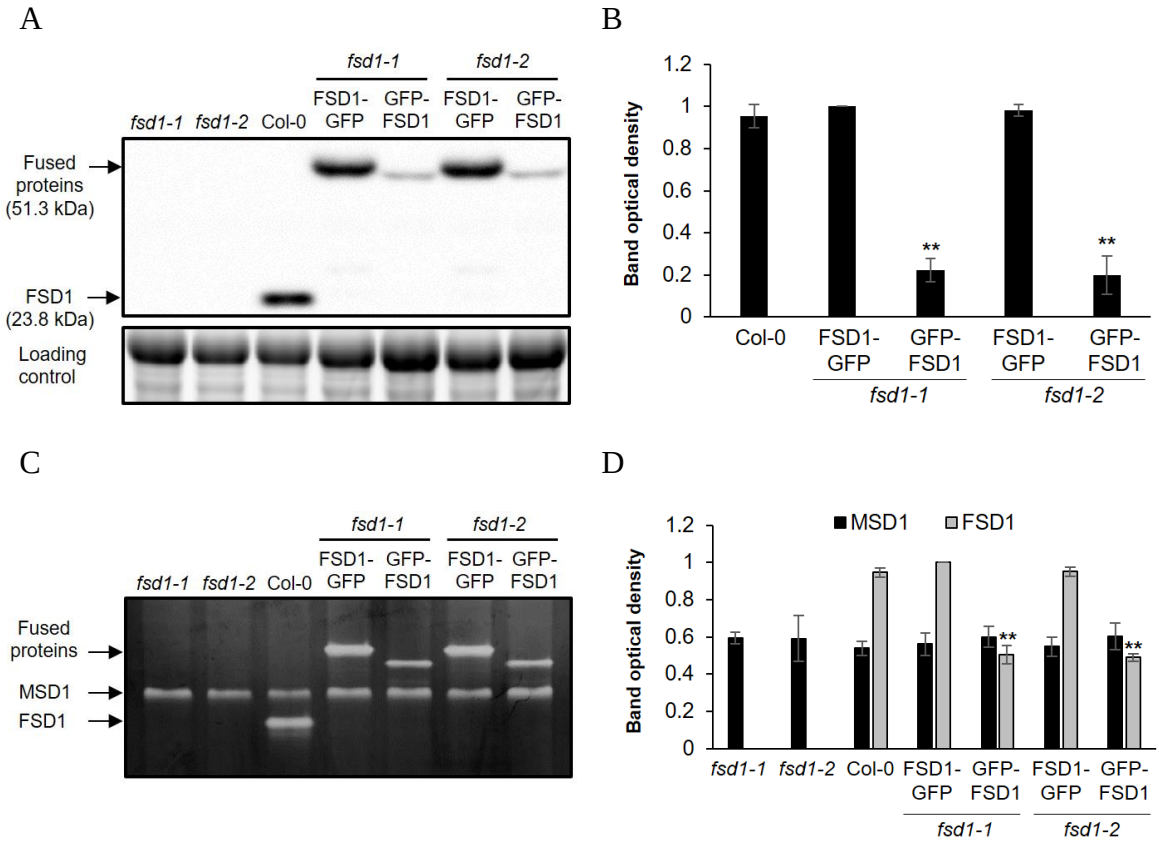

Figure 22 Verification of stably transformed *fsd1* mutant lines by GFP-FSD1 and FSD1-GFP using immunoblotting and SODs activity analysis. (A) Immunoblotting analysis of FSD1, FSD1-GFP and GFP-FSD1 abundance in 14-day-old *fsd1* mutants, Col-0 and complemented *fsd1* mutants using anti-FSD antibody. (B) Quantification of band optical densities in (A). (C) Visualization of SODs isoforms activities on native polyacrylamide gels in indicated plant lines by specific staining. (D) Quantification of optical densities of bands in (C). The optical densities are displayed as relative to the highest value. Error bars represent standard deviation. Stars indicate statistically significant difference as compared to Col-0 (one-way ANOVA, *$p < 0.05$, **$p < 0.01$). Adopted from Dvořák et al. (2021).

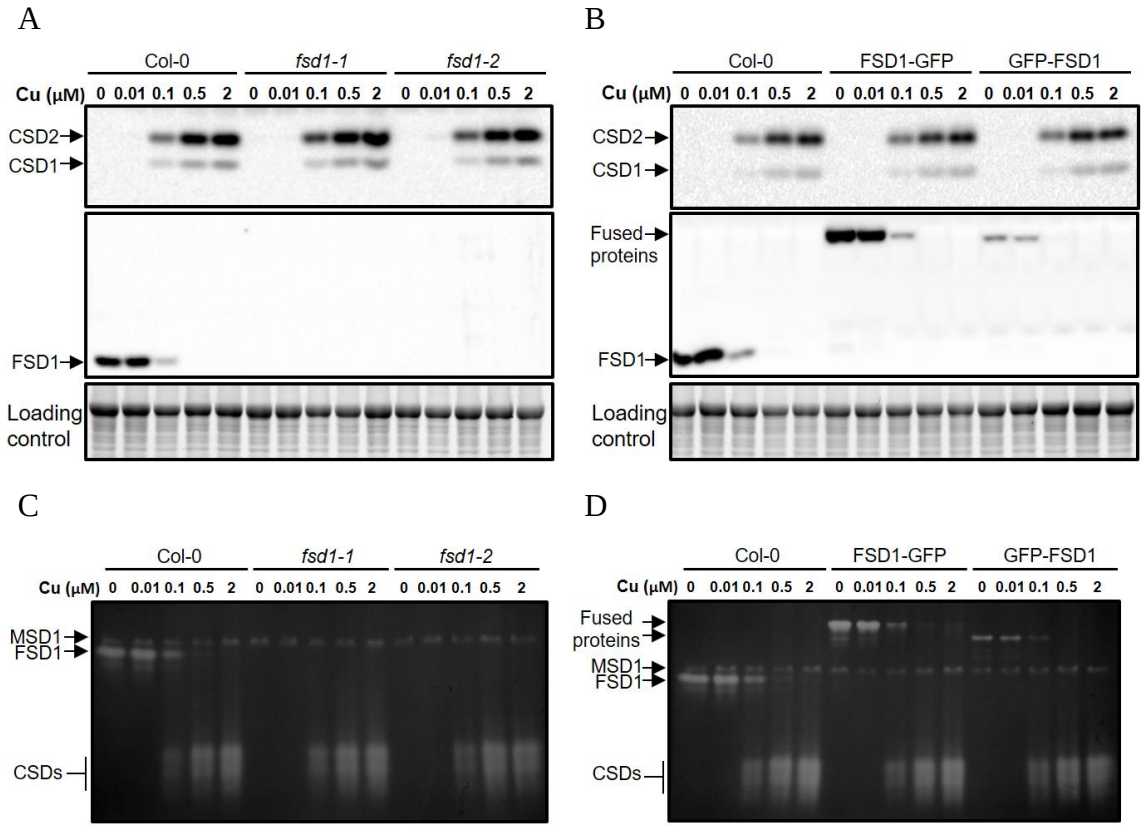

Figure 23 Analysis of abundances and SODs activities in Col-0, *fsd1* mutants and complemented *fsd1-1* mutants carrying FSD1-GFP or GFP-FSD1 in response to different concentrations of Cu^{2+} in growing media. (A-B) Immunoblot analysis using anti-FSD and anti-CSDs antibodies in Col-0 and *fsd1* mutants (A) or Col-0 and complemented *fsd1-1* lines (B). (C-D) Visualization of SOD isoforms activities of Col-0 and *fsd1* mutants (C) or Col-0 and complemented *fsd1* lines (D) on native polyacrylamide gels.

3.2.3 Early developmental and phenotypic analysis *fsd1* mutants and complemented lines

According to the public expression data deposited in the Genevestigator database (presented also in Pilon et al., 2011), *FSD1* is developmentally regulated and is abundantly expressed at early developmental stages. Analysis of FSD1 abundance and activity during *Arabidopsis* early seedling growth revealed that both parameters gradually increased from the 3rd to 13th DAG, but significantly decreased in following days (Figure 24A-D). Possible phenotypic consequences of FSD1 deficiency at early developmental stages were addressed in two independent homozygous T-DNA insertion *fsd1* mutants. It was found that both mutants exhibited reduced lateral root density, while no significant difference was found in the primary root length and seedling fresh weight compared to the wild type (Figure 25A-D). In summary, our data suggest, that FSD1 activity and abundance in *Arabidopsis* depends on the growth phase and its deficiency leads to reduced lateral root numbers.

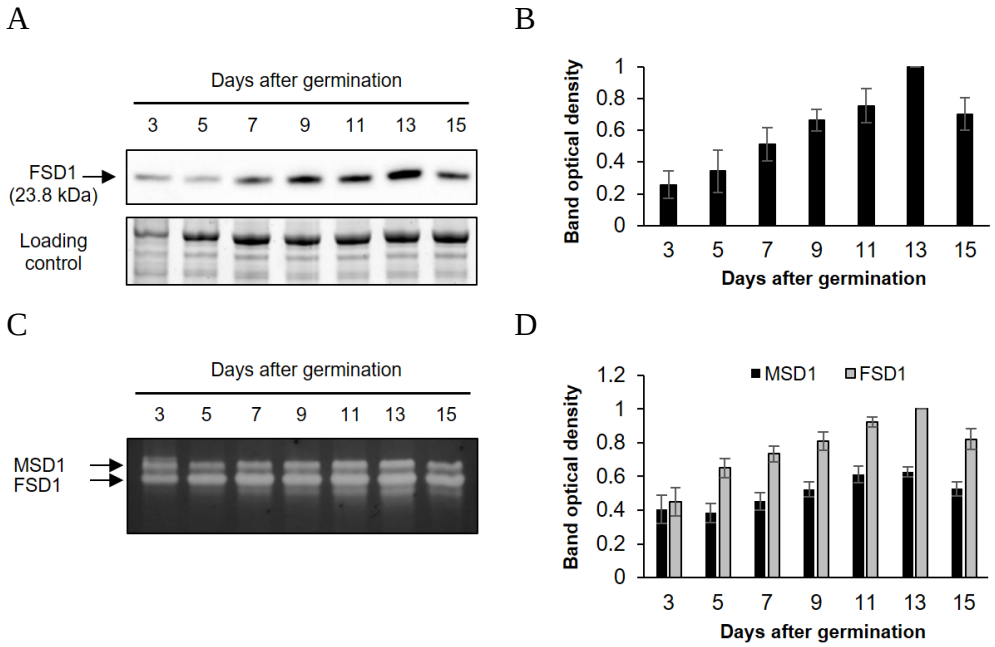

Figure 24 Early developmental analysis of *Arabidopsis* FSD1 using immunoblotting and SODs activity visualization. (A) Measurement of abundance using anti-FSD antibody during early development of wild type seedlings. (B) Quantification of optical densities of bands in (A). (C) Visualization of SOD isoform activities on native polyacrylamide gels during early development of wild type seedlings. (D) Quantification of optical densities of bands in (C). All densities are expressed as relative to the highest value. Error bars represent standard deviation. Adopted from Dvořák et al. (2021).

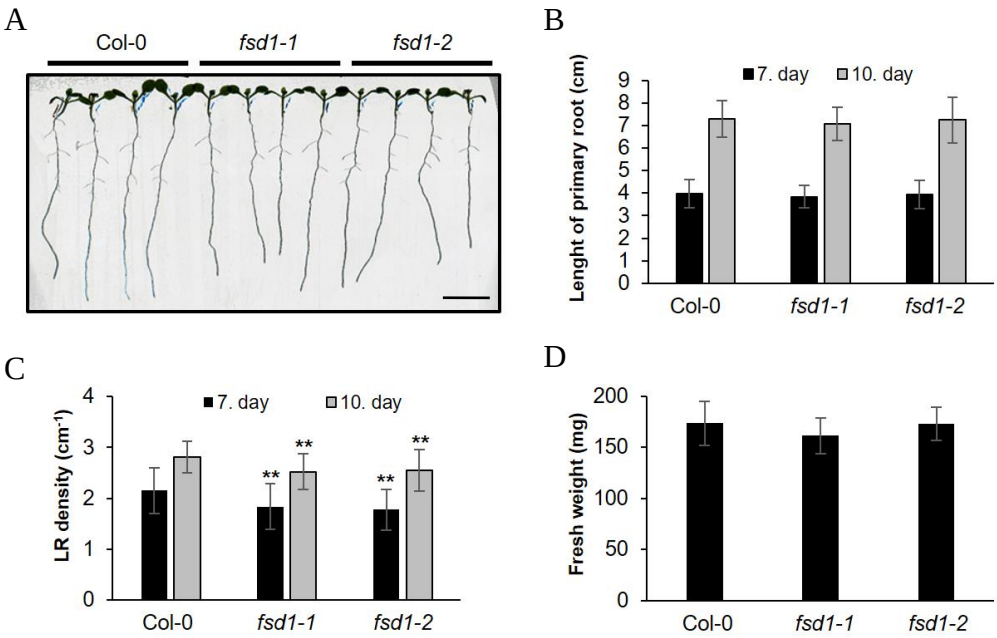

Figure 25 Phenotypical analysis of *fsd1* mutant lines. (A) Representative picture of Col-0 and *fsd1* mutants seedlings on seventh day after germination. (B-D) Quantification of primary root length (B), the lateral root density (C) of indicated 7- or 10-day-old seedlings and fresh weight of 14-day-old seedlings (D). Phenotypic analysis was performed in three repetitions (n = 90). Error bars represent standard deviation. Stars indicate statistically significant difference as compared to Col-0 (one-way ANOVA, **p < 0.01). Scale bar: 1 cm. Adopted from Dvořák et al. (2021).

The complementation of *fsd1-1* via both FSD1-GFP and GFP-FSD1 constructs leads to the reversion of the lateral root phenotypes of *fsd1* mutants (Figure 26A, C). In addition, primary root length (Figure 26B), lateral root density (Figure 26C), and seedling fresh weight (Figure 26D) in complemented lines slightly exceeded the respective values in wild type plants.

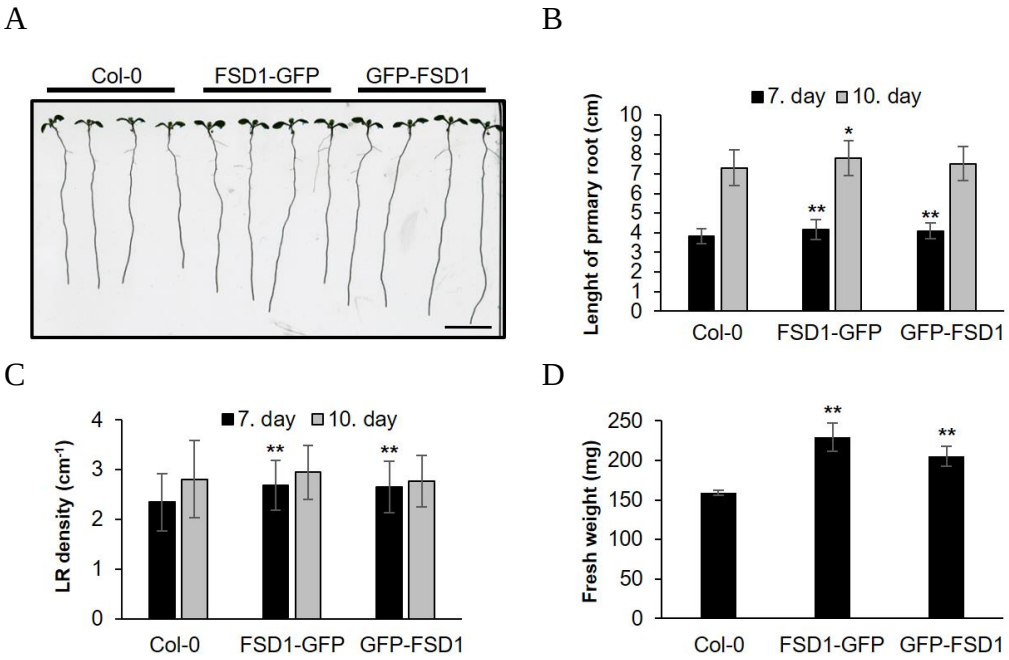

Figure 26 Phenotypical analysis of complemented line of *fsd1* mutant. (A) Representative picture of Col-0 and *fsd1* mutants seedlings by FSD1-GFP and GFP-FSD1 on seventh day after germination. (B-D) Quantification of primary root length (B), lateral root density (C) of indicated 7- or 10-day-old seedlings and fresh weight of 14-day-old seedlings (D). Phenotypic analysis was performed in three repetitions (n = 90). Error bars represent standard deviation. Stars indicatestatistically significant difference as compared to Col-0 (one-way ANOVA, *p < 0.05, **p < 0.01). Scale bar: 1 cm. Adopted from Dvořák et al. (2021).

3.2.4 Monitoring of FSD1-GFP expression during germination and early seedling development

Spatial and temporal patterns of FSD1-GFP expression in the early stages of development were monitored *in vivo* using light-sheet fluorescence microscopy. This allowed the time-lapse monitoring of FSD1-GFP distribution during the whole process of seed germination at nearly environmental conditions (Figure 27; Video S1). Within the first 6 h of seed germination, still before radicle emergence, we observed an increase of FSD1-GFP signal in the micropylar endosperm with a maximum at the future site of radicle protrusion (Figure 27A-G; Video S1). With the endosperm rupture and emergence of the primary root, FSD1-GFP signal gradually decreased in the micropylar endosperm (Figure 27H-J), while a strong FSD1-GFP signal appeared in the fast-

growing primary root (Figure 27K, L; Video S1). Strong expression of FSD1-GFP was visualized in the transition and elongation zones of the primary root (Figure 27L, M; Video S1), which was, however, gradually decreasing in the differentiation zone, particularly after the emergence of the root hairs in the collar region (Figure 27M-O). During seed germination, FSD1-GFP-labelled plastids in endosperm cells showed a high degree of motility (Video S1). Thus, FSD1 may be involved in the process of endosperm rupture during seed germination.

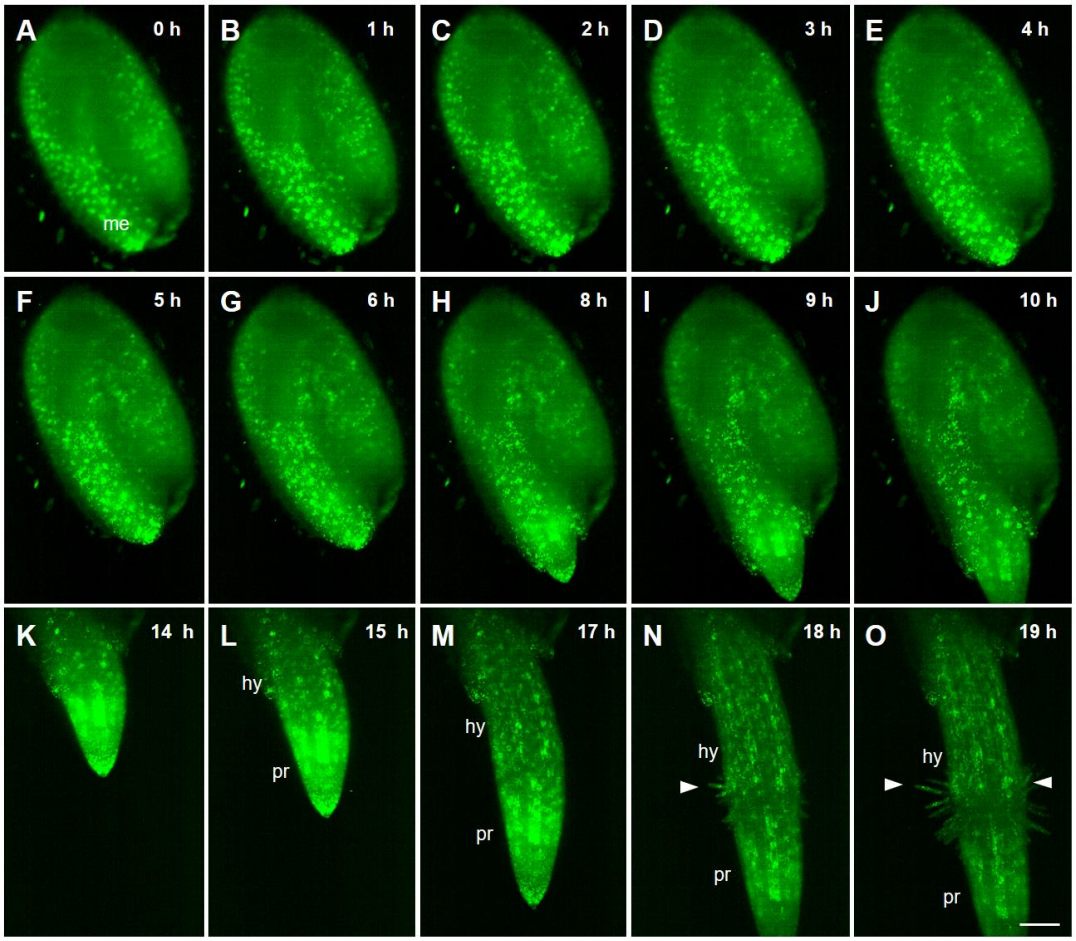

Figure 27 Time-lapse observing of FSD1-GFP expression during seed germination captured by using light-sheet fluorescence microscopy. (A-F) Gradual accumulation and relocation of the signal expression in micropylar endosperm (me) to the site of radicula protrusion. (G-H) endosperm ruptureand radicula protrusion. (I-O) Primary root elongation, (N, O) root hair emergence and elongation. Arrowheads point to the site of root hairs in thecollar region on the border between the elongating primary root (pr) and hypocotyl (hy). Scale bar: 100 µm. Adopted from Dvořák et al. (2021). Miroslav Ovečka and Jasim Basheer performed image acquisition.

After germination, which occurred during the first DAG, growth of the primary root continued and cotyledons were released from the seed coat during the second DAG (Figure S12A, B). Expression levels of FSD1-GFP in emerging cotyledons were high (Figure S12B). Hypocotyl and fully opened cotyledons in developing seedlings at fifth DAG contained moderate amount of FSD1-GFP, while the strongest signal was detectable in the shoot apex and emerging first true leaves (Figure S12C). FSD1-GFP signal considerably increased in the lateral root primordia (Figure S12D-F). Accumulation of FSD1-GFP was still visible in the apices of the lateral roots as well as in the basal parts, at the connection of the lateral roots to the primary root (Figure S12G). In growing apex of the primary root, the strongest FSD1-GFP signal was located in the transition zone (Figure S12H). The FSD1-GFP signal gradually decreased with acceleration of the cell elongation, differentiation, and root hair formation (Figure S12H; Video S2).

3.2.5 Subcellular and tissue-specific localization of GFP-tagged FSD1 in *Arabidopsis* seedling

In the cells of both above- and underground organs of light-exposed seedlings of *fsd1-1* mutants harboring *proFSD1::FSD1:GFP* construct, FSD1-GFP fusion protein was localized in plastids, nuclei, and cytosol, especially in the cortical cytosolic layer in close proximity to the plasma membrane (Video S3). Such localization of FSD1-GFP was consistent in cells of all aboveground organs in light exposed seedlings, such as cotyledon epidermis (mature pavement cells, stomata and their precursors, Figure 28A, B, D-F; Video S3), leaf mesophyll cells (Figure 28G-I; Video S4), hypocotyl epidermis (Figure 28J; Video S5), and first true leaf epidermis with branched trichomes (Figure 28C). In epidermal cells, FSD1-GFP-labelled plastids were located around the nucleus and in the cytosolic strains traversing the vacuole (Figure 28A, B, D, G). Some other FSD1-GFP-labelled plastids located in a close proximity to nuclei in stomata guard cells and adjacent pavement cells, were less dynamic (Video S3). In mesophyll cells, FSD1-GFP-labelled plastids were temporarily contacted and eventually interconnected by the highly dynamic network of tubules and cisternae of the endoplasmic reticulum (Video S4). Moreover, FSD1-GFP maintained the same localization in cotyledon epidermal cells of etiolated *Arabidopsis* seedlings, although it was more intensively accumulated in the cortical cytosol just beneath the plasma membrane as compared to the light

exposed plants (Figure S13). In turn, FSD1-GFP was abundant in etioplasts, showing only basal remaining level of chlorophyll a autofluorescence (Figure S13B, C).

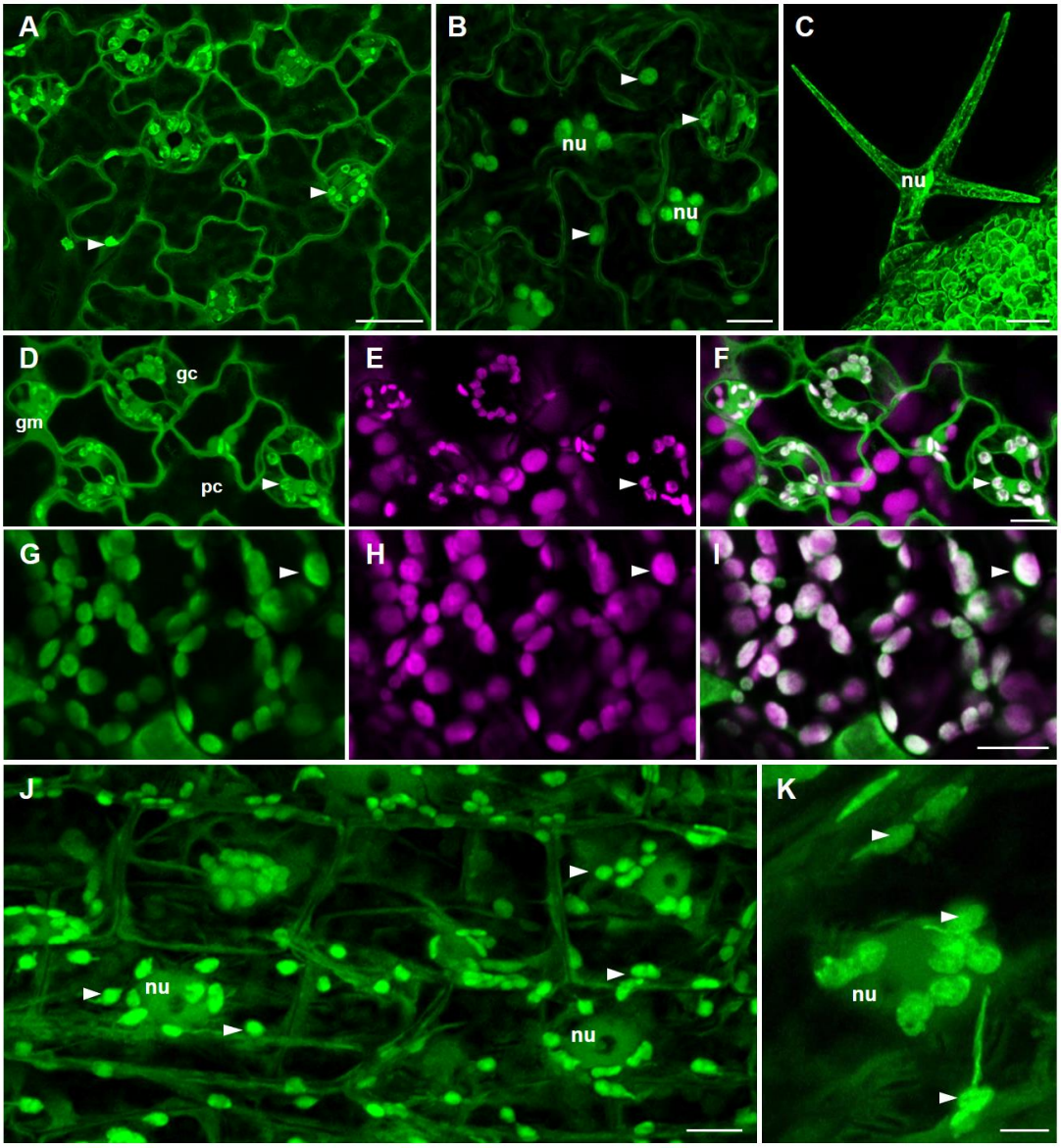

Figure 28 The localization of FSD1-GFP protein in cells of *Arabidopsis* aboveground organs observed using Airyscan confocal laser scanning microscopy. (A-B) FSD1 localization in cotyledon epidermal cells, stomata and leaf epidermal pavement cells and stomata guard cells. (C) Triple-branched leaf trichome. (D-F) Adaxial surface of cotyledons with pavement (pc), guard (gc) and guard mother (gm) cells. (G-I) Leaf mesophyll cells. (J) Hypocotyl cells of epidermis. (K) Magnification of area hypocotyl cells with visible chloroplast stromules. Indications: (nu) nucleus. Arrowheads point on accumulation of FSD1-GFP in plastids. Channels: green – FSD1-GFP; magenta – chlorophyll a autofluorescence. Scale bars: A, C, 20 μm; B, D-J, 10 μm; K, 5 μm. Adopted and modify from Dvořák et al. (2021) and modified.

Plastidic, nuclear and cytosolic localization of FSD1-GFP was detected also in cells of the root apex (Figure 29A; Video S6). This localization pattern was visible in cells of the lateral root cap (Figure 29A, B; Video S7), in meristematic cells (Figure

29A, C), epidermal cells of elongation zone (Figure 29D, E) as well as in trichoblasts within the differentiation zone (Figure 29F) of primary root. It showed lower FSD1-GFP signal intensity in central columella cells (Figure 29A).

Furthermore, accumulation of FSD1-GFP was observed in the LRP emerging from the pericycle (Figure 29K-N). FSD1-GFP signal increased first in cells of forming lateral root primordium still enclosed by tissues of the primary root (Figure 29K). Strong signal of FSD1-GFP was found in cells of the central region, where the apical meristem of the emerging lateral root was established (Figure 29L, M). Considerably high levels of FSD1-GFP also persisted during the release of the lateral root from the primary root tissue (Figure 29N). Established apex of elongating lateral root showed differential pattern of FSD1-GFP expression, with high levels in the endodermis/cortex initials (Video S8), actively dividing cells of the epidermis, cortex and endodermis, and lateral root cap cells. On the other hand, considerably lower levels of FSD1-GFP occurred in cells of the quiescent centre and columella (Video S8).

The process of root hair formation from trichoblasts was connected with the accumulation of FSD1-GFP in the cortical cytosol of the emerging bulge (Figure 29G). In tip-growing root hairs, FSD1-GFP accumulated in the apical and subapical zone (Figure 29H, I; Video S2). It is noteworthy that after the termination of root hair elongation, FSD1-GFP signal dropped at the tip, while typical strong plastidic signal appeared in the cortical cytosol (Figure 29J).

Plastids were the organelles most strongly accumulating FSD1-GFP and located either around the nuclei or distributed throughout the cytosol (Figures 28, 29; Video S3). Typically, plastids in cells of different tissues formed polymorphic stromules, which displayed different tissue-specific shape, length, branching (Figures 28 J, K, 29B-D) and dynamicity (Videos S3-S7). Thus, in lateral root cap cells highly dynamic FSD1-GFP-labelled plastids persistently formed long stromules, touching each other (Figure 29B; Videos S6, S7), while the plastids in isodiametric meristematic cells possessed less stromules (Figure 29C, D). In hypocotyl epidermal cells with active cytosolic streaming, only some plastids were interconnected by stromules (Video S5). Since stromules are tubular plastid extensions filled with stroma (Köhler and Hanson, 2000), FSD1 might be considered as stromal protein. In contrast to FSD2 and FSD3 (Myouga et al., 2008), FSD1 was not detected in the chloroplast nucleoids.

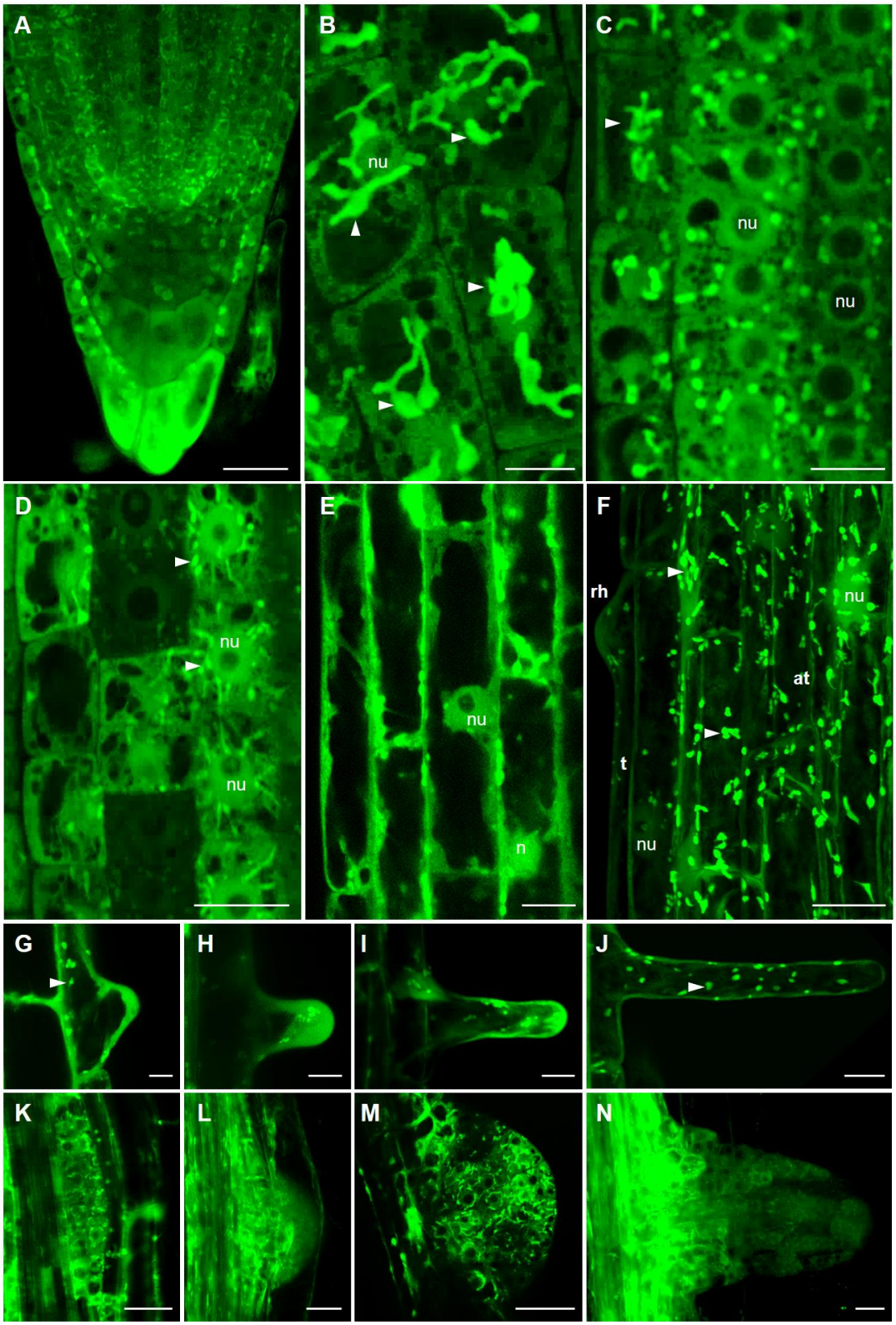

Figure 29 Tissue- and organ-specific subcellular FSD1-GFP presence in *Arabidopsis* roots. (A) Primary root apex (B), root cap cells with GFP-signal in plastids (arrowheads) and nuclei (nu). (C) Epidermal and cortical meristem cells, (D) cortical cells of distal elongation zone, (E) cortical cells of elongation zone. (F) Trichoblasts (t) with an emerging root hair (rh) and atrichoblasts (at) of differentiation zone. (G-J) Mid-plane sections of root hairs, (G) root hair bulge, (H, I) elongating root hair, (J) mature root hair. (K-M) Mid-plane sections of forming lateral root primordia at diverse developmental stages. (N) Emerged lateral root. Scale bars: A, E, F, K-N, 20 μm; B, C, D, G-J, 10 μm. Adopted from Dvořák et al. (2021).

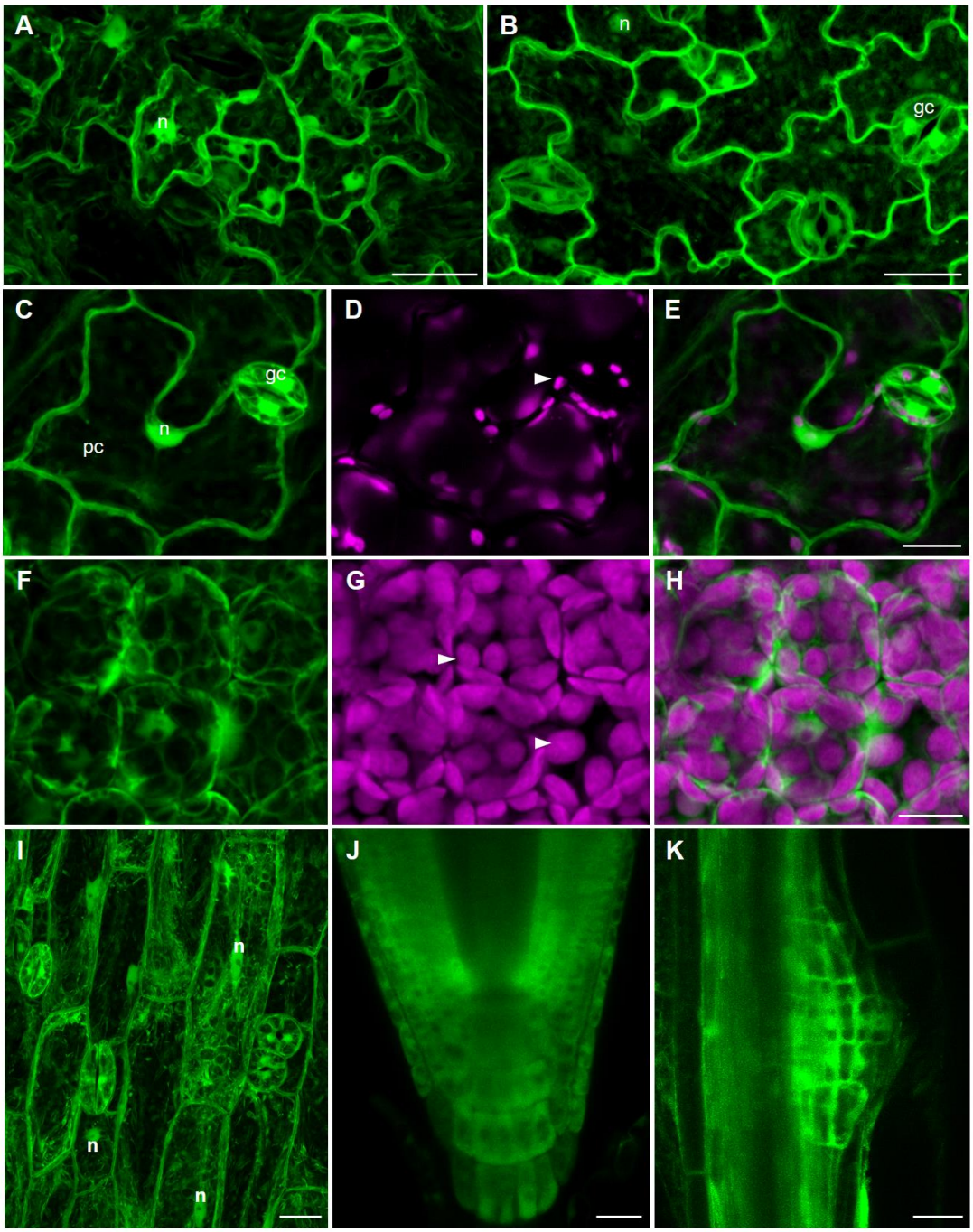

Figure 30 Representative overview of GFP-FSD1 presence in cells of above- and underground organs of *Arabidopsis* seedlings. (A-B) GFP-FSD1 localization in cotyledon epidermal cells, stomata and leaf epidermal pavement cells and stomata guard cells. (C-E) Adaxial surface of cotyledon with pavement (pc) and guard (gc) cells. (F-H) Cotyledon mesophyll cells. (I) Hypocotyl cells, (J) primary root apex, (K) emerging lateral root. Arrowheads indicate plastids. Nuclei is marked as (n). Channels: green – FSD1-GFP; magenta – chlorophyll a autofluorescence. Scale bars: C-H, 10 μm; A, B, I-K 20 μm. Adopted from Dvořák et al. (2021) and modified.

Interestingly, the N-terminal GFP-FSD1 fusion protein was not targeted to plastids, but it was localized both in the nuclei and cytosol. This localization pattern was observed in leaf pavement (Figure 30A, B; Video S9) and stomata guard cells (Figure

30C-E), in cotyledon mesophyll cells (Figure 30F-H) as well as in hypocotyl epidermal cells (Figure 30I). The absence of plastidic localization did not affect the tissue-specific expression pattern of GFP-FSD1 in primary root apex. The strongest signal was located in the epidermis, cortex, endodermis and root cap (Figure 30J). Considerably lower GFP-FSD1 signal was detected in the quiescent center, central columella cells and proliferating tissues of the central cylinder (Figure 30J). Strong accumulation of GFP-FSD1 was typically present in founding cells of the lateral root primordia and adjacent pericycle cells (Figure 30K). Taking into account the strong reduction in FSD1 abundance and activity in transgenic line expressing GFP-FSD1 fusion as compared to FSD1-GFP (Figure 22A-D; Figure S11), the plastidic FSD1 pool may represent around half of the total FSD1 pool in *Arabidopsis* cells.

Subcellular localization pattern of FSD1 was confirmed by the whole mount immunofluorescence localization method in fixed samples using anti-FSD antibody. This technique showed prominent strong immunolocalization of FSD1 to plastids distributed around nuclei and in the cytosol, as well as nuclear and cytosolic localization in meristematic cells of the primary root (Figure 31A-C).

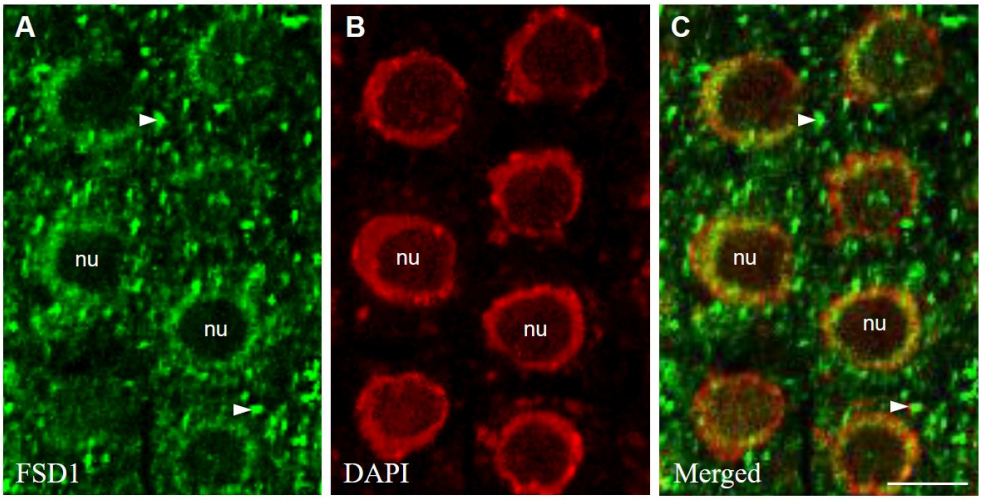

Figure 31 Whole-mount immunofluorescence staining of FSD1 protein by using specific anti-FSD antibody in *Arabidopsis* wild-type seedling. A-C The images of root meristem cells specifically labled agaist FSD1 protein. Green immunolabelling with anti-FSD – Alexa Fluor 488; red pseudocolour – DAPI staining. Arrowheads indicate plastids and (nu) stands for nuclei. Whole-mount immunofluorescence staining and preparation of samples were performed by Yuliya Krasylenko. Adopted from Dvořák et al. (2021) and modified.

Presence of FSD1-GFP in both cytosol and nuclei raises the question of its nucleo-cytoplasmic transport. Predicted size of FSD1-GFP fusion protein, which is approximately 51 kDa, would permit passive diffusion in and out of nucleus, as it is below the exclusion limit of the nuclear pores (typically below 60 kDa). To test this, mobility of FSD1-GFP protein fraction in nuclei was analysed using FRAP in comparison to passive diffusion of free GFP (in the *35S::sGFP* line) with the protein size of 27 kDa. In both transgenic lines bearing FSD1-GFP and free GFP, the whole area of selected nuclei was bleached up to 40–45% of original fluorescence intensity and the rate of fluorescent signal recovery was recorded within the period of 4 min (Figure 32A). While in the case of free GFP the signal was largely recovered within the observation period, the recovery of FSD1-GFP in nuclei was much lower (Figure 32A-C). Data analysis showed that only approximately 13–15% of the nuclear FSD1-GFP fraction is mobile, while mobile nuclear fraction of free GFP represented around 80–86% (Figure 32D). In this respect, immobile fraction of FSD1-GFP in nuclei, which cannot pass through nuclear pores by passive diffusion represented more than 85%. Accordingly, in the case of free GFP this immobile fraction represents only 16% (Figure 32D). Interestingly, the halftime of mobile FSD1-GFP fraction recovery was much shorter (9 s, in average) in comparison to the halftime of mobile free GFP fraction recovery, which was 27 s (Figure 32E). These results, corroborated by quantitative analysis of free GFP movement showing typical passive diffusion, suggest that most of the FSD1-GFP nuclear pool is not imported from or exported to the nuclei by passive diffusion, and stays in the nucleus as an immobile fraction.

3.2.6 Role of FSD1 during salt stress tolerance in *Arabidopsis*

Protective role of FSD1 during the early stages of post-embryonic plant development was tested in *fsd1* mutants and complemented lines on seed germination under salt stress conditions. Seed germination of *fsd1* mutants was strongly reduced by the presence of 150 mM NaCl in the 1/2 MS medium, while FSD1-GFP lines exhibited germination rates comparable to that of wild type (Figure 33A). GFP-FSD1 line showed an insignificantly reduced germination rate on the first day, but germination efficiency was synchronized with wild type and FSD1-GFP line from the second day onwards (Figure 33A). The results indicated that *FSD1* expressed under its own native promoter functionally complemented the salt stress-related deficiency of *fsd1* mutants.

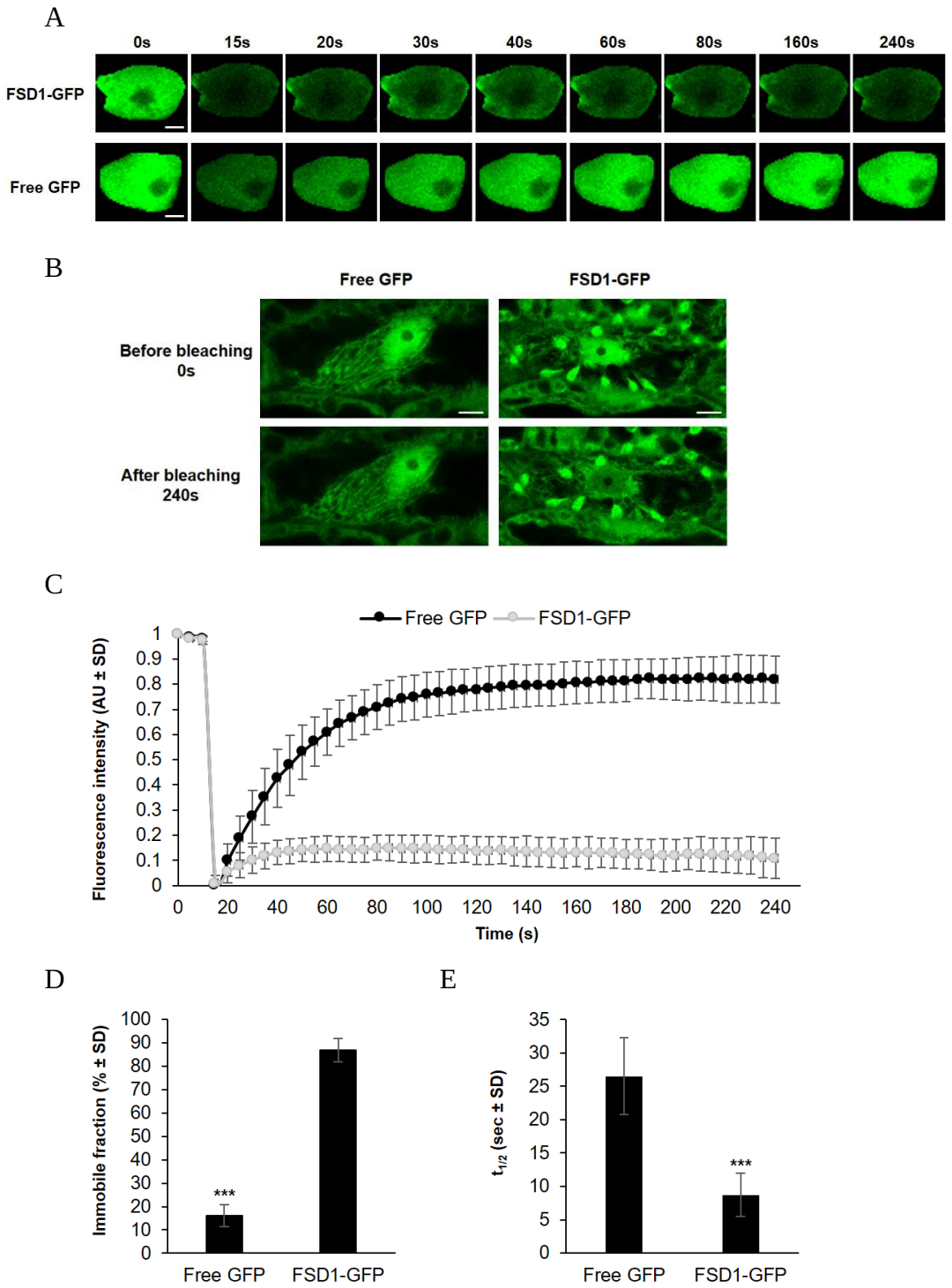

Figure 32 FRAP analysis of FSD1-GFP mobility in nuclei of hypocotyl epidermal cells. Transgenic line producing free GFP were used as a control. (A) Representative pictures of free GFP and FSD1-GFP in nuclei of hypocotyl epidermal cell prior to and after bleaching. Time 0 s shows fluorescence intensity prior to bleaching, time 15 s shows fluorescence intensity immediately after bleaching and time points 20–240 s represent recovery of the fluorescence. (B) Representative pictures of the whole cell before (0 s) and after (240 s) bleaching. (C) Graphycal visualization of signal recovery in analysed nuclei. Values are shown in arbitrary units (AU) after normalization (higest intensity correspond to 1 and to the lowest to 0). (D) Proportion of immobile protein fractions in nuclei. (E) Half-time of signal recovery for examined proteins. Analysis was performed in three repetition (analysed nuclei n = 49). Error bars represent standard deviation (one-way ANOVA; ***$p < 0.001$). Scale bar: 5 μm. Adopted from Dvořák et al. (2021).

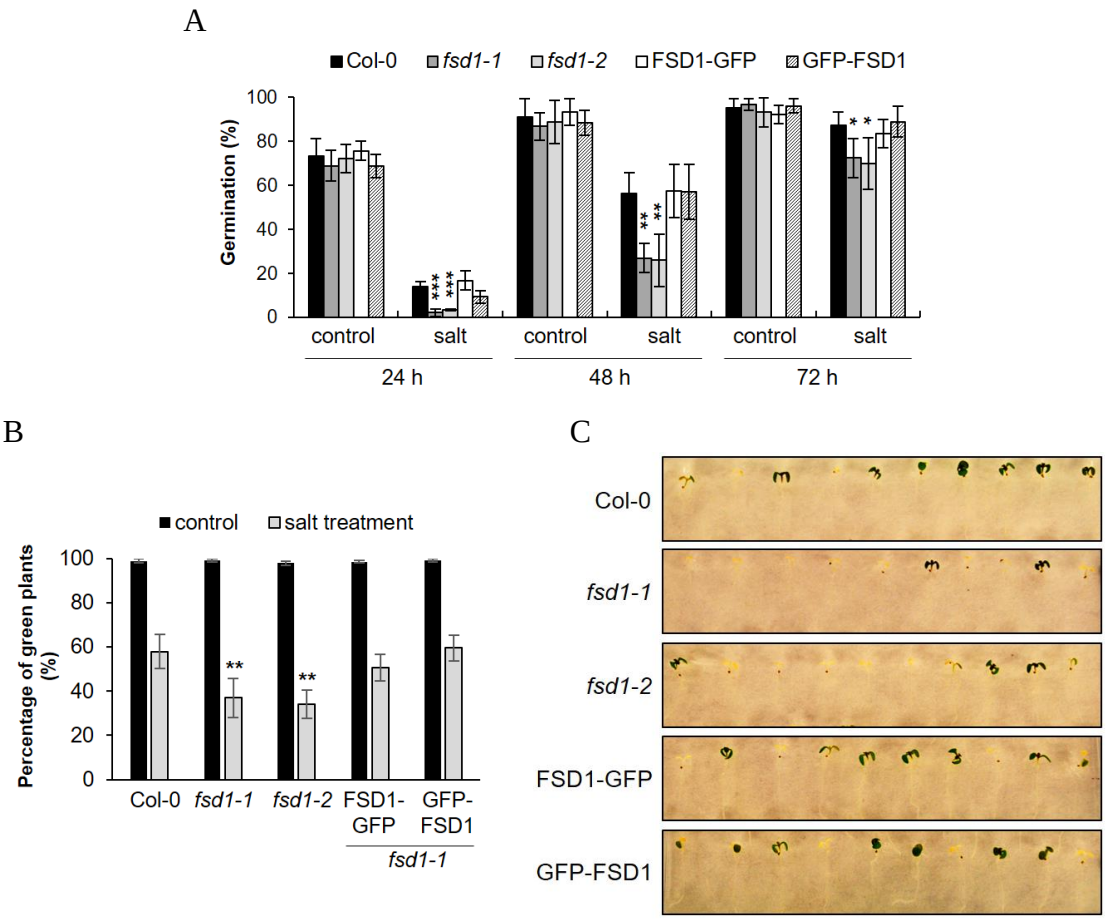

Figure 33 Salt stress response of *fsd1* mutants and complemented mutant lines during germination and aplication stress on young seedlings. (A) Efficiency of seed germination in control and stress conditons induced 150 mM NaCl. Germination is evaluated as a percentage of germinated seeds relative to the total number of examined seeds (n = 120). (B) Viability (fully green cotyledons) of plants on fifth day after the transplantation to the medium with and without 150 mM NaCl. Viability was evaluated as a percentage of seedlings with green cotyledons (n = 120). (C) Representative pictures transplantated seedling growing on 1/2 MS media containing 150 mM NaCl. Error bars in (A) and (B) represent standard deviations. Stars indicate statistically significant difference as compared to Col-0 (one-way ANOVA, *p < 0.05, **p < 0.01, ***p < 0.001). Adopted from Dvořák et al. (2021) and modified.

To further test the new role of FSD1 in salt stress sensitivity, we characterized the response of developing seedlings to the high salt concentration in the culture medium. We found that both *fsd1* mutants showed hypersensitivity to NaCl and exhibited increased cotyledon bleaching. Both FSD1-GFP and GFP-FSD1 fusion proteins efficiently reverted the salt hypersensitivity of *fsd1* mutants (Figure 33B, C). These results supported the new functional role of FSD1 in *Arabidopsis* salt stress tolerance. To gain deeper insight into FSD1 function during plant response to the salt stress, we performed subcellular localization of FSD1-GFP in hypocotyl epidermal cells plasmolysed by 500 mM NaCl (Figure 34A-G; Figure S14A-E). In addition to plastidic, nuclear, and cytosolic localization in untreated cells (Figure 34A), FSD1-GFP was

detected in Hechtian strands and Hechtian reticulum, interconnecting retracted protoplast with the cell wall of plasmolysed cells (Figure 34B-G; Figure S15A, B). Hechtian reticulum located in close proximity to the cell wall (Figure 34D), and thin attachments of Hechtian strands to the cell wall in the form of bright adhesion spots were enriched with FSD1-GFP (Figure 34C, E-G; Figure S14).

Plasmolysed cells showed strong GFP signal at plasma membrane and also contained vesicle-like structures decorated by FSD1-GFP, in their cytosol (Figure S14D) and also within the Hechtian strands (Figure 34F, G). We observed a similar localization pattern in the GFP-FSD1 line. GFP-FSD1 was located in the nuclei and cytosol of untreated cells (Figure 34H), while prominent GFP-FSD1 accumulation was observed at the plasma membrane of retracted protoplasts, in Hechtian strands and Hechtian reticulum after plasmolysis (Figure 34I-N). Peripheral Hechtian reticulum and strands were decorated by spot- and vesicle-like structures labelled with GFP-FSD1 (Figure 34J, N). In contrast, free GFP stably expressed in *Arabidopsis* under 35S promoter did not show localization in the Hechtian strands and Hechtian reticulum (Figure 34O-Q; Figure S14F-J; Figure S15C, D) and prominent accumulation close to the plasma membrane during salt stress (Figure 34P, Q; Figure S14I, J).

Next, we used a fluorescent ROS indicator CellROX Deep Red Reagent, which is preferentially specific to $O_2^{\cdot -}$ and $OH^{\cdot}$ (Alves et al., 2015), to study ROS accumulation in plasmolysed cells. Intense ROS production was detected at the plasma membrane, cytosol, plastids and vesicle-like structures of retracted protoplasts (Figure 35A, D, H, L, P), as well as in Hechtian strands and Hechtian reticulum (Figure 35D, H). We have found that the CellROX Deep Red Reagent fluorescence signal partially colocalised with GFP-FSD1 at the plasma membrane vicinity, Hechtian strands and plastids (Figure 35A-F; Figure S15A, B) after salt-induced plasmolysis in root. We also examined, whether FSD1 deficiency affects the ROS level in *fsd1* mutants upon salt stress. Considerably stronger CellROX Deep Red Reagent fluorescence signal was revealed in both *fsd1* mutants as compared to the wild type (Figure 35G-S). Collectively, these data indicate that salt stressinduced ROS production and accumulation in Hechtian strands and Hechtian reticulum likely depends on *FSD1* expression.

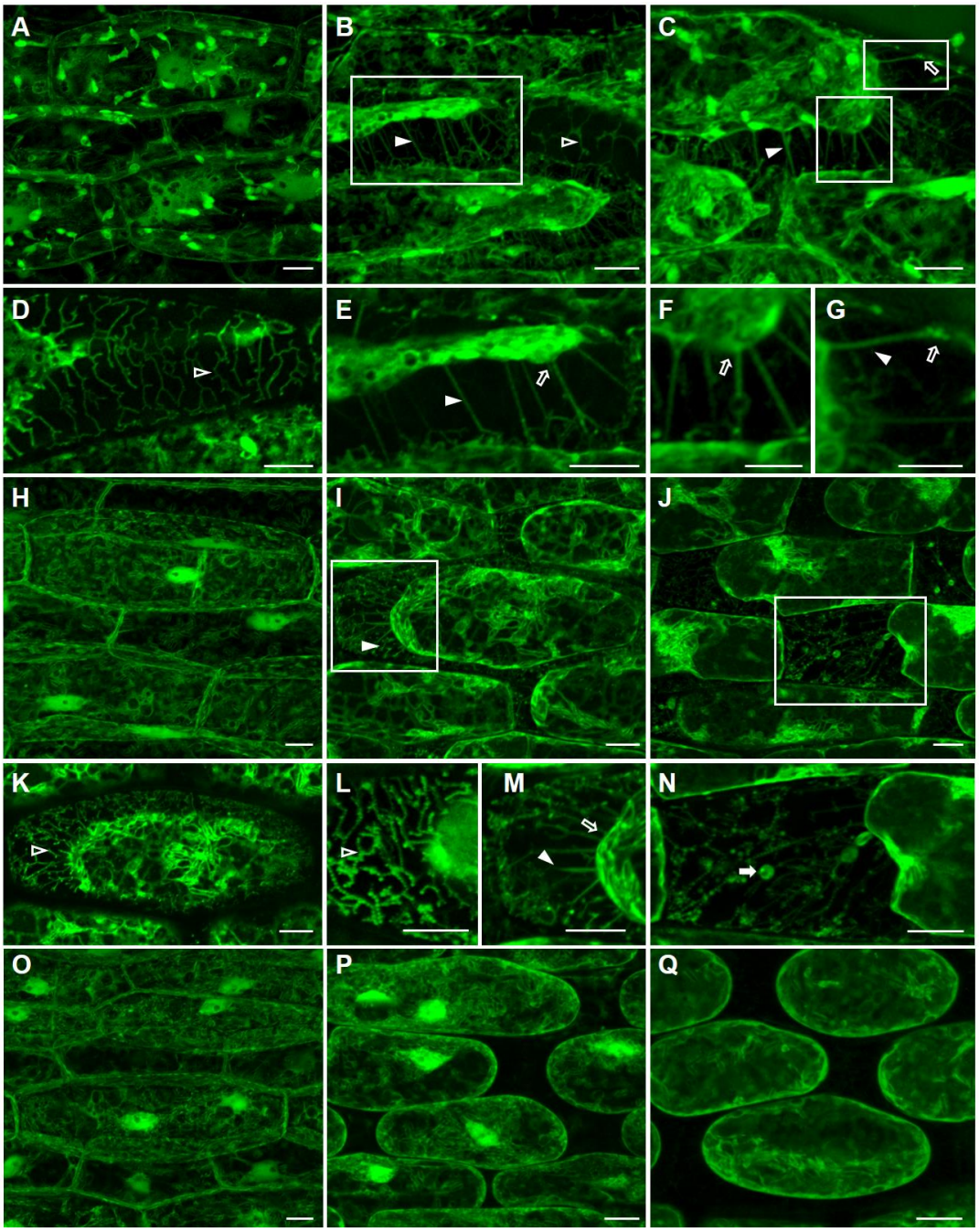

Figure 34 FSD1 localization in plasmolysed hypocotyl epidermal cells treated by salt. (A-G) FSD1-GFP signal in seedlings treated with liquid 1/2 MS media (A) or 1/2 MS media containing 500 mM NaCl (B-G) for 30 min. (B, C) Representative images of plasmolysed cells. (D) Hechtian reticulum. (E-G) Hechtian strands with connections to cell wall, close-ups from pictures (B, C). (H-N) GFP-FSD1 signal in seedlings treated by liquid 1/2 MS media (H) or 1/2 MS media containing 500 mM NaCl (I-N) for 30 min. (I, J) Representative images of plasmolysed cells. (K, L) Hechtian reticulum. (M) Close-up from (I), showing Hechtian strands connected to the cell wall. (N) Close-up from (J), showing disturbed Hechtian reticulum with aggregations. (O-P) Signal from free GFP fluorescence in hypocotyl epidermal cells of transgenic line bearing *35S::sGFP* treated with liquid 1/2 MS media (O) or 1/2 MS media containing 500 mM NaCl (P, Q). Filled arrowheads indicate Hechtian strands; blank arrowheads Hechtian reticulum; filled arrows – globular aggregations; blank arrows – showing Hechtian strands connected to cell wall. Scale bars: A-E, H-Q, 10 μm; F, G, 5 μm. Adopted from Dvořák et al. (2021).

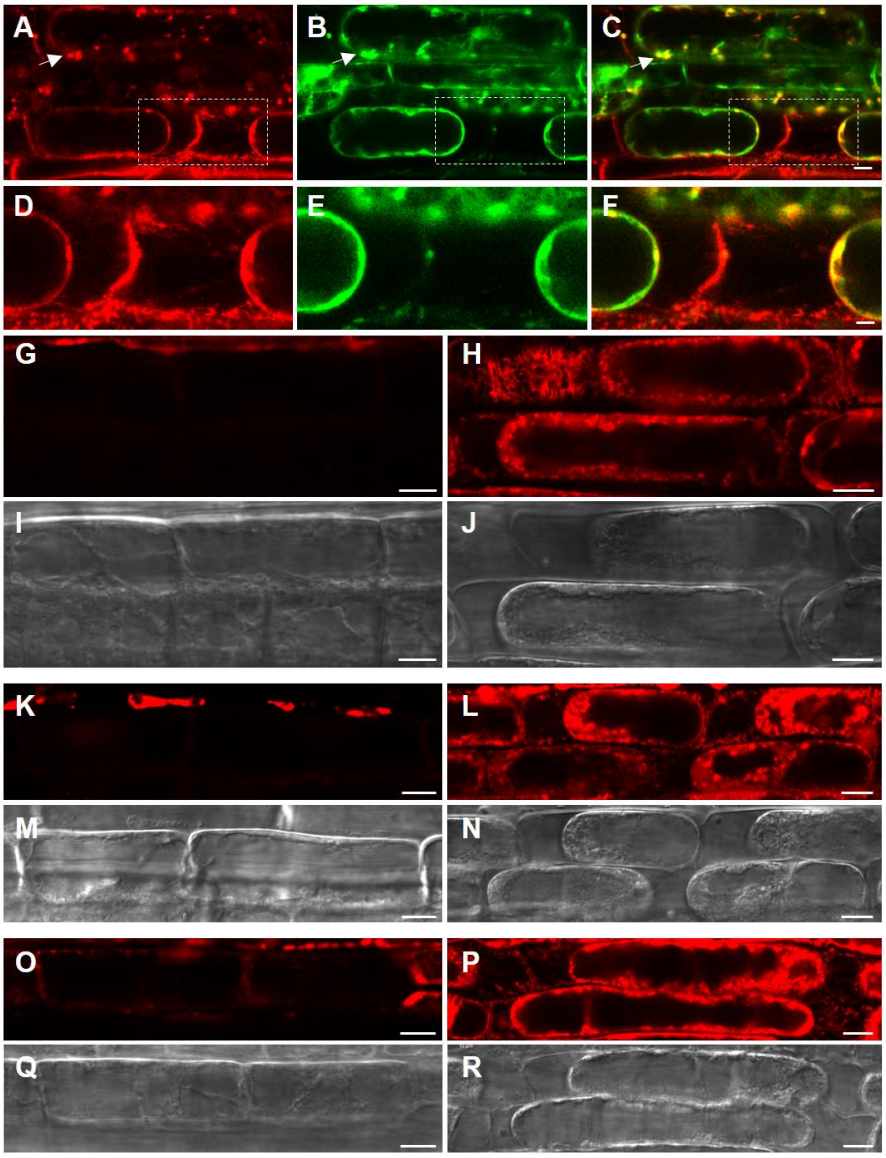

S

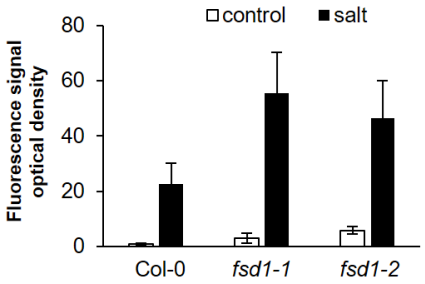

Figure 35 Colocalization of FSD1-GFP with reactive oxygen species (ROS) and their accumulation in primary roots of *Arabidopsis fsd1* mutants in response to salt stress. (A-C) ROS distribution visualized by fluorescent tracker CellRox Deep Red reagent in plasmolysed root cells of FSD1-GFP line (A), GFP fluorescence (B) and superposition of A and B (C). Arrow indicates colocalization in plastid. (D-F) Detailed images of square areas in A-C. (G-R) ROS accumulation in mock treated (G, K, O) and plasmolysed root cells (H, L, P) of Col-0 (G, H), *fsd1-1* mutant (K, L) and *fsd1-2* mutant roots (O, P) visualized by fluorescent tracker CellRox Deep Red reagent. (S) Quantification of CellRox Deep Red reagent fluorescence intensity in images G, H, K, L, O, P. Error bars represent standard deviation. (I, J, M, N, Q, R) Transmitted light. Scale bars: A-F, 20 μm; G-S, 10 μm. Adopted from Dvořák et al. (2021).

3.2.7 Plastidic FSD1 pool is important for oxidative stress tolerance in *Arabidopsis*

In order to reveal the role of FSD1 in scavenging of ROS generated in the chloroplast, we exposed mutant and transgenic lines to MV. Both mutant lines exhibited a hypersensitivity to this agent as estimated by lowest number of fully green cotyledons (Figure 36A, B). The GFP-FSD1 line was hypersensitive as well, but showed slightly elevated number of seedlings with fully green cotyledons when compared to mutants (Figure 36A, B). On the other hand, FSD1-GFP line showed a response resembling the wild type (Figure 36A, B). To better evaluate responses to MV, we measured total chlorophyll content in the cotyledons (Figure 36C). We did not observe any differences in chlorophyll content among the analyzed lines in control conditions (data not shown), being consistent with the data reported previously (Myouga et al., 2008). Chlorophyll content in lines treated with MV positively correlated with the hypersensitivity of the examined lines (Figure 36C). These results show that plastidic FSD1 pool is decisive for acquiring oxidative stress tolerance in *Arabidopsis*.

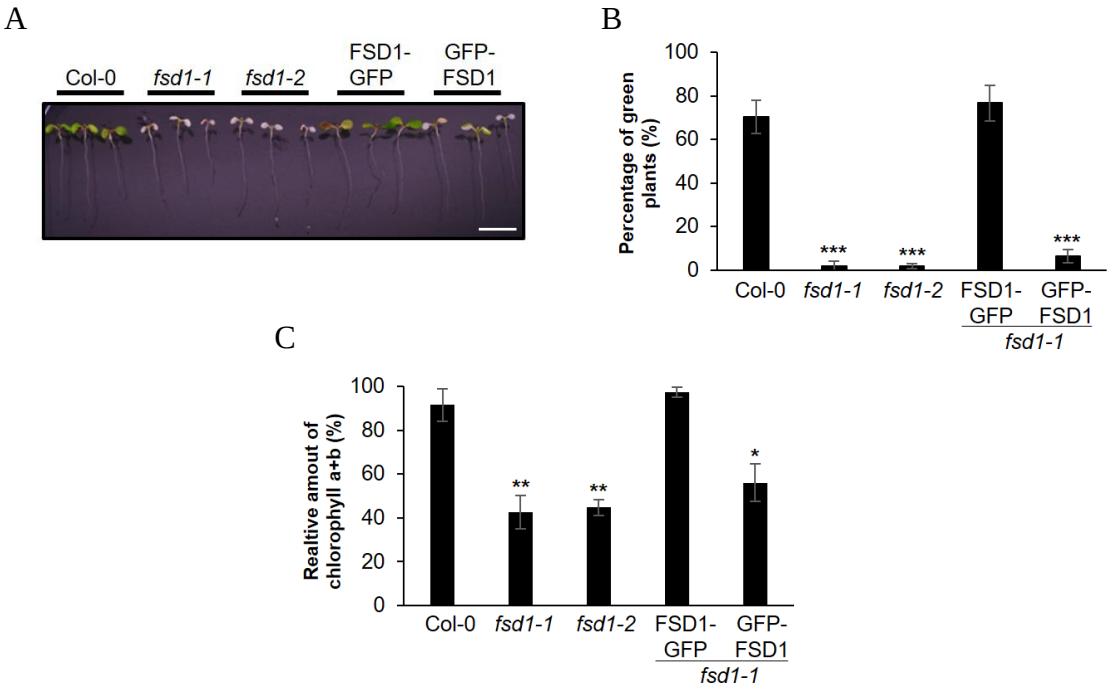

Figure 36 Impact of methyl viologen (MV)-induced oxidative stress on *fsd1* mutant and complemented lines. (A) Representative image of seedlings on fifth day after the transfer to 2 μM MV-containing medium (B) Quantification of seedling with not affected leaves (fully green cotyledons) Measurement was performed in four repetitions (n = 160). (C) Quantification of relative concentration of chlorophylls a and b in seedling growing on 2 μM MV. Measurement was performed in three repetitions (n = 30). Error bars represent standard deviation. Stars indicate statistically significant difference as compared to Col-0 (one-way ANOVA, *p < 0.05, **p < 0.01, ***p < 0.001). Scale bar: 1 cm. Adopted from Dvořák et al. (2021).

3.2.8 Proteomic analysis of FSD1 interactome

The stable expression of FSD1 fused to GFP in *Arabidopsis* offers an opportunity to identify putative interacting partners of FSD1 using co-immunoprecipitation combined with proteomic analysis. The eluates prepared by co-immunoprecipitation on beads bound to anti-GFP antibody from both FSD1-GFP and GFP-FSD1 lines were verified for the presence of fused FSD1 protein using immunoblotting (Figure 37). The different subcellular localization of FSD1 in the transgenic lines allows to find out, how FSD1 absence in chloroplasts affects the interacting partners. The proteomic analysis, which was performed by a commercial service, identified 418 and 105 proteins in FSD1-GFP and GFP-FSD1 line, respectively (4 replicates per line). In order to minimize the presence of unspecific interactors, all proteins previously identified to interact with GFP alone (Takáč et al., unpublished data) were removed. Moreover, proteins, found only in one repetition were eliminated as well. The final list of the 44 selected putative interaction partners including their function and localization is shown in Table 7. Out of them, 36 were identified in FSD1-GFP line, while we found 30 interactors in GFP-FSD1 line. Twenty-one proteins were identified commonly for both lines, including FSD1. These commonly identified proteins included cytosolic proteins (e.g. PLDα1 and 2, HEAT SHOCK 70 KDA PROTEIN 18), several proteins localized to endoplasmic reticulum bodies (e.g. beta glucosidases) and nucleus (e.g. splicing factors, ETHYLENE-RESPONSIVE TRANSCRIPTION FACTOR TINY). Ribosomal (e.g. UBIQUITIN-40S RIBOSOMAL PROTEIN S27A-3, ELONGATION FACTOR 1-ALPHA 1) and one chloroplastic protein (GLYCERALDEHYDE-3-PHOSPHATE DEHYDROGENASE GAPA1, CHLOROPLASTIC) were also identified in both lines. Interactors uniquely found in the FSD1-GFP line (together fifteen proteins) included mainly chloroplastic proteins such as CPN20, which is a known FSD1 interactor (Kuo et al., 2013). We also identified Ca^{2+}-binding CALMODULIN-1 and THIOREDOXIN H3 as putative binding partners of FSD1-GFP. On the other hand, an extracellular protein GLYCINE-RICH PROTEIN 3, or DEHYDRIN HIRD 11, which has cytosolic and nuclear localization were identified solely in GFP-FSD1 interactome. Two nuclear proteins (CAX-INTERACTING PROTEIN 4, G PATCH DOMAIN-CONTAINING PROTEIN TGH) were also found in this subset of interactors. Other proteins showed similarity to those found in FSD1-GFP interactome, or to the commonly found interactors. In general, the interactomes of the transgenic lines differed mainly in the presence of chloroplastic proteins.

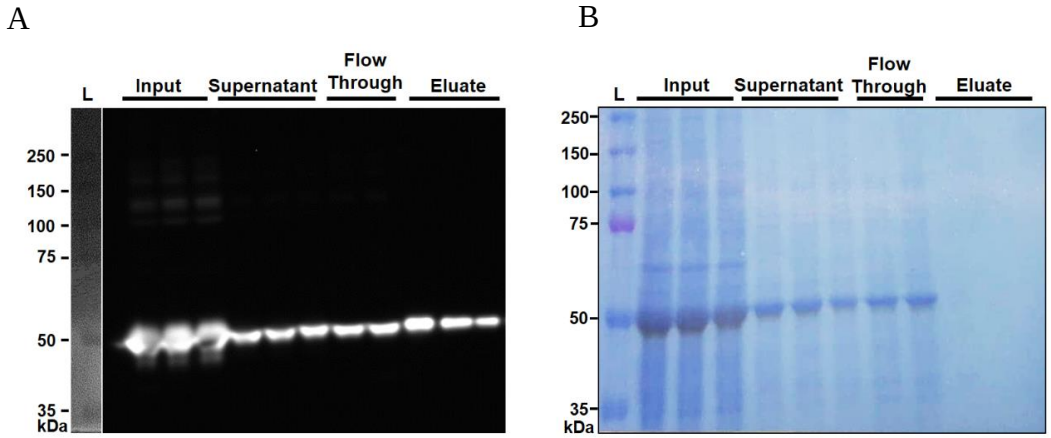

Figure 37 Validation of co-immunoprecititation. (A) Representative immunoblot of fractions obtained during co-immunoprecititation of FSD1-GFP by anti-GFP beads. FSD1-GFP was detected using anti-GFP antibody. (B) Visualization of proteins on the membrane by amido black staining. L – Ladder (Precision Plus Protein™ Dual Color Standards; Bio-Rad; size are given in kDa).

STRING web-based database (Szklarczyk et al., 2015) allows to illustrate protein interaction network among proteins identified as potential FSD1 interactors (Figure 38). This analysis considers either experimentally found physical interactions (including those between homologous and heterologous proteins) as well as coexpression. Five protein clusters were found by STRING, encompassing proteins involved in protein synthesis and folding, photosynthesis, endoplasmic reticulum bodies formation and two with unknown function. Interactions were found by STRING for: 1) Calvin cycle protein CP12-1, Thioredoxin H3 and Glyceraldehyde-3-phosphate dehydrogenase GAPA1; 2) Chlorophyll a-b binding protein CP26 and Chlorophyll a-b binding protein 2; 3) Glyceraldehyde-3-phosphate dehydrogenase and Glycine-rich RNA-binding protein 7; 4) 20 kDa chaperonin and FSD1; 5) Elongation factor 1-alpha 1, 40S ribosomal protein S25-1, Ubiquitin-40S ribosomal protein S27a-1, 40S ribosomal protein S7-1, 40S ribosomal protein S23-1, 60S ribosomal protein L35-2 and Ubiquitin-40S ribosomal protein S27a-3.

Table 7 Putative interacting partners of FSD1 detected by co-immunoprecipitation coupled to mass spectroscopy. Protein localization was either assigned by experimental evidence (as cited in Localization column) or predicted by ARAMEMNON software (Schwacke et al., 2003; http://aramemnon.botanik.uni-koeln.de.). Functions were assigned according to the experimental evidence (as cited in Function column). Abbreviations: C – chloroplast; M – mitochondria; N – nucleus; S – secretory pathway; P – predicted. The consensus prediction score generated using Bayesian analysis of the results from multiple prediction programs (AramLocCon score) indicates the probability of protein localization.

Replicates Identified	Locus	Description	Localization	Function	AramLocCon (Prediction)			
					C	M	N	S
8	At4g25100	Superoxide dismutase [Fe] 1	chloroplast, nucleus, cytosol (Dvořák et al., 2020)	superoxide detoxification, lateral root development, abiotic stress response (Dvořák et al., 2020)	0.3	0.7	-0.2	0.9
8	At3g15730	Phospholipase D alpha 1	cytosol, nuclear surface and plasma membrane (Novák et al., 2018)	abiotic and biotic stress signaling (Hunter et al., 2019; Vadovič et al., 2019).	-1.4	-1.5	-0.4	3.9
8	At1g52570	Phospholipase D alpha 2	cytosol (Urrea Castellanos et al., 2020)	stress signaling (Urrea Castellanos et al., 2020)	-1.5	-1.7	-1.7	2.9
2	At1g78900	V-type proton ATPase catalytic subunit A	plasma membrane, tonoplast (Seidel et al., 2012)	membrane transport (Schumacher and Krebs, 2010)	0	2.4	-2.2	-1.1
5	At1g13440	Glyceraldehyde-3-phosphate dehydrogenase GAPC2	cytosol, nucleus (Vescovi et al., 2013)	glycolysis, response to Cd (Vescovi et al., 2013)	-0.4	4.3	-2.1	1
2	At5g37780	Calmodulin-1	cytosol, nucleus (Moyet et al., 2019)	Ca^{2+} and stress signaling (Zhou et al., 2016)	0.2	0.1	-0.4	1
2	At5g42980	Thioredoxin H3	cytosol (Park et al., 2009)	stress responses, molecular chaperone, redox regulation (Park et al., 2009)	0.9	-1.8	-2.3	1
3	At2g05520	Glycine-rich protein 3	cell wall, plasma membrane (Gramegna et al., 2016)	root development, Al^{3+} stress tolerance (Mangeon et al., 2016); regulator of WAK1 in response to stress (Gramegna et al., 2016; Mangeon et al., 2017)	0.2	-0.9	0.4	31

4	At1g54410	Dehydrin HIRD11	cytosol, nucleus (Jung et al., 2015)	heavy metal and cold stress (Hara et al., 2013; Yokoyama et al., 2020)	-0.9	-2	8.8	-0.9
2	At1g53240	Malate dehydrogenase 1	mitochondria (Gietl, 1992; Kruft et al., 2001)	tricarboxylic acid cycle, seed development and germination (Sew et al., 2016)	5.2	32	-2.2	-1
4	At1g56410	Heat shock 70 kDa protein 18	cytosol (P)	unknown	-1	-1.4	-1.2	-0.5
7	At2g25980	Jacalin-related lectin 20	cytosol (P); apoplast (Nguyen-Kim et al., 2016)	plant development and resistance (Esch and Schaffrath, 2017)	-0.2	-1.5	-1.5	0.2
6	At3g16450	Jacalin-related lectin 33	cytosol (P)	plant development and resistance (Esch and Schaffrath, 2017)	0.7	-1.7	-2	1.3
7	At1g66270	Beta-glucosidase 21	ER bodies (Xu et al., 2004); apoplastic (P)	morphology of the ER bodies (Nagano et al., 2009; Nakano et al., 2017)	1.5	0.4	-1.9	27
5	At1g66280	Beta-glucosidase 22	ER bodies (Xu et al., 2004); apoplastic (P)	morphology of the ER bodies (Nagano et al., 2009; Nakano et al., 2017)	2.9	-1.4	-2.3	28
6	At1g54000	GDSL esterase/lipase 22	vacuole (Heard et al., 2015); apoplast (Nguyen-Kim et al., 2016)	hydrolytic enzymes with broad substrate specificity, regiospecificity, and stereoselectivity (Huang et al., 2015)	-1.2	-1.9	-2.3	32
3	At1g54030	Inactive GDSL esterase/lipase-like protein 25	ER bodies (Nakano et al., 2012)	ER integrity and function (Marti et al., 2010; Nakano et al., 2012)	9.8	-1.6	-1.2	12
4	At3g16430	PYK10-binding protein 2	ER bodies (Nagano et al., 2005)	involved in PYK10 activation, which has β-glucosidase and β-D-fucosidase activities (Nagano et al., 2005; Nakano et al., 2017)	-1.3	-1.9	-1.3	1.5
4	At2g21660	Glycine-rich RNA-binding protein 7	cytosol and nucleus (Xiao et al., 2015)	RNA processing, flowering time control (Xiao et al., 2015)	0.3	-1.5	5.4	1
7	At1g20920	DEAD-box ATP-dependent RNA helicase 42	nucleus (Guan et al., 2013; Lu et al., 2020)	pre-mRNA splicing and cold-response (Guan et al., 2013; Lu et al., 2020)	-0.1	-1	13	0.1
3	At5g02500	Heat shock 70 kDa protein 1	cytosol and nucleus (Leng et al., 2017)	abiotic stress response and protein folding (Leng et al., 2017)	-0.5	-1.8	-0.5	-1

6	At1g44910	Pre-mRNA-processing protein 40A	nucleus (Kang et al., 2009)	mRNA splicing, early steps of spliceosome complex assembly, regulation of flowering time, splicing of abiotic and biotic stress related transcripts (Kang et al., 2009; Hernando et al., 2019)	7.1	1.3	7.9	0.1
7	At4g36690	Splicing factor U2af large subunit A	nucleus (Jang et al., 2014)	mRNA splicing and flowering time (Wang and Brendel, 2006; Jang et al., 2014; Xiong et al., 2019)	0	-0.8	13	-1.3
2	At5g64200	Serine/arginine-rich splicing factor SC35	nuclear speckles (Yan et al., 2017b)	spliceosome assembly, flowering time (Yan et al., 2017b)	-0.9	-0.7	14	0.9
5	At1g60900	Splicing factor U2af large subunit B	nucleus (Xiong et al., 2019)	mRNA splicing, abscisic acid mediated flowering (Wang and Brendel, 2006; Xiong et al., 2019)	-0.2	-1.9	14	-0.8
4	At1g03910	Cactin	nuclear speckles (Baldwin et al., 2013)	function in splicing and is important for embryogenesis (Baldwin et al., 2013)	4.7	2.8	12	-1.6
2	At2g28910	CAX-interacting protein 4	nucleus, cytoplasm (Cheng et al., 2004)	ion transport (Cheng et al., 2004)	0.6	8.7	12	0.2
2	At5g23080	G patch domain-containing protein TGH	subnuclear particles (Calderon-Villalobos et al., 2005)	biogenesis of miRNA and siRNA (Ren et al.,2012)	-0.9	-2	15	0.1
7	At5g25810	Ethylene-responsive transcription factor TINY	nucleus (Xie et al., 2019)	plant growth and response to abiotic stress (Xie et al., 2019)	1.4	-1.9	9.6	-1.4
8	At1g79200	Style cell-cycle inhibitor 1	nucleus (DePaoli et al., 2014)	auxin signaling and cell division (DePaoli et al., 2014)	2.4	1.8	8.4	-1.3
5	At2g16360	40S ribosomal protein S25-1	cytosol (Chang et al., 2005)	component of ribosomal complex (Chang et al., 2005; Carroll, 2013)	6.4	6.5	1.1	-0.3
3	At2g39390	60S ribosomal protein L35-2	cytosol (Chang et al., 2005)	component of ribosomal complex (Chang et al., 2005; Carroll, 2013)	0.7	3	1.5	0.2
5	At3g09680	40S ribosomal protein S23-1	cytosol (Chang et al., 2005)	component of ribosomal complex (Chang et al., 2005; Carroll, 2013)	-0.7	16	-0.9	-1.4
5	At1g48830	40S ribosomal protein S7-1	cytosol (Chang et al., 2005)	component of ribosomal complex (Chang et al., 2005; Carroll, 2013)	-1.3	-1	0.6	0

3	At1g23410	Ubiquitin-40S ribosomal protein S27a-1	cytosol (Chang et al., 2005)	component of the 40S subunit of the ribosome (Montellese et al., 2020)	-1.6	-1	10	-0.6
3	At3g62250	Ubiquitin-40S ribosomal protein S27a-3	cytosol (Chang et al., 2005)	component of the 40S subunit of the ribosome (Montellese et al., 2020)	-1.4	-0.6	8.8	-0.4
3	At1g07940	Elongation factor 1-alpha 1	cytosol (Curie et al., 1993; Suhandono et al., 2014)	translation (Curie et al., 1993)	-1.4	-1.8	-1.3	0.2
2	At5g20720	20 kDa chaperonin, chloroplastic	chloroplast (Kuo et al., 2013)	iron chaperone for superoxide dismutase (Kuo et al., 2013)	26	3.3	-2	-0.7
2	At1g20020	Ferredoxin-NADP reductase, leaf isozyme 2, chloroplastic	chloroplast (Lintala et al., 2007; Benz et al., 2009)	nitrate assimilation (Hanke et al., 2005) and redox reactions (Lintala et al., 2009)	31	-0.7	-2	-0.3
2	At1g11840	Lactoylglutathione lyase GLX1	putative chloroplast (Kaur et al., 2013) and nuclear localization (Kaur et al., 2017)	methylglyoxal detoxification and salt stress tolerance (Batth et al., 2020)	-1.1	0.7	2	-0.5
3	At1g29920	Chlorophyll a-b binding protein 2, chloroplastic	chloroplast (Friso et al., 2004; Mitra et al., 2009)	state transitions (Pietrzykowska et al., 2014)	36	-0.1	-2	1
4	At4g10340	Chlorophyll a-b binding protein CP26, chloroplastic	chloroplast (Ruban et al., 2006)	formation of photosynthetic apparatus (Hou et al., 2015)	36	0.6	-2.2	-0.9
2	At2g47400	Calvin cycle protein CP12-1, chloroplastic	chloroplast (Marri et al., 2010)	photosynthesis (Marri et al., 2005)	15	2.2	-2.1	2.9
5	At3g26650	Glyceraldehyde-3-phosphate dehydrogenase GAPA1, chloroplastic	chloroplast (Zybailov et al., 2008)	photosynthesis (Marri et al., 2005)	19	1.8	-2.4	0.3
8	At5g38410	Ribulose bisphosphate carboxylase small chain 3B, chloroplastic	chloroplast (Zybailov et al., 2008)	photosynthesis (Marri et al., 2005)	29	-0.6	-1.8	3.8

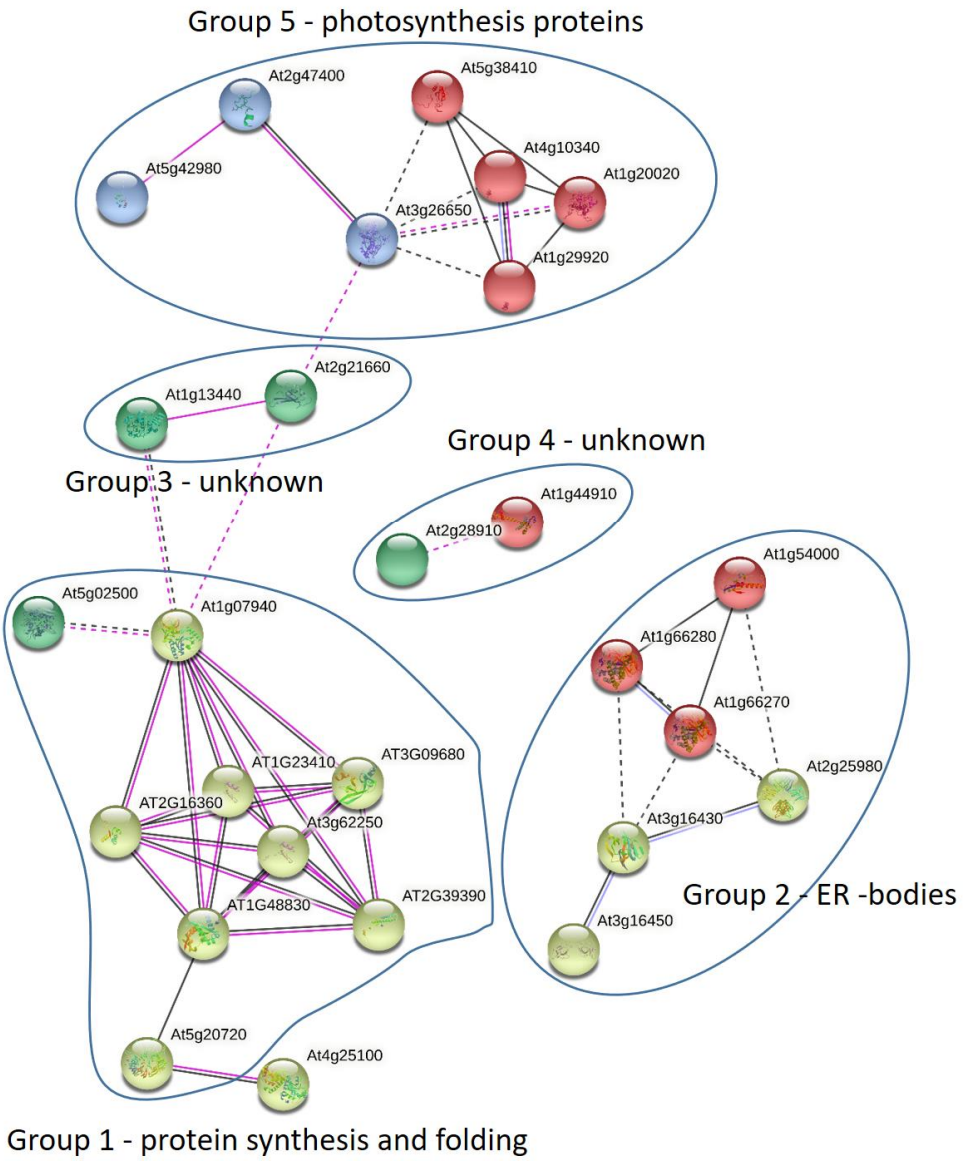

Figure 38 Depiction of protein interaction networks of identified putative interacting partners of FSD1 as constructed using STRING web-based application. Protein-protein interactions based on experimental evidence are considered. AT-codes: group 1 - At5g02500 – HEAT SHOCK 70 kDa PROTEIN 1; At1g07940 – ELONGATION FACTOR 1-α 1; At2g16360 – 40S RIBOSOMAL PROTEIN S25-1; At1g23410 – UBIQUITIN-40S RIBOSOMAL PROTEIN S27a-1; At3g09680 – 40S RIBOSOMAL PROTEIN S23-1; At3g62250 – UBIQUITIN-40S RIBOSOMAL PROTEIN S27a-3; At1g48830 – 40S RIBOSOMAL PROTEIN S7-1; At2g39390 – 60S RIBOSOMAL PROTEIN L35-2; at5g20720 – 20 kDa CHAPERONIN, CHLOROPLASTIC; group 2 - At1g54000 – GDSL ESTERASE/LIPASE 22, At1g66280 – β-GLUCOSIDASE 22, At1g66270 – β-GLUCOSIDASE 21, At2g25980 – JACALIN-RELATED LECTIN 20, At3g16430 – PYK10-BINDING PROTEIN 2, At3g16450 – JACALIN-RELATED LECTIN 33, group 3 - At1g13440 – GLYCERALDEHYDE-3-PHOSPHATE DEHYDROGENASE GAPC2, At2g21660 – GLYCINE-RICH RNA-BINDING PROTEIN 7; group 4 - At2g28910 – CAX-INTERACTING PROTEIN 4, At1g44910 – pre-mRNA-PROCESSING PROTEIN 40A; group 5 - At1g29920 – CHLOROPHYLL a-b BINDING PROTEIN 2, At3g26650 – GLYCERALDEHYDE-3-PHOSPHATE DEHYDROGENASE GAPA1, At1g20020 – FERREDOXIN-NADP REDUCTASE, LEAF ISOZYME 2, At4g10340 – CHLOROPHYLL a-b BINDING PROTEIN CP26, At5g38410 – RIBULOSE BISPHOSPHATE CARBOXYLASE SMALL CHAIN 3B, At2g47400 – CALVIN CYCLE PROTEIN CP12-1, At5g42980 – THIOREDOXIN H3; unclassified - At4g25100 – SUPEROXIDE DISMUTASE [Fe] 1.

Several interesting proteins were identified which were previously described to be involved in stress responses, such as PLDα1 and 2, DEHYDRIN HIRD11, CALMODULIN-1, GLYCINE-RICH PROTEIN 3, LACTOYLGLUTATHIONE LYASE GLX1, ETHYLENE-RESPONSIVE TRANSCRIPTION FACTOR TINY, Pre-mRNA-PROCESSING PROTEIN 40A (Table 7). Interestingly, several proteins involved in pre-mRNA splicing were identified such as pre-mRNA-PROCESSING PROTEIN 40A, SPLICING FACTOR U2AF LARGE SUBUNIT A and B, SERINE/ARGININE-RICH SPLICING FACTOR SC35, CACTIN, DEAD-BOX ATP-DEPENDENT RNA HELICASE 42 (Table 7).

Taken together, the identification of FSD1 interactome changes the view on FSD1 as a conservative antioxidant enzyme. Based on this, new roles in pre-mRNA splicing and regulation of photosynthesis could be suggested for FSD1.

3.2.9 Bioinformatics analysis of potential regulatory mechanisms of FSD1

Proteomic and transcriptomic analyses of MAPKs mutant indicated the MAPK mediated regulation of *FSD1* expression (Frei dit Frey et al., 2014; Takáč et al., 2014; Takáč et al., unpublished results). It is expected that *FSD1* might be controlled by MAPKs transcriptionally by TFs. Modern bioinformatics gives us an opportunity to widen the list of potential TFs controlling *FSD1*, based on expression (transcriptomics) or abundance (proteomics), which has been changed in transgenic lines with modified or absent *MAPK* expression. Based on above mentioned data, we performed the bioinformatics analysis by integrating four different parameters to found potential TFs regulating *FSD1* expression under MPKs control: 1) the presence of *cis*-element(s) in the promoter sequence of *FSD1* gene (predicted by AthaMap; Hehl et al., 2016), (2) TFs co-expressed with *FSD1* and MAPKs (determined by ATTED-II; Obayashi et al., 2018), (3) TFs containing a MAPK-specific phosphorylation site (S(p)P or S(p)T; evaluated by PhosPhat 4.0 and GPS 3.0; Xue et al., 2005; Zulawski et al., 2013), and (4) the presence of a MAPK-specific docking site in the amino acid sequence of the TFs (evaluated by ELM; Kumar et al., 2020). Overall 31 potential TFs have been predicted for the control of *FSD1* expression by MAPKs (Supplementary file 1).

Three candidates belonging to the SPL protein family, namely SPL1, SPL7 and SPL8, were identified as well. SPL7 was described as a TF with direct influence on *FSD1* expression (Yamasaki et al., 2009; Andrés-Colás et al., 2013; Garcia-Molina et al., 2014). We selected SPL1 and SPL7 as the most promising MAPK-phosphorylated TFs regulating *FSD1* expression.

As noted in the introduction, FSD1 activity may be regulated also by phosphorylation. We performed a bioinformatic prediction of phosphorylation sites in the amino acid sequence of FSD1 protein. We found that MAPK is the kinase predicted with the highest probability to phosphorylate FSD1, most likely on EKLKVVKTPNAVNPL peptide. This sequence partially overlapped with the predicted MAPK docking site (KTPNAVNPLVL; Table S6 and S7; Figure S16).

3.2.10 Preparation of recombinant SPL1, SPL7, FSD1, MPKs and phosphorylation experiments by using *in vitro* kinase assay

In order to confirm the hypothesis about MAPK mediated FSD1 regulation, we decided to employ *in vitro* kinase assay, to examine FSD1, SPL1 and SPL7 phosphorylation by MPK3 and MPK6. We prepared constructs for heterologous recombinant protein expression (Figure S17) by using pMAL-p2 or pGEX-6P-1 vectors. Afterward, recombinant proteins were successfully prepared by affinity purification (Figure 39).

The purity of the recombinant proteins was examined by polyacrylamide electrophoresis (Figure 39). The majority of both SPL1 (prepared in GST and MBP tagged versions) and SPL7 (MBP-tagged) was stored in the inclusion bodies and only a minor part remained in the soluble fraction. MBP-SPL1 showed a higher protein yield in comparison with GST-SPL1 (Figure 39A, B). Considerable portion of fused SPL1 and SPL7 stayed attached to affinity beads (Figure 39A, B, C). The expression of MBP-FSD1 showed extensive yields mostly in the soluble fraction (Figure 39D). Finally, recombinant MPK3 and MPK6 with GST fusion were prepared with high quality (Figure 39E, F).

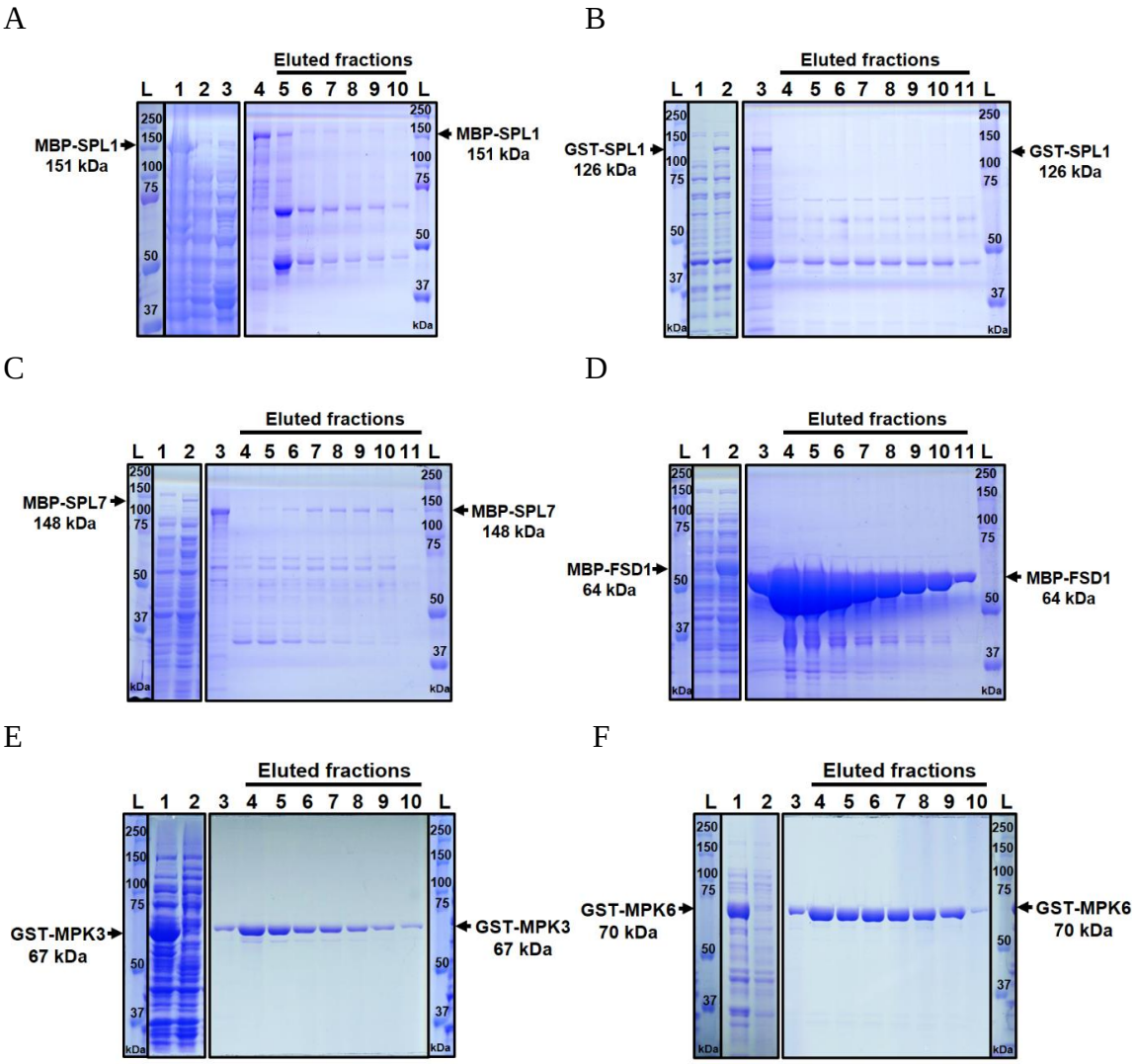

Figure 39 Preparation and purification of recombinant proteins by using the bacterial heterologous system. (A-F) Proteins from various fractions from recombinant protein purification procedure separated on SDS-PAGE gels and stained with Coomassie staining. (A-B) Purification of recombinant SPL1 fused with MPB-tag (A) and GST-tag (B). (A) Lane 1 – proteins derived from non-lysed induced cells. Lanes 2 and 3 – proteins derived from lysed non-induced and induced cells, respectively. Lane 4 – proteins from purification beads with recombinant proteins, which were loaded on the gel. Lanes 4–11 – eluted fractions from affinity purification. The samples in (B) were loaded as in (A) avoiding non-lysed induced cells. (C-F) Purification of recombinant SPL7 (C), FSD1 (D) fused both by MPB-tag; MPK3 (E) and MPK6 (F) both fused with GST-tag. The samples were loaded as in (B). Seven or eight elution fractions were collected. Precision Plus Protein^{TM} Dual Color standards were used as protein size marker (size are given in kDa).

In vitro kinase assay reactions were performed for testing the phosphorylation of SPL1, SPL7, FSD1 by MPK3 (Figure 40A, B) and MPK6 (Figure 40C, D) in two repetitions. MyBP was used as a positive control for the detection of kinase activity. The results showed strong phosphorylation of MyBP control (Figure 40B, D), confirming that prepared recombinant MPKs have kinase activity. However, no radioactive signal was obtained from the area where the recombinant GST-SPL1,

MBP-SPL1, MBP-SPL7 and even MBP-FSD1 were separated (Figure 40A-D). MPK3 (Figure 40A, B) and MPK6 (Figure 40C, D) showed pronounced autophosphorylation. Together, we did not prove the phosphorylation of SPL1, SPL7 and FSD1 by MAPKs in our experiment.

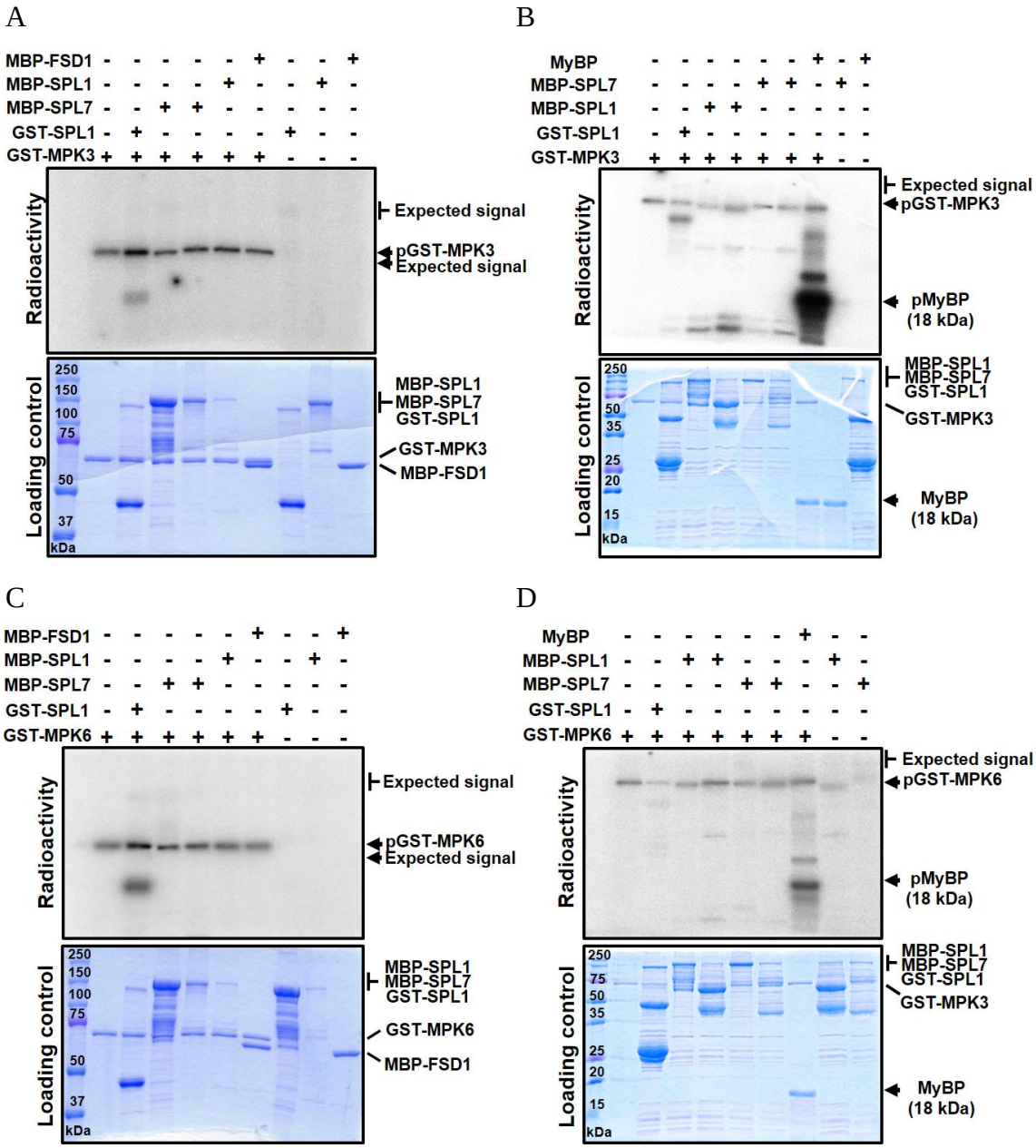

Figure 40 *In vitro* kinase assay of recombinant MPK3 (A, B) and MPK6 (C, D) using predicted recombinant substrates SPL1, SPL7 (both tested in all gels) and FSD1 (A, C). The testing of SPL1 and SPL7 phosphorylation is shown in two repetitions (A, B and C, D, respectively). Gels in (C and D) shows phosphorylation of Myelin basic protein (MyBP) at 18 kDa as a positive control. Arrows mark the area with detected radioactivity and the presence of recombinant protein. The expected Mr of SPL1, SPL7 and FSD1 phosphorylation is indicated by ⊢ and arrows. Gels below the autoradiographs represent the same gels stained by coomassie blue staining.

3.3 Discussion

FSDs were long believed to be chloroplast proteins involved in $O_2^{\cdot-}$ scavenging during photosynthesis. However, the scavenging capacity of *Arabidopsis* FSD1 was challenged, because its transcript levels remained unchanged in response to many environmental conditions (Kliebenstein et al., 1998; Myouga et al., 2008; Xing et al., 2015; Gallie and Chen, 2019). This work shows for the first time that FSD1 is localized not only in plastids, but simultaneously also in the nuclei and cytosol of *Arabidopsis* cells. Moreover, FSD1 accumulates in Hechtian strands and Hechtian reticulum interconnecting retracted protoplast with the cell wall under salt stress conditions.

Using translational fusion constructs with native promoter, GFP-tagged FSD1 exhibited a tissue-specific expression pattern in *Arabidopsis* root tip. This indicates that FSD1 may also have developmental roles that are conditionally determined. Hence, FSD1 might be involved in the regulation of the redox status in dividing cells, like root initials. It is known that the root meristematic activity as well as the quiescent centre organization is maintained by redox homeostasis which acts downstream of the auxin transport (Jiang, 2003; Barlow, 2016; Gallie and Chen, 2019; Horváth et al., 2019). Intriguingly, *FSD1* tissue-dependent expression pattern largely correlates with auxin maxima in the root tip (Petersson et al., 2009; Hayashi et al., 2014), as well as with $O_2^{\cdot-}$ maxima (Dunand et al., 2007). Furthermore, endodermis formation requires SCARECROW (SCR) and SHORTROOT (SHR), two GRAS-type TFs, expressed in the endodermis/cortex initials and quiescent centre (Helariutta et al., 2000; Carlsbecker et al., 2010). FSD1 might also contribute to the regulation of SCR and SHR, which is supported by the high expression of *FSD1* in fluorescence-activated cell sorting-isolated protoplasts expressing endoplasmic reticulum-targeted GFP under the control of the SCR promoter (Geng et al., 2013). This expression was elevated in salt-stressed protoplasts. Considering our results about the role of FSD1 in salt stress tolerance, FSD1 may be involved in the maintenance of redox homeostasis in the endodermis/cortex initials of the root tip.

According to our study, FSD1 is required for proper establishment of lateral roots in *Arabidopsis*. Considering that both N- and C-terminal GFP fusions with FSD1 complemented defective lateral root formation in *fsd1* mutants, one can assume that these fusion proteins are functional and sufficient for full acquisition of lateral root formation capacity in *Arabidopsis*, but further investigation is necessary to verify this

hypothesis. Lateral root formation is dependent on complementary action of multiple regulatory systems governed by auxin (Banda et al., 2019). RBOH-generated ROS are major modulators of this process via cell wall remodeling of overlying parental root tissues (Orman-Ligeza et al., 2016). RBOH activity is controlled by multiple factors including phosphorylation, Ca^{2+}, PA and protein-protein interactions (Ogasawara et al., 2008; Zhang et al., 2009), while ROS accumulation must be controlled in order to ensure proper lateral root formation. As a proof of this concept, we provided experimental evidence showing strong accumulation of FSD1 in LRP, and reduced lateral root number in *fsd1* mutants. Hence, FSD1 appears as an enzyme participating in maintenance of proper redox homeostasis during lateral root formation.

The localization of FSD1 to chloroplasts is determined by an N-terminal transit peptide identified previously (Kuo et al., 2013). According to comparative studies of three *Arabidopsis* isoforms, FSD1 is crucial neither for chloroplast integrity (Myouga et al., 2008), nor for cell protection under photooxidative stress (Gallie and Chen, 2019). It has 3–10 times higher expression compared to *FSD2* and *FSD3* (Pilon et al., 2011) in *Arabidopsis*, depending on developmental stage, and unlike *FSD2* and *FSD3*, it remains insensitive to MV and high light irradiation (Myouga et al., 2008). Evidence was provided for cooperative roles of FSD2 and FSD3 to ensure defense against high light and MV-generated ROS (Myouga et al., 2008; Gallie and Chen, 2019). We show that plastidic pool of FSD1 is important for *Arabidopsis* tolerance against MV-induced oxidative stress, while cytosolic and nuclear pools are inefficient. It is likely that the protective role of FSD1 depends on the severity of the external conditions and might be triggered under harsh stress conditions. The protective roles of FSD1 were reported in transgenic tobacco and maize, where overexpression of this enzyme in chloroplasts enhanced the efficiency of thylakoid and plasma membrane protection (Van Camp et al., 1996; Van Breusegem et al., 1999).

FSD1 is also important for *Arabidopsis* germination under salt stress and for salt stress tolerance in general. As indicated by the FSD1 localization and salt stress response in the complemented lines, cytosolic FSD1, FSD1 in the Hechtian strands and Hechtian reticulum (as discussed below) and likely also nuclear FSD1 pool are crucial for the acquisition of tolerance to salinity during germination. Altogether, our results emphasize the importance of FSD1 in the regulation of cytosolic and also possibly nuclear redox homeostasis in response to salinity stress.

Salt stress causes rapid generation of ROS by NADPH oxidases (Leshem et al., 2007), while it is accompanied by the internalization of RBOH into cytoplasmic structures (Hao et al., 2014). Such salt-induced ROS accumulation has to be tightly controlled in order to avoid damaging consequences. Our results suggest that FSD1 might be involved in the primary plant defense against $O_2^{\cdot-}$ production in the Hechtian strands and Hechtian reticulum during salt stress.

Seed germination is a complex process encompassing multiple events governed by tight phytohormonal regulation. Micropylar endosperm represents the last mechanical barrier constraining the radicle emergence. Endosperm rupture is preceded by its weakening, controlled by the inhibitory effect of ABA and promoting effect of ethylene (Linkies et al., 2009). Furthermore, ROS contribute to this process by oxidizing the cell wall polysaccharides and subsequent cell wall loosening (Müller et al., 2009). Here, we provide data showing FSD1 upregulation and local accumulation in the micropylar endosperm during endosperm weakening and rupture, which is subsequently decreased after primary root emergence.

Such accumulation of FSD1-GFP at the micropylar endosperm before and during endosperm rupture by emerging radicle indicates that it may be involved in the local catalysis of $O_2^{\cdot-}$ conversion to H_2O_2. This assumption is strengthened by increased $O_2^{\cdot-}$ accumulation in *fsd1* mutants and the FSD1-GFP accumulation in the Hechtian strands and Hechtian reticulum interconnecting retracted protoplast with the cell wall. Indeed, *FSD1* shows unique transcriptional changes during seed germination in comparison to other SOD isoforms (Müller et al., 2009), supporting the specific role of FSD1 during endosperm weakening and rupture. Nevertheless, the precise role of FSD1 in endosperm rupture remains to be elucidated.

Our localization data suggest that FSD1 functions are not only restricted to the cytosol and plastids, because we provide here the first evidence on the nuclear localization of SOD in plants. It was previously found that mammalian SOD1 is rapidly relocated to the nucleus upon H_2O_2-triggered oxidative stress (Volkening et al., 2009). In this case, SOD1 binds to specific DNA nucleotide sequences and triggers the expression of genes involved in oxidative resistance and DNA repair. It may also bind to and regulate the stability of specific mRNAs (Volkening et al., 2009). SOD1 nuclear functions are unrelated to its catalyzing of $O_2^{\cdot-}$ removal (Tsang et al., 2014). Nucleotide

sequences of FSD1 as well as structure of FSD1 catalytic and other domains differ considerably from SOD1 (Pilon et al., 2011), nevertheless, a similar role could be expected for plant SODs with localization in the nucleus.

Our FSD1 interactome analysis showed that FSD1 may participate in the regulation and proper function of spliceosome. The interactome included SPLICING FACTOR U2AF LARGE SUBUNIT B, which is involved in ABA-mediated flowering via pre-mRNA splicing of *ABSCISIC ACID-INSENSITIVE 5* and *FLOWERING LOCUS C*, which are both involved in ABA-mediated floral transition (Shu et al., 2016; Xiong et al., 2019). Another component of the spliceosome, SERINE/ARGININE-RICH SPLICING FACTOR SC35 identified in our analysis, has been previously described as regulator of FLOWERING LOCUS C splicing and flowering time (Yan et al., 2017b). Additionally, DEAD-BOX ATP-DEPENDENT RNA HELICASE 42 (Guan et al., 2013; Lu et al., 2020), SPLICING FACTOR U2AF LARGE SUBUNIT A (Wang and Brendel, 2006; Jang et al., 2014), pre-mRNA-PROCESSING PROTEIN 40A (Kang et al., 2009; Hernando et al., 2019) and CACTIN (Baldwin et al., 2013) have been associated with pre-mRNA splicing. Thus FSD1 may likely link ROS signaling to alternative splicing by interacting with the spliceosome complex. This interaction is most probably connected to the control of flowering time, which is also suggested by phenotypes of *fsd1-1* and *fsd1-2* mutants, having delayed flowering (Samakovli et al., unpublished data). FSD1 may also bind STYLE CELL-CYCLE INHIBITOR 1 (DePaoli et al., 2014) and ETHYLENE-RESPONSIVE TRANSCRIPTION FACTOR TINY (Xie et al., 2019), two TFs in our screen. Knowing the previously found function of mammalian SOD as a transcriptional or co-transcriptional factor (Tsang et al., 2014), the presence of TFs in the interactome may imply similar functions also for FSD1. Nevertheless, all these hypotheses need to be experimentally verified and potentially may serve as the basic premise for studies on the nuclear roles of FSD1.

Our phenotypic and microscopic analyses assigned osmoprotective roles to FSD1. In this sense, putative FSD1 interaction with a protein involved in ABA signaling, PLDα1 (found in all of the examined replicates), appears as a very interesting finding. PLDα1 is implicated in plant response to salt stress (Vadovič et al., 2019). Its phospholipid hydrolyzing activity results in the production of PA, an important signaling molecule. It activates MAPKs in response to salt stress (Yu et al., 2010). PLDα1-mediated changes in membrane properties lead to activation of

CYSTEINE-RICH RECEPTOR-LIKE KINASE 2, which relocalizes to plasmodesmata and promotes callose deposition under salt stress (Hunter et al., 2019). Interestingly, FSD1 showed localization very similar to PLDα1 after salt stress and fluorescent signals of both FSD1 and PLDα1 were increased close to the plasma membrane and on Hechtian strands (Novák et al., 2018). The similarity of FSD1 and PLDα1 is apparent also considering the tissue specific expression pattern in the root tip (Novák et al., 2018). These data, together with the ABA responsivity of FSD1 (Müller et al., 2009), support possible interaction between PLDα1 and FSD1 during salt stress. FSD1 may link the ROS signaling (by controlling $O_2^{\cdot -}$ conversion to H_2O_2) with functions of PLDα1 in membrane biophysical properties in order to contribute to osmoprotection.

We also address the question of possible mechanisms of FSD1 regulation. Our bioinformatics pipeline resulted in the identification of 31 putative MAPK-phosphorylated TFs with high potential to bind to *cis*-elements in FSD1 promoter sequence (Supplementary file 1). SPL7 and SPL1 were selected for further studies. The promoter sequences of several *SODs* (*FSD1*, *CSD1*, *CSD3*, *MSD1*) contain the core motif GTAC (Perea-García et al., 2016), specific for SPL binding. More specifically, *FSD1* promoter sequence contains six independent GTAC motifs and three motifs in first intron. Previously, the presence of GTAC motif in the first intron was suggested as a possible binding site for SPL proteins (Yamaguchi et al., 2009). Additionally, the *FSD1* expression is strongly suppressed in *Arabidopsis spl7* mutant (Yamasaki et al., 2009) and mutation of four GTAC motifs in *FSD1* promoter led to significant downregulation of *FSD1* expression (Andrés-Colás et al., 2013). In this sense, the presence of multiple binding motifs may suggest the binding of other SPL isoforms, dependent on developmental stage and stress conditions. As a proof of concept, *spl1/spl12* showed downregulated SOD activity in response to heat stress (Chao et al., 2017). In addition to the transcriptional control of FSD1, the regulation of FSD1 via phosphorylation by MAPKs cannot be excluded, as indicated by our bioinformatics analysis. Previously yeast (Leitch et al., 2012) and human SOD1 (Tsang et al., 2018) has been found phosphorylated and with direct impact on activity and leads to the translocation of this SOD1 to the nucleus. In addition, several isoforms of *Arabidopsis* SODs have been found as phosphorylated by phosphoproteomic methods (Table S1).

The possible phosphorylation of SPL1, SPL7 and FSD1 by MPK3 and MPK6 was tested by *in vitro* kinase assay by using recombinant proteins. Unfortunately, we failed

to prove any of the analyzed phosphorylations. Although we were able to produce a soluble fraction of recombinant SPLs, the majority of the expressed proteins were found in inclusion bodies. This issue is very common for proteins, which are toxic for bacteria and are not properly folded. The bacterial cytoplasm provides a reducing environment, which is not suitable for formation of disulfide bonds. Proteins, which require the formation of disulfide bonds, might be misfolded leading to aggregation and formation of insoluble inclusion bodies (Gąciarz et al., 2017). Indeed, both SPL7 and SPL1 contain in their structure relatively high amount of cysteine and it is possible, that the protein folding was incorrect in *E. coli*. This may affect the access of MPKs to the putatively phosphorylated residues. For this reason, the possible phosphorylation of SPLs by MAPKs cannot be excluded. The SPLs and MAPKs relationship may be studied also by a yeast two-hybrid system, bimolecular fluorescence complementation and localization of fluorescently tagged MAPK and SPLs *in planta*. Furthermore, different heterologous expression systems should be used such as yeast, insect or plants (Tripathi and Shrivastava, 2019) to obtain the recombinant proteins with required properties for repetition of *in vitro* kinase assay.

On the other hand, results of FSD1 phosphorylation by MPK3 and MPK6 showed negative results. In this case, MBP-FSD1 protein purification was working with enormous efficiency. Based on these results, it is highly possible, that FSD1 is not phosphorylated by MPK3 and MPK6 *in planta*.

4 General conclusions

This Ph.D. thesis is focused on the crosstalk of plant MAPKs with ROS signaling. First, we used proteomic, phenotypic and biochemical analyses to examine the impact of MAPKs on the establishment of symbiotic interaction of alfalfa with *S. meliloti*, with accent on antioxidant defense. Secondly, we studied the developmental and protective roles of *Arabidopsis* FSD1 a protein potentially regulated by MAPKs.

Within the theoretical part, a current knowledge about plant MAPK signaling with a focus on abiotic and biotic stresses is summarized. A separate chapter is devoted to MAPK cascades in legumes (mainly alfalfa) and their function during the alfalfa – rhizobia interaction. Next, recent findings connected to ROS signaling and their crosstalk with MAPKs during plant stress response are discussed. The last chapter of the theoretical part addresses antioxidant enzymes, including SODs and mechanisms of their regulation.

In the frame of the experimental part a series of phenotypical, biochemical and proteomic analyses were carried out on alfalfa wild type and transgenic *SIMKK RNAi* line (SIMKKi). The most important results showed that SIMKKi displays significantly decreased number of nodules in comparison with wild type. Combined proteomic and biochemical analyses indicated that SIMKKi may have significant impact on regulation of SODs, bacteria attachment and sterol rearrangements in plasma membrane, all being important for establishment of symbiotic interaction. Together, SIMKK positively regulates the establishment of alfalfa-rhizobia interaction likely through multiple mechanisms.

Since FSD1 was selected as a protein potentially regulated by MAPKs, the second part of experiments was focused on its developmental and protective roles in *Arabidopsis*. FSD1-GFP temporarily accumulated at the site of endosperm rupture during seed germination. In emerged roots, it showed the highest abundance in cells of the lateral root cap, columella, and endodermis/cortex initials. The largest subcellular pool of FSD1-GFP was localized in the plastid stroma, while it was also located in the nuclei and cytosol. The majority of the nuclear FSD1-GFP is immobile as revealed by FRAP. We found that *fsd1* knockout mutants exhibit reduced lateral root number and this phenotype was reverted by genetic complementation. Mutant analysis also revealed a requirement for FSD1 in seed germination during salt stress. Salt stress tolerance was

coupled with the accumulation of FSD1-GFP in Hechtian strands and $O_2^{\cdot-}$ removal. It is likely that the plastidic pool is required for acquiring oxidative stress tolerance in *Arabidopsis*.

The FSD1 interactome identification by using co-immunoprecipitation coupled to proteomic analyses suggested several putative interaction partners of FSD1 and its possible role in pre-mRNA splicing. Finally, we predicted putative TFs controlling FSD1 expression under the control of MAPKs. Among them, putative phosphorylation of two SPL7 and SPL1 TFs by MPK3 and MPK6 was validated by using *in vitro* kinase assay. However, the predicted MAPK-mediated phosphorylation of SPLs was not confirmed. These results suggest a new nuclear, developmental and osmoprotective functions of SODs in plants.

5 References

Abdel-Ghany, S. E., Burkhead, J. L., Gogolin, K. A., Andrés-Colás, N., Bodecker, J. R., Puig, S., et al. (2005). AtCCS is a functional homolog of the yeast copper chaperone Ccs1/Lys7. *FEBS Lett.*, *579*, 2307–2312.

Abercrombie, J. M., Halfhill, M. D., Ranjan, P., Rao, M. R., Saxton, A. M., Yuan, J. S., and Stewart, C. N., Jr. (2008). Transcriptional responses of *Arabidopsis thaliana* plants to As (V) stress. *BMC Plant Biol.*, *8*, 87.

Allu, A. D., Soja, A. M., Wu, A., Szymanski, J., and Balazadeh, S. (2014). Salt stress and senescence: identification of cross-talk regulatory components. *J. Exp. Bot.*, *65*, 3993–4008.

Almagro, L., Gómez Ros, L. V., Belchi-Navarro, S., Bru, R., Ros Barceló, A., and Pedreño, M. A. (2009). Class III peroxidases in plant defence reactions. *J. Exp. Bot.*, *60*, 377–390.

Alvarez, M. E., Pennell, R. I., Meijer, P. J., Ishikawa, A., Dixon, R. A., and Lamb, C. (1998). Reactive oxygen intermediates mediate a systemic signal network in the establishment of plant immunity. *Cell*, *92*, 773–784.

Alves, M. B. R., de Andrade, A. F. C., de Arruda, R. P., Batissaco, L., Rodriguez, S. A. F., Lançoni, R., et al. (2015). An efficient technique to detect sperm reactive oxygen species: The CellRox deep red® fluorescent probe. *Biochem. Physiol.*, *4*, 1–5.

Andrási, N., Rigó, G., Zsigmond, L., Pérez-Salamó, I., Papdi, C., Klement, E., et al. (2019). The mitogen-activated protein kinase 4-phosphorylated heat shock factor A4A regulates responses to combined salt and heat stresses. *J. Exp. Bot.*, *70*, 4903–4918.

Andreasson, E., Jenkins, T., Brodersen, P., Thorgrimsen, S., Petersen, N. H., Zhu, S., et al. (2005). The MAP kinase substrate MKS1 is a regulator of plant defense responses. *EMBO J.*, *24*, 2579–2589.

Andrés-Colás, N., Perea-García, A., Mayo de Andrés, S., Garcia-Molina, A., Dorcey, E., Rodríguez-Navarro, S., et al. (2013). Comparison of global responses to mild deficiency and excess copper levels in Arabidopsis seedlings. *Metallomics*, *5*, 1234–1246.

Andrio, E., Marino, D., Marmeys, A., de Segonzac, M. D., Damiani, I., Genre, A., et al. (2013). Hydrogen peroxide-regulated genes in the Medicago truncatula-Sinorhizobium meliloti symbiosis. *New Phytol.*, *198*, 179–189.

Apel, K., and Hirt, H. (2004). REACTIVE OXYGEN SPECIES: metabolism, oxidative stress, and signal transduction. *Annu. Rev. Plant Biol.*, *55*, 373–399.

Araki, R., Mermod, M., Yamasaki, H., Kamiya, T., Fujiwara, T., and Shikanai, T. (2018). SPL7 locally regulates copper-homeostasis-related genes in *Arabidopsis*. *J. Plant Physiol.*, *224–225*, 137–143.

Aroca, Á., Serna, A., Gotor, C., and Romero, L. C. (2015). S-sulfhydration: a cysteine posttranslational modification in plant systems. *Plant Physiol.*, *168*, 334–342.

Arsova, B., Watt, M., and Usadel, B. (2018). Monitoring of plant protein posttranslational modifications using targeted proteomics. *Front. Plant Sci.*, *9*, 1168.

Asai, S., Ichikawa, T., Nomura, H., Kobayashi, M., Kamiyoshihara, Y., Mori, H., et al. (2013). The variable domain of plant calcium-dependent protein kinase (CDPK) confers subcellular localization and substrate recognition for NADPH oxidase. *J. Biol. Chem.*, *288*, 14332–14340.

Asai, T., Tena, G., Plotnikova, J., Willmann, M. R., Chiu, W. L., Gomez-Gomez, L., et al. (2002). MAP kinase signalling cascade in Arabidopsis innate immunity. *Nature*, *415*, 977–983.

Bailly, C., El-Maarouf-Bouteau, H., and Corbineau, F. (2008). From intracellular signaling networks to cell death: the dual role of reactive oxygen species in seed physiology. *C. R. Biol.*, *331*, 806–814.

Baldwin, K. L., Dinh, E. M., Hart, B. M., and Masson, P. H. (2013). CACTIN is an essential nuclear protein in Arabidopsis and may be associated with the eukaryotic spliceosome. *FEBS Lett.*, *587*, 873–879.

Banci, L., Bertini, I., Calderone, V., Cramaro, F., Del Conte, R., Fantoni, A., et al. (2005). A prokaryotic superoxide dismutase paralog lacking two Cu ligands: From largely unstructured in solution to ordered in the crystal. *Proc. Natl. Acad. Sci. U. S. A.*, *102*, 7541–7546.

Banda, J., Bellande, K., von Wangenheim, D., Goh, T., Guyomarc'h, S., Laplaze, L., and Bennett, M. J. (2019). Lateral root formation in *Arabidopsis*: A well-ordered LRexit. *Trends Plant Sci.*, *24*, 826–839.

Banks, C. J., and Andersen, J. L. (2019). Mechanisms of SOD1 regulation by post-translational modifications. *Redox Biol.*, *26*, 101270.

Bannister, W. H., Bannister, J. V., Barra, D., Bond, J., and Bossa, F. (1991). Evolutionary aspects of superoxide dismutase: the copper/zinc enzyme. Free Radic. Res. Commun., *12–13 Pt 1*, 349–361.

Bardwell, A. J., Frankson, E., and Bardwell, L. (2009). Selectivity of docking sites in MAPK kinases. *J. Biol. Chem.*, *284*, 13165–13173.

Barlow, P. W. (2016). Origin of the concept of the quiescent centre of plant roots. *Protoplasma*, *253*, 1283–1297.

Barnes, J. D., Balaguer, L., Manrique, E., Elvira, S., and Davison, A. W. (1992). A reappraisal of the use of DMSO for the extraction and determination of chlorophylls a and b in lichens and higher plants. *Environ. Exp. Bot.*, *32*, 83–100.

Barreto, P., Okura, V. K., Neshich, I. A., Maia, I., and Arruda, P. (2014). Overexpression of *UCP1* in tobacco induces mitochondrial biogenesis and amplifies a broad stress response. *BMC Plant Biol.*, *14*, 144.

Barreto, P., Yassitepe, J., Wilson, Z. A., and Arruda, P. (2017). Mitochondrial Uncoupling Protein 1 Overexpression Increases Yield in *Nicotiana tabacum* under Drought Stress by Improving Source and Sink Metabolism. *Front. Plant Sci.*, *8*, 1836.

Batth, R., Jain, M., Kumar, A., Nagar, P., Kumari, S., and Mustafiz, A. (2020). Zn^{2+} dependent glyoxalase I plays the major role in methylglyoxal detoxification and salinity stress tolerance in plants. *PLOS ONE*, *15*, e0233493.

Bazin, J., Mariappan, K., Jiang, Y., Blein, T., Voelz, R., Crespi, M., and Hirt, H. (2020). Role of MPK4 in pathogen-associated molecular pattern-triggered alternative splicing in *Arabidopsis*. *PLOS Pathog.*, *16*, e1008401.

Becana, M., Matamoros, M. A., Udvardi, M., and Dalton, D. A. (2010). Recent insights into antioxidant defenses of legume root nodules: Tansley review. *New Phytol.*, *188*, 960–976.

Begara-Morales, J. C., Sánchez-Calvo, B., Chaki, M., Valderrama, R., Mata-Pérez, C., Padilla, M. N., et al. (2016). Antioxidant Systems are Regulated by Nitric Oxide-Mediated Post-translational Modifications (NO-PTMs). *Front. Plant Sci.*, *7*, 152.

Bekešová, S., Komis, G., Křenek, P., Vyplelová, P., Ovečka, M., Luptovčiak, I., et al. (2015). Monitoring protein phosphorylation by acrylamide pendant Phos-Tag™ in various plants. *Front. Plant Sci., 6*, 336.

Benz, J. P., Stengel, A., Lintala, M., Lee, Y. H., Weber, A., Philippar, K., et al. (2009). Arabidopsis Tic62 and ferredoxin-NADP(H) oxidoreductase form light-regulated complexes that are integrated into the chloroplast redox poise. *Plant Cell, 21*, 3965–3983.

Berkholz, D. S., Faber, H. R., Savvides, S. N., and Karplus, P. A. (2008). Catalytic cycle of human glutathione reductase near 1A resolution. *J. Mol. Biol., 382*, 371–384.

Berna, A., and Bernier, F. (1999). Regulation by biotic and abiotic stress of a wheat germin gene encoding oxalate oxidase, a H_2O_2-producing enzyme. *Plant Mol. Biol., 39*, 539–549.

Bethke, G., Unthan, T., Uhrig, J. F., Poschl, Y., Gust, A. A., and Lee, J. (2009). Flg22 regulates the release of an ethylene response factor substrate from MAP kinase 6 in *Arabidopsis thaliana* via ethylene signaling. *Proc. Natl. Acad. Sci. U. S. A., 106*, 8067–8072.

Bheri, M., Mahiwal, S., Sanyal, S. K., and Pandey, G. K. (2020). Plant protein phosphatases: What do we know about their mechanism of action?. *FEBS J.*, 10.1111/febs.15454. Advance online publication.

Bi, G., Zhou, Z., Wang, W., Li, L., Rao, S., Wu, Y., et al. (2018). Receptor-Like Cytoplasmic Kinases Directly Link Diverse Pattern Recognition Receptors to the Activation of Mitogen-Activated Protein Kinase Cascades in Arabidopsis. *Plant Cell, 30*, 1543–1561.

Biondi, R. M., and Nebreda, A. R. (2003). Signalling specificity of Ser/Thr protein kinases through docking-site-mediated interactions. *Biochem. J., 372*, 1–13.

Birkenbihl, R. P., Jach, G., Saedler, H., and Huijser, P. (2005). Functional dissection of the plant-specific SBP-domain: overlap of the DNA-binding and nuclear localization domains. *J. Mol. Biol., 352,* 585–596.

Bleier, L., and Dröse, S. (2013). Superoxide generation by complex III: from mechanistic rationales to functional consequences. *Biochim. Biophys. Acta., 1827,* 1320–1331.

Bögre, L., Calderini, O., Binarova, P., Mattauch, M., Till, S., Kiegerl, S., et al. (1999). A MAP kinase is activated late in plant mitosis and becomes localized to the plane of cell division. *Plant Cell, 11,* 101–113.

Bögre, L., Ligterink, W., Heberle-Bors, E., and Hirt, H. (1996). Mechanosensors in plants. *Nature, 383,* 489–490.

Bögre, L., Ligterink, W., Meskiene, I., Barker, P. J., Heberle-Bors, E., Huskisson, N. S., and Hirt, H. (1997). Wounding Induces the Rapid and Transient Activation of a Specific MAP Kinase Pathway. *Plant Cell, 9*, 75–83.

Bowditch, M. L., and Donaldson, R. P. (1990). Ascorbate free-radical reduction by glyoxysomal membranes. *Plant Physiol., 94*, 531–537.

Bowler, C., van Camp, W., van Montagu, M., and Inze, D. (1994). Superoxide dismutase in plants. *Crit. Rev. Plant Sci., 13,* 199–198.

Burkhead, J. L., Reynolds, K. A., Abdel-Ghany, S. E., Cohu, C. M., and Pilon, M. (2009). Copper homeostasis. *New Phytol., 182,* 799–816.

Bykova, N. V., Egsgaard, H., and Møller, I. M. (2003). Identification of 14 new phosphoproteins involved in important plant mitochondrial processes. *FEBS Lett.*, *540*, 141–146.

Cai, C., Guo, W., and Zhang, B. (2018). Genome-wide identification and characterization of SPL transcription factor family and their evolution and expression profiling analysis in cotton. *Sci. Rep.*, *8*, 762.

Calderon-Villalobos, L. I., Kuhnle, C., Dohmann, E. M., Li, H., Bevan, M., and Schwechheimer, C. (2005). The evolutionarily conserved TOUGH protein is required for proper development of *Arabidopsis thaliana*. *Plant Cell*, *17*, 2473–2485.

Candas, D., Fan, M., Nantajit, D., Vaughan, A. T., Murley, J. S., Woloschak, et al. (2013). CyclinB1/Cdk1 phosphorylates mitochondrial antioxidant MnSOD in cell adaptive response to radiation stress. *J. Mol. Cell Biol.*, *5*, 166–175.

Cardinale, F., Jonak, C., Ligterink, W., Niehaus, K., Boller, T., and Hirt, H. (2000). Differential activation of four specific MAPK pathways by distinct elicitors. *J. Biol. Chem.*, *275*, 36734–36740.

Cardinale, F., Meskiene, I., Ouaked, F., and Hirt, H. (2002). Convergence and divergence of stress-induced mitogen-activated protein kinase signaling pathways at the level of two distinct mitogen-activated protein kinase kinases. *Plant Cell*, *14*, 703–711.

Cardon, G., Höhmann, S., Klein, J., Nettesheim, K., Saedler, H., and Huijser, P. (1999). Molecular characterisation of the Arabidopsis SBP-box genes. *Gene*, *237*, 91–104.

Carlsbecker, A., Lee, J. Y., Roberts, C. J., Dettmer, J., Lehesranta, S., Zhou, J., et al. (2010). Cell signalling by microRNA165/6 directs gene dose-dependent root cell fate. *Nature*, *465*, 316–321.

Carroll, A. J. (2013). The Arabidopsis Cytosolic Ribosomal Proteome: From form to Function. *Front. Plant Sci.*, *4*, 32.

Case, A. J. (2017). On the Origin of Superoxide Dismutase: An Evolutionary Perspective of Superoxide-Mediated Redox Signaling. *Antioxidants*, *6*, 82.

Chan, K. X., Phua, S. Y., Crisp, P., McQuinn, R., and Pogson, B. J. (2016). Learning the languages of the chloroplast: retrograde signaling and beyond. *Annu. Rev. Plant Biol.*, *67*, 25–53.

Chang, R., Jang, C. J., Branco-Price, C., Nghiem, P., and Bailey-Serres, J. (2012). Transient MPK6 activation in response to oxygen deprivation and reoxygenation is mediated by mitochondria and aids seedling survival in *Arabidopsis*. *Plant Mol. Biol.*, *78*, 109–122.

Chang, I. F., Szick-Miranda, K., Pan, S., and Bailey-Serres, J. (2005). Proteomic characterization of evolutionarily conserved and variable proteins of Arabidopsis cytosolic ribosomes. *Plant Physiol.*, *137*, 848–862.

Chao, L. M., Liu, Y. Q., Chen, D. Y., Xue, X. Y., Mao, Y. B., and Chen, X. Y. (2017): *Arabidopsis* Transcription Factors SPL1 and SPL12 Confer Plant Thermotolerance at Reproductive Stage. *Mol. Plant*, *10*, 735–748.

Chaouch, S., Queval, G., and Noctor, G. (2012). AtRbohF is a crucial modulator of defence-associated metabolism and a key actor in the interplay between intracellular oxidative stress and pathogenesis responses in Arabidopsis. *Plant J.*, *69*, 613–627.

Chen, Q., and Yang, G. (2020). Signal Function Studies of ROS, Especially RBOH-Dependent ROS, in Plant Growth, Development and Environmental Stress. *J. Plant Growth Regul., 39*, 157–171.

Chen, T., Zhou, B., Duan, L., Zhu, H., and Zhang, Z. (2017). MtMAPKK4 is an essential gene for growth and reproduction of *Medicago truncatula*. *Physiol. Plant., 159*, 492–503.

Chen, T., Zhu, H., Ke, D., Cai, K., Wang, C., Gou, H., et al. (2012). A MAP kinase kinase interacts with SymRK and regulates nodule organogenesis in *Lotus japonicus*. *Plant Cell, 24*, 823–838.

Cheng, C. Y., Krishnakumar, V., Chan, A. P., Thibaud-Nissen, F., Schobel, S., and Town, C. D. (2017). Araport11: a complete reannotation of the *Arabidopsis thaliana* reference genome. *Plant J.*, 89, 789–804.

Cheng, Z., Li, J. F., Niu, Y., Zhang, X. C., Woody, O. Z., Xiong, Y., et al. (2015). Pathogen-secreted proteases activate a novel plant immune pathway. *Nature, 521*, 213–216.

Cheng, N. H., Liu, J. Z., Nelson, R. S., and Hirschi, K. D. (2004). Characterization of CXIP4, a novel Arabidopsis protein that activates the H^+/Ca^{2+} antiporter, CAX1. *FEBS Lett., 559*, 99–106.

Choi, W. G., Toyota, M., Kim, S. H., Hilleary, R., and Gilroy, S. (2014). Saltstress-induced Ca^{2+} waves are associated with rapid, long-distance rootto-shoot signaling in plants. *Proc. Natl. Acad. Sci. U. S. A., 111*, 6497–6502.

Choudhary, A., Kumar, A., and Kaur, N. (2019). ROS and oxidative burst: Roots in plant development. *Plant Divers., 42*, 33–43.

Ciacka, K., Tymiński, M., Gniazdowska, A., and Krasuska, U. (2020). Carbonylation of proteins-an element of plant ageing. *Planta, 252*, 12.

Clough, S. J., and Bent, A. F. (1998). Floral dip: a simplified method for Agrobacterium-mediated transformation of *Arabidopsis thaliana*. *Plant J., 16*, 735–743.

Cohu, C. M., Abdel-Ghany, S. E., Gogolin Reynolds, K. A., Onofrio, A. M., Bodecker, J. R., Kimbrel, J. A., et al. (2009). Copper delivery by the copper chaperone for chloroplast and cytosolic copper/zinc-superoxide dismutases: regulation and unexpected phenotypes in an *Arabidopsis* mutant. *Mol. Plant, 2*, 1336–1350.

Colombatti, F., Gonzalez, D. H., and Welchen, E. (2014). Plant mitochondria under pathogen attack: a sigh of relief or a last breath?. *Mitochondrion, 19 Pt B*, 238–244.

Considine, M. J., and Foyer, C. H. (2020) Oxygen and reactive oxygen species-dependent regulation of plant growth and development. *Plant Physiol.*, kiaa077.

Corcoran, A., and Cotter, T. G. (2013). Redox regulation of protein kinases. *FEBS J., 280*, 1944–1965.

Csiszár, J., Brunner, S., Horváth, E., Bela, K., Ködmön, P., Riyazuddin, R., et al. (2018). Exogenously applied salicylic acid maintains redox homeostasis in salt-stressed Arabidopsis gr1 mutants expressing cytosolic roGFP1. *Plant Growth Regul., 86*, 181–194.

Cui, F., Brosché, M., Shapiguzov, A., He, X. Q., Vainonen, J. P., Leppälä, J., et al. (2019). Interaction of methyl viologen-induced chloroplast and mitochondrial signalling in *Arabidopsis*. *Free Radic. Biol. Med., 134*, 555–566.

Curie, C., Axelos, M., Bardet, C., Atanassova, R., Chaubet, N., and Lescure, B. (1993). Modular organization and development activity of an *Arabidopsis thaliana* EF-1 alpha gene promoter. *Mol. Gen. Genet.*, *238*, 428–436.

Dalle-Donne, I., Rossi, R., Giustarini, D., Milzani, A., and Colombo, R. (2003). Protein carbonyl groups as biomarkers of oxidative stress. *Clin. Chim. Acta*, *329*, 23–38.

Daneva, A., Gao, Z., Van Durme, M., and Nowack, M. K. (2016). Functions and Regulation of Programmed Cell Death in Plant Development. *Annu. Rev. Cell Dev. Biol.*, *32*, 441–468.

Danquah, A., de Zelicourt, A., Colcombet, J., and Hirt, H. (2014). The role of ABA and MAPK signaling pathways in plant abiotic stress responses. *Biotechnol. Adv.*, *32*, 40–52.

Daudi, A., Cheng, Z., O'Brien, J. A., Mammarella, N., Khan, S., Ausubel, F. M., and Bolwell, G. P. (2012). The apoplastic oxidative burst peroxidase in *Arabidopsis* is a major component of pattern-triggered immunity. *Plant Cell*, *24*, 275–287.

Davis, A. M., Hall, A., Millar, A. J., Darrah, C., and Davis, S. J. (2009). Protocol: Streamlined subprotocols for floral-dip transformation and selection of transformants in *Arabidopsis thaliana*. *Plant Methods*, *5*, 3.

Davletova, S., Rizhsky, L., Liang, H., Shengqiang, Z., Oliver, D. J., Coutu, J., et al. (2005). Cytosolic ascorbate peroxidase 1 is a central component of the reactive oxygen gene network of Arabidopsis. *Plant Cell*, *17*, 268–281.

De Pinto, M. C., Locato, V., and De Gara, L. (2012). Redox regulation in plant programmed cell death: redox regulation in plant PCD. *Plant Cell Environ.*, *35*, 234–244.

De Simone, A., Hubbard, R., de la Torre, N. V., Velappan, Y., Wilson, M., Considine, M. J., et al. (2017). Redox changes during the cell cycle in the embryonic meristem of *Arabidopsis thaliana*. *Antioxid. Redox Signal*, 27, 1505–1519.

Del Río, L. A., and López-Huertas, E. (2016). ROS Generation in Peroxisomes and its Role in Cell Signaling. *Cell Physiol.*, *57*, 1364–1376.

Delledonne, M., Zeier, J., Marocco, A., and Lamb, C. (2001). Signal interactions between nitric oxide and reactive oxygen intermediates in the plant hypersensitive disease resistance response. *Proc. Natl. Acad. Sci. U. S. A.*, *98*, 13454–13459.

DePaoli, H. C., Dornelas, M. C., and Goldman, M. (2014). SCI1 is a component of the auxin-dependent control of cell proliferation in Arabidopsis upper pistil. *Plant Sci.*, *229*, 122–130.

Dhanasekaran, D. N., Kashef, K., Lee, C. M., Xu H., and Reddy, E. P. (2007). Scaffold proteins of MAP-kinase modules. *Oncogene*, *26*, 3185–3202.

Diao, Y., Liu, W., Wong, C. C. L., Wang, X., Lee, K., Cheung, P. Y., et al. (2010). Oxidation-induced intramolecular disulfide bond inactivates mitogenactivated protein kinase 6 by inhibiting ATP binding. *Proc. Natl. Acad. Sci. U. S. A.*, *107*, 20974–20979.

Diaz-Vivancos, P., De Simone, A., Kiddle, G. and Foyer, C. H. (2015). Glutathione- linking cell proliferation to oxidative stress. *Free Radic. Biol. Med*., *89*, 1154–1104.

Dietz, K. J. (2011). Peroxiredoxins in plants and cyanobacteria. *Antioxid. Redox Signal.*, *15*, 1129–1159.

Ding, H., Wang, B., Han, Y., and Li, S. (2020). The pivotal function of dehydroascorbate reductase in glutathione homeostasis in plants. *J. Exp. Bot.*, *71*, 3405–3416.

Dóczi, R., and Bögre, L. (2018). The Quest for MAP Kinase Substrates: Gaining Momentum. *Trends Plant Sci*., *23*, 918–932.

Dóczi, R., Brader, G., Pettkó-Szandtner, A., Rajh, I., Djamei, A., Pitzschke, A., et al. (2007). The Arabidopsis mitogen-activated protein kinase kinase MKK3 is upstream of group C mitogen-activated protein kinases and participates in pathogen signaling. *Plant Cell*, *19*, 3266–3279.

Downie, J. A. (2010). The roles of extracellular proteins, polysaccharides and signals in the interactions of rhizobia with legume roots. *FEMS Microbiol. Rev.*, *34*, 150–170.

Dreyer, B. H., and Schippers, J. H. M. (2019). Copper-zinc superoxide dismutases in plants: Evolution, enzymatic properties, and beyond. *Annu. plant rev. online*, *3*, 933–968.

Du, Y. Y., Wang, P. C., Chen, J., and Song, C. P. (2008). Comprehensive functional analysis of the catalase gene family in *Arabidopsis thaliana*. *J. Integr. Plant Biol.*, *50*, 1318–1326.

Duan, Q., Kita, D., Johnson, E. A., Aggarwal, M., Gates, L., Wu, H. M., and Cheung, A. Y. (2014). Reactive oxygen species mediate pollen tube rupture to release sperm for fertilization in Arabidopsis. *Nat. Commun.*, 5, 3129.

Dugas, D. V., and Bartel, B. (2008). Sucrose induction of *Arabidopsis* miR398 represses two Cu/Zn superoxide dismutases. *Plant Mol. Biol.*, *67*, 403–417.

Dunand, C., Crèvecoeur, M., and Penel, C. (2007). Distribution of superoxide and hydrogen peroxide in *Arabidopsis* root and their influence on root development: Possible interaction with peroxidases. *New Phytol.*, *174*, 332–341.

Dvořák, P., Krasylenko, Y., Ovečka, M., Basheer, J., Zapletalová, V., Šamaj, J., and Takáč, T. (2021). *In vivo* light-sheet microscopy resolves localisation patterns of FSD1, a superoxide dismutase with function in root development and osmoprotection. *Plant Cell Environ.*, *44*, 68–87.

Eastmond, P. J. (2007). *MONODEHYROASCORBATE REDUCTASE4* is required for seed storage oil hydrolysis and postgerminative growth in *Arabidopsis*. *Plant Cell*, *19*, 1376–1387.

Ellinger, D., and Voigt, C. A. (2014). Callose biosynthesis in Arabidopsis with a focus on pathogen response: what we have learned within the last decade. *Ann. Bot.*, *114*, 1349–1358.

Eltayeb, A. E., Kawano, N., Badawi, G. H., Kaminaka, H., Sanekata, T., Shibahara, T., et al. (2007). Overexpression of monodehydroascorbate reductase in transgenic tobacco confers enhanced tolerance to ozone, salt and polyethylene glycol stresses. *Planta*, *225*, 1255–1264.

Eltayeb, A. E., Yamamoto, S., Habora, M. E. E., Yin, L., Tsujimoto, H., and Tanaka, K. (2011). Transgenic potato overexpressing Arabidopsis cytosolic *AtDHAR1* showed higher tolerance to herbicide, drought and salt stresses. *Breed. Sci*., *61*, 3–10.

Erickson, J. L., Kantek, M., and Schattat, M. H. (2017). Plastid-nucleus distance alters the behavior of stromules. *Front. Plant Sci*., *8*, 1135.

Esch, L., and Schaffrath, U. (2017). An Update on Jacalin-Like Lectins and Their Role in Plant Defense. *Int. J. Mol. Sci.*, *18*, 1592.

Estavillo, G. M., Crisp, P. A., Pornsiriwong, W., Wirtz, M., Collinge, D., Carrie, C., et al. (2011). Evidence for a SAL1-PAP chloroplast retrograde pathway that functions in drought and high light signaling in *Arabidopsis*. *Plant Cell*, *23*, 3992–4012.

Eubel, H., Meyer, E. H., Taylor, N. L., Bussell, J. D., O'Toole, N., Heazlewood, J. L., et al. (2008). Novel proteins, putative membrane transporters, and an integrated metabolic network are revealed by quantitative proteomic analysis of Arabidopsis cell culture peroxisomes. *Plant Physiol.*, *148*, 1809–1829.

Evrard, A., Kumar, M., Lecourieux, D., Lucks, J., von Koskull-Döring, P., and Hirt, H. (2013). Regulation of the heat stress response in Arabidopsis by MPK6-targeted phosphorylation of the heat stress factor HsfA2. *PeerJ*, *1*, e59.

Fåhreus, G. (1957). The infection of clover root hairs by nodule bacteria studied by a simple glass slide technique. *J. Gen. Microbiol.*, *16*, 374–381.

Farnese, F. S., Menezes-Silva, P. E., Gusman, G. S., and Oliveira, J. A. (2016). When bad guys become good ones: the key role of reactive oxygen species and nitric oxide in the plant responses to abiotic stress. *Front. Plant Sci.*, *7*, 471.

Farooq, M. A., Niazi, A. K., Akhtar, J., Saifullah, Farooq, M., Souri, Z., et al. (2019). Acquiring control: The evolution of ROS-Induced oxidative stress and redox signaling pathways in plant stress responses. *Plant Physiol. Biochem.*, *141*, 353–369.

Fay, J. M., Zhu, C., Proctor, E. A., Tao, Y., Cui, W., Ke, H., et al. (2016). A phosphomimetic mutation stabilizes SOD1 and rescues cell viability in the context of an ALS-associated mutation. *Structure*, *24*, 1898–1906.

Fehér, A., Otvös, K., Pasternak, T. P., and Szandtner, A. P. (2008). The involvement of reactive oxygen species (ROS) in the cell cycle activation (G0-to-G1 transition) of plant cells. *Plant Signal. Behav.*, *3*, 823–826.

Fernandes, N., and Allbritton, N. L. (2009). Effect of the DEF motif on phosphorylation of peptide substrates by ERK. *Biochem. Biophys. Res. Commun.*, *387*, 414–418.

Fernández-Pérez, F., Pomar, F., Pedreño, M. A., and Novo-Uzal, E. (2015). Suppression of Arabidopsis peroxidase 72 alters cell wall and phenylpropanoid metabolism. *Plant Sci.*, *239*, 192–199.

Fichman, Y., Miller, G., and Mittler, R. (2019). Whole-Plant Live Imaging of Reactive Oxygen Species. *Mol. Plant*, *12*, 1203–1210.

Fichman, Y., and Mittler, R. (2020). Rapid systemic signaling during abiotic and biotic stresses: is the ROS wave master of all trades?. *Plant J.*, *102*, 887–896.

Fischer, B. B., Hideg, É., and Krieger-Liszkay, A. (2013). Production, detection, and signaling of singlet oxygen in photosynthetic organisms. *Antioxid. Redox Signal.*, *18*, 2145–2162.

Flajoulot, S., Ronfort, J., Baudouin, P., Barre, P., Huguet, T., Huyghe, C., et al. (2005). Genetic diversity among alfalfa (*Medicago sativa*) cultivars coming from a breeding program, using SSR markers. *Theor. Appl. Genet.*, *111*, 1420–1429.

Flügel, F., Timm, S., Arrivault, S., Florian, A., Stitt, M., Fernie, A. R., and Bauwe, H. (2017). The Photorespiratory Metabolite 2-Phosphoglycolate Regulates Photosynthesis and Starch Accumulation in Arabidopsis. *Plant Cell*, *29*, 2537–2551.

Foreman, J., Demidchik, V., Bothwell, J. H., Mylona, P., Miedema, H., Torres, M. A., et al. (2003). Reactive oxygen species produced by NADPH oxidase regulate plant cell growth. *Nature*, *422*, 442–446.

Foyer, C. H., and Noctor, G. (2003). Redox sensing and signalling associated with reactive oxygen produced in chloroplasts, peroxisomes, and mitochondria. *Physiol. Plant*, *119*, 355–364.

Foyer, C. H., and Noctor, G. (2005). Oxidant and antioxidant signalling in plants: a re-evaluation of the concept of oxidative stress in a physiological context. *Plant Cell Environ.*, *28*, 1056–1071.

Foyer, C. H., and Noctor, G. (2011). Ascorbate and glutathione: the heart of the redox hub. *Plant Physiol.*, *155*, 2–18.

Foyer, C. H., and Noctor, G. (2020). Redox homeostasis and signaling in a higher-CO_2 world. *Annu. Rev. Plant Biol.*, *71*, 157–182.

Frei dit Frey, N., Garcia, A. V., Bigeard, J., Zaag, R., Bueso, E., Garmier, M., et al. (2014). Functional analysis of Arabidopsis immune-related MAPKs uncovers a role for MPK3 as negative regulator of inducible defences. *Genome Biol.*, *15*, R87.

Fridovich, I. (1978). Superoxide radicals, superoxide dismutases and the aerobic lifestyle. *Photochem. Photobiol.*, *28*, 733–741.

Friso, G., Giacomelli, L., Ytterberg, A. J., Peltier, J. B., Rudella, A., Sun, Q., and Wijk, K. J. (2004). In-depth analysis of the thylakoid membrane proteome of *Arabidopsis thaliana* chloroplasts: new proteins, new functions, and a plastid proteome database. *Plant Cell*, *16*, 478–499.

Frugoli, J. A., Zhong, H. H., Nuccio, M. L., McCourt, P., McPeek, M. A., Thomas, T. L., et al. (1996). Catalase is encoded by a multigene family in *Arabidopsis thaliana* (L.) Heynh. *Plant Physiol.*, *112*, 327–336.

Frye, C. A., Tang, D., and Innes, R. W. (2001). Negative regulation of defense responses in plants by a conserved MAPKK kinase. *Proc. Natl. Acad. Sci. U. S. A.*, *98*, 373–378.

Gąciarz, A., Khatri, N. K., Velez-Suberbie, M. L., Saaranen, M. J., Uchida, Y., Keshavarz-Moore, E., and Ruddock, L. W. (2017). Efficient soluble expression of disulfide bonded proteins in the cytoplasm of *Escherichia coli* in fed-batch fermentations on chemically defined minimal media. *Microb. Cell Fact.*, *16*, 108.

Gallie, D. R., and Chen, Z. (2019). Chloroplast-localized iron superoxide dismutases FSD2 and FSD3 are functionally distinct in Arabidopsis. *PLOS ONE*, *14*, e0220078.

Gao, M., Liu, J., Bi, D., Zhang, Z., Cheng, F., Chen, S., and Zhang, Y. (2008). MEKK1, MKK1/MKK2 and MPK4 function together in a mitogen-activated protein kinase cascade to regulate innate immunity in plants. *Cell Res.*, *18*, 1190–1198.

Gao, J., Wang, Y., Cai, M., Pan, Y., Xu, H., Jiang, J., et al. (2015). Mechanistic insights into EGFR membrane clustering revealed by super-resolution imaging. *Nanoscale*, *7*, 2511–2519.

Garcia-Molina, A., Xing, S., and Huijser, P. (2014). Functional characterisation of *Arabidopsis* SPL7 conserved protein domains suggests novel regulatory mechanisms in the Cu deficiency response. *BMC Plant Biol.*, *14*, 231.

Gaupels, F., Durner, J., and Kogel, K. H. (2017). Production, amplification and systemic propagation of redox messengers in plants? The phloem can do it all! *New Phytol.*, *214*, 554–560.

Gawroński, P., Witoń, D., Vashutina, K., Bederska, M., Betliński, B., Rusaczonek, A., et al. (2014). Mitogen-Activated Protein Kinase 4 is a salicylic acid-independent regulator of growth but not of photosynthesis in *Arabidopsis*. *Mol. Plant*, *7*, 1151–1166.

Gayomba, S. R., Jung, H. I., Yan, J., Danku, J., Rutzke, M. A., Bernal, M., et al. (2013). The CTR/COPT-dependent copper uptake and SPL7-dependent copper deficiency responses are required for basal cadmium tolerance in *A. thaliana*. *Metallomics*, *5*, 1262–1275.

Geng, Y., Wu, R., Wee, C. W., Xie, F., Wei, X., Chan, P. M. Y., et al. (2013). A spatio-temporal understanding of growth regulation during the salt stress response in Arabidopsis. *Plant Cell*, *25*, 2132–2154.

Gietl, C. (1992). Malate dehydrogenase isoenzymes: cellular locations and role in the flow of metabolites between the cytoplasm and cell organelles. *Biochim. Biophys. Acta*, *1100*, 217–234.

Gilroy, S., Białasek, M., Suzuki, N., Górecka, M., Devireddy, A. R., Karpiński, S., and Mittler, R. (2016). ROS, Calcium, and Electric Signals: Key Mediators of Rapid Systemic Signaling in Plants. *Plant Physiol.*, *171*, 1606–1615.

Giraud, E., Ho, L. H., Clifton, R., Carroll, A., Estavillo, G., Tan, Y. F., et al. (2008). The absence of ALTERNATIVE OXIDASE1a in Arabidopsis results in acute sensitivity to combined light and drought stress. *Plant Physiol.*, *147*, 595–610.

Gómez-Gómez, L., and Boller, T. (2000). FLS2: an LRR receptor-like kinase involved in the perception of the bacterial elicitor flagellin in Arabidopsis. *Mol. Cell.*, *5*, 1003–1011.

Good, M. C., Zalatan, J. G., and Lim, W. A. (2011). Scaffold proteins: hubs for controlling the flow of cellular information. *Science*, *332*, 680–686.

Gramegna, G., Modesti, V., Savatin, D. V., Sicilia, F., Cervone, F., and De Lorenzo, G. (2016). *GRP-3* and *KAPP*, encoding interactors of WAK1, negatively affect defense responses induced by oligogalacturonides and local response to wounding. *J. Exp. Bot.*, *67*, 1715–1729.

Granlund, I., Storm, P., Schubert, M., García-Cerdán, J. G., Funk, C., and Schröder, W. P. (2009). The TL29 protein is lumen located, associated with PSII and not an ascorbate peroxidase. *Plant Cell Physiol.*, *50*, 1898–1910.

Guan, Q., Liao, X., He, M., Li, X., Wang, Z., Ma, H., et al. (2017). Tolerance analysis of chloroplast OsCu/Zn-SOD overexpressing rice under NaCl and $NaHCO_3$ stress. *PLOS ONE*, *12*, e0186052.

Guan, Q., Wu, J., Zhang, Y., Jiang, C., Liu, R., Chai, C., and Zhu, J. (2013). A DEAD box RNA helicase is critical for pre-mRNA splicing, cold-responsive gene regulation, and cold tolerance in *Arabidopsis*. *Plant Cell*, *25*, 342–356.

Gudesblat, G. E., Iusem, N. D., and Morris, P. C. (2007). Guard cell-specific inhibition of *Arabidopsis MPK3* expression causes abnormal stomatal responses to abscisic acid and hydrogen peroxide. *New Phytol.*, *173*, 713–721.

Guo, B., Liu, C., Li, H., Yi, K., Ding, N., Li, N., et al. (2016). Endogenous salicylic acid is required for promoting cadmium tolerance of Arabidopsis by modulating glutathione metabolisms. *J. Hazard. Mater.*, *316*, 77–86.

Guo, A. Y., Zhu, Q. H., Gu, X., Ge, S., Yang, J., and Luo, J. (2008). Genome-wide identification and evolutionary analysis of the plant specific SBP-box transcription factor family. *Gene*, *418*, 1–8.

Gupta, A. S., Heinen, J. L., Holaday, A. S., Burke, J. J., and Allen, R. D. (1993). Increased resistance to oxidative stress in transgenic plants that overexpress chloroplastic Cu/Zn superoxide dismutase. Proc. *Natl. Acad. Sci. U. S .A.*, *90*, 1629–1633.

Han, S., Fang, L., Ren, X., Wang, W., and Jiang, J. (2015). MPK6 controls H_2O_2-induced root elongation by mediating Ca^{2+} influx across the plasma membrane of root cells in *Arabidopsis* seedlings. *New Phytol.*, *205*, 695–706.

Haney, C. H., Riely, B. K., Tricoli, D. M., Cook, D. R., Ehrhardt, D. W., and Long, S. R. (2011). Symbiotic rhizobia bacteria trigger a change in localization and dynamics of the *Medicago truncatula* receptor kinase LYK3. *Plant Cell*, *23*, 2774–2787.

Hanke, G. T., Okutani, S., Satomi, Y., Takao, T., Suzuki, A., and Hase, T. (2005). Multiple iso-proteins of FNR in Arabidopsis: evidence for different contributions to chloroplast function and nitrogen assimilation. *Plant Cell Environ.*, *28*, 1146–1157.

Hanson, M. R., and Conklin, P. L. (2020). Stromules, functional extensions of plastids within the plant cell. *Curr. Opin. Plant Biol.*, *58*, 25–32.

Hao, H., Fan, L., Chen, T., Li, R., Li, X., He, Q., et al. (2014). Clathrin and membrane microdomains cooperatively regulate RbohD dynamics and activity in *Arabidopsis*. *Plant Cell*, *26*, 1729–1745.

Hara, M., Kondo, M., and Kato, T. (2013). A KS-type dehydrin and its related domains reduce Cu-promoted radical generation and the histidine residues contribute to the radical-reducing activities. *J. Exp. Bot.*, *64*, 1615–1624.

Hayashi, K., Nakamura, S., Fukunaga, S., Nishimura, T., Jenness, M. K., Murphy, A. S., et al. (2014). Auxin transport sites are visualized in planta using fluorescent auxin analogs. *Proc. Natl. Acad. Sci. U. S. A.*, *111*, 11557–11562.

He, J., Duan, Y., Hua, D., Fan, G., Wang, L., Liu, Y., et al. (2012). DEXH box RNA helicase-mediated mitochondrial reactive oxygen species production in *Arabidopsis* mediates crosstalk between abscisic acid and auxin signaling. *Plant Cell*, *24*, 1815–1833.

He, Y., Zhou, J., Shan, L., and Meng, X. (2018). Plant cell surface receptor-mediated signaling – a common theme amid diversity. *J. Cell Sci.*, *131*, jcs209353.

Heard, W., Sklenář, J., Tomé, D. F., Robatzek, S., and Jones, A. M. (2015). Identification of Regulatory and Cargo Proteins of Endosomal and Secretory Pathways in *Arabidopsis thaliana* by Proteomic Dissection. *Mol. Cell. Proteom.*, *14*, 1796–1813.

Hehl, R., Norval, L., Romanov, A., and Bülow, L. (2016). Boosting AthaMapdatabase content with data from protein binding microarrays. *Plant Cell Physiol.*, 57, e4.

Helariutta, Y., Fukaki, H., Wysocka-Diller, J., Nakajima, K., Jung, J., Sena, G., et al. (2000). The *SHORT-ROOT* gene controls radial patterning of the *Arabidopsis* root through radial signaling. *Cell*, *101*, 555–567.

Hernando, C. E., García Hourquet, M., de Leone, M. J., Careno, D., Iserte, J., Mora Garcia, S., and Yanovsky, M. J. (2019). A role for pre-mRNA-PROCESSING PROTEIN 40C in the control of growth, development, and stress tolerance in *Arabidopsis thaliana*. *Front. Plant Sci.*, *10*, 1019.

Holzmeister, C., Gaupels, F., Geerlof, A., Sarioglu, H., Sattler, M., Durner, J., and Lindermayr, C. (2015). Differential inhibition of Arabidopsis superoxide dismutases by peroxynitrite-mediated tyrosine nitration. *J. Exp. Bot.*, *66*, 989–999.

Horváth, E., Bela, K., Holinka, B., Riyazuddin, R., Gallé, Á., Hajnal, Á., et al. (2019). The *Arabidopsis* glutathione transferases, AtGSTF8 and AtGSTU19 are involved in the maintenance of root redox homeostasis affecting meristem size and salt stress sensitivity. *Plant Sci.*, *283*, 366–374.

Hou, X., Fu, A., Garcia, V. J., Buchanan, B. B., and Luan, S. (2015). PSB27: A thylakoid protein enabling Arabidopsis to adapt to changing light intensity. *Proc. Natl. Acad. Sci. U. S. A.*, *112*, 1613–1618.

Hrbáčková, M., Luptovčiak, I., Hlaváčková, K., Dvořák, P., Tichá, M., Šamajová, O., et al. (2020). Overexpression of alfalfa SIMK promotes root hair growth, nodule clustering and shoot biomass production. *Plant Biotechnol J.*, 1–18. doi: 10.1111/pbi.13503.

Hsu, S. F., Lai, H. C., and Jinn, T. L. (2010). Cytosol-Localized Heat Shock Factor-Binding Protein, AtHSBP, Functions as a Negative Regulator of Heat Shock Response by Translocation to the Nucleus and Is Required for Seed Development in Arabidopsis. *Plant Physiol.*, *153*, 773–784.

Hu, J., Huang, X., Chen, L., Sun, X., Lu, C., Zhang, L., et al. (2015). Site-specific nitrosoproteomic identification of endogenously *S*-nitrosylated proteins in Arabidopsis. *Plant Physiol.*, *167*, 1731–1746.

Hu, C. H., Wang, P. Q., Zhang, P. P., Nie, X. M., Li, B. B., Tai, L., et al. (2020). NADPH Oxidases: The Vital Performers and Center Hubs during Plant Growth and Signaling. *Cells*, *9*, 437.

Huang, C. H., Kuo, W. Y., Weiss, C., and Jinn, T. L. (2012). Copper chaperone-dependent and -independent activation of three copper-zinc superoxide dismutase homologs localized in different cellular compartments in Arabidopsis. *Plant Physiol.*, *158*, 737–746.

Huang, L. M., Lai, C. P., Chen, L. O., Chan, M. T., and Shaw, J. F. (2015). Arabidopsis SFAR4 is a novel GDSL-type esterase involved in fatty acid degradation and glucose tolerance. *Bot. Stud.*, *56*, 33.

Huang, S., Van Aken, O., Schwarzländer, M., Belt, K., and Millar, A. H. (2016). The Roles of Mitochondrial Reactive Oxygen Species in Cellular Signaling and Stress Response in Plants. *Plant Physiol.*, *171*, 1551–1559.

Huang, W., Yang, Y. J., and Zhang, S. B. (2019). The role of water-water cycle in regulating the redox state of photosystem I under fluctuating light. *Biochim. Biophys. Acta*, *1860*, 383–390.

Huang, Y., Yin, C., Liu, J., Feng, B., Ge, D., Kong, L., et al. (2020). A trimeric CrRLK1L-LLG1 complex genetically modulates SUMM2-mediated autoimmunity. *Nat. Commun.*, *11*, 4859.

Huber, S. C. (2007). Exploring the role of protein phosphorylation in plants: from signalling to metabolism. *Biochem. Soc. Trans.*, *35*, 28–32.

Hülskamp, M. (2004). Plant trichomes: a model for cell differentiation. *Nat. Rev. Mol. Cell Biol.*, *5*, 471–480.

Hultquist, J. F., and Dorweiler, J. E. (2008). Feminized tassels of maize *mop1* and *ts1* mutants exhibit altered levels of miR156 and specific SBP-box genes. *Planta*, *229*, 99–113.

Hunter, K., Kimura, S., Rokka, A., Tran, H. C., Toyota, M., Kukkonen, J. P., and Wrzaczek, M. (2019). CRK2 Enhances Salt Tolerance by Regulating Callose Deposition in Connection with PLDα1. *Plant Physiol.*, *180*, 2004–2021.

Ichimura, K., Casais, C., Peck, S. C., Shinozaki, K., and Shirasu, K. (2006). MEKK1 is required for MPK4 activation and regulates tissue-specific and temperature-dependent cell death in *Arabidopsis*. *J. Biol. Chem.*, *281*, 36969–36976.

Ichimura, K., et MAPK Group (2002). Mitogen-activated protein kinase cascades in plants: a new nomenclature. *Trends Plant Sci.*, *7*, 301–308.

Ichimura, K., Mizoguchi, T., Yoshida, R., Yuasa, T., and Shinozaki, K. (2000) Protein phosphorylation and dephosphorylation in environmental stress responses in plants. *Adv. Bot. Res.*, *32*, 355–377.

Jain, A., Wilson, G. T., and Connolly, E. L. (2014). The diverse roles of FRO family metalloreductases in iron and copper homeostasis. *Front. Plant Sci.*, *5*, 100

Jammes, F., Song, C., Shin, D., Munemasa, S., Takeda, K., Gu, D., et al. (2009). MAP kinases MPK9 and MPK12 are preferentially expressed in guard cells and positively regulate ROS-mediated ABA signaling. *Proc. Natl. Acad. Sci. U. S. A.*, *106*, 20520–20525.

Janczarek, M., Rachwał, K., Marzec, A., Grządziel, J., and Palusińska-Szysz, M. (2015). Signal molecules and cell-surface components involved in early stages of the legume–rhizobium interactions. *Appl. Soil Ecol.*, *85*, 94–113.

Jang, Y. H., Park, H. Y., Lee, K. C., Thu, M. P., Kim, S. K., Suh, M. C., et al. (2014). A homolog of splicing factor SF1 is essential for development and is involved in the alternative splicing of pre-mRNA in *Arabidopsis thaliana*. *Plant J.*, *78*, 591–603.

Jia, R. Z., Wang, E. T., Liu, J. H., Li, Y., Gu, J., Yuan, H. L., and Chen, W. X. (2013). Effectiveness of different Ensifermeliloti strain-alfalfa cultivar combinations and their influence on nodulation of native rhizobia. *Soil Biol. Biochem.*, *57*, 960–963.

Jiang, K. (2003). Quiescent center formation in maize roots is associated with an auxin-regulated oxidizing environment. *Development*, *130*, 1429–1438.

Jin, C., Qin, L., Shi, Y., Candas, D., Fan, M., Lu, C. L., et al. (2015). CDK4-mediated MnSOD activation and mitochondrial homeostasis in radioadaptive protection. *Free Radic. Biol. Med.*, *81*, 77–87.

Jonak, C., Kiegerl, S., Ligterink, W., Barker, P. J., Huskisson, N. S., and Hirt, H. (1996). Stress signaling in plants: a mitogen-activated protein kinase pathway is activated by cold and drought. *Proc. Natl. Acad. Sci. U. S. A.*, *93*, 11274–11279.

Jonak, C., Ligterink, W., and Hirt, H. (1999). MAP kinases in plant signal transduction. *Cell. Mol. Life Sci.*, *55*, 204–213.

Jonak, C., Nakagami, H., and Hirt, H. (2004). Heavy metal stress. Activation of distinct mitogen-activated protein kinase pathways by copper and cadmium. *Plant Physiol.*, *136*, 3276–3283.

Joo, J. H., Bae, Y. S., and Lee, J. S. (2001). Role of auxin-induced reactive oxygen species in root gravitropism. *Plant Physiol.*, *126*, 1055–1060.

Joo, J. H., Yoo, H. J., Hwang, I., Lee, J. S., Nam, K. H., and Bae, Y. S. (2005). Auxin-induced reactive oxygen species production requires the activation of phosphatidylinositol 3-kinase. *FEBS Lett.*, *579*, 1243–1248.

Jorgensen, S. A., and Preston, J. C. (2014). Differential *SPL* gene expression patterns reveal candidate genes underlying flowering time and architectural differences in *Mimulus* and *Arabidopsis*. *Mol. Phylogenet. Evol.*, *73*, 129–139.

Jung, H. I., Gayomba, S. R., Rutzke, M. A., Craft, E., Kochian, L. V., and Vatamaniuk, O. K. (2012). COPT6 is a plasma membrane transporter that functions in copper homeostasis in

Arabidopsis and is a novel target of *SQUAMOSA* promoter-binding protein-like 7. *J. Biol. Chem.*, *287*, 33252–33267.

Jung, C. G., Hwang, S. G., Park, Y. C., Park, H. M., Kim, D. S., Park, D. H., and Jang, C. S. (2015). Molecular characterization of the cold- and heat-induced Arabidopsis PXL1 gene and its potential role in transduction pathways under temperature fluctuations. *J. Plant Physiol.*, *176*, 138–146.

Kang, C. H., Feng, Y., Vikram, M., Jeong, I. S., Lee, J. R., Bahk, J. D., et al. (2009). *Arabidopsis thaliana* PRP40s are RNA polymerase II C-terminal domain-associating proteins. *Arch. Biochem. Biophys.*, *484*, 30–38.

Kang, Z., Qin, T., and Zhao, Z. (2019). Thioredoxins and thioredoxin reductase in chloroplasts: A review. *Gene*, *706*, 32–42.

Kang, S., Yang, F., Li, L., Chen, H., Chen, S., and Zhang, J. (2015). The Arabidopsis transcription factor BRASSINOSTEROID INSENSITIVE1-ETHYL METHANESULFONATE-SUPPRESSOR1 is a direct substrate of MITOGEN-ACTIVATED PROTEIN KINASE6 and regulates immunity. *Plant Physiol.*, *167*, 1076–1086.

Kangasjärvi, S., Lepistö, A., Hännikäinen, K., Piippo, M., Luomala, E. M., Aro, E. M., et al. (2008). Diverse roles for chloroplast stromal and thylakoid-bound ascorbate peroxidases in plant stress responses. *Biochem. J.*, *412*, 275–285.

Kärkönen, A., and Kuchitsu, K. (2015). Reactive oxygen species in cell wall metabolism and development in plants. *Phytochemistry*, *112*, 22–32.

Karpinski, S., Escobar, C., Karpinska, B., Creissen, G., and Mullineaux, P. M. (1997). Photosynthetic electron transport regulates the expression of cytosolic ascorbate peroxidase genes in Arabidopsis during excess light stress. *Plant Cell*, *9*, 627–640.

Karpinski, S., Reynolds, H., Karpinska, B., Wingsle, G., Creissen, G., and Mullineaux, P. (1999). Systemic signaling and acclimation in response to excess excitation energy in Arabidopsis. *Science*, *284*, 654–657.

Kataya, A. R., and Reumann, S. (2010). Arabidopsis glutathione reductase 1 is dually targeted to peroxisomes and the cytosol. *Plant Signal. Behav.*, *5*, 171–175.

Kaur, N., and Hu, J. (2011). Defining the plant peroxisomal proteome: from Arabidopsis to rice. *Front. Plant Sci.*, *2*, 103.

Kaur, H., Peel, A., Acosta, K., Gebril, S., Ortega, J. L., and Sengupta-Gopalan, C. (2019). Comparison of alfalfa plants overexpressing glutamine synthetase with those overexpressing sucrose phosphate synthase demonstrates a signaling mechanism integrating carbon and nitrogen metabolism between the leaves and nodules. *Plant Direct*, *3*, e00115.

Kaur, C., Tripathi, A. K., Nutan, K. K., Sharma, S., Ghosh, A., Tripathi, J. K., et al. (2017). A nuclear-localized rice glyoxalase I enzyme, OsGLYI-8, functions in the detoxification of methylglyoxal in the nucleus. *Plant J.*, *89*, 565–576.

Kaur, C., Vishnoi, A., Ariyadasa, T. U., Bhattacharya, A., Singla-Pareek, S. L., and Sopory, S. K. (2013). Episodes of horizontal gene-transfer and gene-fusion led to co-existence of different metal-ion specific glyoxalase I. *Sci. Rep.*, *3*, 3076.

Kawachi, M., Kobae, Y., Mori, H., Tomioka, R., Lee, Y., and Maeshima, M. (2009). A mutant strain *Arabidopsis thaliana* that lacks vacuolar membrane zinc transporter MTP1 revealed the latent tolerance to excessive zinc. *Plant Cell Physiol.*, *50*, 1156–1170.

Keegstra, K. (2010). Plant cell walls. *Plant Physiol.*, *154*, 483–486.

Kerchev, P., Waszczak, C., Lewandowska, A., Willems, P., Shapiguzov, A., Li, Z., et al. (2016). Lack of GLYCOLATE OXIDASE1, but not GLYCOLATE OXIDASE2, attenuates the photorespiratory phenotype of CATALASE2-deficient Arabidopsis. *Plant Physiol.*, *171*, 1704–1719.

Kiegerl, S., Cardinale, F., Siligan, C., Gross, A., Baudouin, E., Liwosz, A., et al. (2000). SIMKK, a mitogen-activated protein kinase (MAPK) kinase, is a specific activator of the salt stress-induced MAPK, SIMK. *Plant Cell*, *12*, 2247–2258.

Kim, S. H., Oikawa, T., Kyozuka, J., Wong, H. L., Umemura, K., Kishi-Kaboshi, M., et al. (2012a). The bHLH Rac Immunity1 (RAI1) Is Activated by OsRac1 via OsMAPK3 and OsMAPK6 in Rice Immunity. *Plant Cell Physiol.*, *53*, 740–754.

Kim, J. M., Woo, D. H., Kim, S. H., Lee, S. Y., Park, H. Y., Seok, H. Y., et al. (2012b). Arabidopsis MKKK20 is involved in osmotic stress response via regulation of MPK6 activity. *Plant Cell Rep.*, *31*, 217–224.

Kimura, S., Kaya, H., Kawarazaki, T., Hiraoka, G., Senzaki, E., Michikawa, M., and Kuchitsu, K. (2012). Protein phosphorylation is a prerequisite for the Ca^{2+}-dependent activation of Arabidopsis NADPH oxidases and may function as a trigger for the positive feedback regulation of Ca^{2+} and reactive oxygen species. *Biochim. Biophys. Acta.*, *1823*, 398–405.

Kimura, S., Waszczak, C., Hunter, K., and Wrzaczek, M. (2017). Bound by Fate: The Role of Reactive Oxygen Species in Receptor-Like Kinase Signaling. *Plant Cell*, *29*, 638–654.

Kliebenstein, D. J., Monde, R. A., and Last, R. L. (1998). Superoxide dismutase in Arabidopsis: an eclectic enzyme family with disparate regulation and protein localization. *Plant Physiol.*, *118*, 637–650.

Köhler, R. H., and Hanson, M. R. (2000). Plastid tubules of higher plants are tissue-specific and developmentally regulated. *J. Cell Sci.*, *113*, 81–89.

Kohli, S. K., Khanna, K., Bhardwaj, R., Abd Allah, E. F., Ahmad, P., and Corpas, F. J. (2019). Assessment of subcellular ROS and NO metabolism in higher plants: multifunctional signaling molecules. *Antioxidants*, *8*, 641.

Kohorn, B. D., Kohorn, S. L., Todorova, T., Baptiste, G., Stansky, K., and McCullough, M. (2012). A dominant allele of *Arabidopsis* pectin-binding wall-associated kinase induces a stress response suppressed by MPK6 but not MPK3 mutations. *Mol. Plant.*, *5*, 841–851.

Kollist, H., Zandalinas, S. I., Sengupta, S., Nuhkat, M., Kangasjärvi, J., and Mittler, R. (2019). Rapid Responses to Abiotic Stress: Priming the Landscape for the Signal Transduction Network. *Trends Plant Sci.*, *24*, 25–37.

Komis, G., Šamajová, O., Ovečka, M., and Šamaj, J. (2018). Cell and Developmental Biology of Plant Mitogen-Activated Protein Kinases. *Annu. Rev. Plant Biol.*, *69*, 237–265.

Kong, Q., Qu, N., Gao, M., Zhang, Z., Ding, X., Yang, F., et al. (2012). The MEKK1-MKK1/MKK2-MPK4 kinase cascade negatively regulates immunity mediated by a mitogen-activated protein kinase kinase kinase in *Arabidopsis*. *Plant Cell*, *24*, 2225–2236.

Kornyeyev, D., Logan, B. A., Payton, P. R., Allen, R. D., and Holaday, A. S. (2003). Elevated chloroplastic glutathione reductase activities decrease chillinginduced photoinhibition by increasing rates of photochemistry, but not thermal energy dissipation, in transgenic cotton. *Funct. Plant Biol.*, *30*, 101–110.

Kosuta, S., Hazledine, S., Sun, J., Miwa, H., Morris, R. J., Downie, J. A., and Oldroyd, G. E. (2008). Differential and chaotic calcium signatures in the symbiosis signaling pathway of legumes. *Proc. Natl Acad. Sci. U. S. A.*, *105*, 9823–9828.

Kovtun, Y., Chiu, W. L., Tena, G., and Sheen, J. (2000). Functional analysis of oxidative stress-activated mitogen-activated protein kinase cascade in plants. *Proc. Natl. Acad. Sci. U. S. A.*, *97*, 2940–2945.

Kropat, J., Tottey, S., Birkenbihl, R. P., Depège, N., Huijser, P., and Merchant, S. (2005). A regulator of nutritional copper signaling in *Chlamydomonas* is an SBP domain protein that recognizes the GTAC core of copper response element. *Proc. Natl. Acad. Sci. U. S. A.*, *102*, 18730–18735.

Kruft, V., Eubel, H., Jänsch, L., Werhahn, W., and Braun, H. P. (2001). Proteomic approach to identify novel mitochondrial proteins in Arabidopsis. *Plant Physiol.*, *127*, 1694–1710.

Kumar, M., Gouw, M., Michael, S., Sámano-Sánchez, H., Pancsa, R., Glavina, J., et al. (2020). ELM-the eukaryotic linear motif resource in 2020. *Nucleic Acids Res.*, 48, D296–D306.

Kuo, W. Y., Huang, C. H., Liu, A. C., Cheng, C. P., Li, S. H., Chang, W. C., et al. (2013). CHAPERONIN 20 mediates iron superoxide dismutase (FeSOD) activity independent of its co-chaperonin role in Arabidopsis chloroplasts. *New Phytol*., *197*, 99–110.

Lagarda-Diaz, I., Guzman-Partida, A., and Vazquez-Moreno, L. (2017). Legume Lectins: Proteins with Diverse Applications. *Int. J. Mol. Sci.*, *18*, 1242.

Lämke, J., Brzezinka, K., and Bäurle, I. (2016). HSFA2 orchestrates transcriptional dynamics after heat stress in *Arabidopsis thaliana*. *Transcription*, *7*, 111–114.

Lang, J., and Colcombet, J. (2020). Sustained Incompatibility between MAPK Signaling and Pathogen Effectors. *Int. J. Mol. Sci.*, *21*, 7954.

Larrainzar, E., Wienkoop, S., Weckwerth, W., Ladrera, R., Arrese-Igor, C., and González, E. M. (2007). *Medicago truncatula* Root Nodule Proteome Analysis Reveals Differential Plant and Bacteroid Responses to Drought Stress. *Plant Physiol.*, *144*, 1495–1507.

Lassig, R., Gutermuth, T., Bey, T. D., Konrad, K. R., and Romeis, T. (2014). Pollen tube NAD(P)H oxidases act as a speed control to dampen growth rate oscillations during polarized cell growth. *Plant J.*, *78*, 94–106.

Lee, H., Kim, J., Im, J. H., Kim, H. B, Oh, C. J., and An, C. S. (2008). Mitogen-activated protein kinase is involved in the symbiotic interaction between *Bradyrhizobium japonicum* USDA110 and soybean. *J. Plant Biol.*, *51*, 291–296.

Leitch, J. M., Li, C. X., Baron, J. A., Matthews, L. M., Cao, X., Hart, P. J., et al. (2012). Post-translational modification of Cu/Zn superoxide dismutase under anaerobic conditions. *Biochemistry*, *51*, 677–685.

Leng, L., Liang, Q., Jiang, J., Zhang, C., Hao, Y., Wang, X., and Su, W. (2017). A subclass of HSP70s regulate development and abiotic stress responses in *Arabidopsis thaliana*. *J. Plant Res.*, *130*, 349–363.

Leshem, Y., Seri, L., and Levine, A. (2007). Induction of phosphatidylinositol 3-kinase-mediated endocytosis by salt stress leads to intracellular production of reactive oxygen species and salt tolerance. *Plant J.*, *51*, 185–197.

Leymarie, J., Vitkauskaite, G., Hoang, H. H., Gendreau, E., Chazoule, V., Meimoun, P., et al. (2012). Role of reactive oxygen species in the regulation of Arabidopsis seed dormancy. *Plant Cell Physiol*., *53*, 96e106.

Li, H., Ding, Y., Shi, Y., Zhang, X., Zhang, S., Gong, Z., and Yang, S. (2017a). MPK3- and MPK6-Mediated ICE1 Phosphorylation Negatively Regulates ICE1 Stability and Freezing Tolerance in *Arabidopsis*. *Dev. Cell*, *43*, 630–642.

Li, Z., Han, X., Song, X., Zhang, Y., Jiang, J., Han, Q., et al. (2017c). Overexpressing the *Sedum alfredii* Cu/Zn superoxide dismutase increased resistance to oxidative stress in transgenic *Arabidopsis*. *Front Plant Sci*., *8*, 1010.

Li, B., Jiang, S., Yu, X., Cheng, C., Chen, S., Cheng, Y., et al. (2015a). Phosphorylation of trihelix transcriptional repressor ASR3 by MAP KINASE4 negatively regulates Arabidopsis immunity. *Plant Cell*, *27*, 839–856.

Li, F., Li, M., Wang, P., Cox, K. L., Jr., Duan, L., Dever, J. K., et al. (2017b). Regulation of cotton (*Gossypium hirsutum*) drought responses by mitogen-activated protein (MAP) kinase cascade-mediated phosphorylation of GhWRKY59. *New Phytol.*, *215*, 1462–1475.

Li, Y., Li, X., Yang, J., and He, Y. (2020). Natural antisense transcripts of MIR398 genes suppress microR398 processing and attenuate plant thermotolerance. *Nat. Commun.*, *11*, 5351.

Li, X. Y., Lin, E. P., Huang, H. H., Niu, M. Y., Tong, Z. K., and Zhang, J. H. (2018). Molecular Characterization of *SQUAMOSA PROMOTER BINDING PROTEIN-LIKE (SPL)* Gene Family in *Betula luminifera*. *Front. Plant Sci.*, *9*, 608.

Li, G., Meng, X., Wang, R., Mao, G., Han, L., Liu, Y., and Zhang, S. (2012a). Dual-level regulation of ACC synthase activity by MPK3/MPK6 cascade and its downstream WRKY transcription factor during ethylene induction in Arabidopsis. *PLOS Genet*., *8*, e1002767.

Li, N., Sun, L., Zhang, L., Song, Y., Hu, P., Li, C., and Hao, F. S. (2015b). AtrbohD and AtrbohF negatively regulate lateral root development by changing the localized accumulation of superoxide in primary roots of Arabidopsis. *Planta*, *241*, 591–602.

Li, C. H., Wang, G., Zhao, J. L., Zhang, L. Q., Ai, L. F., Han, Y. F., et al. (2014). The Receptor-Like Kinase SIT1 Mediates Salt Sensitivity by Activating MAPK3/6 and Regulating Ethylene Homeostasis in Rice. *Plant Cell*, *26*, 2538–2553.

Li, L., Xu, X., Chen, C., and Shen, Z. (2016). Genome-Wide Characterization and Expression Analysis of the Germin-Like Protein Family in Rice and Arabidopsis. *Int. J. Mol. Sci.*, *17*, 1622.

Li, Z., Yue, H., and Xing, D. (2012b). MAP Kinase 6-mediated activation of vacuolar processing enzyme modulates heat shock-induced programmed cell death in Arabidopsis. *New Phytol.*, *195*, 85–96.

Linkies, A., Müller, K., Morris, K., Turečková, V., Wenk, M., Cadman, C. S. C., et al. (2009). Ethylene interacts with abscisic acid to regulate endosperm rupture during germination: A comparative approach using *Lepidium sativum* and *Arabidopsis thaliana*. *Plant Cell*, *21*, 3803–3822.

Lintala, M., Allahverdiyeva, Y., Kidron, H., Piippo, M., Battchikova, N., Suorsa, M., et al. (2007). Structural and functional characterization of ferredoxin-$NADP^+$-oxidoreductase using knock-out mutants of Arabidopsis. *Plant J.*, *49*, 1041–1052.

Lisenbee, C. S., Lingard, M. J., and Trelease, R. N. (2005). Arabidopsis peroxisomes possess functionally redundant membrane and matrix isoforms of monodehydroascorbate reductase. *Plant J*., *43*, 900–914.

Liu, A., Contador, C. A., Fan, K., and Lam, H. M. (2018). Interaction and Regulation of Carbon, Nitrogen, and Phosphorus Metabolisms in Root Nodules of Legumes. *Front Plant Sci.*, *9*, 1860.

Liu, Q., Harberd, N. P., and Fu, X. (2016). SQUAMOSA Promoter Binding Protein-like Transcription Factors: Targets for Improving Cereal Grain Yield. *Mol. Plant*, *9*, 765–767.

Liu, J., Huang, Y., Kong, L., Yu, X., Feng, B., Liu, D., et al. (2020). The malectin-like receptor-like kinase LETUM1 modulates NLR protein SUMM2 activation via MEKK2 scaffolding. *Nat. Plants*, *6*, 1106–1115.

Liu, S., Kracher, B., Ziegler, J., Birkenbihl, R. P., and Somssich, I. E. (2015). Negative regulation of ABA signaling by WRKY33 is critical for Arabidopsis immunity towards Botrytis cinerea 2100. *eLife*, *4*, e07295.

Liu, Y., and Zhang, S. (2004). Phosphorylation of 1-aminocyclopropane-1-carboxylic acid synthase by MPK6, a stress-responsive mitogen-activated protein kinase, induces ethylene biosynthesis in Arabidopsis. *Plant Cell.*, *16*, 3386–3399.

Livanos, P., Galatis, B., Quader, H., and Apostolakos, P. (2012). Disturbance of reactive oxygen species homeostasis induces atypical tubulin polymer formation and affects mitosis in root-tip cells of *Triticum turgidum* and *Arabidopsis thaliana*. *Cytoskeleton*, *69*, 1–21.

Locato, V., Cimini, S., and De Gara, L. (2017). "Glutathione as a key player in plant abiotic stress responses and tolerance," in Glutathione in Plant Growth, Development, and Stress Tolerance, eds M. A. Hossain, M. G. Mostofa, P. Diaz-Vivancos, D. J. Burritt, M. Fujita, and L. S. P. Tran (Cham: Springer International Publishing), 127–145.

Lohar, D. P., Haridas, S., Gantt, J. S., and VandenBosch, K. A. (2007). A transient decrease in reactive oxygen species in roots leads to root hair deformation in the legume-rhizobia symbiosis. *New Phytol.*, *173*, 39–49.

Lopez-Gomez, M., Sandal, N., Stougaard, J., and Boller, T. (2012). Interplay of flg22-induced defence responses and nodulation in *Lotus japonicus*. *J. Exp. Bot.*, *63*, 393–401.

López-Huertas, E., Corpas, F. J., Sandalio, L. M., and del Río, L. A. (1999). Characterization of membrane polypeptides from pea leaf peroxisomes involved in superoxide radical generation. *Biochem. J.*, *337*, 531–536.

Lu, C. A., Huang, C. K., Huang, W. S., Huang, T. S., Liu, H. Y., and Chen, Y. F. (2020). DEAD-Box RNA Helicase 42 Plays a Critical Role in Pre-mRNA Splicing under Cold Stress. *Plant Physiol.*, *182*, 255–271.

Ma, C., Burd, S., and Lers, A. (2015). miR408 is involved in abiotic stress responses in Arabidopsis. *Plant J.*, *84*, 169–187.

Mangeon, A., Menezes-Salgueiro, A. D., and Sachetto-Martins, G. (2017). Start me up: Revision of evidences that AtGRP3 acts as a potential switch for AtWAK1. *Plant Signal. Behav.*, *12*, e1191733.

Mangeon, A., Pardal, R., Menezes-Salgueiro, A. D., Duarte, G. L., de Seixas, R., Cruz, F. P., et al. (2016). AtGRP3 Is Implicated in Root Size and Aluminum Response Pathways in Arabidopsis. *PLOS ONE*, *11*, e0150583.

Mano, S., Hayashi, M., and Nishimura, M. (1999). Light regulates alternative splicing of hydroxypyruvate reductase in pumpkin. *Plant J.*, *17*, 309–320.

Mao, G., Meng, X., Liu, Y., Zheng, Z., Chen, Z., and Zhang, S. (2011). Phosphorylation of a WRKY transcription factor by two pathogen-responsive MAPKs drives phytoalexin biosynthesis in Arabidopsis. *Plant Cell, 23*, 1639–1653.

Marcec, M. J., Gilroy, S., Poovaiah, B. W., and Tanaka, K. (2019). Mutual interplay of Ca^{2+} and ROS signaling in plant immune response. *Plant Sci., 283*, 343–354.

Marino, D., Andrio, E., Danchin, E. G., Oger, E., Gucciardo, S., Lambert, A., et al. (2011). A Medicago truncatula NADPH oxidase is involved in symbiotic nodule functioning. *New Phytol., 189*, 580–592.

Marri, L., Pesaresi, A., Valerio, C., Lamba, D., Pupillo, P., Trost, P., and Sparla, F. (2010). *In vitro* characterization of *Arabidopsis* CP12 isoforms reveals common biochemical and molecular properties. *J. Plant Physiol., 167*, 939–950.

Marri, L., Sparla, F., Pupillo, P., and Trost, P. (2005). Co-ordinated gene expression of photosynthetic glyceraldehyde-3-phosphate dehydrogenase, phosphoribulokinase, and CP12 in *Arabidopsis thaliana*. *J. Exp. Bot., 56*, 73–80.

Marti, L., Stefano, G., Tamura, K., Hawes, C., Renna, L., Held, M. A., and Brandizzi, F. (2010). A missense mutation in the vacuolar protein GOLD36 causes organizational defects in the ER and aberrant protein trafficking in the plant secretory pathway. *Plant J., 63*, 901–913.

Martin, M. V., Distéfano, A. M., Zabaleta, E. J., and Pagnussat, G. C. (2013). New insights into the functional roles of reactive oxygen species during embryo sac development and fertilization in *Arabidopsis thaliana*. *Plant Signal. Behav., 8*, 10.4161/psb.25714.

Marty, L., Bausewein, D., Müller, C., Bangash, S., Moseler, A., Schwarzländer, M., et al. (2019). Arabidopsis glutathione reductase 2 is indispensable in plastids, while mitochondrial glutathione is safeguarded by additional reduction and transport systems. *New Phytol., 224*, 1569–1584.

Maruta, T., Sawa, Y., Shigeoka, S., and Ishikawa, T. (2016). Diversity and evolution of ascorbate peroxidase functions in chloroplasts: more than just a classical antioxidant enzyme? *Plant Cell Physiol., 57*, 1377–1386.

Maruta, T., Tanouchi, A., Tamoi, M., Yabuta, Y., Yoshimura, K., Ishikawa, T., et al. (2010). Arabidopsis chloroplastic ascorbate peroxidase isoenzymes play a dual role in photoprotection and gene regulation under photooxidative stress. *Plant Cell Physiol., 51*, 190–200.

Matamoros, M. A., Kim, A., Peñuelas, M., Ihling, C., Griesser, E., Hoffmann, R., et al. (2018). Protein Carbonylation and Glycation in Legume Nodules. *Plant Physiol., 177*, 1510–1528.

Matsuoka, K., and Nakamura, K. (1991). Propeptide of a precursor to a plant vacuolar protein required for vacuolar targeting. *Proc. Natl. Acad. Sci. U. S. A., 88*, 834–838.

Mattila, H., Khorobrykh, S., Havurinne, V., and Tyystjärvi, E. (2015). Reactive oxygen species: Reactions and detection from photosynthetic tissues. *J. Photochem. Photobiol. B, Biol., 152*, 176–214.

McCord, J. M., Keele, B. B., Jr., and Fridovich, I. (1971). An enzyme-based theory of obligate anaerobiosis: the physiological function of superoxide dismutase. *Proc. Natl. Acad. Sci. U. S. A., 68*, 1024–1027.

McCoy, T. J., and Bingham, E. T. (1988). "Cytology and cytogenetics of alfalfa," in Alfalfa and Alfalfa Improvement, ed. A. A. Hanson (Madison, WI: ASA), 737–776.

Meier, B., Barra, D., Bossa, F., Calabrese, L., and Rotilio, G. (1982). Synthesis of either Fe- or Mn-superoxide dismutase with an apparently identical protein moiety by an anaerobic bacterium dependent on the metal supplied. *J. Biol. Chem.*, *257*, 13977–13980.

Melotto, M., Zhang, L., Oblessuc, P. R., and He, S. Y. (2017). Stomatal Defense a Decade Later. *Plant Physiol.*, *174*, 561–571.

Meng, X., Xu, J., He, Y., Yang, K. Y., Mordorski, B., Liu, Y., and Zhang, S. (2013). Phosphorylation of an ERF transcription factor by *Arabidopsis* MPK3/MPK6 regulates plant defense gene induction and fungal resistance. *Plant Cell*, *25*, 1126–1142.

Meng, X., and Zhang, S. (2013). MAPK cascades in plant disease resistance signaling. *Annu. Rev. Phytopathol.*, *51*, 245–266.

Mermod, M., Takusagawa, M., Kurata, T., Kamiya, T., Fujiwara, T., and Shikanai, T. (2019). SQUAMOSA promoter-binding protein-like 7 mediates copper deficiency response in the presence of high nitrogen in *Arabidopsis thaliana*. *Plant Cell Rep.*, *38*, 835–846.

Mhamdi, A., and Van Breusegem, F. (2018). Reactive oxygen species in plant development. *Development*, *145*, dev164376.

Mignolet-Spruyt, L., Xu, E., Idänheimo, N., Hoeberichts, F. A., Mühlenbock, P., Brosché, M., et al. (2016). Spreading the news: subcellular and organellar reactive oxygen species production and signalling. *J. Exp. Bot.*, *67*, 3831–3844.

Miller, E. W., Dickinson, B. C., and Chang, C. J. (2010). Aquaporin-3 mediates hydrogen peroxide uptake to regulate downstream intracellular signaling. *Proc. Natl. Acad. Sci. U. S. A.*, *107*, 15681–15686.

Miller, G., Schlauch, K., Tam, R., Cortes, D., Torres, M. A., Shulaev, V., et al. (2009). The plant NADPH oxidase RBOHD mediates rapid systemic signaling in response to diverse stimuli. *Sci. Signal.*, *2*, ra45.

Mitra, A., Han, J., Zhang, Z. J., and Mitra, A. (2009). The intergenic region of *Arabidopsis thaliana cab1* and *cab2* divergent genes functions as a bidirectional promoter. *Planta*, *229*, 1015–1022.

Mittler, R. (2017). ROS are good. *Trends Plant Sci.*, *22*, 11–19.

Mittler, R., and Blumwald, E. (2015). The roles of ROS and ABA in systemic acquired acclimation. *Plant Cell*, *27*, 64–70.

Miya, A., Albert, P., Shinya, T., Desaki, Y., Ichimura, K., Shirasu, K., et al. (2007). CERK1, a LysM receptor kinase, is essential for chitin elicitor signaling in Arabidopsis. *Proc. Natl. Acad. Sci. U. S. A.*, *104*, 19613–19618.

Montellese, C., van den Heuvel, J., Ashiono, C., Dörner, K., Melnik, A., Jonas, S., et al. (2020). USP16 counteracts mono-ubiquitination of RPS27a and promotes maturation of the 40S ribosomal subunit. *eLife*, *9*, e54435.

Morgan, M. J., Lehmann, M., Schwarzländer, M., Baxter, C. J., Sienkiewicz-Porzucek, A., Williams, T. C., et al. (2008). Decrease in manganese superoxide dismutase leads to reduced root growth and affects tricarboxylic acid cycle flux and mitochondrial redox homeostasis. *Plant Physiol.*, *147*, 101–114.

Mortier, V., Holsters, M., and Goormachtig, S. (2012). Never too many? How legumes control nodule numbers. *Plant Cell Environ.*, *35*, 245–258.

Moyet, L., Salvi, D., Bouchnak, I., Miras, S., Perrot, L., Seigneurin-Berny, D., et al. (2019). Calmodulin is involved in the dual subcellular location of two chloroplast proteins. *J. Biol. Chem.*, *294*, 17543–17554.

Müller, K., Linkies, A., Vreeburg, R. A. M., Fry, S. C., Krieger-Liszkay, A., and Leubner-Metzger, G. (2009). *In vivo* cell wall loosening by hydroxyl radicals during cress seed germination and elongation growth. *Plant Physiol.*, *150*, 1855–1865.

Müller-Schüssele, S. J., Wang, R., Gütle, D. D., Romer, J., Rodriguez-Franco, M., Scholz, M., et al. (2020). Chloroplasts require glutathione reductase to balance reactive oxygen species and maintain efficient photosynthesis. *Plant J.*, *103*, 1140–1154.

Muñoz, P., and Munné-Bosch, S. (2019). Vitamin E in plants: biosynthesis, transport, and function. *Trends Plant Sci.*, *24*, 1040–1051.

Murgia, I., Tarantino, D., Vannini, C., Bracale, M., Carravieri, S., and Soave, C. (2004). *Arabidopsis thaliana* plants overexpressing thylakoidal ascorbate peroxidase show increased resistance to Paraquat-induced photooxidative stress and to nitric oxide-induced cell death. *Plant J.*, *38*, 940–953.

Murphy, M. P. (2009). How mitochondria produce reactive oxygen species. *Biochem. J.*, *417*, 1–13.

Myouga, F., Hosoda, C., Umezawa, T., Iizumi, H., Kuromori, T., Motohashi, R., et al. (2008). A heterocomplex of iron superoxide dismutases defends chloroplast nucleoids against oxidative stress and is essential for chloroplast development in Arabidopsis. *Plant Cell*, *20*, 3148–3162.

Nagano, A. J., Maekawa, A., Nakano, R. T., Miyahara, M., Higaki, T., Kutsuna, N., et al. (2009). Quantitative analysis of ER body morphology in an Arabidopsis mutant. *Plant Cell Physiol.*, *50*, 2015–2022.

Nagano, A. J., Matsushima, R., and Hara-Nishimura, I. (2005). Activation of an ER-body-localized beta-glucosidase via a cytosolic binding partner in damaged tissues of *Arabidopsis thaliana*. *Plant Cell Physiol.*, *46*, 1140–1148.

Nakagami, H., Soukupová, H., Schikora, A., Zárský, V., and Hirt, H. (2006). A Mitogen-activated protein kinase kinase kinase mediates reactive oxygen species homeostasis in Arabidopsis. *J. Biol. Chem.*, *281*, 38697–38704.

Nakano, R. T., Matsushima, R., Nagano, A. J., Fukao, Y., Fujiwara, M., Kondo, M., et al. (2012). ERMO3/MVP1/GOLD36 is involved in a cell type-specific mechanism for maintaining ER morphology in *Arabidopsis thaliana*. *PLOS ONE*, *7*, e49103.

Nakano, R. T., Piślewska-Bednarek, M., Yamada, K., Edger, P. P., Miyahara, M., Kondo, M., et al. (2017). PYK10 myrosinase reveals a functional coordination between endoplasmic reticulum bodies and glucosinolates in Arabidopsis thaliana. *Plant J.*, *89*, 204–220.

Nguyen-Kim, H., San Clemente, H., Balliau, T., Zivy, M., Dunand, C., Albenne, C., and Jamet, E. (2016). *Arabidopsis thaliana* root cell wall proteomics: Increasing the proteome coverage using a combinatorial peptide ligand library and description of unexpected Hyp in peroxidase amino acid sequences. *Proteomics*, *16*, 491–503.

Niu, L., and Liao, W. (2016). Hydrogen peroxide signaling in plant development and abiotic responses: crosstalk with nitric oxide and calcium. *Front. Plant Sci.*, *7*, 230.

Nivière, V., and Fontecave, M. (2004). Discovery of superoxide reductase: an historical perspective. *J. Biol. Inorg. Chem.*, *9*, 119–123.

Noctor, G., Arisi, A. C. M., Jouanin, L., and Foyer, C. H. (1999). Photorespiratory glycine enhances glutathione accumulation in both the chloroplastic and cytosolic compartments. *J. Exp. Bot.*, *50*, 1157–1167.

Noctor, G., Reichheld, J. P., and Foyer, C. H. (2017). ROS-related redox regulation and signaling in plants. *Cell Dev. Biol.*, *80*, 3–12.

Nodine, M. D., and Bartel, D. P. (2010). MicroRNAs prevent precocious gene expression and enable pattern formation during plant embryogenesis. *Genes Dev.*, *24*, 2678–2692.

Noshi, M., Hatanaka, R., Tanabe, N., Terai, Y., Maruta, T., and Shigeoka, S. (2016). Redox regulation of ascorbate and glutathione by a chloroplastic dehydroascorbate reductase is required for high-light stress tolerance in Arabidopsis. *Biosci. Biotechnol. Biochem.*, *80*, 870–877.

Noshi, M., Yamada, H., Hatanaka, R., Tanabe, N., Tamoi, M., and Shigeoka, S. (2017). Arabidopsis dehydroascorbate reductase 1 and 2 modulate redox states of ascorbate-glutathione cycle in the cytosol in response to photooxidative stress. *Biosci. Biotechnol. Biochem.*, *81*, 523–533.

Novák, D., Vadovič, P., Ovečka, M., Šamajová, O., Komis, G., Colcombet, J., and Šamaj, J. (2018). Gene Expression Pattern and Protein Localization of Arabidopsis Phospholipase D Alpha 1 Revealed by Advanced Light-Sheet and Super-Resolution Microscopy. *Front. Plant Sci.*, *9*, 371.

Obara, K., Sumi, K., and Fukuda, H. (2002). The use of multiple transcription starts causes the dual targeting of Arabidopsis putative monodehydroascorbate reductase to both mitochondria and chloroplasts. *Plant Cell Physiol.*, *43*, 697–705.

Obayashi, T., Aoki, Y., Tadaka, S., Kagaya, Y., and Kinoshita, K. (2018). ATTED-II in 2018: a plant coexpression database based on investigationof thestatistical property of the mutual rank index. *Plant Cell Physiol.*, *59*, e3.

Ogasawara, Y., Kaya, H., Hiraoka, G., Yumoto, F., Kimura, S., Kadota, Y., et al. (2008). Synergistic activation of the Arabidopsis NADPH oxidase AtrbohD by Ca^{2+} and phosphorylation. *J. Biol. Chem.*, *283*, 8885–8892.

Oldroyd, G. E. (2013). Speak, friend, and enter: signalling systems that promote beneficial symbiotic associations in plants. *Nat. Rev. Microbiol.*, *11*, 252–263.

Orman-Ligeza, B., Parizot, B., de Rycke, R., Fernandez, A., Himschoot, E., Van Breusegem, F., et al. (2016). RBOH-mediated ROS production facilitates lateral root emergence in Arabidopsis. *Development*, *143*, 3328–3339.

Ortiz-Masia, D., Perez-Amador, M. A., Carbonell, J., and Marcote, M. J. (2007). Diverse stress signals activate the C1 subgroup MAP kinases of *Arabidopsis*. *FEBS Lett.*, *581*, 1834–1840.

Ott, T. (2017). Membrane nanodomains and microdomains in plant–microbe interactions. *Curr. Opin. Plant Biol.*, *40*, 82–88.

Ott, T., van Dongen, J. T., Günther, C., Krusell, L., Desbrosses, G., Vigeolas, H., et al. (2005). Symbiotic leghemoglobins are crucial for nitrogen fixation in legume root nodules but not for general plant growth and development. *Curr. Biol.*, *15*, 531–535.

Ouaked, F., Rozhon, W., Lecourieux, D., and Hirt, H. (2003). A MAPK pathway mediates ethylene signaling in plants. *EMBO J.*, *22*, 1282–1288.

Ovečka, M., Berson, T., Beck, M., Derksen, J., Šamaj, J., Baluška, F., et al. (2010). Structural sterols are involved in both the initiation and tip growth of root hairs in *Arabidopsis thaliana*. *Plant Cell*., *22*, 2999–3019.

Ovečka, M., Takáč, T., Komis, G., Vadovič, P., Bekešová, S., Doskočilová, A., et al. (2014). Salt-induced subcellular kinase relocation and seedling susceptibility caused by overexpression of *Medicago* SIMKK in *Arabidopsis*. *J. Exp. Bot., 65*, 2335–2350.

Ovečka, M., Vaškebová, L., Komis, G., Luptovčiak, I., Smertenko, A., and Šamaj, J. (2015). Preparation of plants for developmental and cellular imaging by light-sheet microscopy. *Nat. Protoc*., *10*, 1234–1247.

Pallotta, M., Graham, R., Langridge, P., Sparrow, D. H. B., and Barker, S. J. (2000). RFLP mapping of manganese efficiency in barley. *Theor. Appl. Genet., 101*, 1100–1108.

Palma, J. M., Mateos, R. M., López-Jaramillo, J., Rodríguez-Ruiz, M., González- Gordo, S., Lechuga-Sancho, A. M., et al. (2020). Plant catalases as NO and H_2S targets. *Redox Biol*., *34*, 101525.

Pan, R., Liu, J., Wang, S., and Hu, J. (2020). Peroxisomes: versatile organelles with diverse roles in plants. *New Phytol., 225*, 1410–1427.

Park, S. K., Jung, Y. J., Lee, J. R., Lee, Y. M., Jang, H. H., Lee, S. S., et al. (2009). Heat-shock and redox-dependent functional switching of an h-type Arabidopsis thioredoxin from a disulfide reductase to a molecular chaperone. *Plant Physiol., 150*, 552–561.

Passardi, F., Tognolli, M., De Meyer, M., Penel, C., and Dunand, C. (2006). Two cell wall associated peroxidases from Arabidopsis influence root elongation. *Planta, 223*, 965–974.

Pasternak, T. P., Ötvös, K., Domoki, M., and Fehér, A. (2007). Linked activation of cell division and oxidative stress defense in alfalfa leaf protoplast-derived cells is dependent on exogenous auxin. *Plant Growth Regul., 51*, 109–117.

Pathirana, S. M., Vance, C. P., Miller, S. S., and Gantt, J. S. (1992). Alfalfa root nodule phosphoenolpyruvate carboxylase: characterization of the cDNA and expression in effective and plant-controlled ineffective nodules. *Plant Mol. Biol*., *20*, 437–450.

Peck, M. C., Fisher, R. F., and Long, S. R. (2006). Diverse flavonoids stimulate NodD1 binding to nod gene promoters in Sinorhizobium meliloti. *J. Bacteriol., 188*, 5417–5427.

Perea-García, A., Andrés-Bordería, A., Mayo de Andrés, S., Sanz, A., Davis, A. M., Davis, S. J., et al. (2016). Modulation of copper deficiency responses by diurnal and circadian rhythms in *Arabidopsis thaliana*. *J. Exp. Bot., 67*, 391–403.

Petersen, M., Brodersen, P., Naested, H., Andreasson, E., Lindhart, U., Johansen, B., et al. (2000). Arabidopsis map kinase 4 negatively regulates systemic acquired resistance. *Cell, 103*, 1111–1120.

Petersson, S. V., Johansson, A. I., Kowalczyk, M., Makoveychuk, A., Wang, J. Y., Moritz, T., et al. (2009). An auxin gradient and maximum in the Arabidopsis root apex shown by high-resolution cellspecific analysis of IAA distribution and synthesis. *Plant Cell, 21*, 1659–1668.

Pfeilmeier, S., George, J., Morel, A., Roy, S., Smoker, M., Stransfeld, L., et al. (2019). Expression of the Arabidopsis thaliana immune receptor EFR in *Medicago truncatula* reduces infection by a root pathogenic bacterium, but not nitrogen-fixing rhizobial symbiosis. *Plant Biotechnol. J., 17*, 569–579.

Pieterse, C. M. J., Van der Does, D., Zamioudis, C., Leon-Reyes, A., and Van Wees, S. C. M. (2012). Hormonal Modulation of Plant Immunity. *Annu. Rev. Cell Dev. Biol.*, *28*, 489–521.

Pietrzykowska, M., Suorsa, M., Semchonok, D. A., Tikkanen, M., Boekema, E. J., Aro, E. M., and Jansson, S. (2014). The light-harvesting chlorophyll a/b binding proteins Lhcb1 and Lhcb2 play complementary roles during state transitions in Arabidopsis. *Plant Cell*, *26*, 3646–3660.

Pilon, M. (2017). The copper microRNAs. *New Phytol.*, *213*, 1030–1035.

Pilon, M., Ravet, K., and Tapken, W. (2011). The biogenesis and physiological function of chloroplast superoxide dismutases. *Biochim. Biophys. Acta*, *1807*, 989–998.

Pitcher, L. H., and Zilinskas, B. A. (1996). Overexpression of copper/zinc superoxide dismutase in the cytosol of transgenic tobacco confers partial resistance to ozone-induced foliar necrosis. *Plant Physiol.*, *110*, 583–588.

Piterková, J., Luhová, L., Navrátilová, B., Sedlářová, M., and Petřivalský, M. (2015). Early and long-term responses of cucumber cells to high cadmium concentration are modulated by nitric oxide and reactive oxygen species. *Acta Physiol. Plant*, *37*, 19.

Pitzschke, A., Datta, S., and Persak, H. (2014). Salt stress in Arabidopsis: lipid transfer protein AZI1 and its control by mitogen-activated protein kinase MPK3. *Mol. Plant*, *7*, 722–738.

Pitzschke, A., Djamei, A., Bitton, F., and Hirt, H. (2009). A major role of the MEKK1-MKK1/2-MPK4 pathway in ROS signalling. *Mol. Plant*, *2*, 120–137.

Pnueli, L., Liang, H., Rozenberg, M., and Mittler, R. (2003). Growth suppression, altered stomatal responses, and augmented induction of heat shock proteins in cytosolic ascorbate peroxidase (Apx1)-deficient Arabidopsis plants. *Plant J.*, *34*, 187–203.

Podgórska, A., Burian, M., and Szal, B. (2017). Extra-Cellular But Extra-Ordinarily Important for Cells: Apoplastic Reactive Oxygen Species Metabolism. *Front. Plant Sci.*, *8*, 1353.

Pospíšil, P. (2016). Production of Reactive Oxygen Species by Photosystem II as a Response to Light and Temperature Stress. *Front. Plant Sci.*, *7*, 1950.

Prasad, A., Sedlářová, M., Kale, R. S., and Pospíšil, P. (2017). Lipoxygenase in singlet oxygen generation as a response to wounding: in vivo imaging in *Arabidopsis thaliana*. *Sci. Rep.*, *7*, 9831.

Preston, J. C., and Hileman, L. C. (2013). Functional Evolution in the Plant *SQUAMOSA-PROMOTER BINDING PROTEIN-LIKE* (*SPL*) Gene Family. *Front. Plant Sci.*, *4*, 80.

Qi, J., Wang, J., Gong, Z., and Zhou, J. M. (2017). Apoplastic ROS signaling in plant immunity. *Curr. Opin. Plant Biol.*, *38*, 92–100.

Qiu, J. L., Fiil, B. K., Petersen, K., Nielsen, H. B., Botanga, C. J., Thorgrimsen, S., et al. (2008). Arabidopsis MAP kinase 4 regulates gene expression through transcription factor release in the nucleus. *EMBO J.*, *27*, 2214–2221.

Radović, J., Sokolović, D., and Marković, J. (2009). Alfalfa-most important perennial forage legume in animal husbandry. *Biotechnol. Anim. Husb.*, *25*, 465–475.

Rae, T. D., Schmidt, P. J., Pufahl, R. A., Culotta, V. C., and O'Halloran, T. V. (1999). Undetectable intracellular free copper: the requirement of a copper chaperone for superoxide dismutase. *Science*, *284*, 805–808.

Rahantaniaina, M. S., Li, S., Chatel-Innocenti, G., Tuzet, A., Issakidis-Bourguet, E., Mhamdi, A., and Noctor, G. (2017). Cytosolic and chloroplastic DHARs cooperate in oxidative stress-driven activation of the salicylic acid pathway. *Plant Physiol.*, *174*, 956–971.

Ramu, S. K., Peng, H. M., and Cook, D. R. (2002). Nod factor induction of reactive oxygen species production is correlated with expression of the early nodulin gene rip1 in *Medicago truncatula*. *Mol. Plant Microbe Interact.*, *15*, 522–528.

Ranf, S., Eschen-Lippold, L., Pecher, P., Lee, J., and Scheel, D. (2011). Interplay between calcium signalling and early signalling elements during defence responses to microbe- or damage-associated molecular patterns: Calcium signalling in Arabidopsis innate immunity. *Plant J.*, *68*, 100–113.

Rayapuram, N., Bigeard, J., Alhoraibi, H., Bonhomme, L., Hesse, A. M., Vinh, J., et al. (2018). Quantitative phosphoproteomic analysis reveals shared and specific targets of *Arabidopsis* mitogen-activated protein kinases (MAPKs) MPK3, MPK4, and MPK6. *Mol. Cell. Proteom.*, *17*, 61–80.

Rejeb, I. B., Pastor, V., and Mauch-Mani, B. (2014). Plant Responses to Simultaneous Biotic and Abiotic Stress: Molecular Mechanisms. *Plants*, *3*, 458–475.

Ren, G., Xie, M., Dou, Y., Zhang, S., Zhang, C., and Yu, B. (2012). Regulation of miRNA abundance by RNA binding protein TOUGH in Arabidopsis. *Proc. Natl. Acad. Sci. U. S. A.*, *109*, 12817–12821.

Rentel, M. C., Lecourieux, D., Ouaked, F., Usher, S. L., Petersen, L., Okamoto, H., et al. (2004). OXI1 kinase is necessary for oxidative burst-mediated signalling in *Arabidopsis*. *Nature*, *427*, 858–861.

Rhoades, M. W., Reinhart, B. J., Lim, L. P., Burge, C. B., Bartel, B., and Bartel, D. P. (2002). Prediction of plant microRNA targets. *Cell*, *110*, 513–520.

Rhoads, D. M., and Subbaiah, C. C. (2007). Mitochondrial retrograde regulation in plants. *Mitochondrion*, *7*, 177–194.

Rizhsky, L., Liang, H., and Mittler, R. (2003). The water-water cycle is essential for chloroplast protection in the absence of stress. *J. Biol. Chem.*, *278*, 38921–38925.

Rodriguez, M. C., Petersen, M., and Mundy, J. (2010). Mitogen-activated protein kinase signaling in plants. *Annu. Rev. Plant Biol.*, *61*, 621–649.

Rodríguez-Ruiz, M., González-Gordo, S., Cañas, A., Campos, M. J., Paradela, A., Corpas, F. J., and Palma, J. M. (2019). Sweet Pepper (*Capsicum annuum* L.) Fruits Contain an Atypical Peroxisomal Catalase That is Modulated by Reactive Oxygen and Nitrogen Species. *Antioxidants*, *8*, 374.

Rodríguez-Serrano, M., Bárány, I., Prem, D., Coronado, M. J., Risueño, M. C., and Testillano, P. S. (2012). NO, ROS, and cell death associated with caspaselike activity increase in stress-induced microspore embryogenesis of barley. *J. Exp. Bot.*, *63*, 2007–2024.

Rogers, H., and Munné-Bosch, S. (2016). Production and scavenging of reactive oxygen species and redox signaling during leaf and flower senescence: similar but different. *Plant Physiol.*, *171*, 1560–1568.

Roux, M. E., Rasmussen, M. W., Palma, K., Lolle, S., Regué, À. M., Bethke, G., et al. (2015). The mRNA decay factor PAT1 functions in a pathway including MAP kinase 4 and immune receptor SUMM2. *EMBO J.*, *34*, 593–608.

Roux, M., Schwessinger, B., Albrecht, C., Chinchilla, D., Jones, A., Holton, N., et al. (2011). The *Arabidopsis* leucine-rich repeat receptor-like kinases BAK1/SERK3 and BKK1/SERK4 are required for innate immunity to hemibiotrophic and biotrophic pathogens. *Plant Cell*, *23*, 2440–2455.

Roy, S., Liu, W., Nandety, R. S., Crook, A., Mysore, K. S., Pislariu, C. I., et al. (2020). Celebrating 20 Years of Genetic Discoveries in Legume Nodulation and Symbiotic Nitrogen Fixation. *Plant Cell*, *32*, 15–41.

Ruban, A. V., Solovieva, S., Lee, P. J., Ilioaia, C., Wentworth, M., Ganeteg, U., et al. (2006). Plasticity in the composition of the light harvesting antenna of higher plants preserves structural integrity and biological function. *J. Biol. Chem.*, *281*, 14981–14990.

Ruiz-May, E., Segura-Cabrera, A., Elizalde-Contreras, J. M., Shannon, L. M., and Loyola-Vargas, V. M. (2019). A recent advance in the intracellular and extracellular redox post-translational modification of proteins in plants. *J. Mol. Recognit.*, *32*, e2754.

Ryu, H., Laffont, C., Frugier, F., and Hwang, I. (2017). MAP Kinase-Mediated Negative Regulation of Symbiotic Nodule Formation in *Medicago truncatula*. *Mol. Cells*, *40*, 17–23.

Saito, M. A., Sigman, D. M., and Morel, F. M. M. (2003). The bioinorganic chemistry of the ancient ocean: the co-evolution of cyanobacterial metal requirements and biogeochemical cycles at the Archean-Proterozoic boundary? *Inorg. Chim. Acta.*, 356, 308–318.

Salinas, M., Xing, S., Höhmann, S., Berndtgen, R., and Huijser, P. (2012). Genomic organization, phylogenetic comparison and differential expression of the SBP-box family of transcription factors in tomato. *Planta*, *235*, 1171–1184.

Šamaj, J., Ovečka, M., Hlavačka, A., Lecourieux, F., Meskiene, I., Lichtscheidl, I., et al. (2002). Involvement of the mitogen-activated protein kinase SIMK in regulation of root hair tip growth. *EMBO J.*, *21*, 3296–3306.

Šamajová, O., Komis, G., and Šamaj, J. (2014). Immunofluorescent localization of MAPKs and colocalization with microtubules in Arabidopsis seedling whole-mount probes. In G. Komis and J. Šamaj (Eds.), Plant MAP kinases (pp. 107–115). New York, NY: Humana Press.

Šamajová, O., Plíhal, O., Al-Yousif, M., Hirt, H., and Šamaj, J. (2013). Improvement of stress tolerance in plants by genetic manipulation of mitogen-activated protein kinases. *Biotechnol. Adv.*, *31*, 118–128.

Samakovli, D., Tichá, T., Vavrdová, T., Ovečka, M., Luptovčiak, I., Zapletalová, V., et al. (2020). YODA-HSP90 module regulates phosphorylation-dependent inactivation of SPEECHLESS to control stomatal development under acute heat stress in *Arabidopsis*. *Mol. Plant*, *13*, 612–633.

Samis, K., Bowley, S., and McKersie, B. (2002). Pyramiding Mn-superoxide dismutase transgenes to improve persistence and biomass production in alfalfa. *J. Exp. Bot.*, *53*, 1343–1350.

Sandalio, L. M., and Romero-Puertas, M. C. (2015). Peroxisomes sense and respond to environmental cues by regulating ROS and RNS signalling networks. *Ann. Bot.*, *116*, 475–485.

Savatin, D. V., Bisceglia, N. G., Marti, L., Fabbri, C., Cervone, F., and De Lorenzo, G. (2014). The Arabidopsis NUCLEUS- AND PHRAGMOPLASTLOCALIZED KINASE1-related protein kinases are required for elicitorinduced oxidative burst and immunity. *Plant Physiol.*, *165*, 1188–1202.

Schmid, M., Uhlenhaut, N. H., Godard, F., Demar, M., Bressan, R., Weigel, D., and Lohmann, J. U. (2003). Dissection of floral induction pathways using global expression analysis. *Development*, *130*, 6001–6012.

Schmidt, A., Gube, M., Schmidt, A., and Kothe, E. (2009). *In silico* analysis of nickel containing superoxide dismutase evolution and regulation. *J. Basic Microbiol*., *49*, 109–118.

Schmidt, R., Kunkowska, A. B., and Schippers, J. H. M. (2016). Role of reactive oxygen species during cell expansion in leaves. *Plant Physiol*., *172*, 2098–2106.

Schopfer, P., Heyno, E., Drepper, F., and Krieger-Liszkay, A. (2008). Naphthoquinone-dependent generation of superoxide radicals by quinone reductase isolated from the plasma membrane of soybean. *Plant Physiol*., *147*, 864–878.

Schopfer, P., Liszkay, A., Bechtold, M., Frahry, G., and Wagner, A. (2002). Evidence that hydroxyl radicals mediate auxin-induced extension growth. *Planta*, *214*, 821–828.

Schulten, A., Bytomski, L., Quintana, J., Bernal, M., and Krämer, U. (2019). Do Arabidopsis *Squamosa promoter binding Protein-Like* genes act together in plant acclimation to copper or zinc deficiency? *Plant Direct*, *3*, e00150.

Schumacher, K., and Krebs, M. (2010). The V-ATPase: small cargo, large effects. *Curr. Opin. Plant Biol.*, *13*, 724–730.

Schwab, R., Palatnik, J. F., Riester, M., Schommer, C., Schmid, M., and Weigel, D. (2005). Specific effects of microRNAs on the plant transcriptome. *Dev. Cell*, *8*, 517–527.

Schwacke, R., Schneider, A., van der Graaff, E., Fischer, K., Catoni, E., Desimone, M., et al. (2003). ARAMEMNON, a novel database for Arabidopsis integral membrane proteins. *Plant Physiol*,, *131*, 16–26.

Seidel, T., Scholl, S., Krebs, M., Rienmüller, F., Marten, I., Hedrich, R., et al. (2012). Regulation of the V-type ATPase by redox modulation. *Biochem. J.*, *448*, 243–251.

Sew, Y. S., Ströher, E., Fenske, R., and Millar, A. H. (2016). Loss of Mitochondrial Malate Dehydrogenase Activity Alters Seed Metabolism Impairing Seed Maturation and Post-Germination Growth in Arabidopsis. *Plant Physiol.*, *171*, 849–863.

Shafi, A., Chauhan, R., Gill, T., Swarnkar, M. K., Sreenivasulu, Y., Kumar, S., Kumar, N., et al. (2015). Expression of SOD and APX genes positively regulates secondary cell wall biosynthesis and promotes plant growth and yield in Arabidopsis under salt stress. *Plant Mol. Biol.*, *87*, 615–631.

Sheng, Y., Abreu, I. A., Cabelli, D. E., Maroney, M. J., Miller, A. F., Teixeira, M., and Valentine, J. S. (2014). Superoxide dismutases and superoxide reductases. *Chem. Rev.*, *114*, 3854–3918.

Sheridan, D. L., Kong, Y., Parker, S. A., Dalby, K. N., and Turk, B. E. (2008). Substrate discrimination among mitogen-activated protein kinases through distinct docking sequence motifs. *J. Biol. Chem*., *283*, 19511–19520.

Shu, K., Chen, Q., Wu, Y., Liu, R., Zhang, H., Wang, S., et al. (2016). ABSCISIC ACID-INSENSITIVE 4 negatively regulates flowering through directly promoting Arabidopsis FLOWERING LOCUS C transcription. *J. Exp. Bot.*, *67*, 195–205.

Si, L., Chen, J., Huang, X., Gong, H., Luo, J., Hou, Q., et al. (2016). OsSPL13 controls grain size in cultivated rice. *Nat. Genet.*, *48*, 447–456.

Sierla, M., Waszczak, C., Vahisalu, T., and Kangasjärvi, J. (2016). Reactive Oxygen Species in the Regulation of Stomatal Movements. *Plant Physiol., 171*, 1569–1580.

Singh, R., Singh, S., Parihar, P., Mishra, R. K., Tripathi, D. K., Singh, V. P., et al. (2016). Reactive Oxygen Species (ROS): Beneficial Companions of Plants' Developmental Processes. *Front. Plant Sci., 7*, 1299.

Slooten, L., Capiau, K., Van Camp, W., Van Montagu, M., Sybesma, C., and Inze, D. (1995). Factors Affecting the Enhancement of Oxidative Stress Tolerance in Transgenic Tobacco Overexpressing Manganese Superoxide Dismutase in the Chloroplasts. *Plant Physiol., 107*, 737–750.

Smékalová, V., Doskočilová, A., Komis, G., and Šamaj, J. (2014). Crosstalk between secondary messengers, hormones and MAPK modules during abiotic stress signalling in plants. *Biotechnol. Adv., 32*, 2–11.

Smit, P., Limpens, E., Geurts, R., Fedorova, E., Dolgikh, E., Gough, C., et al. (2007). Medicago LYK3, an Entry Receptor in Rhizobial Nodulation Factor Signaling. *Plant Physiol., 145*, 183–191.

Smit, G., Tubbing, D. M. J., Kijne, J. W., and Lugtenberg, B, J. J. (1991). Role of Ca^{2+} in the activity of rhicadhesin from *Rhizobium leguminosarum* biovar *viciae*, which mediates the first step in attachment of *Rhizobiaceae* cells to plant root hair tips. *Arch. Microbiol., 155*, 278–283.

Smith, J. A., Poteet-Smith, C. E., Malarkey, K., and Sturgill, T. W. (1999). Identification of an extracellular signal-regulated kinase (ERK) docking site in ribosomal S6 kinase, a sequence critical for activation by ERK *in vivo*. *J. Biol. Chem., 274*, 2893–2898.

Smokvarska, M., Francis, C., Platre, M. P., Fiche, J. B., Alcon, C., Dumont, X., et al. (2020). A Plasma Membrane Nanodomain Ensures Signal Specificity during Osmotic Signaling in Plants. *Curr. Biol., 30*, 4654–4664.e4.

Soitamo, A. J., Piippo, M., Allahverdiyeva, Y., Battchikova, N., and Aro, E. M. (2008). Light has a specific role in modulating Arabidopsis gene expression at low temperature. *BMC Plant Biol., 8*, 13.

Soto, M. J., Domínguez-Ferreras, A., Pérez-Mendoza, D., Sanjuán, J., and Olivares, J. (2009). Mutualism versus pathogenesis: the give-and-take in plant-bacteria interactions. *Cell Microbiol., 11*, 381–388.

Soukup, A., and Tylová, E. (2018) Apoplastic Barriers: Their Structure and Function from a Historical Perspective. In: Sahi V., Baluška F. (eds) Concepts in Cell Biology - History and Evolution. Plant Cell Monographs, vol 23. Springer, Cham.

Stief, A., Altmann, S., Hoffmann, K., Pant, B. D., Scheible, W. R., and Bäurle, I. (2014). *Arabidopsis* miR156 Regulates Tolerance to Recurring Environmental Stress through SPL Transcription Factors. *Plant Cell, 26*, 1792–1807.

Su, S. H., Suarez-Rodriguez, M. C., and Krysan, P. (2007). Genetic interaction and phenotypic analysis of the Arabidopsis MAP kinase pathway mutations mekk1 and mpk4 suggests signaling pathway complexity. *FEBS Lett.*, 581, 3171–3177.

Su, T., Wang, P., Li, H., Zhao, Y., Lu, Y., Dai, P., et al. (2018). The Arabidopsis catalase triple mutant reveals important roles of catalases and peroxisomederived signaling in plant development. *J. Integr. Plant Biol., 60*, 591–607.

Su, J., Zhang, M., Zhang, L., Sun, T., Liu, Y., Lukowitz, W., et al. (2017). Regulation of Stomatal Immunity by Interdependent Functions of a Pathogen-Responsive MPK3/MPK6 Cascade and Abscisic Acid. *Plant Cell*, *29*, 526–542.

Suarez-Rodriguez, M. C., Adams-Phillips, L., Liu, Y., Wang, H., Su, S. H., Jester, P. J., et al. (2007). MEKK1 is required for flg22-induced MPK4 activation in Arabidopsis plants. *Plant Physiol.*, *143*, 661–669.

Suhandono, S., Apriyanto, A., and Ihsani, N. (2014). Isolation and characterization of three cassava elongation factor 1 alpha (MeEF1A) promoters. *PLOS ONE*, *9*, e84692.

Sultana, S., Khew, C. Y., Morshed, M. M., Namasivayam, P., Napis, S., and Ho, C. L. (2012). Overexpression of monodehydroascorbate reductase from a mangrove plant (AeMDHAR) confers salt tolerance on rice. *J. Plant Physiol.*, *169*, 311–318.

Sumimoto, H. (2008). Structure, regulation and evolution of Nox-family NADPH oxidases that produce reactive oxygen species. *FEBS J.*, *275*, 3249–3277.

Sumugat, M. R., Donahue, J. L., Cortes, D. F., Stromberg, V. K., Grene, R., Shulaev, V., et al. (2010). Seed development and germination in an *Arabidopsis thaliana* line antisense to glutathione reductase 2. *J. New Seeds*, *11*, 104–126.

Sundaravelpandian, K., Chandrika, N. N., and Schmidt, W. (2013). PFT1, a transcriptional Mediator complex subunit, controls root hair differentiation through reactive oxygen species (ROS) distribution in *Arabidopsis*. *New Phytol.*, *197*, 151–161.

Sunkar, R., Kapoor, A., and Zhu, J. K. (2006). Posttranscriptional induction of two Cu/Zn superoxide dismutase genes in Arabidopsis is mediated by downregulation of miR398 and important for oxidative stress tolerance. *Plant Cell*, *18*, 2051–2065.

Suzaki, T., Yoro, E., and Kawaguchi, M. (2015). Leguminous plants: Inventors of root nodules to accommodate symbiotic bacteria. *Int. Rev. Cell Mol. Biol.*, *316*, 111–158.

Suzuki, Y. J., Carini, M., and Butterfield, D. A. (2010). Protein carbonylation. *Antioxid. Redox Signal.*, *12*, 323–325.

Suzuki, N., Miller, G., Salazar, C., Mondal, H. A., Shulaev, E., Cortes, D. F., et al. (2013). Temporal-spatial interaction between reactive oxygen species and abscisic acid regulates rapid systemic acclimation in plants. *Plant Cell*, *25*, 3553–3569.

Swart, S., Logman, T. J., Smit, G., Lugtenberg, B. J., and Kijne, J. W. (1994). Purification and partial characterization of a glycoprotein from pea (*Pisum sativum*) with receptor activity for rhicadhesin, an attachment protein of Rhizobiaceae. *Plant Mol. Biol.*, *24*, 171–183.

Szklarczyk, D., Franceschini, A., Wyder, S., Forslund, K., Heller, D., Huerta-Cepas, J., et al. (2015). STRING v10: protein-protein interaction networks, integrated over the tree of life. *Nucleic Acids Res.*, *43*, D447–D452.

Takáč, T., Obert, B., Rolčík, J., and Šamaj, J. (2016a). Improvement of adventitious root formation in flax using hydrogen peroxide. *New Biotechnol.*, *33*, 728–734.

Takáč, T., and Šamaj, J. (2015). Advantages and limitations of shot-gun proteomic analyses on Arabidopsis plants with altered MAPK signaling. *Front. Plant. Sci.*, *6*, 107.

Takáč, T., Šamajová, O., Pechan, T., Luptovčiak, I., and Šamaj, J. (2017). Feedback Microtubule Control and Microtubule-Actin Cross-talk in *Arabidopsis* Revealed by Integrative Proteomic and Cell Biology Analysis of *KATANIN 1* Mutants. *Mol. Cell Proteomics*, *16*, 1591–1609.

Takáč, T., Šamajová, O., Vadovič, P., Pechan, T., Košútová, P., Ovečka, M., et al. (2014). Proteomic and biochemical analyses show a functional network of proteins involved in antioxidant defense of the *Arabidopsis anp2anp3* double mutant. *J. Proteome Res.*, *13*, 5347–5361.

Takáč, T., Vadovič, P., Pechan, T., Luptovčiak, I., Šamajová, O., and Šamaj, J. (2016b). Comparative proteomic study of Arabidopsis mutants *mpk4* and *mpk6*. *Sci. Rep.*, *6*, 28306.

Takagi, D., Takumi, S., Hashiguchi, M., Sejima, T., and Miyake, C. (2016). Superoxide and Singlet Oxygen Produced within the Thylakoid Membranes Both Cause Photosystem I Photoinhibition. *Plant Physiol.*, *171*, 1626–1634.

Tanoue, T., and Nishida, E. (2003). Molecular recognitions in the MAP kinase cascades. *Cell Signal.*, *15*, 455–462.

Tavormina, P., De Coninck, B., Nikonorova, N., De Smet, I., and Cammue, B. P. (2015). The Plant Peptidome: An Expanding Repertoire of Structural Features and Biological Functions. *Plant Cell*, *27*, 2095–2118.

Teige, M., Scheikl, E., Eulgem, T., Dóczi, R., Ichimura, K., Shinozaki, K., et al. (2004). The MKK2 pathway mediates cold and salt stress signaling in *Arabidopsis*. *Mol. Cell*, *15*, 141–152.

Testa, F., Mastronicola, D., Cabelli, D. E., Bordi, E., Pucillo, L. P., Sarti, P., et al. (2011). The superoxide reductase from the early diverging eukaryote Giardia intestinalis. *Free Radic. Biol. Med.*, *51*, 1567–1574.

Thulasi Devendrakumar, K., Li, X., and Zhang, Y. (2018). MAP kinase signalling: interplays between plant PAMP- and effector-triggered immunity. *Cell. Mol. Life Sci.*, *75*, 2981–2989.

Tian, C. F., Garnerone, A. M., Mathieu-Demazière, C., Masson-Boivin, C., and Batut, J. (2012). Plant-activated bacterial receptor adenylate cyclases modulate epidermal infection in the *Sinorhizobium meliloti–Medicago* symbiosis. *Proc. Natl. Acad. Sci. U. S. A.*, *109*, 6751–6756.

Tognetti, V. B., Van Aken, O., Morreel, K., Vandenbroucke, K., van de Cotte, B., De Clercq, I., et al. (2010). Perturbation of indole-3-butyric acid homeostasis by the UDP-glucosyltransferase *UGT74E2* modulates *Arabidopsis* architecture and water stress tolerance. *Plant Cell*, *22*, 2660–2679.

Torres, M. A., and Dangl, J. L. (2005). Functions of the respiratory burst oxidase in biotic interactions, abiotic stress and development. *Curr. Opin. Plant Biol.*, *8*, 397–403.

Triantaphylidès, C., and Havaux, M. (2009). Singlet oxygen in plants: production, detoxification and signaling. *Trends Plant Sci.*, *14*, 219–228.

Tripathi, R. K., Bregitzer, P., and Singh, J. (2018). Genome-wide analysis of the SPL/miR156 module and its interaction with the AP2/miR172 unit in barley. *Sci. Rep.*, *8*, 7085.

Tripathi, N. K., and Shrivastava, A. (2019). Recent Developments in Bioprocessing of Recombinant Proteins: Expression Hosts and Process Development. *Front. Bioeng. Biotechnol.*, *7*, 420.

Tsang, C. K., Chen, M., Cheng, X., Qi, Y., Chen, Y., Das, I., et al. (2018). SOD1 phosphorylation by mTORC1 couples nutrient sensing and redox regulation. *Mol. Cell*, *70*, 502–515.e8.

Tsang, C. K., Liu, Y., Thomas, J., Zhang, Y., and Zheng, X. F. (2014). Superoxide dismutase 1 acts as a nuclear transcription factor to regulate oxidative stress resistance. *Nat. Commun.*, *5*, 3446.

Tsukagoshi, H. (2012). Defective root growth triggered by oxidative stress is controlled through the expression of cell cycle-related genes. *Plant Sci.*, *197*, 30–39.

Tsukagoshi, H. (2016). Control of root growth and development by reactive oxygen species. *Curr. Opin. Plant Biol.*, *29*, 57–63.

Tuzet, A., Rahantaniaina, M. S., and Noctor, G. (2019). Analyzing the function of catalase and the ascorbate-glutathione pathway in H_2O_2 processing: insights from an experimentally constrained kinetic model. *Antioxid. Redox Signal.*, *30*, 1238–1268.

Urrea Castellanos, R., Friedrich, T., Petrovic, N., Altmann, S., Brzezinka, K., Gorka, M., et al. (2020). FORGETTER2 protein phosphatase and phospholipase D modulate heat stress memory in Arabidopsis. *Plant J.*, *104*, 7–17.

Usami, T., Horiguchi, G., Yano, S., and Tsukaya, H. (2009). The *more and smaller cells* mutants of *Arabidopsis thaliana* identify novel roles for *SQUAMOSA PROMOTER BINDING PROTEIN-LIKE* genes in the control of heteroblasty. *Development*, *136*, 955–964.

Ushimaru, T., Nakagawa, T., Fujioka, Y., Daicho, K., Naito, M., Yamauchi, Y., et al. (2006). Transgenic Arabidopsis plants expressing the rice dehydroascorbate reductase gene are resistant to salt stress. *J. Plant Physiol.*, *163*, 1179–1184.

Vadassery, J., Tripathi, S., Prasad, R., Varma, A., and Oelmüller, R. (2009). Monodehydroascorbate reductase 2 and dehydroascorbate reductase 5 are crucial for a mutualistic interaction between *Piriformospora indica* and *Arabidopsis*. *J. Plant Physiol.*, *166*, 1263–1274.

Vadovič, P., Šamajová, O., Takáč, T., Novák, D., Zapletalová, V., Colcombet, J., and Šamaj, J. (2019). Biochemical and Genetic Interactions of Phospholipase D Alpha 1 and Mitogen-Activated Protein Kinase 3 Affect Arabidopsis Stress Response. *Front. Plant Sci.*, *10*, 275.

Van Aken, O., and Van Breusegem, F. (2015). Licensed to Kill: Mitochondria, Chloroplasts, and Cell Death. *Trends Plant Sci.*, *20*, 754–766.

Van Breusegem, F., and Dat, J. F. (2006). Reactive oxygen species in plant cell death. *Plant Physiol.*, *141*, 384–390.

Van Breusegem, F., Slooten, L., Stassart, J. M., Moens, T., Botterman, J., Van Montagu, M., and Inzé, D. (1999). Overproduction of *Arabidopsis thaliana* FeSOD confers oxidative stress tolerance to transgenic maize. *Plant Cell Physiol.*, *40*, 515–523.

Van Camp, W., Capiau, K., Van Montagu, M., Inzé, D., and Slooten, L. (1996). Enhancement of oxidative stress tolerance in transgenic tobacco plants overproducing Fe-superoxide dismutase in chloroplasts. *Plant Physiol.*, *112*, 1703–1714.

Vance, C. K., and Miller, A. F. (1998). Spectroscopic comparisons of the pH dependencies of Fe-substituted (Mn)superoxide dismutase and Fe-superoxide dismutase. *Biochemistry*, *37*, 5518–5527.

Vance, C. K., and Miller, A. F. (2001). Novel insights into the basis for *Escherichia coli* superoxide dismutase's metal ion specificity from Mn-substituted FeSOD and its very high E_m. *Biochemistry*, *40*, 13079–13087.

Vanlerberghe, G. C. (2013). Alternative oxidase: a mitochondrial respiratory pathway to maintain metabolic and signaling homeostasis during abiotic and biotic stress in plants. *Int. J. Mol. Sci.*, *14*, 6805–6847.

Verbon, E. H., Post, J. A., and Boonstra, J. (2012). The influence of reactive oxygen species on cell cycle progression in mammalian cells. *Gene*, *511*, 1–6.

Vescovi, M., Zaffagnini, M., Festa, M., Trost, P., Lo Schiavo, F., and Costa, A. (2013). Nuclear accumulation of cytosolic glyceraldehyde-3-phosphate dehydrogenase in cadmium-stressed Arabidopsis roots. *Plant Physiol.*, *162*, 333–346.

Vogel, M. O., Moore, M., König, K., Pecher, P., Alsharafa, K., Lee, J., et al. (2014). Fast retrograde signaling in response to high light involves metabolite export, MITOGEN-ACTIVATED PROTEIN KINASE6, and AP2/ERF transcription factors in *Arabidopsis*. *Plant Cell*, *26*, 1151–1165.

Volkening, K., Leystra-Lantz, C., Yang, W., Jaffee, H., and Strong, M. J. (2009). Tar DNA binding protein of 43 kDa (TDP-43), 14-3-3 proteins and copper/zinc superoxide dismutase (SOD1) interact to modulate NFL mRNA stability. Implications for altered RNA processing in amyotrophic lateral sclerosis (ALS). *Brain Res*., *1305*, 168–182.

Vu, L. D., Gevaert, K., and De Smet, I. (2018). Protein language: post-translationalmodifications talking to each other. *Trends Plant Sci*., *23*, 1068–1080.

Wang, B. B., and Brendel, V. (2006). Molecular characterization and phylogeny of U2AF35 homologs in plants. *Plant Physiol.*, *140*, 624–636.

Wang, X. L., Cui, W. J., Feng, X. Y., Zhong, Z. M., Li, Y., Chen, W. X., et al. (2018a). Rhizobia inhabiting nodules and rhizosphere soils of alfalfa: A strong selection of facultative microsymbionts. *Soil Biol. Biochem.*, *116*, 340-350.

Wang, B., Ding, H., Chen, Q., Ouyang, L., Li, S., and Zhang, J. (2019). Enhanced tolerance to methyl viologen-mediated oxidative stress via AtGR2 expression from chloroplast genome. *Front. Plant Sci*., *10*, 1178.

Wang, P., Du, Y., Li, Y., Ren, D., and Song, C. P. (2010a). Hydrogen peroxide-mediated activation of MAP kinase 6 modulates nitric oxide biosynthesis and signal transduction in *Arabidopsis*. *Plant Cell*, *22*, 2981–2998.

Wang, Z., and Gou, X. (2020). Receptor-Like Protein Kinases Function Upstream of MAPKs in Regulating Plant Development. *Int. J. Mol. Sci.*, *21*, 7638.

Wang, P., Hawkins, T. J., and Hussey, P. J. (2017). Connecting membranes to the actin cytoskeleton. *Curr. Opin. Plant Biol.*, *40*, 71–76.

Wang, Y., Li, J., Hou, S., Wang, X., Li, Y., Ren, D., et al. (2010b). A *Pseudomonas syringae* ADP-ribosyltransferase inhibits *Arabidopsis* mitogen-activated protein kinase kinases. *Plant Cell*, *22*, 2033–2044.

Wang, Q., Liu, J., and Zhu, H. (2018b). Genetic and Molecular Mechanisms Underlying Symbiotic Specificity in Legume-Rhizobium Interactions. *Front. Plant Sci.*, *9*, 313.

Wang, Z., Xiao, Y., Chen, W., Tang, K., and Zhang, L. (2010c). Increased vitamin C content accompanied by an enhanced recycling pathway confers oxidative stress tolerance in *Arabidopsis*. *J. Integr. Plant Biol.*, *52*, 400–409.

Wang, P., Xue, L., Batelli, G., Lee, S., Hou, Y. J., Van Oosten, M. J., et al. (2013). Quantitative phosphoproteomics identifies SnRK2 protein kinase substrates and reveals the effectors of abscisic acid action. *Proc. Natl. Acad. Sci. U. S. A.*, *110*, 11205–11210.

Wang, Y., Ying, Y., Chen, J., and Wang, X. (2004). Transgenic *Arabidopsis* overexpressing Mn-SOD enhanced salt-tolerance. *Plant Sci.*, *67*, 671–677.

Wani Z. A., and Ashraf N. (2018). Transcriptomic Studies Revealing Enigma of Plant-Pathogen Interaction. In: Singh A., Singh I. (eds) Molecular Aspects of Plant-Pathogen Interaction. Springer, Singapore.

Waszczak, C., Akter, S., Eeckhout, D., Persiau, G., Wahni, K., Bodra, N., et al. (2014). Sulfenome mining in *Arabidopsis thaliana*. *Proc. Natl. Acad. Sci. U. S. A.*, *111*, 11545–11550.

Waszczak, C., Akter, S., Jacques, S., Huang, J., Messens, J., and Van Breusegem, F. (2015). Oxidative post-translational modifications of cysteine residues in plant signal transduction. *J. Exp. Bot.*, *66*, 2923–2934.

Waszczak, C., Carmody, M., and Kangasjärvi, J. (2018). Reactive Oxygen Species in Plant Signaling. *Annu. Rev. Plant Biol.*, *69*, 209–236.

Waters, B. M., McInturf, S. A., and Stein, R. J. (2012). Rosette iron deficiency transcript and microRNA profiling reveals links between copper and iron homeostasis in *Arabidopsis thaliana*. *J. Exp. Bot.*, *63*, 5903–5918.

Wu, F., Chi, Y., Jiang, Z., Xu, Y., Xie, L., Huang, F., et al. (2020). Hydrogen peroxide sensor HPCA1 is an LRR receptor kinase in *Arabidopsis*. *Nature*, *578*, 577–581.

Wu, T. M., Lin, W. R., Kao, C. H., and Hong, C. Y. (2015). Gene knockout of glutathione reductase 3 results in increased sensitivity to salt stress in rice. *Plant Mol. Biol.*, *87*, 555–564.

Xia, X. J., Zhou, Y. H., Shi, K., Zhou, J., Foyer, C. H., and Yu, J. Q. (2015). Interplay between reactive oxygen species and hormones in the control of plant development and stress tolerance. *J. Exp. Bot.*, *66*, 2839–2856.

Xiang, T., Zong, N., Zou, Y., Wu, Y., Zhang, J., Xing, W., et al. (2008). *Pseudomonas syringae* effector AvrPto blocks innate immunity by targeting receptor kinases. *Curr. Biol.*, *18*, 74–80.

Xiao, J., Li, C., Xu, S., Xing, L., Xu, Y., and Chong, K. (2015). JACALIN-LECTIN LIKE1 Regulates the Nuclear Accumulation of GLYCINE-RICH RNA-BINDING PROTEIN7, Influencing the RNA Processing of *FLOWERING LOCUS C* Antisense Transcripts and Flowering Time in Arabidopsis. *Plant Physiol.*, *169*, 2102–2117.

Xie, Z., Nolan, T., Jiang, H., Tang, B., Zhang, M., Li, Z., and Yin, Y. (2019). The AP2/ERF Transcription Factor TINY Modulates Brassinosteroid-Regulated Plant Growth and Drought Responses in Arabidopsis. *Plant Cell*, *31*, 1788–1806.

Xie, K., Wu, C., and Xiong, L. (2006). Genomic organization, differential expression, and interaction of SQUAMOSA promoter-binding-like transcription factors and microRNA156 in rice. *Plant Physiol.*, *142*, 280–293.

Xing, Y., Cao, Q., Zhang, Q., Qin, L., Jia, W., and Zhang, J. (2013). MKK5 regulates high light-induced gene expression of Cu/Zn superoxide dismutase 1 and 2 in Arabidopsis. *Plant Cell Physiol.*, *54*, 1217–1227.

Xing, Y., Chen, W. H., Jia, W., and Zhang, J. (2015). Mitogen-activated protein kinase kinase 5 (MKK5)-mediated signalling cascade regulates expression of iron superoxide dismutase gene in *Arabidopsis* under salinity stress. *J. Exp. Bot.*, *66*, 5971–5981.

Xing, Y., Jia, W., and Zhang, J. (2007). AtMEK1 mediates stress-induced gene expression of CAT1 catalase by triggering H_2O_2 production in *Arabidopsis*. *J. Exp. Bot.*, *58*, 2969–2981.

Xing, Y., Jia, W., and Zhang, J. (2008). AtMKK1 mediates ABA-induced *CAT1* expression and H_2O_2 production via AtMPK6-coupled signaling in Arabidopsis. *Plant J.*, *54*, 440–451.

Xiong, F., Ren, J. J., Yu, Q., Wang, Y. Y., Lu, C. C., Kong, L. J., et al. (2019). AtU2AF65b functions in abscisic acid mediated flowering via regulating the precursor messenger RNA splicing of *ABI5* and *FLC* in *Arabidopsis*. *New Phytol.*, *223*, 277–292.

Xu, J., and Chua, N. H. (2012). Dehydration stress activates Arabidopsis MPK6 to signal DCP1 phosphorylation. *EMBO J.*, *31*, 1975–1984.

Xu, Z., Escamilla-Treviño, L., Zeng, L., Lalgondar, M., Bevan, D., Winkel, B., et al. (2004). Functional genomic analysis of *Arabidopsis thaliana* glycoside hydrolase family 1. *Plant Mol. Biol.*, *55*, 343–367.

Xu, X. M., Lin, H., Maple, J., Björkblom, B., Alves, G., Larsen, J. P., and Møller, S. G. (2010). The *Arabidopsis* DJ-1a protein confers stress protection through cytosolic SOD activation. *J. Cell Sci.*, *123*, 1644–1651.

Xue, Y., Zhou, F., Zhu, M., Ahmed, K., Chen, G., and Yao, X. (2005). GPS: acomprehensive www server for phosphorylation sites prediction. *Nucleic Acids Res.*, 33, W184–W187.

Yamaguchi, A., Wu, M. F., Yang, L., Wu, G., Poethig, R. S., and Wagner, D. (2009). The microRNA-regulated SBP-Box transcription factor SPL3 is a direct upstream activator of LEAFY, FRUITFULL, and APETALA1. *Dev. Cell.*, *17*, 268–278.

Yamakura, F., and Kawasaki, H. (2010). Post-translational modifications of superoxide dismutase. *Biochim. Biophys. Acta*, *1804*, 318–325.

Yamakura, F., Taka, H., Fujimura, T., and Murayama, K. (1998). Inactivation of human manganese-superoxide dismutase by peroxynitrite is caused by exclusive nitration of tyrosine 34 to 3-nitrotyrosine. *J. Biol. Chem.*, *273*, 14085–14089.

Yamasaki, H., Abdel-Ghany, S. E., Cohu, C. M., Kobayashi, Y., Shikanai, T., and Pilon, M. (2007). Regulation of copper homeostasis by micro-RNA in Arabidopsis. *J. Biol. Chem.*, *282*, 16369–16378.

Yamasaki, H., Hayashi, M., Fukazawa, M., Kobayashi, Y., and Shikanai, T. (2009). SQUAMOSA promoter binding protein-like7 is a central regulator for copper homeostasis in Arabidopsis. *Plant Cell*, *21*, 347–361.

Yamasaki, K., Kigawa, T., Inoue, M., Tateno, M., Yamasaki, T., Yabuki, T., et al. (2004). A novel zinc-binding motif revealed by solution structures of DNA-binding domains of Arabidopsis SBP-family transcription factors. *J. Mol. Biol.*, *337*, 49–63.

Yan, J., Chia, J. C., Sheng, H., Jung, H. I., Zavodna, T. O., Zhang, L., et al. (2017a). Arabidopsis Pollen Fertility Requires the Transcription Factors CITF1 and SPL7 That Regulate Copper Delivery to Anthers and Jasmonic Acid Synthesis. *Plant Cell*, *29*, 3012–3029.

Yan, Q., Xia, X., Sun, Z., and Fang, Y. (2017b). Depletion of *Arabidopsis* SC35 and SC35-like serine/arginine-rich proteins affects the transcription and splicing of a subset of genes. *PLOS Genet.*, *13*, e1006663.

Yang, H., Mu, J., Chen, L., Feng, J., Hu, J., Li, L., et al. (2015). S-Nitrosylation positively regulates ascorbate peroxidase activity during plant stress responses. *Plant Physiol.*, *167*, 1604–1615.

Yang, T., Shad Ali, G., Yang, L., Du, L., Reddy, A. S., and Poovaiah, B. W. (2010). Calcium/calmodulin-regulated receptor-like kinase CRLK1 interacts with MEKK1 in plants. *Plant Signal. Behav.*, *5*, 991–994.

Yang, Z., Wang, X., Gu, S., Hu, Z., Xu, H., and Xu, C. (2008). Comparative study of SBP-box gene family in Arabidopsis and rice. *Gene*, *407*, 1–11.

Yesbergenova, Z., Yang, G., Oron, E., Soffer, D., Fluhr, R., and Sagi, M. (2005). The plant Mo-hydroxylases aldehyde oxidase and xanthine dehydrogenase have distinct reactive oxygen species signatures and are induced by drought and abscisic acid. *Plant J.*, *42*, 862–876.

Yi, D., Alvim Kamei, C. L., Cools, T., Vanderauwera, S., Takahashi, N., Okushima, Y., et al. (2014). The *Arabidopsis* SIAMESE-RELATED cyclin-dependent kinase inhibitors SMR5 and SMR7 regulate the DNA damage checkpoint in response to reactive oxygen species. *Plant Cell*, *26*, 296–309.

Yin, J., Guan, X., Zhang, H., Wang, L., Li, H., Zhang, Q., et al. (2019) An MAP kinase interacts with LHK1 and regulates nodule organogenesis in Lotus japonicus. *Sci. China Life Sci.*, *62*, 1–15.

Yin, L., Mano, J., Tanaka, K., Wang, S., Zhang, M., Deng, X., et al. (2017). High level of reduced glutathione contributes to detoxification of lipid peroxidederived reactive carbonyl species in transgenic Arabidopsis overexpressing glutathione reductase under aluminum stress. *Physiol. Plant.*, *161*, 211–223.

Yin, L., Wang, S., Eltayeb, A. E., Uddin, M. I., Yamamoto, Y., Tsuji, W., et al. (2010). Overexpression of dehydroascorbate reductase, but not monodehydroascorbate reductase, confers tolerance to aluminum stress in transgenic tobacco. *Planta*, *231*, 609–621.

Yokoyama, T., Ohkubo, T., Kamiya, K., and Hara, M. (2020). Cryoprotective activity of Arabidopsis KS-type dehydrin depends on the hydrophobic amino acids of two active segments. *Arch. Biochem. Biophys.*, *691*, 108510.

Yoo, S. D., Cho, Y. H., Tena, G., Xiong, Y., and Sheen, J. (2008). Dual control of nuclear EIN3 by bifurcate MAPK cascades in C_2H_4 signalling. *Nature*, *451*, 789–795.

Yoshida, S., Tamaoki, M., Shikano, T., Nakajima, N., Ogawa, D., Ioki, M., et al. (2006). Cytosolic dehydroascorbate reductase is important for ozone tolerance in *Arabidopsis thaliana*. *Plant Cell Physiol.*, *47*, 304–308.

Yu, L., Nie, J., Cao, C., Jin, Y., Yan, M., Wang, F., et al. (2010). Phosphatidic acid mediates salt stress response by regulation of MPK6 in *Arabidopsis thaliana*. *New Phytol.*, *188*, 762–773.

Yu, X., Pasternak, T., Eiblmeier, M., Ditengou, F., Kochersperger, P., Sun, J., et al. (2013). Plastid-localized glutathione reductase2-regulated glutathione redox status is essential for *Arabidopsis* root apical meristem maintenance. *Plant Cell*, *25*, 4451–4468.

Zandalinas, S. I., Sengupta, S., Burks, D., Azad, R. K., and Mittler, R. (2019). Identification and characterization of a core set of ROS wave-associated transcripts involved in the systemic acquired acclimation response of Arabidopsis to excess light. *Plant J.*, *98*, 126–141.

Zechmann, B. (2018). Compartment-specific importance of ascorbate during environmental stress in plants. Antioxid. *Redox Signal.*, *29*, 1488–1501.

Zeeshan, H. M., Lee, G. H., Kim, H. R., and Chae, H. J. (2016). Endoplasmic Reticulum Stress and Associated ROS. *Int. J. Mol. Sci.*, *17*, 327.

Zeng, L., Velásquez, A. C., Munkvold, K. R., Zhang, J., and Martin, G. B. (2012). A tomato LysM receptor-like kinase promotes immunity and its kinase activity is inhibited by AvrPtoB. *Plant J.*, *69*, 92–103.

Zhang, S., Li, C., Ren, H., Zhao, T., Li, Q., Wang, S., et al. (2020). BAK1 mediates light ibargntensity to phosphorylate and activate catalases to regulate plant growth and development. *Int. J. Mol. Sci.*, *21*, 1437.

Zhang, Z., Liu, Y., Huang, H., Gao, M., Wu, D., Kong, Q., and Zhang, Y. (2017). The NLR protein SUMM2 senses the disruption of an immune signaling MAP kinase cascade via CRCK3. *EMBO Rep.*, *18*, 292–302.

Zhang, B., Liu, X., Zhao, G., Mao, X., Li, A., and Jing, R. (2014). Molecular characterization and expression analysis of Triticum aestivum squamosa-promoter binding protein-box genes involved in ear development. *J. Integr. Plant Biol.*, *56*, 571–581.

Zhang, J., Shao, F., Li, Y., Cui, H., Chen, L., Li, H., et al. (2007). A *Pseudomonas syringae* effector inactivates MAPKs to suppress PAMP-induced immunity in plants. *Cell Host Microbe*, *1*, 175–185.

Zhang, Z., Wu, Y., Gao, M., Zhang, J., Kong, Q., Liu, Y., et al. (2012). Disruption of PAMP-induced MAP kinase cascade by a *Pseudomonas syringae* effector activates plant immunity mediated by the NB-LRR protein SUMM2. *Cell Host Microbe*, *11*, 253–263.

Zhang, Y., Xiao, Y., Du, F., Cao, L., Dong, H., and Ren, H. (2011). Arabidopsis VILLIN4 is involved in root hair growth through regulating actin organization in a Ca^{2+}-dependent manner. *New Phytol.*, *190*, 667–682.

Zhang, H., Zhou, H., Berke, L., Heck, A. J., Mohammed, S., Scheres, B., et al. (2013). Quantitative phosphoproteomics after auxin-stimulated lateral root induction identifies an SNX1 protein phosphorylation site required for growth. *Mol. Cell. Proteomics*, *12*, 1158–1169.

Zhang, T., Zhu, M., Song, W. Y., Harmon, A. C., and Chen, S. (2015). Oxidation and phosphorylation of MAP kinase 4 cause protein aggregation. *Biochim. Biophys. Acta*, *1854*, 156–165.

Zhang, Y., Zhu, H., Zhang, Q., Li, M., Yan, M., Wang, R., et al. (2009). Phospholipase Dα1 and Phosphatidic Acid Regulate NADPH Oxidase Activity and Production of Reactive Oxygen Species in ABA-Mediated Stomatal Closure in Arabidopsis. *Plant Cell*, *21*, 2357–2377.

Zhao, Q., and Guo, H. W. (2011). Paradigms and paradox in the ethylene signaling pathway and interaction network. *Mol Plant.*, *4*, 626–634.

Zhao, C., Wang, P., Si, T., Hsu, C. C., Wang, L., Zayed, O., et al. (2017). MAP Kinase Cascades Regulate the Cold Response by Modulating ICE1 Protein Stability. *Dev. Cell*, *43*, 618–629.e5.

Zhao, Y., Yu, H., Zhou, J. M., Smith, S. M., and Li, J. (2020). Malate Circulation: Linking Chloroplast Metabolism to Mitochondrial ROS. *Trends Plant Sci.*, *25*, 446–454.

Zhong, S., and Chang, C. (2012). Ethylene signalling: The CTR1 protein kinase. In Annual Plant Reviews Volume 44: The Plant Hormone Ethylene, M. T. McManus, ed. (Wiley-Blackwell), pp. 147–168.

Zhong, H. H., and McClung, C. R. (1996). The circadian clock gates expression of two *Arabidopsis* catalase genes to distinct and opposite circadian phases. *Mol. Gen. Genet.*, *251*, 196–203.

Zhong, H. H., Resnick, A. S., Straume, M., and Robertson McClung, C. (1997). Effects of synergistic signaling by phytochrome A and cryptochrome1 on circadian clock-regulated catalase expression. *Plant Cell*, *9*, 947–955.

Zhou, S., Chen, Q., Li, X., and Li, Y. (2017). MAP65-1 is required for the depolymerization and reorganization of cortical microtubules in the response to salt stress in *Arabidopsis*. *Plant Sci.*, *264*, 112–121.

Zhou, S., Jia, L., Chu, H., Wu, D., Peng, X., Liu, X., et al. (2016). *Arabidopsis* CaM1 and CaM4 Promote Nitric Oxide Production and Salt Resistance by Inhibiting *S*-Nitrosoglutathione Reductase via Direct Binding. *PLOS Genet.*, *12*, e1006255.

Zhou, Y. B., Liu, C., Tang, D. Y., Yan, L., Wang, D., Yang, Y. Z., et al. (2018). The receptor-like cytoplasmic kinase STRK1 phosphorylates and activates CatC, thereby regulating H_2O_2 homeostasis and improving salt tolerance in rice. *Plant Cell*, *30*, 1100–1118.

Zhou, J., Wu, S., Chen, X., Liu, C., Sheen, J., Shan, L., and He, P. (2014). The *Pseudomonas syringae* effector HopF2 suppresses Arabidopsis immunity by targeting BAK1. *Plant J.*, *77*, 235–245.

Zipfel, C., Kunze, G., Chinchilla, D., Caniard, A., Jones, J. D., Boller, T., and Felix, G. (2006). Perception of the bacterial PAMP EF-Tu by the receptor EFR restricts *Agrobacterium*-mediated transformation. *Cell*, *125*, 749–760.

Zou, J. J., Li, X. D., Ratnasekera, D., Wang, C., Liu, W. X., Song, L. F., et al. (2015). Arabidopsis CALCIUM-DEPENDENT PROTEIN KINASE8 and CATALASE3 function in abscisic acid-mediated signaling and H_2O_2 homeostasis in stomatal guard cells under drought stress. *Plant Cell*, *27*, 1445–1460.

Zou, M., Ren, H., and Li, J. (2019). An Auxin Transport Inhibitor Targets Villin-Mediated Actin Dynamics to Regulate Polar Auxin Transport. *Plant Physiol.*, *181*, 161–178.

Zulawski, M., Braginets, R., and Schulze, W. X. (2013). PhosPhAtgoeskinases-searchable protein kinase target information in the plantphosphorylation site database PhosPhAt. *Nucleic Acids Res.*, *41*, D1176–D1184.

Zulawski, M., Schulze, G., Braginets, R., Hartmann, S., and Schulze, W. X. (2014). The Arabidopsis Kinome: phylogeny and evolutionary insights into functional diversification. *BMC Genomics*, *15*, 548.

Zwack, P. J., De Clercq, I., Howton, T. C., Hallmark, H. T., Hurny, A., Keshishian, E. A., et al. (2016). Cytokinin Response Factor 6 Represses Cytokinin-Associated Genes during Oxidative Stress. *Plant Physiol*, *172*, 1249–1258.

Zybailov, B., Rutschow, H., Friso, G., Rudella, A., Emanuelsson, O., Sun, Q., and van Wijk, K. J. (2008). Sorting signals, N-terminal modifications and abundance of the chloroplast proteome. *PLOS ONE*, *3*, e1994.

6 Abbreviations

$_1O^2$	Singlet oxygen
ABA	Abscisic acid
ANP	ARABIDOPSIS HOMOLOGUES OF NUCLEUS AND PHRAGMOPLAST LOCALIZED KINASES
AO	Aldehyde oxidase
APX	Ascorbate peroxidase
AU	Arbitrary units
BAK	BRASSINOSTEROID INSENSITIVE 1-ASSOCIATED RECEPTOR KINASE
Bp	Base pair
BSA	Bovine serum albumin
CAT	Catalase
CCS	COPPER CHAPERONE FOR SUPEROXIDE DISMUTASE
CD	Common docking
CDPK	Calcium-dependent protein kinas
CERK	CHITIN ELICITOR RECEPTOR KINASE
CLSM	Confocal laser scanning microscopy
Col-0	Columbia
CPN20	CHAPERONIN 20
CSD	Cu/Zn superoxide dismutase
C-terminal	Carboxy-terminal
CuRE	Copper responsive
D	D-site
DAG	Day after germination
DAMP	Danger-associated molecular patterns
DAP	Differentially abundant protein
DAPI	4,6-diamidino-2-phenylindole
DCP1	DECAPPING 1
DHAR	Dehydroascorbate reductase
DIG	Digoxigenin
ECL	Enhanced chemiluminescence
EFR	ELONGATION FACTOR THERMO UNSTABLE RECEPTOR

EF-Tu	ELONGATION FACTOR THERMO UNSTABLE
ERF	ETHYLENE RESPONSE FACTOR
ETC	Electron transport chain
FEP	Fluorinated ethylene propylene
FLS2	FLAGELLIN SENSING 2
FRAP	Fluorescence recovery after photobleaching
FSD	Fe superoxide dismutase
GFP	GREEN FLUORESCENT PROTEIN
GO	Gene ontology
GR	Glutathione reductase
GST	Glutathione S-transferase
H_2O_2	Hydrogen peroxide
$HO^{\cdot}$	Hydroxyl radical
HPCA1	HYDROGEN-PEROXIDE-INDUCED Ca2+ INCREASES 1
HPLC	High-performance liquid chromatography
HSF	Heat shock transcription factor
HSP	Heat shock protein
IT	Infection thread
JA	Jasmonic acid
kDa	kilodaltons
KO	Knock-out
LRP	Lateral root primordia
LSFM	Light-sheet fluorescence microscopy
LYK3	LYSIN MOTIF RECEPTOR-LIKE KINASE 3
MAMP	Microbe-associated molecular patterns
MAP2K, MEK or MAPKK	Mitogen-activated protein kinase kinase
MAP3K, MEKK or MAPKKK	Mitogen-activated protein kinase kinase kinase
MAPK or MPK	Mitogen-activated protein kinase
MBP	Maltose-binding protein
MDHA	Monodehydroascorbate
MDHAR	Monodehydroascorbate reductase
MKP	MAPK phosphatase

MKS1	MPK4 SUBSTRATE 1
MMS	Root and plant development medium
MS	Murashige and Skoog
MSD	Mn superoxide dismutase
mTORC1	MAMMALIAN TARGET OF RAPAMYCIN COMPLEX 1
MV	Methyl viologen
MyBP	Myelin basic protein
NA	Numerical aperture
NFR	NOD FACTOR RECEPTOR
Nod	Nodulation
NP40	Nonidet P-40
$O_2^{\cdot -}$	Superoxide anion
OD_{600}	Optical density measured at a wavelength of 600 nm
PA	Phosphatidic acid
PAMP	Pathogen-associated molecular patterns
PBS	Phosphate-buffered saline
PCD	Programmed cell death
PDF	Plant defensin
pERK	Anti-phospho ERK antibody
PK	Protein kinase
PLD	Phospholipase D
PM	Plasmatic membrane
PR	Pathogenesis-related
PRKK	PATHOGEN-RESPONSIVE MAPKK
PRR	Pattern-recognition receptors
PS	Photosystem
PTI	Pathogen-triggered immunity
PTM	Posttranslational modification
PVDF	Polyvinylidene difluoride
R	Resistance
RBOH	RESPIRATORY BURST OXIDASE HOMOLOG
RDA	Result dependent acquisition
RHD	Root Hair Defective
RLCK	Receptor-like cytosolic kinase

RLK	Receptor-like kinase
RNS	Reactive nitrogen species
ROI	Regions of interest
ROP	Rho-of-plant
ROS	Reactive oxygen species
rpm	Rotation per minute
RSY	Regen-SY cultivar
RT	Room temperature
SA	Salicylic acid
SAA	Systemic acquired acclimation
SAMK or MMK4	STRESS-ACTIVATED MAPK
SAR	Systemic acquired resistance
SBP	SQUAMOSA PROMOTER BINDING PROTEIN
SCR	SCARECROW
SD	Standard deviation
SDS-PAGE	Sodium dodecyl sulphate-polyacrylamide gel electrophoresis
SHR	SHORTROOT
SIMK or MMK1	STRESS-INDUCED MAPK
SIMKK	STRESS-INDUCED MAPKK
SIMKKi	SIMKK RNAi line
SOD	Superoxide dismutase
SPL	SQUAMOSA-PROMOTER BINDING PROTEIN-LIKE
SSC	Saline-sodium citrate buffer
TBE	Tris/Borate/EDTA buffer
TBS	Tris-buffered-saline
TBS-T	TBS, 0.1% Tween 20
T-DNA	Transfer DNA
TF	Transcription factor
TMR	Transmembrane receptor
UTR	UTR
UV	Ultra violet
YFP	Yellow fluorescent protein

7 Curriculum vitae

Mgr. Petr Dvořák

Address:	Jar. Haška 674/6 Třebíč 67401
Date of birth:	6th February 1991
Place of birth:	Brno
E-mail:	petr.dvorak1@upol.cz
Phone:	+420 734 591 758

Education

Ph.D. study in Biochemistry 2016 – present
Palacký University Olomouc
Title of Ph.D. thesis: Biochemical and proteomic analysis of mitogen-activated protein kinase signaling during oxidative

Master's program in Biochemistry 2014 – 2016
Palacký University Olomouc
Title of Master's thesis: Purification and enzymatic characterization of putative plant adenosine deaminase

Bachelor's programme in Biochemistry 2011 – 2014
Palacký University Olomouc
Title of Bachelor's thesis: Expression and characterization of putative plant adenosine deaminase

Employment

Ph.D. student / academic researcher 09/2018 – present
Centre of the Region Haná for Biotechnological and Agricultural Research, Department of Cell Biology, Faculty of Science, Palacký University Olomouc

Research Internships abroad

University of Helsinki 09/2019 – 11/2019

Faculty of Biological and Environmental Sciences, Organismal and Evolutionary Biology Research Programme, Receptor-Ligand Signaling Group. Laboratory of doc. MSc. Michael Wrzaczek, Ph.D.

Project participation

- "Plants as a tool for sustainable global development" European Regional Development Fund (ERDF), project No. CZ.02.1.01/0.0/0.0/16_019/0000827, position: Ph.D. student / academic researcher. 2018 – present
- "Developmental and subcellular localization of annexin 1 in *Arabidopsis* root using advanced microscopy methods" (IGA_PřF_2018_031), position: Ph.D. student. 2018
- "Analysis of PLDα1, MPK3 and microtubules in plants" (IGA_PřF_2017_026), position: Ph.D. student. 2017
- "Proteomic analysis to study of microtubule severing by katanin in *Arabidopsis*" (IGA_PřF_2016_012), position: Ph.D. student. 2017

Teaching Experience

CRH / PKR Plant tissue culture (practical course) 2016-2019

CRH / TR Transient and stable transformations of plant 2018

List of Attended Conferences

Posters:

- **Dvořák, P**., Takáč, T., Pechan, T., Šamaj, J. (2017) Proteomic and biochemical analysis of mitogen-activated protein kinases in *Arabidopsis* roots during oxidative stress. 4th Meeting on Biotechnology of Plant Products: Green For Good IV - G4G, Olomouc, poster P7.40.
- **Dvořák, P**., Škoríková, M., Šamajová, O., Ovečka, M., Šamaj, J. (2018) Annexin1 localization by light sheet fluorescence microscopy during early root

development of *Arabidopsis*. SEB's Annual Meeting, Florence, Italy. Abstract P7.40.

- **Dvořák, P**., Miroslav, O., Takáč, T., Šamaj, J. (2019). Biochemical analysis and activation of mitogen-activated protein kinases of *Medicago sativa* lines in response to various elicitors and *Sinorhizobium meliloti* treatment. Plant Biotechnology: Green for Good V – G5G, Olomouc, Abstract P 77.
- Takáč, T., **Dvořák, P**., Pechan, T., Šamajová, O., Vadovič, P., Šamaj, J. (2019) Proteomic insights into mitogen activated protein kinase signaling. Plant Biotechnology: Green for Good V – G5G, Olomouc, Abstract P 115.
- **Dvořák, P**., Ovečka, M., Krasylenko, Y., Šamaj, J., Takáč, T. (2019) Developmental expression and subcellular localisation of ironic superoxide dismutase 1 in *Arabidopsis*. Plants in a Changing World Integration of Photosynthesis, Adaptation and Development, Helsinki, 2019, Abstract P8

Fields of interest

Proteomics (differential proteomics, phosphoproteomics), preparation of recombinant protein, *in vitro* kinase assay, microscopy (light microscopy, CLSM, spinning disk microscopy, light-sheet microscopy), molecular biology methods (DNA and RNA isolation, PCR based techniques, GATEWAY and classical cloning, recombinant GFP technology), biochemical methods (protein extraction, SDS-PAGE, western blotting, enzyme activity assay, etc.), co-immunoprecipitation, cytological techniques (whole-mount immunolabelling), plant transformation (transient in *Nicotiana benthamiana* and stable in *Arabidopsis thaliana*), genetics (phenotype studies and backcrosses).

List of publications

Dvořák, P., Krasylenko, Y., Ovečka, M., Basheer, J., Zapletalová, V., Šamaj, J., Takáč, T. *In vivo* light-sheet microscopy resolves localisation patterns of FSD1, a superoxide dismutase with function in root development and osmoprotection. (2021). *Plant, cell & environment*, 44, 68–87. doi: 10.1111/pce.13894.

Dvořák, P., Krasylenko, Y., Zeiner, A., Šamaj, J., Takáč, T. (2021). Signaling Toward Reactive Oxygen Species-Scavenging Enzymes in Plants. *Frontiers in Plant Science*, 11, 618835. doi: 10.3389/fpls.2020.618835.

Hrbáčková, M.*, **Dvořák, P**.*, Takáč, T., Tichá, M., Luptovčiak, I., Šamajová, O., Ovečka, M., Šamaj, J. (2020). Biotechnological perspectives of omics and genetic engineering methods in alfalfa. *Frontiers in Plant Science* 11, 592. doi: 10.3389/fpls.2020.00592. * joined first authors.

Tichá, M., Richter, H., Ovečka, M., Maghelli, N., Hrbáčková, M., **Dvořák, P**., Šamaj, J., Šamajová, O. (2020). Advanced microscopy reveals complex developmental and subcellular localization patterns of ANNEXIN 1 in Arabidopsis. *Frontiers in Plant Science* 11, 1153. doi: 1153.10.3389/fpls.2020.01153.

Hrbáčková, M.*, Luptovčiak, I.*, Hlaváčková, K.*, **Dvořák, P**., Tichá, M., Šamajová, O., Novák, D., Bednarz, H., Niehaus, K., Ovečka, M., Šamaj, J. (2020). Overexpression of alfalfa SIMK promotes root hair growth, nodule clustering and shoot biomass production. *Plant biotechnology journal*, 1–18. doi: 10.1111/pbi.13503. Advance online publication. * joined first authors.

8 Supplements

8.1 Supplement I

8.1.1 Supplementary figures, tables and references

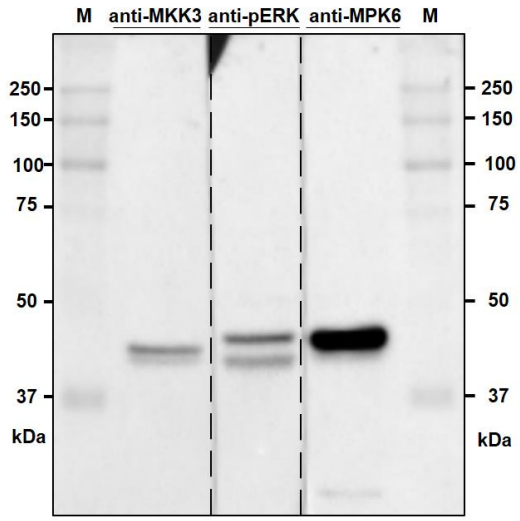

Supplementary figure 1 Immunoblotting analysis of protein extract from alfalfa roots treated by 200nM flg22 for 20 min using phospho-specific anti-pERK, anti-MPK6, and anti-MMK3 antibodies. Samples were loaded in triplicate on one gel and transferred to PVDF membrane. After the transfer, the membrane was cut to individual lanes and they were probed with the above mentioned antibodies. Prior to signal development, the membrane fragments were placed to reconstruct the whole original membrane, allowing the alignment of phosphospecific MAPKs with MMK3 and SIMK. M – marker (Precision Plus ProteinTM Dual Color standards were used as protein size marker).

Supplementary table 1 Phosphorylation sites experimentally found in antioxidant enzymes by mass spectrometry, retrieved from PhosPhat database.

Protein	Description	Modified peptide	Treatment	Position	Referenece
AT2G28190	copper/zinc superoxide dismutase 2	ALTVV(pS)AAK	auxin	S62	Zhang et al., (2013)
AT5G18100	copper/zinc superoxide dismutase 3	GGHKLSK(pS)TGNAGSR	isoxabene	S141	n.a.
AT3G10920	manganese superoxide dismutase 1	NLAPS(pS)EGGGEPPK	isoxabene	S114	n.a.
AT5G51100	Fe superoxide dismutase 2	EQEGTE(pT)EDEENPDDEVPEVYLD(pS)DIDVSEVD	abscisic acid	S297_T280	Wang et al., (2013a)
		EQEGTETEDEENPDDEVPEVYLD(pS)DIDVSEVD	abscisic acid	S297	Wang et al., (2013a)
		EQEG(pT)ETEDEENPDDEVPEVYLD(pS)DIDVSEVD	abscisic acid	S297_T278	Wang et al., (2013a)
		EQEGTE(pT)EDEENPDDEVPEV(pY)LDSDIDVSEVD	abscisic acid	Y294_T280	Wang et al., (2013a)
		EQEGTE(pT)EDEENPDDEVPEVYLDSDIDVSEVD	abscisic acid	T280	Wang et al., (2013a)
		EQEGTETEDEENPDDEVPEV(pY)LDSDIDVSEVD	abscisic acid	Y294	Wang et al., (2013a)
AT1G20630	catalase 1	YPT(pT)PIV(C*)SGNR	cell culture	T409	Sugiyama et al., (2008)
AT4G35090	catalase 2	LNVRP(pS)I		S491	Bhaskara et al., (2017)
			abscisic acid	S491	Umezawa et al., (2013)
		TF(pT)PERQER	ionizing radiation	T439	Roitinger et al., (2015)
AT1G20620	catalase 3	CAEKVP(pT)PTNSYTGIR	flg22	T408	Rayapuram et al., (2018)
					Rayapuram et al., (2014)
			end of day		Reiland et al., (2009)
			flg22		Rayapuram et al., (2018)
			flg22		Rayapuram et al., (2014)
		CAEKVPTP(pT)NSYTGIR	flg22	T410	Rayapuram et al., (2014)
			flg22		Rayapuram et al., (2018)
		VP(pT)PTN(pS)YTGIR	ionizing radiation	T408_S412	Roitinger et al., (2015)
		GFFEVTHDISNL(pT)CADFLR	nitrogen starvation / nitrate resupply	T85	Engelsberger and Schulze, (2012)
		LNVRP(pS)I		S491	Bhaskara et al., (2017)
			abscisic acid		Umezawa et al., (2013)
		(C*)AEKVPTPTNS(pY)TGIR	abscisic acid	Y413	Wang et al., (2013a)

		(C*)AEKVPTPTNSY(pT)GIR	abscisic acid	T414	Wang et al., (2013a)
AT4G08390	stromal ascorbate peroxidase	VDASGPED(C*)PEEGRLPDAGPP(pS)PATHLR		S236	Nakagami et al., (2010)
			nitrate starvation / nitrate resupply	S236	Wang et al., (2012)
			abscisic acid	S236	Wang et al., (2013a)
				S236	Van Leene et al., (2019)
			nitrate starvation / nitrate resupply	S236	Wang et al., (2013b)
		VDASGPED(C*)PEEGRLPDAGPPSPA(pT)HLR	abscisic acid	T239	Wang et al., (2013a)
AT4G32320	ascorbate peroxidase 6	FFEDF(pT)NA(pY)IK	nitrogen starvation / nitrate resupply	T313_Y316	n.a.
AT1G77490	thylakoidal ascorbate peroxidase	ELSD(pS)(oxM)(K*)(K*)	ionizing radiation	S373	Roitinger et al., (2015)
		(oxM)ISPK(C*)AA(pS)DAAQLISAK	flg22	S81	Mithoe et al., (2012)
		LPDAGPP(pS)PADHLR	ionizing radiation	S215	Roitinger et al., (2015)
AT5G16710	dehydroascorbate reductase 1	FQPST(pT)AGVLSASVSRAGFIKR	abscisic acid	T11	Umezawa et al., (2013)
AT1G75270	dehydroascorbate reductase 2	(s)KDANDG(s)EKALVDELEALENHLK	ethylene, ambient air		Li et al., (2009)
AT3G52880	monodehydroascorbate reductase 1	VVGAFMEGG(pS)GDENK		S400	Sugiyama et al., (2008)
			ionizing radiation	S400	Roitinger et al., (2015)
				S400	Nakagami et al., (2010)
				S400	Van Leene et al., (2019)
		ARP(pS)AESLDELVK		S416	Nakagami et al., (2010)
			none	S416	Reiland et al., (2011)
			nitrate starvation / nitrate resupply	S416	Wang et al., (2013c)
			none	S416	Mayank et al., (2012)
				S416	Reiland et al., (2009)
				S416	Bhaskara et al., (2017)
				S416	Van Leene et al., (2019)
			flg22	S416	Rayapuram et al., (2018)

				S416	Choudhary et al., (2015)
			abscisic acid	S416	Wang et al., (2013a)
			abscisic acid	S416	Umezawa et al., (2013)
			Abscisic acid	S416	Xue et al., (2013)
				S416	Sugiyama et al., (2008)
			ionizing radiation	S416	Roitinger et al., (2015)
		ARP(s)AE(s)LDELVKQGI(s)FAAK			Reiland et al., (2009)
		ARP(s)AE(s)LDELVKQGI(s)FAAK	none		Reiland et al., (2011)
		ADLSAK(pS)LVSATGDVFK	abscisic acid	S104	Umezawa et al., (2013)
		ARPSAE(pS)LDELVK	nitrate starvation / nitrate resupply	S419	Wang et al., (2013b)
		GAD(pS)(K*)NILYLR	ionizing radiation	S139	Roitinger et al., (2015)
AT5G03630	monodehydroascorbate reductase 2	AQP(pS)VESLEVLSK	flg22	S417	Rayapuram et al., (2018)
			end of night	S417	Reiland et al., (2009)
			flg22	S417	Rayapuram et al., (2018)
			ionizing radiation	S417	Roitinger et al., (2015)
			flg22	S417	Rayapuram et al., (2014)
			none	S417	Reiland et al., (2011)
			flg22	S417	Rayapuram et al., (2018)
			flg22	S417	Rayapuram et al., (2018)
			end of night	S417	Reiland et al., (2009)
			none	S417	Mayank et al., (2012)
			nitrate starvation / nitrate resupply	S417	Wang et al., (2013b)
			abscisic acid	S417	Wang et al., (2013a)
				S417	Van Leene et al., (2019)
				S417	Sugiyama et al., (2008)
			none	S417	Reiland et al., (2011)

			abscisic acid	S417	Umezawa et al., (2013)
			ethylene	S417	Yang et al., (2013)
			Abscisic acid, mannitol	S417	Xue et al., (2013)
				S417	Choudhary et al., (2015)
		AQP(pS)VE(pS)LEVLSK	flg22	S420_S417	Rayapuram et al., (2018)
		VVGAFLEGG(pS)PEENNAIAK	abscisic acid	S401	Wang et al., (2013a)
AT3G09940	monodehydroascorbate reductase 3	G(pT)VA(pT)GFSTNSDGEVTEVK	epibrassinolide	T228_T231	Lin et al., (2015)
AT3G27820	monodehydroascorbate reductase 4	GTVLTSFEFD(pS)N(K*)(K*)	ionizing radiation	S234	Roitinger et al., (2015)
AT3G54660	glutathione reductase 2	(pT)AAGV	low water potential (PEG)	T561	Bhaskara et al., (2017)

Supplementary table 2 List of proteins with significantly different abundances found in roots of SIMKKi line as compared with wild type. NA means not applicable.

Accession	MW [kDa]	Calc. pI	Description	Ratio (SIMKKi vs WT)	P-value	A-mean (SIMKKi)	A-variance (SIMKKi)	B-mean (WT)	B-variance (WT)
Membrane transport									
922403466	57.4	5	protein HLB1	1.67	0.00028176	501143.003	947970.664	299886.909	22029612.5
922375432	193	5.5	clathrin heavy chain 1	Unique in WT	NA	0	0	7896146.52	2.2622E+11
357498319	25.8	4.77	membrane steroid-binding protein 1	Unique in WT	NA	0	0	1421458.79	5.6969E+11
357517049	43.9	8.9	probable ADP-ribosylation factor GTPase-activating protein AGD8 isoform X1	Unique in WT	NA	0	0	1720747.52	2.7241E+11
357508367	42.8	5.77	V-type proton ATPase subunit C	0.31	0.0091781	5575049.51	8.7745E+12	18183463.5	1.2639E+13
357454943	23.4	5.72	ras-related protein Rab7	0.35	0.0124224	3614845.18	3.9073E+11	10315397.4	7.4609E+11
357473217	98.2	5.21	coatomer subunit gamma	0.24	0.0026019	1146458.02	2.6515E+11	4730728.47	543465212
Cytoskeleton									
922386288	107.2	5.8	villin-4	5.07	0.00496	3842863.85	7431495517	757889.429	8.7685E+10
357508689	49.8	5.1	tubulin alpha-1 chain	0.54	0.0182998	44904944.2	9.5785E+13	83467062.7	2.0515E+14
Defense and symbiosis									
357474991	12.7	4.91	nodulin-related protein 1 (NPR1)	2.91	0.030075	10298568.2	7.3451E+12	3543969.05	5.2609E+12
357441989	23.1	8.75	rhicadhesin receptor	0.46	0.0033805	7400334.18	9.3096E+11	16112086.2	4.9352E+12
922399145	54.5	8.35	allene oxide synthase 3	Unique in WT	NA	0	0	1748720.83	4.7796E+11
922370728	31.6	5.2	tobamovirus multiplication protein 2A	2.38	0.030761	336823.802	2602222034	141291.203	3321242031
922355266	82.7	5.05	far upstream element-binding protein 2	2.12	0.030925	4955443.43	4.4289E+11	2332456.92	3300900360
Oxidative stress and redox homeostasis									
922395795	29.2	6.4	2-Cys peroxiredoxin BAS1, chloroplastic	3.06	0.0084367	12185651.6	721504629	3984065.53	1.7225E+12
357479581	35.7	9.19	peroxidase 16	3.07	0.037102	102586271	1.1548E+15	33368769.7	3.6508E+14
357491415	35.8	9.29	peroxidase 4	2.89	0.00024344	16622636.6	1.0705E+12	5761361.76	1.2491E+12
357476371	35.4	8.92	peroxidase 73	1.82	0.0167196	137440979	6.9062E+13	75351498.1	6.6955E+14

922389034	37.3	5.25	peroxidase A2	1.94	0.049996	324302809	9.0588E+15	167411815	5.1957E+14
922346350	23.2	8.35	peroxiredoxin-2E, chloroplastic	1.45	0.0022371	24270387.6	1.9223E+12	16758409	1.5677E+12
922382612	26.3	8.27	superoxide dismutase [Mn], mitochondrial	2.27	0.043118	7099553.82	2.3531E+12	3132684.2	2.5477E+11
922330211	25.9	9.19	probable phospholipid hydroperoxide glutathione peroxidase	Unique in SIMKKi	NA	12701825.2	8.0584E+13	0	0
922398110	60.5	8.7	L-ascorbate oxidase homolog	0.27	0.00089822	2839054.71	9.0601E+11	10506662.8	1.3411E+12
922384113	56.7	7.3	catalase-4	0.37	0.0063419	19504048.9	1.1029E+14	52520647.9	8.8452E+12
922408443	17.2	5.31	ferredoxin, root R-B1 isoform X1	0.41	0.02838	20171213	1.6068E+14	48870843.9	5.8569E+13
1379613013	38.6	8.31	peroxidase 3	0.55	0.051815	32472476.5	1.7563E+14	58877604.1	1.0262E+14
Protein degradation and processing									
357438145	39.9	7.01	cysteine proteinase 15A	0.47	0.023561	10471307.6	5.2893E+12	22325649.1	2.7953E+13
357451227	53.7	5.15	serine carboxypeptidase II-2	Unique in WT	NA	0	0	7638259.61	1.018E+13
357513145	55.1	6	serine carboxypeptidase-like 20	Unique in WT	NA	0	0	995880.966	3.4973E+10
922400511	55.1	5.58	serine carboxypeptidase-like	Unique in WT	NA	0	0	2481274.18	6.9995E+11
922397880	30.9	5.27	proteasome subunit alpha type-1-B	0.62	0.0029828	15045396	7.0551E+11	24103904.9	5.2243E+12
357483877	17.5	4.65	SKP1-like protein 1B	1.46	0.0192839	21579074.5	2.1088E+12	14826219.5	7.4209E+12
1379758106	35.4	4.34	26S proteasome regulatory subunit RPN13	0.20	0.0062608	620404.593	1549128188	3073711.72	7.4539E+10
357476353	79.8	6.87	subtilisin-like protease SBT1.7	0.52	0.033299	14489529.3	7.5196E+12	27761947.5	4.4496E+13
Heat shock proteins and regulation									
357438459	94.1	4.89	endoplasmin homolog	0.49	0.0120028	19636721.6	6.8962E+12	39975794	5.8209E+13
1379603333	9.9	4.46	heat shock factor-binding protein 1	Unique in SIMKKi	NA	6284227.97	2.7054E+13	0	0
357503161	70.9	5.19	heat shock cognate 70 kDa protein 2	Unique in SIMKKi	NA	384811687	2.6982E+15	0	0
357481949	65.3	5.94	hsp70-Hsp90 organizing protein 3	2.49	0.00010377	33445595	6.8634E+11	13415991.8	4.4817E+12
Apoptosis									
922367163	39.6	9.23	apoptosis-inducing factor homolog A	0.37	0.047722	2425145.14	3.1823E+11	6512772.79	5.9754E+12

922387136	57.9	5.83	serine/threonine protein phosphatase 2A 55 kDa regulatory subunit B beta isoform isoform X1	Unique in WT	NA	0	0	690868.101	3.2444E+10
922334628	44.9	5.11	metacaspase-5	3.52	0.0039988	9519927.84	1.9835E+12	2702500.54	1.9518E+12
WD40 domain proteins									
357449789	55.6	6.57	WD-40 repeat-containing protein MSI4	0.62	0.0177569	2944248.23	2.1729E+11	4723934.88	4.12E+11
357511053	38.3	5.08	protein CIA1	Unique in WT	NA	0	0	1463151.51	2.6637E+10
Stress response									
1379597042	27.2	6.04	universal stress protein PHOS32	0.53	0.029724	15653715.5	3.0517E+12	29480343.6	2.0986E+13
922334512	18	5.55	MLP-like protein 28	1.70	0.0027408	172991322	6.7919E+13	101600319	2.8385E+14
Others									
357479327	92.2	6.25	sucrose synthase	0.45	0.00028241	25459309.8	1.3546E+13	56774611.7	7.1989E+12
1379609395	92.2	6.32	sucrose synthase	0.18	0.0105571	3369672.71	1.2184E+13	18529432.6	2.1371E+13
922379759	29.5	4.73	proliferating cell nuclear antigen	0.41	0.027161	6703926.97	7.6246E+12	16371730.6	1.6566E+13
922389626	18.9	4.79	translationally-controlled tumor protein homolog	1.68	0.044024	36802237.1	2.3019E+13	21845180.5	5.6671E+13
1379755799	89	5.19	probable splicing factor 3A subunit 1	Unique in SIMKKi	NA	2237021.79	1.0532E+11	0	0
922385908	181	6.61	ABC transporter C family member 2	Unique in WT	NA	0	0	2181415.06	2.6359E+11
357513973	22	9.06	auxin-binding protein ABP19b	2.53	0.00075845	10616363.9	8.9622E+11	4198463.38	5.4548E+11
922388448	25.4	5.62	stem-specific protein TSJT1	1.97	0.032179	10073738.8	4.3815E+12	5115822.05	2.7162E+12
922380048	120.9	6.73	protein SMAX1-LIKE 7	Unique in WT	NA	0	0	416249.64	2.205E+10
922354415	65.2	5.03	protein phosphatase PP2A regulatory subunit A	3.31	0.0149436	10355311.7	6.2996E+11	3127733.32	3.3665E+12
1379622079	64.5	7.44	sorting and assembly machinery component 50 homolog B, partial	Unique in WT	NA	0	0	487026.861	6.1032E+10
922398180	72.8	5.52	TOM1-like protein 9	Unique in SIMKKi	NA	344556.318	4.5835E+10	0	0
Translation									
922343213	24.7	10.37	40S ribosomal protein S8	2.66	0.00022262	55770981.7	8.5948E+12	20992968	4.8458E+11

357521277	17.2	10.4	40S ribosomal protein S15-4	1.76	0.035099	15595783	6.6258E+12	8871100.38	7.1989E+12
922346907	21	11.11	60S ribosomal protein L18-3	1.87	0.047443	37434553.7	1.0789E+14	20054160.4	5.4313E+12
922337065	28.3	11.03	small nuclear ribonucleoprotein-associated protein B'	2.74	0.040984	3380204.52	1.3625E+11	1234961.25	2.6553E+11
357520761	62.1	5.68	asparagine-tRNA ligase, cytoplasmic 1	Unique in SIMKKi	NA	4596549.74	1.551E+12	0	0
1379604161	44.5	10.18	60S ribosomal protein L3-1	3.95	0.047721	3761216	1.2107E+12	951588.993	5826222463
			Metabolism						
922400155	48.3	7.99	3-ketoacyl-CoA thiolase 2, peroxisomal	0.51	0.00027825	17850082.9	3.6833E+12	35197794.7	2.5872E+12
922330021	51.3	7.69	bifunctional aspartate aminotransferase and glutamate/aspartate-prephenate aminotransferase	0.48	0.00111641	6794042.36	1.5375E+12	14281441.7	8.6146E+11
357454485	35.2	5.35	probable fructokinase-4	0.56	0.00126498	111675916	1.7011E+14	200931583	1.9525E+14
357447871	46	6.15	fumarylacetoacetase	2.63	0.00131713	19015590	6.7677E+11	7218812.19	1.4662E+12
357453587	64	6.42	dihydroxy-acid dehydratase, chloroplastic	0.23	0.0021813	4967517.3	2.0867E+12	21530426.3	1.467E+13
922368287	35.3	5.34	fructokinase-2	0.54	0.0024174	77031370.7	7.589E+13	142127759	1.9733E+14
357520877	65.3	6.37	NADP-dependent malic enzyme	2.04	0.0024648	164677031	3.0552E+14	80713066.2	1.5451E+14
922391649	41.9	6.86	thiosulfate/3-mercaptopyruvate sulfurtransferase 2	0.25	0.0025004	2159845.36	9.1228E+11	8603149.64	1.8151E+12
922391447	52.5	7.42	citrate synthase, mitochondrial	0.35	0.0026415	8838995.17	9.7381E+12	25449388.7	8.9335E+12
922349977	73.5	7.05	alpha-dioxygenase 1	0.44	0.0035022	11863972.2	6.0438E+12	26691680	1.1284E+13
357502825	37.6	5.86	probable aldo-keto reductase 2	1.54	0.0063419	29985443.6	4.3431E+12	19485270.9	7.707E+12
922383823	34.3	6.67	isoflavone reductase homolog PCBER	1.53	0.0084768	124903655	1.3598E+14	81420837.3	1.0737E+14
1379629476	36.2	6.73	methylecgonone reductase	0.65	0.0086829	4996753.2	2.9016E+11	7649882.39	6.2867E+11
357474575	62.9	6.76	ketol-acid reductoisomerase, chloroplastic	0.46	0.0091961	23148738.1	7.5175E+13	50782821.7	2.779E+13
357451523	44.6	8.44	glyceraldehyde-3-phosphate dehydrogenase GAPCP1, chloroplastic	0.45	0.0104447	32229881.5	1.4323E+14	72302287.3	8.9874E+13
922356654	68.1	5.8	glucose-6-phosphate isomerase 1, chloroplastic	0.28	0.0105048	8241073.76	6.3895E+12	29708304.1	6.0732E+13

357453423	107	7.72	aconitate hydratase, cytoplasmic	0.65	0.0107197	91747940.4	9.1414E+13	142129185	2.8254E+14
357476071	49.9	7.28	LL-diaminopimelate aminotransferase, chloroplastic	0.36	0.0118806	13707094.1	6.1415E+12	38445967.1	8.9593E+13
357477133	52.4	7.18	argininosuccinate synthase, chloroplastic	0.48	0.0128627	11480036.6	2.7857E+12	23885244.7	2.2437E+13
357483533	35.4	5.58	isoflavone reductase	0.55	0.0145606	75469778.9	3.5822E+14	136441053	2.9743E+14
357475593	44.6	6.07	stearoyl-[acyl-carrier-protein] 9-desaturase, chloroplastic isoform X1	2.60	0.0151772	4248038.98	7.5188E+11	1634968.65	4.8238E+11
922369414	53.6	5.87	scopoletin glucosyltransferase	0.29	0.016559	524388.522	2.9918E+10	1820561.52	2.7133E+10
922353879	61.8	5.34	putative 3,4-dihydroxy-2-butanone kinase	2.28	0.0194165	863357.406	9112651708	379067.378	265685284
357518063	41.5	7.08	naringenin,2-oxoglutarate 3-dioxygenase	1.69	0.021604	4083827.26	3.1817E+11	2409762.11	3.0997E+11
1379756023	63.2	5.68	phosphoglucomutase, cytoplasmic	1.63	0.021919	15686011.7	5.9171E+12	9616616.18	2.4127E+12
357469711	79.8	6.93	transketolase, chloroplastic	0.45	0.023181	53135256.8	3.564E+14	116937636	5.9682E+14
1379646350	37.7	5.74	probable fructokinase-7 isoform X1	0.44	0.024339	16011120.6	9.3681E+12	36429209.9	1.1691E+13
357483543	24.2	5.82	soluble inorganic pyrophosphatase PPA1	3.19	0.027463	7058603.81	4.6365E+12	2210258.18	1.4907E+12
922383829	29.3	6.81	gamma carbonic anhydrase 1, mitochondrial	0.46	0.029101	10636976.8	1.4899E+12	23001509.8	3.9867E+13
357481763	52.2	6.13	hydroxymethylglutaryl-CoA synthase	0.54	0.032057	23349711.3	6.5122E+13	43562964.2	5.255E+13
922333770	40.6	7.58	GDSL esterase/lipase 1	4.51	0.035319	19614684.5	2.3708E+13	4350877.01	1.9503E+13
357520447	57.6	6.76	glutamate--cysteine ligase, chloroplastic	0.61	0.035461	11151335.6	8.9723E+12	18321305.9	6.8522E+12
922377798	42.3	9.79	ADP, ATP carrier protein 1, mitochondrial	0.61	0.040455	37562616.3	3.5993E+12	61659574.9	8.5182E+13
1379666067	44.7	6.7	glutamate dehydrogenase 1	0.59	0.040977	16571802.7	1.5949E+13	28276785.6	3.0516E+13
922373013	42.2	8.32	acetyl-CoA acetyltransferase, cytosolic 1	3.48	0.04436	3076367.15	1.4264E+12	885227.863	6.1084E+10
357497367	44.5	6.8	probable glutamate dehydrogenase 3	0.47	0.04666	20220197.6	3.5149E+11	43090769.1	7.8329E+13
357475283	28	5.67	caffeoyl-CoA O-methyltransferase	1.99	0.051422	9734172.21	3.4581E+12	4883164.32	1.6433E+12
922358265	42.8	6.09	chalcone synthase 9	Unique in WT	NA	0	0	17066998.6	9.9349E+12
922330277	53.7	5.57	hexokinase-1	Unique in WT	NA	0	0	3016195.73	1.9846E+12
357446917	63.1	5.95	pyruvate decarboxylase 1	Unique in WT	NA	0	0	1705828.99	5.4311E+11

1379650397	23.9	8.1	polygalacturonase inhibitor 1-like	Unique in SIMKKi	NA	10350192.9	8.6746E+12	0	0
357443443	63	6.8	probable alkaline/neutral invertase D	Unique in WT	NA	0	0	667955.753	2.1146E+11
1379634931	30	8.16	ribulose-phosphate 3-epimerase, chloroplastic	Unique in SIMKKi	NA	3395733.83	5.3043E+11	0	0
357456343	44.2	5.71	3-oxo-Delta(4,5)-steroid 5-beta-reductase	Unique in WT	NA	0	0	2421781.75	1.9836E+12
922370478	57.6	8.78	isoflavone 2'-hydroxylase	Unique in WT	NA	0	0	2198649.97	2.907E+12
922386960	82.2	6.21	4-hydroxy-3-methylbut-2-en-1-yl diphosphate synthase (ferredoxin), chloroplastic	Unique in WT	NA	0	0	1436507.43	2.5886E+11
357502085	40.7	5.44	isoliquiritigenin 2'-O-methyltransferase	Unique in WT	NA	0	0	5683618.47	8.7012E+12
1379608936	90.3	8.03	probable acyl-CoA dehydrogenase IBR3	Unique in WT	NA	0	0	2641867.48	7.4904E+12
357442229	33.2	8.37	ATP-dependent Clp protease proteolytic subunit 5, chloroplastic	Unique in SIMKKi	NA	5002421.77	2.8415E+12	0	0
922335086	110.5	5.88	phosphoenolpyruvate carboxylase, housekeeping isozyme	Unique in WT	NA	0	0	3155671.58	3.4019E+12
357490847	65.8	6.39	asparagine synthetase, root [glutamine-hydrolyzing]	Unique in WT	NA	0	0	5957467.77	1.1764E+12
357445887	56.6	7.84	phospho-2-dehydro-3-deoxyheptonate aldolase 2, chloroplastic	Unique in WT	NA	0	0	6869718.25	5.3237E+13
922397878	29.6	6.43	gamma carbonic anhydrase 1, mitochondrial	Unique in WT	NA	0	0	15581193.1	1.0229E+13
1379594852	75	7.25	trifunctional UDP-glucose 4,6-dehydratase/UDP-4-keto-6-deoxy-D-glucose 3,5-epimerase/UDP-4-keto-L-rhamnose-reductase RHM1	Unique in SIMKKi	NA	21968454.8	6.8381E+13	0	0
357485881	30.4	6.54	carbonic anhydrase 2 isoform X1	Unique in WT	NA	0	0	8512116.31	6.9736E+11
922340153	175.7	6.86	ferredoxin-dependent glutamate synthase, chloroplastic	Unique in WT	NA	0	0	1757133.93	2.2045E+12
1379633979	38.5	6.89	UDP-glucuronic acid decarboxylase 6	Unique in WT	NA	0	0	22385971.6	6.4114E+13
357455121	16.5	6.35	cytochrome c oxidase subunit 5b-2, mitochondrial	Unique in WT	NA	0	0	7197615.02	4.1965E+12

922379121	20	8.82	reactive Intermediate Deaminase A, chloroplastic	Unique in SIMKKi	NA	6227113.52	8.9136E+12	0	0
922374702	20.6	6.19	NADPH:quinone oxidoreductase	Unique in SIMKKi	NA	2548152.52	1.2268E+12	0	0
1379629025	56.3	6.19	LOW QUALITY PROTEIN: bifunctional 3-dehydroquinate dehydratase/shikimate dehydrogenase, chloroplastic	Unique in WT	NA	0	0	1688000.79	1.4436E+11
357485703	53.7	6.04	glutamate--glyoxylate aminotransferase 2	Unique in WT	NA	0	0	3625374.76	4.1071E+11
Unknown									
922370083	24.1	9.17	uncharacterized protein LOC25493282	0.40	0.025459	9869080.04	2.172E+13	24424542.9	8.905E+11
922404662	30.1	5.5	putative bark agglutinin LECRPA3	0.46	0.0149395	36688950.9	2.7578E+14	80140929.6	6.234E+13
922383586	39.4	5.26	bark storage protein A	0.33	0.00042478	6278329.1	3.4251E+12	18928852.2	7.5487E+11
1379622855	33.9	4.94	uncharacterized protein LOC25488885	Unique in WT	NA	0	0	1618259.84	1.2624E+11

Supplementary Table 3 List of proteins with significantly different abundances found in roots of wild type plants treated with *S. meliloti* (6 h) as compared to mock control (6 h). NA means not applicable.

Accession	MW [kDa]	Calc. pI	Description	Ratio (WT mock vs WT sino)	P-value	A-mean (WT mock)	A-variance (WT mock)	B-mean (WT sino)	B-variance (WT sino)
Protein degradation and processing									
1379640387	120.4	5.38	ubiquitin-activating enzyme E1 1-like	0.46	0.028983	2609472.98	4172161430	5674557.21	5.651E+11
357451023	27.2	6.02	proteasome subunit alpha type-6	1.45	0.0189979	19654521.8	5.3977E+12	13577553.8	2.2482E+12
1379630722	46.4	8.21	anamorsin homolog isoform X1	Unique in WT mock	NA	0	0	1795611.74	7.0008E+11
1379627097	36.9	6.1	LOW QUALITY PROTEIN: arginase 1, mitochondrial	0.64	0.051156	1764099.6	9.2297E+10	2769286.42	1.9579E+10
1379671260	110.1	6.61	puromycin-sensitive aminopeptidase isoform X1	0.60	0.04124	4882829.37	2.9317E+12	8096420.62	5.8607E+11

Cytoskeleton									
357521645	50	4.93	tubulin beta chain	0.59	0.022144	11077160.4	1.15E+12	18689978.4	1.505E+12
922383434	57.4	7.93	T-complex protein 1 subunit delta	0.58	0.048222	3646031.64	1.1416E+12	6281088.12	1.493E+12
357469067	50.5	4.83	tubulin beta-2 chain	0.61	0.034624	39684897.4	2.0613E+13	65337816.2	1.7879E+14
Defense response									
357476329	31.8	8.88	protein EXORDIUM-like 2	Unique in WT sino	NA	1343082.82	8.0142E+11	0	0
922370097	83.5	8.27	beta-xylosidase/alpha-L-arabinofuranosidase 2	0.28	0.005201	2008542.63	1.581E+12	7069567.81	9.2574E+11
1379650397	23.9	8.1	polygalacturonase inhibitor 1-like	Unique in WT sino	NA	7733851.9	6.8111E+12	0	0
357448997	40.3	8.72	glucan endo-1,3-beta-glucosidase, basic isoform isoform X1	1.87	0.0257	18079643.4	1.7014E+13	9664949.78	6.7835E+11
357495517	45.1	6.34	fasciclin-like arabinogalactan protein 2	0.55	0.025538	1873536.1	4.3307E+11	3423532.71	1.6482E+11
1379614243	39.6	7.21	UDP-glucuronic acid decarboxylase 6	1.49	0.044683	11456098.8	1.62E+11	7680765.17	4.9673E+12
922358486	26.2	6.27	thaumatin-like protein 1	1.76	0.0152361	45722778.5	2.9726E+13	25989656.4	4.0822E+13
Translation									
922392405	43	6.48	ERBB-3 BINDING PROTEIN 1	Unique in WT mock	NA	0	0	5970569.22	4.3635E+11
922356332	17.3	6.14	eukaryotic translation initiation factor 5A-5 isoform X1	2.18	0.040601	5023376.76	1.8433E+12	2308100.75	6.4172E+11
357502689	12.3	9.54	60S ribosomal protein L30	1.54	0.0120574	7345624.11	3.2543E+11	4776078.36	7.1617E+11
357439781	44.7	10.43	60S ribosomal protein L4	0.46	0.026838	8514046.46	5.028E+12	18535542.1	5.8729E+11
1379648645	15.6	10.77	60S ribosomal protein L32-1	0.55	0.038981	3197647.02	1.4062E+12	5817254.61	8.4407E+11
357516021	29.9	10.23	40S ribosomal protein S4-1	1.69	0.039263	25812325.6	3.4768E+13	15265513.8	1.8859E+12
1379602536	56.6	7.17	serine-tRNA ligase isoform X1	0.55	0.034404	5181468.6	2.9171E+12	9414054.27	2.4882E+12
922401783	11.3	4.54	60S acidic ribosomal protein P2-4	0.56	0.0182399	11342253.7	9.8171E+12	20415192.4	6.8089E+12
357437181	60.5	6.4	aspartate-tRNA ligase 2, cytoplasmic	0.36	0.0134753	3429102.58	2.0531E+12	9649951.42	4.4641E+12

922407961	82.2	6.05	putative mediator of RNA polymerase II transcription subunit 12	0.64	0.0067156	801131.62	2043194213	1260887.15	822805543
Transport									
922350154	30	9.03	outer plastidial membrane protein porin	1.81	0.0183808	38850479.5	3.6181E+13	21436566.6	2.5355E+13
357513537	30.2	9.01	stem 28 kDa glycoprotein	0.45	0.045519	3100760.64	2.0952E+12	6859806.42	3.0552E+12
922389239	32	5.16	coatomer subunit epsilon-2	0.25	0.0039849	839791.22	1.7063E+11	3355848.61	3.6482E+11
357449027	22.1	7.05	GTP-binding protein SAR1A	0.64	0.052599	2707997.09	6.3842E+10	4254521.82	2.091E+11
Stress induced									
1379609444	16.6	5.08	ABA-responsive protein ABR17 isoform X3	Unique in WT mock	NA	0	0	23035812.3	3.0569E+13
357449121	16.6	5.07	ABA-responsive protein ABR17	Unique in WT sino	NA	24292836.2	8.3481E+13	0	0
357449145	16.6	5.08	ABA-responsive protein ABR17 isoform X1	Unique in WT mock	NA	0	0	36217275.7	2.3338E+14
922401091	34.9	5.53	peroxidase A2	1.69	0.0100582	20917275.5	7.1583E+12	12390256.7	2.7248E+11
922362724	21.2	6.58	superoxide dismutase [Cu-Zn], chloroplastic	4.53	0.025502	3464609.98	1.7521E+12	764551.522	6.071E+10
357446059	72.4	5.68	heat shock 70 kDa protein, mitochondrial	0.63	0.0044004	23467142.1	8.309E+11	37418233.5	1.654E+13
357473829	31.7	6.74	L-ascorbate peroxidase 3	2.64	0.033919	7677700.81	6.291E+12	2911973.2	4.9738E+11
922325593	35.7	5.64	annexin D2	1.93	0.036422	17467716.2	1.736E+13	9042922.53	4.8796E+12
922364707	31.9	6.6	S-formylglutathione hydrolase	2.16	0.04884	2062595.87	2.1343E+11	955074.111	852256125
922393670	29.5	4.83	14-3-3-like protein B	1.55	0.043845	32682220.4	2.3618E+13	21024343.7	2.4659E+13
922402503	30.5	5.01	nifU-like protein 4, mitochondrial	2.17	0.042124	2109926.08	1.1815E+11	971991.975	1.6443E+11
357515823	18	5.85	MLP-like protein 43	1.95	0.0028212	30922960	3.128E+12	15862341.3	1.2774E+13
1379627509	31.5	5.26	lactoylglutathione lyase GLX1	Unique in WT mock	NA	0	0	2406904.82	8.7018E+11
Transcription									
357469575	77.3	6.01	ATP-dependent DNA helicase 2 subunit KU80 isoform X1	2.62	0.0040047	756886.221	6154004454	289296.572	3001935198

Sterol and steroid binding									
922406125	24.2	4.61	membrane steroid-binding protein 1	Unique in WT sino	NA	9706152.73	3.144E+13	0	0
357515827	18.2	6.52	MLP-like protein 28	1.65	0.053978	22556764.6	1.4844E+13	13642092.8	7.6202E+12
922343886	52.3	4.97	oxysterol-binding protein-related protein 3A	1.82	0.040981	1625855.21	6.5824E+10	894652.778	3.0204E+10
357465989	10.8	5.15	probable steroid-binding protein 3	Unique in WT mock	NA	0	0	2306590.67	9.547E+11
Unknown									
922398785	72.6	5.87	uncharacterized protein LOC25482515	Unique in WT mock	NA	0	0	2121155.78	3.0837E+12
357496501	45.4	4.93	uncharacterized protein At5g39570	5.65	0.044577	1324184.36	7.3047E+10	234504.296	4.0332E+10
1379620281	29.8	11.25	uncharacterized protein LOC25490772	1.49	0.0029002	39209459	7.707E+12	26250520.4	4.2403E+12
1379756951	56.5	6.54	uncharacterized protein LOC25502183	0.51	0.0084	1997800.44	4.3163E+11	3917240.17	4.0188E+10
Mitochondrion organisation									
357483481	70.5	9.14	ATPase family AAA domain-containing protein 3C	0.31	0.0060838	253880.481	8993624295	816342.285	5530274024
Protein folding									
922328245	89.8	5.14	heat shock protein 90-5, chloroplastic	0.45	0.0081563	3534646.51	2.0945E+12	7844245.84	2.4388E+11
357513317	16.5	7.94	FK506-binding protein 2	1.49	0.0083242	10830343.2	1.0581E+12	7269435.83	5.5785E+11
Miscellaneous									
357463395	20.8	4.93	PLAT domain-containing protein 3	0.53	0.0063383	3656266.15	4.9657E+11	6877868.05	6.3704E+11
Storage									
922388444	45.5	8.16	basic 7S globulin 2	1.97	0.040822	16472376.8	1.872E+13	8373591	3.4692E+12
Amino acid metabolism									
357454545	58.7	8.19	threonine synthase, chloroplastic	2.36	0.044999	3746118.67	1.4015E+12	1589203.47	5.822E+10
357441513	34.3	5.76	cysteine synthase	1.96	0.0041397	25897707	1.0637E+12	13237993	4.0237E+12
Metabolism									
357495429	34.9	6.33	NAD(P)H-dependent 6'-deoxychalcone synthase	2.15	0.0038643	7238422.92	1.1095E+12	3362140.24	1.4016E+11

357479327	92.2	6.25	sucrose synthase	0.55	0.0096379	4989264.89	1.3004E+12	9087738.17	1.0266E+12
922380571	15.7	5.97	deoxyuridine 5'-triphosphate nucleotidohydrolase	0.33	0.0051963	1883634.98	2.74E+11	5726330.78	1.1697E+12
922379161	63.4	6.49	imidazole glycerol phosphate synthase hisHF, chloroplastic isoform X1	2.73	0.021679	5639197.07	2.5692E+12	2067940.95	2.9506E+11
357448501	42.5	8.28	ferredoxin--NADP reductase, root isozyme, chloroplastic	0.45	0.025337	11261133.9	2.5448E+13	24805908.9	1.9979E+13
922369532	40.7	5.88	isoflavone 4'-O-methyltransferase isoform X1	0.51	0.036044	1379819.69	4.4989E+11	2727694.08	1.1545E+11
357484061	39.9	8.02	isocitrate dehydrogenase [NAD] regulatory subunit 1, mitochondrial isoform X1	1.80	0.032421	9244458.64	3.4891E+12	5122621.02	1.4408E+12
357517751	40.2	6.79	isocitrate dehydrogenase [NAD] regulatory subunit 1, mitochondrial	1.67	0.039559	9948589.55	2.934E+12	5954515.69	2.349E+12
357495781	54.5	7.39	isocitrate dehydrogenase [NADP]	0.57	0.043739	9592543.63	1.4449E+11	16838278.4	8.2993E+12
357438399	51.4	7.09	uridine 5'-monophosphate synthase	Unique in WT sino	NA	2356630.5	2.2693E+12	0	0
357455293	28	7.44	NADH dehydrogenase [ubiquinone] flavoprotein 2, mitochondrial	Unique in WT sino	NA	2248895.03	2.331E+12	0	0
Alkaloid production									
1379629476	36.2	6.73	methylecgonone reductase	1.49	0.032505	4130911.17	9.5043E+10	2773758.39	4.4036E+11

Supplementary Table 4 List of proteins with significantly different abundances found in roots of SIMKKi line plants treated with *S. meliloti* (6 h) as compared to mock control (6 h). NA means not applicable.

Accession	MW [kDa]	Calc. pI	Description	Ratio (mock SKIMKKi vs sino SIMKKi)	P-value	A-mean (mock SKIMKKi)	A-variance (mock SKIMKKi)	B-mean (sino SIMKKi)	B-variance (sino SIMKKi)
Protein degradation and processing									
1379623312	48.3	8.32	26S proteasome regulatory subunit 10B homolog A isoform X1	0.46	0.025161	12993390.9	3.6763E+12	28510946.2	5.5692E+13

357473517	29.1	8.51	signal recognition particle receptor subunit beta	Unique in mock SIMKKi	NA	0	0	2434567.35	4.3295E+12
922344961	87.8	7.43	subtilisin-like protease Glyma18g48580	2.25	0.040657	10800091.6	3.207E+12	4800635.73	8.9354E+12
1379757262	54.1	6.09	ubiquitin carboxyl-terminal hydrolase 6	0.65	0.05076	1164730.35	1.3238E+11	1793378.17	2.3065E+10
				Translation					
357480901	29.8	9.86	40S ribosomal protein S3a	0.52	0.046582	5281603.57	1.8779E+12	10145891.1	6.8857E+12
357446651	28.2	10.76	40S ribosomal protein S6	0.50	0.038658	4870812	2.7868E+12	9745608.39	2.0405E+12
922343165	28.2	10.7	40S ribosomal protein S6	0.41	0.049782	4527755.59	6.8261E+12	11111851.3	1.6594E+11
357461283	24.4	9.83	60S ribosomal protein L10a-1	1.74	0.03638	6760942.07	9.5846E+11	3878661.69	143011819
1379609064	23.3	10.35	60S ribosomal protein L18a-2	0.54	0.0170234	3947074.23	1.0238E+12	7268392.95	1.1131E+12
1379604161	44.5	10.18	60S ribosomal protein L3-1	0.31	0.006521	2543485.14	3.7743E+11	8267664.25	3.2597E+12
357439781	44.7	10.43	60S ribosomal protein L4	0.65	0.0059635	14281369.1	3.7079E+12	21969476.5	2.5349E+12
357444829	32.9	10.07	probable mediator of RNA polymerase II transcription subunit 36b	Unique in mock SIMKKi	NA	0	0	3850312.36	3.8854E+11
357475273	71	8.25	polyadenylate-binding protein 8	0.41	0.026783	4248420.69	4.1265E+12	10426250.3	5.6638E+12
1379618197	27.3	10.05	ribonuclease P protein subunit p25-like protein isoform X1	0.40	0.0032212	798292.475	789620821	1999638.11	8556782086
922337065	28.3	11.03	small nuclear ribonucleoprotein-associated protein B'	3.74	0.045082	2260297.35	9.5385E+11	604365.384	3.9019E+10
922335080	45	8.68	UBP1-associated protein 2C	0.48	0.0368	1301136.57	5.4461E+11	2724512.98	9.4577E+10
1379602536	56.6	7.17	serine--tRNA ligase isoform X1	0.55	0.0022557	5507890.97	4.9817E+11	9929336.52	7.159E+11
1379631808	61.4	9.1	probable nucleolar protein 5-1	0.52	0.02472	2151829.35	5.4088E+11	4157543.4	4.3991E+11
1379614964	105.3	5.71	eukaryotic translation initiation factor 3 subunit C-like	Unique in mock SIMKKi	NA	0	0	683265.196	1.6374E+11
				Metabolism					
357453587	64	6.42	dihydroxy-acid dehydratase, chloroplastic	0.61	0.032325	3823421.05	8.3522E+11	6290441.58	9.275E+11
1379666716	41.7	8.9	enoyl-[acyl-carrier-protein] reductase [NADH], chloroplastic	0.50	0.00084389	4351744.17	5.3676E+11	8694159.43	1.6333E+11

922407881	42.6	8.29	fructose-bisphosphate aldolase 3, chloroplastic	0.62	0.037462	18062776.1	2.4551E+13	29253109.2	1.543E+13
922383829	29.3	6.81	gamma carbonic anhydrase 1, mitochondrial	1.61	0.041181	12249623.4	2.2719E+12	7616744.43	5.0323E+12
922332006	37.8	6.65	2-alkenal reductase (NADP(+)-dependent)	0.44	0.048765	2686711.22	6.979E+11	6162549	3.9223E+12
357449387	35.8	6.2	putative glucose-6-phosphate 1-epimerase	0.42	0.02678	3285404.64	1.7031E+12	7875927.81	3.7019E+12
357452533	21.7	6.19	NAD(P)H dehydrogenase (quinone) FQR1	2.39	0.0198967	32222274.1	2.3675E+13	13501778.1	5.0965E+13
1379614868	36.3	7.72	quinone oxidoreductase PIG3	0.01	0.022965	48820.9991	12868564.6	3421396.01	8.1163E+11
357477997	35.9	8.68	NADH-cytochrome b5 reductase-like protein	29.85	0.025221	2507466.71	6.0875E+11	83992.0478	2764085429
357465233	76.8	5.24	NADPH--cytochrome P450 reductase	0.52	0.042843	601036.174	1.7206E+10	1146465.53	3.8055E+10
357444967	23.8	5.47	chalcone--flavonone isomerase 1	1.85	0.0060376	21818637.4	4.3818E+12	11790819.2	6.3064E+12
357467549	49.7	6.57	glutamate-1-semialdehyde 2,1-aminomutase, chloroplastic	0.15	0.0035957	464530.033	1.6488E+11	3008041.47	3.5184E+11
357483875	53.2	7.03	diaminopimelate decarboxylase 1, chloroplastic	1.87	0.029317	8363600.98	3.9154E+12	4478806.92	1.8634E+11
357507415	40.9	8.19	bifunctional L-3-cyanoalanine synthase/cysteine synthase 1, mitochondrial	1.81	0.023025	12477298.9	5.2001E+11	6890731.42	6.7581E+12
1379622546	58.3	8.85	citrate synthase, glyoxysomal isoform X2	2.95	0.046338	3685732.58	4.2548E+11	1249340.31	1.765E+12
357438399	51.4	7.09	uridine 5'-monophosphate synthase	4.83	0.0062956	2634142.97	1.9444E+11	545813.317	6.8647E+10
Cell wall and defense response									
357449115	16.8	4.88	disease resistance response protein Pi49	1.61	0.038785	61460714.2	1.4563E+13	38140545.8	3.0215E+13
922347233	21.7	6.14	wound-induced protein	2.21	0.0131991	8481476.73	6.6941E+11	3835565.58	2.922E+12
357483583	36.6	8.69	peroxidase 72	0.65	0.034176	24951372	4.184E+12	38173581.6	4.8327E+13
922369718	29.7	9.5	non-classical arabinogalactan protein 31	0.61	0.04606	1754711.29	3.685E+11	2893779.14	1.083E+11
357452203	49.4	5.4	epidermis-specific secreted glycoprotein EP1	0.31	4.3189E-05	1845774.56	6016176811	5866398.79	1.9202E+10
357491499	58.1	9.04	trans-cinnamate 4-monooxygenase	0.37	0.031643	520392.412	2784416393	1397250.52	4.829E+10
357495517	45.1	6.34	fasciclin-like arabinogalactan protein 2	0.36	0.032981	1179280.15	5.0413E+11	3240487.42	7.5956E+10

Stress response									
357520323	61.8	4.97	calnexin homolog	Unique in mock SIMKKi	NA	0	0	2996791.27	3.0001E+12
357442955	8.4	6.61	copper transport protein ATX1	2.03	0.013476	10498037.1	1.7459E+12	5164587.79	3.0448E+12
1379642970	36.3	7.55	glyceraldehyde-3-phosphate dehydrogenase 1, cytosolic	Unique in mock SIMKKi	NA	0	0	56920349.7	1.6682E+13
357481917	16.6	4.81	probable calcium-binding protein CML13	5.25	0.027276	9011565.51	4.433E+12	1716450.36	1.058E+11
357505771	26.1	5.77	probable glutathione S-transferase	1.73	0.030884	6733048.38	2.0087E+12	3881679.94	2.7709E+11
922383913	12.8	6.16	thioredoxin H-type	2.54	0.03756	4626487.42	6.0751E+11	1817937.31	1.9153E+12
357517749	47.2	8.06	phosphoserine aminotransferase 2, chloroplastic	1.65	0.037519	24692453.6	2.2492E+13	14941867.4	7.8922E+12
357485917	37.7	5.07	spermidine synthase 1	0.51	0.01972	2037792.82	2.7006E+11	3972415.88	5.228E+11
357512287	37.9	6.46	probable aldo-keto reductase 1 isoform X1	1.87	0.0074358	12875225.6	3.0686E+12	6895127.33	1.2038E+12
357480321	31.4	5.11	lactoylglutathione lyase GLX1	1.78	0.020961	3777009.96	4.0685E+10	2117601.39	7.8498E+10
357447935	28.9	5.6	inositol-phosphate phosphatase	0.55	0.035763	1629882.84	5.1477E+11	2978962.05	4.8642E+10
357443443	63	6.8	probable alkaline/neutral invertase D	0.31	0.0264	174505.721	7304311240	555496.346	674574970
922396253	26.4	6.15	probable glutathione S-transferase	Unique in mock SIMKKi	NA	0	0	6278135.61	2.3944E+11
Signaling									
922368741	65.9	8.38	delta(24)-sterol reductase	0.30	0.0042243	2092190.59	1.5314E+12	6998574.54	5.7047E+11
Transport									
357508367	42.8	5.77	V-type proton ATPase subunit C	0.61	0.037184	4684602.58	2.283E+12	7620528	4.5561E+11
1379756034	51.4	6.74	V-type proton ATPase subunit H	1.66	0.0056404	2686600.04	3.9801E+10	1620296.2	536755530
922385908	181	6.61	ABC transporter C family member 2	0.31	0.0133791	656747.338	2.8126E+11	2148897.87	9.2185E+10
1379631695	27.7	10.1	THO complex subunit 4A	0.35	0.0136042	1990469.85	2.3373E+11	5670949.81	1.3161E+12
922353083	35	6.73	short-chain dehydrogenase TIC 32, chloroplastic	Unique in sino SIMKKi	NA	1127137.24	7.2656E+10	0	0

922400161	36.5	7.69	probable voltage-gated potassium channel subunit beta	1.90	0.034798	3598114.91	3.3397E+11	1893956.42	5.488E+11
922337191	13.6	6.34	nuclear transport factor 2A	Unique in sino SIMKKi	NA	1140156.6	1.4974E+11	0	0
Cytoskeleton									
922386288	107.2	5.8	villin-4	0.54	0.035457	1650742.82	5.6379E+11	3046182.68	3.551E+10
357521645	50	4.93	tubulin beta chain	0.40	0.040722	7703630.78	1.288E+12	19342268.7	1.0457E+13
357469067	50.5	4.83	tubulin beta-2 chain	0.64	0.020001	41782181.2	5.3084E+13	64954659.9	6.1659E+13
Unknown									
1379644347	35.4	8.46	uncharacterized protein LOC11422103 isoform X2	1.84	0.047057	1213547.12	1.9095E+10	658916.012	1.2033E+10
357442239	35.7	8.13	uncharacterized protein LOC11427648	Unique in mock SIMKKi	NA	0	0	3638192.59	4.0762E+12
1379640741	65.6	6.86	uncharacterized protein LOC11437125	0.34	0.0148164	1832149.27	8.5625E+11	5338339.41	8910483039
1379669194	36.3	9.03	uncharacterized protein LOC25499858 isoform X1	0.41	0.0185247	1526429.15	2.0378E+11	3729027.52	3.9294E+11
Mitochondrial function and protein transport									
1379623734	30.3	8.88	prohibitin-3, mitochondrial	2.37	0.052983	8351913.08	3.3833E+12	3524239.93	2.6528E+12
357508379	39.5	9.25	mitochondrial phosphate carrier protein 3, mitochondrial	0.50	0.0082971	7883234.11	1.6011E+12	15838154.2	6.4447E+12
357482601	29.5	9.41	mitochondrial outer membrane protein porin 2	0.62	0.025139	6090979.7	1.5371E+12	9883632.86	2.007E+12
357496297	60.7	7.06	AAA-ATPase ASD, mitochondrial	Unique in mock SIMKKi	NA	0	0	660016.387	1.2031E+10
Aminoacid metabolism									
357437449	114.6	7.31	glycine dehydrogenase (decarboxylating), mitochondrial	0.60	0.030097	3133514.77	9.9823E+10	5205612.58	4.6045E+11
1379621960	86.7	5.11	nudix hydrolase 3	0.39	0.034359	857427.156	1.6046E+10	2180336.85	1.1071E+11
357473151	53.9	6.61	allene oxide synthase 1, chloroplastic	0.52	0.051918	1531914.95	1.6529E+11	2961637.72	6.5163E+11
357441513	34.3	5.76	cysteine synthase	0.63	0.00040459	12960859.6	1.345E+11	20491522.6	2.6744E+11

Methylation									
357509479	29.7	6.06	putative methyltransferase DDB_G0268948	Unique in sino SIMKKi	NA	942131.968	1.2942E+11	0	0
Miscellaneous									
357485093	37.7	4.7	plastoglobulin-1, chloroplastic	2.00	0.0168983	5005357.61	4.2774E+11	2497778.19	7.8469E+11
922328103	40.9	7.85	protein RETICULATA-RELATED 4, chloroplastic	0.38	0.040703	606068.816	9.872E+10	1611882.24	1.0718E+11
DNA replication and cell cycle regulation									
922379759	29.5	4.73	proliferating cell nuclear antigen	0.62	0.042595	6163898.1	3.8665E+12	9893687.32	9.775E+11
357512561	51.3	5.78	replication stress response regulator SDE2	Unique in mock SIMKKi	NA	0	0	3036568.31	2.1481E+12
Transcription regulation									
357469575	77.3	6.01	ATP-dependent DNA helicase 2 subunit KU80 isoform X1	Unique in mock SIMKKi	NA	0	0	610973.443	8.1028E+10
357475063	32.1	5.94	transcription factor Pur-alpha 1	0.54	0.0506	2821405.48	8.9216E+11	5241975.15	1.4073E+12
357442669	20	8.76	methyl-CpG-binding domain-containing protein 4 isoform X1	0.33	0.034699	816662.544	1.5254E+11	2469936.52	6.7678E+11
Glycosylation									
922352199	51	5.45	UDP-glycosyltransferase 74G1	Unique in mock SIMKKi	NA	0	0	1794302.51	4.3767E+11
922352197	51.5	5.66	UDP-glycosyltransferase 74G1	Unique in sino SIMKKi	NA	362123.516	4.1545E+10	0	0
357445733	53.2	5.92	soyasaponin III rhamnosyltransferase	Unique in sino SIMKKi	NA	984542.441	3.9204E+11	0	0
357511215	35.3	7.28	putative GDP-L-fucose synthase 2 isoform X1	Unique in mock SIMKKi	NA	0	0	1435767.68	3.3065E+12
1379611956	49	6.44	LOW QUALITY PROTEIN: epidermis-specific secreted glycoprotein EP1	0.37	0.045218	2432705.43	1.9068E+12	6533202.22	4.1936E+12
1379636646	21.3	6.95	probable mannitol dehydrogenase	Unique in mock SIMKKi	NA	0	0	4623111.06	6.1287E+12

Supplementary Table 5 List of proteins with significantly different abundances found in SIMKKi nodules as compared to wild type nodules. NA means not applicable.

Accession	MW [kDa]	Calc. pI	Description	Ratio (SIMKKi vs WT)	P-value	A-mean (SIMKKi)	A-variance (SIMKKi)	B-mean (WT)	B-variance (WT)
Stress related									
357448423	38.3	7.52	peroxidase E5	0.60	0.052663	23105010.8	4.5621E+12	38448984.2	9.0495E+13
922389034	37.3	5.25	peroxidase A2	Unique in WT	NA	0	0	16492235.8	1.3923E+12
1379615657	39.1	8.22	peroxidase 15	0.61	0.0066247	13943601.6	8.9216E+12	22997382.3	2.611E+11
357452877	34.5	9.04	peroxidase P7	0.32	0.029938	2201785.72	3348071713	6899099.04	2.6105E+12
357470223	46.3	9.03	peroxidase 17	0.47	0.02378	1542788.92	5.9726E+10	3291166.3	2.7388E+11
357500689	17.5	5.87	peroxiredoxin-2B	1.61	0.02668	30391920.1	9.6196E+12	18934311.1	2.3972E+13
357513793	97.7	6.29	linoleate 9S-lipoxygenase	0.46	0.037496	34887731.5	3.8687E+13	76509482.7	5.147E+14
1379597042	27.2	6.04	universal stress protein PHOS32	0.39	0.04518	3281682.88	4.1844E+11	8505465.84	2.2251E+12
357477285	54.3	5.43	betaine aldehyde dehydrogenase 1, chloroplastic	Unique in SIMKKi	NA	4738989.03	2.6088E+11	0	0
1379669869	30	6.57	glyoxylate/succinic semialdehyde reductase 1	Unique in WT	NA	0	0	776200.295	8180851296
922349977	73.5	7.05	alpha-dioxygenase 1	Unique in WT	NA	0	0	3459975.9	1.3788E+12
922378081	26.3	8.62	expansin-A15	Unique in WT	NA	0	0	1431634.75	2.2087E+10
Translation									
922339717	59.7	8.54	DEAD-box ATP-dependent RNA helicase 8	1.82	0.026075	845202.932	7786267946	465235.27	46658204.2
1111670368	31.3	10.65	ribosomal protein L2 (chloroplast) [Medicago falcata]	0.52	0.030863	233482.916	1059037933	447219.236	5007873854
1379647649	31.1	5	U2 small nuclear ribonucleoprotein A'	Unique in WT	NA	0	0	2312084.56	4564281859
Cytoskeleton									
922348988	50.2	5.15	tubulin alpha-3 chain	Unique in WT	NA	0	0	12155081	2.5781E+13
922349606	41.7	5.49	actin-97	Unique in SIMKKi	NA	19431889.6	2.6734E+13	0	0

Protein folding and chaperonines									
922338515	73.7	5.19	luminal-binding protein	1.58	0.00092475	77949245.9	8.3108E+12	49433193	5.9506E+10
922338531	73.6	5.12	luminal-binding protein	1.53	0.00125576	74562044.4	2.7545E+13	48865588.2	2.5055E+12
357495175	80.1	5.03	heat shock cognate protein 80	1.87	0.0053379	54789514.2	4.8336E+13	29229617.3	1.6506E+13
357505883	57.2	5.52	T-complex protein 1 subunit beta	2.05	0.0134762	10666926.5	3.4155E+12	5200522.9	1.6172E+12
922385800	60.4	6.27	T-complex protein 1 subunit gamma	0.27	0.0158828	1756216.92	1.5822E+12	6529570.45	8.8764E+11
357493557	60.2	6.39	T-complex protein 1 subunit eta	Unique in WT	NA	0	0	4471520.18	3.9551E+12
1379617351	15.2	9.41	peptidyl-prolyl cis-trans isomerase NIMA-interacting 4	Unique in WT	NA	0	0	1261907.27	2.08E+10
1379623734	30.3	8.88	prohibitin-3, mitochondrial	Unique in SIMKKi	NA	3399028.16	1.6817E+12	0	0
Membrane transport									
922396563	69.5	5.55	vacuolar-sorting receptor 1	2.33	0.036602	167651.04	515567541	71904.4412	194281718
357519317	49.7	5.88	guanosine nucleotide diphosphate dissociation inhibitor 1	Unique in SIMKKi	NA	4064421.19	8.1611E+12	0	0
Protein degradation and processing									
922328501	55.5	7.59	serine carboxypeptidase-like 40	0.47	0.0159244	1385599.25	2.2256E+10	2969171.57	5.9584E+10
922402459	49.7	6.33	26S proteasome regulatory subunit 4 homolog A	1.84	0.0179596	9604706.43	1.1267E+12	5220993.08	9.8591E+11
357460533	46.4	5.59	26S proteasome regulatory subunit 6B homolog isoform X1	3.30	0.023116	6598673.19	2.2434E+12	2000130.43	2.699E+12
357442229	33.2	8.37	ATP-dependent Clp protease proteolytic subunit 5, chloroplastic	Unique in WT	NA	0	0	1377419.92	4.4531E+11
Aminoacid and nitrogen metabolism									
357507415	40.9	8.19	bifunctional L-3-cyanoalanine synthase/cysteine synthase 1, mitochondrial	2.60	0.0061757	11582305.8	2.8507E+12	4455872.79	2.615E+12
1379629521	42.4	5.54	ervatamin-B	2.76	0.044218	2843625.15	9.8913E+11	1029028.81	3.5075E+10
357460841	39.1	5.59	glutamine synthetase cytosolic isozyme	1.52	0.021458	57707198.1	4.4677E+12	38079111.8	8.1504E+13
1379614636	55	6.44	aspartic proteinase	2.71	0.0069426	6014483.67	5.6552E+11	2221824.87	4.1729E+10

Metabolism									
922400155	48.3	7.99	3-ketoacyl-CoA thiolase 2, peroxisomal	0.41	0.0042019	7050683.06	1.3614E+12	17379224.3	7.9234E+12
357453423	107	7.72	aconitate hydratase, cytoplasmic	0.51	0.0061568	26912225.4	1.8196E+12	52550614	6.881E+13
1379756023	63.2	5.68	phosphoglucomutase, cytoplasmic	2.21	0.0061581	11452300	1.7003E+12	5190083.65	2.5144E+12
922360395	38.2	6.73	fructose-bisphosphate aldolase, cytoplasmic isozyme	1.46	0.0077042	135917816	1.5436E+14	93301964.9	6.7145E+13
357451631	42.4	6.01	phosphoglycerate kinase, cytosolic	0.62	0.0102221	65934642.7	4.4195E+13	106257761	1.8888E+14
357451523	44.6	8.44	glyceraldehyde-3-phosphate dehydrogenase GAPCP1, chloroplastic	0.43	0.024704	9038028.09	2.0728E+11	21023339.4	1.0848E+13
357452217	110.8	6.24	phosphoenolpyruvate carboxylase	0.46	0.036341	43531147.7	2.5612E+14	93754329.1	5.3304E+14
922359584	47.5	6.33	ATP-citrate synthase alpha chain protein 1 isoform X1	Unique in WT	NA	0	0	1497607.56	1.9097E+11
357481763	52.2	6.13	hydroxymethylglutaryl-CoA synthase	2.27	0.044718	6283560.31	3.1844E+12	2774021.59	1.2502E+12
Stress and signaling responce									
1379613055	57.4	7.9	succinate-semialdehyde dehydrogenase, mitochondrial	Unique in WT	NA	0	0	2854480.38	3.138E+11
922349977	73.5	7.05	alpha-dioxygenase 1	Unique in WT	NA	0	0	3459975.9	1.3788E+12
Unknown									
357455159	19	6.15	embryo-specific protein ATS3B isoform X1	Unique in WT	NA	0	0	2114915.58	7.9236E+11
922339073	37.4	6.14	probable aldo-keto reductase 2	Unique in WT	NA	0	0	2598435.91	3.5746E+12
922403709	19.9	5.15	PITH domain-containing protein At3g04780	Unique in WT	NA	0	0	3161053.67	3.212E+12
Gene expression									
1379632523	19.3	6.74	glycine-rich protein 2-like	0.56	0.052861	6175384.49	7.0414E+12	11075935.4	2.6803E+12
922365631	27.5	6.62	uncharacterized protein At5g02240	Unique in WT	NA	0	0	4.6632E+13	2.0456E+12
1379605695	134.4	5.36	LOW QUALITY PROTEIN: spliceosome-associated protein 130 A	Unique in SIMKKi	NA	773584.763	2.0029E+10	0	0

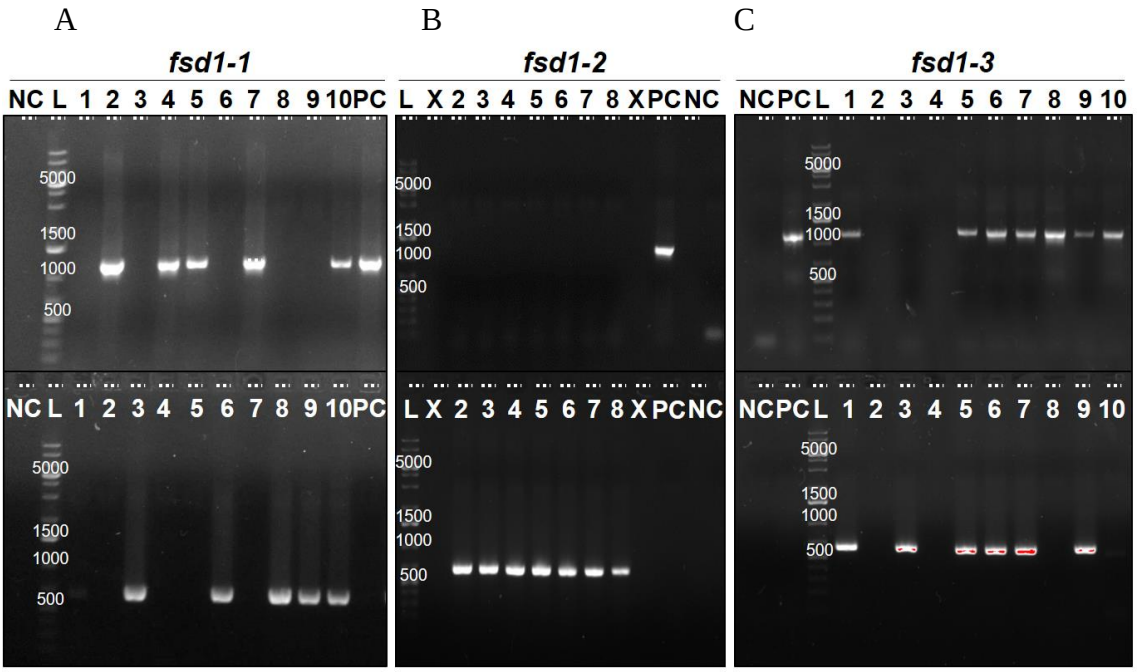

Supplementary figure 2 Electrophoretogram results of PCR-based genotyping of *fsd1* mutant seedlings. (A), (B) and (C) represent three gels, with two sets of samples loaded on top and in the middle. The place of sample loading is indicated by dashed line. In the upper part of the gels, the presence of wild-type genomic DNA fragments with expected size (A) 1141 bp, (B) 1131 bp, (C) 1132 bp was tested using the combination of left genomic primer and right genomic primer. In the lower part of gels, the presence of T-DNA insertion in *fsd1* mutant lines with expected size (A) 529–829 bp, (B) 502–802 bp, (C) 501–801 bp was examined using right genomic primer and left border primer of the T-DNA insertion. Homozygous mutant plants *fsd1*$^{-/-}$ in (A) correspond to lanes 1, 3, 6, 8 and 9; in (B) lanes 2–8; (C) lane 3. Heterozygous individuals of *fsd1*$^{+/-}$ are in (A) lane 10; (B) not found; (C) lanes 1, 5–7, 9 and 10. Lanes 2, 4–5 and 7 (A) and lane 8 (C) were identified as wild type. L – GeneRuler, 1 kb Plus DNA Ladder; sizes are given in bp; NC – negative control (water instead of template DNA), PC – positive control (wild-type DNA), X – empty lanes.

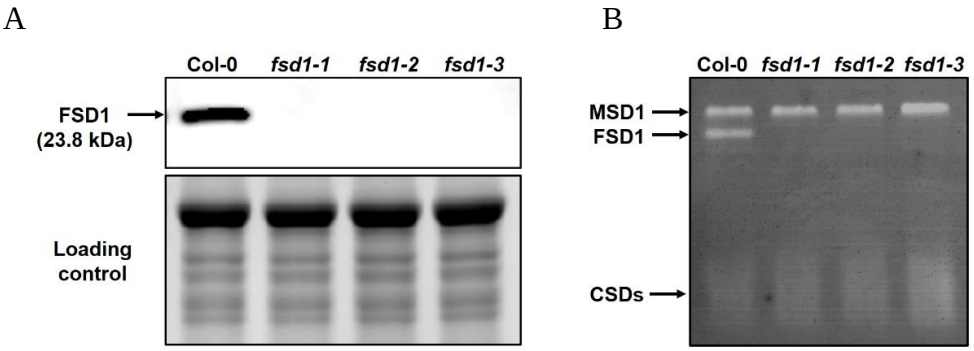

Supplementary figure 3 Verification of *fsd1* mutant lines by immunoblotting and SODs activity analysis. (A) Immunoblot prepared using anti-FSD1 antibody showing the presence of FSD1 (23.8 kDa) in wild type (Col-0) total protein extract and absence in mutant lines. Loading controls are represented by visualization of proteins on TGX membranes using Stain-free technology (BioRad). (B) Visualization of SODs isoforms activities separated on native polyacrylamide gels by specific staining. FSD1 activity was not detected in mutant lines.

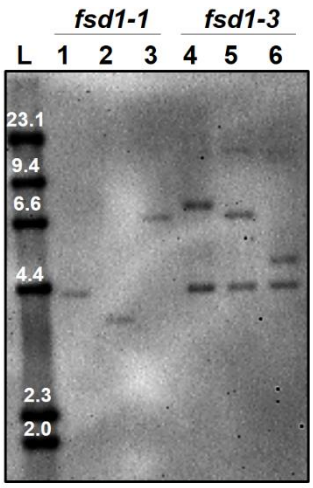

Supplementary figure 4 Verification of T-DNA insertion SALK *fsd1* mutant lines by Southern blot analysis. Isolated genomic DNA from homozygous *fsd1-1* and *fsd1-3* mutants were used to verify number of insertions. Over 10 micrograms of DNA were digested with EcoRI (lines 1, 4), SacI (lines 2, 5), HindIII (lines 3, 6) for both mutants. Overnight cleaved DNAs were separated by electrophoresis and subsequently transferred to a nylon membrane followed by hybridization with a digoxigenin-labeled probe specific to kanamycin resistance, which is inserted in T-DNA. The signal was developed after overnight incubation. Expected size of cleaved genomic DNA of both mutants is approximate: EcoRI – 4 kbp; SacI – 4 kbp; HindIII – 7 kbp, and for *fsd1-3*: EcoRI – 4.4 kbp; SacI – 4 kbp; HindIII – 6.8 kbp L – DNA Molecular Weight Marker II, DIG-labeled, sizes of ladder are given in kbp.

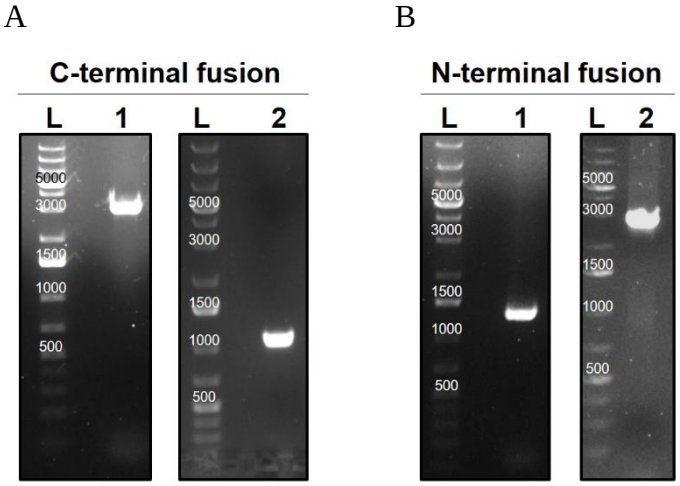

Supplementary figure 5 Representative electrophoretic images of PCR products for preparation of FSD1 entry clones. (A, B) PCR products for BP recombination reaction by MultiSite Gateway®. (A) PCR amplicons of *FSD1* native promoter with *FSD1* gene sequence without stop codon (line 1; 3157 bp) and *FSD1* 3'UTR sequence (line 2; 1070 bp). (B) PCR amplicons of *FSD1* native promoter (line 1; 1270 bp) and *FSD1* gene sequence together with *FSD1* 3'UTR sequence (line 2; 2957 bp). L – GeneRuler, 1 kb Plus DNA Ladder; sizes are given in bp.

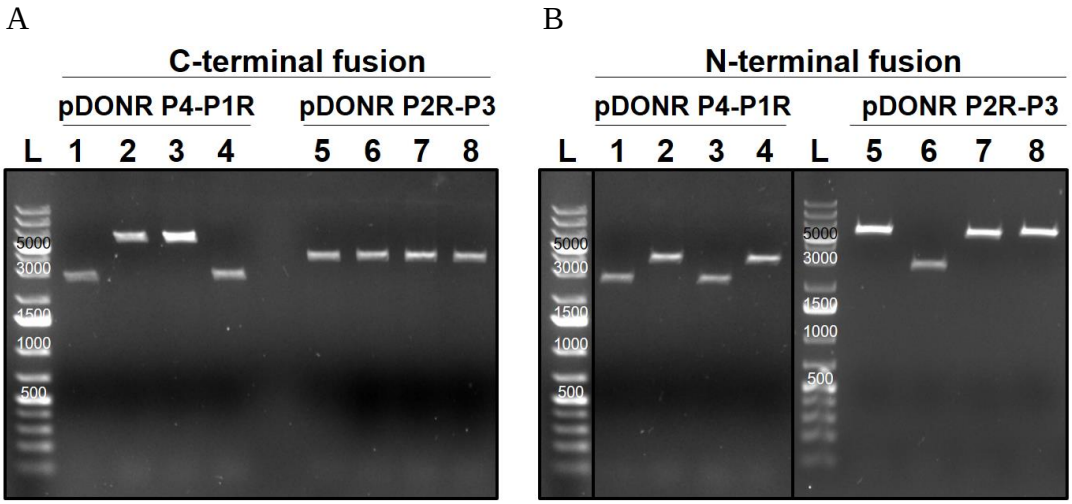

Supplementary figure 6 Selection of positive *E. coli* colonies carrying entry clones for preparation of GFP-fused *FSD1* gene under its own promoter. (A, B) Representative electrophoretic images after enzymatic restriction of DNA. (A) Restriction of entry clones of *FSD1* native promoter with *FSD1* gene sequence without stop codon in pDONR P4-P1R vector cleaved by EcoRI (size of positive product 5769 bp) and *FSD1* 3ˈUTR sequence in pDONR P2R-P3 vector cleaved by EcoRI (size of positive product 3678 bp). Positive products were detected in lines 2, 3 and 5–8. (B) Restriction of entry clones of *FSD1* native promoter in pDONR P4-P1R vector cleaved by EcoRI (size of positive product 3912 bp) and *FSD1* gene sequence together with FSD1 3ˈUTR sequence in pDONR P2R-P3 vector cleaved by EcoRI (size of positive product 5528 bp). Positive products were detected in lines 2, 4 and 5, 7, 8. L – GeneRuler, 1 kb Plus DNA Ladder; sizes are given in bp.

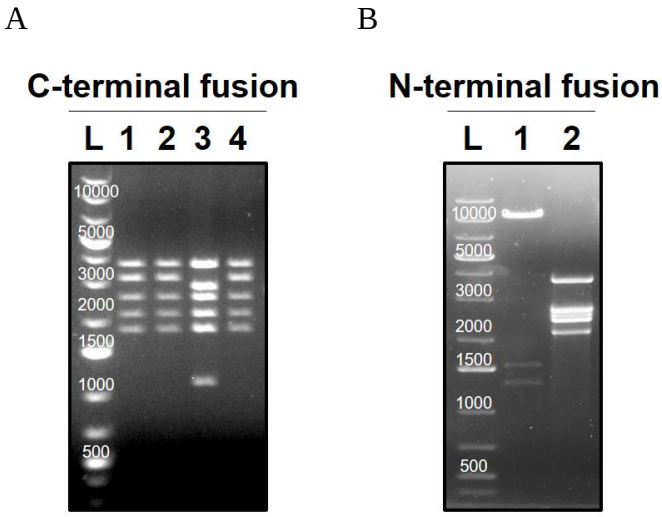

Supplementary figure 7 Selection of positive colonies carrying destination vectors of *GFP*-fused *FSD1* gene under its own promoter. (A, B) Enzymatic cleavage of final products prepared by MultiSite Gateway® LR recombination reaction with destination vector pB7m34GW visualized on electrophoretic images. (A) Restriction analysis of destination vector carrying *pFSD1-gFSD1::GFP:3ˈUTR-FSD1* digested by NdeI (size of positive products 3649, 3161, 2489, 2065, 1855 bp). Positive products were detected in lines 1, 2 and 4. (B) Restriction analysis of destination vector carrying *pFSD1::GFP:gFSD1-3ˈUTR-FSD1* digested by NdeI in line 1 (size of positive products 3649, 2626, 2489, 2387, 2058 bp) and NotI in line 2 (size of positive products 10387, 1532, 1290 bp). Only one colony was grown on culture media. Isolated plasmid DNA was examined by two independent restriction enzymes and both confirmed positive results. L – GeneRuler, 1 kb Plus DNA Ladder; sizes are given in bp.

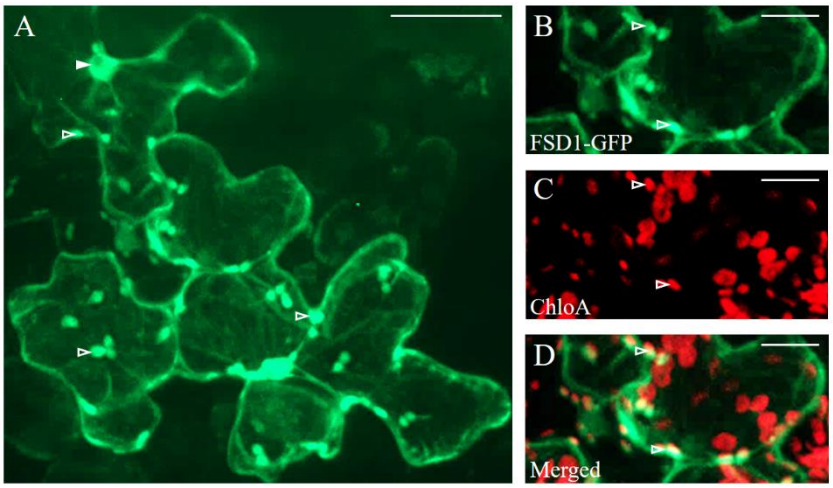

Supplementary figure 8 Transient transformation of *N. benthamiana* leaves by *A. tumefaciens* GW3101 carrying *gFSD1::GFP:3'UTR-FSD1*. (A) Representative image of FSD1-GFP observed by spinning disk microscope (Cell Observer, Carl Zeiss). Note the FSD1-GFP localization in chloroplasts, nuclei, cytosol and in proximity of cytoplasmatic membrane. (B-D) Colocalisation of FSD1-GFP with chloroplasts. (B) FSD1-GFP, (C) chlorophyll a autofluorescence, (D) merged image showing both signals. Filled arrows indicate nuclear signal and blank arrowheads indicate chlorophyll a autofluorescence (green – FSD1-GFP, red – chlorophyll a autofluorescence). Scale bars: A, 50 μm; B-D, 20 μm.

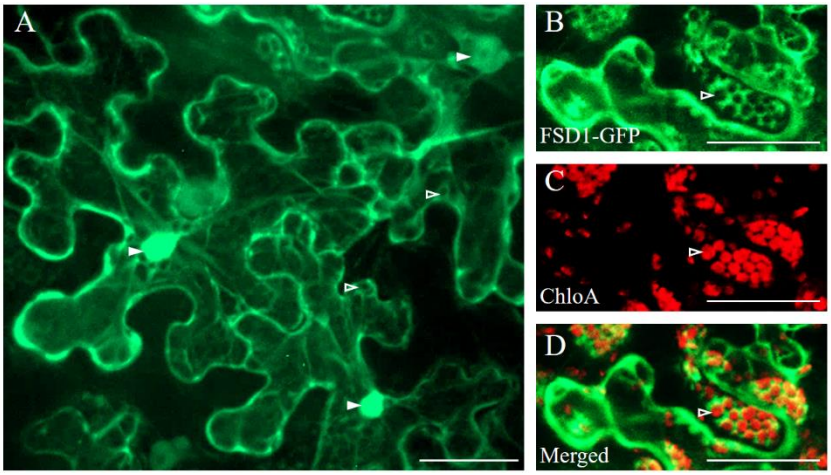

Supplementary figure 9 Transient transformation of *N. benthamiana* leaves by *A. tumefaciens* GW3101 carrying *pFSD1::GFP:gFSD1-3'UTR-FSD1*. (A) Representative image of FSD1-GFP observed by spinning disk microscope (Cell Observer, Carl Zeiss). Note the FSD1-GFP localization in nuclei, cytosol and in proximity of cytoplasmatic membrane. (B-D) Colocalisation of FSD1-GFP with chloroplasts. (B) GFP-FSD1, (C) chlorophyll a autofluorescence, (D) merged image showing both signals. Filled arrows indicate nuclear signal and blank arrowheads indicate chlorophyll a autofluorescence (green – FSD1-GFP, red – chlorophyll a autofluorescence). Scale bars: A, 50 μm; B-D, 20 μm.

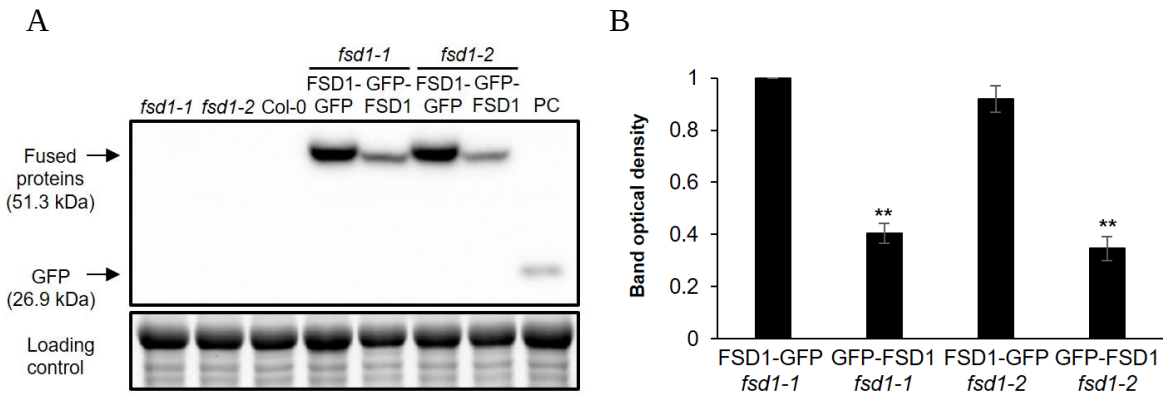

Supplementary figure 10 Detection of GFP fused FSD1 in complemented *fsd1* mutants expressing FSD1-GFP and GFP-FSD1 using anti-GFP antibody. (A) Immunoblots showing the presence of GFP fused FSD1 in 14-days-old complemented *fsd1* mutants expressing FSD1-GFP or GFP-FSD1 and the absence of signal in Col-0 and *fsd1* mutants. *35S::GFP* expressing line was used as positive control. (B) Quantification of optical density of band in (A). The densities are expressed as relative to the highest value. Error bars represent standard deviation. Stars indicate statistically significant difference between GFP-FSD1 and FSD1-GFP abundance (one-way ANOVA, **p < 0.01).

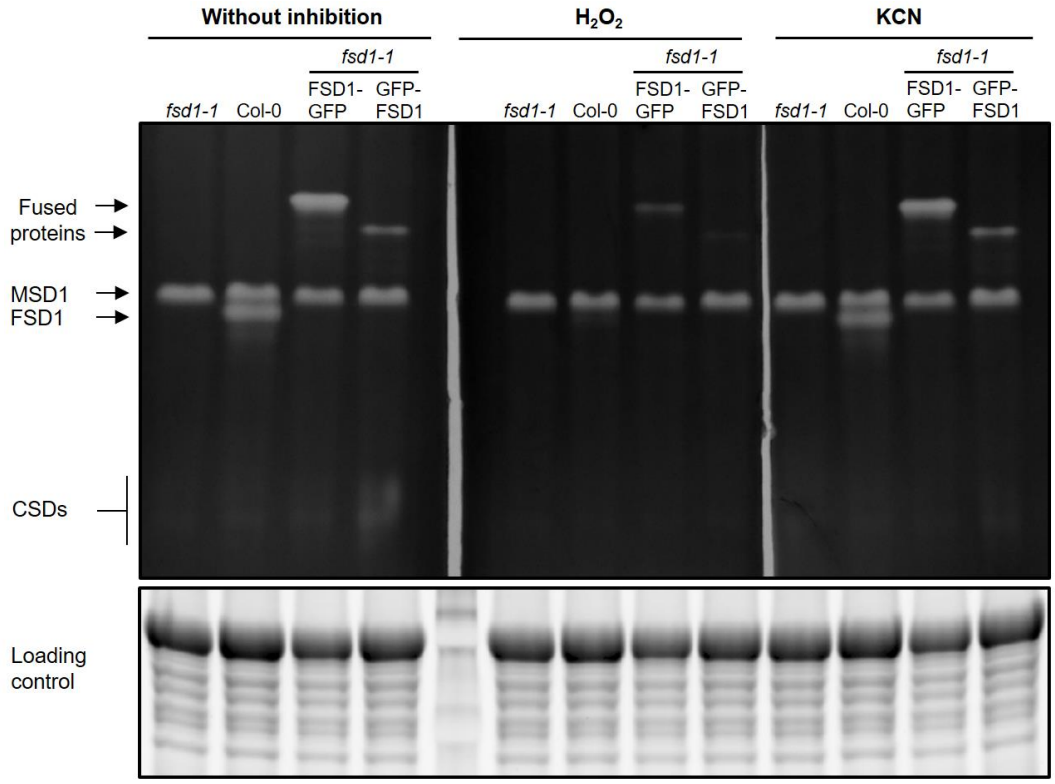

Supplementary figure 11 Identification of SOD isozymes in complemented *fsd1* mutant expressing FSD1-GFP or GFP-FSD1 by specific inhibitors. Visualization of SOD isozymes on native polyacrylamide gel without preincubation, with preincubation in KCN (inhibiting CSDs activity) and with preincubation in H_2O_2 (inhibiting FSD1 and CSDs). Adopted from Dvořák et al. (2021).

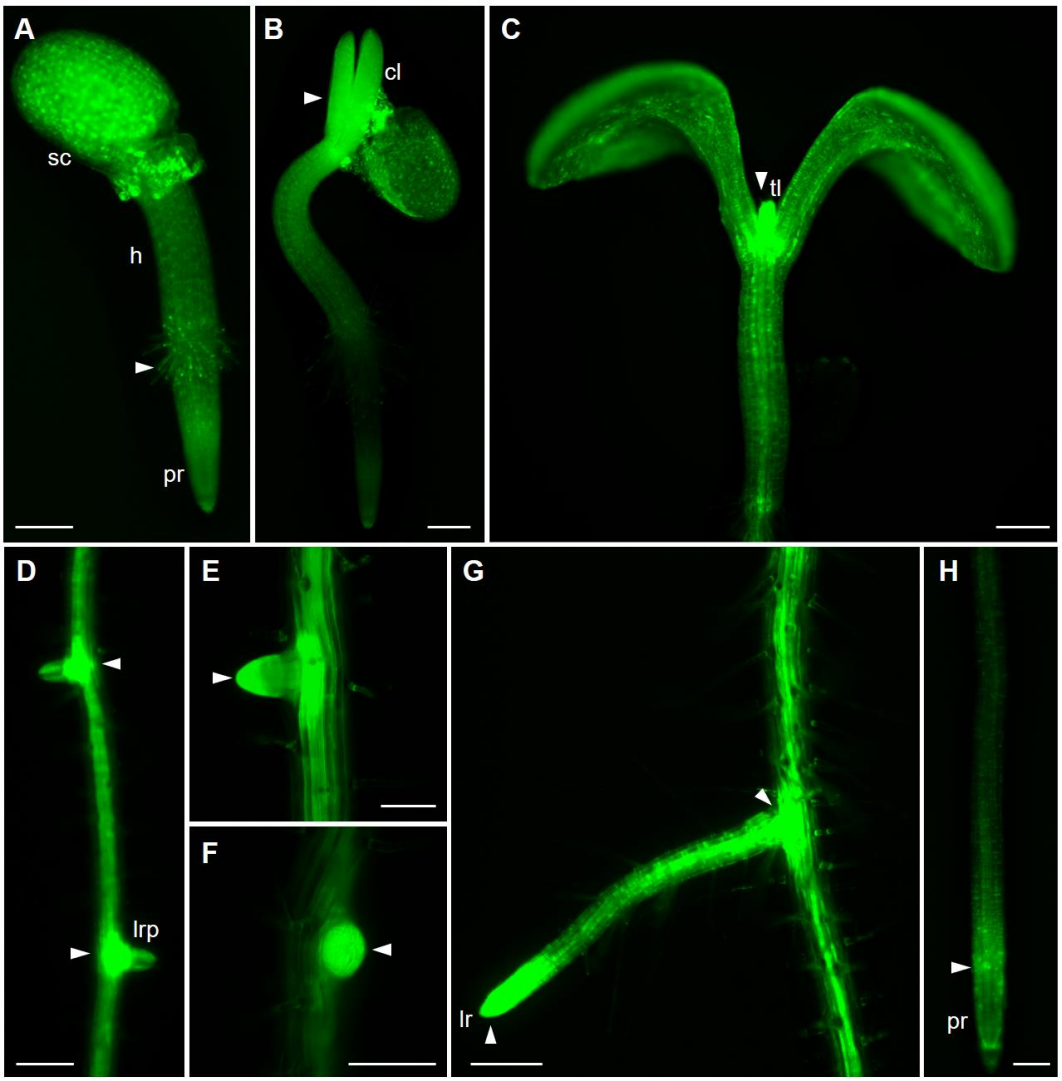

Supplementary figure 12 Localization of FSD1-GFP observed using ZOOM stereomicroscope during different developmental stages of young complemented *fsd1-1* seedlings. (A) Emerged seedling at 1st day after germination emerged from a seed coat (sc), with hypocotyl (h) and primary root (pr). (B) Cotyledons (cl) acquitted from a seed coat at 2nd day after germination. (C) Cotyledons and development first true leaves (tl) at 5th day after germination. (D-F) Lateral root primordia (lrp), 6th day after germination. (G) Fully emerged elongating lateral root on 8th day after germination. (H) Primary root on 8th day after germination. The highest intensity of GFP signal is marked by arrowheads. Scale bars: E, F, 100 μm; A-D, G, H, 200 μm. Adopted from Dvořák et al. (2021).

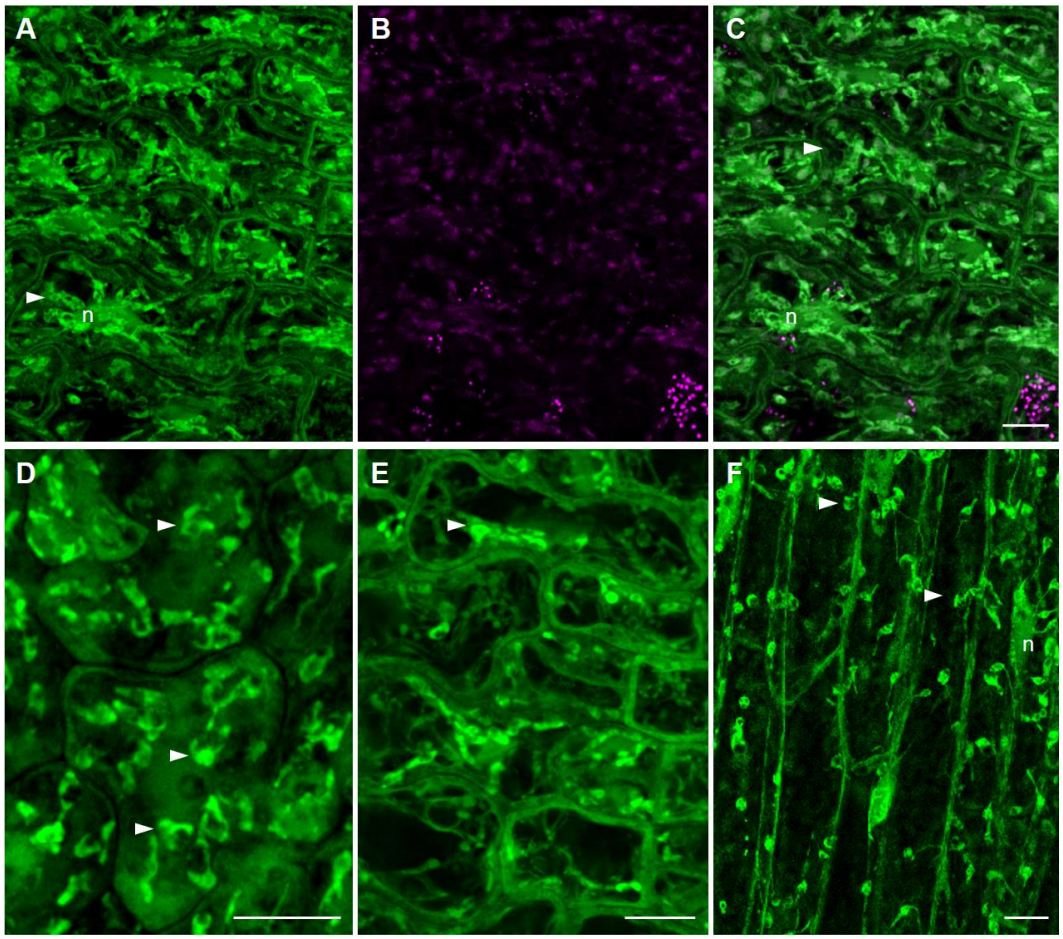

Supplementary figure 13 Microscopy observation of FSD1-GFP localization of etiolated *Arabidopsis* seedlings in epidermal cells. (A-E) cotyledons on 2nd day after germination. (F) Hypocotyl on 2nd day after germination. Arrowheads indicate plastids, (n) stands for nuclei. Channels: green – FSD1-GFP; magenta – chlorophyll a autofluorescence. Scale bars: A-E, 10 μm; F, 20 μm. Adopted from Dvořák et al. (2021).

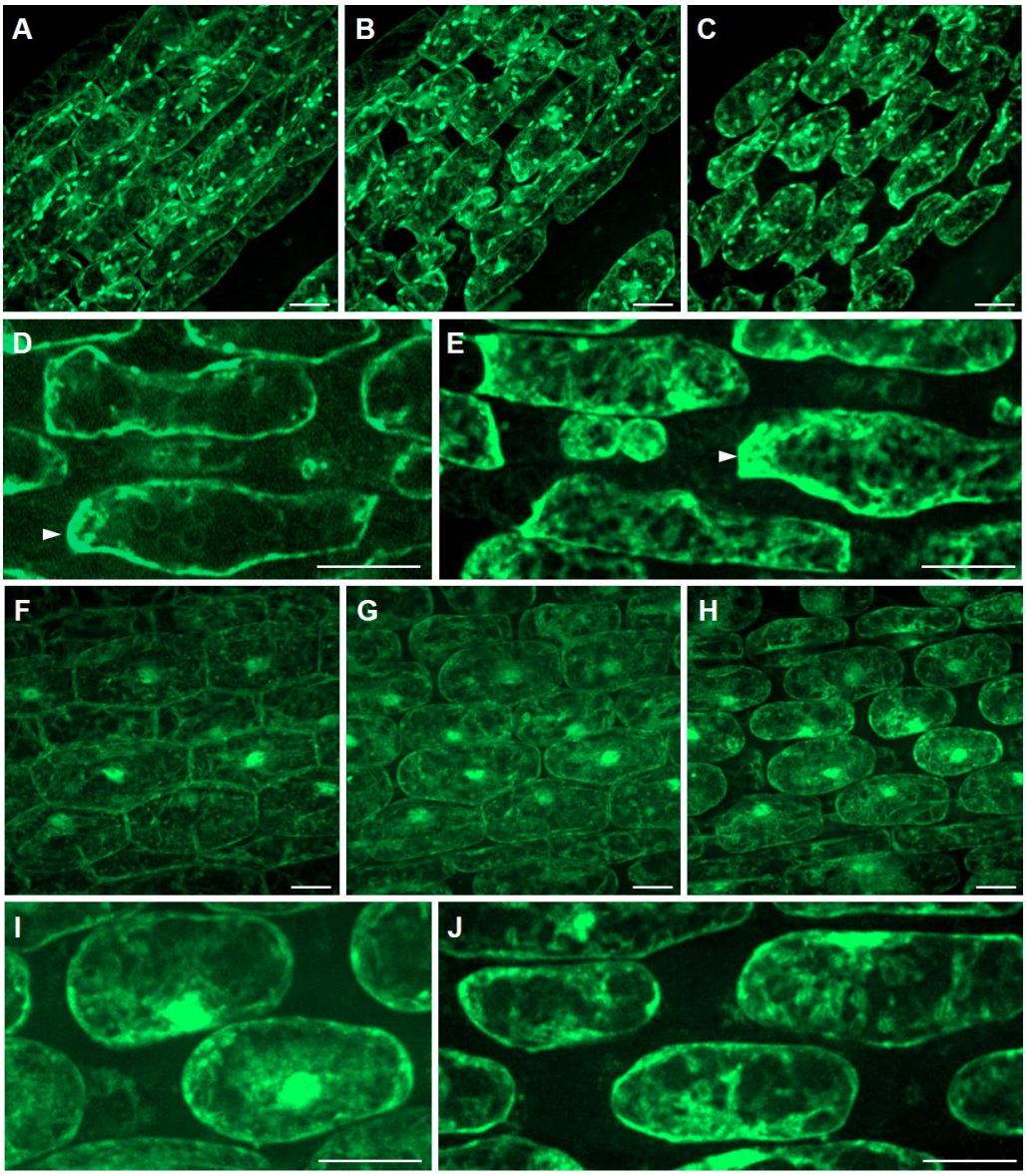

Supplementary figure 14 Time-lapse imaging of induced plasmolysis in hypocotyl epidermal cells of *fsd1-1* mutant carrying FSD1-GFP and wild type line carrying *35S::GFP*. (A-E) The progression of concave and convex plasmolysis in *fsd1-1* mutant line expressing FSD1-GFP. (F-J) The progression of concave and convex plasmolysis in transgenic line expressing *35S::GFP*. (A, F) Cells without treatment, (B, G) 5 min treatment, (C, H) 30 min treatment. (D, E, I, J) Plasmolyzed cells in details. Arrowheads point to FSD1-GFP signal accumulation. Scale bar: 20 μm. Adopted from Dvořák et al. (2021).

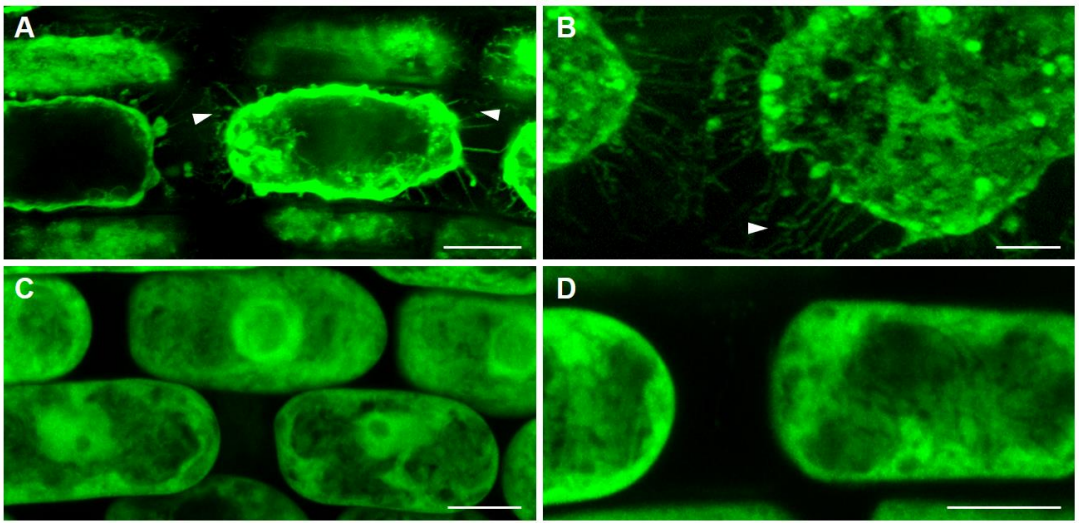

Supplementary figure 15 Salt induced plasmolysis of epidermal cells of primary root elongation zone observed in *fsd1-1* mutant complemented by FSD1-GFP. Plasmolysis of root was observed after treatment by 1/2 MS medium enriched with 250 mM NaCl for 15 min. (A) Concave plasmolysis and Hechtian strands (arrowheads) induced in complemented *fsd1-1* mutant harboring FSD1-GFP. (B) Magnification of Hechtian strands. (C) Concave plasmolysis in epidermal cells of primary root elongation zone in plants of transgenic line carrying *35S::GFP* (D) Magnification of area showing apoplastic space without the presence of Hechtian strands. Scale bars: 10 μm. Adopted from Dvořák et al. (2021).

Supplementary table 6 Prediction of potential kinase responsible for phosphorylation of FSD1 as predicted by GPS 3.0 software (Xue et al., 2005).

Position	Code	Kinase	Peptide	Score	Cutoff
151	T	CMGC/MAPK	EKLKVVKTPNAVNPL	26.883	14.896
211	S	Other/PEK	LEAAKAASA******	18.682	6.12
211	S	CK1/CK1	LEAAKAASA******	13.1	4.847
69	Y	Other/WEE	EHIIHSTYNNGDLLP	12	10
142	S	Other/PEK	GWAWLAYSNEKLKVV	10.773	6.12
4	S	CK1/CK1	****MAASSAVTANY	10.4	4.847
11	Y	STE/STE7	SSAVTANYVLKPPPF	9.688	8.398
117	Y	STE	LERDFTSYEKFYEEF	9.312	7.119
117	Y	STE/STE7	LERDFTSYEKFYEEF	9.312	8.398
43	Y	STE/STE7	WGKHHRAYVDNLKKQ	8.75	8.398
121	Y	AGC	FTSYEKFYEEFNAAA	7.667	6.333
196	S	CAMK/CAMKL	TFMTNLVSWEAVSAR	7.387	6.355
69	Y	AGC	EHIIHSTYNNGDLLP	7	6.333

Supplementary table 7 Identification of probable peptide phosphorylated by MAPK in FSD1 amino acid sequence. MAPK specific phosphopeptide and MAPK specific docking sequences were predicted by GPS 3.0 (Xue et al., 2005), and by ELM (Kumar et al., 2020), respectively.

AGI	Name	Peptide (GPS 3.0)	Docking site (ELM)		
			Name	Sequence	Position
at4g25100	AtFSD1	EKLKVVKTPNAVNPL	DOC_MAPK_DCC_7	KTPNAVNPLVL	150-160

Supplementary figure 16 Prediction of phosphorylation sites in the amino acid sequence of FSD1 protein by using PhosPhAt 3.0 software (25. 10. 2017; Zulawski et al., 2013; http://phosphat.uni-hohenheim.de/).

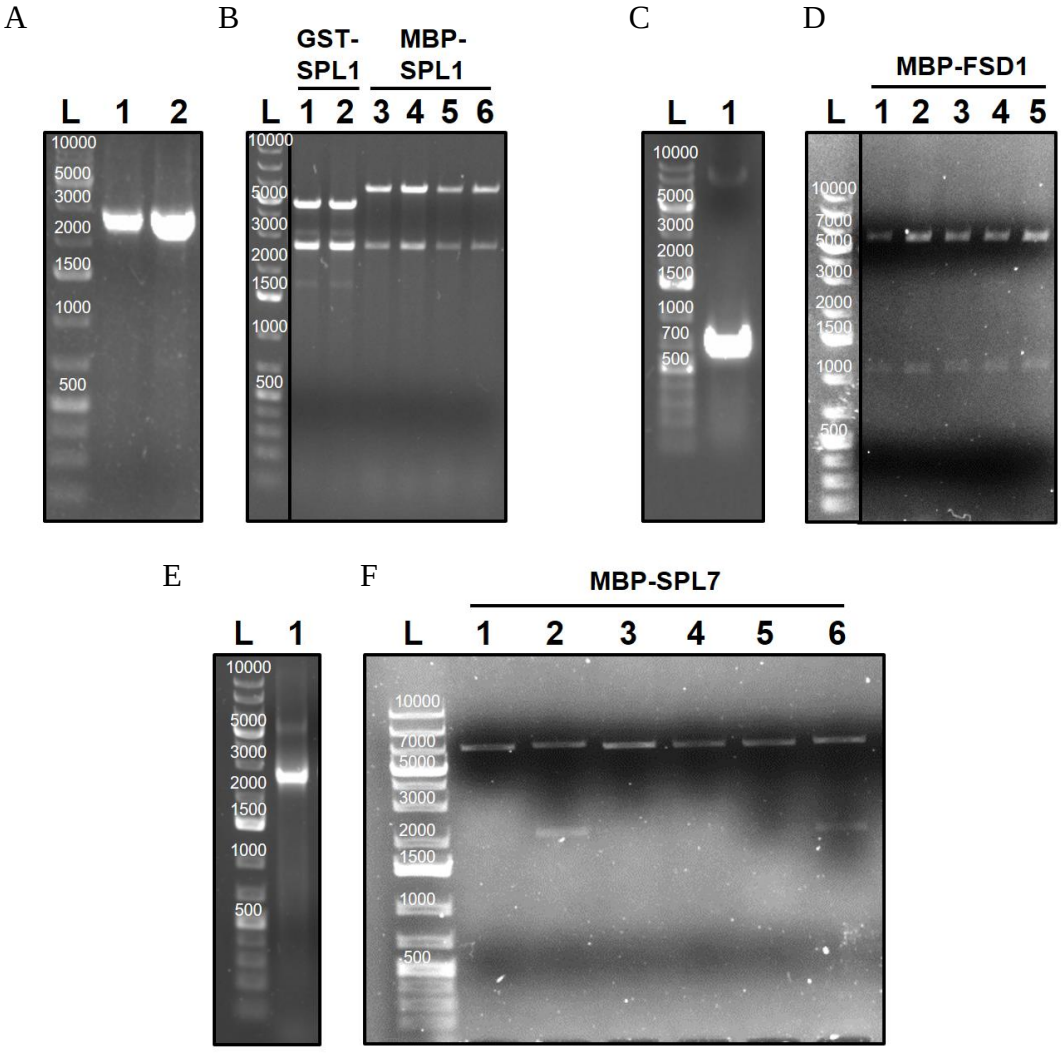

Supplementary figure 17 Preparation of constructs for recombinant protein production. (A, C, E) PCR products of amplified cDNA for SPL1 (A) FSD1 (C, size 675 bp) and SPL7 (E, size 2574 bp). In (A) lane 1 represent PCR product for GST-SPL1 (size 2689 bp), lane 2 MBP-SPL1 (2686 bp). (B, D, F) restriction analysis of prepared constructs GST-SPL1 (B, lane 1, 2, size of positive reaction 4847 bp and 2846 bp), MBP-SPL1 (B, lane 3-6, size of positive reaction 6905 bp and 2891 bp), MBP-FSD1 (D, size of positive reaction 6305 bp and 1201 bp) and SPL7-MBP (F, 7153 bp and 2095 bp). GeneRuler, 1 kb Plus DNA Ladder; sizes are given in bp.

Supplementary references (connected to supplementary table 1):

Bhaskara, G. B., Wen, T. N., Nguyen, T. T., and Verslues, P. E. (2017). Protein phosphatase 2Cs and Microtubule-Associated Stress Protein 1 control microtubule stability, plant growth, and drought response. *Plant Cell, 29,* 169–191.

Choudhary, M. K., Nomura, Y., Wang, L., Nakagami, H., and Somers, D. E. (2015). Quantitative circadian phosphoproteomic analysis of Arabidopsis reveals extensive clock control of key components in physiological, metabolic, and signaling pathways. *Mol. Cell Proteomics*, *14*, 2243–2260.

Engelsberger, W. R., and Schulze, W. X. (2012). Nitrate and ammonium lead to distinct global dynamic phosphorylation patterns when resupplied to nitrogen-starved Arabidopsis seedlings. *Plant J.*, *69*, 978–995.

Li, H., Wong, W. S., Zhu, L., Guo, H. W., Ecker, J., and Li, N. (2009). Phosphoproteomic analysis of ethylene-regulated protein phosphorylation in etiolated seedlings of Arabidopsis mutant *ein2* using two-dimensional separations coupled with a hybrid quadrupole time-of-flight mass spectrometer. *Proteomics*, *9*, 1646–1661.

Lin, L. L., Hsu, C. L., Hu, C.W., Ko, S. Y., Hsieh, H. L., Huang, H. C., et al. (2015). Integrating phosphoproteomics and bioinformatics to study brassinosteroidregulated phosphorylation dynamics in *Arabidopsis*. *BMC Genom*., *16,* 533.

Mayank, P., Grossman, J., Wuest, S., Boisson-Dernier, A., Roschitzki, B., Nanni, P., et al. (2012). Characterization of the phosphoproteome of mature Arabidopsis pollen. *Plant J.*, *72*, 89–101.

Mithoe, S. C., Boersema, P. J., Berke, L., Snel, B., Heck, A. J., and Menke, F. L. (2012). Targeted quantitative phosphoproteomics approach for the detection of phospho-tyrosine signaling in plants. *J. Proteome Res*., *11,* 438–448.

Nakagami, H., Sugiyama, N., Mochida, K., Daudi, A., Yoshida, Y., Toyoda, T., et al. (2010). Large-scale comparative phosphoproteomics identifies conserved phosphorylation sites in plants. *J. Plant Physiol*., *153*, 1161–1174.

Rayapuram, N., Bigeard, J., Alhoraibi, H., Bonhomme, L., Hesse, A. M., Vinh, J., et al. (2018). Quantitative phosphoproteomic analysis reveals shared and specific targets of *Arabidopsis* mitogen-activated protein kinases (MAPKs) MPK3, MPK4, and MPK6. *Mol. Cell. Proteom*., *17*, 61–80.

Rayapuram, N., Bonhomme, L., Bigeard, J., Haddadou, K., Przybylski, C., Hirt, H., et al. (2014). Identification of novel PAMP-triggered phosphorylation and dephosphorylation events in *Arabidopsis thaliana* by quantitative phosphoproteomic analysis. *J. Proteome Res.*, *13*, 2137–2151.

Reiland, S., Finazzi, G., Endler, A., Willig, A., Baerenfaller, K., Grossmann, J., et al. (2011). Comparative phosphoproteome profiling reveals a function of the STN8 kinase in fine-tuning of cyclic electron flow (CEF). *Proc. Natl. Acad. Sci. U. S. A*., *108*, 12955–12960.

Reiland, S., Messerli, G., Baerenfaller, K., Gerrits, B., Endler, A., Grossmann, J., et al. (2009). Large-scale Arabidopsis phosphoproteome profiling reveals novel chloroplast kinase substrates and phosphorylation networks. *Plant Physiol.*, *150*, 889–903.

Roitinger, E., Hofer, M., Köcher, T., Pichler, P., Novatchkova, M., Yang, J., et al. (2015). Quantitative phosphoproteomics of the ataxia telangiectasia-mutated (ATM) and ataxia

telangiectasia-mutated and rad3-related (ATR) dependent DNA damage response in *Arabidopsis thaliana*. *Mol. Cell Proteomics*, *14*, 556–571.

Sugiyama, N., Nakagami, H., Mochida, K., Daudi, A., Tomita, M., Shirasu, K., et al. (2008). Large-scale phosphorylation mapping reveals the extent of tyrosine phosphorylation in *Arabidopsis*. *Mol. Syst. Biol.*, *4*, 193.

Umezawa, T., Sugiyama, N., Takahashi, F., Anderson, J. C., Ishihama, Y., Peck, S. C., et al. (2013). Genetics and phosphoproteomics reveal a protein phosphorylation network in the abscisic acid signaling pathway in *Arabidopsis thaliana*. *Sci. Signal.*, *6*, rs8.

Van Leene, J., Han, C., Gadeyne, A., Eeckhout, D., Matthijs, C., Cannoot, B., et al. (2019). Capturing the phosphorylation and protein interaction landscape of the plant TOR kinase. *Nat. Plants*, *5*, 316–327.

Wang, X., Bian, Y., Cheng, K., Gu, L. F., Ye, M., Zou, H., et al. (2013b). A largescale protein phosphorylation analysis reveals novel phosphorylation motifs and phosphoregulatory networks in Arabidopsis. *J. Proteom.*, *78*, 486–498.

Wang, X., Bian, Y., Cheng, K., Zou, H., Sun, S. S., and He, J. X. (2012). A comprehensive differential proteomic study of nitrate deprivation in *Arabidopsis* reveals complex regulatory networks of plant nitrogen responses. *J. Proteome Res.*, *11*, 2301–2315.

Wang, P., Xue, L., Batelli, G., Lee, S., Hou, Y. J., Van Oosten, M. J., et al. (2013a). Quantitative phosphoproteomics identifies SnRK2 protein kinase substrates and reveals the effectors of abscisic acid action. *Proc. Natl. Acad. Sci. U. S. A.*, *110*, 11205–11210.

Xue, L., Wang, P., Wang, L., Renzi, E., Radivojac, P., Tang, H., et al. (2013). Quantitative measurement of phosphoproteome response to osmotic stress in Arabidopsis based on Library-Assisted eXtracted Ion Chromatogram (LAXIC). *Mol. Cell. Proteomics*, *12*, 2354–2369.

Yang, Z., Guo, G., Zhang, M., Liu, C. Y., Hu, Q., Lam, H., et al. (2013). Stable isotope metabolic labeling-based quantitative phosphoproteomic analysis of Arabidopsis mutants reveals ethylene-regulated time-dependent phosphoproteins and putative substrates of constitutive triple response 1 kinase. *Mol. Cell. Proteom.*, *12*, 3559–3582.

Zhang, H., Zhou, H., Berke, L., Heck, A. J., Mohammed, S., Scheres, B., et al. (2013). Quantitative phosphoproteomics after auxin-stimulated lateral root induction identifies an SNX1 protein phosphorylation site required for growth. *Mol. Cell. Proteomics*, *12*, 1158–1169.

8.1.2 Supplementary videos a files

Supplementary videos and files are attached on CD.

Supplementary video 1 Distribution of FSD1-GFP during *Arabidopsis* seed germination (Light-sheet microscopy).

Supplementary video 2 Real-time primary root growth of FSD1-GFP *Arabidopsis* lines (Light-sheet microscopy).

Supplementary video 3 Dynamic of chloroplasts and nuclei in pavement cells of cotyledons of FSD1-GFP *Arabidopsis* lines (Airyscan fluorescence microscopy).

Supplementary video 4 Dynamic of chloroplasts and their interaction with endoplasmic reticulum bodies in mesophyll cells of FSD1-GFP *Arabidopsis* lines (Airyscan fluorescence microscopy).

Supplementary video 5 Details of cytoplasmic streaming in hypocotyl epidermal cells of FSD1-GFP *Arabidopsis* lines (Airyscan fluorescence microscopy).

Supplementary video 6 FSD1-GFP labeled plastid dynamics in different tissues of root cap (Airyscan fluorescence microscopy).

Supplementary video 7 Dynamic of plastids in lateral cells of root cap of FSD1-GFP *Arabidopsis* in primary root. (Airyscan fluorescence microscopy)

Supplementary video 8 Enhanced FSD1-GFP signal in columella initials of FSD1-GFP *Arabidopsis* lines (Light-sheet microscopy).

Supplementary video 9 Cytoplasmic streaming in pavement cells of cotyledons of FSD1-GFP *Arabidopsis* lines (Airyscan fluorescence microscopy).

Supplementary file 1 Results of prediction putative transcription factors regulation FSD1 expression under the control of MPKs (excel file)

8.2 Supplement II

8.2.1 *In vivo* light-sheet microscopy resolves localisation patterns of FSD1, a superoxide dismutase with function in root development and osmoprotection

Dvořák, P., Krasylenko, Y., Ovečka, M., Basheer, J., Zapletalová, V., Šamaj, J. and Takáč, T. (2021). *In vivo* light-sheet microscopy resolves localisation patterns of FSD1, a superoxide dismutase with function in root development and osmoprotection. *Plant, cell & environment,* 44, 68–87. doi: 10.1111/pce.13894.

Received: 16 April 2020 | Revised: 16 September 2020 | Accepted: 19 September 2020

DOI: 10.1111/pce.13894

ORIGINAL ARTICLE

Plant, Cell & Environment WILEY

In vivo light-sheet microscopy resolves localisation patterns of FSD1, a superoxide dismutase with function in root development and osmoprotection

Petr Dvořák | Yuliya Krasylenko | Miroslav Ovečka | Jasim Basheer | Veronika Zapletalová | Jozef Šamaj | Tomáš Takáč

Department of Cell Biology, Centre of the Region Haná for Biotechnological and Agricultural Research, Faculty of Science, Palacký University Olomouc, Olomouc, Czech Republic

Correspondence
Tomáš Takáč, Department of Cell Biology, Centre of the Region Haná for Biotechnological and Agricultural Research, Faculty of Science, Palacký University, Šlechtitelů 27, 783 71 Olomouc, Czech Republic.
Email: tomas.takac@upol.cz

Funding information
European Regional Development Fund, Grant/Award Number: CZ.02.1.01/0.0/0.0/16_019/0000827; Grantová Agentura České Republiky, Grant/Award Number: 19-00598S

Abstract

Superoxide dismutases (SODs) are enzymes detoxifying superoxide to hydrogen peroxide while temporal developmental expression and subcellular localisation are linked to their functions. Therefore, we aimed here to reveal *in vivo* developmental expression, subcellular, tissue- and organ-specific localisation of iron superoxide dismutase 1 (FSD1) in *Arabidopsis* using light-sheet and Airyscan confocal microscopy. FSD1-GFP temporarily accumulated at the site of endosperm rupture during seed germination. In emerged roots, it showed the highest abundance in cells of the lateral root cap, columella, and endodermis/cortex initials. The largest subcellular pool of FSD1-GFP was localised in the plastid stroma, while it was also located in the nuclei and cytosol. The majority of the nuclear FSD1-GFP is immobile as revealed by fluorescence recovery after photobleaching. We found that *fsd1* knockout mutants exhibit reduced lateral root number and this phenotype was reverted by genetic complementation. Mutant analysis also revealed a requirement for FSD1 in seed germination during salt stress. Salt stress tolerance was coupled with the accumulation of FSD1-GFP in Hechtian strands and superoxide removal. It is likely that the plastidic pool is required for acquiring oxidative stress tolerance in *Arabidopsis*. This study suggests new developmental and osmoprotective functions of SODs in plants.

KEYWORDS

development, FSD1, osmoprotection, oxidative stress, plasmolysis, root, salt stress, seed germination, superoxide dismutase

1 | INTRODUCTION

Plants, as aerobic organisms, have to deal with the harmful by-products of oxidative metabolism named reactive oxygen species (ROS), physiologically produced in organelles (chloroplasts, mitochondria, peroxisomes, glyoxysomes), cytosol and apoplast. Under abiotic stress conditions, the electron leakage to oxygen leads to ROS overproduction mainly in respiratory and photosynthetic electron transport chains in mitochondria and chloroplasts, respectively (Waszczak, Carmody, & Kangasjärvi, 2018; Wrzaczek, Brosché, & Kangasjärvi, 2013). Salt stress causes rapid ROS production by NADPH oxidases (Hao et al., 2014; Leshem, Seri, & Levine, 2007). This plasma membrane-localised enzyme is also responsible for oxidative burst in the course of PAMP (pathogen associated molecular pattern)-triggered plant immunity (Miller et al., 2009).

Moreover, ROS play regulatory and signalling roles during plant development (Mhamdi & van Breusegem, 2018; Mittler, 2017; Orman-Ligeza et al., 2016). Thus, ROS can participate in the regulation of cell cycle (Fehér, Ötvös, Pasternak, & Szandtner, 2008), cell elongation (Liszkay, Kenk, & Schopfer, 2003), embryogenesis (Rodríguez-

Serrano et al., 2012), seed germination (El-Maarouf-Bouteau & Bailly, 2008; Oracz et al., 2009; Schopfer, Plachy, & Frahry, 2001), root hair formation (Foreman et al., 2003), root elongation (Schopfer, Liszkay, Bechtold, Frahry, & Wagner, 2002), lateral and adventitious roots formation (Orman-Ligeza et al., 2016; Pasternak, Potters, Caubergs, & Jansen, 2005) as well as gravitropism (Joo et al., 2005; Joo, Bae, & Lee, 2001). Seed germination might require ROS accumulation (superoxide ($O_2^{\cdot-}$) and hydroxyl radical ($OH^{\cdot}$)), generated in mitochondrial respiratory chain, and in apoplast by peroxidases and likely NADPH oxidase (El-Maarouf-Bouteau & Bailly, 2008). Furthermore, radicle protrusion is accompanied with endosperm weakening, a process linked to ROS-induced cell wall remodelling (Müller et al., 2009). NADPH-oxidase-produced ROS are involved in lateral root formation by promoting cell wall remodelling of overlying parental root tissues (Orman-Ligeza et al., 2016). To regulate ROS levels, plants have developed adaptations and scavenging machineries (Foyer & Noctor, 2005; Noctor, Reichheld, & Foyer, 2018). Due to compartmentalized ROS production, the antioxidant system is present in different cellular compartments. However, the importance of developmental regulations, tissue-specific expression patterns, and subcellular localisations of antioxidant compounds are frequently underestimated in the current literature.

The key antioxidant players, which catalyse the dismutation of $O_2^{\cdot-}$ into hydrogen peroxide (H_2O_2), are superoxide dismutases (EC 1.15.1.1; SODs), metalloenzymes utilizing metal cofactors such as nickel (NiSOD; not present in higher plants), manganese (MnSOD), iron (FeSOD) and zinc-copper (Cu/ZnSOD;Sheng et al., 2014). The *Arabidopsis* genome encodes three Cu/ZnSODs (CSD1, CSD2, CSD3), one MnSOD (MSD1) and three FeSOD (FSD1, FSD2, FSD3) isoforms (Kliebenstein, Monde, & Last, 1998; Pilon, Ravet, & Tapken, 2011).

The subcellular localisation of individual SODs is linked to the detoxification requirements. MSD1 is responsible for scavenging of the $O_2^{\cdot-}$ generated in mitochondria (Kliebenstein et al., 1998). FSD2 and CSD2 are reported to be attached to the thylakoid membrane of chloroplasts (Myouga et al., 2008; Ogawa, Kanematsu, Takabe, & Asada, 1995), while FSD3 is colocalised with the chloroplast nucleoids and protects them against $O_2^{\cdot-}$ through the formation of a heterodimeric protein complex with FSD2 (Myouga et al., 2008). In turn, cytosolic localisation is reported for two isoforms: CSD1 and FSD1 (Kliebenstein et al., 1998; Myouga et al., 2008). Moreover, GFP-fusions suggest that FSD1 can localise to chloroplasts as well and deletion of the 11 amino-terminal nucleotides of FSD1 cDNA sequence restricted this protein to the cytosol (Kuo et al., 2013). However, the above mentioned studies relied on expression in either heterologous systems or protoplast cultures and there are currently no data on FSD1 *in vivo* localisation *in planta*.

The absence or downregulation of some SODs cause phenotypic changes, suggesting their important roles in plant development. Knock-out *fsd2* and *fsd3* mutants display chlorotic phenotypes, abnormal chloroplast morphology and growth inhibition (Myouga et al., 2008). On the other hand, *fsd1* mutant does not show obvious phenotypes in green tissues or altered ROS levels in leaves when transferred into the dark for 2 days (Myouga et al., 2008). Nevertheless, overproduction of *Arabidopsis* FSD1 in *Zea mays* and *Nicotiana tabacum* caused increased tolerance against oxidative stress (Van Breusegem et al., 1999; Van Camp, Capiau, Van Montagu, Inzé, & Slooten, 1996). So far, root phenotypes of *fsd1* mutants have not been comprehensively studied. FSD1 protein shows high level of similarity with FSDs of agriculturally important crops such as *Brassica napus* (93% identity in amino acid sequence), *Solanum lycopersicum* (75%) or *S. tuberosum* (74%), which is higher compared to *Arabidopsis* FSD2 (61%) and FSD3 (56%).

The major factor affecting *FSD1* expression is the availability of copper in the culture medium, while Cu^{2+} homeostasis is mainly regulated by the transcription factor SQUAMOSA promoter binding protein-like 7 (SPL7; Yamasaki, Hayashi, Fukazawa, Kobayashi, & Shikanai, 2009). Upon copper deficiency, SPL7 directly binds GTAC motifs in *FSD1* promoter, thus modulating *FSD1* expression. SPL7 also mediates the downregulation of CSDs mRNA levels by miR398 (Yamasaki et al., 2009). This observation suggests that CSDs activity is replaced by FSD1 under copper deficiency, while under low iron availability the opposite trend was found (Waters, McInturf, & Stein, 2012). The expression of *SPL7* and *FSD1* genes is regulated by circadian and diurnal rhythms (Perea-García et al., 2016). Furthermore, FSD1 activity is mediated by direct interaction with chloroplast chaperonin 20 (CNP20; Kuo et al., 2013) and also by mitogen-activated protein kinases (Takáč et al., 2014).

In the present study, we aimed to gain new insights into the developmental expression and subcellular localisation of FSD1 in *Arabidopsis* using advanced microscopy. We found that *FSD1* expression is developmentally regulated in living plants and at the subcellular level FSD1 localises to the plastids, nuclei, and cytosol. Importantly, FSD1 accumulated in the Hechtian strands and Hechtian reticulum interconnecting retracted protoplast with the cell wall of plasmolysed cells under salt stress conditions. Furthermore, salt induced-ROS production correlated with the FSD1 localisation in roots and was enhanced in *fsd1* mutant plants. Generally, our results provide new evidence for the specific localisation and osmoprotective role for FSD1 in *Arabidopsis*.

2 | MATERIALS AND METHODS

2.1 | Plant material and phenotyping

Arabidopsis seeds were surface sterilized by ethanol and placed on a 1/2 Murashige and Skoog (MS) medium solidified with 0.5% (w/v) gellan gum and stratified at 4°C for 1–2 days, to synchronize germination. For the preparation of 1/2 MS medium with different copper content, final $CuSO_4 \cdot 5H_2O$ concentrations were modified to 0 and 0.5 μM. Seedlings were grown vertically at 21°C, 16/8 hr (light/dark) photoperiod with an illumination intensity of 150 μmol m^{-2} s^{-1} in a phytochamber (Weiss Technik) for 1–15 days prior to imaging. For the preparation of etiolated plants, Petri plates were covered with aluminium foil.

Arabidopsis T-DNA knockout lines were obtained from the European Arabidopsis Stock Centre (http://arabidopsis.info/BasicForm). Two independent mutant lines *fsd1-1* (SALK_029455)

and *fsd1-2* (GABI_740E11) were used, while the T-DNA insertion was confirmed by specific primers designed in the SIGnAL iSect tool (http://signal.salk.edu/tdnaprimers.2.html). Genomic DNA was isolated according to the manufacturer's instructions of the Phire Plant Direct PCR Kit (Thermo Fisher Scientific) and homozygous lines of mutants were confirmed by PCR (primers for genotyping are listed in Table S1).

For the detailed root phenotyping, seedlings were recorded daily and documented using a scanner (ImageScanner III, GE Healthcare, UK) and ZOOM stereo microscope (Axio Zoom.V16; Carl Zeiss, Germany) for 2 weeks. The primary root lengths of 7- and 10-day-old seedlings were measured from the individual scans in ImageJ (http://rsbweb.nih.gov/ij/). Lateral root number was counted on the 7th and 10th day after germination (DAG) and was standardized to the primary root length. The fresh weight of 14-day-old seedlings was measured. Phenotypic measurements were performed in three biological replicates (total examined seedlings 90) and the statistical significance was evaluated by one-way ANOVA test.

2.2 | Preparation of constructs and transgenic lines

Both C- and N-terminal fusion constructs of eGFP (eGFP hereafter designated as GFP) with genomic DNA of *FSD1* (*pFSD1-FSD1::GFP:3′UTR-FSD1* (GFP-FSD1) and *pFSD1::GFP:FSD1-3′UTR-FSD1* (FSD1-GFP)) were cloned under its native promoter from *Arabidopsis* wild type (WT) ecotype Columbia (Col-0). The sequence of the native promoter was taken 1,270 bp upstream of the start codon and for 3′UTR 1,070 bp downstream of the stop codon. MultiSite Gateway Three-Fragment Vector Construction kit (Thermo Fisher Scientific) was used as the cloning method for the preparation of these constructs. Amplified sequences of the promoter, genomic DNA and 3′UTR (primers are listed in Table S1) were recombined into pDONRP4-P1R and pDONRP2R-P3 donor vectors, where plasmids pEN-L1-F-L2 with and without stop-codon were used as B fragment for the subsequent three-fragment vectors LR recombination into the destination vector pB7m34GW. Sequencing-validated cloning products were transformed into *Agrobacterium tumefaciens* GW3101, and used further for floral dip stable transformation of *fsd1-1* and *fsd1-2* mutants. Several transgenic lines possessing intense fluorescent signals have been selected from the T1 generation. Selected lines with one insertion were propagated into T3 homozygous generation and used in further experiments.

Apart from the above mentioned lines, a stably transformed *A. thaliana* transgenic line carrying *35S::sGFP* construct cloned using pMAT037 plasmid (Mano, Hayashi, & Nishimura, 1999; Matsuoka & Nakamura, 1991) was used as a positive control for GFP detection in immunoblotting, microscopic and FRAP analyses.

2.3 | Immunoblotting and SOD activity assay

Immunoblotting of FSD1 abundance was carried out as described in Takáč, Šamajová, Pechan, Luptovčiak, and Šamaj (2017) by anti-FSD primary antibody (Agrisera, Sweden, cat. n. AS06 125; dilution 1:3000 in TBS-T with 3% (w/v) low-fat dry milk) or anti-GFP (Sigma-Aldrich, Germany, dilution 1:1000 in TBS-T with 3% BSA) primary antibody. SOD isoenzymatic activities were performed according to Takáč et al. (2014). Both analyses were performed in three biological replicates and the statistical significance was evaluated using one-way ANOVA test.

2.4 | Quantitative analysis of transcript levels by quantitative real-time PCR

Isolation of total RNA from 14-day-old *Arabidopsis* seedlings (Col-0, *fsd1-1*, *fsd1-2*, FSD1-GFP and GFP-FSD1 transgenic lines in *fsd1-1* background) and subsequent quantitative real-time PCR (qRT-PCR) were performed according to Smékalová et al. (2014). Experiments were run in three biological and three technical replicates. The expression data were normalized to the expression of *ELONGATION FACTOR 1-ALPHA* used as a reference gene (primers are listed in Table S1). Statistical significance was tested by one-way ANOVA test.

2.5 | Whole mount immunofluorescence labelling

Arabidopsis Col-0 grown on 1/2 MS medium were used at third DAG for immunofluorescence labelling of the root tips according to the protocol established by Šamajová, Komis, and Šamaj (2014) with minor modifications. Samples were incubated with anti-FSD (Agrisera) primary antibody diluted at 1:250, in phosphate-buffered saline (PBS) containing 3% (w/v) BSA at 4°C overnight. In the next step, samples were incubated with Alexa-Fluor 488 conjugated goat anti-rabbit secondary antibody diluted at 1:500 in PBS with 3% (w/v) BSA at room temperature for 3 hr. DNA was counterstained with 250 μg/ml 4,6-diamidino-2-phenylindole (DAPI, Sigma-Aldrich) in PBS for 10 min. After a final wash in PBS, the specimens were mounted in an antifade solution (0.5% (w/v) p-phenylenediamine in 90% (v/v) glycerol in PBS or 1 M Tris–HCl, pH 8.0) or in the commercial antifade Vectashield (Vector Laboratories).

2.6 | Salt sensitivity assay and plasmolysis

Germination analysis of Col-0, both *fsd1* mutants and *fsd1-1* complemented lines (GFP-FSD1 and FSD1-GFP) was performed on 1/2 MS medium with and without 150 mM NaCl. Plates with seeds were kept at 4°C for 2 days and incubated as mentioned above. Percentage of germinated seeds (with visible radicle) was counted under stereomicroscope after 24, 48 and 72 hr. Measurements were performed in four repetitions (total examined seeds 120) and statistical significance was tested by one-way ANOVA test.

For salt stress sensitivity determination, 4-day-old seedlings of Col-0, *fsd1* mutants and *fsd1-1* complemented lines (GFP-FSD1 and FSD1-GFP) growing on 1/2 MS medium were transferred to 1/2 MS

medium containing 150 mM NaCl. The ratio of bleached seedlings was counted at the fifth day after transfer. Measurements were performed in four repetitions (total examined seedlings 120) and the statistical significance was evaluated by one-way ANOVA test.

For plasmolysis induction, 4-day-old seedlings of *fsd1-1* complemented lines (FSD1-GFP and GFP-FSD1) and *Arabidopsis* transgenic line expressing *35S::sGFP* were mounted between glass slide and coverslip in liquid 1/2 MS media. Plasmolysis was induced with 500 mM NaCl (hypocotyls) or 250 mM NaCl (roots) in liquid 1/2 MS media applied by perfusion. Plasmolysed cells were observed 5–30 min after the perfusion by confocal laser scanning microscope LSM 880 equipped with an Airyscan detector (Carl Zeiss, Germany) and a spinning disk microscope (Cell Observer, SD, Carl Zeiss).

2.7 | Analysis of oxidative stress tolerance

To determine the sensitivity of examined lines to oxidative stress, 4-day-old seedlings of Col-0, *fsd1* mutants and *fsd1-1* complemented lines (GFP-FSD1 and FSD1-GFP) growing on 1/2 MS medium were transferred to 1/2 MS medium containing 2 μM methyl viologen (MV). The ratio of seedlings with fully green cotyledons was counted at the fifth day after the transfer. Measurements were performed in four repetitions (total examined seedlings 160) and the statistical significance was evaluated by one-way ANOVA test.

The relative amount of chlorophyll *a* and *b* was measured from 30 seedlings of each line according to Barnes, Balaguer, Manrique, Elvira, and Davison (1992). The measurement correlated to the fresh weight of examined seedlings was performed in three repetitions (total examined seedlings 90) and the statistical significance was evaluated by one-way ANOVA test.

2.8 | Fluorescent detection of ROS

ROS in plasmolysed roots were visualised by incubation in 30 μM CellROX Deep Red Reagent (Thermo Fisher Scientific), diluted in 1/2 MS with or without 250 mM NaCl for 15 min in darkness. The emitted signal (excited at 633 nm) was recorded at 652-713 nm using confocal laser scanning microscope LSM 710 (Carl Zeiss). The signal was quantified using ImageJ software. Images were transformed into 8-bit grayscale format and the mean density of the signal was quantified in 6 cells in each of 3 plants per line.

2.9 | Confocal laser scanning microscopy

Three and 8-day-old seedlings of *fsd1-1* mutants carrying recombinant GFP-fused FSD1 were used for microscopy. Imaging of living or fixed samples was performed using a confocal laser scanning microscope LSM710 (Carl Zeiss), LSM880 equipped with an Airyscan (Carl Zeiss) and a spinning disk microscope (Cell Observer, SD, Carl Zeiss). Image acquisition was done with 20× (0.8 NA) dry Plan-Apochromat, 40× (1.4 NA) and 63× (1.4 NA) Plan-Apochromat oil-immersion objectives. Samples were imaged with a 488 nm excitation laser using emission filters BP420-480 + BP495-550 for GFP detection and BP 420–480 + LP 605 for chlorophyll *a* detection. Laser excitation intensity did not exceed 2% of the available laser intensity range. Immunolabelled samples were imaged using the excitation laser line 488 nm and emission spectrum 493–630 nm for Alexa-Fluor 488 fluorescence detection, and excitation laser line 405 nm and emission spectrum 410–495 nm for DAPI. Living 1- and 4-day-old seedlings were stained with 4 μM FM4-64 (Invitrogen) diluted in 1/2 liquid MS medium for 10 min before imaging. Following washing with liquid 1/2 MS medium, samples were observed with excitation laser line 561 nm. Images were processed as single plane maximum intensity projections of Z-stacks in Zen Blue 2012 software (Carl Zeiss), assembled and finalized in Microsoft PowerPoint to final figures.

2.10 | Fluorescence recovery after photobleaching (FRAP)

FRAP analysis of FSD1-GFP (in *fsd1-1* background) and GFP alone in *Arabidopsis* transgenic line expressing *35S::sGFP* was performed in nuclei (selected as regions of interest, ROI) of hypocotyl epidermal cells using confocal laser scanning microscope LSM710 (Carl Zeiss). Argon laser line of 488 nm at 2% laser intensity was used for pre-bleach scans, which was followed by scanning at 100% laser intensity for photobleaching of GPF. Selected regions were scanned each 5 s in total 4 min, where first three scans were pre-bleach scans (0–10 s). Each time point was scanned with 112.5 × 62.5 μm image size and with scaling of 0.21 μm pixel size. Speed of the scanning was 2.41 μs pixel dwell and 3.69 s scan time with 4 time averaging at depth of 16 bit for pre-bleach and post-bleach scanning, and scanning speed of 11.91 μs pixel dwell for bleaching. Quantitative analysis of FRAP experiments was done in ZEN 2011 software (black edition; Carl Zeiss). Briefly, regions of interest for bleaching, reference and background were selected and these areas were scanned. Bleaching was done with full laser power (100%). To keep physiological conditions for examined cells, bleaching was stopped after reaching of 40–45% of the original pre-bleached fluorescence signal intensity. Values of fluorescence intensity were measured in arbitrary units using ZEN 2011 software and they were used for calculations of corresponding half-time of signal recovery and mobile-to-immobile fraction ratios directly in ZEN 2011 software. Data from in total 49 regions of interest were exported to the Microsoft Excel software and normalized to absolute fluorescence intensities, where the highest intensity (before bleaching) was 1 and the lowest intensity (immediately after bleaching) was 0. FRAP measurement was performed in three biological replicates (5 seedlings per one repetition).

2.11 | Light-sheet fluorescence microscopy

Seeds of *fsd1-1* mutant expressing *FSD1-GFP* were surface-sterilized and placed on 1/2 MS medium solidified with 0.5% (w/v) gellan gum and stratified at 4°C for 1–2 days. Subsequently, seeds were transferred

to horizontally-oriented plates with the same culture medium and a height of at least 15 mm. Horizontal cultivation allowed seeds to germinate and roots to grow inside of a solidified medium. Seedlings were inserted into fluorinated ethylene propylene (FEP) tubes with an inner diameter of 2.8 mm and wall thickness of 0.2 mm (Wolf-Technik, Germany), in which roots grew in the block of the culture medium inside the FEP tube, while the upper green part of the seedling developed in an open space of the FEP tube with access to the air (Ovečka et al., 2015). The FEP tube with seedling was inserted into a sample holder and placed into the observation chamber of the light-sheet Z.1 fluorescence microscope (Carl Zeiss). Before insertion of the sample into the microscope, plants were ejected slightly out of the FEP tube allowing for imaging of the root in the block of the solidified culture medium, but without the FEP tube. The sample chamber of the microscope was filled with sterile 1/2 MS medium and tempered to 21°C using the peltier heating/cooling system. Developmental live cell imaging was done with dual-side light-sheet illumination using two LSFM 10×/0.2 NA illumination objectives (Carl Zeiss) with excitation laser line 488 nm, beam splitter LP 560 and with emission filter BP505-545. Image acquisition was done with a W Plan-Apochromat 20×/1.0 NA objective (Carl Zeiss) and images were recorded with the PCO. Edge sCMOS camera (PCO AG, Germany) with an exposure time of 100 ms and imaging frequency of every 2 min in the Z-stack mode for 2–20 hr.

3 | RESULTS

3.1 | FSD1 is developmentally regulated in the early post-germination phase of plant growth

According to the public expression data deposited in the Genevestigator database (presented also in Pilon et al., 2011), *FSD1* is developmentally regulated and is abundantly expressed at early developmental stages. Analysis of FSD1 abundance and activity during *Arabidopsis* early seedling growth revealed that both parameters gradually increased from the 3rd to 13th DAG, but significantly decreased in following days (Figure 1a-d). Note, that the band corresponding to FSD activity on native PAGE gel belongs entirely to FSD1 (Kuo et al., 2013). In order to address the possible phenotypic consequences of FSD1 deficiency at early developmental stages, two independent homozygous T-DNA insertion *fsd1* mutants were analysed (previously characterized by Myouga et al., 2008). It was found that both mutants exhibited reduced lateral root density, while no significant difference was found in the primary root length and seedling fresh weight compared to the WT (Figure 1e-h). In summary, our data suggest, that FSD1 activity and abundance in *Arabidopsis* depends on the growth phase and its deficiency leads to reduced lateral root numbers.

3.2 | Functional complementation of *fsd1* mutants

For the elucidation of FSD1 expression and localisation *in vivo*, we generated stably transformed *fsd1* mutants carrying FSD1 under its own native promoter and fused with GFP to both N- and C-terminus. *FSD1* complementation reverted the lateral root phenotypes of *fsd1* mutants (Figure 2a). In addition, primary root length (Figure 2b), lateral root density (Figure 2c), and seedling fresh weight (Figure 2d) in complemented lines slightly exceeded the respective values in WT plants. Neither FSD1 protein presence, nor enzymatic activity were observed in *fsd1* mutants by biochemical analyses (Figure 2e-h). This confirmed the specificity of the anti-FSD antibody against FSD1 (Figure 2e) as well as that the band corresponding to FSD activity on the native PAGE gel (Figure 2g) is related to FSD1. GFP-tagged FSD1 proteins (FSD1-GFP or GFP-FSD1) were detected in both complemented lines (Figure 2e; Figure S1a). Quantitatively, WT-like level of FSD1 activity and abundance was found in FSD1-GFP complemented plants, as examined by both anti-FSD (Figure 2e, f) and anti-GFP antibodies (Figure S1a, b). On the other hand, strongly reduced (representing 70% and 56% of WT as examined by anti-FSD and anti-GFP antibodies, respectively) protein levels were found in the GFP-FSD1 complemented line (Figure 2e, f; Figure S1a, b). Quantitative PCR analysis showed that *FSD1* transcript levels were similar to WT in GFP-FSD1 line, while three-fold higher mRNA level was found in FSD1-GFP line (Figure S2). Functionality of the FSD1 proteins fused with GFP in both complemented lines was shown by the detection of their activities (Figure 2g, h). Moreover, FSD1 activities and abundances of both GFP-FSD1 and FSD1-GFP were sensitive to copper content in cultivation media, further confirming their functionality (Figure S3a, b).

Inhibition of FSD1 activity by H_2O_2, but not by KCN suggests that the bands on the native PAGE gels correspond to FSD1 proteins fused with GFP (Figure S4). FSD1 activities in the transgenic lines quantitatively correlate with the abundances of the respective fused and native proteins (Figure 2g, h; Figure S4). Interestingly, the band corresponding to GFP-FSD1, migrated in a distinct manner as compared to FSD1-GFP on the native PAGE gel (Figure 2g).

Together, these results suggest that FSD1 is important for the fine-tuning of the lateral root development.

3.3 | Expression pattern of FSD1-GFP during germination and early seedling development

Spatial and temporal patterns of FSD1-GFP expression in the early stages of development were monitored *in vivo* using light-sheet fluorescence microscopy. This allowed the time-lapse monitoring of FSD1-GFP distribution during the whole process of seed germination at nearly environmental conditions (Figure 3; Video S1). Within the first 6 hr of seed germination, still before radicle emergence, we observed an increase of FSD1-GFP signal in the micropylar endosperm with a maximum at the future site of radicle protrusion (Figure 3a-g; Video S1). With the endosperm rupture and emergence of the primary root, FSD1-GFP signal gradually decreased in the micropylar endosperm (Figure 3h-j), while a strong FSD1-GFP signal appeared in the fast-growing primary root (Figure 3k, l; Video S1). Strong expression of FSD1-GFP was visualised in the transition and elongation zones of the primary root (Figure 3l, m; Video S1), which

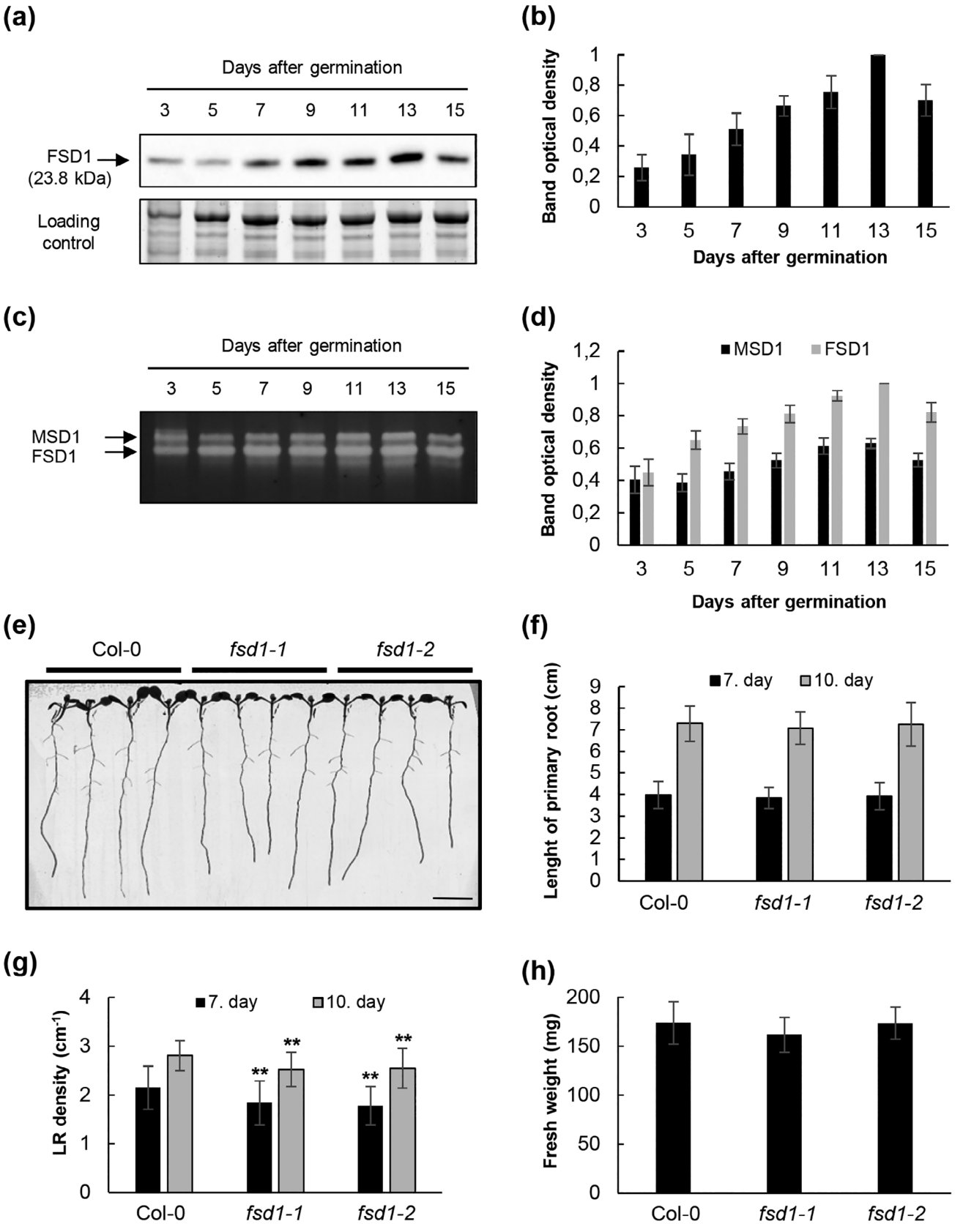

FIGURE 1 Legend on next page.

was, however, gradually decreasing in the differentiation zone, particularly after the emergence of the root hairs in the collar region (Figure 3m-o). During seed germination, FSD1-GFP-labelled plastids in endosperm cells showed a high degree of motility (Video S1). Thus, FSD1 may be involved in the process of endosperm rupture during seed germination. Moreover, FSD1 tissue-specific expression might play a protective role during early root emergence from seeds.

After germination, which occurred during the first DAG, growth of the primary root continued and cotyledons were released from the seed coat during the second DAG (Figure S5a, b). Expression levels of FSD1-GFP in emerging cotyledons were high (Figure S5b). Hypocotyl and fully opened cotyledons in developing seedlings at fifth DAG contained moderate amount of FSD1-GFP, while the strongest signal was detectable in the shoot apex and emerging first true leaves (Figure S5c). FSD1-GFP signal considerably increased in the lateral root primordia (Figure S5d-f). Accumulation of FSD1-GFP was still visible in the apices of the lateral roots as well as in the basal parts, at the connection of the lateral roots to the primary root (Figure S5g). In growing apex of the primary root, the strongest FSD1-GFP signal was located in the transition zone (Figure S5h). The FSD1-GFP signal gradually decreased with acceleration of the cell elongation, differentiation, and root hair formation (Figure S5h; Video S2).

3.4 | Tissue-specific subcellular localisation of GFP-FSD1 and FSD1-GFP in Arabidopsis

In the cells of both above- and underground organs of light-exposed seedlings of *fsd1-1* mutants harbouring *proFSD1::FSD1:GFP* construct, C-terminal FSD1-GFP fusion protein was localised in plastids, nuclei, and cytosol, especially in the cortical cytosolic layer in close proximity to the plasma membrane (Video S3). Such localisation patterns of FSD1-GFP was consistent in cells of all aboveground organs in light-exposed seedlings, such as cotyledon epidermis (mature pavement cells, stomata and their precursors, Figure 4a-c; Video S3), leaf mesophyll cells (Figure 4d-f; Video S4), hypocotyl epidermis (Figure 4g; Video S5), and first true leaf epidermis with branched trichomes (Figure 4h). In epidermal cells, FSD1-GFP-labelled plastids were located around the nucleus and in the cytosolic strains traversing the vacuole (Figure 4a, d). Some other FSD1-GFP-labelled plastids located in a close proximity to nuclei in stomata guard cells and adjacent pavement cells, were less dynamic (Video S3). In mesophyll cells, FSD1-GFP-labelled plastids were temporarily contacted and eventually interconnected by the highly dynamic network of tubules and cisternae of the endoplasmic reticulum (Video S4).

Moreover, FSD1-GFP maintained the same pattern of its localisation in cotyledon epidermal cells of etiolated *Arabidopsis* seedlings, although it was more intensively accumulated in the cortical cytosol just beneath the plasma membrane as compared to the light-exposed plants (Figure S6). In turn, FSD1-GFP was abundant in etioplasts, showing only basal remaining level of chlorophyll *a* autofluorescence (Figure S6b, c).

Plastidic, nuclear and cytosolic localisation of FSD1-GFP was detected also in cells of the root apex (Figure 5a; Video S6). This localisation pattern was visible in cells of the lateral root cap (Figure 5a, b; Video S7), in meristematic cells (Figure 5a, c), epidermal cells of elongation zone (Figure 5d, e) as well as in trichoblasts within the differentiation zone (Figure 5f) of primary root. The selective styryl dye FM4-64 counterstaining of the plasma membrane in root cells helped to reveal tissue-specific FSD1-GFP localisation in the root tip (Figure S7). It showed lower FSD1-GFP signal intensity in central columella cells (Figure 5a; Figure S7).

Furthermore, accumulation of FSD1-GFP was observed in the lateral root primordia emerging from the pericycle (Figure 5k-n). FSD1-GFP signal increased first in cells of forming lateral root primordium still enclosed by tissues of the primary root (Figure 5k; Figure S8a-c). Strong signal of FSD1-GFP was found in cells of the central region, where the apical meristem of the emerging lateral root was established (Figure 5l, m). Considerably high levels of FSD1-GFP also persisted during the release of the lateral root from the primary root tissue (Figure 5n; Figure S8d-f). Established apex of elongating lateral root showed differential pattern of FSD1-GFP expression, with high levels in the endodermis/cortex initials (Figure S8g-i; Video S8), actively dividing cells of the epidermis, cortex and endodermis, and lateral root cap cells (Figure S8g-i). On the other hand, considerably lower levels of FSD1-GFP occurred in cells of the quiescent centre and columella (Figure S8g-i).

The process of root hair formation from trichoblasts was connected with the accumulation of FSD1-GFP in the cortical cytosol of the emerging bulge (Figure 5g). In tip-growing root hairs, FSD1-GFP accumulated in the apical and subapical zone (Figure 5h, i; Video S2). It is noteworthy that after the termination of root hair elongation, FSD1-GFP signal dropped at the tip, while typical strong plastidic signal appeared in the cortical cytosol (Figure 5j).

Subcellular localisation pattern of FSD1 was confirmed by the whole mount immunofluorescence localisation method in fixed

FIGURE 1 Early developmental and phenotypical analysis of iron superoxide dismutase 1 (FSD1). (a) Immunoblotting analysis of FSD1 abundance using anti-FSD antibody during early development of *Arabidopsis* (Col-0) seedlings. (b) Quantification of optical densities of bands in (a). The densities are expressed as relative to the highest value. (c) Visualisation of SOD isoform activities on native polyacrylamide gels during early development of *Arabidopsis* wild type (Col-0) seedlings. (d) Quantification of optical densities of bands in (c). The densities are expressed as relative to the highest value. (e) Representative image of *fsd1-1*, *fsd1-2* mutants and Col-0 seedlings on seventh day after germination. (f-h) Quantification of primary root length (f), lateral root density (g) of indicated 7- and 10-day-old seedlings and fresh weight of 14-day-old seedlings (h). Phenotypic analysis was performed in three repetitions (total examined seedlings 90). Error bars represent standard deviation. Stars indicate statistically significant difference as compared to Col-0 (one-way ANOVA, $^{**}p < .01$). Scale bar: 1 cm

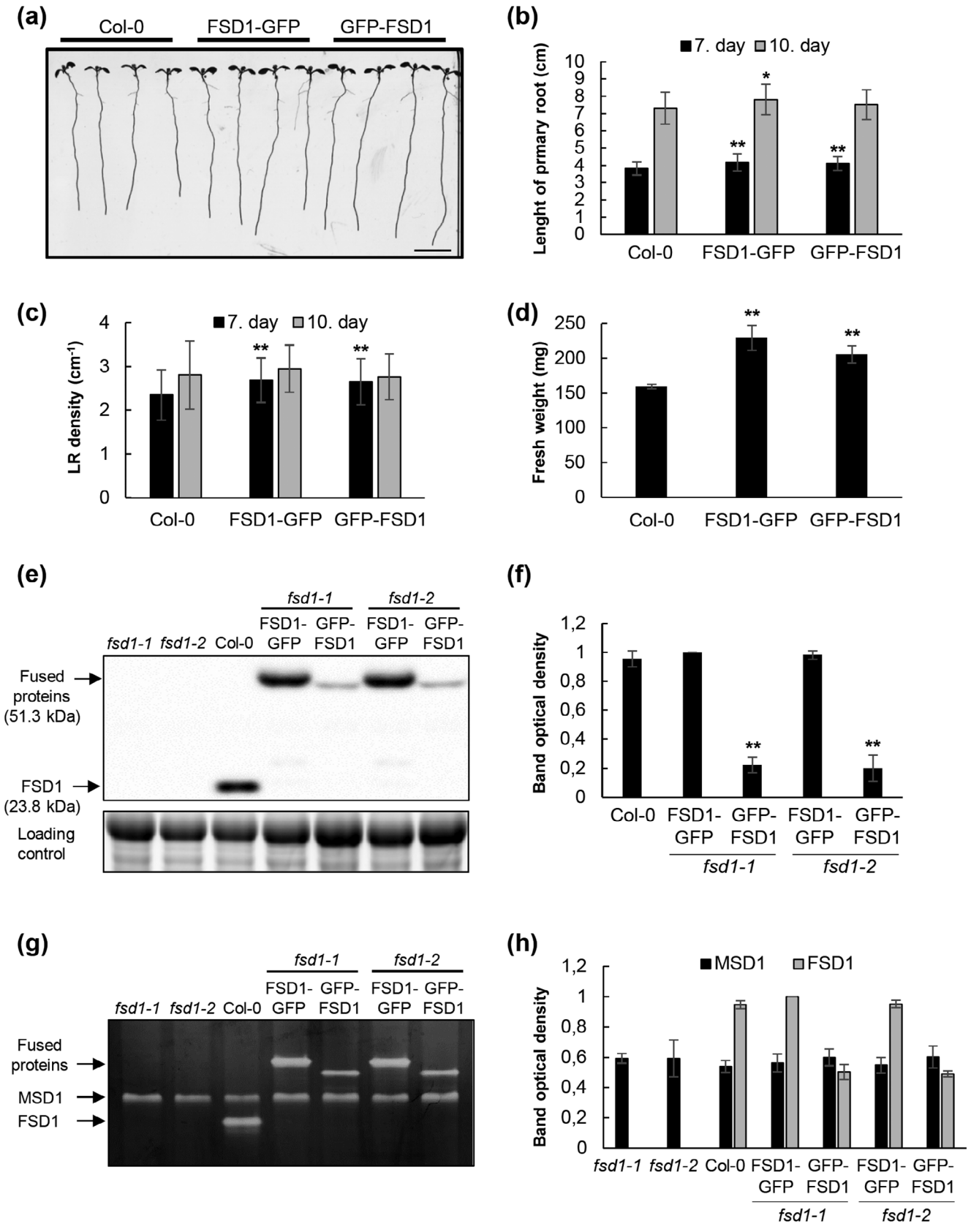

FIGURE 2 Legend on next page.

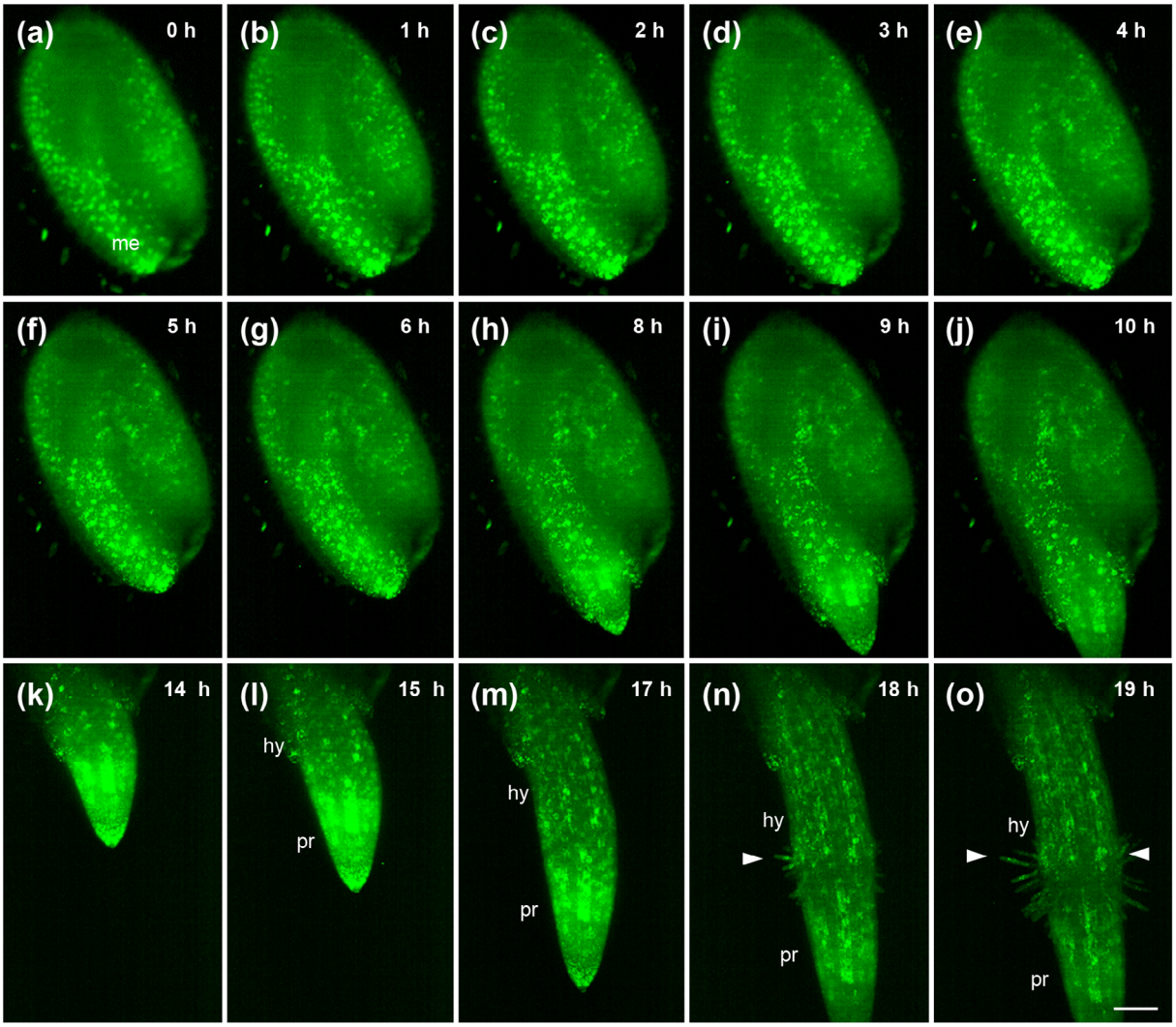

FIGURE 3 Time-lapse monitoring of FSD1-GFP distribution during seed germination obtained using light-sheet fluorescence microscopy. (a-f) Sequential accumulation and relocation of the signal in micropylar endosperm (me) to the site of radicula protrusion. (g, h) endosperm rupture and radicula protrusion. (i-o) Primary root elongation, (n, o) root hair emergence and elongation. Arrowheads point to the site of root hairs in the collar region on the border between the elongating primary root (*pr*) and hypocotyl (*hy*). Scale bar: 100 μm [Colour figure can be viewed at wileyonlinelibrary.com]

samples using anti-FSD antibody. This technique showed prominent strong immunolocalisation of FSD1 to plastids distributed around nuclei and in the cytosol, as well as nuclear and cytosolic localisation in meristematic cells of the primary root (Figure 6a-f).

Presence of FSD1-GFP in both cytosol and nuclei raises the question of its nucleo-cytoplasmic transport. Predicted size of FSD1-GFP fusion protein, which is approximately 51 kDa, would permit passive diffusion in and out of nucleus, as it is below the exclusion limit of the nuclear pores (typically below 60 kDa). To test this, mobility of FSD1-GFP protein fraction in nuclei was analysed using FRAP in comparison to passive diffusion of free GFP (in the *35S::sGFP* line) with the protein size of 27 kDa. In both transgenic lines bearing FSD1-GFP

FIGURE 2 Phenotypic and functional analysis of *fsd1* complemented mutants. (a) Representative image of 7-day-old *Arabidopsis* wild type (Col-0) and *fsd1-1* mutant seedlings carrying FSD1-GFP or GFP-FSD1. (b-d) Quantification of primary root length (b) and lateral root density (c) of indicated 7- and 10-day-old seedlings as well as fresh weight of indicated 14-day-old seedlings (d). Phenotypic analysis was performed in three repetitions (total examined seedlings 90). (e) Immunoblotting analysis of FSD1, FSD1-GFP and GFP-FSD1 abundance in 14-day-old *fsd1* mutants, Col-0 and complemented *fsd1* mutants using anti-FSD antibody. (f) Quantification of band optical densities in (e). (g) Visualisation of activities of SOD isoforms on native polyacrylamide gels in indicated plant lines. (h) Quantification of optical densities of bands in (g). The densities are expressed as relative to the highest value. Error bars represent *standard deviation*. Stars indicate statistically significant difference as compared to Col-0 (one-way ANOVA, $^{*}p < .05$, $^{**}p < .01$,). Scale bar: 1 cm

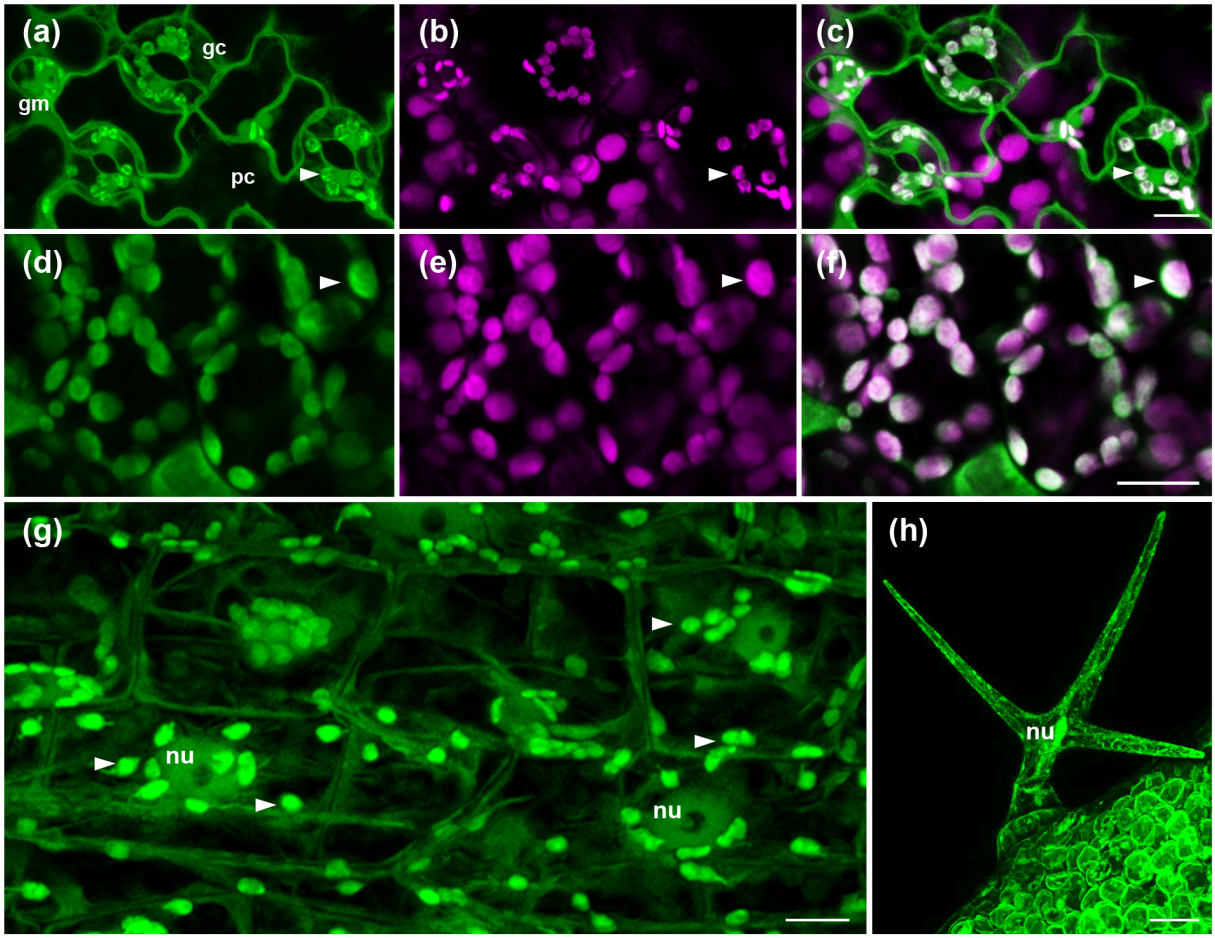

FIGURE 4 FSD1-GFP localisation in cells of *Arabidopsis* aboveground organs revealed by Airyscan confocal laser scanning microscopy. (a-c) Adaxial surface of cotyledons with pavement (*pc*), guard (*gc*) and guard mother (*gm*) cells. (d-f) Leaf mesophyll cells. (g) Epidermal cells of hypocotyls, (h) triple-branched leaf trichome. Indications: (*nu*) nucleus. Arrowheads point on accumulation of FSD1-GFP in plastids. Channels: green—FSD1-GFP; magenta—chlorophyll *a* autofluorescence. Scale bars: a-g, 10 μm; h, 20 μm [Colour figure can be viewed at wileyonlinelibrary.com]

and free GFP, the whole area of selected nuclei was bleached up to 40–45% of original fluorescence intensity and the rate of fluorescent signal recovery was recorded within the period of 4 min (Figure S9a). While in the case of free GFP the signal was largely recovered within the observation period, the recovery of FSD1-GFP in nuclei was much lower (Figure S9a-c). Data analysis showed that only approximately 13–15% of the nuclear FSD1-GFP fraction is mobile, while mobile nuclear fraction of free GFP represented around 80–86% (Figure S9d). In this respect, immobile fraction of FSD1-GFP in nuclei, which cannot pass through nuclear pores by passive diffusion represented more than 85%. Accordingly, in the case of free GFP this immobile fraction represents only 16% (Figure S9d). Interestingly, the halftime of mobile FSD1-GFP fraction recovery was much shorter (9 s, in average) in comparison to the halftime of mobile free GFP fraction recovery, which was 27 s (Figure S9e). These results, corroborated by quantitative analysis of free GFP movement showing typical passive diffusion, suggest that most of the FSD1-GFP nuclear pool is not imported from or exported to the nuclei by passive diffusion, and stays in the nucleus as an immobile fraction.

Interestingly, the N-terminal GFP-FSD1 fusion protein was not targeted to plastids, but it was localised both in the nuclei and cytosol. This localisation pattern was observed in leaf pavement (Video S9) and stomata guard cells (Figure S10a-c), in cotyledon mesophyll cells (Figure S10d-f) as well as in hypocotyl epidermal cells (Figure S10g). The absence of plastidic localisation did not affect the tissue-specific expression pattern of GFP-FSD1 in primary root apex. The strongest signal was located in the epidermis, cortex, endodermis and root cap (Figure S10h). Considerably lower GFP-FSD1 signal was detected in the quiescent center, central columella cells and proliferating tissues of the central cylinder (Figure S10h). Strong accumulation of GFP-FSD1 was typically present in founding cells of the lateral root primordia and adjacent pericycle cells (Figure S10i). Taking into account the strong reduction in FSD1 abundance and activity in transgenic line expressing GFP-FSD1 fusion as compared to FSD1-GFP (Figure 2e-h; Figure S1), the plastidic FSD1 pool may represent around half of the total FSD1 pool in *Arabidopsis* cells.

Plastids were the organelles most strongly accumulating FSD1-GFP and located either around the nuclei or distributed

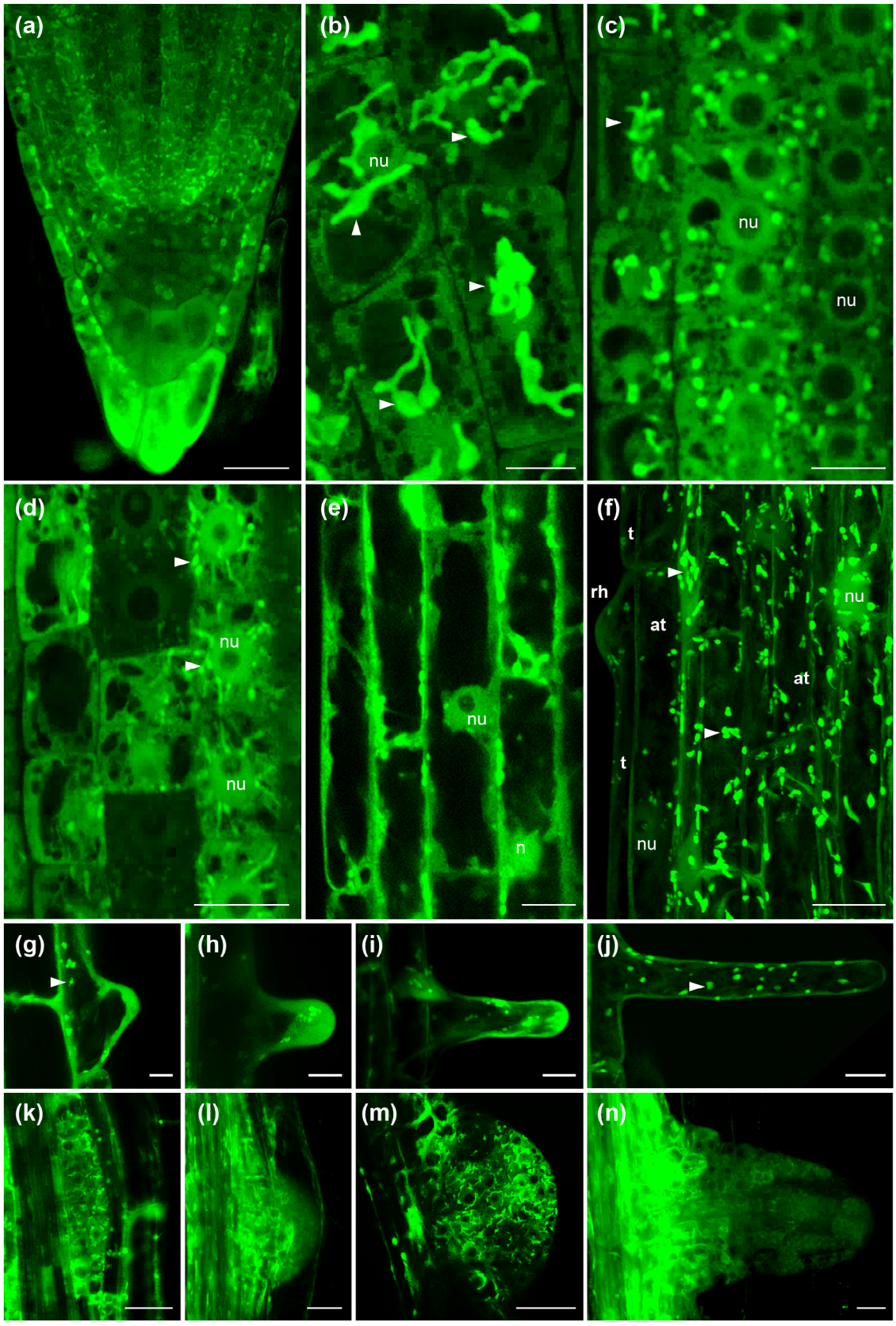

FIGURE 5 Legend on next page.

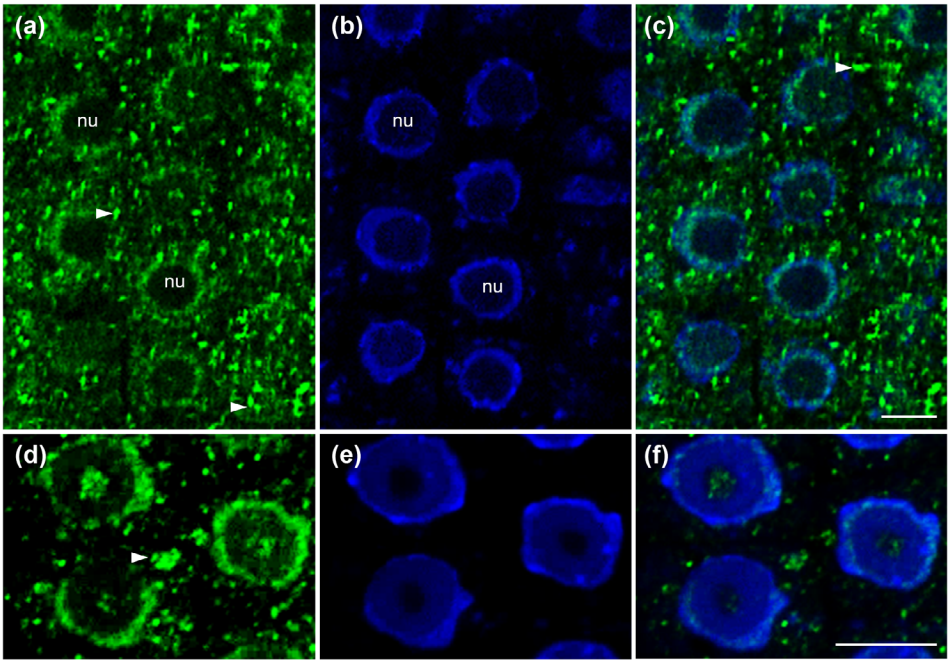

FIGURE 6 Overview of FSD1 immunolocalisation in interphase meristematic cells of *Arabidopsis* (Col-0) primary roots. The images represent maximum intensity projections of 20 optical sections (with thickness of 0.18 μm each) at the mid-plane of root meristem cells with (a-c) or without (d-f) deconvolution in ZEN Blue 2012 software. Green immunolabelling with anti-FSD—Alexa Fluor 488; blue—DAPI staining. Arrowheads indicate plastids. (nu) stands for nuclei. Scale bar: 5 μM [Colour figure can be viewed at wileyonlinelibrary.com]

throughout the cytosol (Figures 4, 5; Figure S6; Video S3). Typically, plastids in cells of different tissues formed polymorphic stromules, which displayed different tissue-specific shape, length, branching (Figures 4, 5) and dynamicity (Videos S3-S7). Thus, in lateral root cap cells highly dynamic FSD1-GFP-labelled plastids persistently formed long stromules, touching each other (Figure 5b; Videos S6, S7), while the plastids in isodiametric meristematic cells possessed less stromules (Figure 5c, d). In hypocotyl epidermal cells with active cytosolic streaming, only some plastids were interconnected by stromules (Video S5). Since stromules are tubular plastid extensions filled with stroma (Köhler & Hanson, 2000), FSD1 might be considered as stromal protein. In contrast to FSD2 and FSD3 (Myouga et al., 2008), FSD1 was not detected in the chloroplast nucleoids.

3.5 | FSD1 contributes to salt stress tolerance in *Arabidopsis*

Protective role of FSD1 during the early stages of post-embryonic plant development was tested in *fsd1* mutants and complemented lines on seed germination under salt stress conditions. Seed germination of *fsd1* mutants was strongly reduced by the presence of 150 mM NaCl in the 1/2 MS medium, while FSD1-GFP lines exhibited germination rates comparable to that of WT (Figure 7a). GFP-FSD1 line showed an insignificantly reduced germination rate on the first day, but germination efficiency was synchronized with WT and FSD1-GFP line from the second day onwards (Figure 7a). The results indicated that *FSD1* expressed under its own native promoter functionally complemented the salt stress-related deficiency of *fsd1* mutants.

To further test the new role of FSD1 in salt stress sensitivity, we characterized the response of developing seedlings to the high salt concentration in the culture medium. We found that both *fsd1* mutants showed hypersensitivity to NaCl and exhibited increased cotyledon bleaching. Both FSD1-GFP and GFP-FSD1 fusion proteins efficiently reverted the salt hypersensitivity of *fsd1* mutants (Figure 7b; Figure S11). These results supported the new functional role of FSD1 in *Arabidopsis* salt stress tolerance.

To gain deeper insight into FSD1 function during plant response to the salt stress, we performed subcellular localisation of FSD1-GFP in hypocotyl epidermal cells plasmolysed by 500 mM NaCl (Figure 7c-i; Figure S12a-e). In addition to plastidic, nuclear, and cytosolic localisation in untreated cells (Figure 7c), FSD1-GFP was detected in Hechtian strands and Hechtian reticulum, interconnecting retracted protoplast with the cell wall of plasmolysed cells (Figure 7d-i; Figure S13a, b). Hechtian reticulum located in close proximity to the cell wall (Figure 7f), and thin attachments of Hechtian strands to the cell wall in the form of bright adhesion spots were enriched with

FIGURE 5 Tissue- and organ-specific subcellular FSD1-GFP localisation in *Arabidopsis* roots revealed by Airyscan confocal laser scanning microscopy. (a) Primary root apex, (b) root cap cells with GFP-signal in plastids (arrowheads) and nuclei (nu). (c) Epidermal and cortical meristem cells, (d) cortical cells of distal elongation zone, (e) cortical cells of elongation zone. (f) Trichoblasts (t) with an emerging root hair (rh) and atrichoblasts (at) of differentiation zone. (g-j) Mid-plane sections of root hairs, (g) root hair bulge, (h, i) elongating root hair, (j) mature root hair. (k-m) Mid-plane sections of forming lateral root primordia at diverse developmental stages. (n) Emerged lateral root. Scale bars: a, e, f, k-n, 20 μm; b, c, d, g-j, 10 μm [Colour figure can be viewed at wileyonlinelibrary.com]

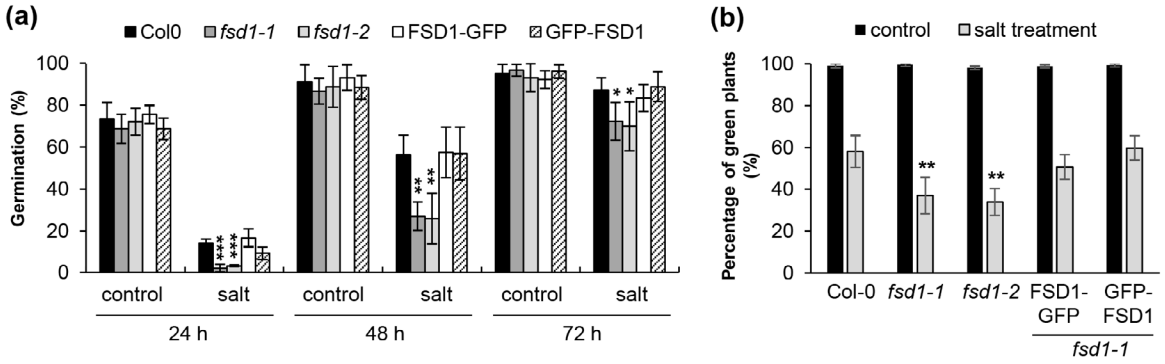

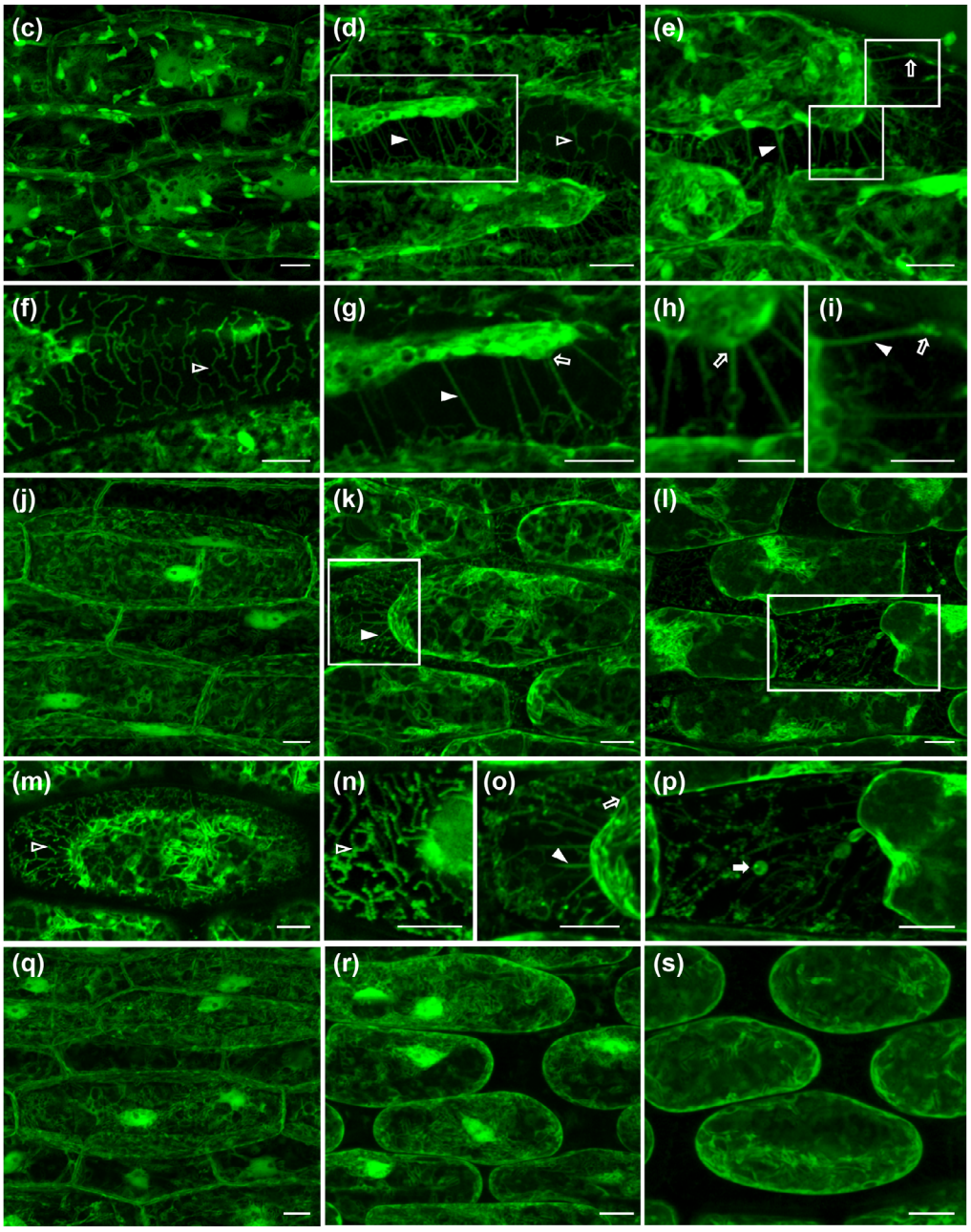

FIGURE 7 Legend on next page.

FSD1-GFP (Figure 7e, g-i; Figure S12). Plasmolysed cells showed strong GFP signal at plasma membrane and also contained vesicle-like structures decorated by FSD1-GFP, in their cytosol (Figure S12d) and also within the Hechtian strands (Figure 7h, i). We observed a similar localisation pattern in the GFP-FSD1 line. GFP-FSD1 was located in the nuclei and cytosol of untreated cells (Figure 7j), while prominent GFP-FSD1 accumulation was observed at the plasma membrane of retracted protoplasts, in Hechtian strands and Hechtian reticulum after plasmolysis (Figure 7k-p). Peripheral Hechtian reticulum and strands were decorated by spot- and vesicle-like structures labelled with GFP-FSD1 (Figure 7l, p). In contrast, free GFP stably expressed in *Arabidopsis* under *35S* promoter did not show localisation in the Hechtian strands and Hechtian reticulum (Figure 7q-s; Figure S12f-j; Figure S13c, d) and prominent accumulation close to the plasma membrane during salt stress (Figure 7r, s; Figure S12i, j).

Next, we used a fluorescent ROS indicator CellROX Deep Red Reagent, which is preferentially specific to $O_2^{\cdot-}$ and $OH^{\cdot}$ (Alves et al., 2015), to study ROS accumulation in plasmolysed cells. Intense ROS production was detected at the plasma membrane, cytosol, plastids and vesicle-like structures of retracted protoplasts (Figure 8a, d, h, l, p), as well as in Hechtian strands and Hechtian reticulum (Figure 8d, h). We have found that the CellROX Deep Red Reagent fluorescence signal partially colocalised with GFP-FSD1 at the plasma membrane vicinity, Hechtian strands and plastids (Figure 8a-f; Figure S13a, b) after salt-induced plasmolysis in root. We also examined, whether *FSD1* deficiency affects the ROS level in *fsd1* mutants upon salt stress. Considerably stronger CellROX Deep Red Reagent fluorescence signal was revealed in both *fsd1* mutants as compared to the WT (Figure 8g-t). Collectively, these data indicate that salt stress-induced ROS production and accumulation in Hechtian strands and Hechtian reticulum likely depends on *FSD1* expression.

3.6 | Plastidic FSD1 pool is important for oxidative stress tolerance in Arabidopsis

In order to reveal the role of FSD1 in scavenging of ROS generated in the chloroplast, we exposed mutant and transgenic lines to MV. Both mutant lines exhibited a hypersensitivity to this agent as estimated by lowest number of fully green cotyledons (Figure 9a-c). The GFP-FSD1 line was hypersensitive as well, but showed slightly elevated number of seedlings with fully green cotyledons when compared to mutants (Figure 9a-c). On the other hand, FSD1-GFP line showed a response resembling the WT (Figure 9a-c). To better evaluate responses to MV, we measured total chlorophyll content in the cotyledons (Figure 9d). We did not observe any differences in chlorophyll content among the analysed lines in control conditions (data not shown), being consistent with the data reported previously (Myouga et al., 2008). Chlorophyll content in lines treated with MV positively correlated with the hypersensitivity of the examined lines (Figure 9d). These results show that plastidic FSD1 pool is decisive for acquiring oxidative stress tolerance in *Arabidopsis*.

4 | DISCUSSION

FSDs were long believed to be chloroplast proteins involved in $O_2^{\cdot-}$ scavenging during photosynthesis. However, the scavenging capacity of *Arabidopsis FSD1* was challenged, because its transcript levels remained unchanged in response to many environmental conditions (Gallie & Chen, 2019; Kliebenstein et al., 1998; Myouga et al., 2008; Xing, Chen, Jia, & Zhang, 2015). Here, we show for the first time that FSD1 is localised not only in plastids, but simultaneously also in the nuclei and cytosol of *Arabidopsis* cells. Moreover, FSD1 accumulates in Hechtian strands and Hechtian reticulum interconnecting retracted protoplast with the cell wall under salt stress conditions.

4.1 | FSD1 might protect root proliferation activity under adverse environmental conditions

Using translational fusion constructs with native promoter, GFP-tagged FSD1 exhibited a tissue-specific expression pattern in *Arabidopsis* root tip. This indicates that FSD1 may also have developmental roles that are conditionally determined. Hence, FSD1 might be involved in the regulation of the redox status in dividing cells, like root initials. It is known that the root meristematic activity as well as the quiescent centre organisation is maintained by redox homeostasis

FIGURE 7 Response of *fsd1* mutants and complemented mutant lines to salt stress. (a) Seed germination efficiency in control conditions and in response to 150 mM NaCl. Germination is evaluated as a percentage of germinated seeds relative to the total number of examined seeds. Experiment was performed in four biological replicates (total examined seeds 120) (b) Viability of seedlings on fifth day after the transfer to solid medium with and without 150 mM NaCl. Viability was evaluated as a percentage of seedlings with green cotyledons. Experiment was performed in four biological replicates (total examined seedlings 120). Error bars in (a) and (b) represent standard deviations. Stars indicate statistically significant difference as compared to Col-0 (one-way ANOVA, $*p < .05$, $**p < .01$, $***p < .001$). (c-i) FSD1-GFP signal in hypocotyl epidermal cells of plants incubated in liquid 1/2 MS media without (c) or with 500 mM NaCl (d-i) for 30 min. (d, e) Overview images of plasmolysed cells. (f) Hechtian reticulum. (g-i) Hechtian strands and their connections to cell wall, close-ups from images (d, e). (j-p) GFP-FSD1 in hypocotyl epidermal cells of plants exposed to liquid 1/2 MS media without (j) or with 500 mM NaCl (k-p) for 30 min. (k, l) Overview images of plasmolysed cells. (m, n) Hechtian reticulum. (o) Close-up from (k), showing Hechtian strands and their connections to cell wall. (p) Close-up from (l), showing disturbed Hechtian reticulum with aggregations. (q-s) GFP fluorescence in hypocotyl epidermal cells of *Arabidopsis* transgenic line expressing *35S::sGFP* exposed to liquid 1/2 MS media without (q) or with 500 mM NaCl for 30 min (r, s). Filled arrowheads indicate Hechtian strands; blank arrowheads - Hechtian reticulum; filled arrows—globular aggregations; blank arrows—connections of Hechtian strands to cell wall. Scale bars: c-g, j-s, 10 μm; h, i, 5 μm [Colour figure can be viewed at wileyonlinelibrary.com]

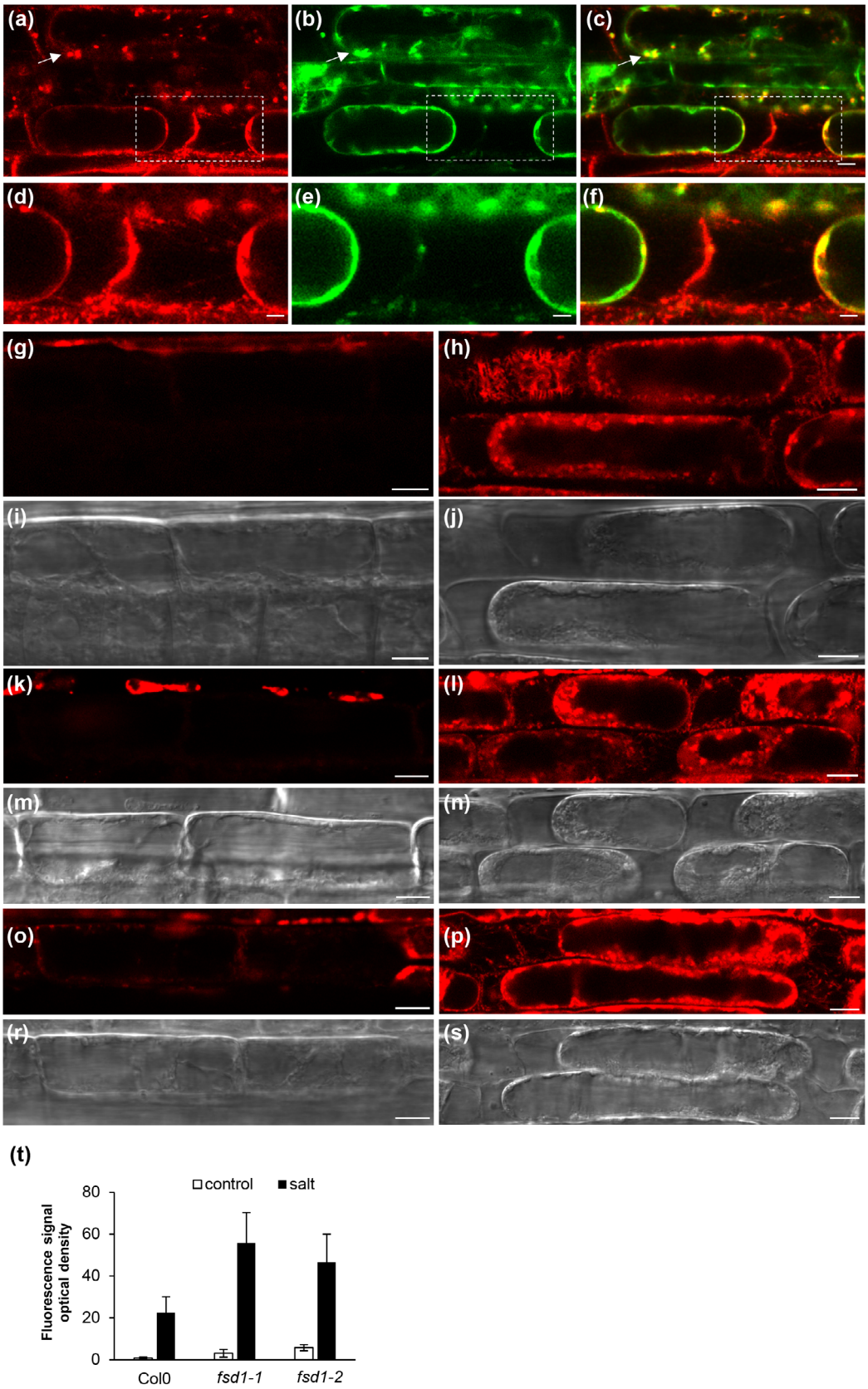

FIGURE 8 Legend on next page.

which acts downstream of the auxin transport (Barlow, 2016; Gallie & Chen, 2019; Horváth et al., 2019; Jiang, 2003). Intriguingly, FSD1 tissue-dependent expression pattern largely correlates with auxin maxima in the root tip (Hayashi et al., 2014; Petersson et al., 2009), as well as with $O_2^{\cdot-}$ maxima (Dunand, Crèvecoeur, & Penel, 2007). Furthermore, endodermis formation requires *SCARECROW (SCR)* and *SHORTROOT (SHR)*, two GRAS-type transcription factors, expressed in the endodermis/cortex initials and quiescent centre (Carlsbecker et al., 2010; Helariutta et al., 2000). FSD1 might also contribute to the regulation of SCR and SHR, which is supported by the high expression of *FSD1* in fluorescence-activated cell sorting (FACS)-isolated protoplasts expressing endoplasmic reticulum-targeted GFP under the control of the SCARECROW promoter (Geng et al., 2013). This expression was elevated in salt-stressed protoplasts. Considering our results about the role of FSD1 in salt stress tolerance, FSD1 may be involved in the maintenance of redox homeostasis in the endodermis/cortex initials of the root tip.

According to our study, FSD1 is required for proper establishment of lateral roots in *Arabidopsis*. Considering that both N- and C-terminal GFP fusions with FSD1 complemented defective lateral root formation in *fsd1* mutants, one can assume that these fusion proteins are functional and sufficient for full acquisition of lateral root formation capacity in *Arabidopsis*, but further investigation is necessary to verify this hypothesis. Lateral root formation is dependent on complementary action of multiple regulatory systems governed by auxin (Banda et al., 2019). RBOH-generated ROS are major modulators of this process via cell wall remodelling of overlying parental root tissues (Orman-Ligeza et al., 2016). RBOH activity is controlled by multiple factors including phosphorylation, Ca^{2+}, phosphatidic acid and protein–protein interactions (Ogasawara et al., 2008; Zhang et al., 2009), while ROS accumulation must be controlled in order to ensure proper lateral root formation. As a proof of this concept, we provided experimental evidence showing strong accumulation of FSD1 in lateral root primordia, and reduced lateral root number in *fsd1* mutants. Hence, FSD1 appears as an enzyme participating in maintenance of proper redox homeostasis during lateral root formation.

4.2 | Arabidopsis response to the salt and oxidative stresses is controlled by different cellular FSD1 pools

Our localisation data suggest that FSD1 functions are not only restricted to the cytosol and plastids, because we provide here the first evidence on the nuclear localisation of SOD in plants. The nuclear localisation is likely driven by bipartite nuclear localisation signal close to the N-terminus of the FSD1 protein, which was predicted by two independent predictors (Figure S14). It was previously found that mammalian SOD1 is rapidly relocated to the nucleus upon H_2O_2-triggered oxidative stress (Volkening, Leystra-Lantz, Yang, Jaffee, & Strong, 2009). In this case, SOD1 binds to specific DNA nucleotide sequences and triggers the expression of genes involved in oxidative resistance and DNA repair. It may also bind to and regulate the stability of specific mRNAs (Volkening et al., 2009). SOD1 nuclear functions are unrelated to its catalysing of $O_2^{\cdot-}$ removal (Tsang, Li, Thomas, Zhang, & Zheng, 2014. Nucleotide sequences of *FSD1* as well as structure of FSD1 catalytic and other domains differ considerably from SOD1 (Pilon et al., 2011). Thus, considering also the immobile nature of nuclear FSD1, the nuclear function of FSD1 cannot be easily anticipated, but it certainly deserves further study.

The localisation of FSD1 to chloroplasts is determined by an N-terminal transit peptide identified previously (Kuo et al., 2013). According to comparative studies of three *Arabidopsis* isoforms, FSD1 is crucial neither for chloroplast integrity (Myouga et al., 2008), nor for cell protection under photooxidative stress (Gallie & Chen, 2019). It has 3–10 times higher expression compared to *FSD2* and *FSD3* (Pilon et al., 2011) in *Arabidopsis*, depending on developmental stage, and unlike *FSD2* and *FSD3*, it remains insensitive to MV and high light irradiation (Myouga et al., 2008). Evidence was provided for cooperative roles of FSD2 and FSD3 to ensure defense against high light and MV-generated ROS (Gallie & Chen, 2019; Myouga et al., 2008). We show that plastidic pool of FSD1 is important for *Arabidopsis* tolerance against MV-induced oxidative stress, while cytosolic and nuclear pools are inefficient. It is likely that the protective role of FSD1 depends on the severity of the external conditions and might be triggered under harsh stress conditions. The protective roles of FSD1 were reported in transgenic tobacco and maize, where overexpression of this enzyme in chloroplasts enhanced the efficiency of thylakoid and plasma membrane protection (Van Breusegem et al., 1999; Van Camp et al., 1996).

FSD1 is also important for *Arabidopsis* germination under salt stress and for salt stress tolerance in general. As indicated by the FSD1 localisation and salt stress response in the complemented lines, cytosolic FSD1, FSD1 in the Hechtian strands and Hechtian reticulum (as discussed below) and likely also nuclear FSD1 pool are crucial for the acquisition of tolerance to salinity during germination. Altogether, our results emphasize the importance of FSD1 in the regulation of cytosolic and also possibly nuclear redox homeostasis in response to salinity stress.

FIGURE 8 Colocalisation of FSD1-GFP with reactive oxygen species (ROS) and their accumulation in primary roots of *Arabidopsis fsd1* mutants in response to salt stress. (a-c) ROS distribution visualised by fluorescent tracker CellRox Deep Red reagent in plasmolysed root cells of FSD1-GFP line (a), GFP fluorescence (b) and superposition of a and b (c). Arrow indicates colocalisation in plastid. (d-f) Detailed images of square areas in a-c. (g-s) ROS accumulation in mock treated (g, k, o) and plasmolysed root cells (h, l, p) of Col-0 (g, h), *fsd1-1* mutant (k, l) and *fsd1-2* mutant roots (o,p) visualised by fluorescent tracker CellRox Deep Red reagent. (t) Quantification of CellRox Deep Red reagent fluorescence intensity in images g, h, k, l, o, p. Error bars represent *standard deviation*. (i, j, m, n, r, s) Transmitted light. Scale bars: a-f, 20 μm; g-s, 10 μm [Colour figure can be viewed at wileyonlinelibrary.com]

Salt stress causes rapid generation of ROS by NADPH oxidases (Leshem et al., 2007), while it is accompanied by the internalization of RBOH into cytoplasmic structures (Hao et al., 2014). Such salt-induced ROS accumulation has to be tightly controlled in order to avoid damaging consequences. Our results suggest that FSD1 might be involved in the primary plant defence against $O_2^{\cdot-}$ production in the Hechtian strands and Hechtian reticulum during salt stress.

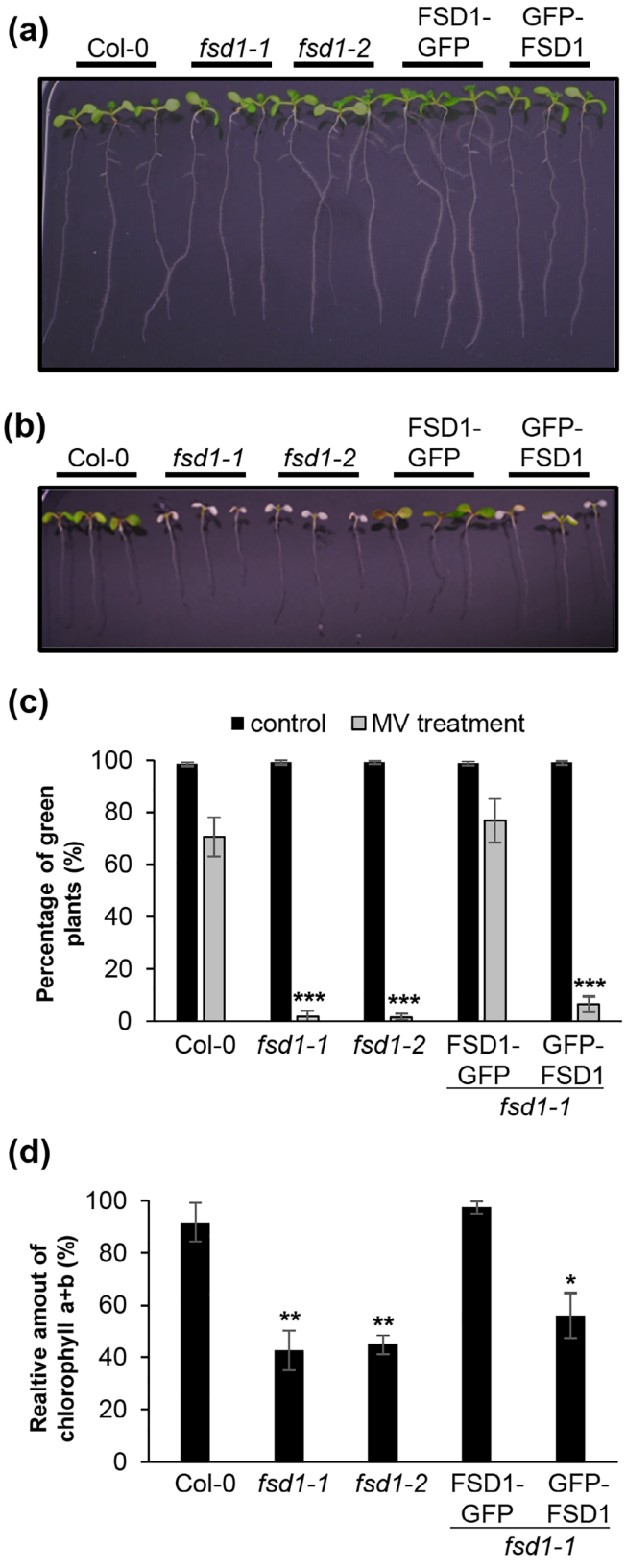

4.3 | FSD1 is likely involved in endosperm rupture during seed germination

Seed germination is a complex process encompassing multiple events governed by tight phytohormonal regulation. Micropylar endosperm represents the last mechanical barrier constraining the radicle emergence. Endosperm rupture is preceded by its weakening, controlled by the inhibitory effect of abscisic acid and promoting effect of ethylene (Linkies et al., 2009). Furthermore, ROS contribute to this process by oxidizing the cell wall polysaccharides and subsequent cell wall loosening (Müller et al., 2009). Here, we provide data showing FSD1 upregulation and local accumulation in the micropylar endosperm during endosperm weakening and rupture, which is subsequently decreased after primary root emergence. Such accumulation of FSD1-GFP at the micropylar endosperm before and during endosperm rupture by emerging radicle indicates that it may be involved in the local catalysis of $O_2^{\cdot-}$ conversion to hydrogen peroxide. This assumption is strengthened by increased $O_2^{\cdot-}$ accumulation in *fsd1* mutants and the FSD1-GFP accumulation in the Hechtian strands and Hechtian reticulum interconnecting retracted protoplast with the cell wall. Indeed, *FSD1* shows unique transcriptional changes during seed germination in comparison to other SOD isoforms (Müller et al., 2009), supporting the specific role of FSD1 during endosperm weakening and rupture. Nevertheless, the precise role of FSD1 in endosperm rupture remains to be elucidated.

In summary, we show developmentally regulated tissue-specific expression pattern, triple subcellular localisation and provide evidence for the new role of FSD1 in the salt stress, which is unique among plant SODs. Its plastidic pool is required for MV-induced oxidative stress in chloroplasts. These new features make FSD1 favourable candidate for potential biotechnological applications.

FIGURE 9 Response of *fsd1* mutants and complemented mutant lines to methyl viologen (MV)-induced chloroplastic oxidative stress. (a-b) Representative pictures of seedlings on fifth day after the transfer to control medium (a) and 2 μM MV-containing medium (b). (c) Quantification of fully green seedlings from total examined number 160 seedlings. Measurement was done in four repetitions. (d) Quantification of relative amount of chlorophylls *a* and *b* in plants treated by 2 μM MV. Measurement was done in three repetitions (one repetition had 30 seedlings of each line). Error bars represent *standard deviation*. Stars indicate statistically significant difference as compared to Col-0 (one-way ANOVA, $*p < .05$, $**p < .01$, $***p < .01$). Scale bar: 1 cm [Colour figure can be viewed at wileyonlinelibrary.com]

ACKNOWLEDGMENTS

We are also thankful to Michael Wrzaczek for critical reading of the manuscript.

This research was funded by Grant No. 19-00598S from the Czech Science Foundation GAČR and by the ERDF project "Plants as a tool for sustainable global development" (No.CZ.02.1.01/0.0/0.0/16_019/0000827).

CONFLICT OF INTEREST

The authors declare that they have no conflict of interest.

AUTHOR CONTRIBUTIONS

Jasim Basheer, Miroslav Ovečka, Petr Dvořák, Tomáš Takáč, Veronika Zapletalová, and Yuliya Krasylenko performed the experiments and analyses. Jozef Šamaj and Tomáš Takáč coordinated the experiments, supervised the project and helped with data assessment. Jozef Šamaj provided the infrastructure and helped with the interpretation of the results. Petr Dvořák, Yuliya Krasylenko and Tomáš Takáč drafted the manuscript which was revised and edited by Miroslav Ovečka and Jozef Šamaj. All authors approved the final version of the manuscript.

ORCID

Petr Dvořák https://orcid.org/0000-0002-2926-7855
Yuliya Krasylenko https://orcid.org/0000-0001-7349-2999
Miroslav Ovečka https://orcid.org/0000-0002-1570-2174
Jasim Basheer https://orcid.org/0000-0001-5557-6152
Veronika Zapletalová https://orcid.org/0000-0002-1484-0778
Jozef Šamaj https://orcid.org/0000-0003-4750-2123
Tomáš Takáč https://orcid.org/0000-0002-1569-1305

REFERENCES

Alves, M. B. R., de Andrade, A. F. C., de Arruda, R. P., Batissaco, L., Rodriguez, S. A. F., Lançoni, R., … Celeghini, E. C. C. (2015). An efficient technique to detect sperm reactive oxygen species: The CellRox deep red® fluorescent probe. *Biochemistry & Physiology: Open Access*, *4*(2), 1–5.

Banda, J., Bellande, K., von Wangenheim, D., Goh, T., Guyomarc'h, S., Laplaze, L., & Bennett, M. J. (2019). Lateral root formation in *Arabidopsis*: A well-ordered LRexit. *Trends in Plant Science*, *24*(9), 826–839.

Barlow, P. W. (2016). Origin of the concept of the quiescent centre of plant roots. *Protoplasma*, *253*(5), 1283–1297.

Barnes, J. D., Balaguer, L., Manrique, E., Elvira, S., & Davison, A. W. (1992). A reappraisal of the use of DMSO for the extraction and determination of chlorophylls *a* and *b* in lichens and higher plants. *Environmental and Experimental Botany*, *32*(2), 83–100.

Carlsbecker, A., Lee, J. Y., Roberts, C. J., Dettmer, J., Lehesranta, S., Zhou, J., … Benfey, P. N. (2010). Cell signalling by microRNA165/6 directs gene dose-dependent root cell fate. *Nature*, *465*(7296), 316–321.

Dunand, C., Crèvecoeur, M., & Penel, C. (2007). Distribution of superoxide and hydrogen peroxide in *Arabidopsis* root and their influence on root development: Possible interaction with peroxidases. *New Phytologist*, *174*(2), 332–341.

El-Maarouf-Bouteau, H., & Bailly, C. (2008). Oxidative signaling in seed germination and dormancy. *Plant Signaling & Behavior*, *3*(3), 175–182.

Fehér, A., Ötvös, K., Pasternak, T. P., & Szandtner, A. P. (2008). The involvement of reactive oxygen species (ROS) in the cell cycle activation (G_0-to-G_1 transition) of plant cells. *Plant Signaling & Behavior*, *3*(10), 823–826.

Foreman, J., Demidchik, V., Bothwell, J. H. F., Mylona, P., Miedema, H., Torres, M. A., … Dolan, L. (2003). Reactive oxygen species produced by NADPH oxidase regulate plant cell growth. *Nature*, *422*(6930), 442–446.

Foyer, C. H., & Noctor, G. (2005). Redox homeostasis and antioxidant signaling: A metabolic interface between stress perception and physiological responses. *The Plant Cell*, *17*(7), 1866–1875.

Gallie, D. R., & Chen, Z. (2019). Chloroplast-localized iron superoxide dismutases FSD2 and FSD3 are functionally distinct in *Arabidopsis*. *PLoS One*, *14*(7), e0220078.

Geng, Y., Wu, R., Wee, C. W., Xie, F., Wei, X., Chan, P. M. Y., … Dinneny, J. R. (2013). A spatio-temporal understanding of growth regulation during the salt stress response in *Arabidopsis*. *The Plant Cell*, *25*(6), 2132–2154.

Hao, H., Fan, L., Chen, T., Li, R., Li, X., He, Q., … Lin, J. (2014). Clathrin and membrane microdomains cooperatively regulate RbohD dynamics and activity in *Arabidopsis*. *The Plant Cell*, *26*(4), 1729–1745.

Hayashi, K., Nakamura, S., Fukunaga, S., Nishimura, T., Jenness, M. K., Murphy, A. S., … Aoyama, T. (2014). Auxin transport sites are visualized in planta using fluorescent auxin analogs. *Proceedings of the National Academy of Sciences*, *111*(31), 11557–11562.

Helariutta, Y., Fukaki, H., Wysocka-Diller, J., Nakajima, K., Jung, J., Sena, G., … Benfey, P. N. (2000). The *SHORT-ROOT* gene controls radial patterning of the *Arabidopsis* root through radial signaling. *Cell*, *101*(5), 555–567.

Horváth, E., Bela, K., Holinka, B., Riyazuddin, R., Gallé, Á., Hajnal, Á., … Csiszár, J. (2019). The *Arabidopsis* glutathione transferases, AtGSTF8 and AtGSTU19 are involved in the maintenance of root redox homeostasis affecting meristem size and salt stress sensitivity. *Plant Science*, *283*, 366–374.

Jiang, K. (2003). Quiescent center formation in maize roots is associated with an auxin-regulated oxidizing environment. *Development*, *130*(7), 1429–1438.

Joo, J. H., Bae, Y. S., & Lee, J. S. (2001). Role of auxin-induced reactive oxygen species in root gravitropism. *Plant Physiology*, *126*(3), 1055–1060.

Joo, J. H., Yoo, H. J., Hwang, I., Lee, J. S., Nam, K. H., & Bae, Y. S. (2005). Auxin-induced reactive oxygen species production requires the activation of phosphatidylinositol 3-kinase. *FEBS Letters*, *579*(5), 1243–1248.

Kliebenstein, D. J., Monde, R. A., & Last, R. L. (1998). Superoxide dismutase in *Arabidopsis*: An eclectic enzyme family with disparate regulation and protein localization. *Plant Physiology*, *118*(2), 637–650.

Köhler, R. H., & Hanson, M. R. (2000). Plastid tubules of higher plants are tissue-specific and developmentally regulated. *Journal of Cell Science*, *113*(1), 81–89.

Kuo, W. Y., Huang, C. H., Liu, A. C., Cheng, C. P., Li, S. H., Chang, W. C., … Jinn, T. L. (2013). CHAPERONIN 20 mediates iron superoxide dismutase (FeSOD) activity independent of its co-chaperonin role in *Arabidopsis* chloroplasts. *New Phytologist*, *197*(1), 99–110.

Leshem, Y., Seri, L., & Levine, A. (2007). Induction of phosphatidylinositol 3-kinase-mediated endocytosis by salt stress leads to intracellular production of reactive oxygen species and salt tolerance. *The Plant Journal*, *51*(2), 185–197.

Linkies, A., Müller, K., Morris, K., Turečková, V., Wenk, M., Cadman, C. S. C., … Leubner-Metzger, G. (2009). Ethylene interacts with abscisic acid to regulate endosperm rupture during germination: A comparative approach using *Lepidium sativum* and *Arabidopsis thaliana*. *The Plant Cell*, *21*(12), 3803–3822.

Liszkay, A., Kenk, B., & Schopfer, P. (2003). Evidence for the involvement of cell wall peroxidase in the generation of hydroxyl radicals mediating extension growth. *Planta*, *217*(4), 658–667.

Mano, S., Hayashi, M., & Nishimura, M. (1999). Light regulates alternative splicing of hydroxypyruvate reductase in pumpkin. *The Plant Journal*, *17*(3), 309–320.

Matsuoka, K., & Nakamura, K. (1991). Propeptide of a precursor to a plant vacuolar protein required for vacuolar targeting. *Proceedings of the National Academy of Sciences of the United States of America*, *88*(3), 834–838.

Mhamdi, A., & Van Breusegem, F. (2018). Reactive oxygen species in plant development. *Development*, *145*(15), dev164376.

Miller, G., Schlauch, K., Tam, R., Cortes, D., Torres, M. A., Shulaev, V., … Mittler, R. (2009). The plant NADPH oxidase RBOHD mediates rapid systemic signaling in response to diverse stimuli. *Science Signaling*, *2* (84), ra45.

Mittler, R. (2017). ROS are good. *Trends in Plant Science*, *22*(1), 11–19.

Müller, K., Linkies, A., Vreeburg, R. A. M., Fry, S. C., Krieger-Liszkay, A., & Leubner-Metzger, G. (2009). *In vivo* cell wall loosening by hydroxyl radicals during cress seed germination and elongation growth. *Plant Physiology*, *150*(4), 1855–1865.

Myouga, F., Hosoda, C., Umezawa, T., Iizumi, H., Kuromori, T., Motohashi, R., … Shinozaki, K. (2008). A heterocomplex of iron superoxide dismutases defends chloroplast nucleoids against oxidative stress and is essential for chloroplast development in *Arabidopsis*. *The Plant Cell*, *20*(11), 3148–3162.

Noctor, G., Reichheld, J. P., & Foyer, C. H. (2018). ROS-related redox regulation and signaling in plants. *Seminars in Cell & Developmental Biology*, *80*, 3–12.

Ogasawara, Y., Kaya, H., Hiraoka, G., Yumoto, F., Kimura, S., Kadota, Y., … Kuchitsu, K. (2008). Synergistic activation of the *Arabidopsis* NADPH oxidase AtrbohD by Ca^{2+} and phosphorylation. *Journal of Biological Chemistry*, *283*(14), 8885–8892.

Ogawa, K., Kanematsu, S., Takabe, K., & Asada, K. (1995). Attachment of CuZn-superoxide dismutase to thylakoid membranes at the site of superoxide generation (PS I) in spinach chloroplasts: Detection of immuno-gold labeling after rapid freezing and substitution method. *Plant and Cell Physiology*, *36*(4), 565–573.

Oracz, K., El-Maarouf-Bouteau, H., Kranner, I., Bogatek, R., Corbineau, F., & Bailly, C. (2009). The mechanisms involved in seed dormancy alleviation by hydrogen cyanide unravel the role of reactive oxygen species as key factors of cellular signaling during germination. *Plant Physiology*, *150*(1), 494–505.

Orman-Ligeza, B., Parizot, B., de Rycke, R., Fernandez, A., Himschoot, E., Van Breusegem, F., … Draye, X. (2016). RBOH-mediated ROS production facilitates lateral root emergence in *Arabidopsis*. *Development*, *143* (18), 3328–3339.

Ovečka, M., Vaškebová, L., Komis, G., Luptovčiak, I., Smertenko, A., & Šamaj, J. (2015). Preparation of plants for developmental and cellular imaging by light-sheet microscopy. *Nature Protocols*, *10*(8), 1234–1247.

Pasternak, T., Potters, G., Caubergs, R., & Jansen, M. A. (2005). Complementary interactions between oxidative stress and auxins control plant growth responses at plant, organ, and cellular level. *Journal of Experimental Botany*, *56*(418), 1991–2001.

Perea-García, A., Andrés-Bordería, A., Mayo de Andrés, S., Sanz, A., Davis, A. M., Davis, S. J., … Peñarrubia, L. (2016). Modulation of copper deficiency responses by diurnal and circadian rhythms in *Arabidopsis thaliana*. *Journal of Experimental Botany*, *67*(1), 391–403.

Petersson, S. V., Johansson, A. I., Kowalczyk, M., Makoveychuk, A., Wang, J. Y., Moritz, T., … Ljung, K. (2009). An auxin gradient and maximum in the *Arabidopsis* root apex shown by high-resolution cell-specific analysis of IAA distribution and synthesis. *The Plant Cell*, *21*(6), 1659–1668.

Pilon, M., Ravet, K., & Tapken, W. (2011). The biogenesis and physiological function of chloroplast superoxide dismutases. *Biochimica et Biophysica Acta (BBA)—Bioenergetics*, *1807*(8), 989–998.

Rodríguez-Serrano, M., Bárány, I., Prem, D., Coronado, M. J., Risueño, M. C., & Testillano, P. S. (2012). NO, ROS, and cell death associated with caspase-like activity increase in stress-induced microspore embryogenesis of barley. *Journal of Experimental Botany*, *63*(5), 2007–2024.

Šamajová, O., Komis, G., & Šamaj, J. (2014). Immunofluorescent localization of MAPKs and colocalization with microtubules in *Arabidopsis* seedling whole-mount probes. In G. Komis & J. Šamaj (Eds.), *Plant MAP kinases* (pp. 107–115). New York, NY: Humana Press.

Schopfer, P., Liszkay, A., Bechtold, M., Frahry, G., & Wagner, A. (2002). Evidence that hydroxyl radicals mediate auxin-induced extension growth. *Planta*, *214*(6), 821–828.

Schopfer, P., Plachy, C., & Frahry, G. (2001). Release of reactive oxygen intermediates (superoxide radicals, hydrogen peroxide, and hydroxyl radicals) and peroxidase in germinating radish seeds controlled by light, gibberellin, and abscisic acid. *Plant Physiology*, *125*(4), 1591–1602.

Sheng, Y., Abreu, I. A., Cabelli, D. E., Maroney, M. J., Miller, A.-F., Teixeira, M., & Valentine, J. S. (2014). Superoxide dismutases and superoxide reductases. *Chemical Reviews*, *114*(7), 3854–3918.

Smékalová, V., Luptovčiak, I., Komis, G., Šamajová, O., Ovečka, M., Doskočilová, A., … Šamaj, J. (2014). Involvement of YODA and mitogen activated protein kinase 6 in *Arabidopsis* post-embryogenic root development through auxin up-regulation and cell division plane orientation. *New Phytologist*, *203*(4), 1175–1193.

Takáč, T., Šamajová, O., Pechan, T., Luptovčiak, I., & Šamaj, J. (2017). Feedback microtubule control and microtubule-actin cross-talk in *Arabidopsis* revealed by integrative proteomic and cell biology analysis of KATANIN 1 mutants. *Molecular & Cellular Proteomics*, *16*, 1591–1609.

Takáč, T., Šamajová, O., Vadovič, P., Pechan, T., Košútová, P., Ovečka, M., … Šamaj, J. (2014). Proteomic and biochemical analyses show functional network of proteins involved in antioxidant defense of *Arabidopsis anp2anp3* double mutant. *Journal of Proteome Research*, *13*(12), 5347–5361.

Tsang, C. K., Li, Y., Thomas, J., Zhang, Y., & Zheng, X. F. S. (2014). Superoxide dismutase 1 acts as a nuclear transcription factor to regulate oxidative stress resistance. *Nature Communications*, *5*, 3446.

Van Breusegem, F., Slooten, L., Stassart, J. M., Moens, T., Botterman, J., Van Montagu, M., & Inzé, D. (1999). Overproduction of *Arabidopsis thaliana* FeSOD confers oxidative stress tolerance to transgenic maize. *Plant & Cell Physiology*, *40*(5), 515–523.

Van Camp, W., Capiau, K., Van Montagu, M., Inzé, D., & Slooten, L. (1996). Enhancement of oxidative stress tolerance in transgenic tobacco plants overproducing Fe-superoxide dismutase in chloroplasts. *Plant Physiology*, *112*(4), 1703–1714.

Volkening, K., Leystra-Lantz, C., Yang, W., Jaffee, H., & Strong, M. J. (2009). Tar DNA binding protein of 43 kDa (TDP-43), 14-3-3 proteins and copper/zinc superoxide dismutase (SOD1) interact to modulate NFL mRNA stability. Implications for altered RNA processing in amyotrophic lateral sclerosis (ALS). *Brain Research*, *1305*, 168–182.

Waszczak, C., Carmody, M., & Kangasjärvi, J. (2018). Reactive oxygen species in plant signaling. *Annual Review of Plant Biology*, *69*, 209–236.

Waters, B. M., McInturf, S. A., & Stein, R. J. (2012). Rosette iron deficiency transcript and microRNA profiling reveals links between copper and iron homeostasis in *Arabidopsis thaliana*. *Journal of Experimental Botany*, *63*(16), 5903–5918.

Wrzaczek, M., Brosché, M., & Kangasjärvi, J. (2013). ROS signaling loops—Production, perception, regulation. *Current Opinion in Plant Biology*, *16* (5), 575–582.

Xing, Y., Chen, W., Jia, W., & Zhang, J. (2015). Mitogen-activated protein kinase kinase 5 (MKK5)-mediated signalling cascade regulates expression of iron superoxide dismutase gene in *Arabidopsis* under salinity stress. *Journal of Experimental Botany*, *66*(19), 5971–5981.

Yamasaki, H., Hayashi, M., Fukazawa, M., Kobayashi, Y., & Shikanai, T. (2009). SQUAMOSA promoter binding protein-like7 is a central regulator for copper homeostasis in *Arabidopsis*. *The Plant Cell*, *21*(1), 347–361.

Zhang, Y., Zhu, H., Zhang, Q., Li, M., Yan, M., Wang, R., … Wang, X. (2009). Phospholipase Dα1 and phosphatidic acid regulate NADPH oxidase activity and production of reactive oxygen species in ABA-mediated stomatal closure in *Arabidopsis*. *The Plant Cell*, *21*(8), 2357–2377.

SUPPORTING INFORMATION

Additional supporting information may be found online in the Supporting Information section at the end of this article.

How to cite this article: Dvořák P, Krasylenko Y, Ovečka M, et al. *In vivo* light-sheet microscopy resolves localisation patterns of FSD1, a superoxide dismutase with function in root development and osmoprotection. *Plant Cell Environ*. 2020;1–20. https://doi.org/10.1111/pce.13894

8.3 Supplement III

8.3.1 Signaling Toward Reactive Oxygen Species-Scavenging Enzymes in Plants

Dvořák, P., Krasylenko, Y., Zeiner, A., Šamaj, J. and Takáč, T. (2021). Signaling Toward Reactive Oxygen Species-Scavenging Enzymes in Plants. *Frontiers in Plant Science*, 11, 618835. doi: 10.3389/fpls.2020.618835.

frontiers in Plant Science

REVIEW
published: 01 February 2021
doi: 10.3389/fpls.2020.618835

Signaling Toward Reactive Oxygen Species-Scavenging Enzymes in Plants

*Petr Dvořák, Yuliya Krasylenko, Adam Zeiner, Jozef Šamaj and Tomáš Takáč**

Department of Cell Biology, Centre of the Region Haná for Biotechnological and Agricultural Research, Faculty of Science, Palacký University, Olomouc, Czechia

Reactive oxygen species (ROS) are signaling molecules essential for plant responses to abiotic and biotic stimuli as well as for multiple developmental processes. They are produced as byproducts of aerobic metabolism and are affected by adverse environmental conditions. The ROS content is controlled on the side of their production but also by scavenging machinery. Antioxidant enzymes represent a major ROS-scavenging force and are crucial for stress tolerance in plants. Enzymatic antioxidant defense occurs as a series of redox reactions for ROS elimination. Therefore, the deregulation of the antioxidant machinery may lead to the overaccumulation of ROS in plants, with negative consequences both in terms of plant development and resistance to environmental challenges. The transcriptional activation of antioxidant enzymes accompanies the long-term exposure of plants to unfavorable environmental conditions. Fast ROS production requires the immediate mobilization of the antioxidant defense system, which may occur *via* retrograde signaling, redox-based modifications, and the phosphorylation of ROS detoxifying enzymes. This review aimed to summarize the current knowledge on signaling processes regulating the enzymatic antioxidant capacity of plants.

Keywords: signaling, stress, oxidative stress, plants, mitogen-activated protein kinases, calcium, antioxidant enzymes, reactive oxygen species

OPEN ACCESS

Edited by:
Luisa M. Sandalio, Departamento de Bioquímica, Biología Celular y Molecular de Plantas, Estación Experimental del Zaidín (EEZ), Spain

Reviewed by:
Rosa M. Rivero, Spanish National Research Council, Spain
Mirza Hasanuzzaman, Sher-e-Bangla Agricultural University, Bangladesh

****Correspondence:***
Tomáš Takáč
tomas.takac@upol.cz

Specialty section:
This article was submitted to Plant Abiotic Stress, a section of the journal Frontiers in Plant Science

Received: *18 October 2020*
Accepted: *11 December 2020*
Published: *01 February 2021*

Citation:
Dvořák P, Krasylenko Y, Zeiner A, Šamaj J and Takáč T (2021) Signaling Toward Reactive Oxygen Species-Scavenging Enzymes in Plants. Front. Plant Sci. 11:618835. doi: 10.3389/fpls.2020.618835

INTRODUCTION

Reactive oxygen species (ROS), as unavoidable byproducts of metabolism, have important signaling roles in living organisms under optimal and adverse environmental conditions (Apel and Hirt, 2004; Baxter et al., 2014; Waszczak et al., 2018). ROS are produced from atmospheric oxygen by its partial monovalent reduction, which occurs in the presence of electron donors. Plant ROS are generated mainly by electron transport chains in chloroplasts (Pospíšil, 2016; Foyer, 2018) and mitochondria (Gleason et al., 2011) as well as during photorespiration in peroxisomes (del Río et al., 2006; del Río and López-Huertas, 2016). Apoplastic ROS are produced by plasma membrane-localized NADPH oxidase [NOX, in plants encoded by *RESPIRATORY BURST OXIDASE HOMOLOG (RBOH)* genes; Sagi and Fluhr, 2006], oxalate oxidase (Voothuluru and Sharp, 2013), or by the degradation of spermidine by polyamine oxidase (Geilfus et al., 2015). Apoplastic peroxidases also possess ROS generating capacity (Bindschedler et al., 2006). Only four ROS, namely singlet oxygen ($_1O^2$), superoxide ($O_2^{\cdot -}$), hydrogen peroxide (H_2O_2), and hydroxyl radical ($OH^{\cdot}$), are more abundant and stable. They quickly interconvert, thus providing a high level of functional variability. However, they differ

in their stability, reactivity, and ability to be transported across membranes. H_2O_2 is the most stable ROS transported actively across membranes by aquaporins (Miller et al., 2010; Mittler, 2017; Smirnoff and Arnaud, 2019).

Depending on the generated ROS concentration, severity of stress, antioxidant capacity, and cellular energetic status, different cellular and physiological outcomes may be obtained. In small concentrations, ROS exert signaling functions, leading to the expression of stress-responsive genes. Upon extensive accumulation, ROS reactivity may cause damaging oxidative effects on lipids, nucleic acids, and proteins, eventually resulting in cell death. Moreover, ROS are involved in strictly regulated programmed cell death (Lehmann et al., 2015; Petrov et al., 2015). A very important feature of ROS signaling is that it can be propagated from cell to cell and transduce signals for long distances in a process known as the ROS wave (Mittler et al., 2011). This is mediated by the interplay between NOX, calcium (Ca^{2+}) channels, and oxidative stress-induced Ca^{2+} fluxes (Gilroy et al., 2016). The ROS wave, together with other hormone- or electric signal-mediated signaling mechanisms, is implicated in systemic acquired acclimation, in which the locally generated stress signal is transported into sites not being directly affected by the stress. Systemic acquired acclimation is accompanied by rapid and dramatic transcriptional reprogramming (Zandalinas et al., 2019, 2020).

In addition to plant stress responses, ROS are widely involved in developmental processes (Considine and Foyer, 2014; Xia et al., 2015; Mhamdi and Van Breusegem, 2018), regulating morphogenetic processes in the close interplay of phytohormones such as auxins and cytokinins (Xia et al., 2015; Zwack et al., 2016). Interestingly, auxin and abscisic acid (ABA) can promote ROS production by activating NOX (Joo et al., 2001; Schopfer et al., 2002; Pasternak et al., 2007). In turn, ROS may affect auxin levels (Takáč et al., 2016a) and homeostasis leading to altered shoot branching and leaf rosette shapes (Tognetti et al., 2010).

This review aimed to summarize recent findings on the regulation of major ROS-decomposing enzymes. First, we introduce the major antioxidant enzymes and provide an overview of the mechanisms by which ROS affect signaling in plants. Next, we summarize recent knowledge on the redox regulation of major antioxidant enzymes and elaborate on their modulation by mitogen-activated protein kinase (MAPK) and Ca^{2+} signaling pathways. The transcriptional activation of antioxidant enzymes, including metabolite-driven retrograde signaling, is discussed as well. Finally, we point out the importance of their post-translational regulation by reversible phosphorylation and reactive nitrogen species (RNS).

CHARACTERIZATION OF KEY ANTIOXIDANT ENZYMES

Generally, enzymatic antioxidant capacity inevitably contributes to plant survival in adverse conditions, especially when the stress pressure exceeds the mechanisms preventing ROS overaccumulation. The significance of antioxidant enzymes has been documented many times by genetic studies reporting on the positive correlation between the expression of these enzymes and plant stress tolerance. Contrarily, the deregulation of these enzymes is connected with plant hypersensitivity to stress and programmed cell death (De Pinto et al., 2012).

ROS scavenging is performed enzymatic or *via* non-enzymatic antioxidant defense pathways, which control the regulation of ROS levels through strict compartmentalization (Mignolet-Spruyt et al., 2016; Noctor et al., 2017; Foyer and Noctor, 2020). Non-enzymatic antioxidant defense is mainly mediated by low molecular-weight metabolites such as ascorbate, glutathione, α-tocopherol, carotenoids, and flavonoids (Locato et al., 2017; Smirnoff, 2018; Zechmann, 2018; Muñoz and Munné-Bosch, 2019; Foyer and Noctor, 2020). Superoxide dismutases (SODs), catalases (CATs), ascorbate peroxidases (APXs), dehydroascorbate reductases (DHARs), monodehydroascorbate reductases (MDHARs), and glutathione reductases (GRs) are among the main antioxidant enzyme classes. Furthermore, glutathione peroxidases, peroxidases, and thio-, gluta-, and peroxiredoxins are potent ROS scavengers as well (Dietz, 2011; Kang et al., 2019; Foyer and Noctor, 2020). Within this section, we briefly characterize the key enzymatic antioxidants in plants.

Major enzymatic antioxidants are plastidic, cytosolic, mitochondrial, and peroxisomal SODs, which decompose $O_2^{\cdot -}$ to H_2O_2 (Kliebenstein et al., 1998; Alscher et al., 2002; Pilon et al., 2011). Based on the presence of metal cofactors in their active site, four different SODs are recognized in living organisms, namely FeSOD, MnSOD, NiSOD (not present in higher plants), and Cu/ZnSOD. In the *Arabidopsis thaliana* genome, three *FeSOD* (*FSD1*, *FSD2*, and *FSD3*), one *MnSOD* (*MSD1*), and three *Cu/ZnSOD* (*CSD1*, *CSD2*, and *CSD3*; Kliebenstein et al., 1998; Pilon et al., 2011) genes have been identified. Individual SOD isozymes are compartmentalized into mitochondria (MSD1; Morgan et al., 2008), peroxisomes (CSD3; Kliebenstein et al., 1998), cytosol (CSD1 and FSD1; Kliebenstein et al., 1998, Dvořák et al., 2020), the chloroplast stroma (FSD1; Kuo et al., 2013; Dvořák et al., 2020), and thylakoids (CSD2, FSD2, and FSD3; Kliebenstein et al., 1998; Myouga et al., 2008). Recently, it was discovered that FSD1 is also localized to the nucleus (Dvořák et al., 2020). In addition to their antioxidative role during salt, oxidative (Myouga et al., 2008; Shafi et al., 2015; Dvořák et al., 2020), and photooxidative stresses (Myouga et al., 2008; Xing et al., 2013; Gallie and Chen, 2019), SODs also have developmental functions during lateral root growth (Morgan et al., 2008; Dvořák et al., 2020), germination (Dvořák et al., 2020), chloroplast development, and flowering (Rizhsky et al., 2003; Myouga et al., 2008).

CATs are responsible for the detoxification of the overproduced H_2O_2, which occurs owing to their kinetic properties (Tuzet et al., 2019). As iron-containing homotetrameric proteins, CATs catalyze the decomposition of H_2O_2 to H_2O and O_2, predominantly produced during photorespiration. Three genes (*CAT1*, *CAT2*, and *CAT3*) encoding CATs have been found in the *Arabidopsis* genome. CAT isozymes are localized in peroxisomes (Frugoli et al., 1996; Du et al., 2008) and play important roles under unfavorable conditions for plants. For example, all three CAT isoforms

are required for the plant response to photooxidative stress (Vandenabeele et al., 2004; Bueso et al., 2007; Zhang S. et al., 2020). CAT2 is involved in plant responses to heat, heavy metal (Corpas and Barroso, 2017; Ono et al., 2020), cold, and salt stresses (Bueso et al., 2007). CAT3 participates in the drought stress response (Zou et al., 2015), whereas CAT1 is implicated in the drought and salt stress responses (Xing et al., 2007). Surprisingly, H_2O_2-induced CAT2, likely together with CAT1 and CAT3, generates a signal promoting autophagy-dependent cell death during plant immune responses (Hackenberg et al., 2013; Teh and Hofius, 2014). In addition, tobacco NbCAT1 is relocalized to nuclei after interaction with CRINKLING- AND NECROSIS-INDUCING PROTEIN 63 (CRN63) secreted by *Phytophthora sojae* under attack as found in the transient assay. This mechanism was reported to regulate pathogen-induced cell death in tobacco (Zhang M. et al., 2015). CATs are involved in root growth (Yang et al., 2019), leaf development and senescence (Mhamdi et al., 2010; Zhang Y. et al., 2020), as well as shoot, ovule, pollen, and seed development (Sharma and Ahmad, 2014; Su et al., 2018; Palma et al., 2020).

Balance in cellular H_2O_2 levels is also maintained by enzymes of the ascorbate–glutathione cycle, such as APX, MDHAR, DHAR, and GR. APXs, as heme-containing peroxidases, detoxify H_2O_2 *via* the electron transfer from ascorbate to form monodehydroascorbate (MDHA) and H_2O. The presence of nine putative *APX* genes has been described in the *Arabidopsis* genome; nevertheless, the *APX4* gene product is lacking H_2O_2 decomposing activity, and *APX7* is annotated as a pseudogene (Granlund et al., 2009). Cytosolic (APX1, APX2 and APX6), chloroplast (stromal sAPX and thylakoid tAPX), peroxisomal (APX3 and APX5) APXs have been recognized in *Arabidopsis* (Maruta et al., 2012, 2016), while sAPX is targeted also to mitochondria (Chew et al., 2003). Chloroplastic APX isozymes are involved in the water-water cycle, which decomposes H_2O_2 generated by $O_2^{\cdot -}$ dismutation (Huang et al., 2019). They are therefore crucial for photoprotection (Murgia et al., 2004; Kangasjärvi et al., 2008; Maruta et al., 2010). Remarkably, the chloroplastic H_2O_2 detoxification turns to be inactive in plants depleted of cytosolic APX1 (Davletova et al., 2005a, Pnueli et al., 2003). APX1 is also involved in plant responses to heat and drought stress (Koussevitzky et al., 2008; Vanderauwera et al., 2011) and to wounding (Maruta et al., 2012). The importance of cytosolic APX2 was shown during high light, heat, salinity, and drought stresses using *apx2* and *apx1/apx2* mutants (Rossel et al., 2006; Suzuki et al., 2013). Additionally, both cytosolic APXs play important roles during cold stress (van Buer et al., 2016). Mutants in peroxisomal *APX3* do not display any phenotype upon salt treatment and exposure to low or high temperature (Narendra et al., 2006). Finally, APXs also play essential roles as enzymatic regulators of H_2O_2 signaling during plant development (Chen et al., 2014; Pandey et al., 2017; Chin et al., 2019).

The reverse reduction of MDHA to ascorbate, catalyzed by MDHAR, occurs in the presence of NAD(P)H as a reductant (Foyer and Noctor, 2011). Overall, five *Arabidopsis* genes encode six functional proteins of MDHARs (Obara et al., 2002). Cytosolic localization is confirmed for MDHAR2 and 3, whereas MDHAR1 has been found also in peroxisomes. MDHAR4 is located in peroxisomal membrane (Lisenbee et al., 2005; Eubel et al., 2008; Kaur and Hu, 2011). The *MDHAR6* gene is expressed in two splicing variants, producing two protein products localized either in mitochondria (MDHAR5) or chloroplasts (MDHAR6; Obara et al., 2002). The overexpression of *Arabidopsis MDHAR1* in tobacco leads to increased tolerance to ozone, salt, and osmotic stresses (Eltayeb et al., 2007). The overexpression of cytosolic *Acanthus ebracteatus* MDHAR in rice confers increased resistance to salt stress and higher germination rate and grain weight (Sultana et al., 2012). A study exploiting the genetic manipulation of *MDHAR4* suggests that it is implicated in plant germination, post-germination growth, and possibly in senescence (Eastmond, 2007). MDHAR2 and MDHAR5 play important roles during the interaction of *Arabidopsis* with plant growth-promoting endophyte *Piriformospora indica* (Vadassery et al., 2009).

Dehydroascorbate (DHA) is enzymatically reduced by DHAR by using glutathione as an electron donor, which is oxidized to glutathione disulfide. DHARs are soluble monomeric enzymes, and their thiol group participates in the catalyzed reaction. Three functional genes are present in the *Arabidopsis* genome. Their protein products are localized either in the cytosol (DHAR1, DHAR2) or chloroplasts (DHAR3; Rahantaniaina et al., 2017). Recently, their role in the regulation of ascorbate and glutathione homeostasis was described during plant developmental processes (reviewed in Ding et al., 2020). The overexpression of *DHAR1* protects *Arabidopsis* from methyl viologen-induced oxidative, high temperature, and high light stresses (Ushimaru et al., 2006; Wang et al., 2010; Noshi et al., 2017). DHAR2 has an antioxidant role in plant responses to ozone (Yoshida et al., 2006), drought, salt, and polyethylene glycol (Yin et al., 2010; Eltayeb et al., 2011), whereas DHAR3 is involved in the high light response (Noshi et al., 2016).

The pool of reduced glutathione consumed by DHAR activity is recovered by GR in a NADPH-dependent reaction, which is essential for glutathione homeostasis. Structurally, the GR protein contains a FAD-binding domain, a dimerization domain, and a NADPH-binding domain, crucial for proper enzymatic activity (Berkholz et al., 2008). Two isozymes were described in *Arabidopsis*, showing dual localization in the cytosol and peroxisomes for GR1 and in chloroplasts and mitochondria for GR2 (Kataya and Reumann, 2010; Marty et al., 2019). GR1 is involved in the tolerance of *Arabidopsis* to high light (Müller-Schüssele et al., 2020), heavy metals (Guo et al., 2016; Yin et al., 2017), and salt stress (Csiszár et al., 2018). GR2 is involved in methyl viologen-induced oxidative stress (Wang et al., 2019), chilling stress (Kornyeyev et al., 2003), and high light stress (Karpinski et al., 1997) but also in developmental processes such as root growth, root apical meristem maintenance (Yu et al., 2013), embryo development (Marty et al., 2019), and seed germination (Sumugat et al., 2010). In addition, the knockout mutation of *GR3* confers salt stress sensitivity in rice (Wu et al., 2015).

REGULATION OF ANTIOXIDANT ENZYMES

Plants can percept, transduce, and then translate the ROS signal into appropriate cellular responses. The key consequence of ROS

accumulation is the modification of the potential signaling targets [e.g., kinases, transcription factors (TFs), and stress response-related proteins] by their oxidizing properties. ROS can modulate signaling through their capability to affect the protein redox status *via* the oxidation of methionine residues and thiol groups of cysteines. This leads to the activation/deactivation, structure alteration, and loss-/gain-of-function of ROS targets (Waszczak et al., 2015). Redox-related processes are strictly regulated by such proteins as thio- and glutaredoxins, which can undergo reversible oxidation/reduction and can be activated/inactivated in response to the cellular redox state (Waszczak et al., 2015, 2018). Recently, a redox-based sensing mechanism was introduced for H_2O_2, including cell-surface H_2O_2 receptor capable of transducing signal from extracellularly produced ROS into intracellular signaling cascades (Wu et al., 2020). HYDROGEN-PEROXIDE-INDUCED Ca^{2+} INCREASES 1 (HPCA1) is a membrane-spanning enzyme belonging to a protein family of leucine-rich repeat (LRR) receptor kinases, which percepts apoplastic H_2O_2 *via* the oxidation of two pairs of cysteine residues in its extracellular domain, leading to its autophosphorylation. This promotes the acceleration of Ca^{2+} influx through Ca^{2+}-channels and the subsequent closure of stomata (Wu et al., 2020).

ROS can also cause carbonylation, a type of protein oxidation, where the carbonyl groups (aldehydes and ketones) are attached to protein side chains at proline, arginine, lysine and threonine residues (Yalcinkaya et al., 2019). Carbonylation alters protein stability and might enhance their susceptibility to proteolysis (Dalle-Donne et al., 2003; Suzuki et al., 2010; Ciacka et al., 2020).

Redox perturbations, driven by ROS produced in chloroplasts and mitochondria, are transduced by metabolic signals to activate rapid adaptive mechanisms by retrograde signaling (Chan et al., 2016; Cui et al., 2019). As of late, ROS were also introduced as mediators of retrograde signaling directed from the plastids to the nucleus. Thus, H_2O_2 generated in plastids is transported to the nucleus to activate the defense gene expression (Exposito-Rodriguez et al., 2017).

In addition, ROS can cross talk with other key secondary messengers, such as Ca^{2+} and RNS. Owing to their strong oxidation potential, ROS interact with such ubiquitous messengers as nitric oxide (NO), leading to the formation of RNS, including radical nitric oxide ($NO^{\cdot}$), nitric dioxide ($NO_2^{\cdot}$), and nitrate radical ($NO_3^{\cdot}$) as well as non-radical peroxynitrite ($ONOO^-$), nitrosonium cation (NO^+), nitroxyl anion (NO^-), nitrous acid (HNO_2), and other NO_x species involved in plant development, metabolism, (a)biotic stress responses, or stomatal closure (del Río, 2015; Lindermayr and Durner, 2015; Piterková et al., 2015; Farnese et al., 2016; Niu and Liao, 2016). The first evidence of NO and H_2O_2 interplay was related to cytotoxic effects during plant hypersensitive responses (Delledonne et al., 2001). Generally, the ROS cross talk with RNS is concentration-dependent and organelle- and even microcompartment-specific and might have beneficial or deleterious effects on plant cells (Kohli et al., 2019).

In general, an increased production of ROS caused by various environmental cues rapidly triggers antioxidant defense by multiple mechanisms, including retrograde signaling, transcriptional control, post-transcriptional regulation, post-translational redox modifications or phosphorylation, and protein–protein interactions.

Redox Regulation

The cellular antioxidant capacity is tightly coupled with the maintenance of redox homeostasis by redox buffers such as ascorbate and glutathione (Karpinski et al., 1997; Foyer and Noctor, 2011). Both compounds may directly decompose ROS and are essential for preserving the ROS content at physiological levels. In addition, they serve as co-substrates for enzymes of the ascorbate–glutathione cycle. The high reduction state of both compounds is connected to enhanced plant tolerance to adverse stress conditions and increased antioxidant capacity (Foyer and Noctor, 2011). The flexibility and rapid response of antioxidant enzymes to changing external conditions are primarily controlled by the redox state of thiol groups in their amino acid sequences, regulated by thio-, peroxi-, and glutaredoxins or other oxidoreductases (Meyer et al., in press). One of them, NUCLEOREDOXIN 1 (NRX1), can target several important antioxidant enzymes, including CAT1, CAT2, and CAT3, GLUTATHIONE S-TRANSFERASE (GST), APX1, GLUTAREDOXIN FAMILY PROTEIN, and METHIONINE SULFOXIDE REDUCTASE (MSR) B2. The expression of antioxidant enzymes depends on the proper functioning of NRX1 that has an impact on plant oxidative stress tolerance (Kneeshaw et al., 2017). A similar proteomic elucidation of thioredoxin mitochondrial targets using affinity chromatography revealed that mitochondrial MSD1, thio- and peroxiredoxins, MSR isoforms, and GLUTATHIONE PEROXIDASE 6 act in a thioredoxin-dependent manner (Yoshida et al., 2013). Multiple antioxidant enzymes including chloroplastic CSD2, CAT3, MDHAR6, PEROXIREDOXIN TPx1, GST isoforms, and MSR-LIKE PROTEIN have also been detected as targets of THIOREDOXIN y1, a plastidic thioredoxin isoform in roots (Marchand et al., 2010). These data indicate that the redox regulation of antioxidant plant defense is quite complex and requires both spatial and temporal coordination.

Mitogen-Activated Protein Kinase Signaling, Reactive Oxygen Species, and Antioxidants

Reactive Oxygen Species-Induced Mitogen-Activated Protein Kinase Signaling Pathways

A very significant feature of ROS is their capability to activate MAPKs, representing key signal transduction proteins triggered by a plethora of environmental and developmental factors (Colcombet and Hirt, 2008; Šamajová et al., 2013; Smékalová et al., 2014, Komis et al., 2018). MAPK signaling cascades consist of MAPKKKs (MAP3Ks), MAPKKs (MAP2Ks), and MAPKs, which are consecutively phosphorylated, leading to the activation/inactivation of a wide range of target proteins, including TFs (Liu and He, 2017). It is well-known that MAPK signaling pathways are activated by ROS accumulated during plant responses to either abiotic stresses or pathogen attack.

So far, two kinds of MAP3Ks were identified to be activated by ROS, namely ARABIDOPSIS HOMOLOGS OF NUCLEUS AND PHRAGMOPLAST LOCALIZED KINASES (ANPs) and MITOGEN-ACTIVATED PROTEIN KINASE KINASE KINASE 1 (MAPKKK1 or MEKK1). ANPs are required for the plant immune response (Kovtun et al., 2000; Savatin et al., 2014), whereas the ROS-triggered signal is further transduced *via* MITOGEN-ACTIVATED PROTEIN KINASE 3 (MPK3) and MPK6 (Kovtun et al., 2000; Nakagami et al., 2006). The full activation of MPK3 and MPK6 is preconditioned by the presence of OXIDATIVE SIGNAL INDUCIBLE 1 kinase (OXI1), which is an essential component of this signal transduction pathway (Rentel et al., 2004). Another ROS-activated MAPK cascade consists of MEKK1, MKK1/2, and MPK4 (Nakagami et al., 2006; Pitzschke et al., 2009). This pathway is also important for basal plant defense against pathogen attack (Zhang et al., 2012). Moreover, a pathogen-induced oxidative burst activates the MPK7 downstream of MKK3 (MAP2K), thus triggering the expression of pathogenesis-related (PR) genes, independently of flagellin receptor FLAGELLIN SENSING 2 (Dóczi et al., 2007).

Furthermore, MPK1 and MPK2 are activated by oxidative stress and jasmonic acid (JA), ABA, and wounding (Ortiz-Masia et al., 2007). In turn, ABA and ROS-activated MPK9 and MPK12 act upstream of anion channels in guard cells, thus regulating stomatal closure (Jammes et al., 2009). MPK3 was found as another principal player in guard cell signaling *via* ABA and H_2O_2 perception in guard cells, which leads to stomatal closure (Gudesblat et al., 2007). Thus, MAPK signaling activated by ABA-induced ROS accumulation is generally implicated in stomatal movements (Danquah et al., 2014; Sierla et al., 2016).

MAPKs also respond to ROS produced in chloroplasts and mitochondria. In this respect, MPK6 is implicated in chloroplast to nucleus-directed retrograde signaling upon intense light exposure. The activation of MPK6 under such conditions is preceded by the export of Calvin–Benson cycle intermediate dihydroxyacetone phosphate (DHAP) from chloroplasts to the cytosol. These events lead to the rapid (within several minutes) expression of *APETALA2/ETHYLENE-RESPONSIVE ELEMENT BINDING FACTOR (AP2/ERF)* TFs and other downstream genes, such as *CHLOROPLAST PROTEIN KINASE LIKE* (*ChlPK-like*), *CHITINASE FAMILY PROTEIN* (*CHFP*), *HEAT SHOCK PROTEIN 20 LIKE* (*HSP20-like*), and *PR1* (Vogel et al., 2014). Similarly, MPK4 orchestrates plastid retrograde signaling in a salicylic acid-dependent manner (Gawroński et al., 2014). Mitochondrial ROS production induced by oxygen deprivation activates MPK6 and subsequent retrograde signaling toward the nucleus, leading to transcriptional reprogramming and triggering plant defense mechanisms (Chang et al., 2012).

Several studies report on the regulation of MAPKs by direct interactions with ROS. Waszczak et al. (2014) identified MPK2, MPK4, and MPK7 as capable of being sulfenylated in an H_2O_2-dependent manner. Another example pertains to *Brassica napus* BnMPK4, an ortholog of *Arabidopsis* MPK4, activated by H_2O_2 and undergoes aggregation upon the H_2O_2-dependent oxidation of the Cys232 residue (Zhang T. et al., 2015). Thus, it is obvious that MAPKs could be modified on cysteine residues by direct oxidation, affecting their stability, aggregation, and probably protein–protein interactions. It is noteworthy that the redox regulation of MAPKs may lead either to their activation or inactivation. The oxidation of kinase amino acid residues was reported to interfere with ATP binding and cause inactivation (Diao et al., 2010) but may also lead to their super-activation state (Corcoran and Cotter, 2013).

Regulation of Antioxidant Enzymes by Mitogen-Activated Protein Kinase Signaling

MAPKs appear as essential regulators of antioxidant defense, as their genetic modifications can alter the expression profile of many antioxidant enzymes under diverse environmental conditions.

Under high light intensity (Xing et al., 2013) and hypersalinity (Xing et al., 2015), the expression of *Arabidopsis* SODs is regulated by MKK5 (MAP2K). The expression of *CSD1* and *CSD2* increases under enhanced light exposure. Interestingly, the transcript levels of both *CSD* genes remain unchanged under these conditions in a transgenic *Arabidopsis* line with downregulated *MKK5*, which is hypersensitive to high light. In contrast, a transgenic *Arabidopsis* line overexpressing *MKK5* is resistant to high light stress and shows the increased activity of both CSDs. Moreover, the downregulation of *MKK5* negatively affects the activation of MPK3 and MPK6 under these conditions, thereby implying that these two MAPKs act downstream of MKK5 (Xing et al., 2013). It is worth mentioning that MKK5, acting downstream of MEKK1 and upstream of MPK6, is also essential for the expression of chloroplastic *FSD2* and *FSD3* during salt stress (Xing et al., 2015). In addition, MKK1 mediates the transcriptional activation of *CAT1*, but not of *CAT2* and *CAT3*, during salt stress, and after drought and ABA treatments (Xing et al., 2007). CAT1 is important for the regulation of ABA-mediated H_2O_2 production, whereas its expression is activated by MPK6 operating downstream of MKK1 (Xing et al., 2008).

A MAPK cascade activated by ROS includes ANPs, MPK3, and MPK6 (Kovtun et al., 2000). A shotgun proteomic analysis of *Arabidopsis anp2/anp3* double mutant revealed the overabundance and/or increased activity of several proteins important for plant antioxidative defense, including FSD1, MSD1, and enzymes of the ascorbate–glutathione cycle, such as APX and DHAR. Consequently, this double mutant showed enhanced resistance to the methyl viologen-induced oxidative stress. Thus, it might be concluded that ANPs negatively regulate *Arabidopsis* tolerance to oxidative stress (Takáč et al., 2014). ANPs are likely master regulators of plant antioxidant defense. Contrarily, they also confer resistance to *Arabidopsis* against necrotrophic fungus *Botrytis cinerea* (Savatin et al., 2014), suggesting the functional divergence of ANPs in *Arabidopsis*.

The genetic modification of the MEKK1-MKK1/MKK2-MPK4 signaling pathway also deregulates the expression of several antioxidant enzymes. Notably, *Arabidopsis* mutants in genes encoding individual constituents of this cascade show diverse patterns of *CSD1*, *APX1*, *GR*, *CAT1*, and *CAT2* expression. The upregulation of *CAT1* and *CAT3* in *mekk1* and *mkk1/mkk2* mutants, but not in the *mpk4* mutant points, to the complexity of MAPK signaling toward antioxidant genes suggests possible cross talk of diverse MAPK signaling pathways (Pitzschke et al.,

2009). According to another study, MPK4 is required for the homeostasis of ROS scavenging proteins in a salicylic acid-dependent manner (Gawroński et al., 2014). Apart from its signaling role during pathogen defense, salicylic acid positively regulates the expression of diverse abiotic stress-related proteins, including antioxidant enzymes, thus contributing to plant stress tolerance (Horváth et al., 2007; Khan et al., 2015). The double mutant in *MPK4* and *ISOCHRISMATE SYNTHASE 1*, encoding an enzyme involved in the synthesis of salicylic acid, results in the deregulated expression of *FSDs*, *CSD2*, *GR2*, and *APXs*. Therefore, the cross talk of salicylic acid and MAPK signaling is important for the expression of enzymes with antioxidant functions (Gawroński et al., 2014).

Thus, MEKK1 appears as an important regulator of antioxidant defense, capable of activation of MKK1/2 and MKK5 and subsequently MPK3/6 and MPK4. According to the current knowledge, MAPKs acting downstream of MEKK1 (MKK1/2/5; MPK3/4/6) may serve as proteins providing signal specificity toward individual antioxidant enzymes (**Figure 1**).

The MAPK-mediated transcriptional remodeling of oxidative stress-related genes occurs *via* the phosphorylation of TFs. For example, a TF called MYB44 (Persak and Pitzschke, 2013, 2014) and HEAT SHOCK TRANSCRIPTION FACTOR A4A (HSFA4A; Pérez-Salamó et al., 2014) are phosphorylated by MPK3 or MPK6. Heat shock TFs are known to play important roles during plant responses to several abiotic stresses. Thus, the overexpression of *HSFA4A* reduces the H_2O_2 content and lipid peroxidation, whereas it increases the activity of APX1 after salt treatment. Moreover, it leads to transcriptional changes in a large set of genes responsive to oxidative stress. The same study also confirmed that HSFA4A is involved in the transcriptional activation of genes encoding other TFs, such as *WRKY30*, *ZAT12*, *CRK13*, *HSP17.6A*, *ZAT6,* and *CTP1*, which are known to play essential roles in plant responses to biotic and abiotic stresses (Pérez-Salamó et al., 2014). Furthermore, MPK6 phosphorylates AP2/ERF6 (Wang et al., 2013a; Vogel et al., 2014) and AP2/ERF104 (Bethke et al., 2009) during oxidative stress. After activation, ERF6 specifically binds to the ROS-responsive cis-acting element 7 (ROSE7/GCC box), thus inducing the expression of ROS-responsive genes under intense illumination. ROSE are sorted into seven groups according to their *cis*-acting motives and core sequences showing different responses to stress conditions (Wang et al., 2013a).

Thus, MAPKs can activate an array of TFs controlling the expression of antioxidant enzymes. Modern bioinformatics provides an opportunity to broaden the list of potential TF-regulating antioxidants, which show altered expression (transcriptomics) or abundance (proteomics) in transgenic lines with a modified or missing expression of particular *MAPK* genes. This may be carried out by integrating four different parameters: (1) the presence of *cis*-element(s) in the promoter sequence of the gene encoding the target antioxidant enzyme (predicted by AthaMap; Hehl et al., 2016), (2) TFs co-expressed with target antioxidants and MAPKs (determined by ATTED II; Obayashi et al., 2018), (3) TFs containing a MAPK-specific phosphorylation site [S(p)P or S(p)T; evaluated by PhosPhat 4.0 and GPS 3.0; Xue et al., 2005; Zulawski et al., 2013], and (4) the presence of a MAPK-specific docking site in the amino acid sequence of the TF (evaluated by ELM; Kumar et al., 2020). As an example, we provide a list of TFs potentially responsible for the expression of *FSD1*, *DHAR1*, and *APX1* under the regulation of MPK3, MPK4, and MPK6 (**Figure 2**; **Supplementary Tables 1**–**3**). Previously, these three enzymes showed significant changes in their abundance in *mpk4* (Takáč et al., 2016b) and *anp2/anp3* mutants (Takáč et al., 2014). Some predicted TFs have already been reported as regulators of antioxidant enzymes, including SPL7 regulating *FSD1*. The data set also includes HSFB2A, which has been predicted as a general TF for all three examined enzymes (**Supplementary Table 1**).

Finally, it should be noted that MAPK signaling can also affect the expression of *NOXs*. MEK2 cascade phosphorylates WRKY TFs (WRKY7/WRKY8/WRKY9/WRKY11), binding to the *cis*-element of the *RBOHB* promoter sequence during the exposure of *Nicotiana benthamiana* to bacterial protein elicitor INF1 and effector R3a/AVR3a (Adachi et al., 2015). In *Zea mays*, the activation of ZmMAPK5 is related to the increased expression of *NOX* and apoplastic ROS production in response to brassinosteroid and ABA treatments (Lin et al., 2009; Zhang et al., 2010). Nevertheless, the precise mechanism controlling the homeostasis between MAPK-induced ROS production and decomposition remains unknown.

Ca^{2+} Signaling, Reactive Oxygen Species, and Antioxidants

Cross Talk of Reactive Oxygen Species With Ca^{2+} Signaling

Cytosolic Ca^{2+} is an important secondary messenger functioning in intra- and extracellular signaling networks involved in abiotic stress responses and plant innate immunity (Schulz et al., 2013; Demidchik et al., 2018; Tian et al., 2020). The rapidly fluctuating cytosolic content of Ca^{2+} is regulated by environmental cues, which activate Ca^{2+} channels, ion pumps, or plasma membrane- or organelle-membrane-embedded Ca^{2+} transporters (Chmielowska-Bak et al., 2014; Tian et al., 2020), as well as by Ca^{2+}-binding proteins, such as calmodulin, calcineurin B-like proteins (CBL), and various Ca^{2+}-dependent protein kinases (CPKs or CDPKs; Gilroy et al., 2014; Zhang et al., 2018). Plant- and protozoan-specific Ser-/Thr-CDPKs are key players of stress-mediated signaling networks, represented by a large number of members in the multigene family in diverse plant species [34 in *Arabidopsis*, 29 in rice, 20 in wheat, and 30 in poplar and *Brachypodium distachyon* (Zhang et al., 2018; reviewed in Atif et al., 2019; Wen et al., 2020)].

The interplay between Ca^{2+} and ROS is mutual because the cytosolic Ca^{2+} content is regulated by ROS, and *vice versa*, Ca^{2+} is crucial for ROS production (Choi et al., 2014; Gaupels et al., 2017). Therefore, Ca^{2+}-dependent ROS signaling through NOXs as key signaling hubs and ROS-dependent Ca^{2+} signaling through the direct regulation of Ca^{2+} channels and sensors amplify each other during plant immune responses (reviewed by Marcec et al., 2019). The auto-propagating ROS wave generated by Ca^{2+}-dependent NOX is directly linked to the Ca^{2+} wave during the systemic response of plants to pathogen

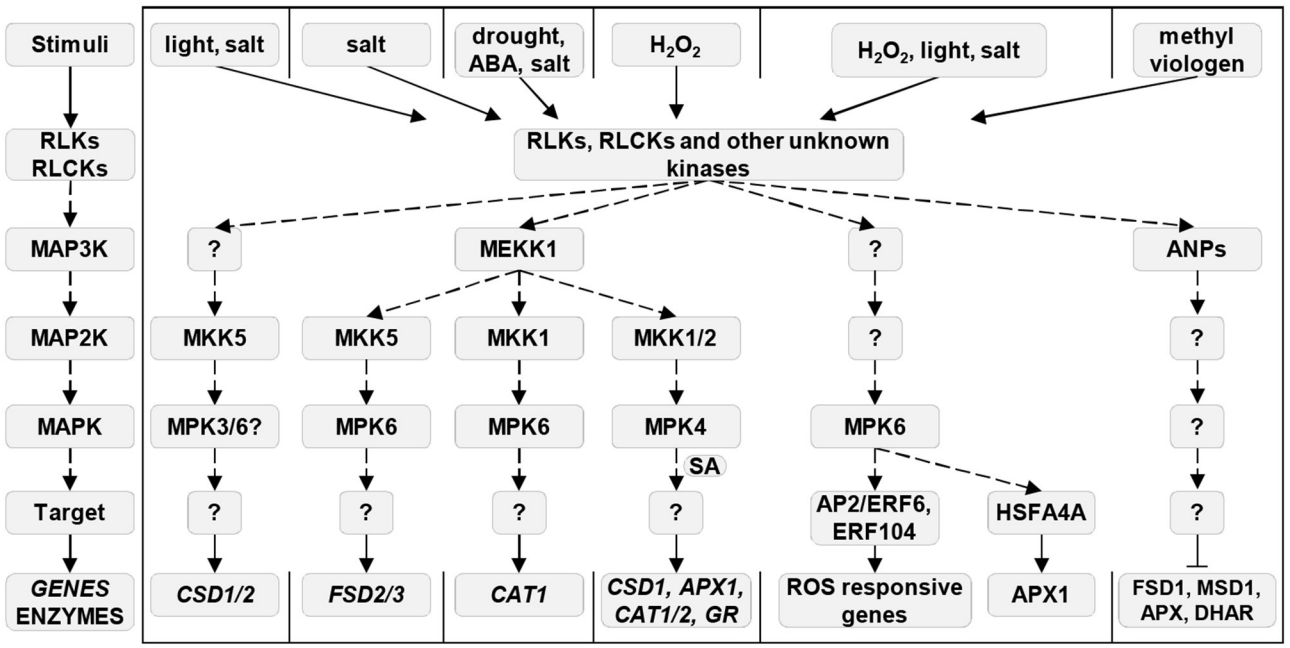

FIGURE 1 | MAPK-dependent regulation of antioxidant enzymes during plant stress responses. Most left pathway shows the universal order of a MAP3K/MAP2K/MAPK cascade. Solid arrows indicate induction, dashed arrows show phosphorylation, and ⊥ indicates negative regulation. Question mark means an unknown component of the pathway. ABA, abscisic acid; ANPs, Arabidopsis nucleus- and phragmoplast-localized kinases; AP2/ERF6, Apetala2/Ethylene-responsive element binding factor 6; APX, ascorbate peroxidase; CAT, catalase; CSD, Cu/Zn superoxide dismutase; DHAR, dehydroascorbate reductase; ERF104, Ethylene-responsive element binding factor 104; FSD, Fe superoxide dismutase; GR, glutathione reductase; HSFA4A, Heat shock transcription factor A4A; MAPK, mitogen-activated protein kinase; MAP2K, mitogen-activated protein kinase kinase; MAP3K, mitogen-activated protein kinase kinase kinase; MSD, Mn superoxide dismutase; RLCKs, receptor-like cytoplasmic kinases; RLKs, receptor-like kinases; ROS, reactive oxygen species; SA, salicylic acid.

A

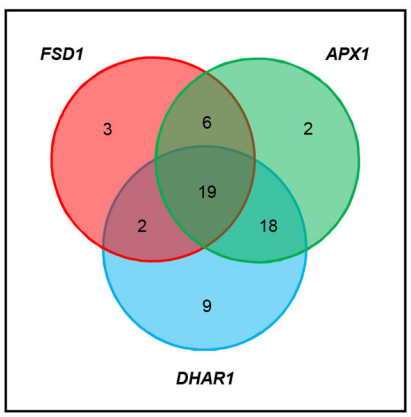

B

	Number of TFs	TFs
TFs common for *APX1*, *DHAR1* and *FSD1*	19	SCAP1, HSFB2A, TOE1, MYC3, TOE2, RVE1, RR10, MYB83, SPL7, AHL12, ASL18, AGF1, AHL20, MYB59, ARR11, MYB46, NAC058, RAV1, GLK1
TFs common for *APX1-FSD1*	6	LEC2, NAC046, AGL15, Putative C2H2-zinc-finger-type (AT3G53600), MYB52, YAB1
TFs common for *DHAR1-FSD1*	2	Putative C2H2-zinc-finger-type (AT5G03510), STY1
TFs common for *APX1-DHAR1*	18	HB15, MYB61, KAN4, ARF3, HB51, GATA12, DEAR3, GT2L, HSFC1, DAZ1, MYB55, WOX13, ZAT6, Putative C2H2-zinc-finger-type (AT4G35610), DAG2, KAN1, Putative F-box/kelch-repeat protein (AT1G12870), CCA1
TFs specific for *FSD1*	3	BZIP60, SPL8, TGA2
TFs specific for *APX1*	2	TCP16, TCP15
TFs specific for *DHAR1*	9	TGA1, ORA47, MYC2, WRKY38, WRKY12, WRKY18, REM1, HB, WRI1

FIGURE 2 | Graphical **(A)** and tabular **(B)** overview of common transcription factors (TFs) predicted to regulate the expression of *FSD1*, *APX1*, and *DHAR1* under the regulation of mitogen-activated protein kinases.

infection, as CDPKs modulate the activity of RBOHD (reviewed by Gilroy et al., 2016). Both Ca^{2+} and ROS waves may be integrated *via* RBOHs, Ca^{2+} channel TWO-PORE CHANNEL 1, and CDPKs such as CPK/CBL-CIPKs (CBL-interacting protein kinases; Choi et al., 2014; Gilroy et al., 2016). Moreover, NOXs possess a special hydrophilic N-terminal Ca^{2+}-binding site, the so called EF-hand motif, activated by Ca^{2+} (reviewed by Hu et al., 2020).

Under drought stress, ion channels in the plasma membrane are activated by ROS (Pei et al., 2000; Dodd et al., 2010), whereas H_2O_2 can induce the channel activity of *Arabidopsis* ANNEXIN 1 (AtANN1) and STELAR K^+ OUTWARD RECTIFIER (SKOR;

Richards et al., 2014; reviewed by Demidchik, 2018). In turn, CDPKs regulate the production of ROS by the phosphorylation of serine residues at the C-terminus of NOXs in a Ca^{2+}-dependent manner (Kobayashi et al., 2007).

Moreover, *Arabidopsis* CPK5 and RBOHD are key components of a self-propagating activation circuit mediating cell-to-cell communication in plant immunity responses (Dubiella et al., 2013). Further, a plasma membrane anchored AtCPK27 is required for the plant response to salt stress, as its disruption causes oxidative burst and H_2O_2 accumulation in primary roots (Zhao et al., 2015). CPK4, CPK5, CPK6, and CPK11 regulate ROS production in *Arabidopsis*, possibly by the direct phosphorylation of RBOHB (Boudsocq et al., 2010). Finally, endoplasmic reticulum membrane-localized *B. napus* CPK2 interacts with RBOHD during cell death, accompanied by ROS accumulation (Wang et al., 2018).

Therefore, reciprocal ROS and Ca^{2+} signaling pathways orchestrate the production and accumulation of these secondary messengers and play vital roles in plant adaptation to adverse environmental conditions.

Modulation of Antioxidant Enzymes by Ca^{2+} Signaling

The impact of Ca^{2+} signaling on antioxidant enzymes was demonstrated by experiments with exogenous Ca^{2+} or the genetic manipulation of Ca^{2+} transporters. For example, $CaCl_2$ enhances the tolerance of rice seedlings to arsenic stress by the reduction of ROS content and the stimulation of MDHAR, DHAR, CAT, GLUTATHIONE PEROXIDASE, and SOD (Rahman et al., 2015). Ca^{2+}-dependent ATPases are Ca^{2+} transporters involved in multiple stress signaling pathways, physiological processes such as stomatal closure and programmed cell death, and ROS homeostasis (reviewed by Marcec et al., 2019). Furthermore, OsACA6, a Ca^{2+}-ATPase from rice, can modulate ROS levels under salinity and drought stresses by the upregulation of CAT, APX, and GR activities, whereas plants overexpressing *OsACA6* show enhanced tolerance to these abiotic stress factors (Huda et al., 2013).

It is known that CDPKs/CPKs are crucial for the regulation of both ROS generation and metabolism under both abiotic and biotic stress conditions and are closely related to enhanced antioxidant enzyme activities in plants, e.g., under the attack of herbivores or microbial pathogens (Romeis and Herde, 2014; Marcec et al., 2019). For instance, AtCPK8 is a component of the ABA- and Ca^{2+}-mediated signaling pathway, which phosphorylates and activates CAT3 at Ser261 in stomatal guard cells during drought stress (Zou et al., 2015). The CPK-mediated regulation of CAT activity was reported under salt stress conditions, namely CPK12 controls ion homeostasis and ROS accumulation *via* CAT, APX, and SOD activities, thereby impacting *Arabidopsis* salt stress tolerance (Zhang et al., 2018). CPKs also affect other components of the ROS-decomposing machinery. Thus, OsCPK12 from rice enhances salt stress tolerance through decreasing the ROS content, owing to the elevated expression of *OsAPX2, OsAPX8*, and reduced expression of NOX called *OsBOHI* but, at the same time, negatively modulates blast disease resistance (Asano et al., 2012). Ca^{2+}-regulated expression of *APX* was also observed in maize, as Ca^{2+} activation of ZmCCaMK (Ca^{2+}/calmodulin-dependent protein kinase from *Z. mays*) is required for the expression and activation of *APX2* (and also *SOD4*) in response to brassinosteroids (Yan et al., 2015).

Hence, Ca^{2+} homeostasis and subsequent Ca^{2+} signal transduction *via* CDPKs (**Figure 3**) play an inevitable role in the regulation of antioxidant protection machinery by enhancing plant plasticity and resistance to environmental challenges.

Reactive Nitrogen Species-Mediated Regulation of Antioxidant Enzymes

RNS interplay with ROS-signaling pathway by both direct and indirect modulation of antioxidant enzymes activity (Lindermayr and Durner, 2015; Farnese et al., 2016). Thus, exogenous NO donor sodium nitroprusside (SNP) alleviates the detrimental effects of arsenic stress by stimulating the SOD, CAT, GST, and APX activities (Shukla and Singh, 2015). Potentiated action of SNP and silicon (Si) significantly increased the activities of SOD, guaiacol peroxidase, APX, GR, and GST in arsenic-stressed *B. juncea* plants (Ahmad et al., 2020). SNP also alleviates cadmium (Cd^{2+})-induced oxidative damage in *O. sativa* by the pronounced enhancement of the SOD, APX, guaiacol peroxidase, and CAT activities (He et al., 2014). A similar mechanism of the protective effects of SNP under nickel stress by upregulating the transcript levels of CAT, guaiacol peroxidase, APX, GR, and SOD genes was described (Rizwan et al., 2018). Both NO and H_2O_2 are involved in the regulation of ascorbate and glutathione metabolism by JA in *Agropyron cristatum* leaves, as JA stimulates the production of both secondary messengers and enhances the activities of APX, GR, MDHAR, DHAR, and enzymes of ascorbate biosynthesis (Shan and Yang, 2017). The link between NO and glutathione exists as well, as SNP modulates glutathione synthesis in *Medicago truncatula* roots by upregulation of *GAMMA-GLUTAMYLCYSTEINE SYNTHETASE* and *GLUTATHIONE SYNTHETASE* but not *HOMOGLUTATHIONE SYNTHETASE* (Innocenti et al., 2007).

Covalent loss- and/or gain-of-function NO-induced post-translational modifications (PTM) of antioxidant enzymes such as S-nitrosylation and tyrosine nitration reciprocally regulate ROS homeostasis, thereby preserving the balance between ROS production and scavenging in plant cells under natural and stress conditions (Yang et al., 2015; Romero-Puertas and Sandalio, 2016; Kohli et al., 2019). Thus, S-nitrosylation at Cys32 increases the activity of cytosolic APX1 under salinity stress (Begara-Morales et al., 2014), enhances the plant resistance to methyl viologen, but negatively modulates the plant immune response triggered by flagellin elicitor peptide flg22 (Yang et al., 2015). ROS reduces the degree of S-nitrosylation through inhibition of S-nitrosoglutathione reductase (GSNOR), a Zn^{2+}-dependent class III alcohol dehydrogenase enzyme controlling the pool of S-nitrosoglutathione (GSNO)-the storage and long-distance transport NO form. This mechanism leads to higher

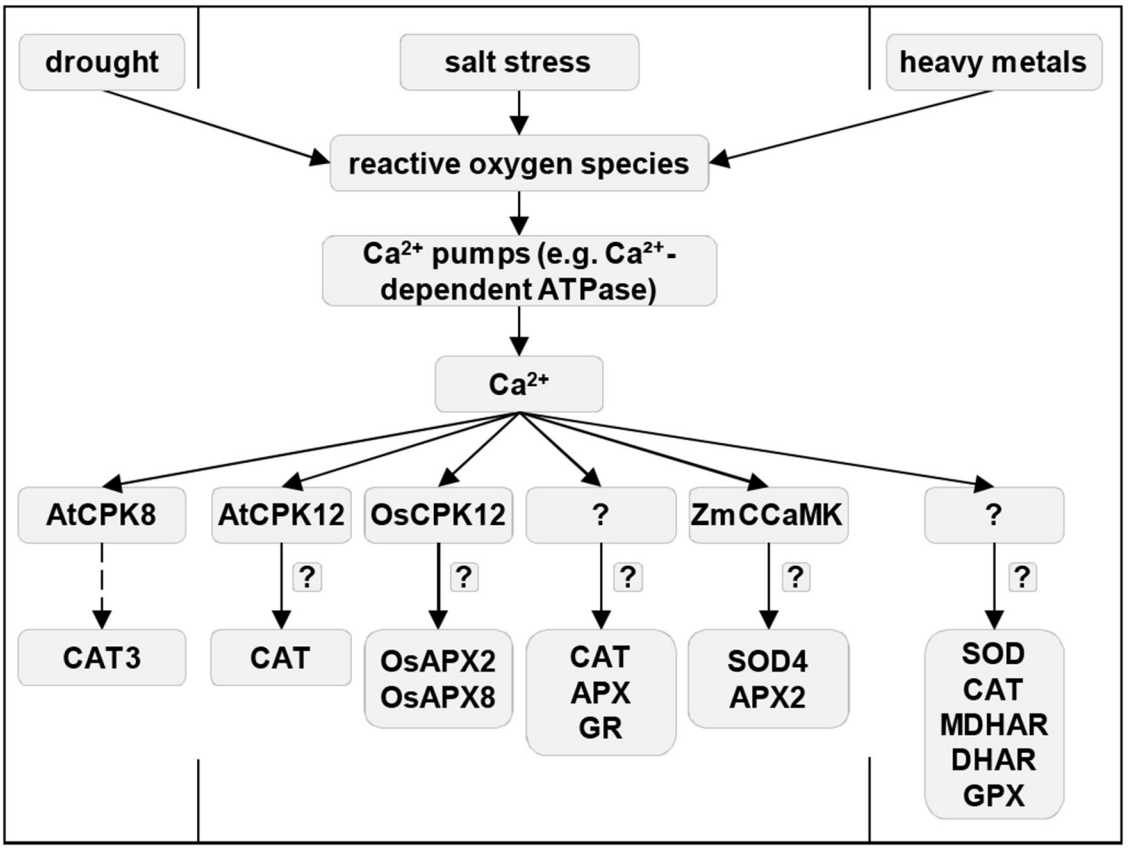

FIGURE 3 | Mechanisms of Ca^{2+}-mediated regulation of antioxidant enzymes during stress in plants. Solid arrows indicate induction, and dashed arrows show phosphorylation. Question mark means an unknown regulation. APX, ascorbate peroxidases; CAT, catalase; CPK, Ca^{2+}-dependent protein kinases; DHAR, dehydroascorbate reductase; GPX, glutathione peroxidase; GR, glutathione reductase; MDHAR, monodehydroascorbate reductase; SOD, superoxide dismutase; ZmCCaM, Ca^{2+}/calmodulin-dependent protein kinase from *Zea mays*.

glutathione levels, transcripts, and activities of glutathione-dependent antioxidant enzymes (Kovacs et al., 2016). This PTM at Cys230 inhibits CAT1 activity in response to Cd^{2+} in pea leaves (Ortega-Galisteo et al., 2012). In turn, another NO-induced PTM, namely $ONOO^-$-induced tyrosine nitration, inhibits the activity of APX (Begara-Morales et al., 2014), MDHAR (Begara-Morales et al., 2015), CAT (Chaki et al., 2015), MSD1, peroxisomal CSD3, and chloroplastic FSD3 (Holzmeister et al., 2015). It is noteworthy that CAT activity is affected not only by S-nitrosylation but also by H_2S-induced persulfidation (Palma et al., 2020).

GSNOR is apparently a significant convergence point between ROS- and RNS-signaling, as ROS inhibits GSNOR activity by oxidation or the Zn^{2+}-release from the GSNOR structure (Tichá et al., 2017; Lindermayr, 2018). The activity and stability of GSNOR1 are also regulated by ROG1 (REPRESSOR OF GSNOR1)-mediated transnitrosylation at Cys10, which, by this mechanism, affects NO-based redox signaling in plants. Surprisingly, ROG1 is identical to CAT3 (Chen et al., 2020), assigning unexpected roles to this antioxidant enzyme. Last but not least, ROS and RNS cooperatively regulate MAPK signaling in a broad range of abiotic stresses, such as heavy metal exposure as well as drought and osmotic stress (reviewed by Farnese et al., 2016).

In summary, the expression and activity of antioxidant enzymes indispensably depend on their RNS mediated PTMs (**Figure 4**).

Transcriptional and Post-transcriptional Regulation of Antioxidant Enzymes

Antioxidant enzymes are also regulated at the level of transcription, which is mediated by diverse TFs, not necessarily acting downstream of MAPKs. They are rapidly activated by redox perturbations in photosynthetic electron transport during retrograde signaling from plastid to nucleus encompassing metabolites (e.g., phosphoadenosines, tetrapyrroles, carotenoid oxidation products, carbohydrate metabolites, and isoprenoid precursors) and ROS (Chan et al., 2016; Exposito-Rodriguez et al., 2017). The rapid activation of MAPK cascades conditions this signaling process. Furthermore, TFs alone might be controlled by redox modifications (Dietz, 2014).

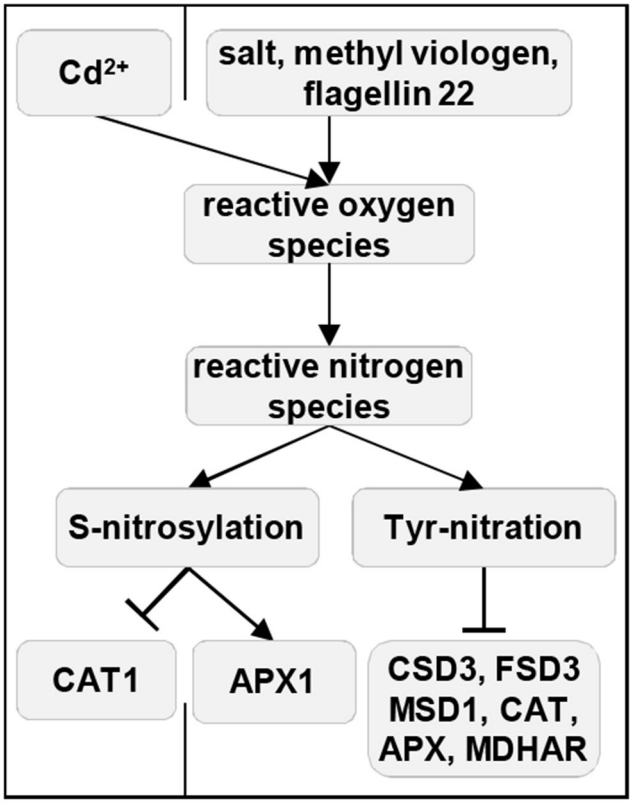

FIGURE 4 | Reactive nitrogen species-mediated direct regulation of antioxidant enzymes during plant stress responses. Solid arrows indicate induction, and ⊥ indicates negative regulation. APX, ascorbate peroxidase; CAT, catalase; FSD, Fe superoxide dismutase; MDHAR, monodehydroacorbate reductase; MSD, Mn superoxide dismutase.

Compelling evidence suggests the transcriptional remodeling of ROS-responsive genes (reviewed in He et al., 2018; Li et al., 2018). Gadjev et al. (2006) performed a microarray transcriptomic analysis focused on the expression of exogenous ROS-induced TFs. More than 500 annotated *Arabidopsis* TFs showed a distinct expression pattern upon ROS, and some of them displayed the ability to modulate the expression of antioxidant enzymes (Gadjev et al., 2006). TF families most often connected to the transcriptional control of antioxidants in response to ROS include WRKY, Zinc finger (Znf), NAC, AP2/ERF, DREB, MYB, or bZIP (Khedia et al., 2019).

In general, numerous reports demonstrate the altered expression of antioxidant enzymes in transgenic or mutant plants with modified TF expression. Contrarily, only a few studies demonstrate the direct binding of TFs to the promoter sequences of antioxidant enzymes. It is known that *FSD1* and *CSD*s are transcriptionally orchestrated *via* a TF called SQUAMOSA PROMOTER BINDING PROTEIN-LIKE 7 (SPL7; Yamasaki et al., 2007, 2009; Garcia-Molina et al., 2014) in a Cu-dependent manner. Under copper deficiency, SPL7 binds to an SPL-specific SBP (SQUAMOSA PROMOTER BINDING PROTEIN DOMAIN) promoter sequence and induces the expression of *FSD1*, leading to increased abundance and activity of the FSD1 enzyme. At the same time, *CSD1*, *CSD2*, and COPPER CHAPERONE FOR SOD (*CCS*) are post-transcriptionally downregulated by miR398, which is induced by the binding of SPL7 to its promoter sequence (Cohu et al., 2009; Yamasaki et al., 2009). Therefore, SPL7 is an important modulator of copper balance *via* Cu-responsive proteins and miRNAs (reviewed by Pilon et al., 2011; Pilon, 2017; Araki et al., 2018). In turn, miR398 suppresses the mRNA of *CSD1* and *CSD2* after treatment with high sucrose content in the culture medium (Dugas and Bartel, 2008). Importantly, miR398 levels are downregulated to allow the post-transcriptional *CSD1* and *CSD2* mRNA accumulation leading to elevated (oxidative) stress tolerance (Sunkar et al., 2006; Khraiwesh et al., 2012). SPL7 is also implicated in the circadian regulation of *FSD1* expression (Perea-García et al., 2016). Further, *CSD1* and *CSD2* expression is also regulated by miR408 (Ma et al., 2015), illustrating that the post-transcriptional control of *SOD* expression is quite complex.

The equilibrium between *CSDs* and *FSD1* is influenced by *ZAT12* (Znf protein) because its overexpression leads to the increased expression of *CSD1*, *CSD2,* and *CCS*, while *FSD1* is downregulated (Davletova et al., 2005b). The induction of *ZAT12* expression is reported as an abiotic stress marker during high light exposure, low temperature, oxidative stress (triggered by H_2O_2 and methyl viologen), and osmotic and salinity stress (Kreps et al., 2002; Rizhsky et al., 2004a; Davletova et al., 2005b; Vogel et al., 2005; Xu et al., 2017). Furthermore, the expression of *FSD1*, *APX1,* and *APX2* depends on ZAT10 (Mittler et al., 2006) and RELATED TO APETALA-2.6L (RAP2.6L; Liu et al., 2012), while this positive regulation determines the resistance of *Arabidopsis* to abiotic stresses.

MYB49 has been reported to be an important TF for plant responses to drought, salt, and heavy metal stresses (Cui et al., 2018; Zhang et al., 2019; Zhang P. et al., 2020). In this respect, a transgenic tomato line overexpressing *MYB49* showed higher resistance to drought and salt stresses and increased its SOD and peroxidase activity (Cui et al., 2018). Additionally, an *Arabidopsis* transgenic line overexpressing functional repressor of MYB49, a chimeric AtMYB49-SRDX called SRDX49, showed downregulation of *CSD2* and several peroxidases (Zhang P. et al., 2020). Nevertheless, the binding of the TFs of ZAT, RAP, or MYB families to the promoter sequence of SODs has not been confirmed yet.

The expression patterns of *CATs* are closely correlated with plant senescence, and they contribute to the redox control of this process (Zimmermann et al., 2006; Mhamdi et al., 2012). The transcriptional regulation of *CATs* is complex and requires several TFs. *CATs* are directly controlled by WRKY53, which works downstream of redox-sensitive regulatory factor WRKY25 during senescence and oxidative stress response (Miao et al., 2004; Doll et al., 2020). *Arabidopsis wrky25/cat2* double mutant exhibit upregulated H_2O_2 levels in comparison with the wild-type or *cat2* single mutant (Doll et al., 2020). This ROS inducible WRKY25-WRKY53-CAT signaling hub can cross talk with MEKK1, which interacts with and phosphorylates

TABLE 1 | Phosphorylation sites experimentally found in antioxidant enzymes by mass spectrometry, retrieved from PhosPhat database.

Protein	Description	Modified peptide	Treatment	Position	References
AT2G28190	Copper/zinc superoxide dismutase 2	ALTVV(pS)AAK	Auxin	S62	Zhang et al., 2013
AT5G18100	Copper/zinc superoxide dismutase 3	GGHKLSK(pS)TGNAGSR	Isoxabene	S141	n.a.
AT3G10920	Manganese superoxide dismutase 1	NLAPS(pS)EGGGEPPK	Isoxabene	S114	n.a.
AT5G51100	Iron superoxide dismutase 2	EQEGTE(pT)EDEENPDDEVPEVYLD(pS)DIDVSEVD	Abscisic acid	S297_T280	Wang et al., 2013b
		EQEGTETEDEENPDDEVPEVYLD(pS)DIDVSEVD	Abscisic acid	S297	Wang et al., 2013b
		EQEG(pT)ETEDEENPDDEVPEVYLD(pS)DIDVSEVD	Abscisic acid	S297_T278	Wang et al., 2013b
		EQEGTE(pT)EDEENPDDEVPEV(pY)LDSDIDVSEVD	Abscisic acid	Y294_T280	Wang et al., 2013b
		EQEGTE(pT)EDEENPDDEVPEVYLDSDIDVSEVD	Abscisic acid	T280	Wang et al., 2013b
		EQEGTETEDEENPDDEVPEV(pY)LDSDIDVSEVD	Abscisic acid	Y294	Wang et al., 2013b
AT1G20630	Catalase 1	YPT(pT)PIV(C*)SGNR	Cell culture	T409	Sugiyama et al., 2008
AT4G35090	Catalase 2	LNVRP(pS)I		S491	Bhaskara et al., 2017
			Abscisic acid	S491	Umezawa et al., 2013
		TF(pT)PERQER	Ionizing radiation	T439	Roitinger et al., 2015
AT1G20620	Catalase 3	CAEKVP(pT)PTNSYTGIR	flg22	T408	Rayapuram et al., 2018
					Rayapuram et al., 2014
			End of day		Reiland et al., 2009
			flg22		Rayapuram et al., 2018
			flg22		Rayapuram et al., 2014
		CAEKVPTP(pT)NSYTGIR	flg22	T410	Rayapuram et al., 2014
			flg22		Rayapuram et al., 2018
		VP(pT)PTN(pS)YTGIR	Ionizing radiation	T408_S412	Roitinger et al., 2015
		GFFEVTHDISNL(pT)CADFLR	Nitrogen starvation/nitrate resupply	T85	
					Engelsberger and Schulze, 2012
		LNVRP(pS)I		S491	Bhaskara et al., 2017
			Abscisic acid		Umezawa et al., 2013
		(C*)AEKVPTPTNS(pY)TGIR	Abscisic acid	Y413	Wang et al., 2013b
		(C*)AEKVPTPTNSY(pT)GIR	Abscisic acid	T414	Wang et al., 2013b
AT4G08390	Stromal ascorbate peroxidase	VDASGPED(C*)PEEGRLPDAGPP(pS)PATHLR		S236	Nakagami et al., 2010
			Nitrate starvation/nitrate resupply	S236	Wang et al., 2012
			Abscisic acid	S236	Wang et al., 2013b
				S236	Van Leene et al., 2019
			Nitrate starvation/nitrate resupply	S236	Wang et al., 2013c
		VDASGPED(C*)PEEGRLPDAGPPSPA(pT)HLR	Abscisic acid	T239	Wang et al., 2013b
AT4G32320	Ascorbate peroxidase 6	FFEDF(pT)NA(pY)IK	Nitrogen starvation/nitrate resupply	T313_Y316	n.a.
AT1G77490	Thylakoidal ascorbate peroxidase	ELSD(pS)(oxM)(K*)(K*)	Ionizing radiation	S373	Roitinger et al., 2015
		(oxM)ISPK(C*)AA(pS)DAAQLISAK	flg22	S81	Mithoe et al., 2012
		LPDAGPP(pS)PADHLR	Ionizing radiation	S215	Roitinger et al., 2015
AT5G16710	Dehydroascorbate reductase 1	FQPST(pT)AGVLSASVSRAGFIKR	Abscisic acid	T11	Umezawa et al., 2013

(Continued)

TABLE 1 | Continued

Protein	Description	Modified peptide	Treatment	Position	References
AT1G75270	Dehydroascorbate reductase 2	(s)KDANDG(s)EKALVDELEALENHLK	Ethylene, ambient air		Li et al., 2009
AT3G52880	Monodehydroascorbate reductase 1	VVGAFMEGG(pS)GDENK		S400	Sugiyama et al., 2008
			Ionizing radiation	S400	Roitinger et al., 2015
				S400	Nakagami et al., 2010
				S400	Van Leene et al., 2019
		ARP(pS)AESLDELVK		S416	Nakagami et al., 2010
			None	S416	Reiland et al., 2011
			Nitrate starvation/nitrate resupply	S416	Wang et al., 2013c
			None	S416	Mayank et al., 2012
				S416	Reiland et al., 2009
				S416	Bhaskara et al., 2017
				S416	Van Leene et al., 2019
			flg22	S416	Rayapuram et al., 2018
				S416	Choudhary et al., 2015
			Abscisic acid	S416	Wang et al., 2013b
			Abscisic acid	S416	Umezawa et al., 2013
			Abscisic acid	S416	Xue et al., 2013
				S416	Sugiyama et al., 2008
			Ionizing radiation	S416	Roitinger et al., 2015
		ARP(s)AE(s)LDELVKQGI(s)FAAK			Reiland et al., 2009
		ARP(s)AE(s)LDELVKQGI(s)FAAK	None		Reiland et al., 2011
		ADLSAK(pS)LVSATGDVFK	Abscisic acid	S104	Umezawa et al., 2013
		ARPSAE(pS)LDELVK	Nitrate starvation/nitrate resupply	S419	Wang et al., 2013c
		GAD(pS)(K*)NILYLR	Ionizing radiation	S139	Roitinger et al., 2015
AT5G03630	Monodehydroascorbate reductase 2	AQP(pS)VESLEVLSK	flg22	S417	Rayapuram et al., 2018
			End of night	S417	Reiland et al., 2009
			flg22	S417	Rayapuram et al., 2018
			Ionizing radiation	S417	Roitinger et al., 2015
			flg22	S417	Rayapuram et al., 2014
			None	S417	Reiland et al., 2011
			flg22	S417	Rayapuram et al., 2018
			flg22	S417	Rayapuram et al., 2018
			End of night	S417	Reiland et al., 2009
			None	S417	Mayank et al., 2012
			Nitrate starvation/nitrate resupply	S417	Wang et al., 2013c
			Abscisic acid	S417	Wang et al., 2013b
				S417	Van Leene et al., 2019

(Continued)

TABLE 1 | Continued

Protein	Description	Modified peptide	Treatment	Position	References
				S417	Sugiyama et al., 2008
			None	S417	Reiland et al., 2011
			Abscisic acid	S417	Umezawa et al., 2013
			Ethylene	S417	Yang et al., 2013
			Abscisic acid, mannitol	S417	Xue et al., 2013
				S417	Choudhary et al., 2015
		AQP(pS)VE(pS)LEVLSK	flg22	S420_S417	Rayapuram et al., 2018
		VVGAFLEGG(pS)PEENNAIAK	Abscisic acid	S401	Wang et al., 2013b
AT3G09940	Monodehydroascorbate reductase 3	G(pT)VA(pT)GFSTNSDGEVTEVK	Epibrassinolide	T228_T231	Lin et al., 2015
AT3G27820	Monodehydroascorbate reductase 4	GTVLTSFEFD(pS)N(K*)(K*)	Ionizing radiation	S234	Roitinger et al., 2015
AT3G54660	Glutathione reductase 2	(pT)AAGV	drought stress	T561	Bhaskara et al., 2017

WRKY53 (Miao et al., 2007). In addition, the *CAT2* promoter interacts with WRKY75, leading to *CAT2* downregulation depending on plant age, senescence, salicylic acid, H_2O_2, and multiple plant hormones (Guo et al., 2017). The *CAT3* expression is directly induced by two isoforms of AP2/ERF4 family TFs, having a different impact on plant senescence according to the alternative polyadenylation of pre-mRNAs. The age-dependent expression of *CAT3* and plant senescence are controlled by the expression ratio of *ERF4-A* (inducer) and *ERF4-R* (repressor) isoforms (Riester et al., 2019). Recently, MYC2 was experimentally approved to bind to the promoter of *Arabidopsis CAT2,* leading to its downregulation during leaf senescence in a JA-dependent manner. Such downregulation promotes H_2O_2 accumulation and the activation of senescence-associated genes (Zhang Y. et al., 2020). Finally, *CAT2* expression is also regulated by CDF4 (CYCLING DOF FACTOR 4) during senescence (Xu et al., 2020).

The ascorbate–glutathione cycle represents a very sensitive and efficient system for H_2O_2 decomposition, requiring not only strict redox control but also the synchronized expression of respective enzymes. APXs are major components of the ascorbate–glutathione cycle and comprise chloroplastic, peroxisomal, mitochondrial, and cytosolic isoforms, which efficiently eliminate excessive H_2O_2 by using ascorbate as an electron donor (Foyer and Noctor, 2011). The transcriptional control of *APXs* relies on multiple TFs, whereas RAP2s (also known as ERF-VIIs) exhibit the highest affinity toward both chloroplastic and cytosolic *APXs*. Chloroplastic stromal and thylakoid *APX* isoforms (Rudnik et al., 2017) and *2-Cys PEROXIREDOXIN A* (Shaikhali et al., 2008; Rudnik et al., 2017) are regulated by redox-sensitive RAP2.4a directly interacting with their promoters under photooxidative stress and increased ROS levels. Seven additional members of the RAP2.4 family also demonstrate an ability to bind to the promoters of the genes mentioned earlier and to fine-tune their expression (Rudnik et al., 2017). In addition, RADICAL-INDUCED CELL DEATH 1 (RCD1), a protein integrating mitochondrial and chloroplastic ROS signals with pleiotropic functions (Shapiguzov et al., 2019), interacts with RAP2.4 under mild and severe oxidative stress and promotes the activation of downstream genes (Hiltscher et al., 2014). The preference of RAP2 for *APXs* regulation has also been demonstrated for RAP2.6L because the overexpression of this TF causes the overexpression of cytosolic *APX1* and improves plant tolerance against waterlogging stress (Liu et al., 2012). Besides RAP2.6L, ZAT12, ZAT7, and WRKY25 are also required for the proper expression of cytosolic *APX1* during oxidative stress (H_2O_2, methyl viologen, heat shock, or wounding; Rizhsky et al., 2004b). *APX2* and *APX7* are expressed under the control of HSFA3, downstream of a TF named DEHYDRATION-RESPONSIVE ELEMENT-BINDING 2C (DREB2C), having an impact on plant resistance to oxidative stress (Hwang et al., 2012; Song et al., 2016). The induction of *APX2* transcription as a response to high light initiates photosynthetic redox homeostasis alterations occurring upon the nuclear accumulation and activation of HSFA1D (Jung et al., 2013). C2H2-type zinc finger protein ZFP36 is among the important *APX* regulators, as this TF binds to the promoter

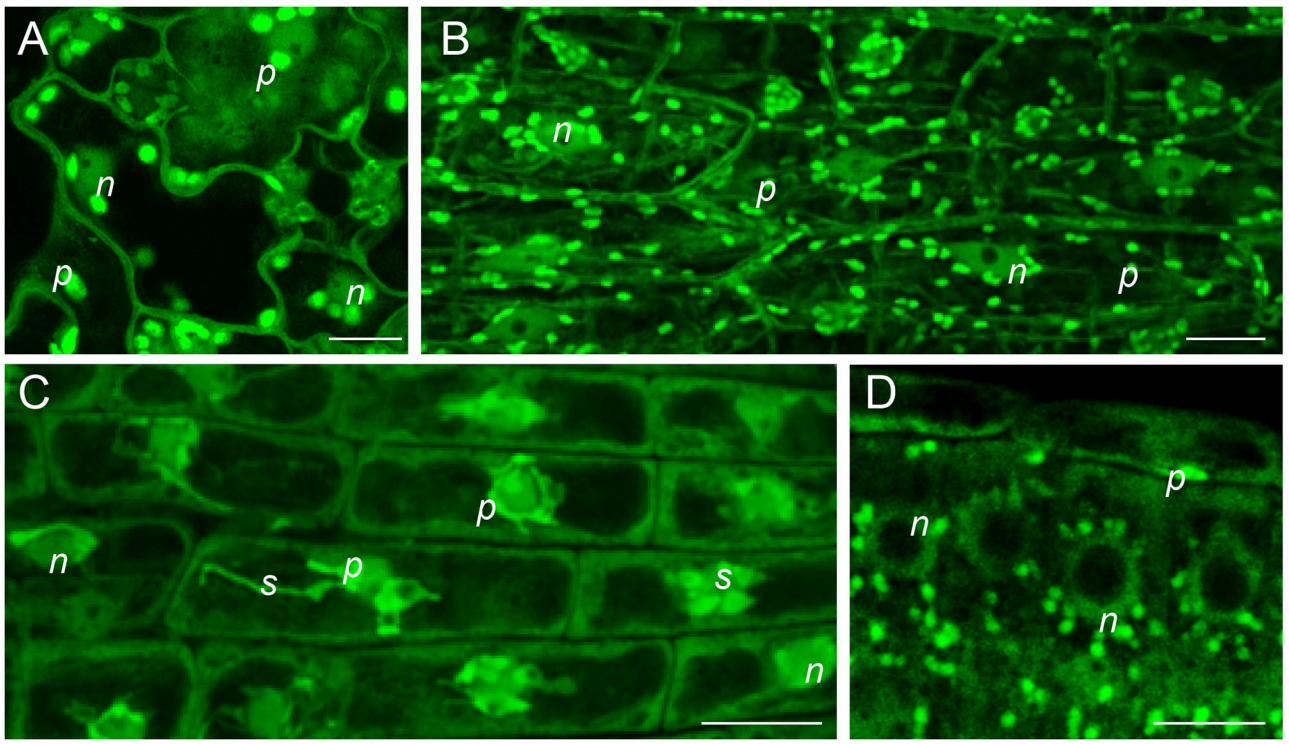

FIGURE 5 | *In vivo* subcellular localization of FSD1-GFP in plastids, nuclei and cytoplasm of 4-day-old *Arabidopsis fsd1-1* mutant harboring *proFSD1::FSD1:GFP* construct (Dvořák et al., 2020) as revealed by confocal laser scanning microscope equipped with an Airyscan detector. **(A)** Pavement cells of leaf epidermis; **(B)** epidermal cells of hypocotyl; **(C)** lateral root cap cells; **(D)** root meristematic cells. n, nucleus; p, plastid; s, stromule. Scale bars: **(A**, **C**, **D)** 10 μm; **(B)** 20 μm.

sequence and activates the *OsAPX1* gene in rice. This activation is enhanced by LATE EMBRYOGENESIS ABUNDANT 5 (OsLEA5), a protein interacting with ZFP36, which regulates *OsAPX1* expression during seed germination (Huang et al., 2018). In addition, ZFP36 was found to be important during rice responses to oxidative and abiotic stresses (Zhang et al., 2014). Another TF called ANAC089 has been reported as a negative regulator of stromal *APX* in *Arabidopsis* and can play different roles during plant acclimation to low, normal, and high light conditions. ANAC089 decreases the expression of stromal *APX* under highly reducing conditions induced by a DTT treatment (Klein et al., 2012).

Knowledge on the transcriptional control of *DHARs*, *MHARs,* and *GRs*, encoding enzymes implicated in ascorbate regeneration during the ascorbate–glutathione cycle, is limited. The mutant analysis of an AP2/ERF domain-containing TF showed the upregulation of *DHAR1* and the downregulation of *MDHAR3* in response to H_2O_2 treatment (Sewelam et al., 2013). Recently, R2R3-type MYB from *Pyrus betulaefolia* (PbrMYB5) was reported as TF important for the expression of *PbrDHAR2*. The genetic manipulation of PbrMYB5 in tobacco positively correlates with chilling when overexpressor lines show a higher expression of *NtDHAR2* and elevated levels of ascorbate (Xing et al., 2019). Finally, regulation by miRNA (PN-2013) interference was reported for wheat *MDHAR* (Feng et al., 2014).

Phosphorylation of Antioxidant Enzymes

PTMs of proteins represent versatile, dynamic, and flexible regulatory mechanisms for the reprogramming of a wide range of cellular functions. For example, these processes ensure the fast and targeted activation of plant immune responses upon pathogen attacks. Generally, PTMs affect enzymatic activities, subcellular localization, protein interactions, and stability (reviewed in Withers and Dong, 2017; Ruiz-May et al., 2019; Vu et al., 2018;). Among PTMs, the reversible phosphorylation of proteins represents a driving force of signaling processes during plant development and stress challenges (Arsova et al., 2018). Several antioxidant proteins are modified by direct phosphorylation, mainly by proteomic approaches (**Table 1**).

Although the phosphorylation of SODs has been documented for human SOD1 (Fay et al., 2016; Tsang et al., 2018) and SOD2 (Candas et al., 2013; Jin et al., 2015), mouse SOD2 (Candas et al., 2013), or yeast SOD1 (Leitch et al., 2012; Tsang et al., 2014), the phosphorylation of SOD isoforms in plants has not been approved by genetic means so far. Mammalian SOD1 is phosphorylated at Thr2 (Fay et al., 2016) and Thr40 (Tsang et al., 2018), having a pronounced impact on its activity. For example, the mammalian target of rapamycin complex 1 (mTORC1) is a negative regulator of SOD1 activity under nutrient-rich conditions by reversible phosphorylation at Thr40 (Tsang et al., 2018). Yeast SOD1 is phosphorylated at Ser38 under low oxygen conditions, which allows its interaction with CCS

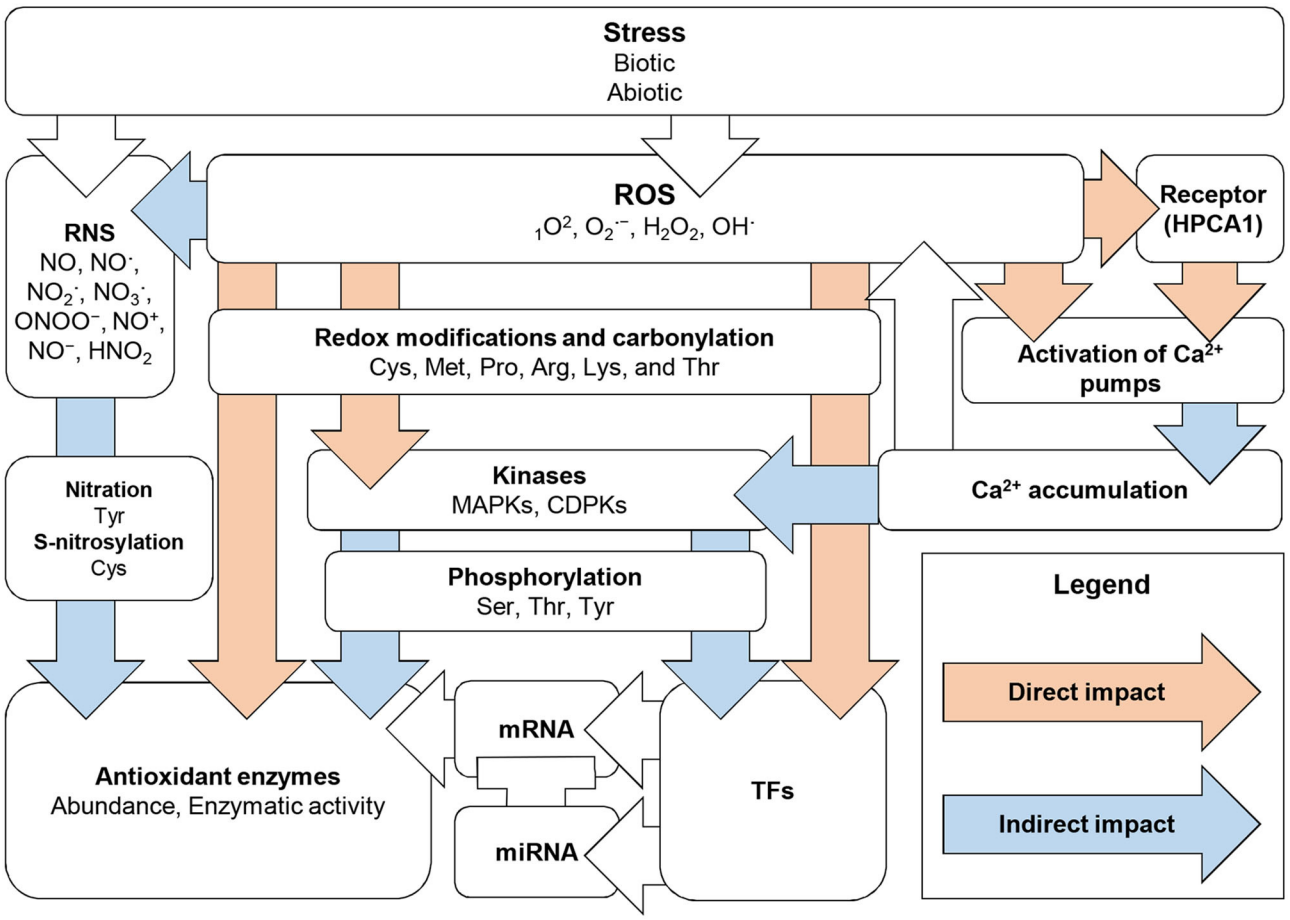

FIGURE 6 | Overview of direct and indirect mechanisms of antioxidant enzyme regulation in response to stress-induced ROS generation.

and, consequently, proper folding and activation (Leitch et al., 2012). Contrarily, the double phosphorylation of yeast SOD1 at Ser60 and Ser99 by a DNA damage checkpoint kinase Dun1 during oxidative stress leads to the translocation of this SOD to the nucleus, where it binds to the promoters and activates ROS-responsive and DNA repair genes (Tsang et al., 2014). Recently, the first *in planta* evidence of the nuclear localization of SODs was reported in plants (Dvořák et al., 2020). Thus, in addition to well-known protective functions during oxidative stress, plant SODs might have similar functions in the nucleus as yeast SOD1 (**Figure 5**). However, this working hypothesis needs to be experimentally tested in the future. Rarely, phosphoproteomic studies have reported on the detection of phosphorylated amino acid residues in plant SODs. A gel-based study on mitochondrial phosphoproteomes identified phosphorylated MSD1 (Bykova et al., 2003). In addition, CSD2 and CSD3 were found to be phosphorylated in response to auxin and isoxaben, respectively (Zhang et al., 2013; **Table 1**). Multiple phosphorylation sites were also detected in FSD2 after ABA treatment (Wang et al., 2013b). These findings demonstrate that the phosphorylation of plant SODs may have some important functions that need to be elucidated in future studies.

On the other side, there is quite rich phosphoproteomic evidence on the phosphorylation of CAT isoforms in plants (**Table 1**). CAT phosphorylation has been broadly documented in human research (Kumar et al., 2010; Rafikov et al., 2014). A recent study suggested that high light-induced H_2O_2 is regulated by the interaction between CAT isoforms and BRASSINOSTEROID-INSENSITIVE 1 ASSOCIATED RECEPTOR KINASE 1 (BAK1), leading to CAT1 phosphorylation and activation (Zhang S. et al., 2020). CAT3 activity is enhanced through phosphorylation by CPK8, leading to H_2O_2 decomposition under drought stress (Zou et al., 2015). In rice, the CATC isoform is phosphorylated by SALT TOLERANCE RECEPTOR-LIKE CYTOPLASMIC KINASE 1 (STRK1), which acts as a positive regulator of salt and oxidative stress tolerance (Zhou et al., 2018). STRK1 is anchored in the plasma membrane *via* palmitoylation, where it interacts and phosphorylates the CATC isoform at Tyr210 (Zhou et al., 2018).

Notably, H_2O_2 decomposition is controlled by phosphorylation also within the ascorbate–glutathione cycle. Based on phosphoproteomic data, the stromal and thylakoid APX and MDAR1, MDAR2, and GR2 are enzymes prone to phosphorylation (**Table 1**). Thylakoid APX is negatively

regulated by WHEAT KINASE START1 (WKS1)-dependent phosphorylation in wheat infected by stripe rust-inducing fungi *Puccinia striiformis* f. sp. *tritici*. Such decreased activity of thylakoid APX leads to the enhanced accumulation of peroxides, causing cell death upon pathogen attacks (Gou et al., 2015).

CONCLUSION AND FUTURE PROSPECTS

In summary, the expression and activities of antioxidant enzymes are controlled both directly and indirectly at multiple levels with the involvement of ubiquitous secondary messengers (ROS, RNS, and Ca^{2+}), PTMs (phosphorylation and redox-dependent ones), TFs, and other precise mechanisms (**Figure 6**). Currently, data on the coordination of the transcriptional and post-translational regulation of these enzymes are scarce. Moreover, the impact of protein–protein interactions on the functionality of antioxidant enzymes should not be underestimated. The complexity is increased by the requirement for rapid and spatially-specific antioxidant activation, which has to occur in subcellular- and tissue-dependent manners.

Further proteomic, genetic, cell, and molecular biology integrative investigations are necessary to uncover precise spatiotemporal regulations of individual antioxidant enzymes during plant development and stress responses. In addition, up-to-date proteomic, phospho- and redox-proteomic approaches might uncover new MAPK and CDPK targets modulating antioxidant defense during oxidative stress. The use of these techniques on transgenic plant lines with modified abundances of certain antioxidant enzymes may significantly contribute to the elucidation of their developmental and stress-related functions.

AUTHOR CONTRIBUTIONS

PD and AZ performed the bioinformatic prediction. PD and YK drafted the manuscript, which was revised and edited by TT and JŠ. All authors approved the final version of the manuscript.

FUNDING

This research was funded by grant no. 19-00598S from the Czech Science Foundation GACR and by the ERDF project Plants as a tool for sustainable global development (No. CZ.02.1.01/0.0/0.0/16_019/0000827).

SUPPLEMENTARY MATERIAL

The Supplementary Material for this article can be found online at: https://www.frontiersin.org/articles/10.3389/fpls.2020.618835/full#supplementary-material

REFERENCES

Adachi, H., Nakano, T., Miyagawa, N., Ishihama, N., Yoshioka, M., Katou, Y., et al. (2015). WRKY transcription factors phosphorylated by MAPK regulate a plant immune NADPH oxidase in *Nicotiana benthamiana*. *Plant Cell* 27, 2645–2663. doi: 10.1105/tpc.15.00213

Ahmad, A., Khan, W. U., Shah, A. A., Yasin, N. A., Naz, S., Ali, A., et al. (2020). Synergistic effects of nitric oxide and silicon on promoting plant growth, oxidative stress tolerance and reduction of arsenic uptake in *Brassica juncea*. *Chemosphere* 262:128384. doi: 10.1016/j.chemosphere.2020.128384

Alscher, R. G., Erturk, N., and Heath, L. S. (2002). Role of superoxide dismutases (SODs) in controlling oxidative stress in plants. *J. Exp. Bot.* 53, 1331–1341. doi: 10.1093/jexbot/53.372.1331

Apel, K., and Hirt, H. (2004). REACTIVE OXYGEN SPECIES: metabolism, oxidative stress, and signal transduction. *Annu. Rev. Plant Biol.* 55, 373–399. doi: 10.1146/annurev.arplant.55.031903.141701

Araki, R., Mermod, M., Yamasaki, H., Kamiya, T., Fujiwara, T., and Shikanai, T. (2018). SPL7 locally regulates copper-homeostasis-related genes in *Arabidopsis*. *J. Plant Physiol.* 224–225, 137–143. doi: 10.1016/j.jplph.2018.03.014

Arsova, B., Watt, M., and Usadel, B. (2018). Monitoring of plant protein post-translational modifications using targeted proteomics. *Front. Plant Sci.* 9:1168. doi: 10.3389/fpls.2018.01168

Asano, T., Hayashi, N., Kobayashi, M., Aoki, N., Miyao, A., Mitsuhara, I., et al. (2012). A rice calcium-dependent protein kinase OsCPK12 oppositely modulates salt-stress tolerance and blast disease resistance. *Plant J.* 69, 26–36. doi: 10.1111/j.1365-313X.2011.04766.x

Atif, R. M., Shahid, L., Waqas, M., Ali, B., Rashid, M. A. R., Azeem, F., et al. (2019). Insights on calcium-dependent protein kinases (CPKs) signaling for abiotic stress tolerance in plants. *Int. J. Mol. Sci.* 20:5298. doi: 10.3390/ijms20215298

Baxter, A., Mittler, R., and Suzuki, N. (2014). ROS as key players in plant stress signalling. *J. Exp. Bot.* 65, 1229–1240. doi: 10.1093/jxb/ert375

Begara-Morales, J. C., Sánchez-Calvo, B., Chaki, M., Mata-Pérez, C., Valderrama, R., Padilla, M. N., et al. (2015). Differential molecular response of monodehydroascorbate reductase and glutathione reductase by nitration and *S* -nitrosylation. *J. Exp. Bot.* 66, 5983–5996. doi: 10.1093/jxb/erv306

Begara-Morales, J. C., Sánchez-Calvo, B., Chaki, M., Valderrama, R., Mata-Pérez, C., López-Jaramillo, J., et al. (2014). Dual regulation of cytosolic ascorbate peroxidase (APX) by tyrosine nitration and S-nitrosylation. *J. Exp. Bot.* 65, 527–538. doi: 10.1093/jxb/ert396

Berkholz, D. S., Faber, H. R., Savvides, S. N., and Karplus, P. A. (2008). Catalytic cycle of human glutathione reductase near 1 A resolution. *J. Mol. Biol.* 382, 371–384. doi: 10.1016/j.jmb.2008.06.083

Bethke, G., Unthan, T., Uhrig, J. F., Pöschl, Y., Gust, A. A., Scheel, D., et al. (2009). Flg22 regulates the release of an ethylene response factor substrate from MAP kinase 6 in *Arabidopsis thaliana* via ethylene signaling. *Proc. Natl. Acad. Sci. U.S.A.* 106, 8067–8072. doi: 10.1073/pnas.0810206106

Bhaskara, G. B., Wen, T. N., Nguyen, T. T., and Verslues, P. E. (2017). Protein phosphatase 2Cs and *Microtubule-Associated Stress Protein 1* control microtubule stability, plant growth, and drought response. *Plant Cell* 29, 169–191. doi: 10.1105/tpc.16.00847

Bindschedler, L. V., Dewdney, J., Blee, K. A., Stone, J. M., Asai, T., Plotnikov, J., et al. (2006). Peroxidase-dependent apoplastic oxidative burst in *Arabidopsis* required for pathogen resistance. *Plant J.* 47, 851–863. doi: 10.1111/j.1365-313X.2006.02837.x

Boudsocq, M., Willmann, M. R., McCormack, M., Lee, H., Shan, L., He, P., et al. (2010). Differential innate immune signalling via Ca^{2+} sensor protein kinases. *Nature* 464, 418–422. doi: 10.1038/nature08794

Bueso, E., Alejandro, S., Carbonell, P., Perez-Amador, M. A., Fayos, J., Bellés, J. M., et al. (2007). The lithium tolerance of the *Arabidopsis cat2* mutant reveals a cross-talk between oxidative stress and ethylene. *Plant J.* 52, 1052–1065. doi: 10.1111/j.1365-313X.2007.03305.x

Bykova, N. V., Egsgaard, H., and Møller, I. M. (2003). Identification of 14 new phosphoproteins involved in important plant mitochondrial processes. *FEBS Lett.* 540, 141–146. doi: 10.1016/s0014-5793(03)00250-3

Candas, D., Fan, M., Nantajit, D., Vaughan, A. T., Murley, J. S., Woloschak, et al. (2013). CyclinB1/Cdk1 phosphorylates mitochondrial antioxidant MnSOD

in cell adaptive response to radiation stress. *J. Mol. Cell Biol.* 5, 166–175. doi: 10.1093/jmcb/mjs062

Chaki, M., Álvarez de Morales, P., Ruiz, C., Begara-Morales, J. C., Barroso, J. B., Corpas, F. J., et al. (2015). Ripening of pepper (*Capsicum annuum*) fruit is characterized by an enhancement of protein tyrosine nitration. *Ann. Bot.* 116, 637–647. doi: 10.1093/aob/mcv016

Chan, K. X., Phua, S. Y., Crisp, P., McQuinn, R., and Pogson, B. J. (2016). Learning the languages of the chloroplast: retrograde signaling and beyond. *Annu. Rev. Plant Biol.* 67, 25–53. doi: 10.1146/annurev-arplant-043015-111854

Chang, R., Jang, C. J., Branco-Price, C., Nghiem, P., and Bailey-Serres, J. (2012). Transient MPK6 activation in response to oxygen deprivation and reoxygenation is mediated by mitochondria and aids seedling survival in *Arabidopsis*. *Plant Mol. Biol.* 78, 109–122. doi: 10.1007/s11103-011-9850-5

Chen, C., Letnik, I., Hacham, Y., Dobrev, P., Ben-Daniel, B. H., Vanková, R., et al. (2014). ASCORBATE PEROXIDASE6 protects *Arabidopsis* desiccating and germinating seeds from stress and mediates cross talk between reactive oxygen species, abscisic acid, and auxin. *Plant Physiol.* 166, 370–383. doi: 10.1104/pp.114.245324

Chen, L., Wu, R., Feng, J., Feng, T., Wang, C., Hu, J., et al. (2020). Transnitrosylation mediated by the non-canonical catalase ROG1 regulates nitric oxide signaling in plants. *Dev. Cell* 53, 444–457.e5. doi: 10.1016/j.devcel.2020.03.020

Chew, O., Whelan, J., and Millar, A. H. (2003). Molecular definition of the ascorbate-glutathione cycle in *Arabidopsis* mitochondria reveals dual targeting of antioxidant defenses in plants. *J. Biol. Chem.* 278, 46869–46877. doi: 10.1074/jbc.M307525200

Chin, D. C., Senthil Kumar, R., Suen, C. S., Chien, C. Y., Hwang, M. J., Hsu, C. H., et al. (2019). Plant cytosolic ascorbate peroxidase with dual catalytic activity modulates abiotic stress tolerances. *iScience* 16, 31–49. doi: 10.1016/j.isci.2019.05.014

Chmielowska-Bak, J., Gzyl, J., Rucińska-Sobkowiak, R., Arasimowicz-Jelonek, M., and Deckert, J. (2014). The new insights into cadmium sensing. *Front. Plant Sci.* 5:245. doi: 10.3389/fpls.2014.00245

Choi, W. G., Toyota, M., Kim, S. H., Hilleary, R., and Gilroy, S. (2014). Salt stress-induced Ca^{2+} waves are associated with rapid, long-distance root-to-shoot signaling in plants. *Proc. Natl. Acad. Sci. U.S.A.* 111, 6497–6502. doi: 10.1073/pnas.1319955111

Choudhary, M. K., Nomura, Y., Wang, L., Nakagami, H., and Somers, D. E. (2015). Quantitative circadian phosphoproteomic analysis of *Arabidopsis* reveals extensive clock control of key components in physiological, metabolic, and signaling pathways. *Mol. Cell Proteomics* 14, 2243–2260. doi: 10.1074/mcp.M114.047183

Ciacka, K., Tymiński, M., Gniazdowska, A., and Krasuska, U. (2020). Carbonylation of proteins-an element of plant ageing. *Planta* 252:12. doi: 10.1007/s00425-020-03414-1

Cohu, C. M., Abdel-Ghany, S. E., Gogolin Reynolds, K. A., Onofrio, A. M., Bodecker, J. R., Kimbrel, J. A., et al. (2009). Copper delivery by the copper chaperone for chloroplast and cytosolic copper/zinc-superoxide dismutases: regulation and unexpected phenotypes in an *Arabidopsis* mutant. *Mol. Plant.* 2, 1336–1350. doi: 10.1093/mp/ssp084

Colcombet, J., and Hirt, H. (2008). *Arabidopsis* MAPKs: a complex signalling network involved in multiple biological processes. *Biochem. J.* 413, 217–226. doi: 10.1042/BJ20080625

Considine, M. J., and Foyer, C. H. (2014). Redox regulation of plant development. *Antioxid. Redox Signal.* 21, 1305–1326. doi: 10.1089/ars.2013.5665

Corcoran, A., and Cotter, T. G. (2013). Redox regulation of protein kinases. *FEBS J.* 280, 1944–1965. doi: 10.1111/febs.12224

Corpas, F. J., and Barroso, J. B. (2017). Lead-induced stress, which triggers the production of nitric oxide (NO) and superoxide anion ($O^{2\cdot-}$) in *Arabidopsis* peroxisomes, affects catalase activity. *Nitric Oxide* 68, 103–110. doi: 10.1016/j.niox.2016.12.010

Csiszár, J., Brunner, S., Horváth, E., Bela, K., Ködmön, P., Riyazuddin, R., et al. (2018). Exogenously applied salicylic acid maintains redox homeostasis in salt-stressed *Arabidopsis gr1* mutants expressing cytosolic roGFP1. *Plant Growth Regul.* 86, 181–194. doi: 10.1007/s10725-018-0420-6

Cui, F., Brosché, M., Shapiguzov, A., He, X. Q., Vainonen, J. P., Leppälä, J., et al. (2019). Interaction of methyl viologen-induced chloroplast and mitochondrial signalling in *Arabidopsis*. *Free Radic. Biol. Med.* 134, 555–566. doi: 10.1016/j.freeradbiomed.2019.02.006

Cui, J., Jiang, N., Zhou, X., Hou, X., Yang, G., Meng, J., et al. (2018). Tomato MYB49 enhances resistance to *Phytophthora infestans* and tolerance to water deficit and salt stress. *Planta* 248, 1487–1503. doi: 10.1007/s00425-018-2987-6

Dalle-Donne, I., Rossi, R., Giustarini, D., Milzani, A., and Colombo, R. (2003). Protein carbonyl groups as biomarkers of oxidative stress. *Clin. Chim. Acta* 329, 23–38. doi: 10.1016/s0009-8981(03)00003-2

Danquah, A., de Zelicourt, A., Colcombet, J., and Hirt, H. (2014). The role of ABA and MAPK signaling pathways in plant abiotic stress responses. *Biotechnol. Adv.* 32, 40–52. doi: 10.1016/j.biotechadv.2013.09.006

Davletova, S., Rizhsky, L., Liang, H., Shengqiang, Z., Oliver, D. J., Coutu, J., et al. (2005a). Cytosolic ascorbate peroxidase 1 is a central component of the reactive oxygen gene network of *Arabidopsis*. *Plant Cell* 17, 268–281. doi: 10.1105/tpc.104.026971

Davletova, S., Schlauch, K., Coutu, J., and Mittler, R. (2005b). The zinc-finger protein Zat12 plays a central role in reactive oxygen and abiotic stress signaling in *Arabidopsis*. *Plant Physiol.* 139, 847–856. doi: 10.1104/pp.105.068254

De Pinto, M. C., Locato, V., and De Gara, L. (2012). Redox regulation in plant programmed cell death: redox regulation in plant PCD. *Plant Cell Environ.* 35, 234–244. doi: 10.1111/j.1365-3040.2011.02387.x

del Río, L. A. (2015). ROS and RNS in plant physiology: an overview. *J. Exp. Bot.* 66, 2827–2837. doi: 10.1093/jxb/erv099

del Río, L. A., and López-Huertas, E. (2016). ROS Generation in peroxisomes and its role in cell signaling. *Plant Cell Physiol.* 57, 1364–1376. doi: 10.1093/pcp/pcw076

del Río, L. A., Sandalio, L. M., Corpas, F. J., Palma, J. M., and Barroso, J. B. (2006). Reactive oxygen species and reactive nitrogen species in peroxisomes. Production, scavenging, and role in cell signaling. *Plant Physiol.* 141, 330–335. doi: 10.1104/pp.106.078204

Delledonne, M., Zeier, J., Marocco, A., and Lamb, C. (2001). Signal interactions between nitric oxide and reactive oxygen intermediates in the plant hypersensitive disease resistance response. *Proc. Natl. Acad. Sci. U.S.A.* 98, 13454–13459. doi: 10.1073/pnas.231178298

Demidchik, V. (2018). ROS-Activated ion channels in plants: biophysical characteristics, physiological functions and molecular nature. *Int. J. Mol. Sci.* 19, 1263. doi: 10.3390/ijms19041263

Demidchik, V., Shabala, S., Isayenkov, S., Cuin, T. A., and Pottosin, I. (2018). Calcium transport across plant membranes: mechanisms and functions. *New Phytol.* 220, 49–69. doi: 10.1111/nph.15266

Diao, Y., Liu, W., Wong, C. C. L., Wang, X., Lee, K., Cheung, P.-Y., et al. (2010). Oxidation-induced intramolecular disulfide bond inactivates mitogen-activated protein kinase 6 by inhibiting ATP binding. *Proc. Natl. Acad. Sci. U.S.A.* 107, 20974–20979. doi: 10.1073/pnas.1007225107

Dietz, K.-J. (2011). Peroxiredoxins in plants and cyanobacteria. *Antioxid. Redox Signal.* 15, 1129–1159. doi: 10.1089/ars.2010.3657

Dietz, K.-J. (2014). Redox regulation of transcription factors in plant stress acclimation and development. *Antioxid. Redox Signal.* 21, 1356–1372. doi: 10.1089/ars.2013.5672

Ding, H., Wang, B., Han, Y., and Li, S. (2020). The pivotal function of dehydroascorbate reductase in glutathione homeostasis in plants. *J. Exp. Bot.* 71, 3405–3416. doi: 10.1093/jxb/eraa107

Dóczi, R., Brader, G., Pettkó-Szandtner, A., Rajh, I., Djamei, A., Pitzschke, A., et al. (2007). The *Arabidopsis* mitogen-activated protein kinase kinase MKK3 is upstream of group C mitogen-activated protein kinases and participates in pathogen signaling. *Plant Cell* 19, 3266–3279. doi: 10.1105/tpc.106.050039

Dodd, A. N., Kudla, J., and Sanders, D. (2010). The language of calcium signaling. *Annu. Rev. Plant Biol.* 61, 593–620. doi: 10.1146/annurev-arplant-070109-104628

Doll, J., Muth, M., Riester, L., Nebel, S., Bresson, J., Lee, H. C., et al. (2020). *Arabidopsis thaliana WRKY25* transcription factor mediates oxidative stress tolerance and regulates senescence in a redox-dependent manner. *Front. Plant Sci.* 10:1734. doi: 10.3389/fpls.2019.01734

Du, Y. Y., Wang, P. C., Chen, J., and Song, C. P. (2008). Comprehensive functional analysis of the catalase gene family in *Arabidopsis thaliana*. *J. Integr. Plant Biol.* 50, 1318–1326. doi: 10.1111/j.1744-7909.2008.00741.x

Dubiella, U., Seybold, H., Durian, G., Komander, E., Lassig, R., Witte, C.-P., et al. (2013). Calcium-dependent protein kinase/NADPH oxidase activation circuit

is required for rapid defense signal propagation. *Proc. Natl. Acad. Sci. U.S.A.* 110, 8744–8749. doi: 10.1073/pnas.1221294110

Dugas, D. V., and Bartel, B. (2008). Sucrose induction of *Arabidopsis* miR398 represses two Cu/Zn superoxide dismutases. *Plant Mol. Biol.* 67, 403–417. doi: 10.1007/s11103-008-9329-1

Dvořák, P., Krasylenko, Y., Ovečka, M., Basheer, J., Zapletalová, V., Šamaj, J., et al. (2020). *In-vivo* light-sheet microscopy resolves localisation patterns of FSD1, a superoxide dismutase with function in root development and osmoprotection. *Plant Cell Environ.* 44, 68–87. doi: 10.1111/pce.13894

Eastmond, P. J. (2007). MONODEHYROASCORBATE REDUCTASE4 is required for seed storage oil hydrolysis and postgerminative growth in *Arabidopsis*. *Plant Cell* 19, 1376–1387. doi: 10.1105/tpc.106.043992

Eltayeb, A. E., Kawano, N., Badawi, G. H., Kaminaka, H., Sanekata, T., Shibahara, T., et al. (2007). Overexpression of monodehydroascorbate reductase in transgenic tobacco confers enhanced tolerance to ozone, salt and polyethylene glycol stresses. *Planta* 225, 1255–1264. doi: 10.1007/s00425-006-0417-7

Eltayeb, A. E., Yamamoto, S., Habora, M. E. E., Yin, L., Tsujimoto, H., and Tanaka, K. (2011). Transgenic potato overexpressing *Arabidopsis* cytosolic AtDHAR1 showed higher tolerance to herbicide, drought and salt stresses. *Breed. Sci.* 61, 3–10. doi: 10.1270/jsbbs.61.3

Engelsberger, W. R., and Schulze, W. X. (2012). Nitrate and ammonium lead to distinct global dynamic phosphorylation patterns when resupplied to nitrogen-starved *Arabidopsis* seedlings. *Plant J.* 69, 978–995. doi: 10.1111/j.1365-313X.2011.04848.x

Eubel, H., Meyer, E. H., Taylor, N. L., Bussell, J. D., O'Toole, N., Heazlewood, J. L., et al. (2008). Novel proteins, putative membrane transporters, and an integrated metabolic network are revealed by quantitative proteomic analysis of *Arabidopsis* cell culture peroxisomes. *Plant Physiol.* 148, 1809–1829. doi: 10.1104/pp.108.129999

Exposito-Rodriguez, M., Laissue, P. P., Yvon-Durocher, G., Smirnoff, N., and Mullineaux, P. M. (2017). Photosynthesis-dependent H_2O_2 transfer from chloroplasts to nuclei provides a high-light signalling mechanism. *Nat. Commun.* 8:49. doi: 10.1038/s41467-017-00074-w

Farnese, F. S., Menezes-Silva, P. E., Gusman, G. S., and Oliveira, J. A. (2016). When bad guys become good ones: the key role of reactive oxygen species and nitric oxide in the plant responses to abiotic stress. *Front. Plant Sci.* 7:471. doi: 10.3389/fpls.2016.00471

Fay, J. M., Zhu, C., Proctor, E. A., Tao, Y., Cui, W., Ke, H., et al. (2016). A phosphomimetic mutation stabilizes SOD1 and rescues cell viability in the context of an ALS-associated mutation. *Structure* 24, 1898–1906. doi: 10.1016/j.str.2016.08.011

Feng, H., Wang, X., Zhang, Q., Fu, Y., Feng, C., Wang, B., et al. (2014). Monodehydroascorbate reductase gene, regulated by the wheat PN-2013 miRNA, contributes to adult wheat plant resistance to stripe rust through ROS metabolism. *Biochim. Biophys. Acta* 1839, 1–12. doi: 10.1016/j.bbagrm.2013.11.001

Foyer, C. H. (2018). Reactive oxygen species, oxidative signaling and the regulation of photosynthesis. *Environ. Exp. Bot.* 154, 134–142. doi: 10.1016/j.envexpbot.2018.05.003

Foyer, C. H., and Noctor, G. (2011). Ascorbate and glutathione: the heart of the redox hub. *Plant Physiol.* 155, 2–18. doi: 10.1104/pp.110.167569

Foyer, C. H., and Noctor, G. (2020). Redox homeostasis and signaling in a higher-CO_2 world. *Annu. Rev. Plant Biol.* 71, 157–182. doi: 10.1146/annurev-arplant-050718-095955

Frugoli, J. A., Zhong, H. H., Nuccio, M. L., McCourt, P., McPeek, M. A., Thomas, T. L., et al. (1996). Catalase is encoded by a multigene family in *Arabidopsis thaliana* (L.) Heynh. *Plant Physiol.* 112, 327–336. doi: 10.1104/pp.112.1.327

Gadjev, I., Vanderauwera, S., Gechev, T. S., Laloi, C., Minkov, I. N., Shulaev, V., et al. (2006). Transcriptomic footprints disclose specificity of reactive oxygen species signaling in *Arabidopsis*. *Plant Physiol.* 141, 436–445. doi: 10.1104/pp.106.078717

Gallie, D. R., and Chen, Z. (2019). Chloroplast-localized iron superoxide dismutases FSD2 and FSD3 are functionally distinct in *Arabidopsis*. *PLoS ONE* 14:e0220078. doi: 10.1371/journal.pone.0220078

Garcia-Molina, A., Xing, S., and Huijser, P. (2014). Functional characterisation of *Arabidopsis* SPL7 conserved protein domains suggests novel regulatory mechanisms in the Cu deficiency response. *BMC Plant Biol.* 14:231. doi: 10.1186/s12870-014-0231-5

Gaupels, F., Durner, J., and Kogel, K.-H. (2017). Production, amplification and systemic propagation of redox messengers in plants? The phloem can do it all! *New Phytol.* 214, 554–560. doi: 10.1111/nph.14399

Gawroński, P., Witoń, D., Vashutina, K., Bederska, M., Betliński, B., Rusaczonek, A., et al. (2014). Mitogen-activated protein kinase 4 is a salicylic acid-independent regulator of growth but not of photosynthesis in *Arabidopsis*. *Mol. Plant.* 7, 1151–1166. doi: 10.1093/mp/ssu060

Geilfus, C.-M., Niehaus, K., Gödde, V., Hasler, M., Zörb, C., Gorzolka, K., et al. (2015). Fast responses of metabolites in *Vicia faba* L. to moderate NaCl stress. *Plant Physiol. Biochem.* 92, 19–29. doi: 10.1016/j.plaphy.2015.04.008

Gilroy, S., Białasek, M., Suzuki, N., Górecka, M., Devireddy, A. R., Karpiński, S., et al. (2016). ROS, calcium, and electric signals: key mediators of rapid systemic signaling in plants. *Plant Physiol.* 171, 1606–1615. doi: 10.1104/pp.16.00434

Gilroy, S., Suzuki, N., Miller, G., Choi, W.-G., Toyota, M., Devireddy, A. R., et al. (2014). A tidal wave of signals: calcium and ROS at the forefront of rapid systemic signaling. *Trends Plant Sci.* 19, 623–630. doi: 10.1016/j.tplants.2014.06.013

Gleason, C., Huang, S., Thatcher, L. F., Foley, R. C., Anderson, C. R., Carroll, A. J., et al. (2011). Mitochondrial complex II has a key role in mitochondrial-derived reactive oxygen species influence on plant stress gene regulation and defense. *Proc. Natl. Acad. Sci. U.S.A.* 108, 10768–10773. doi: 10.1073/pnas.1016060108

Gou, J. Y., Li, K., Wu, K., Wang, X., Lin, H., Cantu, D., et al. (2015). Wheat stripe rust resistance protein WKS1 reduces the ability of the thylakoid-associated ascorbate peroxidase to detoxify reactive oxygen species. *Plant Cell* 27, 1755–1770. doi: 10.1105/tpc.114.134296

Granlund, I., Storm, P., Schubert, M., García-Cerdán, J. G., Funk, C., and Schröder, W. P. (2009). The TL29 protein is lumen located, associated with PSII and not an ascorbate peroxidase. *Plant Cell Physiol.* 50, 1898–1910. doi: 10.1093/pcp/pcp134

Gudesblat, G. E., Iusem, N. D., and Morris, P. C. (2007). Guard cell-specific inhibition of *Arabidopsis* MPK3 expression causes abnormal stomatal responses to abscisic acid and hydrogen peroxide. *New Phytol.* 173, 713–721. doi: 10.1111/j.1469-8137.2006.01953.x

Guo, B., Liu, C., Li, H., Yi, K., Ding, N., Li, N., et al. (2016). Endogenous salicylic acid is required for promoting cadmium tolerance of *Arabidopsis* by modulating glutathione metabolisms. *J. Hazard. Mater.* 316, 77–86. doi: 10.1016/j.jhazmat.2016.05.032

Guo, P., Li, Z., Huang, P., Li, B., Fang, S., Chu, J., et al. (2017). A tripartite amplification loop involving the transcription factor WRKY75, salicylic acid, and reactive oxygen species accelerates leaf senescence. *Plant Cell* 29, 2854–2870. doi: 10.1105/tpc.17.00438

Hackenberg, T., Juul, T., Auzina, A., Gwizdz, S., Malolepszy, A., Van Der Kelen, K., et al. (2013). Catalase and NO CATALASE ACTIVITY1 promote autophagy-dependent cell death in *Arabidopsis*. *Plant Cell* 25, 4616–4626. doi: 10.1105/tpc.113.117192

He, H., Van Breusegem, F., and Mhamdi, A. (2018). Redox-dependent control of nuclear transcription in plants. *J. Exp. Bot.* 69, 3359–3372. doi: 10.1093/jxb/ery130

He, J., Ren, Y., Chen, X., and Chen, H. (2014). Protective roles of nitric oxide on seed germination and seedling growth of rice (*Oryza sativa* L.) under cadmium stress. *Ecotoxicol. Environ. Saf.* 108, 114–119. doi: 10.1016/j.ecoenv.2014.05.021

Hehl, R., Norval, L., Romanov, A., and Bülow, L. (2016). Boosting AthaMap database content with data from protein binding microarrays. *Plant Cell Physiol.* 57:e4. doi: 10.1093/pcp/pcv156

Hiltscher, H., Rudnik, R., Shaikhali, J., Heiber, I., Mellenthin, M., Duarte, I. M., et al. (2014). The radical induced cell death protein 1 (RCD1) supports transcriptional activation of genes for chloroplast antioxidant enzymes. *Front. Plant Sci.* 5:475. doi: 10.3389/fpls.2014.00475

Holzmeister, C., Gaupels, F., Geerlof, A., Sarioglu, H., Sattler, M., Durner, J., et al. (2015). Differential inhibition of *Arabidopsis* superoxide dismutases by peroxynitrite-mediated tyrosine nitration. *J. Exp. Bot.* 66, 989–999. doi: 10.1093/jxb/eru458

Horváth, E., Szalai, G., and Janda, T. (2007). Induction of abiotic stress tolerance by salicylic acid signaling. *J. Plant Growth Regul.* 26, 290–300. doi: 10.1007/s00344-007-9017-4

Hu, C.-H., Wang, P.-Q., Zhang, P.-P., Nie, X.-M., Li, B.-B., Tai, L., et al. (2020). NADPH Oxidases: the vital performers and center hubs during plant growth and signaling. *Cells* 9:437. doi: 10.3390/cells9020437

Huang, L., Jia, J., Zhao, X., Zhang, M., Huang, X., Ji, E., et al. (2018). The ascorbate peroxidase APX1 is a direct target of a zinc finger transcription factor ZFP36 and a late embryogenesis abundant protein OsLEA5 interacts with ZFP36 to co-regulate OsAPX1 in seed germination in rice. *Biochem. Biophys. Res. Commun.* 495, 339–345. doi: 10.1016/j.bbrc.2017.10.128

Huang, W., Yang, Y.-J., and Zhang, S.-B. (2019). The role of water-water cycle in regulating the redox state of photosystem I under fluctuating light. *Biochim. Biophys. Acta* 1860, 383–390. doi: 10.1016/j.bbabio.2019.03.007

Huda, K. M. K., Banu, M. S. A., Garg, B., Tula, S., Tuteja, R., and Tuteja, N. (2013). OsACA6, a P-type IIB Ca^{2+} ATPase promotes salinity and drought stress tolerance in tobacco by ROS scavenging and enhancing the expression of stress-responsive genes. *Plant J.* 76, 997–1015. doi: 10.1111/tpj.12352

Hwang, J. E., Lim, C. J., Chen, H., Je, J., Song, C., and Lim, C. O. (2012). Overexpression of *Arabidopsis* dehydration- responsive element-binding protein 2C confers tolerance to oxidative stress. *Mol. Cells* 33, 135–140. doi: 10.1007/s10059-012-2188-2

Innocenti, G., Pucciariello, C., Le Gleuher, M., Hopkins, J., de Stefano, M., Delledonne, M., et al. (2007). Glutathione synthesis is regulated by nitric oxide in *Medicago truncatula* roots. *Planta* 225, 1597–1602. doi: 10.1007/s00425-006-0461-3

Jammes, F., Song, C., Shin, D., Munemasa, S., Takeda, K., Gu, D., et al. (2009). MAP kinases MPK9 and MPK12 are preferentially expressed in guard cells and positively regulate ROS-mediated ABA signaling. *Proc. Natl. Acad. Sci. U.S.A.* 106, 20520–20525. doi: 10.1073/pnas.0907205106

Jin, C., Qin, L., Shi, Y., Candas, D., Fan, M., Lu, C. L., et al. (2015). CDK4-mediated MnSOD activation and mitochondrial homeostasis in radioadaptive protection. *Free Radic. Biol. Med.* 81, 77–87. doi: 10.1016/j.freeradbiomed.2014.12.026

Joo, J. H., Bae, Y. S., and Lee, J. S. (2001). Role of auxin-induced reactive oxygen species in root gravitropism. *Plant Physiol.* 126, 1055–1060. doi: 10.1104/pp.126.3.1055

Jung, H. S., Crisp, P. A., Estavillo, G. M., Cole, B., Hong, F., Mockler, T. C., et al. (2013). Subset of heat-shock transcription factors required for the early response of *Arabidopsis* to excess light. *Proc. Natl. Acad. Sci. U.S.A.* 110, 14474–14479. doi: 10.1073/pnas.1311632110

Kang, Z., Qin, T., and Zhao, Z. (2019). Thioredoxins and thioredoxin reductase in chloroplasts: a review. *Gene* 706, 32–42. doi: 10.1016/j.gene.2019.04.041

Kangasjärvi, S., Lepistö, A., Hännikäinen, K., Piippo, M., Luomala, E. M., Aro, E. M., et al. (2008). Diverse roles for chloroplast stromal and thylakoid-bound ascorbate peroxidases in plant stress responses. *Biochem. J.* 412, 275–285. doi: 10.1042/BJ20080030

Karpinski, S., Escobar, C., Karpinska, B., Creissen, G., and Mullineaux, P. M. (1997). Photosynthetic electron transport regulates the expression of cytosolic ascorbate peroxidase genes in *Arabidopsis* during excess light stress. *Plant Cell* 9, 627–640. doi: 10.1105/tpc.9.4.627

Kataya, A. R., and Reumann, S. (2010). *Arabidopsis* glutathione reductase 1 is dually targeted to peroxisomes and the cytosol. *Plant Signal. Behav.* 5, 171–175. doi: 10.4161/psb.5.2.10527

Kaur, N., and Hu, J. (2011). Defining the plant peroxisomal proteome: from *Arabidopsis* to rice. *Front. Plant Sci.* 2:103. doi: 10.3389/fpls.2011.00103

Khan, M. I., Fatma, M., Per, T. S., Anjum, N. A., and Khan, N. A. (2015). Salicylic acid-induced abiotic stress tolerance and underlying mechanisms in plants. *Front. Plant Sci.* 6:462. doi: 10.3389/fpls.2015.00462

Khedia, J., Agarwal, P., and Agarwal, P. K. (2019). Deciphering hydrogen peroxide-induced signalling towards stress tolerance in plants. *3 Biotech* 9, 395. doi: 10.1007/s13205-019-1924-0

Khraiwesh, B., Zhu, J. K., and Zhu, J. (2012). Role of miRNAs and siRNAs in biotic and abiotic stress responses of plants. *Biochim. Biophys. Acta* 1819, 137–148. doi: 10.1016/j.bbagrm.2011.05.001

Klein, P., Seidel, T., Stöcker, B., and Dietz, K. J. (2012). The membrane-tethered transcription factor ANAC089 serves as redox-dependent suppressor of stromal ascorbate peroxidase gene expression. *Front. Plant Sci.* 3:247. doi: 10.3389/fpls.2012.00247

Kliebenstein, D. J., Monde, R. A., and Last, R. L. (1998). Superoxide dismutase in *Arabidopsis*: an eclectic enzyme family with disparate regulation and protein localization. *Plant Physiol.* 118, 637–650. doi: 10.1104/pp.118.2.637

Kneeshaw, S., Keyani, R., Delorme-Hinoux, V., Imrie, L., Loake, G. J., Le Bihan, T., et al. (2017). Nucleoredoxin guards against oxidative stress by protecting antioxidant enzymes. *Proc. Natl. Acad. Sci. U.S.A.* 114, 8414–8419. doi: 10.1073/pnas.1703344114

Kobayashi, M., Ohura, I., Kawakita, K., Yokota, N., Fujiwara, M., Shimamoto, K., et al. (2007). Calcium-dependent protein kinases regulate the production of reactive oxygen species by potato NADPH oxidase. *Plant Cell* 19, 1065–1080. doi: 10.1105/tpc.106.048884

Kohli, S. K., Khanna, K., Bhardwaj, R., Abd Allah, E. F., Ahmad, P., and Corpas, F. J. (2019). Assessment of subcellular ROS and NO metabolism in higher plants: multifunctional signaling molecules. *Antioxidants* 8:641. doi: 10.3390/antiox8120641

Komis, G., Šamajová, O., Ovečka, M., and Šamaj, J. (2018). Cell and developmental biology of plant mitogen-activated protein kinases. *Annu. Rev. Plant Biol.* 69, 237–265. doi: 10.1146/annurev-arplant-042817-040314

Kornyeyev, D., Logan, B. A., Payton, P. R., Allen, R. D., and Holaday, A. S. (2003). Elevated chloroplastic glutathione reductase activities decrease chilling-induced photoinhibition by increasing rates of photochemistry, but not thermal energy dissipation, in transgenic cotton. *Funct. Plant Biol.* 30, 101–110. doi: 10.1071/FP02144

Koussevitzky, S., Suzuki, N., Huntington, S., Armijo, L., Sha, W., Cortes, D., et al. (2008). Ascorbate peroxidase 1 plays a key role in the response of *Arabidopsis thaliana* to stress combination. *J. Biol. Chem.* 283, 34197–34203. doi: 10.1074/jbc.M806337200

Kovacs, I., Holzmeister, C., Wirtz, M., Geerlof, A., Fröhlich, T., Römling, G., et al. (2016). ROS-mediated inhibition of S-nitrosoglutathione reductase contributes to the activation of anti-oxidative Mechanisms. *Front. Plant Sci.* 7:1669. doi: 10.3389/fpls.2016.01669

Kovtun, Y., Chiu, W. L., Tena, G., and Sheen, J. (2000). Functional analysis of oxidative stress-activated mitogen-activated protein kinase cascade in plants. *Proc. Natl. Acad. Sci. U.S.A.* 97, 2940–2945. doi: 10.1073/pnas.97.6.2940

Kreps, J. A., Wu, Y., Chang, H. S., Zhu, T., Wang, X., and Harper, J. F. (2002). Transcriptome changes for *Arabidopsis* in response to salt, osmotic, and cold stress. *Plant Physiol.* 130, 2129–2141. doi: 10.1104/pp.008532

Kumar, M., Gouw, M., Michael, S., Sámano-Sánchez, H., Pancsa, R., Glavina, J., et al. (2020). ELM-the eukaryotic linear motif resource in 2020. *Nucleic Acids Res.* 48, D296–D306. doi: 10.1093/nar/gkz1030

Kumar, S., Sud, N., Fonseca, F. V., Hou, Y., and Black, S. M. (2010). Shear stress stimulates nitric oxide signaling in pulmonary arterial endothelial cells via a reduction in catalase activity: role of protein kinase C delta. *Am. J. Physiol. Lung Cell Mol. Physiol.* 298, L105–L116. doi: 10.1152/ajplung.00290.2009

Kuo, W. Y., Huang, C. H., Liu, A. C., Cheng, C. P., Li, S. H., Chang, W. C., et al. (2013). CHAPERONIN 20 mediates iron superoxide dismutase (FeSOD) activity independent of its co-chaperonin role in *Arabidopsis* chloroplasts. *New Phytol.* 197, 99–110. doi: 10.1111/j.1469-8137.2012.04369.x

Lehmann, S., Serrano, M., L'Haridon, F., Tjamos, S. E., and Metraux, J.-P. (2015). Reactive oxygen species and plant resistance to fungal pathogens. *Phytochemistry* 112, 54–62. doi: 10.1016/j.phytochem.2014.08.027

Leitch, J. M., Li, C. X., Baron, J. A., Matthews, L. M., Cao, X., Hart, P. J., et al. (2012). Post-translational modification of Cu/Zn superoxide dismutase under anaerobic conditions. *Biochemistry* 51, 677–685. doi: 10.1021/bi201353y

Li, H., Wong, W. S., Zhu, L., Guo, H. W., Ecker, J., and Li, N. (2009). Phosphoproteomic analysis of ethylene-regulated protein phosphorylation in etiolated seedlings of *Arabidopsis* mutant ein2 using two-dimensional separations coupled with a hybrid quadrupole time-of-flight mass spectrometer. *Proteomics* 9, 1646–1661. doi: 10.1002/pmic.200800420

Li, X., Makavitskaya, M., Samokhina, V., Mackievic, V., Navaselsky, I., Hryvusevich, P., et al. (2018). Effects of exogenously-applied L-ascorbic acid on root expansive growth and viability of the border-like cells. *Plant Signal. Behav.* 13:e1514895. doi: 10.1080/15592324.2018.1514895

Lin, F., Ding, H., Wang, J., Zhang, H., Zhang, A., Zhang, Y., et al. (2009). Positive feedback regulation of maize NADPH oxidase by mitogen-activated protein kinase cascade in abscisic acid signalling. *J. Exp. Bot.* 60, 3221–3238. doi: 10.1093/jxb/erp157

Lin, L. L., Hsu, C. L., Hu, C. W., Ko, S. Y., Hsieh, H. L., Huang, H. C., et al. (2015). Integrating phosphoproteomics and bioinformatics to study brassinosteroid-regulated phosphorylation dynamics in *Arabidopsis*. *BMC Genom.* 16, 533. doi: 10.1186/s12864-015-1753-4

Lindermayr, C. (2018). Crosstalk between reactive oxygen species and nitric oxide in plants: key role of S-nitrosoglutathione reductase. *Free Radic. Biol. Med*. 122, 110–115. doi: 10.1016/j.freeradbiomed.2017.11.027

Lindermayr, C., and Durner, J. (2015). Interplay of reactive oxygen species and nitric oxide: nitric oxide coordinates reactive oxygen species homeostasis. *Plant Physiol*. 167, 1209–1210. doi: 10.1104/pp.15.00293

Lisenbee, C. S., Lingard, M. J., and Trelease, R. N. (2005). *Arabidopsis* peroxisomes possess functionally redundant membrane and matrix isoforms of monodehydroascorbate reductase. *Plant J*. 43, 900–914. doi: 10.1111/j.1365-313X.2005.02503.x

Liu, P., Sun, F., Gao, R., and Dong, H. (2012). RAP2.6L overexpression delays waterlogging induced premature senescence by increasing stomatal closure more than antioxidant enzyme activity. *Plant Mol. Biol*. 79, 609–622. doi: 10.1007/s11103-012-9936-8

Liu, Y., and He, C. (2017). A review of redox signaling and the control of MAP kinase pathway in plants. *Redox Biol*. 11, 192–204. doi: 10.1016/j.redox.2016.12.009

Locato, V., Cimini, S., and De Gara, L. (2017). "Glutathione as a key player in plant abiotic stress responses and tolerance," in *Glutathione in Plant Growth, Development, and Stress Tolerance*, eds M. A. Hossain, M. G. Mostofa, P. Diaz-Vivancos, D. J. Burritt, M. Fujita, and L.-S. P. Tran (Cham: Springer International Publishing), 127–145. doi: 10.1007/978-3-319-66682-2_6

Ma, C., Burd, S., and Lers, A. (2015). miR408 is involved in abiotic stress responses in *Arabidopsis*. *Plant J*. 84, 169–187. doi: 10.1111/tpj.12999

Marcec, M. J., Gilroy, S., Poovaiah, B. W., and Tanaka, K. (2019). Mutual interplay of Ca^{2+} and ROS signaling in plant immune response. *Plant Sci*. 283, 343–354. doi: 10.1016/j.plantsci.2019.03.004

Marchand, C. H., Vanacker, H., Collin, V., Issakidis-Bourguet, E., Maréchal, P. L., and Decottignies, P. (2010). Thioredoxin targets in *Arabidopsis* roots. *Proteomics* 10, 2418–2428. doi: 10.1002/pmic.200900835

Marty, L., Bausewein, D., Müller, C., Bangash, S., Moseler, A., Schwarzländer, M., et al. (2019). *Arabidopsis* glutathione reductase 2 is indispensable in plastids, while mitochondrial glutathione is safeguarded by additional reduction and transport systems. *New Phytol*. 224, 1569–1584. doi: 10.1111/nph.16086

Maruta, T., Inoue, T., Noshi, M., Tamoi, M., Yabuta, Y., Yoshimura, K., et al. (2012). Cytosolic ascorbate peroxidase 1 protects organelles against oxidative stress by wounding- and jasmonate-induced H_2O_2 in *Arabidopsis* plants. *Biochim. Biophys. Acta* 1820, 1901–1907. doi: 10.1016/j.bbagen.2012.08.003

Maruta, T., Sawa, Y., Shigeoka, S., and Ishikawa, T. (2016). Diversity and evolution of ascorbate peroxidase functions in chloroplasts: more than just a classical antioxidant enzyme? *Plant Cell Physiol*. 57, 1377–1386. doi: 10.1093/pcp/pcv203

Maruta, T., Tanouchi, A., Tamoi, M., Yabuta, Y., Yoshimura, K., Ishikawa, T., et al. (2010). *Arabidopsis* chloroplastic ascorbate peroxidase isoenzymes play a dual role in photoprotection and gene regulation under photooxidative stress. *Plant Cell Physiol*. 51, 190–200. doi: 10.1093/pcp/pcp177

Mayank, P., Grossman, J., Wuest, S., Boisson-Dernier, A., Roschitzki, B., Nanni, P., et al. (2012). Characterization of the phosphoproteome of mature *Arabidopsis* pollen. *Plant J*. 72, 89–101. doi: 10.1111/j.1365-313X.2012.05061.x

Meyer, A. J., Dreyer, A., Ugalde, J. M., Feitosa-Araujo, E., Dietz, K.-J., and Schwarzländer, M. (in press). Shifting paradigms and novel players in Cys-based redox regulation and ROS signaling in plants - and where to go next. *Biol. Chem*. doi: 10.1515/hsz-2020-0291

Mhamdi, A., Noctor, G., and Baker, A. (2012). Plant catalases: peroxisomal redox guardians. *Arch. Biochem. Biophys*. 525, 181–194. doi: 10.1016/j.abb.2012.04.015

Mhamdi, A., Queval, G., Chaouch, S., Vanderauwera, S., Van Breusegem, F., and Noctor, G. (2010). Catalase function in plants: a focus on *Arabidopsis* mutants as stress-mimic models. *J. Exp. Bot*. 61, 4197–4220. doi: 10.1093/jxb/erq282

Mhamdi, A., and Van Breusegem, F. (2018). Reactive oxygen species in plant development. *Development* 145:dev164376. doi: 10.1242/dev.164376

Miao, Y., Laun, T., Zimmermann, P., and Zentgraf, U. (2004). Targets of the WRKY53 transcription factor and its role during leaf senescence in *Arabidopsis*. *Plant Mol. Biol*. 55, 853–867. doi: 10.1007/s11103-004-2142-6

Miao, Y., Laun, T. M., Smykowski, A., and Zentgraf, U. (2007). *Arabidopsis* MEKK1 can take a short cut: it can directly interact with senescence-related WRKY53 transcription factor on the protein level and can bind to its promoter. *Plant Mol. Biol*. 65, 63–76. doi: 10.1007/s11103-007-9198-z

Mignolet-Spruyt, L., Xu, E., Idänheimo, N., Hoeberichts, F. A., Mühlenbock, P., Brosché, M., et al. (2016). Spreading the news: subcellular and organellar reactive oxygen species production and signalling. *J. Exp. Bot*. 67, 3831–3844. doi: 10.1093/jxb/erw080

Miller, E. W., Dickinson, B. C., and Chang, C. J. (2010). Aquaporin-3 mediates hydrogen peroxide uptake to regulate downstream intracellular signaling. *Proc. Natl. Acad. Sci. U.S.A*. 107, 15681–15686. doi: 10.1073/pnas.1005776107

Mithoe, S. C., Boersema, P. J., Berke, L., Snel, B., Heck, A. J., and Menke, F. L. (2012). Targeted quantitative phosphoproteomics approach for the detection of phospho-tyrosine signaling in plants. *J. Proteome Res*. 11, 438–448. doi: 10.1021/pr200893k

Mittler, R. (2017). ROS are good. *Trends Plant Sci*. 22, 11–19. doi: 10.1016/j.tplants.2016.08.002

Mittler, R., Kim, Y., Song, L., Coutu, J., Coutu, A., Ciftci-Yilmaz, S., et al. (2006). Gain- and loss-of-function mutations in Zat10 enhance the tolerance of plants to abiotic stress. *FEBS Lett*. 580, 6537–6542. doi: 10.1016/j.febslet.2006.11.002

Mittler, R., Vanderauwera, S., Suzuki, N., Miller, G., Tognetti, V. B., Vandepoele, K., et al. (2011). ROS signaling: the new wave? *Trends Plant Sci*. 16, 300–309. doi: 10.1016/j.tplants.2011.03.007

Morgan, M. J., Lehmann, M., Schwarzländer, M., Baxter, C. J., Sienkiewicz-Porzucek, A., Williams, T. C., et al. (2008). Decrease in manganese superoxide dismutase leads to reduced root growth and affects tricarboxylic acid cycle flux and mitochondrial redox homeostasis. *Plant Physiol*. 147, 101–114. doi: 10.1104/pp.107.113613

Müller-Schüssele, S. J., Wang, R., Gütle, D. D., Romer, J., Rodriguez-Franco, M., Scholz, M., et al. (2020). Chloroplasts require glutathione reductase to balance reactive oxygen species and maintain efficient photosynthesis. *Plant J*. 103, 1140–1154. doi: 10.1111/tpj.14791

Muñoz, P., and Munné-Bosch, S. (2019). Vitamin E in plants: biosynthesis, transport, and function. *Trends Plant Sci*. 24, 1040–1051. doi: 10.1016/j.tplants.2019.08.006

Murgia, I., Tarantino, D., Vannini, C., Bracale, M., Carravieri, S., and Soave, C. (2004). *Arabidopsis thaliana* plants overexpressing thylakoidal ascorbate peroxidase show increased resistance to Paraquat-induced photooxidative stress and to nitric oxide-induced cell death. *Plant J*. 38, 940–953. doi: 10.1111/j.1365-313X.2004.02092.x

Myouga, F., Hosoda, C., Umezawa, T., Iizumi, H., Kuromori, T., Motohashi, R., et al. (2008). A heterocomplex of iron superoxide dismutases defends chloroplast nucleoids against oxidative stress and is essential for chloroplast development in *Arabidopsis*. *Plant Cell* 20, 3148–3162. doi: 10.1105/tpc.108.061341

Nakagami, H., Soukupová, H., Schikora, A., Zárský, V., and Hirt, H. (2006). A Mitogen-activated protein kinase kinase kinase mediates reactive oxygen species homeostasis in *Arabidopsis*. *J. Biol. Chem*. 281, 38697–38704. doi: 10.1074/jbc.M605293200

Nakagami, H., Sugiyama, N., Mochida, K., Daudi, A., Yoshida, Y., Toyoda, T., et al. (2010). Large-scale comparative phosphoproteomics identifies conserved phosphorylation sites in plants. *J. Plant Physiol*. 153, 1161–1174. doi: 10.1104/pp.110.157347

Narendra, S., Venkataramani, S., Shen, G., Wang, J., Pasapula, V., Lin, Y., et al. (2006). The *Arabidopsis* ascorbate peroxidase 3 is a peroxisomal membrane-bound antioxidant enzyme and is dispensable for *Arabidopsis* growth and development. *J. Exp. Bot*. 57, 3033–3042. doi: 10.1093/jxb/erl060

Niu, L., and Liao, W. (2016). Hydrogen peroxide signaling in plant development and abiotic responses: crosstalk with nitric oxide and calcium. *Front Plant Sci*. 7:230. doi: 10.3389/fpls.2016.00230

Noctor, G., Reichheld, J.-P., and Foyer, C. H. (2017). ROS-related redox regulation and signaling in plants. *Cell Dev. Biol*. 80, 3–12. doi: 10.1016/j.semcdb.2017.07.013

Noshi, M., Hatanaka, R., Tanabe, N., Terai, Y., Maruta, T., and Shigeoka, S. (2016). Redox regulation of ascorbate and glutathione by a chloroplastic dehydroascorbate reductase is required for high-light stress tolerance in *Arabidopsis*. *Biosci. Biotechnol. Biochem*. 80, 870–877. doi: 10.1080/09168451.2015.1135042

Noshi, M., Yamada, H., Hatanaka, R., Tanabe, N., Tamoi, M., and Shigeoka, S. (2017). *Arabidopsis* dehydroascorbate reductase 1 and 2 modulate redox states of ascorbate-glutathione cycle in the cytosol in response

to photooxidative stress. *Biosci. Biotechnol. Biochem*. 81, 523–533. doi: 10.1080/09168451.2016.1256759

Obara, K., Sumi, K., and Fukuda, H. (2002). The use of multiple transcription starts causes the dual targeting of *Arabidopsis* putative monodehydroascorbate reductase to both mitochondria and chloroplasts. *Plant Cell Physiol*. 43, 697–705. doi: 10.1093/pcp/pcf103

Obayashi, T., Aoki, Y., Tadaka, S., Kagaya, Y., and Kinoshita, K. (2018). ATTED-II in 2018: a plant coexpression database based on investigation of the statistical property of the mutual rank index. *Plant Cell Physiol*. 59:e3. doi: 10.1093/pcp/pcx191

Ono, M., Isono, K., Sakata, Y., and Taji, T. (2020). CATALASE2 plays a crucial role in long-term heat tolerance of *Arabidopsis thaliana*. *Biochem. Biophys. Res. Commun*. 534, 747–751. doi: 10.1016/j.bbrc.2020.11.006

Ortega-Galisteo, A. P., Rodríguez-Serrano, M., Pazmiño, D. M., Gupta, D. K., Sandalio, L. M., and Romero-Puertas, M. C. (2012). S-Nitrosylated proteins in pea (*Pisum sativum* L.) leaf peroxisomes: changes under abiotic stress. *J. Exp. Bot*. 63, 2089–2103. doi: 10.1093/jxb/err414

Ortiz-Masia, D., Perez-Amador, M. A., Carbonell, J., and Marcote, M. J. (2007). Diverse stress signals activate the C1 subgroup MAP kinases of *Arabidopsis*. *FEBS Lett*. 581, 1834–1840. doi: 10.1016/j.febslet.2007.03.075

Palma, J. M., Mateos, R. M., López-Jaramillo, J., Rodríguez-Ruiz, M., González-Gordo, S., Lechuga-Sancho, A. M., et al. (2020). Plant catalases as NO and H_2S targets. *Redox Biol*. 34:101525. doi: 10.1016/j.redox.2020.101525

Pandey, S., Fartyal, D., Agarwal, A., Shukla, T., James, D., Kaul, T., et al. (2017). Abiotic stress tolerance in plants: myriad roles of ascorbate peroxidase. *Front. Plant Sci*. 8:581. doi: 10.3389/fpls.2017.00581

Pasternak, T. P., Ötvös, K., Domoki, M., and Fehér, A. (2007). Linked activation of cell division and oxidative stress defense in alfalfa leaf protoplast-derived cells is dependent on exogenous auxin. *Plant Growth Regul*. 51, 109–117. doi: 10.1007/s10725-006-9152-0

Pei, Z.-M., Murata, Y., Benning, G., Thomine, S., Klüsener, B., Allen, G. J., et al. (2000). Calcium channels activated by hydrogen peroxide mediate abscisic acid signalling in guard cells. *Nature* 406, 731–734. doi: 10.1038/35021067

Perea-García, A., Andrés-Bordería, A., Mayo de Andrés, S., Sanz, A., Davis, A. M., Davis, S., et al. (2016). Modulation of copper deficiency responses by diurnal and circadian rhythms in *Arabidopsis thaliana*. *J. Exp. Bot*. 67, 391–403. doi: 10.1093/jxb/erv474

Pérez-Salamó, I., Papdi, C., Rigó, G., Zsigmond, L., Vilela, B., Lumbreras, V., et al. (2014). The heat shock factor A4A confers salt tolerance and is regulated by oxidative stress and the mitogen-activated protein kinases MPK3 and MPK6. *Plant Physiol*. 165, 319–334. doi: 10.1104/pp.114.237891

Persak, H., and Pitzschke, A. (2013). Tight interconnection and multi-level control of *Arabidopsis* MYB44 in MAPK cascade signalling. *PLoS ONE* 8:e57547. doi: 10.1371/journal.pone.0057547

Persak, H., and Pitzschke, A. (2014). Dominant repression by *Arabidopsis* transcription factor MYB44 causes oxidative damage and hypersensitivity to abiotic stress. *Int. J. Mol. Sci*. 15, 2517–2537. doi: 10.3390/ijms15022517

Petrov, V., Hille, J., Mueller-Roeber, B., and Gechev, T. S. (2015). ROS-mediated abiotic stress-induced programmed cell death in plants. *Front. Plant Sci*. 6:69. doi: 10.3389/fpls.2015.00069

Pilon, M. (2017). The copper microRNAs. *New Phytol*. 213, 1030–1035. doi: 10.1111/nph.14244

Pilon, M., Ravet, K., and Tapken, W. (2011). The biogenesis and physiological function of chloroplast superoxide dismutases. *Biochim. Biophys. Acta* 1807, 989–998. doi: 10.1016/j.bbabio.2010.11.002

Piterková, J., Luhová, L., Navrátilová, B., Sedlárová, M., and Petrivalsky, M. (2015). Early and long-term responses of cucumber cells to high cadmium concentration are modulated by nitric oxide and reactive oxygen species. *Acta Physiol. Plant* 37:19. doi: 10.1007/s11738-014-1756-9

Pitzschke, A., Djamei, A., Bitton, F., and Hirt, H. (2009). A major role of the MEKK1-MKK1/2-MPK4 pathway in ROS signalling. *Mol. Plant* 2, 120–137. doi: 10.1093/mp/ssn079

Pnueli, L., Liang, H., Rozenberg, M., and Mittler, R. (2003). Growth suppression, altered stomatal responses, and augmented induction of heat shock proteins in cytosolic ascorbate peroxidase (*Apx1*)-deficient *Arabidopsis* plants. *Plant J*. 34, 187–203. doi: 10.1046/j.1365-313x.2003.01715.x

Pospíšil, P. (2016). Production of reactive oxygen species by photosystem II as a response to light and temperature stress. *Front. Plant Sci*. 7:1950. doi: 10.3389/fpls.2016.01950

Rafikov, R., Kumar, S., Aggarwal, S., Hou, Y., Kangath, A., Pardo, D., et al. (2014). Endothelin-1 stimulates catalase activity through the PKCδ-mediated phosphorylation of serine 167. *Free Radic. Biol. Med*. 67, 255–264. doi: 10.1016/j.freeradbiomed.2013.10.814

Rahantaniaina, M.-S., Li, S., Chatel-Innocenti, G., Tuzet, A., Issakidis-Bourguet, E., Mhamdi, A., et al. (2017). Cytosolic and chloroplastic DHARs cooperate in oxidative stress-driven activation of the salicylic acid pathway. *Plant Physiol*. 174, 956–971. doi: 10.1104/pp.17.00317

Rahman, A., Mostofa, M. G., Alam, M. M., Nahar, K., Hasanuzzaman, M., and Fujita, M. (2015). Calcium mitigates arsenic toxicity in rice seedlings by reducing arsenic uptake and modulating the antioxidant defense and glyoxalase systems and stress markers. *Biomed Res. Int*. 2015:340812. doi: 10.1155/2015/340812

Rayapuram, N., Bigeard, J., Alhoraibi, H., Bonhomme, L., Hesse, A. M., Vinh, J., et al. (2018). Quantitative phosphoproteomic analysis reveals shared and specific targets of Arabidopsis mitogen-activated protein kinases (MAPKs) MPK3, MPK4, and MPK6. *Mol. Cell. Proteom*. 17, 61–80. doi: 10.1074/mcp.RA117.000135

Rayapuram, N., Bonhomme, L., Bigeard, J., Haddadou, K., Przybylski, C., Hirt, H., et al. (2014). Identification of novel PAMP-triggered phosphorylation and dephosphorylation events in *Arabidopsis thaliana* by quantitative phosphoproteomic analysis. *J. Proteome Res*. 13, 2137–2151. doi: 10.1021/pr401268v

Reiland, S., Finazzi, G., Endler, A., Willig, A., Baerenfaller, K., Grossmann, J., et al. (2011). Comparative phosphoproteome profiling reveals a function of the STN8 kinase in fine-tuning of cyclic electron flow (CEF). *Proc. Natl. Acad. Sci. U.S.A*. 108, 12955–12960. doi: 10.1073/pnas.1104734108

Reiland, S., Messerli, G., Baerenfaller, K., Gerrits, B., Endler, A., Grossmann, J., et al. (2009). Large-scale *Arabidopsis* phosphoproteome profiling reveals novel chloroplast kinase substrates and phosphorylation networks. *Plant Physiol*. 150, 889–903. doi: 10.1104/pp.109.138677

Rentel, M. C., Lecourieux, D., Ouaked, F., Usher, S. L., Petersen, L., Okamoto, H., et al. (2004). OXI1 kinase is necessary for oxidative burst-mediated signalling in *Arabidopsis*. *Nature* 427, 858–861. doi: 10.1038/nature02353

Richards, S. L., Laohavisit, A., Mortimer, J. C., Shabala, L., Swarbreck, S. M., Shabala, S., et al. (2014). Annexin 1 regulates the H_2O_2-induced calcium signature in *Arabidopsis thaliana* roots. *Plant J*. 77, 136–145. doi: 10.1111/tpj.12372

Riester, L., Köster-Hofmann, S., Doll, J., Berendzen, K. W., and Zentgraf, U. (2019). Impact of alternatively polyadenylated isoforms of ETHYLENE RESPONSE FACTOR4 with activator and repressor function on senescence in *Arabidopsis thaliana* L. *Genes* 10:91. doi: 10.3390/genes10020091

Rizhsky, L., Davletova, S., Liang, H., and Mittler, R. (2004b). The zinc finger protein Zat12 is required for cytosolic ascorbate peroxidase 1 expression during oxidative stress in Arabidopsis. *J. Biol. Chem*. 279, 11736–11743. doi: 10.1074/jbc.M313350200

Rizhsky, L., Liang, H., and Mittler, R. (2003). The water-water cycle is essential for chloroplast protection in the absence of stress. *J. Biol. Chem*. 278, 38921–38925. doi: 10.1074/jbc.M304987200

Rizhsky, L., Liang, H., Shuman, J., Shulaev, V., Davletova, S., and Mittler, R. (2004a). When defense pathways collide. The response of Arabidopsis to a combination of drought and heat stress. *Plant Physiol*. 134, 1683–1696. doi: 10.1104/pp.103.033431

Rizwan, M., Mostofa, M. G., Ahmad, M. Z., Imtiaz, M., Mehmood, S., Adeel, M., et al. (2018). Nitric oxide induces rice tolerance to excessive nickel by regulating nickel uptake, reactive oxygen species detoxification and defense-related gene expression. *Chemosphere* 191, 23–35. doi: 10.1016/j.chemosphere.2017.09.068

Roitinger, E., Hofer, M., Köcher, T., Pichler, P., Novatchkova, M., Yang, J., et al. (2015). Quantitative phosphoproteomics of the ataxia telangiectasia-mutated (ATM) and ataxia telangiectasia-mutated and rad3-related (ATR) dependent DNA damage response in *Arabidopsis thaliana*. *Mol. Cell Proteomics* 14, 556–571. doi: 10.1074/mcp.M114.040352

Romeis, T., and Herde, M. (2014). From local to global: CDPKs in systemic defense signaling upon microbial and herbivore attack. *Curr. Opin. Plant Biol*. 20, 1–10. doi: 10.1016/j.pbi.2014.03.002

Romero-Puertas, M. C., and Sandalio, L. M. (2016). Nitric oxide level is self-regulating and also regulates its ROS partners. *Front. Plant Sci*. 7:316. doi: 10.3389/fpls.2016.00316

Rossel, J. B., Walter, P. B., Hendrickson, L., Chow, W. S., Poole, A., Mullineaux, P. M., et al. (2006). A mutation affecting ASCORBATE PEROXIDASE 2 gene expression reveals a link between responses to high light and drought tolerance. *Plant Cell Environ*. 29, 269–281. doi: 10.1111/j.1365-3040.2005.01419.x

Rudnik, R., Bulcha, J. T., Reifschneider, E., Ellersiek, U., and Baier, M. (2017). Specificity versus redundancy in the RAP2.4 transcription factor family of *Arabidopsis thaliana*: transcriptional regulation of genes for chloroplast peroxidases. *BMC Plant Biol*. 17:144. doi: 10.1186/s12870-017-1092-5

Ruiz-May, E., Segura-Cabrera, A., Elizalde-Contreras, J. M., Shannon, L. M., and Loyola-Vargas, V. M. (2019). A recent advance in the intracellular and extracellular redox post-translational modification of proteins in plants. *J. Mol. Recogn*. 32:e2754. doi: 10.1002/jmr.2754

Sagi, M., and Fluhr, R. (2006). Production of reactive oxygen species by plant NADPH oxidases. *Plant Physiol*. 141, 336–340. doi: 10.1104/pp.106.078089

Šamajová, O., Plíhal, O., Al-Yousif, M., Hirt, H., and Šamaj, J. (2013). Improvement of stress tolerance in plants by genetic manipulation of mitogen-activated protein kinases. *Biotechnol. Adv*. 31, 118–128. doi: 10.1016/j.biotechadv.2011.12.002

Savatin, D. V., Bisceglia, N. G., Marti, L., Fabbri, C., Cervone, F., and De Lorenzo, G. (2014). The *Arabidopsis* NUCLEUS- AND PHRAGMOPLAST-LOCALIZED KINASE1-related protein kinases are required for elicitor-induced oxidative burst and immunity. *Plant Physiol*. 165, 1188–1202. doi: 10.1104/pp.114.236901

Schopfer, P., Liszkay, A., Bechtold, M., Frahry, G., and Wagner, A. (2002). Evidence that hydroxyl radicals mediate auxin-induced extension growth. *Planta* 214, 821–828. doi: 10.1007/s00425-001-0699-8

Schulz, P., Herde, M., and Romeis, T. (2013). Calcium-dependent protein kinases: hubs in plant stress signaling and development. *Plant Physiol*. 163, 523–530. doi: 10.1104/pp.113.222539

Sewelam, N., Kazan, K., Thomas-Hall, S. R., Kidd, B. N., Manners, J. M., and Schenk, P. M. (2013). Ethylene response factor 6 is a regulator of reactive oxygen species signaling in *Arabidopsis*. *PLoS ONE* 8:e70289. doi: 10.1371/journal.pone.0070289

Shafi, A., Chauhan, R., Gill, T., Swarnkar, M. K., Sreenivasulu, Y., Kumar, S., et al. (2015). Expression of SOD and APX genes positively regulates secondary cell wall biosynthesis and promotes plant growth and yield in *Arabidopsis* under salt stress. *Plant Mol. Biol*. 87, 615–631. doi: 10.1007/s11103-015-0301-6

Shaikhali, J., Heiber, I., Seidel, T., Ströher, E., Hiltscher, H., Birkmann, S., et al. (2008). The redox-sensitive transcription factor Rap2.4a controls nuclear expression of 2-Cys peroxiredoxin A and other chloroplast antioxidant enzymes. *BMC Plant Biol*. 8:48. doi: 10.1186/1471-2229-8-48

Shan, C., and Yang, T. (2017). Nitric oxide acts downstream of hydrogen peroxide in the regulation of ascorbate and glutathione metabolism by jasmonic acid in *Agropyron cristatum* leaves. *Biol. Plant*. 61, 779–784. doi: 10.1007/s10535-017-0708-9

Shapiguzov, A., Vainonen, J. P., Hunter, K., Tossavainen, H., Tiwari, A., Järvi, S., et al. (2019). *Arabidopsis* RCD1 coordinates chloroplast and mitochondrial functions through interaction with ANAC transcription factors. *Elife* 8:e43284. doi: 10.7554/eLife.43284

Sharma, I., and Ahmad, P. (2014). "Catalase: a versatile antioxidant in plants," in *Oxidative Damage to Plants*, ed P. Ahmad (Srinagar: S.P. College), 131–148.

Shukla, P., and Singh, A. K. (2015). Nitric oxide mitigates arsenic-induced oxidative stress and genotoxicity in *Vicia faba* L. *Environ. Sci. Pollut. Res*. 22, 13881–13891. doi: 10.1007/s11356-015-4501-z

Sierla, M., Waszczak, C., Vahisalu, T., and Kangasjärvi, J. (2016). Reactive oxygen species in the regulation of stomatal movements. *Plant Physiol*. 171, 1569–1580. doi: 10.1104/pp.16.00328

Smékalová, V., Doskočilová, A., Komis, G., and Šamaj, J. (2014). Crosstalk between secondary messengers, hormones and MAPK modules during abiotic stress signalling in plants. *Biotechnol. Adv*. 32, 2–11. doi: 10.1016/j.biotechadv.2013.07.009

Smirnoff, N. (2018). Ascorbic acid metabolism and functions: a comparison of plants and mammals. *Free Radic. Biol. Med*. 122, 116–129. doi: 10.1016/j.freeradbiomed.2018.03.033

Smirnoff, N., and Arnaud, D. (2019). Hydrogen peroxide metabolism and functions in plants. *New Phytol*. 221, 1197–1214. doi: 10.1111/nph.15488

Song, C., Chung, W. S., and Lim, C. O. (2016). Overexpression of heat shock factor gene HsfA3 increases galactinol levels and oxidative stress tolerance in *Arabidopsis*. *Mol. Cells* 39, 477–483. doi: 10.14348/molcells.2016.0027

Su, T., Wang, P., Li, H., Zhao, Y., Lu, Y., Dai, P., et al. (2018). The *Arabidopsis* catalase triple mutant reveals important roles of catalases and peroxisome-derived signaling in plant development. *J. Integr. Plant Biol*. 60, 591–607. doi: 10.1111/jipb.12649

Sugiyama, N., Nakagami, H., Mochida, K., Daudi, A., Tomita, M., Shirasu, K., et al. (2008). Large-scale phosphorylation mapping reveals the extent of tyrosine phosphorylation in *Arabidopsis*. *Mol. Syst. Biol*. 4:193. doi: 10.1038/msb.2008.32

Sultana, S., Khew, C. Y., Morshed, M. M., Namasivayam, P., Napis, S., and Ho, C. L. (2012). Overexpression of monodehydroascorbate reductase from a mangrove plant (AeMDHAR) confers salt tolerance on rice. *J. Plant Physiol*. 169, 311–318. doi: 10.1016/j.jplph.2011.09.004

Sumugat, M. R., Donahue, J. L., Cortes, D. F., Stromberg, V. K., Grene, R., Shulaev, V., et al. (2010). Seed development and germination in an *Arabidopsis thaliana* line antisense to glutathione reductase 2. *J. New Seeds* 11, 104–126. doi: 10.1080/15228861003776175

Sunkar, R., Kapoor, A., and Zhu, J. K. (2006). Posttranscriptional induction of two Cu/Zn superoxide dismutase genes in *Arabidopsis* is mediated by downregulation of miR398 and important for oxidative stress tolerance. *Plant Cell* 18, 2051–2065. doi: 10.1105/tpc.106.041673

Suzuki, N., Miller, G., Sejima, H., Harper, J., and Mittler, R. (2013). Enhanced seed production under prolonged heat stress conditions in *Arabidopsis thaliana* plants deficient in cytosolic ascorbate peroxidase 2. *J. Exp. Bot*. 64, 253–263. doi: 10.1093/jxb/ers335

Suzuki, Y. J., Carini, M., and Butterfield, D. A. (2010). Protein carbonylation. *Antioxid. Redox Signal*. 12, 323–325. doi: 10.1089/ars.2009.2887

Takáč, T., Obert, B., Rolčík, J., and Šamaj, J. (2016a). Improvement of adventitious root formation in flax using hydrogen peroxide. *N. Biotechnol*. 33, 728–734. doi: 10.1016/j.nbt.2016.02.008

Takáč, T., Šamajová, O., Vadovič, P., Pechan, T., Košútová, P., Ovečka, M., et al. (2014). Proteomic and biochemical analyses show a functional network of proteins involved in antioxidant defense of the *Arabidopsis anp2anp3* double mutant. *J. Proteome Res*. 13, 5347–5361. doi: 10.1021/pr500588c

Takáč, T., Vadovič, P., Pechan, T., Luptovčiak, I., Šamajová, O., Šamaj, J. (2016b). Comparative proteomic study of *Arabidopsis* mutants mpk4 and mpk6. *Sci. Rep*. 6:28306. doi: 10.1038/srep28306

Teh, O.-K., and Hofius, D. (2014). Membrane trafficking and autophagy in pathogen-triggered cell death and immunity. *J. Exp. Bot*. 65, 1297–1312. doi: 10.1093/jxb/ert441

Tian, W., Wang, C., Gao, Q., Li, L., and Luan, S. (2020). Calcium spikes, waves and oscillations in plant development and biotic interactions. *Nat. Plants* 6, 750–759. doi: 10.1038/s41477-020-0667-6

Tichá, T., Lochman, J., Cinčalová, L., Luhová, L., and Petrivalský, M. (2017). Redox regulation of plant S-nitrosoglutathione reductase activity through post-translational modifications of cysteine residues. *Biochem. Biophys. Res. Commun*. 494, 27–33. doi: 10.1016/j.bbrc.2017.10.090

Tognetti, V. B., Van Aken, O., Morreel, K., Vandenbroucke, K., van de Cotte, B., De Clercq, I., et al. (2010). Perturbation of indole-3-butyric acid homeostasis by the UDP-glucosyltransferase UGT74E2 modulates *Arabidopsis* architecture and water stress tolerance. *Plant Cell* 22, 2660–2679. doi: 10.1105/tpc.109.071316

Tsang, C. K., Chen, M., Cheng, X., Qi, Y., Chen, Y., Das, I., et al. (2018). SOD1 phosphorylation by mTORC1 couples nutrient sensing and redox regulation. *Mol. Cell* 70, 502–515.e8. doi: 10.1016/j.molcel.2018.03.029

Tsang, C. K., Liu, Y., Thomas, J., Zhang, Y., and Zheng, X. F. (2014). Superoxide dismutase 1 acts as a nuclear transcription factor to regulate oxidative stress resistance. *Nat. Commun*. 5:3446. doi: 10.1038/ncomms4446

Tuzet, A., Rahantaniaina, M. S., and Noctor, G. (2019). Analyzing the function of catalase and the ascorbate-glutathione pathway in H_2O_2 processing: insights from an experimentally constrained kinetic model. *Antioxid. Redox Signal*. 30, 1238–1268. doi: 10.1089/ars.2018.7601

Umezawa, T., Sugiyama, N., Takahashi, F., Anderson, J. C., Ishihama, Y., Peck, S. C., et al. (2013). Genetics and phosphoproteomics reveal a protein phosphorylation network in the abscisic acid signaling pathway in *Arabidopsis thaliana*. *Sci. Signal*. 6:rs8. doi: 10.1126/scisignal.2003509

Ushimaru, T., Nakagawa, T., Fujioka, Y., Daicho, K., Naito, M., Yamauchi, Y., et al. (2006). Transgenic *Arabidopsis* plants expressing the rice dehydroascorbate reductase gene are resistant to salt stress. *J. Plant Physiol.* 163, 1179–1184. doi: 10.1016/j.jplph.2005.10.002

Vadassery, J., Tripathi, S., Prasad, R., Varma, A., and Oelmüller, R. (2009). Monodehydroascorbate reductase 2 and dehydroascorbate reductase 5 are crucial for a mutualistic interaction between *Piriformospora indica* and *Arabidopsis*. *J. Plant Physiol.* 166, 1263–1274. doi: 10.1016/j.jplph.2008.12.016

van Buer, J., Cvetkovic, J., and Baier, M. (2016). Cold regulation of plastid ascorbate peroxidases serves as a priming hub controlling ROS signaling in *Arabidopsis thaliana*. *BMC Plant Biol.* 16:163. doi: 10.1186/s12870-016-0856-7

Van Leene, J., Han, C., Gadeyne, A., Eeckhout, D., Matthijs, C., Cannoot, B., et al. (2019). Capturing the phosphorylation and protein interaction landscape of the plant TOR kinase. *Nat. Plants* 5, 316–327. doi: 10.1038/s41477-019-0378-z

Vandenabeele, S., Vanderauwera, S., Vuylsteke, M., Rombauts, S., Langebartels, C., Seidlitz, H. K., et al. (2004). Catalase deficiency drastically affects gene expression induced by high light in *Arabidopsis thaliana*. *Plant J.* 39, 45–58. doi: 10.1111/j.1365-313X.2004.02105.x

Vanderauwera, S., Suzuki, N., Miller, G., van de Cotte, B., Morsa, S., Ravanat, J. L., et al. (2011). Extranuclear protection of chromosomal DNA from oxidative stress. *Proc. Natl. Acad. Sci. U.S.A.* 108, 1711–1716. doi: 10.1073/pnas.101835910

Vogel, J. T., Zarka, D. G., Van Buskirk, H. A., Fowler, S. G., and Thomashow, M. F. (2005). Roles of the CBF2 and ZAT12 transcription factors in configuring the low temperature transcriptome of *Arabidopsis*. *Plant J.* 41, 195–211. doi: 10.1111/j.1365-313X.2004.02288.x

Vogel, M. O., Moore, M., König, K., Pecher, P., Alsharafa, K., Lee, J., et al. (2014). Fast retrograde signaling in response to high light involves metabolite export, MITOGEN-ACTIVATED PROTEIN KINASE6, and AP2/ERF transcription factors in *Arabidopsis*. *Plant cell* 26, 1151–1165. doi: 10.1105/tpc.113.121061

Voothuluru, P., and Sharp, R. E. (2013). Apoplastic hydrogen peroxide in the growth zone of the maize primary root under water stress. *I.* Increased levels are specific to the apical region of growth maintenance. *J. Exp. Bot.* 64, 1223–1233. doi: 10.1093/jxb/ers277

Vu, L. D., Gevaert, K., and De Smet, I. (2018). Protein language: post-translational modifications talking to each other. *Trends Plant Sci.* 23, 1068–1080. doi: 10.1016/j.tplants.2018.09.004

Wang, B., Ding, H., Chen, Q., Ouyang, L., Li, S., and Zhang, J. (2019). Enhanced tolerance to methyl viologen-mediated oxidative stress via *AtGR2* expression from chloroplast genome. *Front. Plant Sci.* 10:1178. doi: 10.3389/fpls.2019.01178

Wang, P., Du, Y., Zhao, X., Miao, Y., and Song, C. P. (2013a). The MPK6-ERF6-ROS-responsive cis-acting Element7/GCC box complex modulates oxidative gene transcription and the oxidative response in *Arabidopsis*. *Plant Physiol.* 161, 1392–1408. doi: 10.1104/pp.112.210724

Wang, P., Xue, L., Batelli, G., Lee, S., Hou, Y. J., Van Oosten, M. J., et al. (2013b). Quantitative phosphoproteomics identifies SnRK2 protein kinase substrates and reveals the effectors of abscisic acid action. *Proc. Natl. Acad. Sci. U.S.A.* 110, 11205–11210. doi: 10.1073/pnas.1308974110

Wang, W., Zhang, H., Wei, X., Yang, L., Yang, B., Zhang, L., et al. (2018). Functional characterization of calcium-dependent protein kinase (CPK) 2 gene from oilseed rape (*Brassica napus* L.) in regulating reactive oxygen species signaling and cell death control. *Gene* 651, 49–56. doi: 10.1016/j.gene.2018.02.006

Wang, X., Bian, Y., Cheng, K., Gu, L. F., Ye, M., Zou, H., et al. (2013c). A large-scale protein phosphorylation analysis reveals novel phosphorylation motifs and phosphoregulatory networks in *Arabidopsis*. *J. Proteom.* 78, 486–498. doi: 10.1016/j.jprot.2012.10.018

Wang, X., Bian, Y., Cheng, K., Zou, H., Sun, S. S., and He, J. X. (2012). A comprehensive differential proteomic study of nitrate deprivation in *Arabidopsis* reveals complex regulatory networks of plant nitrogen responses. *J. Proteome Res.* 11, 2301–2315. doi: 10.1021/pr2010764

Wang, Z., Xiao, Y., Chen, W., Tang, K., and Zhang, L. (2010). Increased vitamin C content accompanied by an enhanced recycling pathway confers oxidative stress tolerance in *Arabidopsis*. *J. Integr. Plant Biol.* 52, 400–409. doi: 10.1111/j.1744-7909.2010.00921.x

Waszczak, C., Akter, S., Eeckhout, D., Persiau, G., Wahni, K., Bodra, N., et al. (2014). Sulfenome mining in *Arabidopsis thaliana*. *Proc. Natl. Acad. Sci. U.S.A.* 111, 11545–11550. doi: 10.1073/pnas.1411607111

Waszczak, C., Akter, S., Jacques, S., Huang, J., Messens, J., and Van Breusegem, F. (2015). Oxidative post-translational modifications of cysteine residues in plant signal transduction. *J. Exp. Bot.* 66, 2923–2934. doi: 10.1093/jxb/erv084

Waszczak, C., Carmody, M., and Kangasjärvi, J. (2018). Reactive oxygen species in plant signaling. *Annu. Rev. Plant Biol.* 69, 209–236. doi: 10.1146/annurev-arplant-042817-040322

Wen, F., Ye, F., Xiao, Z., Liao, L., Li, T., Jia, M., et al. (2020). Genome-wide survey and expression analysis of calcium-dependent protein kinase (CDPK) in grass *Brachypodium distachyon*. *BMC Genomics* 21:53. doi: 10.1186/s12864-020-6475-6

Withers, J., and Dong, X. (2017). Post-translational regulation of plant immunity. *Curr. Opin. Plant Biol.* 38, 124–132. doi: 10.1016/j.pbi.2017.05.004

Wu, F., Chi, Y., Jiang, Z., Xu, Y., Xie, L., Huang, F., et al. (2020). Hydrogen peroxide sensor HPCA1 is an LRR receptor kinase in *Arabidopsis*. *Nature* 578, 577–581. doi: 10.1038/s41586-020-2032-3

Wu, T. M., Lin, W. R., Kao, C. H., and Hong, C. Y. (2015). Gene knockout of *glutathione reductase 3* results in increased sensitivity to salt stress in rice. *Plant Mol. Biol.* 87, 555–564. doi: 10.1007/s11103-015-0290-5

Xia, X.-J., Zhou, Y.-H., Shi, K., Zhou, J., Foyer, C. H., and Yu, J.-Q. (2015). Interplay between reactive oxygen species and hormones in the control of plant development and stress tolerance. *J. Exp. Bot.* 66, 2839–2856. doi: 10.1093/jxb/erv089

Xing, C., Liu, Y., Zhao, L., Zhang, S., and Huang, X. (2019). A novel MYB transcription factor regulates ascorbic acid synthesis and affects cold tolerance. *Plant Cell Environ.* 42, 832–845. doi: 10.1111/pce.13387

Xing, Y., Cao, Q., Zhang, Q., Qin, L., Jia, W., and Zhang, J. (2013). MKK5 regulates high light-induced gene expression of Cu/Zn superoxide dismutase 1 and 2 in *Arabidopsis*. *Plant Cell Physiol.* 54, 1217–1227. doi: 10.1093/pcp/pct072

Xing, Y., Chen, W. H., Jia, W., and Zhang, J. (2015). Mitogen-activated protein kinase kinase 5 (MKK5)-mediated signalling cascade regulates expression of iron superoxide dismutase gene in *Arabidopsis* under salinity stress. *J. Exp. Bot.* 66, 5971–5981. doi: 10.1093/jxb/erv305

Xing, Y., Jia, W., and Zhang, J. (2007). AtMEK1 mediates stress-induced gene expression of CAT1 catalase by triggering H_2O_2 production in *Arabidopsis*. *J. Exp. Bot.* 58, 2969–2981. doi: 10.1093/jxb/erm144

Xing, Y., Jia, W., and Zhang, J. (2008). AtMKK1 mediates ABA-induced *CAT1* expression and H_2O_2 production via AtMPK6-coupled signaling in *Arabidopsis*. *Plant J.* 54, 440–451. doi: 10.1111/j.1365-313X.2008.03433.x

Xu, J., Tran, T., Padilla Marcia, C. S., Braun, D. M., and Goggin, F. L. (2017). Superoxide-responsive gene expression in *Arabidopsis thaliana* and *Zea mays*. *Plant Physiol. Biochem.* 117, 51–60. doi: 10.1016/j.plaphy.2017.05.018

Xu, P., Chen, H., and Cai, W. (2020). Transcription factor CDF4 promotes leaf senescence and floral organ abscission by regulating abscisic acid and reactive oxygen species pathways in *Arabidopsis*. *EMBO Rep.* 21:e48967. doi: 10.15252/embr.201948967

Xue, L., Wang, P., Wang, L., Renzi, E., Radivojac, P., Tang, H., et al. (2013). Quantitative measurement of phosphoproteome response to osmotic stress in *Arabidopsis* based on Library-Assisted eXtracted Ion Chromatogram (LAXIC). *Mol. Cell. Proteomics* 12, 2354–2369. doi: 10.1074/mcp.O113.027284

Xue, Y., Zhou, F., Zhu, M., Ahmed, K., Chen, G., and Yao, X. (2005). GPS: a comprehensive www server for phosphorylation sites prediction. *Nucleic Acids Res.* 33, W184–W187. doi: 10.1093/nar/gki393

Yalcinkaya, T., Uzilday, B., Ozgur, R., Turkan, I., and Mano, J. (2019). Lipid peroxidation-derived reactive carbonyl species (RCS): their interaction with ROS and cellular redox during environmental stresses. *Environ. Exp. Bot.* 165, 139–149. doi: 10.1016/j.envexpbot.2019.06.004

Yamasaki, H., Abdel-Ghany, S. E., Cohu, C. M., Kobayashi, Y., Shikanai, T., and Pilon, M. (2007). Regulation of copper homeostasis by micro-RNA in *Arabidopsis*. *J. Biol. Chem.* 282, 16369–16378. doi: 10.1074/jbc.M700138200

Yamasaki, H., Hayashi, M., Fukazawa, M., Kobayashi, Y., and Shikanai, T. (2009). SQUAMOSA promoter binding protein-like7 is a central regulator for copper homeostasis in *Arabidopsis*. *Plant Cell* 21, 347–361. doi: 10.1105/tpc.108.060137

Yan, J., Guan, L., Sun, Y., Zhu, Y., Liu, L., Lu, R., et al. (2015). Calcium and ZmCCaMK are involved in brassinosteroid-induced antioxidant defense in maize leaves. *Plant Cell Physiol.* 56, 883–896. doi: 10.1093/pcp/pcv014

Yang, H., Mu, J., Chen, L., Feng, J., Hu, J., Li, L., et al. (2015). S-Nitrosylation positively regulates ascorbate peroxidase activity during plant stress responses. *Plant Physiol.* 167, 1604–1615. doi: 10.1104/pp.114.255216

Yang, Z., Guo, G., Zhang, M., Liu, C. Y., Hu, Q., Lam, H., et al. (2013). Stable isotope metabolic labeling-based quantitative phosphoproteomic analysis of *Arabidopsis* mutants reveals ethylene-regulated time-dependent phosphoproteins and putative substrates of constitutive triple response 1 kinase. *Mol. Cell. Proteom.* 12, 3559–3582. doi: 10.1074/mcp.M113.031633

Yang, Z., Mhamdi, A., and Noctor, G. (2019). Analysis of catalase mutants underscores the essential role of CATALASE2 for plant growth and day length-dependent oxidative signalling. *Plant Cell Environ.* 42, 688–700. doi: 10.1111/pce.13453

Yin, L., Mano, J., Tanaka, K., Wang, S., Zhang, M., Deng, X., et al. (2017). High level of reduced glutathione contributes to detoxification of lipid peroxide-derived reactive carbonyl species in transgenic *Arabidopsis* overexpressing glutathione reductase under aluminum stress. *Physiol. Plant.* 161, 211–223. doi: 10.1111/ppl.12583

Yin, L., Wang, S., Eltayeb, A. E., Uddin, M. I., Yamamoto, Y., Tsuji, W., et al. (2010). Overexpression of dehydroascorbate reductase, but not monodehydroascorbate reductase, confers tolerance to aluminum stress in transgenic tobacco. *Planta* 231, 609–621. doi: 10.1007/s00425-009-1075-3

Yoshida, K., Noguchi, K., Motohashi, K., and Hisabori, T. (2013). Systematic exploration of thioredoxin target proteins in plant mitochondria. *Plant Cell Physiol.* 54, 875–892. doi: 10.1093/pcp/pct037

Yoshida, S., Tamaoki, M., Shikano, T., Nakajima, N., Ogawa, D., Ioki, M., et al. (2006). Cytosolic dehydroascorbate reductase is important for ozone tolerance in *Arabidopsis thaliana*. *Plant Cell Physiol.* 47, 304–308. doi: 10.1093/pcp/pci246

Yu, X., Pasternak, T., Eiblmeier, M., Ditengou, F., Kochersperger, P., Sun, J., et al. (2013). Plastid-localized glutathione reductase2-regulated glutathione redox status is essential for *Arabidopsis* root apical meristem maintenance. *Plant Cell* 25, 4451–4468. doi: 10.1105/tpc.113.11702

Zandalinas, S. I., Fichman, Y., Devireddy, A. R., Sengupta, S., Azad, R. K., and Mittler, R. (2020). Systemic signaling during abiotic stress combination in plants. *Proc. Natl. Acad. Sci. U.S.A.* 117, 13810–13820. doi: 10.1073/pnas.2005077117

Zandalinas, S. I., Sengupta, S., Burks, D., Azad, R. K., and Mittler, R. (2019). Identification and characterization of a core set of ROS wave-associated transcripts involved in the systemic acquired acclimation response of *Arabidopsis* to excess light. *Plant J.* 98, 126–141. doi: 10.1111/tpj.14205

Zechmann, B. (2018). Compartment-specific importance of ascorbate during environmental stress in plants. *Antioxid. Redox Signal.* 29, 1488–1501. doi: 10.1089/ars.2017.7232

Zhang, A., Zhang, J., Ye, N., Cao, J., Tan, M., Zhang, J., et al. (2010). ZmMPK5 is required for the NADPH oxidase-mediated self-propagation of apoplastic H_2O_2 in brassinosteroid-induced antioxidant defence in leaves of maize. *J. Exp. Bot.* 61, 4399–4411. doi: 10.1093/jxb/erq243

Zhang, H., Liu, Y., Wen, F., Yao, D., Wang, L., Guo, J., et al. (2014). A novel rice C2H2-type zinc finger protein, ZFP36, is a key player involved in abscisic acid-induced antioxidant defence and oxidative stress tolerance in rice. *J. Exp. Bot.* 65, 5795–5809. doi: 10.1093/jxb/eru313

Zhang, H., Zhang, Y., Deng, C., Deng, S., Li, N., Zhao, C., et al. (2018). The *Arabidopsis* Ca^{2+}-dependent protein kinase CPK12 is involved in plant response to salt stress. *Int. J. Mol. Sci.* 19:4062. doi: 10.3390/ijms19124062

Zhang, H., Zhou, H., Berke, L., Heck, A. J., Mohammed, S., Scheres, B., et al. (2013). Quantitative phosphoproteomics after auxin-stimulated lateral root induction identifies an SNX1 protein phosphorylation site required for growth. *Mol. Cell. Proteomics* 12, 1158–1169. doi: 10.1074/mcp.M112.021220

Zhang, M., Li, Q., Liu, T., Liu, L., Shen, D., Zhu, Y., et al. (2015). Two cytoplasmic effectors of *Phytophthora sojae* regulate plant cell death via interactions with plant catalases. *Plant Physiol.* 167, 164–175. doi: 10.1104/pp.114.252437

Zhang, P., Wang, R., Ju, Q., Li, W., Tran, L. P., and Xu, J. (2019). The R2R3-MYB transcription factor MYB49 regulates cadmium accumulation. *Plant Physiol.* 180, 529–542. doi: 10.1104/pp.18.01380

Zhang, P., Wang, R., Yang, X., Ju, Q., Li, W., Lü, S., et al. (2020). The R2R3-MYB transcription factor AtMYB49 modulates salt tolerance in *Arabidopsis* by modulating the cuticle formation and antioxidant defence. *Plant Cell Environ.* 43, 1925–1943. doi: 10.1111/pce.13784

Zhang, S., Li, C., Ren, H., Zhao, T., Li, Q., Wang, S., et al. (2020). BAK1 mediates light intensity to phosphorylate and activate catalases to regulate plant growth and development. *Int. J. Mol. Sci.* 21:1437. doi: 10.3390/ijms21041437

Zhang, T., Zhu, M., Song, W. Y., Harmon, A. C., and Chen, S. (2015). Oxidation and phosphorylation of MAP kinase 4 cause protein aggregation. *Biochim. Biophys. Acta* 1854, 156–165. doi: 10.1016/j.bbapap.2014.11.006

Zhang, Y., Ji, T. T., Li, T. T., Tian, Y. Y., Wang, L. F., and Liu, W. C. (2020). Jasmonic acid promotes leaf senescence through MYC2-mediated repression of *CATALASE2* expression in *Arabidopsis*. *Plant Sci.* 299:110604. doi: 10.1016/j.plantsci.2020.110604

Zhang, Z., Wu, Y., Gao, M., Zhang, J., Kong, Q., Liu, Y., et al. (2012). Disruption of PAMP-induced MAP kinase cascade by a *Pseudomonas syringae* effector activates plant immunity mediated by the NB-LRR protein SUMM2. *Cell Host Microbe* 11, 253–263. doi: 10.1016/j.chom.2012.01.015

Zhao, R., Sun, H., Zhao, N., Jing, X., Shen, X., and Chen, S. (2015). The *Arabidopsis* Ca^{2+}-dependent protein kinase CPK27 is required for plant response to salt-stress. *Gene* 563, 203–214. doi: 10.1016/j.gene.2015.03.024

Zhou, Y. B., Liu, C., Tang, D. Y., Yan, L., Wang, D., Yang, Y. Z., et al. (2018). The receptor-like cytoplasmic kinase STRK1 phosphorylates and activates CatC, thereby regulating H_2O_2 homeostasis and improving salt tolerance in rice. *Plant Cell* 30, 1100–1118. doi: 10.1105/tpc.17.01000

Zimmermann, P., Heinlein, C., Orendi, G., and Zentgraf, U. (2006). Senescence-specific regulation of catalases in *Arabidopsis thaliana* (L.) Heynh. *Plant Cell Environ.* 29, 1049–1060. doi: 10.1111/j.1365-3040.2005.01459.x

Zou, J.-J., Li, X.-D., Ratnasekera, D., Wang, C., Liu, W.-X., Song, L.-F., et al. (2015). *Arabidopsis* CALCIUM-DEPENDENT PROTEIN KINASE8 and CATALASE3 function in abscisic acid-mediated signaling and H_2O_2 homeostasis in stomatal guard cells under drought stress. *Plant Cell* 27, 1445–1460. doi: 10.1105/tpc.15.00144

Zulawski, M., Braginets, R., and Schulze, W. X. (2013). PhosPhAt goes kinases-searchable protein kinase target information in the plant phosphorylation site database PhosPhAt. *Nucleic Acids Res.* 41, D1176–D1184. doi: 10.1093/nar/gks1081

Zwack, P. J., De Clercq, I., Howton, T. C., Hallmark, H. T., Hurny, A., Keshishian, E. A., et al. (2016). Cytokinin response factor 6 represses cytokinin-associated genes during oxidative stress. *Plant Physiol.* 172, 1249–1258. doi: 10.1104/pp.16.00415

Conflict of Interest: The authors declare that the research was conducted in the absence of any commercial or financial relationships that could be construed as a potential conflict of interest.

8.4 Supplement IV

8.4.1 Biotechnological Perspectives of Omics and Genetic Engineering Methods in Alfalfa

Hrbáčková, M.*, **Dvořák, P**.*, Takáč, T., Tichá, M., Luptovčiak, I., Šamajová, O., Ovečka, M., Šamaj, J. (2020). Biotechnological perspectives of omics and genetic engineering methods in alfalfa. *Frontiers in Plant Science* 11, 592. doi: 10.3389/fpls.2020.00592. * joined first authors

frontiers in Plant Science

REVIEW
published: 21 May 2020
doi: 10.3389/fpls.2020.00592

Biotechnological Perspectives of Omics and Genetic Engineering Methods in Alfalfa

*Miroslava Hrbáčková†, Petr Dvořák†, Tomáš Takáč, Michaela Tichá, Ivan Luptovčiak, Olga Šamajová, Miroslav Ovečka and Jozef Šamaj**

Department of Cell Biology, Centre of the Region Haná for Biotechnological and Agricultural Research, Faculty of Science, Palacký University Olomouc, Olomouc, Czechia

OPEN ACCESS

Edited by:
Agnieszka Ludwików, Adam Mickiewicz University, Poland

Reviewed by:
Tianzuo Wang, Institute of Botany, Chinese Academy of Sciences, China
Rui-Cai Long, Institute of Animal Sciences, Chinese Academy of Agricultural Sciences, China
Taras P. Pasternak, University of Freiburg, Germany

***Correspondence:**
Jozef Šamaj
jozef.samaj@upol.cz

† These authors have contributed equally to this work

Specialty section:
This article was submitted to Plant Biotechnology, a section of the journal Frontiers in Plant Science

Received: *27 February 2020*
Accepted: *20 April 2020*
Published: *21 May 2020*

Citation:
Hrbáčková M, Dvořák P, Takáč T, Tichá M, Luptovčiak I, Šamajová O, Ovečka M and Šamaj J (2020) Biotechnological Perspectives of Omics and Genetic Engineering Methods in Alfalfa. Front. Plant Sci. 11:592. doi: 10.3389/fpls.2020.00592

For several decades, researchers are working to develop improved major crops with better adaptability and tolerance to environmental stresses. Forage legumes have been widely spread in the world due to their great ecological and economic values. Abiotic and biotic stresses are main factors limiting legume production, however, alfalfa (*Medicago sativa* L.) shows relatively high level of tolerance to drought and salt stress. Efforts focused on alfalfa improvements have led to the release of cultivars with new traits of agronomic importance such as high yield, better stress tolerance or forage quality. Alfalfa has very high nutritional value due to its efficient symbiotic association with nitrogen-fixing bacteria, while deep root system can help to prevent soil water loss in dry lands. The use of modern biotechnology tools is challenging in alfalfa since full genome, unlike to its close relative barrel medic (*Medicago truncatula* Gaertn.), was not released yet. Identification, isolation, and improvement of genes involved in abiotic or biotic stress response significantly contributed to the progress of our understanding how crop plants cope with these environmental challenges. In this review, we provide an overview of the progress that has been made in high-throughput sequencing, characterization of genes for abiotic or biotic stress tolerance, gene editing, as well as proteomic and metabolomics techniques bearing biotechnological potential for alfalfa improvement.

Keywords: alfalfa, *Medicago sativa*, genomics, metabolomics, proteomics, stress resistance genes

INTRODUCTION

Legumes are important food crops for the exponentially growing population, owing to their micronutrient, macronutrient, and secondary metabolite content (Le et al., 2007). Some of these organic compounds (e.g., phytoalexins and chitinases) play roles in plant defense against pathogens and pests (He and Dixon, 2000). Moreover, Fabaceae is one of the most studied plant families, and it has gained high agricultural importance, especially owing to its ability to fix nitrogen in symbiosis with rhizobia (Doyle and Luckow, 2003).

Medicago sativa L., commonly known as alfalfa or "lucerne," belongs to Fabaceae, and its first cultivated form most likely originates from western Persia. It then spread to many regions in Asia, Europe, and America. In addition, Rashmi et al. (1997) and Samac and Temple (2004) reported that alfalfa ranks fourth in terms of acreage and economic value, following corn, soybean, and wheat.

The genus *Medicago* includes both perennial and annual species. Alfalfa is a highly valuable perennial deep-rooted forage legume, especially because of its widespread production, soil protection, and ability to improve nitrogen-limited soils (Radović et al., 2009). It is also widely cultivated for livestock feed (Flajoulot et al., 2005), and is used as a biofuel feedstock for ethanol production, either as hay or silage (McCoy and Bingham, 1988). The biological and agronomical potential of alfalfa, like all other members of the whole legume family, is extraordinary because it requires little to no nitrogen fertilizer for optimal growth (Ebert, 2007). In addition, alfalfa plays an important role as a free fertilizer providing nitrogen to subsequent crops (Triboi and Triboi-Blondel, 2014).

Alfalfa shows a high content of proteins, enzymes (amylase, coagulase, peroxidase, erepsin, lipase, invertase, and pectinase), antioxidants, minerals, and vitamins A, C, K, and E, as well as valuable phytopharmaceutical components (Bora and Sharma, 2011 and references therein). Moreover, alfalfa and some other species of Fabaceae family possess two different thiol redox compounds, namely glutathione (GSH) and the homoglutathione (hGSH), with higher content of hGSH (Klapheck, 1988; Baldacci-Cresp et al., 2012). More specifically, alfalfa shows different ratios of hGSH/GSH in diverse organs such as leaves, stems, and roots (Pasternak et al., 2014). Thus, alfalfa represents one of the most valuable and important forage crops, and can also be used in grasslands as a cover crop for improved weed control. Finally, alfalfa is also suitable for use in the production of recombinant pharmaceutical proteins (Fu et al., 2015) and in phytoremediation (Nirola et al., 2016).

The tetraploid genome of alfalfa and outbreeding mating systems have made selective breeding harder (Zhou et al., 2011; Annicchiarico et al., 2015). Advanced methods such as genomic, proteomic, and metabolomic approaches, as well as gene editing, could lead to the practical applications of genes that have biotechnological value for alfalfa improvement, especially if applied in an integrated and targeted manner. As a result, single or multiple genes might show desirable effects on several agronomically important alfalfa traits, which can significantly accelerate research in comparison to conventional breeding (Singer et al., 2018). Alfalfa is a major source of proteins in the livestock and dairy industries. In the last years, alfalfa production has been displaced to saline environments by major cereals. Therefore, the incorporation of transgenic traits into alfalfa with varying degrees of tolerance to salinity has been developed and this robust approach can improve the productivity and quality of nitrogen-fixing crops (Kang et al., 2016; Stritzler et al., 2018). Genetically engineered glyphosate-resistant alfalfa was commercialized in the United States in 2010. Another alfalfa variety with reduced lignin content stacked to glyphosate resistance trait has been available since 2015. Reduced lignin content in forage legumes can improve their digestibility by animals, thus it is an important forage quality trait (Li et al., 2016; Barros et al., 2019).

The purpose of this review is to provide a perspective on the current state of alfalfa biotechnology research. It focuses mainly on the biotechnological potential of genomic and transcriptomic approaches, biotechnologically valuable genes, gene editing, proteomics, and metabolomics. When appropriate it is compared to barrel medic.

GENOMIC APPROACHES

The identification of genes that affect legume crop production represents an important aim of current genomic studies (Bevan et al., 2017), and this requires knowledge of their full genomic sequences. Technologies for sequencing DNA and RNA have undergone revolutionary improvements (Ari and Arikan, 2016). It is known that after the evolutionary split between monocots and eudicots, several whole genome duplications and triplications had occurred in legumes (Severin et al., 2011; Masonbrink et al., 2017), which might delay whole genome sequencing efforts. The major strength of next-generation sequencing (NGS) is its ability to detect abnormalities across the entire genome. NGS is less costly and has a faster turnaround time compared to classical sequencing methods. New NGS platforms, such as the Roche/454 system (Margulies et al., 2005), Illumina platform (Wang et al., 2012), real-time DNA sequencing by Pacific Biosciences (Eid et al., 2009), Oxford Nanopore system (Lu et al., 2016), and Ion Torrent system (Rothberg et al., 2011), were used for sequencing crop and legume genomes. They have had a major impact on plant research, since they enable the understanding of genomic complexity as well as the identification of genomic variations, such as single nucleotide polymorphisms (SNPs) or insertions/deletions (INDELs; Valliyodan et al., 2017; Abdelrahman et al., 2018). NGS and bioinformatics approaches for high-throughput data analysis are major tools in modern plant breeding programs (Abdelrahman et al., 2015, 2017a,b; Pavlovich, 2017). These modern technologies are also used in legume research, and several recent studies have been devoted to alfalfa genomics using high-throughput genome sequencing (reviewed by Hawkins and Yu, 2018).

High-Throughput NGS in Genomics and Transcriptomics

Genome sequencing and assembly have been applied to many plant species, including crops. Such genome assemblies serve as common references for alignment with re-sequenced plants (Huang et al., 2012; Schreiber et al., 2018). Large-scale systematic genome sequencing has been carried out in leguminous plants such as *Lotus japonicus* (Sato et al., 2008), *M. truncatula* (release 3.0)[1], and *Glycine max* (Schmutz et al., 2010). The genome sequence of alfalfa has not yet been published, and current transcriptomic studies and SNP discoveries rely on the barrel medic genome sequence alignment (genome version[2] *Mt4*.0v1; Young et al., 2011; Tang et al., 2014). Currently, the most advanced genome sequencing method is NGS. It has become the major tool for the development of new molecular markers and for gene identification (Edwards and Batley, 2010). Together with the rapid development of NGS, the number of plants with completely sequenced genomes has dramatically increased (Van et al., 2013;

[1]https://www.jcvi.org/research/medicago-truncatula-genome-database
[2]phytozome.jgi.doe.gov/pz/portal.html#!info?alias=Org_Mtruncatula

Le Nguyen et al., 2018; Kersey, 2019). Advantages of NGS include lower costs and shorter time requirements. The development of NGS technology contributed to the identification of new genes that had evolved by whole-genome duplication and structural variations in chromosomes (Barabaschi et al., 2012; Van et al., 2013). Reference genome sequences of several legume and crop species are now available, and candidate genes of important SNPs can be rapidly and easily identified (Gao et al., 2012; Van et al., 2013; Le Nguyen et al., 2018; Scheben et al., 2019). Alfalfa is an outbred, tetrasomic tetraploid ($2n = 4x = 32$) with eight basic chromosomes and a genome size of 800–1000 Mbp (Blondon et al., 1994). Genetic and genomic resources have been widely explored and developed, but in the absence of a fully sequenced and assembled reference genome for alfalfa, genome of closely related barrel medic is used as a model organism (Zhou et al., 2011). Barrel medic is a diploid species ($2n = 2x = 16$) with smaller genome (about 550 Mbp; Piano and Pecetti, 2010). NGS technologies could speed up the discovery of quantitative trait loci (QTLs) and candidate SNPs, which represent common sequence variations among plants and are functionally important. Numerous molecular markers are used in high-throughput genotyping by sequencing (GBS) platforms associated with alfalfa mapping (Hawkins and Yu, 2018), population diversity studies (Herrmann et al., 2018), and genomic selection (Annicchiarico et al., 2016). In the past years, low density linkage maps were constructed on diploid alfalfa (Brummer et al., 1993; Kiss et al., 1993; Echt et al., 1994; Julier et al., 2003). Although several genetic linkage maps have been constructed for tetraploid alfalfa, most of them were framework maps with only few markers (Brouwer and Osborn, 1999; Julier et al., 2003; Musial et al., 2007; Robins et al., 2007; Khu et al., 2013). Li X. et al. (2014) have constructed a saturated genetic linkage map of autotetraploid alfalfa by using GBS. They have shown high synteny between linkage groups of alfalfa and barrel medic, and clearly identified translocations between chromosomes 4 and 8, and small inversion on chromosome 1. The high-density linkage maps contained 3,591 SNP markers on 64 linkage groups across both maternal and paternal genomes of an autotetraploid alfalfa F_1 population (Li X. et al., 2014).

Genome-wide associated studies (GWAS) are a modern and powerful strategy that can be used to overcome the limitations of conventional QTL mapping. GWAS map genetic loci in a breeding population, relying on linkage disequilibrium (LD; Liu X. P. et al., 2019). Recently, GWAS have been used in the identification of genetic loci in crop species such as soybean (Hwang et al., 2014), maize (Olukolu et al., 2016), barrel medic (Kang et al., 2015), and alfalfa. Zhang T. et al. (2015) evaluated two important features associated with drought resistance, namely drought resistance index (DRI) and relative leaf water content (RWC) under greenhouse conditions in 198 alfalfa cultivars and landraces. These results were then correlated with genomic data obtained through GBS. Subsequent to the QTL mapping approach, GWAS provided identification of 15 loci associated with DRI and RWC. Markers associated with DRI are located at all chromosomes, whereas markers associated with RWC are located at chromosomes 1, 2, 3, 4, 5, 6, and 7. Co-localization of markers for DRI and WRC were found on chromosomes 3, 5, and 7 (Zhang T. et al., 2015). A GWAS approach using more than 15,000 genome-wide SNPs obtained through GBS was applied to examine forage yield and nutritive value-related traits. Five genes, containing known SNPs aligned to the barrel medic genome, were found as candidates in determining fall dry matter yield (*TUBBY-LIKE PROTEIN*), summer dry matter yield (*E3 SUMO-PROTEIN LIGASE SIZ1, RNA-DEPENDENT RNA POLYMERASE FAMILY PROTEIN*), fall stem weight (*UBIQUITIN-LIKE-SPECIFIC PROTEASE ESD4-LIKE PROTEIN*), and cell wall biogenesis (*NUCLEOTIDE-DIPHOSPHO-SUGAR TRANSFERASE FAMILY PROTEIN*; Sakiroglu and Brummer, 2017). Aiming to find markers for alfalfa forage quality, 154 plants originating from the second generation prepared by the outcrossing of three alfalfa cultivars were subjected to GBS, while their half-sib progenies were phenotyped for forage quality parameters under three different growing conditions. Subsequently, GWAS of SNPs was carried out using barrel medic as a reference genome, confirming a polygenic control of quality traits and indicating a substantially different genetic control of a given trait in stems and leaves (Biazzi et al., 2017). Important alfalfa loci for salt tolerance during germination were identified by similar marker-trait association using a GWAS approach (Yu et al., 2016). Remarkably, they used 198 different accessions with potential drought tolerance, whereas DNA libraries were sequenced in two lanes of an Illumina Hi-Seq2000 instrument. Identified SNP markers were located on all chromosomes, with the exception of chromosome 3. Several alfalfa loci showed similar genetic locations to the reported QTLs associated with salt tolerance in barrel medic. The results suggest the similarity of mechanisms controlling salt stress responses in these two species. This study resulted in the identification of 14 genes connected to 23 markers associated with salt tolerance during germination. These include *PEROXYGENASE, B3 DNA-BINDING PROTEIN,* and *CPR5 PROTEIN*, which are linked to cuticle wax biosynthesis and ABA signaling (Yu et al., 2016).

Over the last two decades, several methods have been developed that allowed the examination of global transcriptional changes. The most used ones are the hybridization of cDNAs (DNA microarrays) and the deep sequencing of cDNA (RNA-Seq; Schena et al., 1995; Wang et al., 2009; Lardi and Pessi, 2018). RNA-Seq, a massive parallel sequencing method for transcriptome analysis, was developed 10 years ago (Wang et al., 2009). Transcriptomic studies analyze only the transcribed portion of the genome and provides in-depth sequencing coverage and additional qualitative information such as isoform-specific expression (Abdelrahman et al., 2018). In contrast to microarrays, ribosomal RNA (rRNA) does not hybridize to the chip, as homologous probes are not present. In RNA-Seq, the abundant rRNA is removed (Lardi and Pessi, 2018). Originally, transcriptomic studies were based on Sanger sequencing of expressed sequence tags (ESTs) or microarrays, which was used in alfalfa and barrel medic (Aziz et al., 2005; Cheung et al., 2006; Yang et al., 2010). It has also been applied for other legumes such as *G. max* (Le et al., 2012; Ha et al., 2015; Tripathi et al., 2016), *L. japonicus* (Asamizu et al., 2004), and *Cicer arietinum* (Deokar et al., 2011).

Several studies contributed to the transcriptome sequencing of alfalfa with various coverage. These studies relied on NGS technologies such as 454 technology (Han et al., 2011) or RNA-Seq (Yang et al., 2011; Li and Brummer, 2012; Liu et al., 2013; O'Rourke et al., 2015). Liu et al. (2013) performed *de novo* transcriptome sequencing of *M. sativa* L. subsp. *sativa* using Illumina paired-end sequencing. Plant material included 15 tissue types, and the transcriptome coverage was 5.64 Gbp of clean nucleotides. About 40,433 unigenes were obtained, and 1649 potential expressed sequence tags simple sequence repeat markers (EST-SSRs) were annotated by alignment with the following databases: the National Center for Biotechnology Information (NCBI) nonredundant protein (Nr) database, the NCBI non-redundant nucleotide sequence (Nt) database, Swiss-Prot, The Kyoto Encyclopedia of Genes and Genomes (KEGG), the Clusters of Orthologous Group (COG), Translated EMBL (TrEMBL), and the InterPro (Ipr) database (Liu et al., 2013). RNA-Seq analysis of two alfalfa subspecies, namely *M. sativa* ssp. *sativa* (B47) and *M. sativa* ssp. *falcata* (F56) using roots, nitrogen-fixing root nodules, leaves, flowers, elongating stem internodes, and post-elongation stem internodes resulted in 112,626 unique transcript sequences, which were assembled into the alfalfa Gene Index 1.2 (MSGI 1.2; O'Rourke et al., 2015). Chao et al. (2019) used PacBio SMRT technology and identified 72,606 open reading frames (ORFs) including 46,616 full-length ORFs, 1670 transcription factors and 44,040 SSRs. A total of 7568 alternative splicing events and 17,740 long non-coding RNAs supported the feasibility of deep sequencing full length RNA from alfalfa transcriptome on a single-molecule level (Chao et al., 2019). Another approach developed to provide long-read sequencing of transcripts is Oxford Nanopore Technologies®. The MinION device, which was developed by Oxford Nanopore, is a portable apparatus compatible with a PC or laptop (Jain et al., 2016; Lu et al., 2016). Fleming et al. (2018) evaluated changes in mRNA in dry soybean seeds with use of MinION-based pipeline technology. Li et al. (2019) used MinION-based technology for high-throughput mapping of transgenic alleles in soybean. They rapidly mapped the transgene insertion positions in 51 transgenic soybean plants in a single 1D sequencing run. This method was optimized using a population of soybean lines, but it can be adapted to map the transgenes in any other crops.

TRANSCRIPTOMIC APPROACHES AND GENE EXPRESSION MODIFICATIONS

Resistance to Abiotic Stress

Salinity stress interferes with plant growth because it causes two main stresses on plants: hyperosmotic pressure and ion toxicity, especially due to Na^+ (Volkov et al., 2004). High salinity often triggers an increase in cytosolic Ca^{2+}, reactive oxygen species (ROS), abscisic acid (ABA), and mitogen activated protein kinase (MAPK) signaling (Ovečka et al., 2014; Mittler and Blumwald, 2015). These activated signal molecules affect plant transcriptomes by regulating transcription factors (Xiong et al., 2002; Zhu, 2002). One of the basic strategies in plant stress responses is the accumulation of water-soluble compounds of low molecular weight, such as betaines, polyols, sugars, and amino acids (Chen and Murata, 2002). These compounds accumulate to high concentrations under water or salt stress and protect plants via ROS detoxification and membrane integrity maintenance (Bohnert and Jensen, 1996). For example, glycinebetaine (GB) is a particularly effective protectant against abiotic stress (Chen and Murata, 2008), and accumulates rapidly in plants exposed to salt, drought, and low temperature stresses (Rhodes and Hanson, 1993).

Previous studies have shown that overexpression of stress-related genes caused enhanced tolerance of alfalfa to the salinity stress (Luo et al., 2019b). Li H. et al. (2014) successfully targeted *CHOLINE OXIDASE A* (*CODA)* cDNA derived from *Agrobacterium globiformis* to alfalfa chloroplasts under the control of the strong stress inducible *SWEETPOTATO PEROXIDASE ANIONIC 2* (*SWPA2*) promoter (Kim et al., 2003). Such transgenic alfalfa plants exhibited increased tolerance to oxidative, drought, and salt stress. Because salinity also causes cellular ionic imbalances, the Na^+/H^+ antiporter in the plasma membrane (SOS1 – SALT OVERLAY SENSITIVE 1) and tonoplast (NHX2 – SODIUM/HYDROGEN EXCHANGER 2) can maintain higher K^+/Na^+ ratios in the cytoplasm as a protection against sodium toxicity (Fukuda et al., 1999; Xia et al., 2002; Zhang L. Q. et al., 2014). Moreover, the expression of foreign genes, such as *TaNHX2* (*Triticum aestivum NHX2*), *AhBADH* (*Atriplex hortensis BETAINE ALDEHYDE DEHYDROGENASE*), *SsNHX1 (Suaeda salsa NHX1),* and *GmDREB1* (*G. max DEHYDRATION-RESPONSIVE ELEMENT BINDING PROTEIN 1*), can increase salt tolerance in transgenic alfalfa plants (Zhang et al., 2012). As such, Zhang L. Q. et al. (2014) transformed the exogenous gene *SeNHX1* (*Salicornia europaea NHX1*) into alfalfa using *Agrobacterium*-mediated transformation; this enhanced tolerance to salt stress was manifested by improved photosynthesis and membrane stability. Another attempt to improve salt tolerance in alfalfa was reported by Jin et al. (2010) using transformation with the soybean *DREB* ortholog, *GmDREB1*, under the control of *Arabidopsis* stress-inducible *RD29A* (*RD – RESPONSIVE TO DESICCATION)* promoter. Ion leakage, chlorophyll fluorescence, total soluble sugars, transcript level of *Δ1-PYRROLINE-5-CARBOXYLATE SYNTHASE* (*P5CS*), and free proline contents were correlated with the higher salt tolerance of transgenic lines (Jin et al., 2010). Wang et al. (2014) generated and characterized transgenic alfalfa plants with heterologous expression of *AtNDPK2* (*NUCLEOSIDE DIPHOSPHATE KINASE 2*) under the control of oxidative stress inducible *SWPA2* promoter. These transgenic plants showed increased tolerance to oxidative, high temperature, salt and drought stresses. Such enhanced tolerance was mediated by activation of ROS scavenging, enhanced activity of NDPK2 enzyme, improved protection of membrane integrity, and increased proline accumulation (Wang et al., 2014).

First studies on drought responses of alfalfa started in the 1990s (Luo et al., 1991, 1992; Laberge et al., 1993). Metabolite profiling and proteomic approaches identified soluble sugars, amino acids, and proteins that respond to drought in leaves and nodules of alfalfa variety Magali (Aranjuelo et al., 2011). Simultaneously, Kang et al. (2011) have shown systematic analysis of two alfalfa varieties, Wisfal and Chilean, with different tolerance/sensitivity to the drought stress. They have

identified many genes involved in adaptation to the drought stress, including genes encoding transcription and regulatory factors, or genes involved in the biosynthesis of osmolytes and antioxidants. Knowledge of such genes can help in breeding programs. A number of microRNAs have been used to improve various crop species via genetic engineering (Macovei et al., 2012; Zhou and Luo, 2013; Aung et al., 2015). Researchers also characterized microRNAs and their target genes that respond to hypoxia, wounding, heat or oxidative stress (Zhao et al., 2007; Budak et al., 2015). Recent study by Arshad et al. (2017) suggested that overexpression of microRNA156 (*miR156OE*) is an emerging tool to improve drought tolerance of alfalfa since it silenced *SQUAMOSA PROMOTER BINDING PROTEIN-LIKE 13 (SPL13i)* leading to reduced water loss and enhanced stomatal conductance and photosynthetic assimilation. Another study proposed a role of *miR156OE* and *SPL13i* in heat stress tolerance since plants carrying these constructs showed increased antioxidant levels (Matthews et al., 2019). As found by NGS, plants possessing *miR156OE* exhibited broad changes in gene expression, including genes involved in nodulation, root development and phytohormone biosynthesis (Aung et al., 2017). Taking together, miR156 can improve drought or heat stress tolerance in alfalfa, at least partially by silencing *SPL13* (Feyissa et al., 2019; Matthews et al., 2019).

RNA-Seq analysis was utilized in the transcriptome profiling of alfalfa in order to study the molecular mechanisms underlying frost (Song et al., 2016), salinity (Postnikova et al., 2013; An et al., 2016; Lei et al., 2018), drought (Arshad et al., 2018), resistance to aluminum (Liu W. et al., 2017), lead (Xu et al., 2017) and waterlogging (Zeng et al., 2019), or fall dormancy (Zhang S. et al., 2015). For example, genes encoding membrane proteins, and proteins of hormonal signal transduction, and ubiquitin-mediated proteolysis pathways contribute to the freezing adaptation mechanisms in alfalfa (Song et al., 2016). Using high-throughput sequencing technology, Postnikova et al. (2013) have demonstrated that salinity stress affects a variety of alfalfa genes. Among the most affected ones were genes of known function, such as *DIHYDROFLAVONOL REDUCTASE* (*DFR)*, transcription factor *MYB59*, *SUGAR TRANSPORTER ERD6-like 16* (*ERD – EARLY RESPONSE TO DEHYDRATION*), and *INOSITOL-145-TRISPHOSPHATE 5-PHOSPHATASE* (*IP5P2*). This study revealed that 86 transcription factors responded to salinity stress; among them are those belonging to GRAS, ARR, JUMONJI, and MYB families that were preferentially upregulated in the tolerant alfalfa cultivar (Postnikova et al., 2013). Alfalfa fall dormancy is determined by genes involved in auxin (e.g., *AUXIN-INDUCED PROTEIN 5NG4)* and ethylene signaling (ethylene responsive TF *RAP2-11)* and carbohydrate transport *(ERD6-LIKE PROTEIN*; Zhang S. et al., 2015). Genes encoding *BETA-AMYLASE*, *ETHYLENE RESPONSE FACTOR (ERF)*, *CALCINEURIN B-LIKE (CBL) INTERACTING PROTEIN KINASES (CIPKs)*, *GLUTATHIONE PEROXIDASE (GPX)*, and *GLUTATHIONE S-TRANSFERASE (GST)* are among those important for waterlogging stress resistance in alfalfa (Zeng et al., 2019).

Plant damage caused by saline stress is usually divided into three categories: high pH damage, osmotic shock, and toxic cation stress. Nutrient solution pH variation significantly affected growth of alfalfa seedlings with the optimal pH values in the range between 5.0 and 6.0, as estimated by length and fresh weight of roots, hypocotyls, epicotyls, first leaf petioles, and leaf blades (Köpp et al., 2011). Alfalfa is a saline-alkaline stress-tolerant species (Zhu, 2001; Wong et al., 2006; Gong et al., 2014; An et al., 2016). An et al. (2016) performed transcriptomic analysis of whole alfalfa seedlings treated with saline-alkaline solutions using ion torrent sequencing technology to study changes in the gene expression pattern. This method detects hydrogen ions that are released during DNA polymerization. DEG profiles were obtained and annotated using two methods. Firstly, generated reads were mapped to barrel medic, which has a sequence that is highly homologous to alfalfa. Secondly, functional annotations of assembled unigenes were performed using BLASTX search against the Swiss-Prot databases of barrel medic, thale cress, and soybean. Gene ontology analysis revealed 14 highly enriched pathways. Specific responses of peroxidases, the expression level of *RUBISCO*, and flavonoids indicated antioxidant capacity as one of the main mechanisms behind the saline-alkaline stress tolerance in alfalfa (An et al., 2016). Another study provided a comprehensive transcriptome analysis of alfalfa roots under prolonged ABA treatment (Luo et al., 2019a). Sequences were assembled for many isoforms and were analyzed for their potential role. Differentially expressed isoforms (DEIs) regulated by ABA were mainly involved in transcriptional regulation, plant immunity, plant hormone signal transduction, and anti-oxidative defense.

Nevertheless, these studies were mainly focused on genotype-specific stress mechanisms. Functional and structural genomics studies are fundamental for the understanding of plant biology. Access to high-quality genome and transcriptome sequences is important to perform studies of this kind. Recently, the third-generation sequencing technology PacBio RSII has emerged as a unique method for constructing full-length transcripts (Dong et al., 2015; Nakano et al., 2017). PacBio RSII is an ideal tool for whole genome sequencing, targeted sequencing, RNA-Seq, and epigenetic characterization. This technique allows the sequencing of single DNA molecules in real-time (SMRT) without amplification by PCR (Dong et al., 2015). Using PacBio RSII, Luo et al. (2019b) studied salt stress as a major environmental factor that impacts alfalfa development and production (Zhang S. et al., 2015). They have constructed the first full-length transcriptome database of alfalfa root tips treated with mannitol (a non-ionic osmotic stress) and NaCl (an ionic osmotic stress), which provided evidence that the response to salinity stress includes both osmotic and ionic components. They have found 8,016 mannitol-regulated DEGs and 8,861 NaCl-regulated DEGs. These DEGs are involved in signal transduction, transcriptional regulation, anti-oxidative defense, and signal perceptions (Luo et al., 2019b).

Resistance to Biotic Stress

Biotic stress also considerably affects alfalfa growth and yield. Current methods of plant protection focus mostly on the elimination of pathogenic organisms using pesticides (Shafique et al., 2014). However, the improvement of plant resistance against such pathogens seems like a more beneficial alternative, since it might be more effective and more environmentally

friendly (Kudapa et al., 2013; Varshney and Kudapa, 2013). It is expected that climatic changes are linked to the spread of diseases and emergence of new ones and can raise the threat of parasites and pests (Kudapa et al., 2013; Shafique et al., 2014). Therefore, disease-resilient plants could provide higher production and yield, reflecting the importance of genetically engineering specific genes (de Zélicourt et al., 2011).

Disease resistance mechanisms in plants after encountering a pathogen have been well-described (Roumen, 1994; Zipfel, 2014; Rubiales et al., 2015). Plant infection is facilitated by effector molecules produced by pathogens, which can overcome the first line of plant defense, which is the pathogen−associated molecular pattern (PAMP) triggered immunity; subsequently, plant resistance is suppressed. On the other hand, specific plant resistance (R) proteins have been evolutionarily developed and can provide protection against specific pathogen effectors (Jones and Dangl, 2006; Singer et al., 2018). Nowadays, genes encoding R proteins are widely manipulated for introducing plant resistance to a specific pathogen (Rubiales et al., 2015).

Generally, the most frequently occurring pathogens are bacteria and fungi belonging to Ascomycetes and Basidiomycetes; these obtain nutrients by attacking various parts of the plant body (Shafique et al., 2014). Considerable declines in alfalfa production have been observed mostly due to root infections leading to wilting caused by the bacterium *Clavibacter michiganensis*, fungi *Fusarium oxysporum* and *Verticillium alfalfae*, and microscopic fungus *Phytophthora medicaginis*, or due to leaves infected by *Colletotrichum trifolii* (Nutter et al., 2002; Singer et al., 2018). Alfalfa varieties resistant to these diseases have been obtained by common breeding methods over decades (Toth and Bakheit, 1983; Elgin et al., 1988; Pratt and Rowe, 2002). However, it may not be enough to cover the world demand for crop yields, considering the influence of a retrogressive living environment. Because of alfalfa autopolyploidy and its out-crossing nature (Zhang T. et al., 2015; Yu et al., 2017), the comprehension of molecular and genetic mechanisms during pathogenesis leading to the introduction of specific resistance can be a demanding task. For this reason, barrel medic is widely used for such purposes. Different transcriptomic methods (Gao et al., 2012; Van et al., 2013; Le Nguyen et al., 2018; Scheben et al., 2019) were used to identify barrel medic loci correlated with QTLs, providing resistance to diseases caused by fungi such as *Uromyces striatus* and *Erysiphe pisi* (Bustos-Sanmamed et al., 2013).

C. trifolii is an agent of a highly destructive and prevalent foliar disease, anthracnose (Annicchiarico et al., 2015), which can cause up to 30% decrease in alfalfa yield (Yang et al., 2008). Recognition of this pathogen and induction of response in alfalfa are understudied and need further characterization by cloning techniques. Nevertheless, Yang et al. (2008) found out that overexpression of the gene for intracellular R protein, *RCT1* encoding TIR-NBS-LRR (TOLL/INTERLEUKIN-1 RECEPTOR NUCLEOTIDE BINDING SITE LEUCINE-RICH REPEAT) from barrel medic, ensured anthracnose resistance in alfalfa. Mackie et al. (2007) and Tesfaye et al. (2007) identified tetrasomic dominant *ANTHOCYANIN* genes *AN1* and *AN2* regulating resistance against *C. trifolii* (Elgin and Ostazeski, 1985). Mackie et al. (2007) mapped locations of QTLs for *C. trifolii* traits 1, 2, and 4 in autotetraploid alfalfa clone W126, which is resistant to this pest. Interactions between particular QTLs and phenotypic variations for three *C. trifolii* traits have been described. Obtained markers may be usable in alfalfa breeding for introducing multiple sources of resistance. Although genes for a specific resistance have been identified, new pathotypes of *C. trifolii* are still being discovered; therefore, the generation of new, long-lasting resistant plants is more difficult (Shafique et al., 2014).

Using the suppression subtractive hybridization library, Bustos-Sanmamed et al. (2013) proved the importance of pathogenesis-related (PR) proteins of group 10, as well as proteins engaged in ABA signaling for resistance against harmful fungi, e.g., *Aphanomyces enteiches*. Bahramnejad et al. (2010) designated and isolated the *MsPR10.1A* gene in alfalfa based on its homology to *PR10* genes from other Fabaceae plants, e.g., *Lupinus luteus* (Zhang, 2004). Expression levels of *MsPR10.1A* under different conditions such as ABA treatment, heat shock, wounding, and pathogen attack, were compared with the expression levels of a previously described gene, *PPRG2* (termed as *MsPR10.1B;* Borsics and Lados, 2002). Bahramnejad et al. (2010) observed faster induction of *MsPR10.1A* gene expression than that of *MsPR10.1B* gene after ABA and ethylene treatment, and after application of the pathogenic bacterium *Xanthomonas campestris*. However, inoculation of alfalfa leaves with compatible *X. campestris* led to markedly higher expression of both genes. On the other hand, gene *AAB41557* from the alfalfa *PR10* group did not respond to *X. campestris* inoculation (Esnault et al., 1993). Generally, most examples regarding *PR10* induction due to bacterial inoculation involve incompatible bacteria, such as activation of alfalfa genes *AAB41557* (Esnault et al., 1993) and *MsPR10.1B* (Borsics and Lados, 2002) after *Pseudomonas syringae pv. pisi* inoculation. The promoter of *YPR-10* (of the *RIBONUCLEASE-LIKE PR PROTEIN-10* gene) from *G. max* fused with *GUS* showed activity in the vasculature of *Nicotiana benthamiana* leaves after transient transformation (Walter et al., 1996). Moreover, Bahramnejad et al. (2010) suggested the importance of *MsPR10.1A* promoter expression in the leaf vasculature, resulting in resistance against diseases. *MsPR10.1A* and *MsPR10.1B* promoters have many similar functions in stress responses, but notable differences were found in their reactions to wounding. Thus, promoters of *PR10* genes may be potentially used in biotechnological applications for directing transgene expression in proper tissues.

Plant defense peptides are composed of five main groups: proteases, α-amylase inhibitors, lectins, chitinases, and polyphenol oxidases (Fürstenberg-Hägg et al., 2013). Singer et al. (2018) summarized several genes for the biosynthesis of substances with anti-pathogen effect, such as *AGLUL* encoding β-1,3-glucanase (Masoud et al., 1996), *IOMT* – Isoflavone-*O*-methyltransferase (He and Dixon, 2000), *LF* – encoding lactoferrin (Stefanova et al., 2013) and *RS* – encoding resveratrol synthase (Hipskind and Paiva, 2000). Highly effective protectants, such as protease inhibitors, naturally occur in plants, and they can inhibit proteolytic enzymes in the digestive system of insects or nematodes. Consequently, plant material is not digestible, leading to pathogen starvation and removal from the plant. Inhibitors of cysteine proteases called phytocystatins

were identified in many plants, showing potential in conferring resistance against pathogens. Rice *ORYZACYSTATIN-I* (*OC-I*) and *ORYZACYSTATIN II* (*OC-II*) genes driven by a potato wound-inducible promoter (*Protease inhibitor II*, *PinII*) were transferred to alfalfa attacked by root lesion nematode and leaf beetle. Such transgenic plants revealed a reduction in the *Pratylenchus penetrans* population and enhanced mortality of *Phytodecta fornicata* larvae (Ninković et al., 1995; Samac and Smigocki, 2003).

Tesfaye et al. (2005) generated alfalfa plants that secreted a fungal endochitinase (ECH42). These transgenic plants showed up to 25.7 times increased chitinase activity in vegetative organs and root exudates. Such secreted endochitinases not only retained the lytic activity against glycol chitin, but also showed antifungal activity by the inhibition of spore germination of two fungal pathogens, namely, *Phoma medicaginis* and *C. trifolii* (Tesfaye et al., 2005).

Based on the expression distribution of *SNAKIN* gene *StSN1* in *Solanum tuberosum*, Segura et al. (1999) hypothesized *SN1* as a component of constitutive defense barriers in reproductive and storage plant organs. *StSN2* is induced locally after wounding and pathogen attack; accordingly, it could play an important role in constitutive and inducible defense barriers (Kovalskaya and Hammond, 2009; Guzman-Rodriguez et al., 2013). Next, García et al. (2014) proposed SNAKIN proteins as antimicrobial compounds in plant innate immunity. Indeed, alfalfa transgenic plants carrying *SNAKIN-1* (*MsSN1*) under the control of a constitutive promoter showed improved tolerance against pathogenic fungi. Three independent transgenic lines carrying the *CaMV35S:MsSN1* construct showed significantly lower amounts of infected leaves than wild type plants when treated by *C. trifolii* and with the oomycete *P. medicaginis* (García et al., 2014).

Finally, it is worth mentioning that the genetic transformation of alfalfa with *Bacillus thuringiensis* gene *Cry1C* coding for δ-endotoxin has also been shown to be an effective protective strategy. After transformation, alfalfa was more resistant to *Nemapogon granellus* and *Spodoptera exigua* (Strizhov et al., 1996).

Transcriptomic studies contributed to the knowledge of alfalfa resistance to aphids, strips, and nematodes. Aphids are major insect pests causing a significant decrease of alfalfa yield. Tu et al. (2018b) performed a transcriptomic analysis of two alfalfa cultivars differing in aphid resistance. Genes involved in salicylic acid biosynthesis represented an important defense mechanism in both cultivars. The alfalfa resistance against aphids was mainly determined by induction of genes involved in linoleic acid synthesis important for jasmonic acid and flavonoid biosynthesis (Tu et al., 2018b). Genes participating in jasmonic acid biosynthesis, such as *LIPOXYGENASE, SERINE PROTEINASE INHIBITOR*, and *SEED LINOLEATE 9S-LIPOXYGENASE* were also important for alfalfa resistance to strips infestation. Moreover, genes involved in fatty acid degradation, chloroalkane and chloroalkene degradation, beta-alanine and phenylalanine metabolism and flavonoid biosynthesis also contributed to this resistance (Tu et al., 2018a). Another comparative transcriptomic analysis aimed to screen for genes determining alfalfa resistance to root-knot nematode *Meloidogyne incognita* (Postnikova et al., 2015). *LRR AND NB-ARC DOMAIN DISEASE RESISTANCE PROTEIN* (Medtr3g023030.1), *RECEPTOR-LIKE PROTEIN* (Medtr5g087320.1) and *DISEASE RESISTANCE PROTEIN* (TIR-NBS-LRR class, Medtr0277s0020.3) were up-regulated in the resistant cultivar, while susceptible one showed their down-regulation (Postnikova et al., 2015).

From the biotechnological point of view, ideal alfalfa cultivars should have better nutritional quality, enhanced biomass production and yield, and better resistance to biotic and abiotic stress. All such traits mentioned should be sustainable over a long period of time. Several experimental studies have been conducted to improve alfalfa, but detailed characterization and relationships between desired traits need further genetic and molecular research.

PROTEOMICS AND METABOLOMICS

Owing to its beneficial agronomical traits, alfalfa has been attracting substantial interest in the fields of proteomics and metabolomics during the past two decades. A strong effort was invested in the discovery of new proteins and metabolites involved in alfalfa development and abiotic stress response. In this section, we attempt to summarize the recent achievements of current alfalfa proteomic and metabolomic research. We also aim to highlight the relevance of these investigations for putative biotechnological applications.

Nitrogen and Carbon Metabolism in Alfalfa From a Proteomic Perspective

Proteomics and metabolomics have a remarkable capability to examine the balance between carbon and nitrogen metabolism under stress conditions in alfalfa during interactions with nitrogen-fixing bacteria (Aranjuelo et al., 2011, 2013). Water stress limits nitrogen fixation in nodules by the reduction of nitrogenase activity (Carter and Sheaffer, 1983; Aranjuelo et al., 2011) and Rubisco availability in leaves (Aranjuelo et al., 2005, 2011). The latter likely occurs due to Rubisco-enhanced proteolysis and lower abundance of RUBISCO ACTIVASE. Water stress also affected ammonia assimilation into amino acids, as evidenced by the upregulation of glutamine synthetase and decreased levels of glutamic acid and asparagine in leaves. The effects of water stress were followed by elevated photorespiration (exemplified by increased abundances of photorespiratory enzymes), lower demand for carbohydrates, and accumulation of soluble sugars. In nodules, water deprivation caused the attenuation of respiration, leading to CO_2 recycling by PHOSPHOENOLPYRUVATE CARBOXYLASE. This likely occurred in order to support carbon skeletons for amino acid biosynthesis. The reduced respiration may also be a consequence of increased demand for compounds with osmoregulation capacity such as glycerol (Aranjuelo et al., 2013). The dynamic behavior of ammonia assimilation seems to be important for abiotic stress tolerance. It is likely that nitrogen is relocated from glutamic acid and asparagine, which are the main nitrogen sources in control conditions,

to proline under stress conditions. Thus, proline might be an alternative nitrogen source under osmotic stress, and it seems that alfalfa may easily switch between proline biosynthesis and degradation (Zhang and Shi, 2018). Abiotic stresses caused accumulation of enzymes of nitrogen assimilation, such as GLUTAMINE SYNTHETASE and FERREDOXIN-DEPENDENT GLUTAMATE SYNTHASE (Rahman et al., 2016) as well as GLUTAMATE DEHYDROGENASE (Dai et al., 2017). Remarkably, heat stress positively affected the abundance of ASPARTATE AMINOTRANSFERASE and GLUTAMINE SYNTHETASE, indicating an enhancement of nitrogen metabolism (Li W. et al., 2013).

Clearly, Rubisco availability and homeostasis between carbon and nitrogen metabolism is crucial for plant performance under unfavorable environmental conditions. For this reason, the proteins regulating C and N metabolism, as well as stress related proteins (**Table 1**), appear to be prospective candidates for the biotechnological improvement of alfalfa.

Proteins and Pathways Found by Proteomics as Promising Candidates for Alfalfa Abiotic Stress Resistance Improvement

Seed priming involves a complex array of physiological as well as molecular processes leading to an improved ability of plants to withstand adverse environment (Paparella et al., 2015). A gel-based proteomic approach was employed to investigate proteome remodeling during osmoprimed alfalfa seed germination. This process was accompanied by intense accumulation of storage proteins (such as vicilins), proteins involved in protein folding, UDP glucose and methionine biosynthesis, annexins, and antioxidant enzymes, compared to seeds that were not osmoprimed. Osmopriming was also followed by remarkable induction of stress-related proteins and proteasome components (**Table 1**) (Yacoubi et al., 2011). A follow-up article highlighted that osmopriming has remarkable consequences on the proteome of seeds germinating under saline conditions. An increased seed vigor associated with osmopriming was related to the accumulation of storage proteins, annexins and RNA-BINDING PROTEIN. The last one indicated the possible importance of posttranscriptional regulation in the seedlings exposed to salt stress. On the other hand, seeds without osmopriming accumulated HEAT SHOCK PROTEINS (HSP), LATE EMBRYOGENESIS ABUNDANT (LEA) PROTEINS, SEED MATURATION PROTEINS, GLUTATHIONE *S*-TRANSFERASE 9, and HEME OXIDASE (**Table 1**) (Yacoubi et al., 2013). These data indicate that the transient genetic modification of genes encoding the above-mentioned stress-related proteins (for instance, by expression under an inducible tissue-specific promoter), might be of biotechnological importance.

Tolerance of alfalfa to the polyethylene glycol (PEG)-induced osmotic stress was accompanied by enhanced carbohydrate metabolism and energy production. Stress-related proteins such as glutathione *S*-transferases and LEA proteins are also correlated with osmotic stress tolerance (**Table 1**) (Zhang and Shi, 2018), and both represent promising candidates for biotechnological applications. A similar study revealed that proteins involved in protein folding (DISULFIDE ISOMERASE), NAD production (NAD SYNTHASE), methylation (ADENOSINE KINASE, *S*-ADENOSYL-METHIONINE) and antioxidant defense (represented mainly by peroxidases), are candidates to determine alfalfa salt tolerance (Rahman et al., 2015). Overabundance of proteins involved in the enzymatic antioxidant defense was commonly associated with an increased tolerance of alfalfa not only to the salt, but also to the drought and osmotic stresses (**Table 1**) (Rahman et al., 2015; Long et al., 2018; Zhang and Shi, 2018). According to a proteomic study, water stress increased the abundance of AGAMOUS-LIKE 65 and bHLH TRANSCRIPTION FACTORS, while it reduced the abundance of JADE-1 and JADE-3, transcriptional regulators belonging to a PHD (plant homeodomain)-type zinc fingers family (**Table 1**) (Rahman et al., 2016). These intriguing findings of transcriptional factors involved in water stress deserve further biotechnological investigations. Genetic modifications of hormone biosynthesis belong also to promising biotechnological approaches, since water stress elevated the abundances of ABA (9-*CIS*-EPOXYCAROTENOID DIOXYGENASE) and auxin (AUXIN-INDEPENDENT GROWTH PROMOTER) biosynthetic proteins in alfalfa (Rahman et al., 2016). In this regard, local stress-induced changes in the turnover of auxin regulatory proteins could modify plant developmental processes, such as cell elongation, lateral roots emergence, transition from cell division to cell differentiation, enabling plants to rapidly adapt to adverse environmental conditions (Korver et al., 2018). On the other hand, drought stress caused some common but also distinct responses when compared to salt stress at the level of the alfalfa proteome. Interestingly, both stresses targeted proteasome complex and translation. Nevertheless, the proteasome complex exhibits different sensitivity to these stressors, since the abundance of 26S PROTEASOME REGULATORY SUBUNIT 6 was increased by drought but subsequently reduced by salt stress (Ma et al., 2017).

Comparative proteomic studies point out to obvious similarities between alfalfa and barrel medic in their response to environmental stimuli. Proteome-wide comparison of salt-tolerant alfalfa and salt-sensitive barrel medic indicated that both species are capable of keeping photosynthetic activity during salt stress. Only heat shock protein (gi357476131) was differentially regulated under salt stress in these two Medicago species. It was upregulated in alfalfa but downregulated in barrel medic (Long et al., 2016), indicating its potential biotechnological significance for salt tolerance. A proteomic analysis of these two species at the early post-germination stage showed an important role of antioxidant defense, cell wall metabolism, and jasmonic acid biosynthesis during response to salt (Long et al., 2018). Enhanced salt tolerance of alfalfa, compared to salt sensitive barrel medic, was reflected by higher numbers of differentially regulated proteins, also suggesting higher proteome plasticity (Long et al., 2016, 2018).

Differences in the composition of differentially abundant proteins between two alfalfa cultivars with contrasting freezing tolerance were reported after cold stress treatment (Chen et al.,

2015). Freezing-tolerant cultivar exhibited higher abundances of Rubisco subunits as compared to the freezing susceptible one, but showed downregulation of proteins involved in methionine, lignin and terpenoid biosynthesis, and energy metabolism under cold stress (Chen et al., 2015). Heat stress caused an upregulation of proteins involved in energy production, signaling, and intracellular transport and defense, including chaperones, antioxidant enzymes and PR proteins (Li W. et al., 2013). Interestingly, only prolonged heat stress caused downregulation of Rubisco and photosynthetic enzyme activities. Lower abundance of photosynthetic proteins was associated with altered abundance of proteins involved in plastid protein import.

It is known that the external application of bioactive molecules such as hydrogen (H_2; Jin et al., 2013) may remarkably increase plant survival rate under adverse environmental conditions. Proteomic elucidation of the beneficial effects of H_2 on the alfalfa response to cadmium revealed that this is mainly determined by the modification of proteins involved in the cellular redox homeostasis. Among these proteins, enzymes involved in cysteine biosynthesis and CYSTEINE DESULFURYLASE are elevated by external H_2. Cysteine is a precursor for GSH and hGSH, an important redox buffering compounds (Baldacci-Cresp et al., 2012; Diaz-Vivancos et al., 2015), hGSH is specifically produced in species of Fabaceae family including alfalfa, in higher rate compared to GSH, having important role in nodulation (Klapheck, 1988; Matamoros et al., 1999; Frendo et al., 2005; Baldacci-Cresp et al., 2012; Pasternak et al., 2014). Similarly, the abundance of CuZn SUPEROXIDE DISMUTASE (SOD) increased along with a positive effect of external H_2 treatment on alfalfa Cd tolerance. Gaseous H_2 also enhances the abundance of defense related proteins such as PATHOGENESIS-RELATED PROTEIN BET V I FAMILY PROTEIN and PATHOGENESIS-RELATED THAUMATIN FAMILY PROTEIN (Dai et al., 2017). Such induction of defense related proteins, including chitinases and enzymes involved in cell wall modification, was also observed in alfalfa stems and leaves exposed to long-term Cd stress (Gutsch et al., 2018a,b). Remarkably, chitinases are also employed in the alfalfa response to osmotic stress and waterlogging (**Table 1**) (Zhang and Shi, 2018; Zeng et al., 2019). This implies that genetic modification of cell walls might improve alfalfa tolerance to multiple stresses.

Proteins Implicated in Development-Associated Agronomical Traits

Proteomics has also been proven as valuable for the evaluation of metabolic activities during alfalfa stem development. The apical region characterized by fiber development showed an overabundance of proteins involved in chloroplast protein synthesis and carbon fixation. The mature stem part possessed a pool of proteins involved in redox homeostasis (Printz et al., 2015). Moreover, the stem is an organ highly sensitive to perturbations of mineral nutrition. This was highlighted by recent proteomic studies reporting that copper availability greatly influenced the abundance of proteins involved in cell wall biogenesis, and in pectin and lignin biosynthesis (Printz et al., 2016). Thus, mineral homeostasis seems to be a crucial factor affecting alfalfa stem growth and rigidity, and also eventually affecting drought tolerance and pathogen resistance.

Flowering represents a critical developmental stage in alfalfa, mainly in terms of seed yield and quality. Pollination and post-pollination processes in alfalfa are linked to altered homeostasis of stress-related proteins such as DUAL SPECIFICITY KINASE SPLA-LIKE PROTEIN, NADPH: QUINONE OXIDOREDUCTASE-LIKE PROTEIN, and CARBONIC ANHYDRASE (Chen et al., 2016). Moreover, PROTEIN DISULFIDE ISOMERASE-LIKE PROTEIN, ASCORBATE PEROXIDASE, GLUTAREDOXIN, and PEROXIREDOXINS also showed fluctuations in their abundances. In addition, metabolic activity was enhanced during pollination and declined afterward.

Fall dormancy is a crucial phenomenon influencing alfalfa performance in autumn, but also during the following season. Based on a comparative proteomic study of terminal buds isolated from two alfalfa cultivars with contrasting fall dormancy, several new proteins were discovered as important for this physiological process (Du et al., 2018). It was suggested that lower abundance of L-ASPARAGINASE and CINNAMYL ALCOHOL DEHYDROGENASES may contribute to fall dormancy. In addition, CHALCONE AND STILBENE SYNTHASE FAMILY PROTEIN (a protein involved in flavonoid biosynthesis) and GLUTAREDOXIN S17 seemed to be important for shoot apical meristem maintenance. Both proteins also have a role in polar auxin transport (**Table 1**) (Du et al., 2018).

Finally, the nutritional value of alfalfa depends on the developmental stage. Cutting of alfalfa in later developmental stages, such as in full flowering, leads to increased fiber and decreased protein content in the biomass (Fan et al., 2018). Combined proteomic and metabolomic analyses underpinned this finding and showed changes in amino acid composition. These unfeasible nutritional changes are accompanied by increased hemicellulose content, due to the accumulation of D-mannose and higher abundance of ALPHA GLUCOSIDASE, ALPHA AMYLASE, and UDP-GLUCURONIC ACID DECARBOXYLASE, as well as lignin, due to the higher levels of lignin precursors and proteins involved in lignin biosynthesis (**Table 1**) (Fan et al., 2018).

GENE EDITING USING TALEN AND CRISPR/Cas TECHNOLOGIES

The process of gene editing is based on sequence-specific nucleases (SSNs) creating *in vivo* loci-specific DNA double-stranded breaks (DSBs) that are subsequently repaired. There are two main DNA repair systems: homology-directed repair (HDR), and the more efficient but less precise non-homologous end joining (NHEJ). NHEJ can result in the insertion or deletion (indel) of nucleotides and a frameshift mutation, which can consequently create a premature stop codon, thus rendering the gene non-functional and creating a genetic knockout. Gene targeting technologies include meganucleases, zinc finger nucleases (ZFNs), transcription activator-like effector nucleases

TABLE 1 | Overview of proteins and metabolites important for biotechnological improvement of alfalfa as revealed by proteomic and metabolomic studies.

Treatment, stress, condition	Sample	Methodological approach	Proteins and metabolites of biotechnological importance	References
Seed germination and osmopriming	Seeds	2-D gel electrophoresis (nano-LC MS/MS)	**Carbohydrate metabolism:** UDP glucose pyrophosphorylase **Protein destination and storage:** HSP70 and HSP20, GroEL-like chaperone, ATPase, vicilin, protein disulfide-isomerase precursor **Stress response:** annexin, peroxiredoxins, manganese superoxide dismutase, glyoxalase, lipoxygenase, glutathione *S*-transferase, thioredoxin **Proteolysis:** peptidase T1A, proteasome beta subunit, peptidase A1 pepsin	Yacoubi et al. (2011)
Osmoprimed seeds germinating under salt stress	Seeds	2-D gel electrophoresis (nano-LC MS/MS)	**Small HSPs:** 18.2 kDa class I HSP **Methionine synthesis:** methionine synthase, cysteine synthase **Dehydration defense:** LEA proteins, PM22 **Others:** annexin, RNA-binding protein, heme oxygenase, glutathione *S*-transferase 9	Yacoubi et al. (2013)
PEG-induced osmotic stress	Roots of varieties contrasting in drought tolerance	iTRAQ (strong cation exchange fractionation and LC MS/MS)	**Stress and defense:** glutathione *S*-transferases, disease resistance response protein, epoxide hydrolase, chitinase, reticuline oxidase-like protein, low-temperature-induced 65 kDa protein, aldo/keto reductase, pirin-like plant protein, glucan endo-1,3-beta-glucosidase **Protein metabolism:** HSPs, lysine-ketoglutarate reductase/saccharopine dehydrogenase, phosphatidylethanolamine-binding protein, homoglutathione synthetase **Signal transduction:** monooxygenases, cysteine-rich RLK (receptor-like kinase) protein, 12-oxophytodienoate reductase **Cell wall:** beta xylosidase, xyloglucan-specific endoglucanase inhibitor protein, expansin-B1-like protein	Zhang and Shi (2018)
Salt stress	Roots of two cultivars contrasting in salt resistance	2-D gel electrophoresis (MALDI TOF/TOF)	**Oxidative stress:** peroxidase, peroxiredoxin **Protein folding:** protein disulfide isomerase **Metabolism:** NAD synthetase, UTP-glucose 1 phosphate uridylyltransferase **Fatty acid metabolism:** biotin carboxylase 3 **Membrane transport:** V-ATPase	Rahman et al. (2015)
Salt and drought stress	Seedlings	2-D gel electrophoresis (MALDI TOF-MS/MS)	**Salt stress:** caffeoyl-CoA 3-*O*-methyltransferase, peroxiredoxin, ubiquitin-conjugating enzyme, UV excision repair protein rad23, glutathione peroxidase **Drought stress:** ubiquitin-conjugating enzyme, putative alcohol dehydrogenase, chaperonin 10	Ma et al. (2017)
Drought stress	Leaves of plants inoculated by *S. meliloti*	Proteomics: 2-D gel electrophoresis (LCMS/MS analysis) Metabolomics: GC TOF-MS	**Rubisco availability and regeneration:** rubisco activase, sedoheptulose-1,7-bisphosphatase, ribulose-phosphate 3-epimerase and phosphoribulokinase **Nitrogen metabolism:** glutamine synthetase **Stress and defense response:** superoxide dismutase, dehydroascorbate reductase, 2-cys peroxiredoxin-like protein, 14-3-3-like protein **Osmoprotectant metabolites:** proline, pinitol	Aranjuelo et al. (2011)
Drought stress	Nodules, roots, leaves	Proteomics: 2-D gel electrophoresis (LCMS/MS analysis) Metabolomics: GC TOF-MS	**Nodule proteome:** alpha 1,4-glucan protein synthase, lipoxygenase, PEP-carboxylase **Nodule N containing metabolites:** glutamine, asparagine **Nodule osmoprotectant metabolites:** glycerol, galactinol, myo-inositol, proline, sucrose, raffinose, fumaric acid and malate **Nodule metabolites with antioxidant capacity:** ascorbate, threonate	Aranjuelo et al. (2013)
Water deficit stress	Roots	2-D gel electrophoresis (MALDI TOF)	**Nitrogen metabolism:** glutamine synthetase, ferredoxin-dependent glutamate synthase **ABA biosynthesis:** 9-*cis*-epoxycarotenoid dioxygenase **Stress response and oxidative stress:** ascorbate peroxidase, peroxiredoxin, calreticulin, stress-induced phosphoprotein, annexin **Transcription:** basic helix-loop-helix (bHLH) transcription factor, agamous-like 65 **Other functions:** inward-rectifying potassium channel, auxin-independent growth promoter	Rahman et al. (2016)
Heat stress	Leaves	2-D gel electrophoresis (MALDI TOF/TOF)	**Rubisco availability:** Rubisco activase isoforms **Nitrogen metabolism:** aspartate aminotransferase and glutamine synthetase **Protein synthesis and processing:** peptidyl-prolyl *cis–trans* isomerases, protein disulfide isomerase-like protein precursor, porin, proteasome subunit β type, eukaryotic translation initiation factor 3 subunit I, BiP isoform A/glycine max, cysteine proteinase, outer plastidial membrane protein porin **Intracellular traffic, cell structure:** protein TOC75, translocon Tic40, profilin	Li W. et al. (2013)

(Continued)

TABLE 1 | Continued

Treatment, stress, condition	Sample	Methodological approach	Proteins and metabolites of biotechnological importance	Reference
			Defense response: 17 kDa HSP, 18.2 kDa class I HSP, 20 kDa chaperonin, HSP23, HSP70, thaumatin-like protein, ubiquitin, ascorbate peroxidases, glucan endo-1,3-beta-glucosidase	
Cold acclimation	Leaves of cultivars tolerant or sensitive to freezing	2-D gel electrophoresis (MALDI TOF/TOF)	**Oxidative stress:** monodehydroascorbate reductase, glutathione peroxidase, peptide methionine sulfoxide reductases A3, thioredoxin-like protein CDSP32, 2-cys peroxiredoxin BAS1-like	Chen et al. (2015)
			Methionine biosynthesis: 5-methyltetrahydropteroyltriglutamate-homocysteine methyltransferase	
			Lignin and terpenoid biosynthesis: cinnamoyl-CoA reductase, 1-deoxy-D-xylulose 5-phosphate reductoisomerase	
			Photosynthesis and Rubisco availability: Rubisco large subunit-binding protein subunit beta, Rubisco activase B, chlorophyll A/B binding protein, oxygen-evolving enhancer protein 1, cytochrome b6-f complex iron-sulfur subunit	
			Protein folding and disassembling: chaperone protein ClpC, GTPase, peptidyl-prolyl *cis–trans* isomerase CYP20-3	
Cadmium stress	Cell walls and soluble proteins from stems	2-D DIGE (MALDI TOF/TOF)	**Cell wall modification:** sucrose synthase, pectinesterase/pectinesterase inhibitor, polygalacturonase non-catalytic protein, polygalacturonase-inhibiting protein 1, b-xylosidase/alpha-L-arabinofuranosidase, trichome birefringence-like protein, xyloglucan endotransglucosylase/hydrolase family protein, dirigent protein 21-like	Gutsch et al. (2018a)
			Defense: chitinase (Class Ib)/hevein, chitinase, class I chitinase, disease resistance response protein, pathogenesis-related protein 1, pathogenesis-related thaumatin family protein, plant basic secretory protein (BSP) family protein, pre-hevein-like protein, stromal 70 kDa heat shock-related protein, CAP, cysteine-rich secretory protein, antigen 5	
			Oxidation-reduction process: anionic peroxidase swpb3 protein, class III peroxidase, peroxidase family protein, peroxidase1b, peroxidase2	
Cadmium stress	Stems (soluble and cell wall enriched proteins)	2-D DIGE (MALDI TOF/TOF)	**Cell wall modification:** pectinesterase/pectinesterase inhibitor, polygalacturonase non-catalytic protein, polygalacturonase-inhibiting protein 1 **Chloroplast protein degradation:** chloroplastic aspartyl protease isoforms **Cell wall:** class III peroxidase, lignin biosynthetic peroxidase, chitinases	Gutsch et al. (2018b)
Stem growth	Different regions of stems (apical, intermediate, and basal)	2-D gel electrophoresis (MALDI TOF/TOF)	**Chloroplast protein synthesis:** CSP41-b, EF-Tu, EF-G, Cpn 60, HSP70 **Lignin biosynthesis:** transketolase, enolase **Cytoplasmic protein synthesis:** eIF-5a, endoplasmic protein disulfide isomerase, HSP90, ribosomal protein P3-like	Printz et al. (2015)
			Vesicular trafficking: clathrin light chain	
			Stress response: peroxisomal membrane protein, monodehydroascorbate reductase, flavoprotein wrbA-like, Pprg2	
			Sieve element development: sieve element occlusion by forisomes 3	
Cadmium stress and hydrogen-rich water	Roots	iTRAQ (nano-LC MS/MS)	**Defense response:** mitogen-activated protein kinase, pathogenesis-related thaumatin family protein, pathogenesis-related protein bet V I family protein, disease-resistance response protein **Nitrogen metabolism:** glutamate dehydrogenase **Sulfur compound metabolic process:** cysteine synthase, ATP sulfurylase	Dai et al. (2017)
			Secondary metabolism: chalcone-flavonone isomerase family protein	
Waterlogging	Leaves of two cultivars contrasting in tolerance to waterlogging	iTRAQ (reverse-phase HPLC fractionation and LC-MS/MS)	**Cell wall and defense response:** acidic endochitinase, expansin-like B1, early nodulin-like protein 2, thaumatin-like protein, 1,4 alpha-glucan-branching enzyme 1, pathogenesis-related protein **Stress response:** glutathione *S*-transferase, protein C2-DOMAIN ABA-RELATED 9, aldo-keto reductase family 4 member C9, Fe superoxide dismutase 2, 1 aminocyclopropane-1-carboxylate oxidase homolog 5,	Zeng et al. (2019)
			Proteolysis: vacuolar-processing enzyme	
Different developmental stages (budding and mid-flowering)	Leaves	TMT labeling (nano-LC MS/MS)	**Metabolites:** D-mannose hemicellulose precursor (upregulated in mid flowering), L-phenylalanine, L-tyrosine, L-phenylalanine **Metabolism:** alpha glucosidase, alpha amylase **Cell wall modification:** UDP-glucuronic acid decarboxylase (xylan production), cinnamyl alcohol dehydrogenase (lignin biosynthesis)	Fan et al. (2018)
Fall dormancy	Terminal buds of fall dormant and non-fall dormant cultivars	iTRAQ (SCX fractionation, LC MS/MS)	**Nitrogen metabolism:** L-asparaginase **Auxin polar transport:** stilbene synthase family protein, monothiol glutaredoxin-S17 protein **Lignin biosynthesis:** cinnamyl alcohol dehydrogenase **Pyruvate metabolism and transport:** pyruvate carrier protein	Du et al. (2018)
			Vitamin B1 metabolism: thiazole biosynthetic enzyme	

(TAL effector nucleases or TALENs), and clustered regularly interspaced short palindromic repeat/CRISPR–associated protein 9 (CRISPR/Cas9). Among these, TALENs and CRISPR/Cas9 are the preferred SSNs for research purposes (Kanaar et al., 1998; Pastwa and Blasiak, 2003; Smith et al., 2006; Pâques and Duchateau, 2007; Hartlerode and Scully, 2009; Sander et al., 2011; Qi, 2015; Steinert et al., 2016; Malzahn et al., 2017; Shan et al., 2020).

The history of gene targeting technologies started in 1988 when the first gene-targeting experiment was performed on tobacco (*Nicotiana tabacum*) protoplasts (Paszkowski et al., 1988). Later, Puchta et al. (1993) discovered that gene-targeting efficiency can be improved by DSBs in plant cells. More than a decade later, ZFNs were adapted in tobacco and were used in a few plant species for trait improvement (Wright et al., 2005). Subsequently, TALENs were introduced into the group of plant genome editing technologies (Christian et al., 2010). Finally, CRISPR/Cas9 technology has been used in plants such as *Arabidopsis thaliana*, *N. benthamiana*, *Oryza sativa*, and *T. aestivum* (Li J. F. et al., 2013; Nekrasov et al., 2013; Shan et al., 2013, 2020).

TALENs

TALENs are created by the fusion of DNA binding TALE repeats to the Fok1 nuclease domain. TALENs are less toxic and are easier to engineer than ZFNs. Each of these two platforms has unique limitations, and they are not routinely used in plants. The main advantages of TALENs over CRISPR are that they have less off-target effects due to their ∼30 bp target requirement, as well as their lack of PAM requirement, as unlike CRISPR, TALENs are able to target any sequence. On the other hand, TALENs have more disadvantages: an increased time and financial investment due to the difficulty in protein engineering, a highly variable efficiency for each construct, an inability to target methylated DNA, and the difficulties in engineering nickase (Christian et al., 2010; Li et al., 2011; Mahfouz et al., 2011; Miller et al., 2011; Malzahn et al., 2017; Chen et al., 2019). So far, a successful application of TALEN technology has not been published for either alfalfa or barrel medic. Nevertheless, TALENs have been used for the targeted mutagenesis of another legume, namely soybean (Haun et al., 2014; Demorest et al., 2016; Du et al., 2016; Curtin et al., 2018). The use of TALENs for the mutagenesis of higher plants was recently reviewed by Malzahn et al. (2017) and Khan et al. (2017).

CRISPR/Cas9

In bacteria and archaea, CRISPR and Cas9 function together against invading phages, plasmids, and viruses in adaptive immune system by cleaving the invader's nucleic acids. The first component is single guide RNA (sgRNA) that associates with a Cas9 protein a Cas9/sgRNA complex. The second component Cas9 belongs to the single-protein effectors of Class 2 CRISPR-Cas systems and is composed of two endonuclease domains, namely, the RuvC-like domain and the HNH, each cutting one strand of DNA. The CRISPR/Cas9 constituents can be transformed into plant cells by different strategies, including *Agrobacterium*-mediated delivery, gene gun (biolistic delivery), or using virus-based guide RNA (gRNA). Out of the primary SSN classes, CRISPR/Cas9 technology has been the most used and adopted in recent years (Barrangou et al., 2007; Marraffini and Sontheimer, 2008; Wiedenheft et al., 2012; Graham and Root, 2015; Schiml and Puchta, 2016; Makarova et al., 2017; Malzahn et al., 2017; Chen et al., 2019). The CRISPR/Cas system has the potential for numerous applications, such as fusing dCas9 (deactivated Cas9) with other proteins, which can be used for DNA imaging, epigenome editing, gene regulation, and genomic labeling (Chen et al., 2019). One of the main limitations of CRISPR/Cas9 technology might be the generation of undesired off-target effects. Nevertheless, whole-genome sequencing revealed very limited off-target effect mutations in *Arabidopsis* (Feng et al., 2013), rice (Zhang H. et al., 2014; Tang et al., 2018), and tomato (Nekrasov et al., 2017). Using software tools such as CRISPR-P (Liu H. et al., 2017) and CRISPRGE (Xie et al., 2017) can further decrease any potential off-target occurrence by designing highly specific guide RNAs. Finally, breeding processes may remove any off-target mutations that have negative effects and may keep positive or neutral off-target mutations (Mao et al., 2019).

CRISPR/Cas9 in Alfalfa

CRISPR/Cas9 technology was very recently used for targeted mutagenesis in alfalfa. Selected *SQUAMOSA PROMOTER BINDING PROTEIN-LIKE 9* (*SPL9*) gene was successfully mutagenized and transgenic lines were pre-selected by using droplet digital PCR (ddPCR) for high-throughput screening of large populations. It was further confirmed by restriction enzyme digestion after PCR amplification and sequencing of sub-clones. Comparison of editing efficiency with available data on barrel medic showed lower efficiency in alfalfa, which might be related to its tetraploid genome possessing highly repeated clusters (Meng et al., 2017, 2019; Gao et al., 2018). Gao et al. (2018) concluded that CRISPR/Cas9-mediated modifications of tetraploid alfalfa genome have been successfully performed, but there is still a need to improve editing efficiency. Alfalfa plants with silenced *SPL9* had no visible phenotype so ddPCR-based estimation of concentration of the event per μl was a direct indicator of the genome editing rate. Sequencing analysis showed no off-target effects in the alfalfa genome and proved that the sgRNAs of *SPL9* were highly specific to the recognition site. In other legumes such as barrel medic, CRISPR/Cas9 technology has been used as well (Michno et al., 2015; Meng et al., 2017, 2019; Curtin et al., 2018; Wen et al., 2019; Yin et al., 2020). Recently, Meng et al. (2019) developed an optimized *Agrobacterium*-dependent CRISPR/Cas9 system and successfully edited an endogenous *PHYTOENE DESATURASE* (*MtPDS)* gene. CRISPR/Cas9 technology for the mutagenesis was also used in *L. japonicus* (Wang et al., 2016, 2019), and *G. max* (Cai et al., 2015; Jacobs et al., 2015; Li et al., 2015; Sun et al., 2015; Du et al., 2016; Tang et al., 2016; Curtin et al., 2018; Bao et al., 2019; Wang et al., 2020). Utilization of CRISPR/Cas9-based mutagenesis in several non-leguminous plant species, including data on delivery method, integration into the genome, and editing efficiency, has been reviewed recently (Belhaj et al., 2013; Jaganathan et al., 2018; Liu X. et al., 2019; Kuluev et al., 2019; Mao et al., 2019;

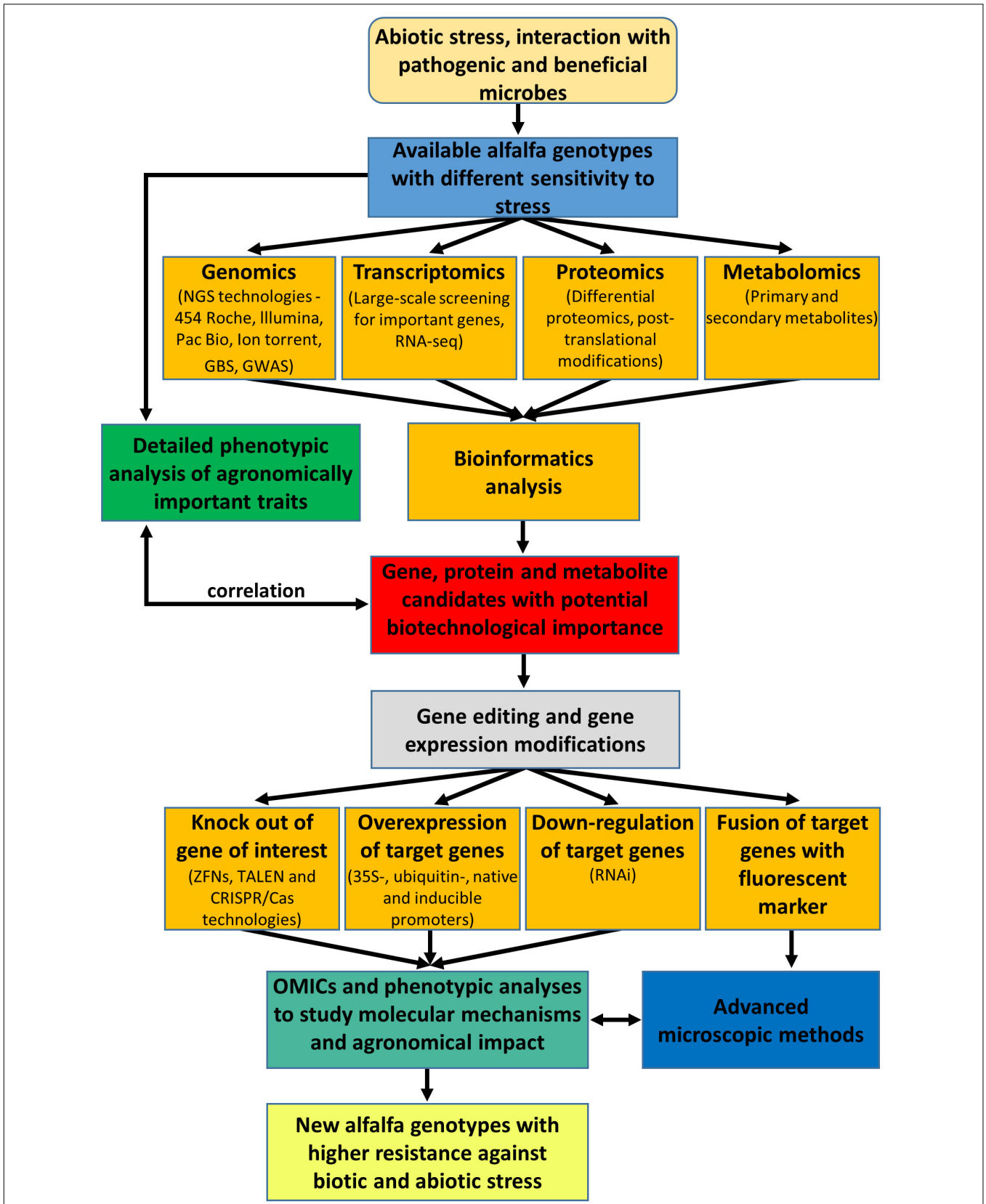

FIGURE 1 | Overview and integration of omics and molecular genetics approaches aiming to improve agronomic traits and performance of alfalfa.

Moradpour and Abdulah, 2020; Shan et al., 2020). Approaches such as transgene integration and gene stacking developed for diploid crop species (e.g., corn, cotton, soybean) might be less suitable for alfalfa due to its auto-tetraploid character (Kumar et al., 2018), but the CRISPR/Cas9 technology seems to work well.

PHOSPHORYLATION-DEPENDENT POST-TRANSLATIONAL MODIFICATION BY MAPKs

Multiple abiotic stress stimuli, such as wounding, cold, salinity, or drought, are perceived by plants through the activation of MAPKs (Šamajová et al., 2013b). Activated MAPKs phosphorylate, and thereby regulate, several intracellular targets including other protein kinases, cytoskeletal components, nuclear transcription factors, and proteins involved in vesicular trafficking (Komis et al., 2011; Šamajová et al., 2013a). In alfalfa, STRESS-INDUCED MAPK (SIMK), was identified as a salt- and elicitor- stress induced MAPK (Cardinale et al., 2002). SIMK in response to salt stress is specifically activated by upstream STRESS-INDUCED MAPKK (SIMKK; Kiegerl et al., 2000; Bekešová et al., 2015). SIMK is localized to nuclei and cytoplasm of root cells, while in developing root hairs it relocated from the nucleus to the growing tip (Šamaj et al., 2002). Moreover, stimulus-dependent activation and the subsequent subcellular relocation of both SIMK and its upstream SIMKK were induced by salt stress (Ovečka et al., 2014). Such activity-dependent and coordinated relocation of SIMK-SIMKK module from the nucleus to cytoplasm under salt stress were observed in alfalfa and thale cress. Transgenic thale cress plants stably producing SIMKK-YFP exhibited enhanced MITOGEN-ACTIVATED PROTEIN KINASE 3 (MPK3) and MITOGEN-ACTIVATED PROTEIN KINASE 6 (MPK6) activation and conferred altered sensitivity to salt stress. These data suggested that SIMKK may serve as a negative regulator of the salt stress response in alfalfa (Ovečka et al., 2014).

CONCLUSION AND PERSPECTIVES

Alfalfa is a perennial, cross-pollinated, autotetraploid ($2n = 4x = 32$) plant with genome size of 800–900 Mbp. It is often mentioned as the "queen of forages" due to the very high production potential as hay, silage or as a biofuel feedstock for ethanol production (Blondon et al., 1994). However, tetraploid nature made understanding and improving of alfalfa by traditional breeding methods rather challenging. Therefore, the use of modern biotechnological, omics and genetic engineering approaches for alfalfa improvement is highly actual and desirable task for crop researchers.

This review provides an overview of the biotechnological potential of alfalfa based on the integration of various omics and molecular tools as depicted in the **Figure 1**. Recent advances in high-throughput sequencing technology have opened another scientific boundary, and many species, including economically important crops, have been subjected to whole-genome sequencing by *de novo* assembly and resequencing. Several novel genes have been identified owing to whole-genome duplications and structural variations in chromosomes (Van et al., 2013). Since plant responses to stresses are often very specific, proteomic and transcriptomic approaches should be targeted to individual cell types and tissues at different developmental stages. Such approach was already reported for root hairs and root border cells of barrel medic (Breakspear et al., 2014; Watson et al., 2015). In this respect, the integration of fast-developing omics methods and bioinformatics into systems biology at the single cell level might bring new opportunities to improve plant stress tolerance (Libault et al., 2017).

Biotechnological approaches provide a great potential to increase crop production for the constantly growing global population. Introducing tolerance to environmental abiotic and biotic stresses is crucial for improving the productivity of crop legumes (Farooq et al., 2017). Extensive research conducted on alfalfa stress tolerance suggests that it is able to cope with abiotic stresses using general mechanisms such as antioxidant defense, protein folding, and cell wall remodeling. Research in the field of alfalfa biotechnology also aimed to identify genes involved in the energy production pathway or in enhancing environmental tolerance (Pennycooke et al., 2008; Aranjuelo et al., 2011; Mo et al., 2011). Scientists grew alfalfa plants under different conditions in order to analyze gene expression profiles and to identify crucial genes and proteins, as well as to understand global correlations between genes, proteins, and metabolites using omics approaches.

The potentials of these methods have only partially been exploited in alfalfa research. Continued research toward the development of alfalfa proteome studies (Komatsu and Ahsan, 2009) should permit the rapid comparison of alfalfa cultivars, mutants, and transgenic lines.

AUTHOR CONTRIBUTIONS

All authors listed have made a substantial, direct and intellectual contribution to the work, and approved it for publication. MH, PD, TT, MT, and IL drafted the review which was coordinated by OŠ, MO, and finally edited by JŠ.

FUNDING

This work was funded by the European Regional Development Fund, European Union (ERDF) project "Plants as a tool for sustainable global development" (CZ.02.1.01/0.0/0.0/16_019/0000827).

ACKNOWLEDGMENTS

We would like to thank Editage (www.editage.com) for English language editing.

REFERENCES

Abdelrahman, M., El-Sayed, M., Sato, S., Hirakawa, H., Ito, S. I., Tanaka, K., et al. (2017a). RNA-sequencing-based transcriptome and biochemical analyses of steroidal saponin pathway in a complete set of *Allium fistulosum*-A. cepa monosomic addition lines. *PLoS One* 12:e0181784. doi: 10.1371/journal.pone.0181784

Abdelrahman, M., Suzumura, N., Mitoma, M., Matsuo, S., Ikeuchi, T., Mori, M., et al. (2017b). Comparative de novo transcriptome profiles in *Asparagus officinalis* and A. kiusianus during the early stage of *Phomopsis asparagi* infection. *Sci. Rep.* 7:2608. doi: 10.1038/s41598-017-02566-7

Abdelrahman, M., Jogaiah, S., Burritt, D. J., and Tran, L. S. P. (2018). Legume genetic resources and transcriptome dynamics under abiotic stress conditions. *Plant Cell Environ.* 41, 1972–1983. doi: 10.1111/pce.13123

Abdelrahman, M., Sawada, Y., Nakabayashi, R., Sato, S., Hirakawa, H., El-Sayed, M., et al. (2015). Integrating transcriptome and target metabolome variability in doubled haploids of *Allium cepa* for abiotic stress protection. *Mol. Breed.* 35:195. doi: 10.1007/s11032-015-0378-2

An, Y. M., Song, L. L., Liu, Y. R., Shu, Y. J., and Guo, C. H. (2016). De novo transcriptional analysis of alfalfa in response to saline-alkaline stress. *Front. Plant Sci.* 7:931. doi: 10.3389/fpls.2016.00931

Annicchiarico, P., Barrett, B., Brummer, E. C., Julier, B., and Marshall, A. H. (2015). Achievements and challenges in improving temperate perennial forage legumes. *Crit. Rev. Plant Sci.* 34, 327–380. doi: 10.1080/07352689.2014.898462

Annicchiarico, P., Nazzicari, N., and Brummer, E. C. (2016). ""Alfalfa genomic selection: challenges, strategies, transnational cooperation"," in *Breeding in a World of Scarcity*, eds I. Roldán-Ruiz, J. Baert, and D. Reheul (Cham: Springer), 145–149. doi: 10.1007/978-3-319-28932-8_22

Aranjuelo, I., Molero, G., Erice, G., Avice, J. C., and Nogués, S. (2011). Plant physiology and proteomics reveals the leaf response to drought in alfalfa (*Medicago sativa* L.). *J. Exp. Bot.* 62, 111–123. doi: 10.1093/jxb/erq249

Aranjuelo, I., Perez, P., Hernandez, L., Irigoyen, J. J., Zita, G., Martinez-Carrasco, R., et al. (2005). The response of nodulated alfalfa to water supply, temperature and elevated CO2: photosynthetic downregulation. *Physiol. Plant.* 123, 348–358. doi: 10.1111/j.1399-3054.2005.00459.x

Aranjuelo, I., Tcherkez, G., Molero, G., Gilard, F., Avice, J.-C., and Nogués, S. (2013). Concerted changes in N and C primary metabolism in alfalfa (*Medicago sativa*) under water restriction. *J. Exp. Bot.* 64, 885–897. doi: 10.1093/jxb/ers367

Ari, Ş, and Arikan, M. (2016). "Next-generation sequencing: advantages, disadvantages, and future," in *Plant Omics: Trends and Applications*, eds K. Hakeem, H. Tombuloglu, and G. Tombuloglu (Cham: Springer), 109–135. doi: 10.1007/978-3-319-31703-8_5

Arshad, M., Feyissa, B. A., Amyot, L., Aung, B., and Hannoufa, A. (2017). MicroRNA156 improves drought stress tolerance in alfalfa (*Medicago sativa*) by silencing SPL13. *Plant Sci.* 258, 122–136. doi: 10.1016/j.plantsci.2017.01.018

Arshad, M., Gruber, M. Y., and Hannoufa, A. (2018). Transcriptome analysis of microRNA156 overexpression alfalfa roots under drought stress. *Sci. Rep.* 8:9363. doi: 10.1038/s41598-018-27088-8

Asamizu, E., Nakamura, Y., Sato, S., and Tabata, S. (2004). Characteristics of the Lotus japonicus gene repertoire deduced from large-scale expressed sequence tag (EST) analysis. *Plant Mol. Biol.* 54, 405–414. doi: 10.1023/B:PLAN.0000036372.46942.b8

Aung, B., Gao, R., Gruber, M. Y., Yuan, Z. C., Sumarah, M., and Hannoufa, A. (2017). MsmiR156 affects global gene expression and promotes root regenerative capacity and nitrogen fixation activity in alfalfa. *Transgenic Res.* 26, 541–557. doi: 10.1007/s11248-017-0024-3

Aung, B., Gruber, M. Y., Amyot, L., Omari, K., Bertrand, A., and Hannoufa, A. (2015). Micro RNA 156 as a promising tool for alfalfa improvement. *Plant Biotechnol. J.* 13, 779–790. doi: 10.1111/pbi.12308

Aziz, N., Paiva, N. L., May, G. D., and Dixon, R. A. (2005). Transcriptome analysis of alfalfa glandular trichomes. *Planta* 221, 28–38. doi: 10.1007/s00425-004-1424-1

Bahramnejad, B., Goodwin, P. H., Zhang, J., Atnaseo, C., and Erickson, L. R. (2010). A comparison of two class 10 pathogenesis-related genes from alfalfa and their activation by multiple stresses and stress-related signaling molecules. *Plant Cell Rep.* 29, 1235–1250. doi: 10.1007/s00299-010-0909-6

Baldacci-Cresp, F., Chang, C., Maucourt, M., Deborde, C., Hopkins, J., Lecomte, P., et al. (2012). Homoglutathione deficiency impairs root-knot nematode development in *Medicago truncatula*. *PLoS Pathog.* 8:2471. doi: 10.1371/journal.ppat.1002471

Bao, A., Chen, H., Chen, L., Chen, S., Hao, Q., Guo, W., et al. (2019). CRISPR/Cas9-mediated targeted mutagenesis of *GmSPL9* genes alters plant architecture in soybean. *BMC Plant Biol.* 19:131. doi: 10.1186/s12870-019-1746-6

Barabaschi, D., Guerra, D., Lacrima, K., Laino, P., Michelotti, V., Urso, S., et al. (2012). Emerging knowledge from genome sequencing of crop species. *Mol. Biotech.* 50, 250–266. doi: 10.1007/s12033-011-9443-1

Barrangou, R., Fremaux, C., Deveau, H., Richards, M., Boyaval, P., Moineau, S., et al. (2007). CRISPR provides acquired resistance against viruses in prokaryotes. *Science* 315, 1709–1712. doi: 10.1126/science.1138140

Barros, J., Temple, S., and Dixon, R. A. (2019). Development and commercialization of reduced lignin alfalfa. *Curr. Opin. Biotech.* 56, 48–54. doi: 10.1016/j.copbio.2018.09.003

Bekešová, S., Komis, G., Křenek, P., Vyplelová, P., Ovečka, M., Luptovčiak, I., et al. (2015). Monitoring protein phosphorylation by acrylamide pendant Phos-TagTM in various plants. *Front. Plant Sci.* 6:336. doi: 10.3389/fpls.2015.00336

Belhaj, K., Chaparro-Garcia, A., Kamoun, S., and Nekrasov, V. (2013). Plant genome editing made easy: targeted mutagenesis in model and crop plants using the CRISPR/Cas system. *Plant Methods* 9:39. doi: 10.1186/1746-4811-9-39

Bevan, M. W., Uauy, C., Wulff, B. B., Zhou, J., Krasileva, K., and Clark, M. D. (2017). Genomic innovation for crop improvement. *Nature* 543, 346–354. doi: 10.1038/nature22011

Biazzi, E., Nazzicari, N., Pecetti, L., Brummer, E. C., Palmonari, A., Tava, A., et al. (2017). Genome-wide association mapping and genomic selection for alfalfa (*Medicago sativa*) forage quality traits. *PLoS One* 12:e0169234. doi: 10.1371/journal.pone.0169234

Blondon, F., Marie, D., Brown, S., and Kondorosi, A. (1994). Genome size and base composition in *Medicago sativa* and M. *truncatula species*. *Genome* 37, 264–270. doi: 10.1139/g94-037

Bohnert, H. J., and Jensen, R. G. (1996). Strategies for engineering water-stress tolerance in plants. *Trends Biotechnol.* 14, 89–97. doi: 10.1016/0167-7799(96)80929-2

Bora, K. S., and Sharma, A. (2011). Phytochemical and pharmacological potential of *Medicago sativa*: a review. *Pharm. Biol.* 49, 211–220. doi: 10.3109/13880209.2010.504732

Borsics, T., and Lados, M. (2002). Dodder infection induces the expression of a pathogenesis-related gene of the family PR-10 in alfalfa. *J. Exp. Bot.* 53, 1831–1832. doi: 10.1093/jxb/erf039

Breakspear, A., Liu, C., Roy, S., Stacey, N., Rogers, C., Trick, M., et al. (2014). The root hair "infectome" of *Medicago truncatula* uncovers changes in cell cycle genes and reveals a requirement for auxin signaling in rhizobial infection. *Plant Cell* 26, 4680–4701. doi: 10.1105/tpc.114.133496

Brouwer, D. J., and Osborn, T. C. (1999). A molecular marker linkage map of tetraploid alfalfa (*Medicago sativa* L.). *Theor. Appl. Gen.* 99, 1194–1200. doi: 10.1007/s001220051324

Brummer, E. C., Bouton, J. H., and Kochert, G. (1993). Development of an RFLP map in diploid alfalfa. *Theor. Appl. Gen.* 86, 329–332. doi: 10.1007/BF00222097

Budak, H., Kantar, M., Bulut, R., and Akpinar, B. A. (2015). Stress responsive miRNAs and isomiRs in cereals. *Plant Sci.* 235, 1–13. doi: 10.1016/j.plantsci.2015.02.008

Bustos-Sanmamed, P., Mao, G., Deng, Y., Elouet, M., Khan, G. A., Bazin, J., et al. (2013). Overexpression of miR160 affects root growth and nitrogen-fixing nodule number in *Medicago truncatula*. *Funct. Plant Biol.* 40, 1208–1220. doi: 10.1071/FP13123

Cai, Y., Chen, L., Liu, X., Sun, S., Wu, C., Jiang, B., et al. (2015). CRISPR/Cas9-mediated genome editing in soybean hairy roots. *PLoS One* 10:e0136064. doi: 10.1371/journal.pone.0136064

Cardinale, F., Meskiene, I., Ouaked, F., and Hirt, H. (2002). Convergence and divergence of stress-induced mitogen-activated protein kinase signaling pathways at the level of two distinct mitogen-activated protein kinase kinases. *Plant Cell* 14, 703–711. doi: 10.1105/tpc.010256

Carter, P. R., and Sheaffer, C. C. (1983). Alfalfa response to soil water deficits. III. Nodulation and N2 fixation. *Crop Sci.* 23, 985–990. doi: 10.2135/cropsci1983.0011183X002300050041x

Chao, Y., Yuan, J., Guo, T., Xu, L., Mu, Z., and Han, L. (2019). Analysis of transcripts and splice isoforms in *Medicago sativa* L. by single-molecule

long-read sequencing. *Plant Mol. Biol.* 99, 219–235. doi: 10.1007/s11103-018-0813-y

Chen, J., Han, G., Shang, C., Li, J., Zhang, H., Liu, F., et al. (2015). Proteomic analyses reveal differences in cold acclimation mechanisms in freezing-tolerant and freezing-sensitive cultivars of alfalfa. *Front. Plant Sci.* 6:105. doi: 10.3389/fpls.2015.00105

Chen, K., Wang, Y., Zhang, R., Zhang, H., and Gao, C. (2019). CRISPR/Cas genome editing and precision plant breeding in agriculture. *Annu. Rev. Plant Biol.* 70, 667–697. doi: 10.1146/annurev-arplant-050718-100049

Chen, L., Chen, Q., Zhu, Y., Hou, L., and Mao, P. (2016). Proteomic identification of differentially expressed proteins during alfalfa (*Medicago sativa* L.) flower development. *Front. Plant Sci.* 7:1502. doi: 10.3389/fpls.2016.01502

Chen, T. H., and Murata, N. (2002). Enhancement of tolerance of abiotic stress by metabolic engineering of betaines and other compatible solutes. *Curr. Opin. Plant Biol.* 5, 250–257. doi: 10.1016/s1369-5266(02)00255-8

Chen, T. H., and Murata, N. (2008). Glycinebetaine: an effective protectant against abiotic stress in plants. *Trends Plant Sci.* 13, 499–505. doi: 10.1016/j.tplants.2008.06.007

Cheung, F., Haas, B. J., Goldberg, S. M. D., May, G. D., Xiao, Y., and Town, C. D. (2006). Sequencing *Medicago truncatula* expressed sequenced tags using 454 Life Sciences technology. *BMC Genom.* 7:272. doi: 10.1186/1471-2164-7-272

Christian, M., Cermak, T., Doyle, E. L., Schmidt, C., Zhang, F., Hummel, A., et al. (2010). Targeting DNA double-strand breaks with TAL effector nucleases. *Genetics* 186, 757–761. doi: 10.1534/genetics.110.120717

Curtin, S. J., Xiong, Y., Michno, J. M., Campbell, B. W., Stec, A. O., Čermák, T., et al. (2018). CRISPR/Cas9 and TALENs generate heritable mutations for genes involved in small RNA processing of Glycine max and *Medicago truncatula*. *Plant Biotech. J.* 16, 1125–1137. doi: 10.1111/pbi.12857

Dai, C., Cui, W., Pan, J., Xie, Y., Wang, J., and Shen, W. (2017). Proteomic analysis provides insights into the molecular bases of hydrogen gas-induced cadmium resistance in *Medicago sativa*. *J. Proteom.* 152, 109–120. doi: 10.1016/j.jprot.2016.10.013

de Zélicourt, A., Diet, A., Marion, J., Laffont, C., Ariel, F., Moison, M., et al. (2011). Dual involvement of a *Medicago truncatula* NAC transcription factor in root abiotic stress response and symbiotic nodule senescence. *Plant J.* 70, 220–230. doi: 10.1111/j.1365-313X.2011.04859.x

Demorest, Z. L., Coffman, A., Baltes, N. J., Stoddard, T. J., Clasen, B. M., Luo, S., et al. (2016). Direct stacking of sequence-specific nuclease-induced mutations to produce high oleic and low linolenic soybean oil. *BMC Plant Biol.* 16:225. doi: 10.1186/s12870-016-0906-1

Deokar, A. A., Kondawar, V., Jain, P. K., Karuppayil, S. M., Raju, N. L., Vadez, V., et al. (2011). Comparative analysis of expressed sequence tags (ESTs) between drought-tolerant and -susceptible genotypes of chickpea under terminal drought stress. *BMC Plant Biol.* 11:70. doi: 10.1186/1471-2229-11-70

Diaz-Vivancos, P., de Simone, A., Kiddle, G., and Foyer, C. H. (2015). Glutathione–linking cell proliferation to oxidative stress. *Free Radical Biol. Med.* 89, 1154–1164. doi: 10.1016/j.freeradbiomed.2015.09.023

Dong, L., Liu, H., Zhang, J., Yang, S., Kong, G., Chu, J. S., et al. (2015). Single-molecule real-time transcript sequencing facilitates common wheat genome annotation and grain transcriptome research. *BMC Genom.* 16:1039. doi: 10.1186/s12864-015-2257-y

Doyle, J. J., and Luckow, M. A. (2003). The rest of the iceberg. Legume diversity and evolution in a phylogenetic context. *Plant Physiol.* 131, 900–910. doi: 10.1104/pp.102.018150

Du, H., Shi, Y., Li, D., Fan, W., Wang, Y., Wang, G., et al. (2018). Proteomics reveals key proteins participating in growth difference between fall dormant and non-dormant alfalfa in terminal buds. *J. Proteom.* 173, 126–138. doi: 10.1016/j.jprot.2017.11.029

Du, H., Zeng, X., Zhao, M., Cui, X., Wang, Q., Yang, H., et al. (2016). Efficient targeted mutagenesis in soybean by TALENs and CRISPR/Cas9. *J. Biotechnol.* 217, 90–97. doi: 10.1016/j.jbiotec.2015.11.005

Ebert, J. (2007). Alfalfa's bioenergy appeal. *Ethanol Prod. Mag.* 88–94.

Echt, C. S., Kidwell, K. K., Knapp, S. J., Osborn, T. C., and McCoy, T. J. (1994). Linkage mapping in diploid alfalfa (*Medicago sativa*). *Genome* 37, 61–71. doi: 10.1139/g94-008

Edwards, D., and Batley, J. (2010). Plant genome sequencing: applications for crop improvement. *Plant Biotechnol. J.* 8, 2–9. doi: 10.1111/j.1467-7652.2009.00459.x

Eid, J., Fehr, A., Gray, J., Luong, K., Lyle, J., Otto, G., et al. (2009). Real-time DNA sequencing from single polymerase molecules. *Science* 323, 133–138. doi: 10.1126/science

Elgin, J. H. Jr., and Ostazeski, S. A. (1985). Inheritance of resistance to race 1 and race 2 anthracnose in Arc and Saranac AR alfalfa. *Crop Sci.* 25, 861–865. doi: 10.2135/cropsci1985.0011183X002500050032x

Elgin, J. H. Jr., Welty, R. E., and Gilchrist, D. B. (1988). Breeding for disease and nematode resistance. *Alfalfa Alfalfa Impr.* 29, 827–858. doi: 10.2134/agronmonogr29.c27

Esnault, R., Buffard, D., Breda, C., Sallaud, C., Turk, J., and Kondorosi, A. (1993). Pathological and molecular characterizations of alfalfa interactions with compatible and incompatible bacteria, Xanthomonas campestris pv. alfalfae and *Pseudomonas* syringae pv. pisi. *Mol. Plant Microbe Interact.* 6, 655–664. doi: 10.1094/MPMI-6-655

Fan, W., Ge, G., Liu, Y., Wang, W., Liu, L., and Jia, Y. (2018). Proteomics integrated with metabolomics: analysis of the internal causes of nutrient changes in alfalfa at different growth stages. *BMC Plant Biol.* 18:78. doi: 10.1186/s12870-018-1291-8

Farooq, M., Gogoi, N., Hussain, M., Barthakur, S., Paul, S., Bharadwaj, N., et al. (2017). Effects, tolerance mechanisms and management of salt stress in grain legumes. *Plant Physiol. Biochem.* 118, 199–217. doi: 10.1105/10.1016/j.plaphy.2017.06.020

Feng, Z., Zhang, B., Ding, W., Liu, X., Yang, D. L., Wei, P., et al. (2013). Efficient genome editing in plants using a CRISPR/Cas system. *Cell Res.* 23, 1229–1232. doi: 10.1038/cr.2013.114

Feyissa, B. A., Arshad, M., Gruber, M. Y., Kohalmi, S. E., and Hannoufa, A. (2019). The interplay between miR156/SPL13 and DFR/WD40–1 regulate drought tolerance in alfalfa. *BMC plant Biol.* 19:2059. doi: 10.1186/s12870-019-2059-5

Flajoulot, S., Ronfort, J., Baudouin, P., Barre, P., Huguet, T., Huyghe, C., et al. (2005). Genetic diversity among alfalfa (*Medicago sativa*) cultivars coming from a breeding program, using SSR markers. *Theor. Appl. Genet.* 111, 1420–1429. doi: 10.1007/s00122-005-0074-4

Fleming, M. B., Patterson, E. L., Reeves, P. A., Richards, C. M., Gaines, T. A., and Walters, C. (2018). Exploring the fate of mRNA in aging seeds: protection, destruction, or slow decay? *J. Exp. Bot.* 69, 4309–4321. doi: 10.1093/jxb/ery215

Frendo, P., Harrison, J., Norman, C., and Jiménez, M. J. H. (2005). Glutathione and homoglutathione play a critical role in the nodulation process of *Medicago truncatula*. *Mol. Plant-Mic. Int.* 18, 254–259. doi: 10.1094/MPMI-18-0254

Fu, G., Grbic, V., Ma, S., and Tian, L. (2015). Evaluation of somatic embryos of alfalfa for recombinant protein expression. *Plant Cell Rep.* 34, 211–221. doi: 10.1007/s00299-014-1700-x

Fukuda, A., Nakamura, A., and Tanaka, Y. (1999). Molecular cloning and expression of the Na+/H+ exchanger gene in *Oryza sativa*. *Biochem. Biophys. Acta* 1446, 149–155. doi: 10.1016/s0167-4781(99)00065-2

Fürstenberg-Hägg, J., Zagrobelny, M., and Bak, S. (2013). Plant defense against insect herbivores. *Int. J. Mol. Sci.* 14, 10242–10297. doi: 10.3390/ijms140510242

Gao, R., Feyissa, B. A., Croft, M., and Hannoufa, A. (2018). Gene editing by CRISPR/Cas9 in the obligatory outcrossing *Medicago sativa*. *Planta* 247, 1043–1050. doi: 10.1007/s00425-018-2866-1

Gao, Z., Luo, W., Liu, H., Zeng, C., Liu, X., Yi, S., et al. (2012). Transcriptome analysis and SSR/SNP markers information of the blunt snout bream (*Megalobrama amblycephala*). *PLoS One* 7:42637. doi: 10.1371/journal.pone.0042637

García, A. N., Ayub, N. D., Fox, A. R., Gómez, M. C., Diéguez, M. J., Pagano, E. M., et al. (2014). Alfalfa snakin-1 prevents fungal colonization and probably coevolved with rhizobia. *BMC Plant Biol.* 14:248. doi: 10.1186/s12870-014-0248-9

Gong, B., Li, X., Bloszies, S., Wen, D., Sun, S., and Wei, M. (2014). Sodic alkaline stress mitigation by interaction of nitric oxide and polyamines involves antioxidants and physiological strategies in *Solanum lycopersicum*. *Free Radic. Biol. Med.* 71, 36–48. doi: 10.1016/j.freeradbiomed.2014.02.018

Graham, D. B., and Root, D. E. (2015). Resources for the design of CRISPR gene editing experiments. *Genome Biol.* 16:26. doi: 10.1186/s13059-015-0823-x

Gutsch, A., Keunen, E., Guerriero, G., Renaut, J., Cuypers, A., Hausman, J. F., et al. (2018b). Long-term cadmium exposure influences the abundance of proteins that impact the cell wall structure in *Medicago sativa* stems. *Plant Biol.* 20, 1023–1035. doi: 10.1111/plb.12865

Gutsch, A., Zouaghi, S., Renaut, J., Cuypers, A., Hausman, J. F., and Sergeant, K. (2018a). Changes in the proteome of *Medicago sativa* leaves in response to long-term cadmium exposure using a cell-wall targeted approach. *Int. J. Mol. Sci.* 19:2498. doi: 10.3390/ijms19092498

Guzman-Rodriguez, J. J., Ibarra-Laclette, E., Herrera-Estrella, L., Ochoa-Zarzosa, A., Suarez-Rodriguez, L. M., Rodriguez-Zapata, L. C., et al. (2013). Analysis of expressed sequence tags (ESTs) from avocado seed (*Persea americana* var. drymifolia) reveals abundant expression of the gene encoding the antimicrobial peptide snakin. *Plant Physiol. Biochem.* 70, 318–324. doi: 10.1016/j.plaphy.2013.05.045

Ha, C. V., Watanabe, Y., Tran, U. T., Le, D. T., Tanaka, M., Nguyen, K. H., et al. (2015). Comparative analysis of root transcriptomes from two contrasting drought-responsive Williams 82 and DT2008 soybean cultivars under normal and dehydration conditions. *Front. Plant Sci.* 6:551. doi: 10.3389/fpls.2015.00551

Han, Y., Kang, Y., Torres-Jerez, I., Cheung, F., Town, C. D., Zhao, P. X., et al. (2011). Genome-wide SNP discovery in tetraploid alfalfa using 454 sequencing and high resolution melting analysis. *BMC Genom.* 12:350. doi: 10.1186/1471-2164-12-350

Hartlerode, A. J., and Scully, R. (2009). Mechanisms of double-strand break repair in somatic mammalian cells. *Biochem. J.* 423, 157–168. doi: 10.1042/BJ20090942

Haun, W., Coffman, A., Clasen, B. M., Demorest, Z. L., Lowy, A., Ray, E., et al. (2014). Improved soybean oil quality by targeted mutagenesis of the fatty acid desaturase 2 gene family. *Plant Biotechnol. J.* 12, 934–940. doi: 10.1111/pbi.12201

Hawkins, C., and Yu, L. X. (2018). Recent progress in alfalfa (*Medicago sativa* L.) *genomics and genomic selection*. *Crop J.* 6, 565–575. doi: 10.1016/j.cj.2018.01.006

He, X. Z., and Dixon, R. A. (2000). Genetic manipulation of isoflavone 7-O-methyltransferase enhances biosynthesis of 4'-O-methylated isoflavonoid phytoalexins and disease resistance in alfalfa. *Plant Cell* 12, 1689–1702. doi: 10.1105/tpc.12.9.1689

Herrmann, D., Flajoulot, S., Barre, P., Huyghe, C., Ronfort, J., and Julier, B. (2018). Comparison of morphological traits and molecular markers to analyse diversity and structure of alfalfa (*Medicago sativa* L.) *cultivars*. *Gen. Res. Crop Evol.* 65, 527–540. doi: 10.1007/s10722-017-0551-z

Hipskind, J. D., and Paiva, N. L. (2000). Constitutive accumulation of a resveratrol-glucoside in transgenic alfalfa increases resistance to Phoma medicaginis. *Mol. Plant Microbe Int.* 13, 551–556. doi: 10.1094/MPMI.2000.13.5.551

Huang, X., Kurata, N., Wang, Z. X., Wang, A., Zhao, Q., Zhao, Y., et al. (2012). A map of rice genome variation reveals the origin of cultivated rice. *Nature* 490, 497–501. doi: 10.1038/nature11532

Hwang, E. Y., Song, Q., Jia, G., Specht, J. E., Hyten, D. L., Costa, J., et al. (2014). A genome-wide association study of seed protein and oil content in soybean. *BMC Genom.* 15:2164. doi: 10.1186/1471-2164-15-1

Jacobs, T. B., LaFayette, P. R., Schmitz, R. J., and Parrott, W. A. (2015). Targeted genome modifications in soybean with CRISPR/Cas9. *BMC Biotechnol.* 15:16. doi: 10.1186/s12896-015-0131-2

Jaganathan, D., Ramasamy, K., Sellamuthu, G., Jayabalan, S., and Venkataraman, G. (2018). CRISPR for crop improvement: an update review. *Front. Plant Sci.* 9:985. doi: 10.3389/fpls.2018.00985

Jain, M., Olsen, H. E., Paten, B., and Akeson, M. (2016). The Oxford Nanopore MinION: delivery of nanopore sequencing to the genomics community. *Gen. Biol.* 17:239. doi: 10.1186/s13059-016-1103-0

Jin, Q., Zhu, K., Cui, W., Xie, Y., Han, B., and Shen, W. (2013). Hydrogen gas acts as a novel bioactive molecule in enhancing plant tolerance to paraquat-induced oxidative stress via the modulation of heme oxygenase-1 signalling system. *Plant Cell Environ.* 36, 956–969. doi: 10.1111/pce.12029

Jin, T., Chang, Q., Li, W., Yin, D., Li, Z., Wang, D., et al. (2010). Stress-inducible expression of GmDREB1 conferred salt tolerance in transgenic alfalfa. *Plant Cell Trans. Organ Cult.* 100, 219–227. doi: 10.1007/s11240-009-9628-5

Jones, J. D. G., and Dangl, J. L. (2006). The plant immune system. *Nature* 444, 323–329. doi: 10.1038/nature05286

Julier, B., Flajoulot, S., Barre, P., Cardinet, G., Santoni, S., Huguet, T., et al. (2003). Construction of two genetic linkage maps in cultivated tetraploid alfalfa (*Medicago sativa*) using microsatellite and AFLP markers. *BMC Plant B.* 3:9. doi: 10.1186/1471-2229-3-9

Kanaar, R., Hoeijmakers, J. H., and van Gent, D. C. (1998). Molecular mechanisms of DNA double strand break repair. *Trends Cell. Biol.* 8, 483–489. doi: 10.1016/S0962-8924(98)01383-X

Kang, P., Bao, A. K., Kumar, T., Pan, Y. Q., Bao, Z., Wang, F., et al. (2016). Assessment of stress tolerance, productivity, and forage quality in T1 transgenic alfalfa co-overexpressing ZxNHX and ZxVP1-1 from *Zygophyllum xanthoxylum*. *Front. Plant Sci.* 7:1598. doi: 10.3389/fpls.2016.01598

Kang, Y., Han, Y., Torres-Jerez, I., Wang, M., Tang, Y., Monteros, M., et al. (2011). System responses to long-term drought and re-watering of two contrasting alfalfa varieties. *Plant J.* 68, 871–889. doi: 10.1111/j.1365-313X.2011.04738.x

Kang, Y., Sakiroglu, M., Krom, N., Stanton-Geddes, J., Wang, M., Lee, Y. C., et al. (2015). Genome-wide association of drought-related and biomass traits with HapMap SNPs in *Medicago truncatula*. *Plant Cell Environ.* 38, 1997–2011. doi: 10.1111/pce.12520

Kersey, P. J. (2019). Plant genome sequences: past, present, future. *Curr. Opin. Plant Biol.* 48, 1–8. doi: 10.1016/j.pbi.2018.11.001

Khan, Z., Khan, S. H., Mubarik, M. S., Sadia, B., and Ahmad, A. (2017). Use of TALEs and TALEN technology for genetic improvement of plants. *Plant Mol. Biol. Rep.* 35, 1–19. doi: 10.1007/s11105-016-0997-8

Khu, D. M., Reyno, R., Han, Y., Zhao, P. X., Bouton, J. H., Brummer, E. C., et al. (2013). Identification of aluminum tolerance quantitative trait loci in tetraploid alfalfa. *Crop Sci.* 53, 148–163. doi: 10.2135/cropsci2012.03.0181

Kiegerl, S., Cardinale, F., Siligan, C., Gross, A., Baudouin, E., Liwosz, A., et al. (2000). SIMKK, a mitogen-activated protein kinase (MAPK) kinase, is a specific activator of the salt stress–induced MAPK, SIMK. *Plant Cell* 12, 2247–2258. doi: 10.1105/tpc.12.11.2247

Kim, K. Y., Kwon, S. Y., Lee, H. S., Hur, Y., Bang, J. W., and Kwak, S. S. (2003). A novel oxidative stress-inducible peroxidase promoter from sweetpotato: molecular cloning and characterization in transgenic tobacco plants and cultured cells. *Plant Mol. Biol.* 51, 831–838. doi: 10.1023/a:1023045218815

Kiss, G. B., Csanádi, G., Kálmán, K., Kaló, P., and Ökrész, L. (1993). Construction of a basic genetic map for alfalfa using RFLP, RAPD, isozyme and morphological markers. *Mol. Gen. Gen.* 238, 129–137. doi: 10.1007/BF00279539

Klapheck, S. (1988). Homoglutathione: isolation, quantification and occurrence in legumes. *Physiol. Plant.* 74, 727–732. doi: 10.1111/j.1399-3054.1988.tb02044.x

Komatsu, S., and Ahsan, N. (2009). Soybean proteomics and its application to functional analysis. *J. Proteomics* 72, 325–336. doi: 10.1016/j.jprot.2008.10.001

Komis, G., Illés, P., Beck, M., and Šamaj, J. (2011). Microtubules and mitogen-activated protein kinase signalling. *Curr. Oppin. Plant Biol.* 14, 650–657. doi: 10.1016/j.pbi.2011.07.008

Köpp, M., Passos, L., Verneue, R., Lédo, F. J., Coimbra, J. L., and de Oliveira, A. (2011). Effects of nutrient solution pH on growth parameters of alfalfa (*Medicago sativa* L.) *genotypes*. *Comun. Sci.e* 2, 135–141. doi: 10.14295/cs.v2i3.39

Korver, R. A., Koevoets, I. T., and Testerink, C. (2018). Out of shape during stress: a key role for auxin. *Trends Plant Sci.* 23, 783–793. doi: 10.1016/j.tplants.2018.05.011

Kovalskaya, N., and Hammond, R. W. (2009). Expression and functional characterization of the plant antimicrobial snakin-1 and defensin recombinant proteins. *Protein Expr. Purif.* 63, 12–17. doi: 10.1016/j.pep.2008.08.013

Kudapa, H., Ramalingam, A., Nayakoti, S., Chen, W., Zhuang, W., Liang, X., et al. (2013). Functional genomics to study stress responses in crop legumes: progress and prospects. *Funct. Plant Biol.* 40, 1221–1233. doi: 10.1071/FP13191

Kuluev, B. R., Gumerova, G. R., Mikhaylova, E. V., Gerashchenkov, G. A., Rozhnova, N. A., Vershinina, Z. R., et al. (2019). Delivery of CRISPR/Cas components into higher plant cells for genome editing. *Russ. J. Plant. Physl.* 66, 694–706. doi: 10.1134/S102144371905011X

Kumar, T., Bao, A. K., Bao, Z., Wang, F., Gao, L., and Wang, S. M. (2018). The progress of genetic improvement in alfalfa (*Medicago sativa* L.). *Czech. J. Genet. Plant Breed.* 54, 41–51. doi: 10.17221/46/2017-CJGPB

Laberge, S., Castonguay, Y., and Vézina, L. P. (1993). New cold-and drought-regulated gene from *Medicago sativa*. *Plant Physiol.* 101, 1411–1411. doi: 10.1104/pp.101.4.1411

Lardi, M., and Pessi, G. (2018). Functional genomics approaches to studying symbioses between legumes and nitrogen-fixing rhizobia. *High Throughput.* 7:15. doi: 10.3390/ht7020015

Le, B. H., Wagmaister, J. A., Kawashima, T., Bui, A. Q., Harada, J. J., and Goldberg, R. B. (2007). Using genomics to study legume seed development. *Plant Physiol.* 144, 562–574. doi: 10.1104/pp.107.100362

Le, D. T., Nishiyama, R., Watanabe, Y., Tanaka, M., Seki, M., Ham, L. H., et al. (2012). Differential gene expression in soybean leaf tissues at late developmental stages under drought stress revealed by genome-wide transcriptome analysis. *PLoS One* 7:e49522. doi: 10.1371/journal.pone.0049522

Le Nguyen, K., Grondin, A., Courtois, B., and Gantet, P. (2018). Next-generation sequencing accelerates crop gene discovery. *Trends Plant Sci.* 24, 8. doi: 10.1016/j.tplants.2018.11.008

Lei, Y., Xu, Y., Hettenhausen, C., Lu, C., Shen, G., Zhang, C., et al. (2018). Comparative analysis of alfalfa (*Medicago sativa* L.) leaf transcriptomes reveals genotype-specific salt tolerance mechanisms. *BMC Plant Biol.* 18:35. doi: 10.1186/s12870-018-1250-4

Li, H., Wang, Z., Ke, Q., Ji, C. Y., Jeong, J. C., Lee, H. S., et al. (2014). Overexpression of codA gene confers enhanced tolerance to abiotic stresses in alfalfa. *Plant Physiol. Biochem.* 85, 31–40. doi: 10.1016/j.plaphy.2014.10.010

Li, J. F., Norville, J. E., Aach, J., McCormack, M., Zhang, D., Bush, J., et al. (2013). Multiplex and homologous recombination-mediated genome editing in Arabidopsis and Nicotiana benthamiana using guide RNA and Cas9. *Nat. Biotechnol.* 31, 688–691. doi: 10.1038/nbt.2654

Li, S., Jia, S., Hou, L., Nguyen, H., Sato, S., Holding, D., et al. (2019). Mapping of transgenic alleles in soybean using a nanopore-based sequencing strategy. *J. Exp. Bot.* 70, 3825–3833. doi: 10.1093/jxb/erz202

Li, T., Huang, S., Jiang, W. Z., Wright, D., Spalding, M. H., Weeks, D. P., et al. (2011). TAL nucleases (TALNs): hybrid proteins composed of TAL effectors and FokI DNA-cleavage domain. *Nucleic Acids Res.* 39, 359–372. doi: 10.1093/nar/gkq704

Li, W., Wei, Z., Qiao, Z., Wu, Z., Cheng, L., and Wang, Y. (2013). Proteomics analysis of alfalfa response to heat stress. *PLoS One* 8:e82725. doi: 10.1371/journal.pone.0082725

Li, X., and Brummer, E. C. (2012). Applied genetics and genomics in alfalfa breeding. *Agronomy* 2, 40–61. doi: 10.3390/agronomy2010040

Li, X., Hannoufa, A., Zhang, Y., and Yu, P. (2016). Gene-silencing-induced changes in carbohydrate conformation in relation to bioenergy value and carbohydrate subfractions in modeled plant (*Medicago sativa*) with down-regulation of HB12 and TT8 transcription factors. *Int. J. Mol. Sci.* 17:720. doi: 10.3390/ijms17050720

Li, X., Wei, Y., Acharya, A., Jiang, Q., Kang, J., and Brummer, E. C. (2014). A saturated genetic linkage map of autotetraploid alfalfa (*Medicago sativa* L.) developed using genotyping-by-sequencing is highly syntenous with the *Medicago truncatula* genome. *G3* 4, 1971–1979. doi: 10.1534/g3.114.012245

Li, Z., Liu, Z. B., Xing, A., Moon, B. P., Koellhoffer, J. P., Huang, L., et al. (2015). Cas9-guide RNA directed genome editing in soybean. *Plant Physiol.* 169, 960–970. doi: 10.1104/pp.15.00783

Libault, M., Pingault, L., Zogli, P., and Schiefelbein, J. (2017). Plant systems biology at the single-cell level. *T. Plant Sci.* 22, 949–960. doi: 10.1016/j.tplants.2017.08.006

Liu, H., Ding, Y., Zhou, Y., Jin, W., Xie, K., and Chen, L. L. (2017). CRISPR-P 2.0: *an improved CRISPR-Cas*9 tool for genome editing in plants. *Mol. Plant* 10, 530–532. doi: 10.1016/j.molp.2017.01.003

Liu, W., Xiong, C., Yan, L., Zhang, Z., Ma, L., Wang, Y., et al. (2017). Transcriptome analyses reveal candidate genes potentially involved in al stress response in alfalfa. *Front. Plant Sci.* 8:26. doi: 10.3389/fpls.2017.00026

Liu, X., Wu, S., Xu, J., Sui, C., and Wei, J. (2019). Application of CRISPR/Cas9 in plant biology. *Acta Pharm. Sin. B.* 7, 292–302. doi: 10.1016/j.apsb.2017.01.002

Liu, X. P., Hawkins, C., Peel, M. D., and Yu, L. X. (2019). Genetic loci associated with salt tolerance in advanced breeding populations of tetraploid alfalfa using genome-wide association studies. *Plant Genome* 12:26. doi: 10.3835/plantgenome2018.05.0026

Liu, Z., Chen, T., Ma, L., Zhao, Z., Zhao, P. X., Nan, Z., et al. (2013). Global transcriptome sequencing using the Illumina platform and the development of EST-SSR markers in autotetraploid alfalfa. *PLoS One* 8:e83549. doi: 10.1371/journal.pone.0083549

Long, R., Gao, Y., Sun, H., Zhang, T., Li, X., Li, M., et al. (2018). Quantitative proteomic analysis using iTRAQ to identify salt-responsive proteins during the germination stage of two Medicago species. *Sci. Rep.* 8:9553. doi: 10.1038/s41598-018-27935-8

Long, R., Li, M., Zhang, T., Kang, J., Sun, Y., Cong, L., et al. (2016). Comparative proteomic analysis reveals differential root proteins in *Medicago sativa* and *Medicago truncatula* in response to salt stress. *Front. Plant Sci.* 7:424. doi: 10.3389/fpls.2016.00424

Lu, H., Giordano, F., and Ning, Z. (2016). Oxford Nanopore MinION sequencing and genome assembly. *Genom. Proteom. Bioinf.* 14, 265–279. doi: 10.1016/j.gpb.2016.05.004

Luo, D., Wu, Y., Liu, J., Zhou, Q., Liu, W., Wang, Y., et al. (2019a). Comparative transcriptomic and physiological analyses of *Medicago sativa* L. indicates that multiple regulatory networks are activated during continuous aba treatment. *Int. J. Mol. Sci.* 20:E47. doi: 10.3390/ijms20010047

Luo, D., Zhou, Q., Wu, Y., Chai, X., Liu, W., Wang, Y., et al. (2019b). Full-length transcript sequencing and comparative transcriptomic analysis to evaluate the contribution of osmotic and ionic stress components towards salinity tolerance in the roots of cultivated alfalfa (*Medicago sativa* L.). *BMC Plant Biol.* 19:32. doi: 10.1186/s12870-019-1630-4

Luo, M., Lin, L., Hill, R. D., and Mohapatra, S. S. (1991). Primary structure of an environmental stress and abscisic acid-inducible alfalfa protein. *Plant Mol. Biol.* 17, 1267–1269. doi: 10.1007/bf00028745

Luo, M., Liu, J. H., Mohapatra, S., Hill, R. D., and Mohapatra, S. S. (1992). Characterization of a gene family encoding abscisic acid-and environmental stress-inducible proteins of alfalfa. *J. Biol. Chem.* 267, 15367–15374.

Ma, Q., Kang, J., Long, R., Zhang, T., Xiong, J., Zhang, K., et al. (2017). Comparative proteomic analysis of alfalfa revealed new salt and drought stress-related factors involved in seed germination. *Mol. Biol. Rep.* 44, 261–272. doi: 10.1007/s11033-017-4104-5

Mackie, J. M., Musial, J. M., Armour, D. J., Phan, H. T. T., and Ellwood, S. E. (2007). Identification of QTL for reaction to three races of *Colletotrichum trifolii* and further analysis of inheritance of resistance in autotetraploid lucerne. *Theor. Appl. Genet.* 114, 1417–1426. doi: 10.1007/s00122-007-0527-z

Macovei, A., Gill, S. S., and Tuteja, N. (2012). microRNAs as promising tools for improving stress tolerance in rice. *Plant Sig. Beh.* 7, 1296–1301. doi: 10.4161/psb.21586

Mahfouz, M. M., Li, L., Shamimuzzaman, M., Wibowo, A., Fang, X., and Zhu, J. K. (2011). De novo-engineered transcription activator-like effector (TALE) hybrid nuclease with novel DNA binding specificity creates double-strand breaks. *Proc. Natl. Acad. Sci. U.S.A.* 108, 2623–2628. doi: 10.1073/pnas.1019533108

Makarova, K. S., Zhang, F., and Koonin, E. V. (2017). SnapShot: Class 2 CRISPR-Cas systems. *Cell* 168, 328–328. doi: 10.1016/j.cell.2016.12.038

Malzahn, A., Lowder, L., and Qil, Y. (2017). Plant genome editing with TALEN and CRISPR. *Cell Biosci.* 7:21. doi: 10.1186/s13578-017-0148-4

Mao, Y. F., Botella, J. R., Liu, Y. G., and Zhu, J. K. (2019). Gene editing in plants: progress and challenges. *Natl. Sci. Rev.* 6, 421–437. doi: 10.1093/nsr/nwz005

Margulies, M., Egholm, M., Altman, W. E., Attiya, S., Bader, J. S., Bemben, L. A., et al. (2005). Genome sequencing in microfabricated high-density picolitre reactors. *Nature* 437, 376–380. doi: 10.1038/nature03959

Marraffini, L. A., and Sontheimer, E. J. (2008). CRISPR interference limits horizontal gene transfer in staphylococci by targeting DNA. *Science* 322, 1843–1845. doi: 10.1126/science.1165771

Masonbrink, R. E., Severin, A. J., and Seetharam, A. S. (2017). "Comparative genomics of soybean and other legumes," in *The Soybean Genome*, eds H. Nguyen and M. Bhattacharyya (Cham: Springer), 83–93. doi: 10.1007/978-3-319-64198-0_6

Masoud, S. A., Zhu, Q., Lamb, C., and Dixon, R. A. (1996). Constitutive expression of an inducible β-1,3-glucanase in alfalfa reduces disease severity caused by the oomycete pathogen *Phytophthora megasperma* f. sp. medicaginis, but does not reduce disease severity of chitin-containing fungi. *Transgenic Res.* 5, 313–323. doi: 10.1007/BF01968941

Matamoros, M. A., Moran, J. F., Iturbe-Ormaetxe, I., Rubio, M. C., and Becana, M. (1999). Glutathione and homoglutathione synthesis in legume root nodules. *Plant Physiol.* 121, 879–888. doi: 10.1104/pp.121.3.879

Matthews, C., Arshad, M., and Hannoufa, A. (2019). Alfalfa response to heat stress is modulated by microRNA156. *Physiol. Plant.* 165, 830–842. doi: 10.1111/ppl.12787

McCoy, T. J., and Bingham, E. T. (1988). "Cytology and cytogenetics of alfalfa," in *Alfalfa and Alfalfa Improvement*, ed. A. A. Hanson (Madison, WI: ASA), 737–776.

Meng, Y., Wang, C., Yin, P., Zhu, B., Zhang, P., Niu, L., et al. (2019). "Targeted mutagenesis by an optimized agrobacterium-delivered CRISPR/Cas 9 system in the model legume *Medicago truncatula*," in *The Model Legume Medicago truncatula*, ed. F. D. Bruijn (Hoboken, NJ: Wiley), 1015–1018. doi: 10.1002/9781119409144.ch130

Meng, Y. Y., Hou, Y. L., Wang, H., Ji, R. H., Liu, B., Wen, J. Q., et al. (2017). Targeted mutagenesis by CRISPR/Cas9 system in the model legume *Medicago truncatula*. *Plant Cell Rep.* 36, 371–374. doi: 10.1007/s00299-016-2069-9

Michno, J. M., Wang, X., Liu, J., Curtin, S. J., Kono, T. J., and Stupar, R. M. (2015). CRISPR/Cas mutagenesis of soybean and *Medicago truncatula* using a new web-tool and a modified Cas9 enzyme. *GM Crops Food* 6, 243–252. doi: 10.1080/21645698.2015.1106063

Miller, J. C., Tan, S., Qiao, G., Barlow, K. A., Wang, J., Xia, D. F., et al. (2011). A TALE nuclease architecture for efficient genome editing. *Nat. Biotechnol.* 29, 143–148. doi: 10.1038/nbt.1755

Mittler, R., and Blumwald, E. (2015). The roles of ROS and ABA in systemic acquired acclimation. *Plant Cell* 27, 64–70. doi: 10.1105/tpc.114.133090

Mo, Y., Liang, G., Shi, W., and Xie, J. (2011). Metabolic responses of alfalfa (*Medicago Sativa* L.) leaves to low and high temperature induced stresses. *Afr. J. Biotechnol.* 10, 1117–1124. doi: 10.5897/AJB10.1433

Moradpour, M., and Abdulah, S. N. A. (2020). CRISPR/dCas9 platforms in plants: strategies and applications beyond genome editing. *Plant Biotechnol. J.* 18, 32–44. doi: 10.1111/pbi.13232

Musial, J. M., Mackie, J. M., Armour, D. J., Phan, H. T. T., Ellwood, S. E., Aitken, K. S., et al. (2007). Identification of QTL for resistance and susceptibility to *Stagonospora meliloti* in autotetraploid lucerne. *Theor. Appl. Gen.* 114, 1427–1435. doi: 10.1007/s00122-007-0528-y

Nakano, K., Shiroma, A., Shimoji, M., Tamotsu, H., Ashimine, N., Ohki, S., et al. (2017). Advantages of genome sequencing by long-read sequencer using SMRT technology in medical area. *Hum. Cell* 30, 149–161. doi: 10.1007/s13577-017-0168-8

Nekrasov, V., Staskawicz, B., Weigel, D., Jones, J. D., and Kamoun, S. (2013). Targeted mutagenesis in the model plant Nicotiana benthamiana using Cas9 RNA-guided endonuclease. *Nat. Biotechnol.* 31, 691–693. doi: 10.1038/nbt.2655

Nekrasov, V., Wang, C. M., and Win, J. (2017). Rapid generation of a transgene-free powdery mildew resistant tomato by genome deletion. *Sci. Rep.* 7:482. doi: 10.1038/s41598-017-00578-x

Ninković, S., Miljuš-Đukić, J., and Nešković, M. (1995). Genetic transformation of alfalfa somatic embryos and their clonal propagation through repetitive somatic embryogenesis. *Plant Cell T. Organ Cult.* 42, 255–260. doi: 10.1007/BF00029996

Nirola, R., Megharaj, M., Beecham, S., Aryal, R., Thavamani, P., Vankateswarlu, K., et al. (2016). Remediation of metalliferous mines, revegetation challenges and emerging prospects in semi-arid and arid conditions. *Env. Sci. Poll. Res.* 23, 20131–20150. doi: 10.1007/s11356-016-7372-z

Nutter, F. W., Guan, J., Gotlieb, A. R., Rhodes, L. H., Grau, C. R., and Sulc, R. M. (2002). Quantifying alfalfa yield losses caused by foliar diseases in Iowa, Ohio, Wisconsin, and Vermont. *Plant Dis.* 863, 269–277. doi: 10.1094/PDIS.2002.86.3.269

Olukolu, B. A., Tracy, W. F., Wisser, R., De Vries, B., and Balint-Kurti, P. J. (2016). A genome-wide association study for partial resistance to maize common rust. *Phytopath.* 106, 745–751. doi: 10.1094/PHYTO-11-15-0305-R

O'Rourke, J. A., Fu, F., Bucciarelli, B., Yang, S. S., Samac, D. A., Lamb, J. F. S., et al. (2015). The *Medicago sativa* gene index 1.2: a web-accessible gene expression atlas for investigating expression differences between *Medicago sativa* subspecies. *BMC Genom.* 16:502. doi: 10.1186/s12864-015-1718-7

Ovečka, M., Takáč, T., Komis, G., Vadovič, P., Bekešová, S., Doskočilová, A., et al. (2014). Salt-induced subcellular kinase relocation and seedling susceptibility caused by overexpression of Medicago SIMKK in *Arabidopsis*. *J. Exp. Bot.* 65, 2335–2350. doi: 10.1093/jxb/eru115

Paparella, S., Araújo, S. S., Rossi, G., Wijayasinghe, M., Carbonera, D., and Balestrazzi, A. (2015). Seed priming: state of the art and new perspectives. *Plant Cell Rep.* 34, 1281–1293. doi: 10.1007/s00299-015-1784-y

Pâques, F., and Duchateau, P. (2007). Meganucleases and DNA double-strand break-induced recombination: perspectives for gene therapy. *Curr. Gene Ther.* 7, 49–66. doi: 10.2174/156652307779940216

Pasternak, T., Asard, H., Potters, G., and Jansen, M. A. (2014). The thiol compounds glutathione and homoglutathione differentially affect cell development in alfalfa (*Medicago sativa* L.). *Plant Phys. Biochem.* 74, 16–23. doi: 10.1016/j.plaphy.2013.10.028

Pastwa, E., and Blasiak, J. (2003). Non-homologous DNA end joining. *Acta. Biochim. Pol.* 50, 891–908. doi: 10.18388/abp.2003_3622

Paszkowski, J., Baur, M., Bogucki, A., and Potrykus, I. (1988). Gene targeting in plants. *EMBO J.* 7, 4021–4026. doi: 10.1002/j.1460-2075.1988.tb03295.x

Pavlovich, M. (2017). Computing in biotechnology: omics and beyond. *Trends Biotechnol.* 35, 450–497. doi: 10.1016/j.tibtech.2017.03.011

Pennycooke, J. C., Cheng, H., and Stockinger, E. J. (2008). Comparative genomic sequence and expression analyses of *Medicago truncatula* and alfalfa subspecies falcata COLD-ACCLIMATION-SPECIFIC genes. *Plant Physiol.* 146, 1242–1254.

Piano, E., and Pecetti, L. (2010). "Minor legume species," in *Fodder Crops and Amenity Grassesm Handbook of Plant Breeding*, Vol. 5, eds B. Boller, U. K. Posselt, and F. Veronesi (NewYork, NY: Springer), 477–500. doi: 10.1007/978-1-4419-0760-8_20

Postnikova, O. A., Hult, M., Shao, J., Skantar, A., and Nemchinov, L. G. (2015). Transcriptome analysis of resistant and susceptible alfalfa cultivars infected with root-knot nematode Meloidogyne incognita. *PLoS One* 10:e0123157. doi: 10.1371/journal.pone.0118269

Postnikova, O. A., Shao, J., and Nemchinov, L. G. (2013). Analysis of the alfalfa root transcriptome in response to salinity stress. *Plant Cell Physiol.* 54, 1041–1055. doi: 10.1093/pcp/pct056

Pratt, R. G., and Rowe, D. E. (2002). Enhanced resistance to *Sclerotium rolfsii* in populations of alfalfa selected for quantitative resistance to *Sclerotinia trifoliorum*. *Phytopathology* 92, 204–209. doi: 10.1094/PHYTO.2002.92.2.204

Printz, B., Guerriero, G., Sergeant, K., Audinot, J. N., Guignard, C., Renaut, J., et al. (2016). Combining-omics to unravel the impact of copper nutrition on alfalfa (*Medicago sativa*) stem metabolism. *Plant Cell Physiol.* 57, 407–422. doi: 10.1093/pcp/pcw001

Printz, B., Guerriero, G., Sergeant, K., Renaut, J., Lutts, S., and Hausman, J. F. (2015). Ups and downs in alfalfa: proteomic and metabolic changes occurring in the growing stem. *Plant Sci.* 238, 13–25. doi: 10.1016/j.plantsci.2015.05.014

Puchta, H., Dujon, B., and Hohn, B. (1993). Homologous recombination in plant cells is enhanced by in vivo induction of double strand breaks into DNA by a site-specific endonuclease. *Nucleic Acids Res.* 21, 5034–5040. doi: 10.1093/nar/21.22.5034

Qi, Y. (2015). "High efficient genome modification by designed zinc finger nuclease," in *Advances in New Technology for Targeted Modification of Plant Genomes*, eds F. Zhang, H. Puchta, and J. G. Thomson (New York, NY: Springer), 39–53. doi: 10.1007/978-1-4939-2556-8_3

Radović, J., Sokolović, D., and Marković, J. (2009). Alfalfa-most important perennial forage legume in animal husbandry. *Biotechnol. Anim. Husb.* 25, 465–475. doi: 10.2298/BAH0906465R

Rahman, M. A., Alam, I., Kim, Y. G., Ahn, N. Y., Heo, S. H., Lee, D. G., et al. (2015). Screening for salt-responsive proteins in two contrasting alfalfa cultivars using a comparative proteome approach. *Plant Physiol. Biochem.* 89, 112–122. doi: 10.1016/j.plaphy.2015.02.015

Rahman, M. A., Yong-Goo, K., Iftekhar, A., Liu, G., Hyoshin, L., Joo, L. J., et al. (2016). Proteome analysis of alfalfa roots in response to water deficit stress. *J. Integr. Agric.* 15, 1275–1285. doi: 10.1016/S2095-3119(15)61255-2

Rashmi, R., Sarkar, M., and Vikramaditya, T. (1997). Cultivaton of alfalfa (*Medicago sativa* L.). *Anc. Sci. Life* 17, 117–119.

Rhodes, D., and Hanson, A. D. (1993). Quaternary ammonium and tertiary sulfonium compounds in higher plants. *Ann. Rev. Plant Biol.* 44, 357–384. doi: 10.1146/annurev.pp.44.060193.002041

Robins, J. G., Luth, D., Campbell, T. A., Bauchan, G. R., He, C., Viands, D. R., et al. (2007). Genetic mapping of biomass production in tetraploid alfalfa. *Crop Sci.* 47, 1–10. doi: 10.2135/cropsci2005.11.0401

Rothberg, J. M., Hinz, W., Rearick, T. M., Schultz, J., Mileski, W., Davey, M., et al. (2011). An integrated semiconductor device enabling non-optical genome sequencing. *Nature* 475, 348–352. doi: 10.1038/nature10242

Roumen, E. C. (1994). "A strategy for accumulating genes for partial resistance to blast disease in rice within a conventional breeding program," in *Rice Blast Disease*, eds R. S. Zeigler, S. A. Leong, and P. S. Teng (Cambridge: CAB International), 245–265.

Rubiales, D., Fondevilla, S., Chen, W., Gentzbittel, L., Higgins, T. J. V., Castillejo, M. A., et al. (2015). Achievements and challenges in legume breeding for pest and disease resistance. *CRC Crit. Rev. Plant Sci.* 34, 195–236. doi: 10.1080/07352689.2014.898445

Sakiroglu, M., and Brummer, E. C. (2017). Identification of loci controlling forage yield and nutritive value in diploid alfalfa using GBS-GWAS. *Theor. Appl. Gen.* 130, 261–268. doi: 10.1007/s00122-016-2782-3

Samac, D., and Smigocki, A. (2003). Expression of oryzacystatin I and II in alfalfa increases resistance to the root-lesion nematode. *Phytopathology* 93, 799–804. doi: 10.1094/PHYTO.2003.93.7.799

Samac, D. A., and Temple, S. J. (2004). "Development and utilization of transformation in Medicago species," in *Genetically Modified Crops, Their Development, Uses and Risks*, eds G. H. Liang and D. Z. Skinner (New York, NY: The Haworth Press), 165–202.

Šamaj, J., Ovečka, M., Hlavačka, A., Lecourieux, F., Meskiene, I., Lichtscheidl, I., et al. (2002). Involvement of the mitogen-activated protein kinase SIMK in regulation of root hair tip growth. *EMBO J.* 21, 3296–3306. doi: 10.1093/emboj/cdf349

Šamajová, O., Komis, G., and Šamaj, J. (2013a). Emerging topics in the cell biology of mitogen-activated protein kinases. *Trans. Plant Sci.* 18, 140–148. doi: 10.1016/j.tplants.2012.11.004

Šamajová, O., Plíhal, O., Al-Yousif, M., Hirt, H., and Šamaj, J. (2013b). Improvement of stress tolerance in plants by genetic manipulation of mitogen-activated protein kinases. *Biotech. A.* 31, 118–128. doi: 10.1016/j.biotechadv.2011.12.002

Sander, J. D., Dahlborg, E. J., Goodwin, M. J., Cade, L., Zhang, F., Cifuentes, D., et al. (2011). Selection-free zinc-finger-nuclease engineering by context-dependent assembly (CoDA). *Nat. Methods* 8, 67–69. doi: 10.1038/nmeth.1542

Sato, S., Nakamura, Y., Kaneko, T., Asamizu, E., Kato, T., Nakao, M., et al. (2008). Genome structure of the legume, *Lotus japonicus*. *DNA Res.* 15, 227–239. doi: 10.1093/dnares/dsn008

Scheben, A., Verpaalen, B., Lawley, C. T., Chan, C. K. K., Bayer, P. E., Batley, J., et al. (2019). CropSNPdb: a database of SNP array data for Brassica crops and hexaploid bread wheat. *Plant J.* 98, 142–152. doi: 10.1111/tpj.14194

Schena, M., Shalon, D., Davis, R. W., and Brown, P. O. (1995). Quantitative monitoring of gene expression patterns with a complementary DNA microarray. *Science* 270, 467–470. doi: 10.1126/science.270.5235.467

Schiml, S., and Puchta, H. (2016). Revolutionizing plant biology: multiple ways of genome engineering by CRISPR/Cas. *Plant Methods* 12:8. doi: 10.1186/s13007-016-0103-0

Schmutz, J., Cannon, S. B., Schlueter, J., Ma, J., Mitros, T., Nelson, W., et al. (2010). Genome sequence of the palaeopolyploid soybean. *Nature* 463, 178–183. doi: 10.1038/nature08670

Schreiber, M., Stein, N., and Mascher, M. (2018). Genomic approaches for studying crop evolution. *Genome Biol.* 19:140. doi: 10.1186/s13059-018-1528-8

Segura, A., Moreno, M., Madueno, F., Molina, A., and Garcia-Olmedo, F. (1999). Snakin-1, a peptide from potato that is active against plant pathogens. *Mol. Plant Microbe Interact.* 12, 16–23. doi: 10.1094/MPMI.1999.12.1.16

Severin, A. J., Cannon, S. B., Graham, M. M., Grant, D., and Shoemaker, R. C. (2011). Changes in twelve homoeologous genomic regions in soybean following three rounds of polyploidy. *Plant Cell* 23, 3129–3136. doi: 10.1105/tpc.111.089573

Shafique, A., Rehman, A., Khan, A., and Kazi, A. G. (2014). "Chapter 1 - Improvement of legume crop production under environmental stresses through biotechnological intervention," in *Emerging Technologies and Management of Crop Stress Tolerance: Volume II - A Sustainable Approach*, eds P. Ahmad and S. Rehman (San Diego: Accademic Press), 1–22. doi: 10.1016/B978-0-12-800875-1.00001-6

Shan, Q., Wang, Y., Li, J., Zhang, Y., Chen, K., Liang, Z., et al. (2013). Targeted genome modification of crop plants using a CRISPR-Cas system. *Nat. Biotechnol.* 31, 686–688. doi: 10.1038/nbt.2650

Shan, S., Soltis, P. S., Soltis, D. E., and Yang, B. (2020). Considerations in adapting CRISPR/Cas9 in nongenetic model plant systems. *Appl. Plant Sci.* 8, e11314. doi: 10.1002/aps3.11314

Singer, S. D., Hannoufa, A., and Acharya, S. (2018). Molecular improvement of alfalfa for enhanced productivity and adaptability in a changing environment. *Plant Cell Environ.* 41, 1955–1971. doi: 10.1111/pce.13090

Smith, J., Grizot, S., Arnould, S., Duclert, A., Epinat, J. C., Chames, P., et al. (2006). A combinatorial approach to create artificial homing endonucleases cleaving chosen sequences. *Nucleic Acids Res.* 34, e149. doi: 10.1093/nar/gkl720

Song, L., Jiang, L., Chen, Y., Shu, Y., Bai, Y., and Guo, C. (2016). Deep-sequencing transcriptome analysis of field-grown *Medicago sativa* L. crown buds acclimated to freezing stress. *Func. Integr. Genomics* 16, 495–511. doi: 10.1007/s10142-016-0500-5

Stefanova, G., Slavov, S., Gecheff, K., Vlahova, M., and Atanassov, A. (2013). Expression of recombinant human lactoferrin in transgenic alfalfa plants. *Biol. Plant.* 57, 457–464. doi: 10.1007/s10535-013-0305-5

Steinert, J., Schiml, S., and Puchta, H. (2016). Homology-based double-strand break-induced genome engineering in plants. *Plant Cell Rep.* 35, 1429–1438. doi: 10.1007/s00299-016-1981-3

Strizhov, N., Keller, M., Mathur, J., Koncz-Kálmán, Z., Bosch, D., Prudovsky, E., et al. (1996). A synthetic *cryIC* gene, encoding a *Bacillus thuringiensis* δ-endotoxin, confers *Spodoptera* resistance in alfalfa and tobacco.ă*Proc. Natl. Acad. Sci. U.S.A.* 93, 15012–15017. doi: 10.1073/pnas.93.26.15012

Stritzler, M., Elba, P., Berini, C., Gomez, C., Ayub, N., and Soto, G. (2018). High-quality forage production under salinity by using a salt-tolerant AtNXH1-expressing transgenic alfalfa combined with a natural stress-resistant nitrogen-fixing bacterium. *J. Biotechnol.* 276, 42–45. doi: 10.1016/j.jbiotec.2018.04.013

Sun, X., Hu, Z., Chen, R., Jiang, Q., Song, G., Zhang, H., et al. (2015). Targeted mutagenesis in soybean using the CRISPR-Cas9 system. *Sci. Rep.* 5:10342. doi: 10.1038/srep10342

Tang, F., Yang, S., Liu, J., and Zhu, H. (2016). Rj4, a gene controlling nodulation specificity in soybeans, encodes a thaumatin-like protein but not the one previously reported. *Plant Physiol.* 170, 26–32. doi: 10.1104/pp.15.01661

Tang, H., Krishnakumar, V., Bidwell, S., Rosen, B., Chan, A., Zhou, S., et al. (2014). An improved genome release (version Mt4. 0) for the model legume *Medicago truncatula*. *BMC genom.* 15:312. doi: 10.1186/1471-2164-15-312

Tang, X., Liu, G. Q., Zhou, J. P., Ren, Q., You, Q., Tian, L., et al. (2018). A large-scale whole-genome sequencing analysis reveals highly specific genome editing by both Cas9 and Cpf1 (Cas12a) nucleases in rice. *Genome Biol.* 19:84. doi: 10.1186/s13059-018-1458-5

Tesfaye, M., Denton, M. D., Samac, D. A., and Vance, C. P. (2005). Transgenic alfalfa secretes a fungal endochitinase protein to the rhizosphere. *Plant Soil* 269, 233–243. doi: 10.1007/s11104-004-0520-0

Tesfaye, M., Liu, J., and Vance, C. P. (2007). Genomic and genetic control of phosphate stress in legumes. *Plant Physiol.* 144, 594–603. doi: 10.1104/pp.107.097386

Toth, E., and Bakheit, B. R. (1983). Results of resistance breeding in alfalfa. II. Resistance to Verticillium wilt. *Acta Biol. Hung.* 32, 78–85.

Triboi, E., and Triboi-Blondel, A. M. (2014). "Towards sustainable, self-supporting agriculture: biological nitrogen factories as a key for future cropping systems," in *Soil as World Heritage*, ed. D. Dent (Dordrecht: Springer), 329–342. doi: 10.1007/978-94-007-6187-2_32

Tripathi, P., Rabara, R. C., Reese, R. N., Miller, M. A., Rohila, J. S., Subramanian, S., et al. (2016). A toolbox of genes, proteins, metabolites and promoters for improving drought tolerance in soybean includes the metabolite coumestrol and stomatal development genes. *BMC Genom.* 17:102. doi: 10.1186/s12864-016-2420-0

Tu, X., Liu, Z., and Zhang, Z. (2018a). Comparative transcriptomic analysis of resistant and susceptible alfalfa cultivars (*Medicago sativa* L.) after thrips infestation. *BMC Genom.* 19:116. doi: 10.1186/s12864-018-4495-2

Tu, X., Zhao, H., and Zhang, Z. (2018b). Transcriptome approach to understand the potential mechanisms of resistant and susceptible alfalfa (*Medicago sativa* L.) cultivars in response to aphid feeding. *J. Integr. Agric.* 17, 2518–2527. doi: 10.1016/S2095-3119(17)61843-4

Valliyodan, B., Ye, H., Song, L., Murphy, M., Shannon, J. G., and Nguyen, H. T. (2017). Genetic diversity and genomic strategies for improving drought and

waterlogging tolerance in soybeans. *J. Exp. Bot.* 68, 1835–1849. doi: 10.1093/jxb/erw433

Van, K., Rastogi, K., Kim, K. H., and Lee, S. H. (2013). Next-generation sequencing technology for crop improvement. *SABRAO J. Breed. Genet.* 45, 84–99. doi: 10.3389/fpls.2014.00367

Varshney, R. K., and Kudapa, H. (2013). Legume biology: the basis for crop improvement. *Funct. Plant Biol.* 40, 5–8. doi: 10.1071/FPv40n12_FO

Volkov, V., Wang, B., Dominy, P. J., Fricke, W., and Amtmann, A. (2004). Thellungiella halophila, a salt-tolerant relative of *Arabidopsis thaliana*, possesses effective mechanisms to discriminate between potassium and sodium. *Plant Cell Environ.* 27, 1–14. doi: 10.1046/j.0016-8025.2003.01116.x

Walter, M. H., Liu, J. W., Wünn, J., and Hess, D. (1996). Bean ribonuclease-like pathogenesis-related protein genes Ypr10 display complex patterns of developmental, dark-induced and exogenous-stimulus-dependent expression. *Eur. J. Biochem.* 239, 281–293. doi: 10.1111/j.1432-1033.1996.0281u.x

Wang, K., Wang, Z., Li, F., Ye, W., and Wang, J. (2012). The draft genome of a diploid cotton *Gossypium raimondii*. *Nature Gen.* 44, 1098–1103. doi: 10.1038/ng.2371

Wang, L., Rubio, M. C., Xin, X., Zhang, B., Fan, Q., Wang, Q., et al. (2019). CRISPR/Cas9 knockout of leghemoglobin genes in *Lotus japonicus* uncovers their synergistic roles in symbiotic nitrogen fixation. *New Phytol.* 224, 818–832. doi: 10.1111/nph.16077

Wang, L., Sun, S., Wu, T., Liu, L., Sun, X., Cai, Y., et al. (2020). Natural variation and CRISPR/Cas9-mediated mutation in *GmPRR37* affect photoperiodic flowering and contribute to regional adaptation of soybean. *Plant Biotechnol. J.* 1–13. doi: 10.1111/pbi.13346

Wang, L., Wang, L., Tan, Q., Fan, Q., Zhu, H., Hong, Z., et al. (2016). Efficient inactivation of symbiotic nitrogen fixation related genes in *Lotus japonicus* using CRISPR-Cas9. *Front. Plant Sci.* 7:1333. doi: 10.3389/fpls.2016.01333

Wang, Z., Gerstein, M., and Snyder, M. (2009). RNA-Seq: a revolutionary tool for transcriptomics. *Nat. Rev. Genet.* 10, 57–63. doi: 10.1038/nrg2484

Wang, Z., Li, H., Ke, Q., Jeong, J. C., Lee, H. S., Xu, B., et al. (2014). Transgenic alfalfa plants expressing AtNDPK2 exhibit increased growth and tolerance to abiotic stresses. *Plant Physiol. Biochem.* 84, 67–77. doi: 10.1016/j.plaphy.2014.08.025

Watson, B. S., Bedair, M. F., Urbanczyk-Wochniak, E., Huhman, D. V., Yang, D. S., Allen, S. N., et al. (2015). Integrated metabolomics and transcriptomics reveal enhanced specialized metabolism in *Medicago truncatula* root border cells. *Plant Physiol.* 167, 1699–1716. doi: 10.1093/jxb/erx308

Wen, L., Chen, Y., Schnabel, E., Crook, A., and Frugoli, J. (2019). Comparison of efficiency and time to regeneration of Agrobacterium-mediated transformation methods in *Medicago truncatula*. *Plant Met.* 15:20. doi: 10.1186/s13007-019-0404-1

Wiedenheft, B., Sternberg, S. H., and Doudna, J. A. (2012). RNA-guided genetic silencing systems in bacteria and archaea. *Nature* 482, 331–338. doi: 10.1038/nature10886

Wong, C. E., Li, Y., and Moffatt, B. A. (2006). Transcriptional profiling implicates novel interactions between abiotic stress and hormonal responses in *Thellungiella*, a close relative of *Arabidopsis*. *Plant Physiol.* 140, 1437–1450. doi: 10.1104/pp.105.070508

Wright, D. A., Townsend, J. A., Winfrey, R. J. Jr., Irwin, P. A., and Rajagopal, J. (2005). High-frequency homologous recombination in plants mediated by zinc-finger nucleases. *Plant J.* 44, 693–705. doi: 10.1111/j.1365-313X.2005.02551.x

Xia, T., Apse, M. P., Aharon, G. S., and Blumwald, E. (2002). Identification and characterization of a NaCl-inducible vacuolar Na+/H+ antiporter in *Beta vulgaris*. *Physiol. Plant.* 116, 206–212. doi: 10.1034/j.1399-3054.2002.1160210.x

Xie, X., Ma, X., Zhu, Q., Zeng, D., Li, G., and Liu, Y. G. (2017). CRISPR-GE: a convenient software toolkit for CRISPR-based genome editing. *Mol. Plant.* 10, 1246–1249. doi: 10.1016/j.molp.2017.06.004

Xiong, L., Lee, H., Ishitani, M., and Zhu, J. K. (2002). Regulation of osmotic stress-responsive gene expression by theLOS6/ABA1 locus in *Arabidopsis*. *J. Biol. Chem.* 277, 8588–8596. doi: 10.1074/jbc.M109275200

Xu, B., Wang, Y., Zhang, S., Guo, Q., Jin, Y., Chen, J., et al. (2017). Transcriptomic and physiological analyses of *Medicago sativa* L. roots in response to lead stress. *PLoS One* 12:e0175307. doi: 10.1371/journal.pone.0175307

Yacoubi, R., Job, C., Belghazi, M., Chaibi, W., and Job, D. (2011). Toward characterizing seed vigor in alfalfa through proteomic analysis of germination and priming. *J. Proteome Res.* 10, 3891–3903. doi: 10.1021/pr101274f

Yacoubi, R., Job, C., Belghazi, M., Chaibi, W., and Job, D. (2013). Proteomic analysis of the enhancement of seed vigour in osmoprimed alfalfa seeds germinated under salinity stress. *Seed Sci. Res.* 23, 99–110. doi: 10.1017/S0960258513000093

Yang, S., Gao, M., Xu, C., Gao, J., Deshpande, S., Lin, S., et al. (2008). Alfalfa benefits from *Medicago truncatula*: the RCT1 gene from M. truncatula confers broad-spectrum resistance to anthracnose in alfalfa. *Proc. Natl. Acad. Sci. U.S.A.* 105, 12164–12169. doi: 10.1073/pnas.0802518105

Yang, S. S., Tu, Z. J., Cheung, F., Xu, W. W., Lamb, J. F., Jung, H. J. G., et al. (2011). Using RNA-Seq for gene identification, polymorphism detection and transcript profiling in two alfalfa genotypes with divergent cell wall composition in stems. *BMC genom.* 12:199. doi: 10.1186/1471-2164-12

Yang, S. S., Xu, W. W., Tesfaye, M., Lamb, J. F., Jung, H. J. G., VandenBosch, K. A., et al. (2010). Transcript profiling of two alfalfa genotypes with contrasting cell wall composition in stems using a cross-species platform: optimizing analysis by masking biased probes. *BMC genom.* 11:323. doi: 10.1186/1471-2164-11-323

Yin, P., Ma, Q., Wang, H., Feng, D., Wang, X., Pei, Y., et al. (2020). SMALL Leaf and BUSHY1 controls organ size and lateral branching by modulating the stability of BIG SEEDS1 in *Medicago truncatula*. *New Phytol.* [Epub ahead of print]. doi: 10.1111/nph.16449

Young, N. D., Debellé, F., Oldroyd, G. E., Geurts, R., Cannon, S. B., Udvardi, M. K., et al. (2011). The medicago genome provides insight into the evolution of rhizobial symbioses. *Nature* 480, 520–524. doi: 10.1038/nature10625

Yu, L. X., Liu, X., Boge, W., and Liu, X. P. (2016). Genome-wide association study identifies loci for salt tolerance during germination in autotetraploid alfalfa (*Medicago sativa* L.) using genotyping-by-sequencing. *Front. Plant Sci.* 7:956. doi: 10.3389/fpls.2016.00956

Yu, L. X., Zheng, P., Zhang, T., Rodringuez, J., and Main, D. (2017). Genotyping-by-sequencing-based genome-wide association studies on *Verticillium* wilt resistance in autotetraploid alfalfa (*Medicago sativa* L.). *Mol. Plant Pathol.* 18, 187–194. doi: 10.1111/mpp.12389

Zeng, N., Yang, Z., Zhang, Z., Hu, L., and Chen, L. (2019). Comparative transcriptome combined with proteome analyses revealed key factors involved in alfalfa (*Medicago sativa*) response to waterlogging stress. *Int. J. Mol. Sci.* 20:1359. doi: 10.3390/ijms20061359

Zhang, C., and Shi, S. (2018). Physiological and proteomic responses of contrasting alfalfa (*Medicago sativa* L.) varieties to PEG-induced osmotic stress. *Front Plant Sci.* 9:242. doi: 10.3389/fpls.2018.00242

Zhang, H., Zhang, J., and Wei, P. (2014). The CRISPR/Cas9 system produces specific and homozygous targeted gene editing in rice in one generation. *Plant Biotechnol. J.* 12, 797–807. doi: 10.1111/pbi.12200

Zhang, J. (2004). *Harvesting Inducible Gene And Promoters In Alfalfa*. Dissertation thesis, University of Guelph, Guelph, ON.

Zhang, L. Q., Niu, Y. D., Huridu, H., Hao, J. F., Qi, Z., and Hasi, A. (2014). Salicornia europaea L. Na+/H+ antiporter gene improves salt tolerance in transgenic alfalfa (*Medicago sativa* L.). *Genet. Mol. Res.* 13, 5350–5360. doi: 10.4238/2014.July.24.14

Zhang, S., Shi, Y., Cheng, N., Du, H., Fan, W., and Wang, C. (2015). *De novo* characterization of fall dormant and nondormant alfalfa (*Medicago sativa L.*) leaf transcriptome and identification of candidate genes related to fall dormancy. *PloS One* 10:e0122170. doi: 10.1371/journal.pone.0122170

Zhang, T., Yu, L. X., Zheng, P., Li, Y., Rivera, M., Main, D., et al. (2015). Identification of loci associated with drought resistance traits in heterozygous autotetraploid alfalfa (*Medicago sativa* L.) using genome-wide association studies with genotyping by sequencing. *PLoS One* 10:e0138931. doi: 10.1371/journal.pone.0138931

Zhang, Y. M., Liu, Z. H., Wen, Z. Y., Zhang, H. M., Yang, F., and Guo, X. L. (2012). The vacuolar Na+- H+ antiport gene TaNHX2 confers salt tolerance on transgenic alfalfa (*Medicago sativa*). *Funct. Plant Biol.* 39, 708–716. doi: 10.1071/FP12095

Zhao, B., Liang, R., Ge, L., Li, W., Xiao, H., Lin, H., et al. (2007). Identification of drought-induced microRNAs in rice. *Biochem. Biophys. Res. Comm.* 354, 585–590. doi: 10.1016/j.bbrc.2007.01.022

Zhou, C., Han, L., Pislariu, C., Nakashima, J., Fu, C., Jiang, Q., et al. (2011). From model to crop: functional analysis of a STAY-GREEN gene in the model legume *Medicago truncatula* and effective use of the gene

for alfalfa improvement. *Plant Physiol.* 157, 1483–1496. doi: 10.1104/pp.111.185140

Zhou, M., and Luo, H. (2013). MicroRNA-mediated gene regulation: potential applications for plant genetic engineering. *Plant Mol. Biol.* 83, 59–75. doi: 10.1007/s11103-013-0089-1

Zhu, J. K. (2001). Plant salt tolerance. *Trends Plant Sci.* 6, 66–71. doi: 10.1016/S1360-1385(00)01838-0

Zhu, J. K. (2002). Salt and drought stress signal transduction in plants. *Ann. Rev. Plant Biol.* 53, 247–273. doi: 10.1146/annurev.arplant.53.091401.143329

Zipfel, C. (2014). Plant pattern-recognition receptors. *Trends Immunol.* 35, 345–351. doi: 10.1016/j.it.2014.05.004

Conflict of Interest: The authors declare that the research was conducted in the absence of any commercial or financial relationships that could be construed as a potential conflict of interest.

PALACKÝ UNIVERSITY OLOMOUC

Faculty of Science

Department of Biochemistry

Biochemical and proteomic analysis of mitogen-activated protein kinase signaling during oxidative stress

Ph.D. Thesis summary

Doctoral study program in biochemistry – P1406

Mgr. Petr Dvořák

Olomouc

2021

This Ph.D. thesis was prepared as a part of a full-time doctoral study program in biochemistry P1406 at the Department of Cell Biology, Centre of the Region Haná for Biotechnological and Agricultural Research, Faculty of Science, Palacký University Olomouc in the period 2016–2021 under the supervision of doc. Ing. Tomáš Takáč, Ph.D.

Ph.D. Candidate: **Mgr. Petr Dvořák**
Department of Cell Biology, Centre of the Region Haná for Biotechnological and Agricultural Research
Faculty of Science, Palacký University Olomouc,
Šlechtitelů 241/27, 783 71, Olomouc, Czech Republic

Supervisor: **doc. Ing. Tomáš Takáč, Ph.D.**
Department of Cell Biology, Centre of the Region Haná for Biotechnological and Agricultural Research
Faculty of Science, Palacký University Olomouc
Šlechtitelů 241/27, 783 71, Olomouc, Czech Republic

Opponents: **doc. Mgr. Ildikó Matušíková, Ph.D.**
Department of Ecochemistry and Radioecology
Faculty of Natural Sciences
University of St. Cyril and Methodius in Trnava
Nám. J. Herdu 2, 917 01, Trnava, Slovak Republic

doc. Mgr. Aleš Pečinka, Ph.D.
Institute of Experimental Botany, v. v. i. (IEB)
Centre of the Region Haná for Biotechnological and Agricultural Research
Šlechtitelů 31, 783 71, Olomouc, Czech Republic

The evaluation of the Ph.D. thesis was prepared by the Department of Cell Biology, CRH, Faculty of Science, Palacký University Olomouc.

The summary of the Ph.D. thesis was sent for distribution on …… The oral defense will take place at the Faculty of Science, Palacký University in Olomouc, Šlechtitelů 27 on ……

The Ph.D. thesis is available at the Biology Branch Library in Holice of the Faculty of Science, Šlechtitelů 27, Olomouc.

Prof. RNDr. Ivo Frébort, CSc., Ph.D.
Chairman of Doctoral Study Board in Biochemistry

Content

1 Abstract

Mitogen-activated protein kinase (MAPK) cascades are evolutionarily highly conserved signaling pathways that play an important role in many cellular processes. One of their main functions is to transmit the signal received from the external environment through receptors by intra and intercellular signaling. They also play an irreplaceable signaling role during the establishment of pathogenic or symbiotic relationships between the plants and microorganisms. Plant cells exposed to biotic and abiotic stress conditions accumulate reactive oxygen species (ROS) causing oxidative stress, which in extreme cases can lead to cell death. ROS plays a critical role in cell signaling and plant developmental processes. Increased accumulation of ROS activates MAPKs, which in turn regulate several cellular processes, including antioxidant enzymes such as superoxide dismutases (SODs).

The main aim of the first part of this thesis is to examine the role of MAPK during the initiation of symbiotic relationships of *Medicago sativa* with the beneficial bacteria *Sinorhizobium meliloti* and subsequent nodulation. Biochemical, phenotypic and proteomic analyses of the *M. sativa* transgenic SIMKK RNAi line with reduced expression of MAPK kinase SIMKK revealed the possible involvement of MAPK cascades in these processes. SIMKK RNAi line displayed a reduced number of nodules compared to the wild type. Subsequent biochemical and proteomic analysis showed that this phenotype could be caused by defects in bacterial adhesion to the root surface, plasma membrane remodeling, and redox regulation, including the abundance of antioxidant proteins. The nodules of the transgenic line show an affected nitrogen and carbon metabolism.

Within the second part, the developmental roles and localization of the SOD isoenzyme FSD1 in *Arabidopsis thaliana* were examined. Moreover, possible mechanisms of its regulation by MAPK were suggested. We found that FSD1 is involved in the development of lateral roots and it has a protective role during oxidative stress and salt stress. FSD1 localizes in the cytoplasm, chloroplasts and, surprisingly, in the nucleus, as revealed by advanced microscopy. It temporarily accumulates at the site of endosperm rupture during seed germination. With the help of co-immunoprecipitation, potential interaction partners of FSD1 were identified by mass spectrometry and possible functions of FSD1 were proposed. Finally, experiments were conducted in order to reveal the possible involvement of MPK3 and MPK6 in the regulation of FSD1 expression through SPL transcription factors.

With the increasing demands of humanity and at the same time there are dynamically changing environmental conditions, conventional agriculture is nearing its limitations. The understanding of the symbiotic relationships and especially its initial signaling pathways can lead to subsequent biotechnological advances and thus increase crop yields. A feasible alternative is also a genetic modification of antioxidant enzymes, which would lead to higher resistance of plants to both biotic and abiotic stress. However, for their targeted modification, it is important to understand their functions in plants. This work contributes to the understanding of the role of MAPK cascades and FSD1 protein in plants and supports the claim for their possible involvement in biotechnological applications in agriculture.

2 Aims of thesis

- Summary of current knowledge on oxidative stress in plants, mitogen-activated protein kinases (MAPKs) and their role in response to biotic and abiotic stress, superoxide dismutases (SODs), and regulation of SODs by SQUAMOSA PROMOTER-BINDING PROTEIN-LIKE proteins (SPLs), symbiotic interaction of alfalfa and the role of MAPK during nodulation.

- Proteomic analysis of the role of SIMKK during symbiotic interaction between alfalfa and rhizobia, with focus on ROS regulation.

- Developmental and biochemical characterization of FeSOD1.

- Examination of the relationship between superoxide dismutase (especially FeSOD1) and MAPK.

3 PART I – Genereal introduction

3.1 Mitogen activated protein kinases

Due to their sessile nature, plants must cope with unfavorable environmental conditions by rapid signal perception ensuring proper physiological responses and adaptation. Thus, plants have stress responses that are coordinated via complex networks of densely interconnected signaling pathways. Phosphorylation is the key post-translational modification (PTM) of proteins allowing immediate signal transduction in response to various environmental or developmental cues (Ichimura et al., 2000). Protein phosphorylation, which is catalyzed by protein kinases, may cause enzyme activation or inactivation, a change in the substrate specificity, protein stability, protein-protein interaciton and localization as well as the ability to bind protein partners (Huber, 2007; Vu et al., 2018). Around 4–5% of the *Arabidopsis* genome encodes protein kinases (Zulawski et al., 2014). Mitogen-activated protein kinases (MAPK) hold a leading position among kinases ensuring transduction of the signal generated by environmental and developmental factors (Šamajová et al., 2013; Komis et al., 2018). MAPK signaling cascades consist of MAPK kinase kinase (named also MAP3Ks, MEKKs or MAPKKKs), MAPK kinase (MAP2Ks, MEKs or MAPKK and MKKs), and MAPKs (MPKs), which are consecutively phosphorylated leading to the activation/inactivation of a wide range of target proteins including transcription factors (TFs), enzymes or other kinases (Dóczi and Bögre, 2018; Figure 1). MAPK cascades are highly conserved in eukaryotes. *Arabidopsis* genome encodes 60 putative MAP3Ks, 10 MAP2Ks, and 20 MAPKs (Rodriguez et al., 2010).

Activation of MAPK cascade is initiated by phosphorylation of MAP3K either by receptor-like kinases (RLKs), receptor-like cytoplasmic kinases (RLCK; Bi et al., 2018; Wang et al., 2020) or other protein kinases (e.g. BRASSINOSTEROID-INSENSITIVE 2; Kim et al., 2012). Activated MAP3Ks phosphorylate MAP2Ks at a conserved S/T-$X_{3–5}$-S/T motif. Subsequently, MAPKs are double phosphorylated at a conserved TXY motif by MAP2Ks (Tanoue and Nishida, 2003). Deactivation of MAPKs is mediated by protein phosphatases (Bheri et al., 2020).

Judging from the differences in the number of MAP3K, MAP2K and MAPK representatives, it is obvious that there is a broad crosstalk and redundancy in signaling. It means, that multiple MAP3K/MAP2Ks activate individual MAPKs in response to various stimuli. On the other hand, various MAPKs may be initiated by a single stimulus activating only a specific MAP3K/MAP2K (Smékalová et al., 2014). High variability of MAPK signaling cascades allows the generation of specific response to the perceived signal. Another mechanism ensuring the specificity of signaling are adaptors or scaffold proteins, which provide organizing platforms for integration of kinase modules in a complex. Thus, scaffold proteins enable operative utilization of MAPK modules for various signaling outputs, and prevent crosstalking with other signaling pathways (Dhanasekaran et al., 2007; Good et al., 2011). The best-studied example in plants is the MAPK scaffolding protein named RECEPTOR FOR ACTIVATED C KINASE 1, which is responsible for scaffolding of MEKK1-MKK4/MKK5-MPK3/MPK6 module activated by the involvement of heterotrimeric GTPases in response to *P. aeruginosa* in *Arabidopsis* (Cheng et al., 2015).

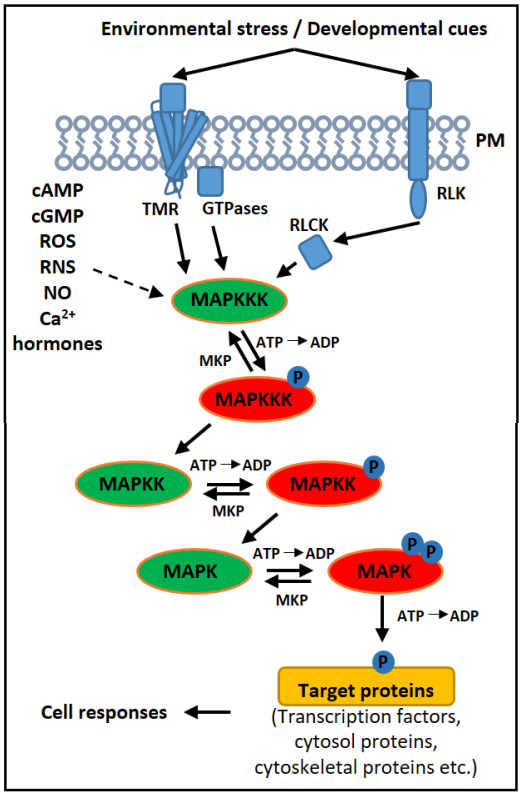

Figure 1 Schematic depiction of general MAPK cascade activation and its targets. MAPK cascades are initiated by extracellular stimuli through receptors, leading to consecutive phosphorylation of individual MAPK members. This occurs upon vital crosstalk with second messengers such as ROS. Terminal MAPK phosphorylates diverse proteins including transcription factors, enzymes, cytoskeletal proteins and others. Abbreviations: Ca^{2+} – calcium ions, cAMP – cyclic adenosine monophosphate, cGMP – cyclic guanosine monophosphate, MAPK – mitogen activated protein kinase, MAPKK – mitogen activated protein kinase kinase, MAPKKK – mitogen activated protein kinase kinase kinase, MKP – MAPK phosphatase, NO – nitric oxide, PK – protein kinase, PM – plasmatic membrane, RLCK – receptor-like cytosolic kinase, RLK – receptor-like kinase, RNS – reactive nitrogen species, ROS – reactive oxygen species, TMR – transmembrane receptor.

3.1.1 MAPK signaling during biotic and abiotic stress

The central consequence of plant elicitation by pathogenic or beneficial organisms is the activation of MAPK signaling (Meng and Zhang, 2013). Currently, two MAPK cascades are known to be initiated during pathogen-triggered immunity. One is composed of MEKK3/5-MKK4/5-MPK3/6 (Bi et al., 2018). Previously, MEKK1 was also suggested as an upstream activator of the MKK4/5-MPK3/6 pathway (Asai et al., 2002), however, later studies uncovered that treatment with flg22 led to the activation of MPK3 and MPK6 in *mekk1* T-DNA insertion mutants (Suarez-Rodriguez et al., 2007). The second independent cascade leads to activation of MPK4 downstream of MEKK1 and MKK1/2 (Gao et al., 2008). Based on genetic studies, MPK3 and MPK6 have a positive role on activation of plant immunity, while MPK4 is a positive and negative regulator (Kong et al., 2012; Thulasi Devendrakumar et al., 2018; Huang et al., 2020).

The regulation of pathogen defense by *Arabidopsis* MPK3 and MPK6 is multilevel and affects stomatal immunity, hormone biosynthesis and signaling as well as gene expression. MPK3 and MPK6 regulate stomatal closure, which prevents fungal invasion, by two mechanisms, either by metabolic shift of organic acids such as malate and citrate (Su et al., 2017) or by phosphorylation of nitric oxide producing enzyme NITRATE REDUCTASE 2 (Wang et al., 2010). MPK3 and MPK6 phosphorylate TFs belonging to the WRKY family, such

as WRKY22/WRKY29 (Asai et al., 2002) or WRKY33 (Mao et al., 2011) and other such as ETHYLENE-INSENSITIVE 3 (Yoo et al., 2008), BRASSINOSTEROID INSENSITIVE1-ETHYL METHANESULFONATE SUPPRESSOR 1 (Kang et al., 2015), ERF6 and 104 in response to biotic stress. Their activation is connected with expression of plant defensins (PDF; Bethke et al., 2009; Meng et al., 2013), camalexin biosynthesis (Mao et al., 2011), and enzymes of ethylene biosynthesis (Li et al., 2012).

MPK4 is involved in immune response through multiple mechanisms. MPK4 phosphorylates MPK4 SUBSTRATE 1 (MKS1; Andreasson et al., 2005), causing the release of MKS1-WRKY33 complex. Activation of MPK4 promotes JA-dependent gene expression (e.g. *PDF1.2* and a pathogenesis related gene *THIONIN 2.1;* Petersen et al., 2000), while it has a negative impact on SA-dependent immune response (Kong et al., 2012). It was found that the autoimmune response is caused by over-activation of a defense, mediated by a nucleotide-binding and leucine-rich repeat receptor protein *SUPPRESSOR OF MKK1/MKK2 2* (Zhang et al., 2012). More recent studies uncovered complex interactions behind MPK4 directed autoimmunity among *Catharanthus roseus* RECEPTOR-LIKE KINASE 1-like-LLG1 complex (Huang et al., 2020), CALMODULIN-BINDING RECEPTOR-LIKE CYTOPLASMIC KINASE 3 (Zhang et al., 2017) and malectin-like RLK LETUM 1 (Liu et al., 2020).

Abiotic stresses such as osmotic and temperature stress, drought, heavy metals, high light or UV irradiation belong to the most important factors limiting plant growth and crop production. All of these conditions lead to the production of secondary messengers such as ROS, Ca^{2+} and phytohormones. Their crosstalk and ability to activate signaling cascades is the main driving force of plant stress adaptation (Smékalová et al., 2014).

Cold stress activates two MAPK pathways involving either MKK2 (Ichimura et al., 2000; Teige et al., 2004) or MKK4/5 as MAP2Ks (Li et al., 2017a; Zhao et al., 2017). MKK2 is phosphorylated by MEKK1 and activates MPK4 (Ichimura et al., 2000; Teige et al., 2004). MKK4/5 acting upstream of MPK3/6 negatively affect cold stress response, because phosphorylation of INDUCER OF CBF EXPRESSION 1 transcriptional activator leads to its degradation (Li et al., 2017a; Zhao et al., 2017).

Heat shock TFs (HSFs) are MAPK targets, as for example MPK6 phosphorylates HSFA2 on its Thr-249 residue, which then relocalizes from the cytoplasm to the nucleus (Evrard et al., 2013). HSFA4A is phosphorylated by MPK3, MPK4 and MPK6 on Ser-309 and promotes expression of heat shock protein (HSP) *HSP17.6A* and TFs *WRKY30* and *ZAT12* (Andrási et al., 2019). Heat stress responsive proteins HSP90s interact and activate YODA (MAP3K)-MPK3/6 cascade under heat stress. Subsequently, both MPK3/6 inhibit the activity of TF SPEECHLESS, which is responsible for stomatal development (Samakovli et al., 2020).

MAPKs are involved in drought stress responses through crosstalk with abscisic acid (ABA) as well as phosphatidic acid (PA) signaling. ABA and ROS-activated MPK9 and MPK12 act upstream of anion channels in guard cells, thus regulating a stomatal closure (Jammes et al., 2009). MPK6 (downstream of MAPKKK15-MKK4) has also impact on drought responsive gene expression through phosphorylation of WRKY59, which promotes the expression of *DEHYDRATION-RESPONSIVE ELEMENT BINDING PROTEIN 2* in response to drought stress (Li et al., 2017b).

Osmotic stress activates MAPK signaling, particularly MPK3 and MPK6 upstream of MKK9 (Zhao and Guo, 2011) or MKKK20 (Kim et al., 2012). It leads also to activation of

MEKK1 (Su et al., 2007) and MMK2, upstream of MPK4 and MPK6 (Teige et al., 2004). A previous study identified a lectin receptor-like kinase SALT INTOLERANCE 1 to be an upstream activator of MPK3 and MPK6 in response to salt stress. However, SALT INTOLERANCE 1-MPK3/6 complex is a negative regulator of salt stress response by affecting ROS, ethylene homeostasis and signaling (Li et al., 2014).

3.1.2 MAPKs in *Medicago sativa*

Medicago sativa L., also known as alfalfa or lucerne, is a perennial world's leading forage legume, with extensive green biomass production and rich root system providing beneficial impact on soil agronomical properties (Radović et al., 2009). Alfalfa and other legumes are characterized by their ability to interact with nitrogen-fixing bacteria named rhizobia (e.g. *Bradyrhizobium* or *Sinorhizobium*) and their interaction can lead to a reduction of atmospheric nitrogen into ammonium in specialized organs called root nodules (Oldroyd, 2013; Wang et al., 2018). This may contribute up to 60% of the entire nitrogen nutritional requirement of alfalfa.

The symbiotic interaction is initiated by the release of flavonoid compounds by plant roots to the rhizosphere, which are sensed by bacteria. As a response, the bacteria produce extracellular lipochitooligosaccharides, known as nodulation (Nod) factors (Oldroyd, 2013). Nod factors are sensed by specific receptor-like kinase complexes, which consist e.g. of NOD FACTOR RECEPTOR (LjNFR1)/LYSIN MOTIF RECEPTOR-LIKE KINASE 3 (MtLYK3) heterodimer and NOD FACTOR PERCEPTION 5 (LjNFR5/MtNFP; Roy et al., 2020). Nod factor recognition triggers specific symbiosis signaling pathways (Roy et al., 2020). Entry of bacteria into the root system is associated with curling of the root hair tip, and trapping the bacteria inside the root hair curl. Rhizobia are reproduced in the hair curl and penetrate to the root system through a specialized structure called infection thread (IT; Suzaki et al., 2015). Thanks to the rapidly dividing bacteria, IT elongates, allowing the bacteria to reach cortical cells and initiate nodule formation. ITs expand and branch within the cortical cells, which accelerate the bacterial colonization and development of the nodule primordium (Tian et al., 2012). Later, rhizobia are released from IT inside the cells of the nodule, and they differentiate to individual bacteroids, which form the basic nitrogen-fixing unit.

MAPKs plays an important role during stress signaling (Jonak et al., 1996 and 2004; Cardinale et al., 2002; Lopez-Gomez et al., 2012), development (Bögre et al., 1999; Šamaj et al., 2002; Chen et al., 2017) along with establishing a symbiotic relationship (Lee et al., 2008; Chen et al., 2012; Ryu et al., 2017; Yin et al., 2019) in *Fabaceae*. So far, four MAPKs known as SIMK (STRESS-INDUCED MAPK or MMK1), MMK2, MMK3, and SAMK (STRESS-ACTIVATED MAPK or MMK4), were identified in alfalfa (Jonak et al., 1999). SIMK is a salt and elicitor stress-induced MAPK orthologous to *Arabidopsis* MPK6 (Cardinale et al., 2002), which is activated in response to salt stress by upstream STRESS-INDUCED MAPKK (SIMKK; Kiegerl et al., 2000). In addition to that, SIMK is localized to the nucleus and cytoplasm of the root cells, while it relocates from the nucleus to the growing tip of the developing root hairs (Šamaj et al., 2002). Activation and the subsequent sub-cellular relocation from nucleus to cytoplasmic compartments of both SIMK and its upstream SIMKK were induced by salt stress (Ovečka et al., 2014). The actin-dependent relocalization of SIMK and SIMKK to the root tip, along with their activity, is required for proper root hair formation and elongation in alfalfa (Šamaj et al, 2002). Recently, it was revealed, that their genetic modification is linked to defects in IT generation (Hrbáčková et al., 2020), which suggests the important role of the SIMKK-SIMK module in nodulation. SIMK can be activated also by

upstream PATHOGEN-RESPONSIVE MAPKK (PRKK) in response to Pep13 elicitor (Cardinale et al., 2002).

3.2. Reactive oxygen species

The common feature of all aerobic organisms is the exploitation of O_2 in metabolism, which is powered by energy-producing reactions that lead to the generation of ROS by electron or energy leakage to O_2 (Fischer et al., 2013). ROS are defined as molecules displaying higher chemical reactivity than O_2 and about 1% of O_2 utilized by plants is turned to their production. The most important ROS in higher plants include singlet oxygen ($_1O^2$), superoxide anion ($O_2^{\cdot -}$), hydrogen peroxide (H_2O_2) and hydroxyl radical ($HO^{\cdot}$). The high reactivity of ROS may cause damaging oxidative effects on lipids, nucleic acids, and proteins eventually resulting in cell death. Individual ROS are characterized by different reactivity, which is closely related to the time of their existence (Mittler, 2017; Waszczak et al., 2018). H_2O_2 could be transported by membrane-localized aquaporins and cause rapid and reversible oxidation of redox-sensitive proteins (Miller et al., 2010; Mittler, 2017). All these features make H_2O_2 a suitable candidate for signaling roles under both optimal and adverse environmental conditions (Apel and Hirt, 2004; Waszczak et al., 2018). Chloroplasts and peroxisomes are the main ROS producers in photosynthesizing organisms. The contribution of mitochondria (and other places of ROS production such as apoplast, endoplasmic reticulum, cytosol) to ROS production is relatively small in photosynthetic tissues in comparison with chloroplasts. Currently, ROS are recognized as universal signaling metabolites playing an important role during stress responses (Noctor et al., 2017) and development (Mhamdi and Van Breusegem, 2018).

3.2.1 Signaling roles of ROS

The production of ROS is strictly regulated by a complex antioxidant system, which is keeping ROS in physiological concentrations. Depending on the generated ROS concentration, severity of stress, antioxidant capacity, and cellular energetic status, different cellular and physiological outcomes may be obtained. In higher concentrations, ROS shift the compartmental redox balance toward an oxidized state and this change can be sensed by various compartment-specific systems (Noctor et al., 2017). The key consequence of ROS accumulation is the modification of signaling targets (e.g. kinases, TFs, stress response proteins) by their oxidizing properties (Waszczak et al., 2014). ROS can modulate signaling through their capability to affect protein redox status via oxidation of methionine residues and thiol groups of cysteines. This leads to activation, inactivation, or alters the structure and function of the target proteins (Waszczak et al., 2015). These modifications are strictly regulated by redox-sensitive proteins such as thioredoxins, peroxiredoxins and glutaredoxins, which can undergo reversible oxidation/reduction and are activated/inactivated in the response to the cellular redox state (Waszczak et al., 2015 and 2018). The oxidation of Cys-residue as a regulatory mechanism is employed also for sensing of extracellular H_2O_2 by leucine-rich repeat receptor kinase HYDROGEN-PEROXIDE-INDUCED Ca^{2+} INCREASES 1 (Wu et al., 2020).

Redox perturbations driven by ROS production in chloroplasts and mitochondria are transduced by metabolic signals to the nucleus in order to activate rapid adaptive mechanisms within retrograde signaling (Chan et al., 2016; Cui et al., 2019). Moreover, chloroplastic H_2O_2 itself is transported to the nucleus by stromules in order to activate the expression of defense genes (Erickson et al., 2017; Hanson and Conklin, 2020).

The perception of the apoplastic ROS is a crucial source of the signaling information for plants. Apoplastic ROS are involved in stress responses (Chaouch et al., 2012; Qi et al., 2017), long-

distance signaling (Gilroy et al., 2016; Fichman and Mittler, 2020), various developmental processes (Orman-Ligeza et al., 2016; Mhamdi and Van Breusegem, 2018; Choudhary et al., 2019), and induction of cell death (Van Breusegem and Dat, 2006). They are sensed either by their recognition by above mentioned membrane receptors (Wu et al., 2020), or by recognition of oxidized apoplastic peptides, ligands and metabolites (Tavormina et al., 2015; Kimura et al., 2017; Waszczak et al., 2018). Alternatively ROS are sensed by oxidative PTMs of intracellular signaling proteins (Waszczak et al., 2015).

3.2.2 ROS-induced MAPK signaling pathways

It is well-known that MAPK signaling pathways are activated by ROS accumulated during plant responses to either abiotic stresses or biotic interactions. So far, two MAP3Ks were identified to be activated by ROS, namely ARABIDOPSIS HOMOLOGUES OF NUCLEUS AND PHRAGMOPLAST LOCALIZED KINASES (ANPs), and MAPKKK1 (or MEKK1). ANPs are required for the plant immune response (Kovtun et al., 2000; Savatin et al., 2014), while the ROS-triggered signal is further transduced via MPK3 and MPK6 (Kovtun et al., 2000; Nakagami et al., 2006).

Another ROS-activated MAPK cascade consists of MEKK1, MKK1/2, and MPK4 (Nakagami et al., 2006; Pitzschke et al., 2009). This pathway is also important for basal plant defense against a pathogen attack (Zhang et al., 2012). Moreover, a pathogen-induced oxidative burst activates the MPK7 downstream of MKK3 (MAP2K), thus triggering the expression of *PR* genes, independently of flagellin receptor FLS2 (Dóczi et al., 2007).

Furthermore, MPK1 and MPK2 are activated by oxidative stress, as well as by JA, ABA, and wounding (Ortiz-Masia et al., 2007). In turn, ABA and ROS-activated MPK9 and MPK12 act upstream of anion channels in guard cells, thus regulating stomatal closure (Jammes et al., 2009). MPK3 was found as another principal player in guard cell signaling via ABA and H_2O_2 perception in guard cells, which leads to stomatal closure (Gudesblat et al., 2007).

Several studies report on the regulation of MAPKs by direct interactions with ROS. Waszczak et al. (2014) identified MPK2, MPK4, and MPK7 as capable of being sulfenylated in an H_2O_2-dependent manner. Another example pertains to *Brassica napus* BnMPK4, an ortholog of *Arabidopsis* MPK4, which is activated by H_2O_2 and undergoes aggregation upon the H_2O_2-dependent oxidation of the Cys-232 residue (Zhang et al., 2015).

3.2.3 Developmental roles of ROS

ROS are widely involved in plant growth and developmental processes (Xia et al., 2015; Mhamdi and Van Breusegem, 2018; Considine and Foyer, 2020). Proper plant growth in both normal and stress conditions is ensured by precise regulation of cell cycle, proliferation, and expansion, which are affected by ROS or redox-dependent mechanisms (Tsukagoshi, 2012; Diaz-Vivancos et al., 2015; De Simone et al., 2017). ROS produced by RBOHC control cell proliferation by affecting assembly/disassembly of mitotic microtubule structures (Livanos et al., 2012). ROS-orchestrated PCD plays an important role in the development of various tissues and organs, such as the tapetum, seed coat, lateral root cap and endosperm (Daneva et al., 2016).

Initial stages of seed germination are accompanied with the accumulation of ROS after water imbibition, which is important for proficient germination and radicle protrusion (Bailly et al., 2008; Müller et al., 2009; Singh et al., 2016). Various studies showed the influence of ROS during primary root, lateral root and root hair growth (Foreman et al., 2003; Li et al., 2015;

Tsukagoshi, 2016). RBOH-mediated ROS production promotes lateral root primordia (LRP) formation by inducing cell wall remodeling of overlying parental tissues and via crosstalk between ROS and auxin signaling pathways. Genetic manipulation of RBOHD showed an increased number of LRP in overexpressing lines and decreased in knockout (KO) mutant lines (Orman-Ligeza et al., 2016). Root hair elongation is promoted by ROS produced by RBOH (specifically by RBOHC) in root hair tip (Foreman et al., 2003).

3.3 Antioxidant defense in plants with focus on superoxide dismutases

Generally, enzymatic antioxidant capacity inevitably contributes to plant survival in adverse conditions, especially when the stress pressure exceeds the mechanisms preventing ROS over-accumulation. The significance of antioxidant enzymes has been documented by genetic studies reporting on the positive correlation between their expression and plant stress tolerance. By contrast, the downregulation of these enzymes is connected with plant hypersensitivity to stress and PCD (De Pinto et al., 2012).

ROS scavenging is performed via enzymatic or non-enzymatic antioxidant defense pathways, which control the regulation of ROS levels through strict compartmentalization (Mignolet-Spruyt et al., 2016; Foyer and Noctor, 2020). Non-enzymatic antioxidant defense is mainly mediated by low molecular-weight metabolites such as ascorbate, glutathione, α-tocopherol, carotenoids, and flavonoids. (Locato et al., 2017; Zechmann, 2018; Muñoz and Munné-Bosch, 2019; Foyer and Noctor, 2020).

Superoxide dismutases (SODs), catalases (CATs), ascorbate peroxidases (APXs), dehydroascorbate reductases (DHARs), monodehydroascorbate reductases (MDHARs), and glutathione reductases (GRs) are among the main antioxidant enzyme classes. Furthermore, glutathione peroxidases, peroxidases, and thio-, gluta-, and peroxiredoxins are potent ROS scavengers as well (Dietz, 2011; Kang et al., 2019; Foyer and Noctor, 2020).

3.3.1 Superoxide dismutases

SODs (EC 1.15.1.1) are antioxidant metalloenzymes expressed in all living organisms (McCord et al., 1971; Fridovich, 1978; Foyer and Noctor, 2005). SODs catalyze the dismutation of $O_2^{\cdot-}$ to molecular oxygen and less toxic H_2O_2 ($2O_2^{\cdot-} + 2H^+ \leftrightarrow H_2O_2 + O_2$). The enzymatic dismutation of $O_2^{\cdot-}$ by SODs is an extremely effective reaction, occurring at the almost diffusion-limited rate of $\approx 10^9$ $M^{-1} \cdot s^{-1}$ (Sheng et al., 2014). $O_2^{\cdot-}$ can be also spontaneously dismutated to H_2O_2. However, this reaction is 10^4 times slower in comparison with the catalyzed reaction and the rate is highly dependent on the concentration of $O_2^{\cdot-}$ (Table 1; Murphy, 2009; Sheng et al., 2014).

Table 1 Comparison of catalyzed and spontaneous $O_2^{\cdot-}$ dismutation at different concentrations of substrate and SOD. Adopted from Sheng et al. (2014).

Concentration		Half life	Acceleration factor
$O_2^{\bullet-}$	SOD		
10^{-6}	None	3000 ms	
10^{-6}	10^{-9}	175 ms	20x
10^{-9}	None	Hours	
10^{-9}	10^{-9}	175 ms	10 000x
10^{-9}	10^{-6}	0.175 ms	10 000 000x

Based on the presence of metal cofactors in their active site, four different SODs exist in living organisms, namely NiSOD, FeSOD, MnSOD, and Cu/ZnSOD.

Plant SODs compartmentalize into the main compartments of $O_2^{\cdot-}$ production: chloroplast and plastids, cytosol, mitochondria, peroxisome, and apoplast (Kliebenstein et al., 1998). In the genome of *Arabidopsis*, three *FeSOD* (*FSD1*, *FSD2*, and *FSD3*), one *MnSOD* (*MSD1*), and three *Cu/ZnSOD* (*CSD1*, *CSD2*, and *CSD3*; Kliebenstein et al., 1998; Pilon et al., 2011) gene isoforms have been identified. Mitochondrial $O_2^{\cdot-}$ is eliminated by MSD1 (Morgan et al., 2008), peroxisomes contain CSD3 (Kliebenstein et al., 1998) and cytosolic $O_2^{\cdot-}$ is decomposed by CSD1 and FSD1 (Kliebenstein et al., 1998, Myouga et al., 2008). Photosynthetic $O_2^{\cdot-}$ is decomposed by FSD1 in the chloroplast stroma (Kuo et al., 2013), and by CSD2, FSD2, and FSD3 in thylakoids (Kliebenstein et al., 1998; Myouga et al., 2008).

3.3.1.1 FSDs

Interestingly, all *Arabidopsis* FSD isoforms are localized in chloroplast while FSD1 has dual localization in the cytosol and chloroplast as shown in *Arabidopsis* protoplasts (Kuo et al., 2013) and tobacco leaves transiently transformed by particle bombardment (Myouga et al., 2008).

Although FSD1 is the most abundant SOD in *Arabidopsis* with more than 10 times higher expression than *FSD2* and *FSD3*, *fsd1* T-DNA mutants do not exhibit obvious phenotypic defects. Contrariwise, the leaves of *fsd2* and *fsd3* mutants are pale-green in color, with abnormalities in chloroplast development and impaired growth (Myouga et al., 2008). The phenotype of *fsd2*/*fsd3* double mutant is even more pronounced, suggesting that FSD2 and FSD3 have complementary functions. Both *fsd2* and *fsd3* mutants show a higher accumulation of $O_2^{\cdot-}$ in normal conditions and high sensitivity to high light, while *fsd1* has a similar response as wild type. Additionally, *fsd2* mutant displays decreased chlorophyll concentrations, decreased PSII efficiency followed by reduced rate of CO_2 assimilation under normal conditions. On the other hand, *FSD2* and *FSD3* overexpression confer on increased oxidative tolerance induced by MV (Myouga et al., 2008; Gallie and Chen, 2019). These mentioned reverse genetic studies have questioned the role of FSD1 in oxidative stress tolerance. Interestingly, heterologous overexpression of *Arabidopsis FSD1* in tobacco and maize led to an increased tolerance against MV and in maize also to increased growth rates (Van Camp et al., 1996; Van Breusegem et al., 1999).

The main factors affecting *FSD1* expression and activity are the availability of Fe^{2+} (Waters et al., 2012), Cu^{2+} (Cohu et al., 2009; Yamasaki et al., 2009), nitrogen (Mermod et al., 2019), and sucrose (Dugas and Bartel, 2008). FSD1 expression/abundance increases upon low Cu^{2+} availability, in parallel with the drop of expression of *CSD1* and *CSD2* and Cu^{2+} is redirected into housekeeping proteins and compounds as plastocyanin and cytochrome-c oxidase (Burkhead et al., 2009; Cohu et al., 2009; Pilon, 2017). By contrast, in conditions of Cu^{2+} sufficiency, CSD1 and CSD2 abundance rises and FSD1 abundance drops to minimal levels (Cohu et al., 2009; Yamasaki et al., 2009). The expression of *FSD1* and both *CSD1* and *CSD2* is also similarly affected by sucrose (Dugas and Bartel, 2008) and nitrogen availability (Mermod et al., 2019). The expression of *FSD2* and *FSD3*, but not *FSD1* is sensitive to stress conditions as high light and oxidative stress (Kliebenstein et al., 1998; Myouga et al., 2008), heavy metals (Abdel-Ghany et al., 2005; Abercrombie et al., 2008), ozone (Kliebenstein et al., 1998) and cold (Soitamo et al., 2008).

3.4 SQUAMOSA-PROMOTER BINDING PROTEIN-LIKE proteins

A characteristic feature of SPLs protein family is the presence of the SQUAMOSA PROMOTER BINDING PROTEIN (SBP) domain, which consists of a highly conserved region of 76 amino acids. This domain is responsible for nuclear import and binding to the specific promoter regions by two unconventional zinc fingers formed of eight conserved histidine and cysteine residues (Yamasaki et al., 2004; Birkenbihl et al., 2005; Guo et al., 2008). The structural motif recognized in the promoter sequence is known as TNCGTACAA *cis*-element (Cardon et al., 1999; Yamasaki et al., 2004), nevertheless, the sequence GTAC is the essential core indispensable for binding SPLs as TFs (Birkenbihl et al., 2005; Kropat et al., 2005). The size, structure, and presence of other structural domains may vary significantly among SPLs.

SPL genes are expressed in green plants, green algae and mosses (Preston and Hileman, 2013). *Arabidopsis* genome encodes 17 *SPL* genes, however, *SPL13A* and *SPL13B* emerged as a tandem duplication (Yang et al., 2008). SPLs show high variability in length of their amino acid sequence, which range in *Arabidopsis* from 131 (SPL3) to 1037 (SPL14) amino acids. Depending on protein domain composition (e.g. the presence of transmembrane domain and ankyrine repetition), SPLs are subclassified into structurally more complex large SPLs (SPL1/7/12/14/16), and small SPLs.

SPLs are involved in root and rosette development (Yang et al., 2008), generative growth (Schmid et al., 2003), flower formation (Salinas et al., 2012; Jorgensen and Preston, 2014), embryo development and seed germination (Nodine and Bartel, 2010). They contribute to plant responses to abiotic and biotic stresses (Stief et al., 2014; Chao et al., 2017; Cai et al., 2018) along with heteroblasty (Usami et al., 2009).

3.4.1 SPL7

SPL7 together with Cu-DEFICIENCY INDUCED TRANSCRIPTION FACTOR 1 are the master regulators of Cu^{2+} homeostasis (Yamasaki et al., 2009; Yan et al., 2017) and regulators of JA biosynthetic genes under Cu^{2+} deficiency (Yan et al., 2017). Besides *miRNA389* and *FSD1* promoters, SPL7 targets also *FERRIC REDUCTASE OXIDASES* (Jain et al., 2014), *COPPER TRANSPORTERS FAMILY* (Jung et al., 2012; Gayomba et al., 2013), *Cu-RESPONSIVE miRNAs*, and others (Yamasaki et al., 2009; Yan et al., 2017).

As mentioned before, *FSD1*, *CSD1* and *CSD2* are transcriptionally and post-transcriptionally regulated by SPL7 in a Cu-dependent manner (Yamasaki et al., 2007 and 2009; Garcia-Molina et al., 2014). Under Cu^{2+} deficiency, SPL7 binds to Cu^{2+} responsive (CuRE) promoter sequence and induces the expression of *FSD1*, leading to increased abundance and activity of the FSD1 enzyme. At the same time, *CSD1*, *CSD2*, and *CCS* are post-transcriptionally downregulated by miRNA398, which is induced by the SPL7-positive regulation in the promoter sequence (Cohu et al., 2009; Yamasaki et al., 2009). Therefore, SPL7 is an important modulator of Cu^{2+} balance via Cu^{2+}-responsive proteins and miRNAs (Burkhead et al., 2009; Araki et al., 2018). All of these important roles are supported by studies employing *spl7* mutant, which accumulates less Cu^{2+} and it has developmental defects unless higher Cu^{2+} concentration is added in the growth medium (Yamasaki et al., 2009; Gayomba et al., 2013; Schulten et al., 2019). SPL7 is also implicated in the circadian regulation of *FSD1* expression, since changes in amplitude of a FSD1 classical clock output were found in *spl7* mutants (Perea-García et al., 2016).

4 PART II – MAPK activation and function in response to elicitation and symbiotic bacteria

4.1 Materials and methods

Used material and methods are briefly introduced here. All detailed information are described in the Ph.D. thesis.

The study is focused on wild type and transgenic *Medicago sativa* cv. Regen-SY (RSY) line *SIMKK RNAi line* (SIMKKi) with strong downregulation of SIMKK and SIMK (as described in Bekešová et al. (2015)). Indicated lines were treated with 200 nM flg22 or bacterial culture of *Sinorhizobium meliloti* SM2011 (OD_{600} 0.5). MAPK activation assay (after flg22 and *S. meliloti* treatment), proteomic and evaluation of nodule generation analysis was performed (after *S. meliloti* treatment).

For immunoblot analysis material was homogenized into fine powder in a mortar with liquid nitrogen. Proteins were extracted in E-buffer and the extract was centrifuged 15 min at 13 000 g at 4°C. Equal amounts of proteins were mixed with 4x concentrated LB (Bio-Rad) and boiled at 95°C for 5 min. SDS-PAGE was performed on 10% TGX Stain-Free™ Fast-Cast™ gels (Bio-Rad). Proteins were transferred to a polyvinylidene difluoride (PVDF) membrane (GE Healthcare) using a wet tank unit (Bio-Rad). Membranes were blocked by overnight incubation of the membrane either in 5% BSA (for detection of anti-phospho ERK Ab (pERK)), or in 4% BSA and 4% low-fat dry milk (for detection of HSP70 Ab), or in 5% low-fat dry milk (for detection of MMK3 Ab, MnSOD1 Ab, CAT Ab), in TBS-T. Subsequently, the membranes were incubated with anti-pERK (1:1000; Cell signaling), anti-MnSOD (1:3000; Agrisera), anti-HSP70 (1:5000; Sigma) and anti-CAT (1:1000; Agrisera) primary antibodies in TBS-T containing 1% BSA at 4°C overnight. Membranes were incubated with a secondary antibody diluted in TBS-T containing 1% BSA for 1.5 h. Horseradish peroxidase-conjugated goat anti-rabbit and anti-mouse IgG secondary antibodies (both diluted 1:5000; Thermo Scientific) were used for the detection.

For the analysis of SOD isoenzymes activities, roots (non-treated and *S. meliloti* treated alfalfa) were homogenized in liquid nitrogen and subjected to protein extraction using 50 mM sodium phosphate buffer. The extract was cleaned by centrifugation at 13 000 g at 4°C for 15 min, followed by measurement of the protein concentration. Samples of equal protein content were loaded on a 10% native PAGE gel and separated at constant 20 mA/gel for 2 h. Gels were preincubated in 50 mM sodium phosphate buffer, pH 7.8 for 10 min after separation. SOD isoform activities and their specific inhibition were visualized as described by Takáč et al. (2014).

Both immunoblotting and enzyme activity analyses were performed in three biological replicates and the statistical significance was evaluated using one-way ANOVA test.

Extraction of proteins for proteomic analysis was performed according to Takáč et al. (2017) with slight modification. Fresh material from 1g of roots and 500 mg of nodules was homogenized in liquid nitrogen with 1 ml of cold extraction medium (0.9 M sucrose, 0.1 M Tris-HCl (pH 8.8), 10 mM EDTA, 100 mM KCl, and 0.4% (v/v) 2-mercaptoethanol) and an equal amount of Tris-HCl-buffered phenol. The following steps were carried out as described in Takáč et al. (2017). The nano-liquid chromatography followed by tandem mass spectrometry analysis

(nLC-MS/MS) was performed in the laboratory of Dr. Tibor Pechan (Mississippi University, Starkville) as a service.

4.2 Results

4.2.1 MAPK activation in SIMKKi line in response to elicitation and *Sinorhizobium meliloti*

Within the following experiments, we aimed to monitor the abundance and activation of SIMK, a MAPK acting downstream of SIMKK, in response to flg22 elicitation, and in response to *S. meliloti* inoculation. Afterward, we attempted to uncover proteins, metabolic processes or signaling events occurring downstream of SIMKK in response to symbiotic bacteria *S. meliloti* by comparative shot-gun proteomic analysis.

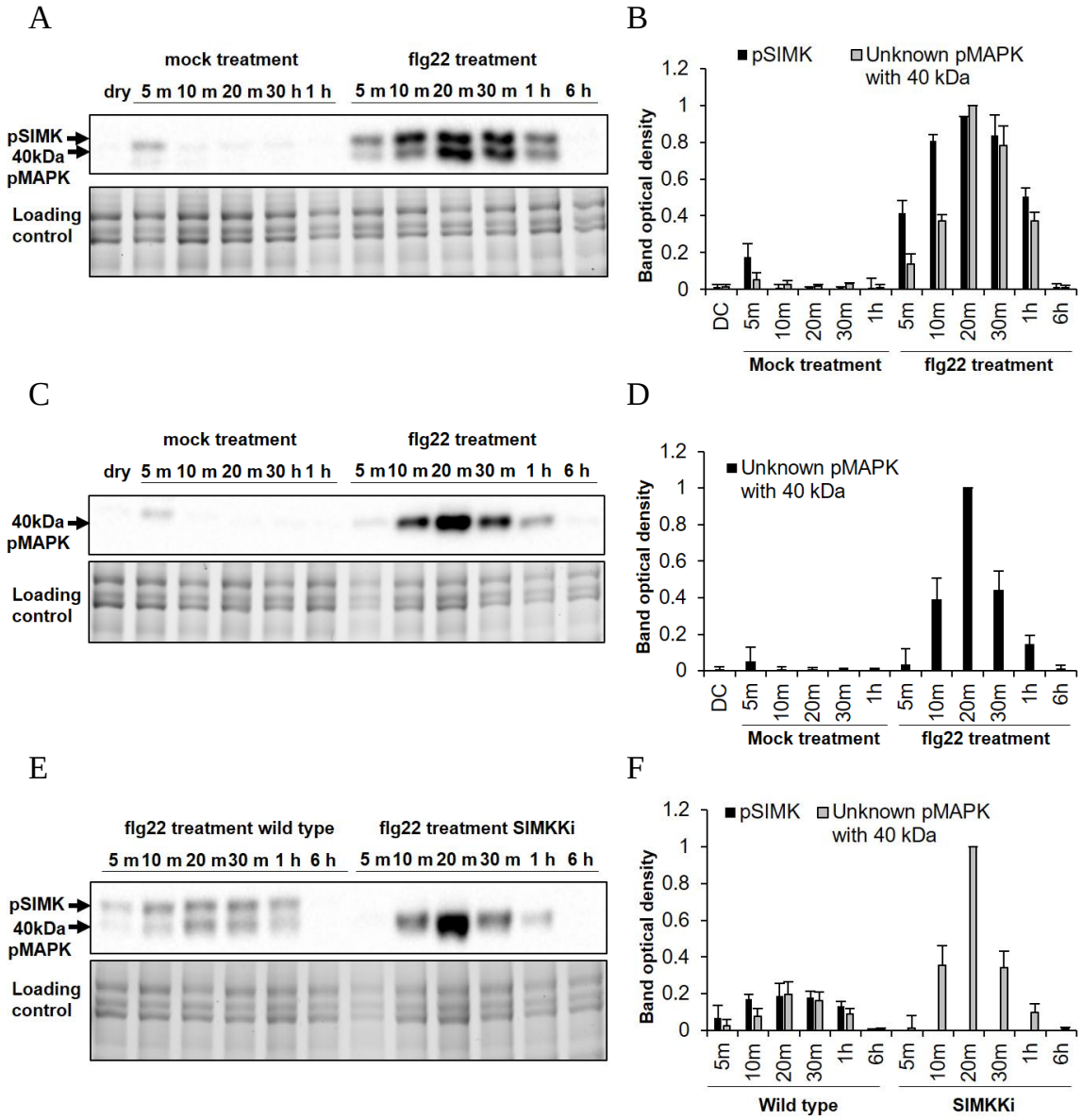

Figure 2 Effect of flg22 on activation of MAPKs in roots of alfalfa wild type and SIMKKi line. Fifteen-days-old wild type (RSY) and SIMKKi plants were treated by 200 nM flg22 for different time periods. (A, C, E) Immunoblot analysis of MAPK activation by using phosphospecific anti-pERK antibody on root protein extracts. (A) Treatment of wild type with mock treatment and flg22. (C) Treatment of SIMKKi line with mock treatment and flg22. (E) Comparison of wild type and SIMKKi line after flg22. (B, D, F) Quantification of band optical densities of phosphorylated MAPKs. All densities are expressed as relative to the highest value. Error bars represent standard deviation.

Flg22 treatment lead to appearance of two bands with 46 kDa and 40 kDa on immunoblots prepared using pERK antibody in wild type roots (Figure 2). Time course observation of MAPK activation showed that the intensity of both bands peaked after 20 min of flg22 treatment, followed by continuous decrease (deactivation). SIMK activation showed a steeper rise compared to the 40 kDa band. Immunoblotting analysis indicated that SIMK abundance did not change after 20 min flg22 treatment (Figure 3). Very similar results were obtained upon inoculation of wild type plants with *S. meliloti* suspension culture (Figure 4), thus confirming the common initial signaling events for pathogenic and symbiotic plant-bacteria interactions.

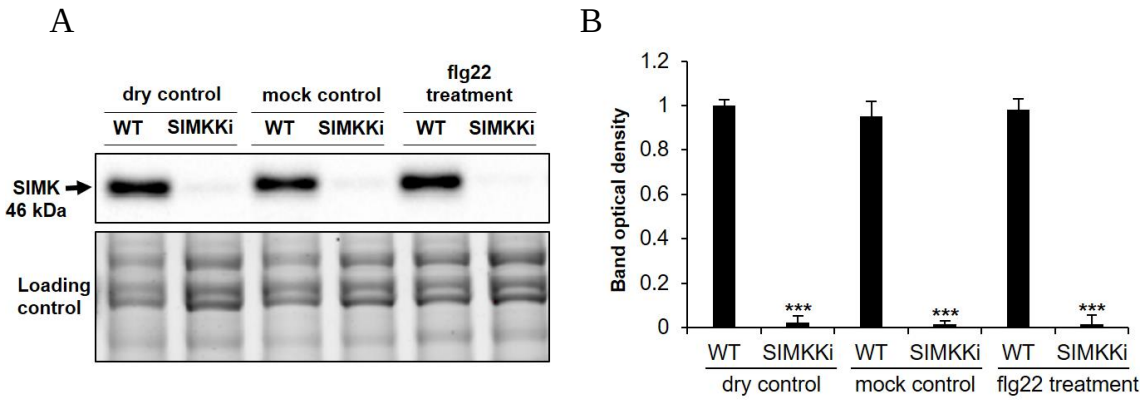

Figure 3 Effect of flg22 on SIMK abundance in roots of alfalfa wild type and SIMKKi line. Fifteen-days-old wild type (RSY) and SIMKKi line plants were treated by 200 nM flg22 or MS medium for 20 min. (A) Immunoblot analysis of SIMK abundance by using anti-MPK6 antibody in root protein extracts. (B) Quantification of band optical densities. All densities are expressed as relative to the highest value. Error bars represent standard deviation. Stars indicate statistically significant difference (one-way ANOVA, ***p < 0.001).

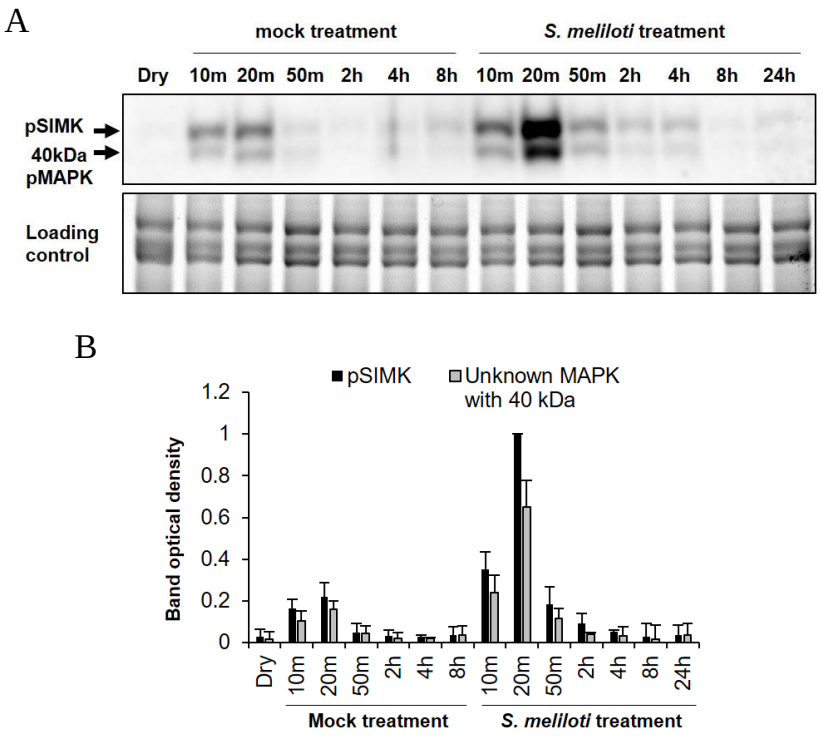

Figure 4 Activation of MAPKs after *S. meliloti* treatment in roots of alfalfa wild type. Fifteen-days-old plants were treated by *S. meliloti* for different time periods. (A) Immunoblot analysis of MAPK activation by using phosphospecific anti-pERK antibody in root protein extracts. (B) Quantification of band optical densities of phosphorylated MAPKs. All densities are expressed as relative to the highest value. Error bars represent standard deviation

As expected from the previously published results (Bekešová et al., 2015), only one band (with 40 kDa) was resolved on immunoblots prepared from SIMKKi line (Figure 2). The band corresponding to SIMK was not present in SIMKKi line, owing to its strong downregulation (Figure 3; Bekešová et al., 2015). To compare the rate of activation of MAPK with 40 kDa in wild type and SIMKKi line, both samples were loaded on one gel keeping equal protein loading. This experiment showed that the examined MAPK was over-activated in SIMKKi line (Figure 2E, F) suggesting possible a compensatory mechanism.

Next, we wanted to elucidate the impact of SIMKK downregulation on nodule formation. The quantitative phenotypic analysis showed that the SIMKKi line formed roughly half of the nodules as compared to wild type (Figure 5), suggesting that SIMKK and SIMK are involved in nodulation evoked by *S. meliloti*.

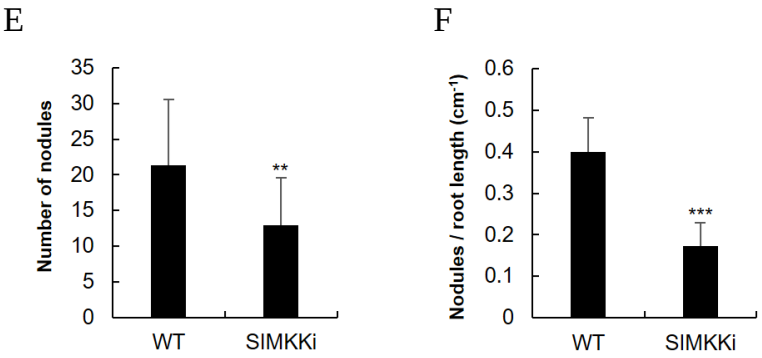

Figure 5 Nodule formation in roots of alfalfa wild type and SIMKKi seedlings inoculated with *S. meliloti*. (A) Quantification of the number of nodules and (B) number of nodules per root length (cm^{-1}) at 20 days after inoculation. Phenotypic analysis was performed in three repetitions (n = 30). Error bars represent standard deviation. Stars indicate statistically significant difference (one-way ANOVA, **p < 0.01; ***p < 0.001).

4.2.2 Proteome-wide examination of processes regulated by SIMKK

Within the following experiments, comparative shotgun proteomic analyses were employed to gain more insights into the processes regulated by SIMKK in alfalfa.

First, we compared root proteomes of wild type with SIMKKi line, and the differential proteome was evaluated using bioinformatics. Prior to proteomic analysis, we successfully proved the SIMK downregulation in SIMKKi plants using immunoblotting (Figure 6).

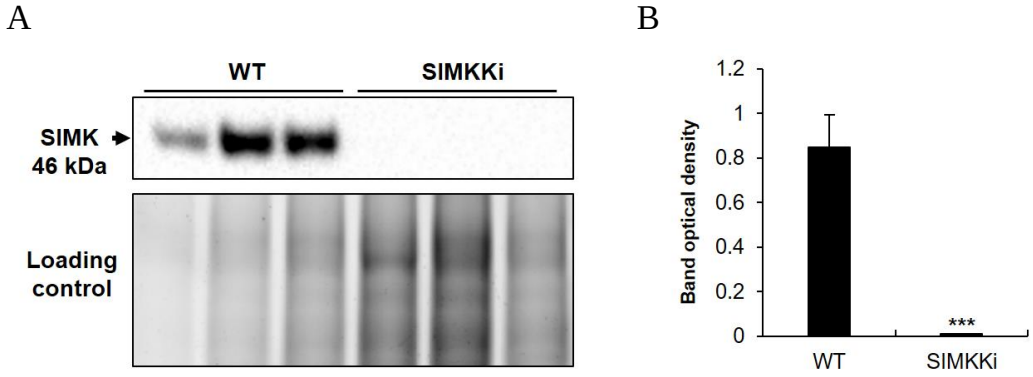

Figure 6 Analysis of SIMK abundance in *S. meliloti*-treated wild type and SIMKKi line in roots. (A) Immunoblot analysis by using anti-MPK6 antibody on three replicates of wild type and SIMKKi line. The anti-MPK6 antibody specifically recognizes SIMK. (B) Quantification of band optical densities. Densities are expressed as relative to the highest value and normalized according to loading control differences. Error bars represent standard deviation. Stars indicate statistically significant difference (one-way ANOVA, ***p < 0.001).

Together 129 differentially abundant proteins (DAPs) were identified and evaluated. Among them, 49 proteins were more abundant and 36 were less abundant in SIMKKi line. Twelve proteins were unique for SIMKKi line, while 32 proteins were found solely in the wild type. DAPs are mostly assigned to metabolic GO annotations, while catabolic and biosynthetic processes appeared as balanced. Substantial number of DAPs are involved in response to stimulus, stress as well as chemical. Fourteen proteins belong to GO annotation called establishment of localization and 13 to transport. In terms of cellular compartment, DAPs were mostly localized in cytoplasm, but we detected also membranous, plastidic, nucleolar and extracellular proteins. Remarkably, SIMKK downregulation may lead to the disturbance of protein complexes.

Eleven DAPs belong to NAD(P)-binding domain superfamily, indicating that processes connected to redox homeostasis might be affected in the transgenic line. Haem peroxidases, thiolases and aldolase type TIM barrel family of proteins were also abundant within the DAPs. KEGG pathway analysis allows acquiring insight into the status of metabolic processes in the studied material. SIMKK downregulation negatively affected the starch and glucose metabolism as well as glycolysis/gluconeogenesis. In addition, carbon fixation, amino acid metabolism, galactose pyruvate and glyoxylate and dicarboxylate metabolism were affected as well. SIMKKi line show also downregulation of proteins involved in nitrogen metabolism, such as two isoforms of glutamate dehydrogenase, CARBONIC ANHYDRASE 2 ISOFORM X1 and FERREDOXIN-DEPENDENT GLUTAMATE SYNTHASE. Closer inspection of stress related proteins showed that some important proteins involved in redox homeostasis and oxidative stress were upregulated including 4 peroxidase isoforms, two peroxiredoxin isoforms and MnSOD in SIMKKi line. On the other hand, CATALASE 4, PEROXIDASE 3 and L-ASCORBATE OXIDASE HOMOLOG were downregulated. This data indicates the involvement of SIMKK in redox homeostasis regulation.

Other remarkable findings are the downregulation of RHICADHESIN RECEPTOR, SUCROSE SYNTHASE and upregulation of NODULIN RELATED PROTEIN 1, all participating in the symbiotic interaction. Membrane transport is apparently deregulated in SIMKKi, as proposed by the downregulation of the seven proteins (for example CLATHRIN HEAVY CHAIN 1, V-TYPE PROTON ATPASE SUBUNIT C, RAS-RELATED PROTEIN RAB 7, COATOMER SUBUNIT GAMMA) involved in this process. Interestingly, the SIMKK downregulation had an impact on the differential abundance of HEAT SHOCK FACTOR-BINDING PROTEIN 1, HEAT SHOCK COGNATE 70kDa PROTEIN 2, HSP70-HSP90 ORGANIZING PROTEIN 3 indicating the involvement of SIMKK in heat stress response. In order to validate the proteomic data, immunoblotting analysis using specific primary antibodies against HSP70, catalase and MnSOD was carried out. The obtained differences in protein abundance were in agreement with the proteomic data (Figure 7A-D and 8A, B). We also tested whether increased abundance of MnSOD will be reflected in the level of MnSOD activity in the SIMKKi line using SOD activity staining on native PAGE gels. This analysis confirmed the significantly increased MnSOD activity in the transgenic line (Figure 8C, D). Other SODs isoforms did not show significant difference in activity.

Our results show, that SIMKK downregulation leads to disturbance in homeostasis of proteins involved in metabolism, redox regulation, abiotic and biotic stress response as well as membrane transport. The functional links of these proteins to SIMKK signaling and phenotypes of SIMKKi line are discussed in the Discussion section.

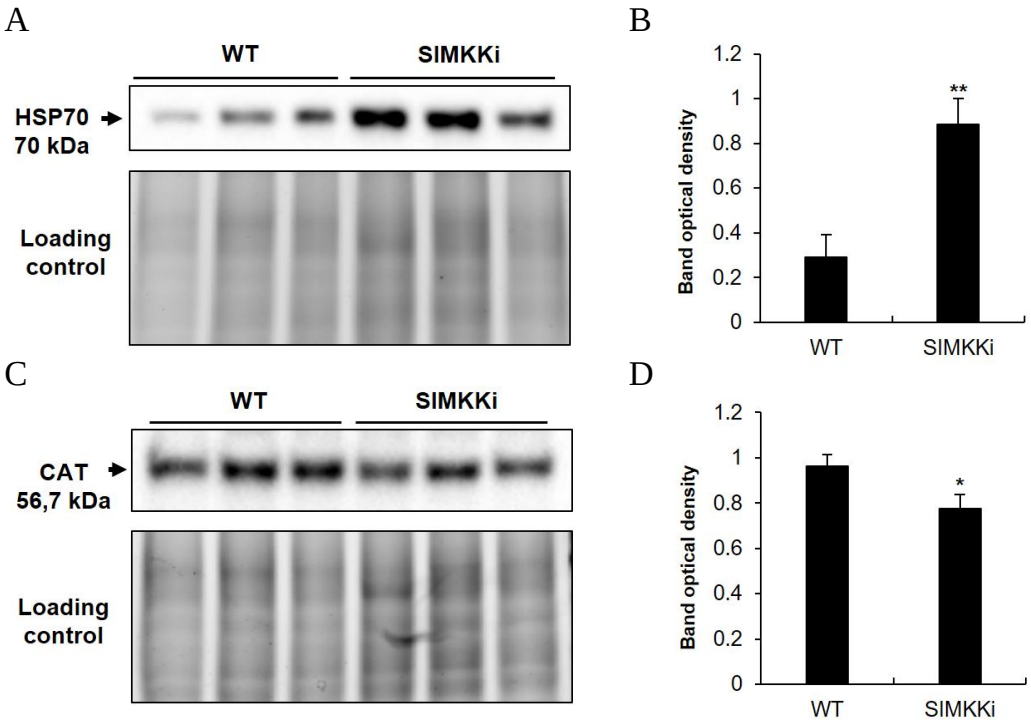

Figure 7 Analysis of HSP70 and catalase abundances in non-treated alfalfa wild type and SIMKKi line roots. (A, C) Immunoblot analysis by using anti-HSP70 antibody (A) and anti-CAT antibody (C) on three replicates of wild type and SIMKKi line. (B) Quantification of band optical densities in (A). (D) Quantification of band optical densities in (C). Densities are expressed as relative to the highest value. Error bars represent standard deviation. Stars indicate statistically significant difference (one-way ANOVA, *p < 0.05, **p < 0.01).

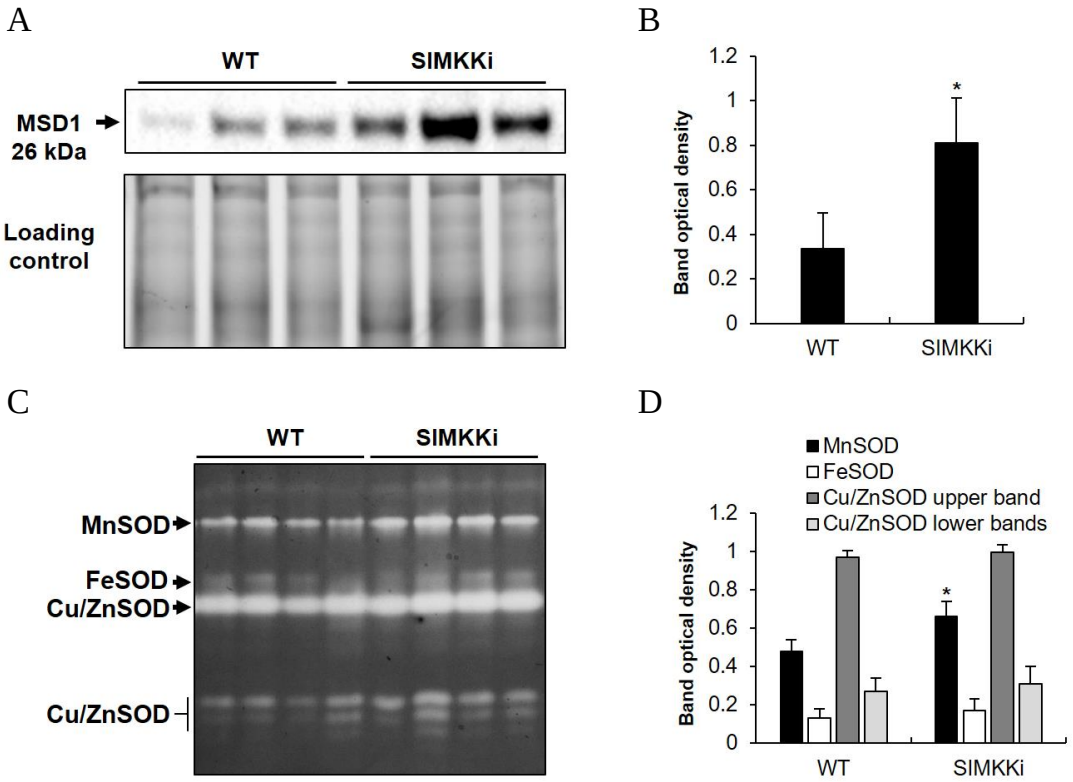

Figure 8 Analysis of MnSOD abundance and SOD isoenzymes activities in non-treated alfalfa wild type and SIMKKi line roots. (A) Immunoblot analysis by using anti-MnSOD antibody on three replicates of wild type and SIMKKi line. (B) Quantification of band optical densities in (A). (C) Visualization of SOD isoenzymes activities on native polyacrylamide gels by specific staining. (D) Quantification of band optical densities in (C). Densities are expressed as relative to the highest value. Error bars represent standard deviation. Stars indicate statistically significant difference in individual isoforms between SIMKKi and wild type (one-way ANOVA, *p < 0.05).

Within the next experiment, we compared the responses of both lines to 6 h long *S. meliloti* inoculation to monitor the impact of SIMKK downregulation on the initial events undergoing upon alfalfa-rhizobia interaction. We have identified 70 and 92 differentially abundant proteins in wild type and SIMKKi line, respectively. Similar to the previous experiment, we adopted GO annotation and compared the differential proteomes of both lines. The *S. meliloti* inoculation led to differential regulation of metabolic proteins, mainly in favor of biosynthetic, compared to catabolic processes in both lines. Proteins involved in response to stress, gene expression, translation and transport were substantially affected as well. In terms of cellular compartment, the differential proteome consisted mainly from cytoplasmic, membranous, nuclear, mitochondrial proteins as well as proteins in protein complexes. Most striking differences between the examined lines were observed in GO annotations named cellular nitrogen compound metabolic process, organic cyclic compound metabolic process and response to stress, all being prevalently abundant in wild type. Proteins localized in mitochondria and the endomembrane system were more affected in wild type. Concerning protein families, *S. meliloti* treatment affected 7 proteins belonging to NAD(P) binding domain superfamily, while just one was found in wild type. Oppositely, 4 and 1 protein belonging to START-like domain superfamily were found in wild type and SIMKKi, respectively. Transgenic line exhibited also more proteins from thioredoxin superfamily, RNA binding domain superfamily or pyridoxal phosphate dependent transferase domain family.

Detailed views on the differential proteomes showed that wild type responded to *S. meliloti* by upregulation of antioxidant defense, as exemplified by increased abundance of Cu/Zn SUPEROXIDASE DISMUTASE, L-ASCORBATE PEROXIDASE 3 and PEROXIDASE A2. This is confirmed also by the staining of SOD specific activity on native gels indicating dramatically increased activities of Cu/ZnSODs in the 6 h after inoculation by *S. meliloti* in wild type plants, which is not observed in SIMKKi line (Figure 9A, B). These antioxidant enzymes were not detected as significantly affected in SIMKKi. Nevertheless, signs of favorable redox regulation are present also in SIMKKi differential proteome by increased abundance of THIOREDOXIN H TYPE. The abundance of two glutathione S-transferases had opposing abundances in SIMKKi line. These data may indicate that different from SIMKKi, wild type plants effectively responded to ROS generated by *S. meliloti* inoculation by upregulation of ROS scavenging mechanism.

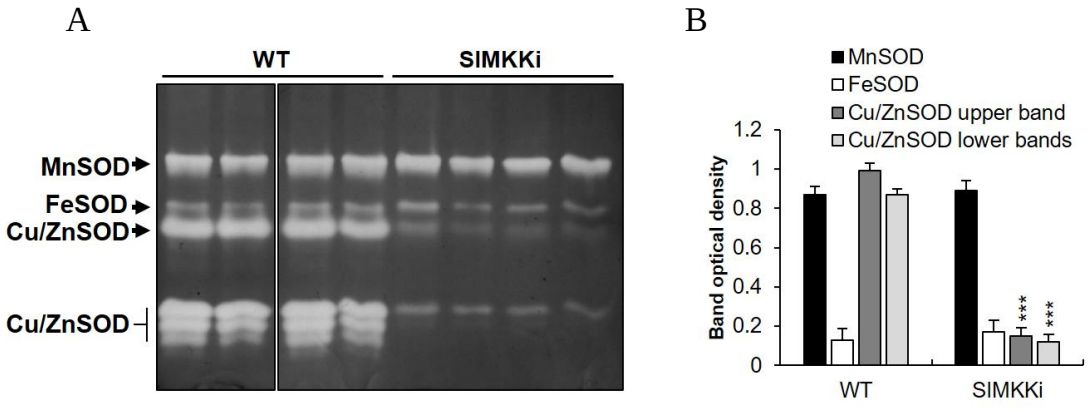

Figure 9 Comparison of individual SODs activity in *S. meliloti* treated wild type and SIMKKi line alfalfa roots. Treatment of indicated plants was performed with *S. meliloti* for 6 h. (A) Visualization of SODs isoforms activities on native polyacrylamide gels in indicated plant lines by specific staining. (B) Quantification of optical densities of bands in (A). The optical densities are displayed as relative to the highest value. Error bars represent standard deviation. Stars indicate statistically significant difference of in individual isoforms between SIMKKi and wild type (one-way ANOVA, ***$p < 0.001$).

We also found several defense related proteins to be upregulated in wild type. These include protein EXORDIUM-like 2, POLYGALACTURONASE INHIBITOR 1-LIKE, GLUCAN ENDO-1,3-BETA-GLUCOSIDASE BASIC ISOFORM ISOFORM X 1, UDP-GLUCURONIC ACID DECARBOXYLASE 6, THAUMATIN-LIKE PROTEIN 1. This upregulation was not so evident in SIMKKi line possessing rather downregulation of majority of defense related proteins. Differently to SIMKKi line, *S. meliloti* treatment disturbed the sterol homeostasis in wild type as shown by 4 sterol or steroid binding proteins.

The interrogation of nodule proteomes of wild type and SIMKKi may shed light on SIMKK regulated biochemical processes undergoing in nodules. We again examined the abundance of SIMK in nodules of wild type and SIMKKi showing downregulation in SIMKKi nodules (Figure 10A, B).

Similar to the previous experiments, the differential proteome of SIMKKi nodules also included mostly proteins involved in metabolic processes, including nitrogen compound, oxoacid, lipid, protein and carbohydrates. More of the DAPs were involved in catabolic processes compared to biosynthetic ones. Proteins involved in response to stimulus, stress and chemical were affected as well. Proteins localized to compartments such as cytosol, membrane, extracellular space, nucleus and mitochondrion were the most abundant. The peroxidase protein family was the most affected among the DAPs. Remarkably, all peroxidases were downregulated in the transgenic line.

The central enzyme of nitrogen assimilation, CYTOSOLIC GLUTAMINE SYNTHETASE shows increased abundance in the mutant. Interestingly, SIMKK downregulation leads to deregulation of endoplasmic reticulum proteins involved in protein folding. This may indicate the onset of endoplasmic reticulum stress in the SIMKKi line.

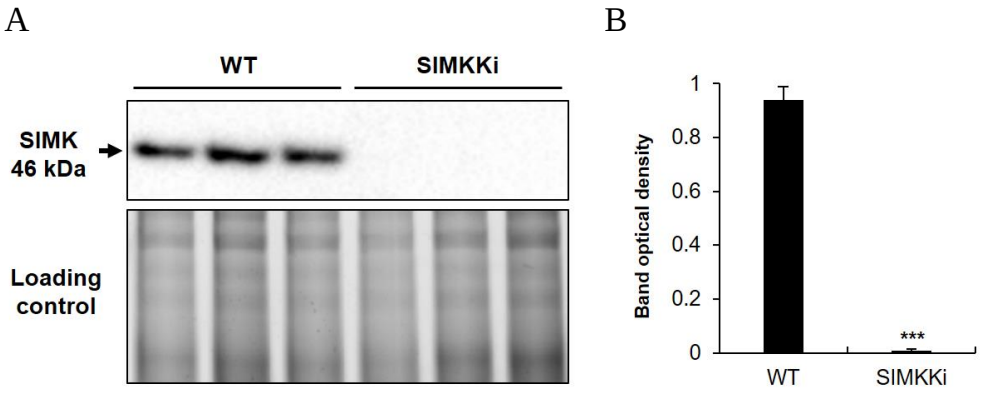

Figure 10 Analysis of SIMK abundance in nodules of wild type and SIMKKi line. (A) Immunoblot analysis by using anti-MPK6 antibody in three replicates of wild type and SIMKKi line. The anti-MPK6 antibody specifically recognizes SIMK. (B) Quantification of band optical densities. Densities are expressed as relative to the highest value. Error bars represent standard deviation. Stars indicate statistically significant difference (one-way ANOVA, ***$p < 0.001$).

KEGG pathway analysis showed that SIMKK downregulation in nodules affected processes connected with carbon processing and assimilation such as glycolysis/gluconeogenesis, carbon fixation, pentose phosphate pathway, and pyruvate, glyoxylate and dicarboxylate metabolism. SIMKKi line show also downregulation of proteins involved in nitrogen metabolism.

4.3 Discussion

SIMKK is a stress induced alfalfa MAPKK acting upstream of SIMK (Kiegerl et al., 2000). Interestingly, SIMKK downregulation leads to almost complete silencing of SIMK in SIMKKi plants (Bekešová et al., 2015; Hrbáčková et al., 2020, our study). SIMK is activated by bacterial elicitation (Cardinale et al., 2000) or salt stress (Ovečka et al., 2014). Its heterologous overexpression in *Arabidopsis* leads to hypersensitivity to salt stress, which was consistent with the constitutive proteome of the SIMKK-YFP (yellow fluorescent protein) overexpressing *Arabidopsis* plants (Ovečka et al., 2014).

MAPK mutants often possess altered expression and abundances of stress related proteins and this may be explained by their essential role in regulation of stress responses (Frei dit Frey et al., 2014; Takáč and Šamaj, 2015). Our results show upregulation of enzymes involved in antioxidant defense in SIMKKi line, including four isoforms of secretory peroxidases, MnSOD, PEROXIREDOXIN-2E and 2-Cys PEROXIREDOXIN BAS 1, thus underlining the SIMKK and SIMK mediated regulation of antioxidant defense in alfalfa. This might indicate that SIMKK negatively regulates the expression of *MnSOD*, *PEROXIREDOXIN-2E* and *2-Cys PEROXIREDOXIN BAS1*. So far, evidence exists about the MPK6 mediated control of *FSD2*, *FSD3* (Xing et al., 2015) and *CSD1*, *CSD2* expression (Xing et al., 2013) which are located in cytosol (CSD1), and plastids (FSD2, FSD3, CSD2). The possible link between MAPKs and mitochondrial MSD1 was not reported yet. We hypothesize, that SIMK regulates *MnSOD* on expression level via mitochondrial retrograde signaling. Mitochondrial proteins represented a substantial portion of the differential proteome of SIMKKi line. Furthermore, SIMK ortholog MPK6 was shown to transduce the mitochondria generated retrograde signal in *Arabidopsis* (Chang et al., 2012).

This elevated antioxidant defense, in hand with the hypersensitivity of the SIMKK-YFP overexpressing *Arabidopsis* (Ovečka et al., 2014), may suggest better survival of SIMKKi transgenes under abiotic stress. Anticipating from our differential proteome, heat stress is another promising candidate, because SIMKKi line show elevated levels of HEAT SHOCK FACTOR-BINDING PROTEIN 1, HEAT SHOCK COGNATE 70 kDa PROTEIN 2 and HSP70-HSP90 ORGANIZING PROTEIN 3, all implicated in heat stress response (Hsu et al., 2010). In this case, alfalfa SIMKK-SIMK signaling module may have roles resembling *Arabidopsis* MPK6, which phosphorylates heat stress factor HSFA2 during heat stress response (Evrard et al., 2013).

Secretory peroxidases are ubiquitous enzymes with multiple functions. Except for their antioxidant roles, they have also an ability to generate H_2O_2, thus contributing to cell wall loosening in order to promote cell elongation (Passardi et al., 2006; Almagro et al., 2009). This function of peroxidases is connected to MAPKs, as MPK6 can control the expression of *PEROXIDASE 34* to regulate *Arabidopsis* root elongation (Han et al., 2015). This again supports the close similarity of *Arabidopsis* MPK6 and SIMK.

MAPK signaling cascades were earlier showed to be activated upon plant infection with symbiotic rhizobia (Lopez-Gomez et al., 2012). A well-described example is MAPKK SIP2 form *Lotus japonicus*, which interacts with SYMBIOSIS RECEPTOR-LIKE KINASE SymRK (Chen et al., 2012). Moreover, SIP2 is an upstream activator of LjMPK6 and the SymRK-SIP2-MPK6 cascade is an important signaling transduction module during nodulation in *L. japonicus* (Yin et al., 2019). Additionally, MKK4 from *Medicago truncatula* is an orthologue of SIP2 and it is important for root nodule formation. MMK4 interacts with MtMPK3 and MtMPK6 (Chen et

al., 2017). Alfalfa SIMKK showed 88% amino acid identity with LjSIP2 (Chen et al., 2012), and shares a high amino acid similarity with MtMKK4 (Chen et al., 2017). SIMKK and SIMK regulate root hair growth (Šamaj et al., 2002, Hrbáčková et al., 2020), formation of infection threads as well as nodules (Hrbáčková et al., 2020). MKK5 from *M. truncatula,* which interacts with both MtMPK3 and MtMPK6 acts as negative player in the symbiotic nodule formation (Ryu et al., 2017).

Multiple molecular processes determine the successful establishment of plant-rhizobia interaction, including the attraction of bacteria by plant derived flavonoids, and attachment of bacteria on root hairs followed by root hair curling and subsequent signaling events (Oldroyd, 2013). The bacteria attachment is mainly facilitated by specific plant cell wall components such as lectins, arabinogalactan like proteins, but also bacterial surface components such as adhesins, glucomannans and lipopolysacharides (Downie, 2010; Janczarek et al., 2015). Ricadhesin was previously identified as a bacterial surface polysaccharide present in one of the bacterial poles with a role in rhizobacteria attachment (Smit et al., 1991). Moreover, a glycoprotein with putative rhicadhesin receptor activity was identified in pea (Swart et al, 1994). A protein named RHICADHESIN RECEPTOR was substantially downregulated in SIMKKi line, indicating the possible defects in rhizobia attachment on the surface of its root hairs. The possible defects in bacterial adhesion in SIMKKi line are also supported by decreased abundance of PUTATIVE BARK AGGLUTININ LECRP A 3, bearing a legume lectin beta domain. Proteins with legume lectin domain bind to rhizobia and contribute to the bacteria attachment (Lagarda-Diaz et al., 2017). Furthermore, SIMKKi line specific deregulation of lectins is observable also after *S. meliloti* inoculation, as shown by downregulation of EPIDERMIS-SPECIFIC SECRETED GLYCOPROTEIN EP 1, a protein with bulb-type lectin domain. Altered ability for bacterial attachment likely contributes to the reduced nodulation in SIMKKi line.

SIMKK and SIMK are implicated in root hair growth and development (Šamaj et al., 2002; Hrbáčková et al., 2020). SIMK is relocalizing from nucleus to the cytoplasmic vesicles, which accumulate in tips of growing root hairs in actin dependent manner (Ovečka et al., 2014). Cytoskeletal inhibitor mediated modifications of actin disturb the SIMK distribution in the root hairs and negatively affect the root hair development (Šamaj et al., 2002). VILLIN 4, actin-binding protein highly homologous to *Arabidopsis* VILLIN 4, is considerably upregulated in SIMKKi line compared to wild type. *Arabidopsis* VILLIN 4 is involved in root elongation and root hair development by regulation of actin organization in Ca^{2+} dependent manner (Zhang et al., 2011). Furthermore, VILLIN 4 was substantially downregulated in SIMKKi line after *S. meliloti* treatment, but not in wild type. These data indicate the close link between SIMKK and VILLIN 4 in alfalfa. Villins were also identified as MAPK phosphorylation targets (Rayapuram et al., 2018), further supporting the hypothesis about the villin-mediated defects of root hair development in SIMKKi plants.

The dynamicity of membrane transport is crucially dependent on proper functioning of actin cytoskeleton (Wang et al., 2017). Therefore, actin disturbances, as those caused by villin modifications have obvious effect on membrane trafficking (Zou et al., 2019). It is reasonable to claim that SIMKK-mediated VILLIN 4 disturbances are connected to robust changes in membrane transport associated proteins, which also might participate on root hair defects in SIMKKi line. Root hair formation and elongation is tightly connected also to structural sterols, which accumulate in trichoblasts during the prebulging and bulge stages and show a polar accumulation in the tip during root hair elongation (Ovečka et al., 2010). Notably, *S. meliloti* treatment caused changes in abundances of MEMBRANE STEROID-BINDING PROTEIN 1,

OXYSTEROL-BINDING PROTEIN-RELATED PROTEIN 3 A and PROBABLE STEROID-BINDING PROTEIN 3 in wild type, while sterol metabolism was less affected in SIMKKi line. The altered homeostasis of plasma membrane sterol composition alters the protein clustering into microdomains (Gao et al., 2015) a site of localization of LYK3 an entry receptor for alfalfa infection by rhizobia (Smit et al., 2007). Our results imply plasma membrane sterol content rearrangements in wild type. This is in agreement with changes in LYK3 localization in response to bacterial inoculation (Haney et al., 2011), in a time scale comparable to the length of treatment in our experiment. It was suggested that LYK3 undergoes endocytosis similar to other receptors, such as FLS2 (Ott, 2017). Our data suggest possible differences in sterol rearrangements upon *S. meliloti* inoculation between SIMKKi and wild type line with possible impact on nodule formation.

Proteomic analyses is a powerful tool to uncover processes undergoing in nodules including nitrogen and carbohydrate metabolism as well as redox homeostasis (Larrainzar et al., 2007). Nitrogen fixation requires a constant supply of energy, which is provided by high metabolic rate (Becana et al., 2010). This leads to increased production of ROS leading to protein oxidative modifications (Matamoros et al., 2018). To avoid the negative effects of ROS, nodules are equipped with a broad battery of antioxidants (Becana et al., 2010). We have found that SIMKKi directed downregulation increased the abundance of PEROXIREDOXIN-2B, a redox buffering protein positively contributing to redox homeostasis (Dietz, 2011) indicating the suppressed regulation redox homeostasis in SIMKKi nodules. An intriguing finding is the downregulation of 5 secretory peroxidases in SIMKKi nodules. As noted above, they may contribute to apoplastic ROS production and thus affect cell wall modifications and defense responses (Fernández-Pérez et al., 2015). These results suggest that SIMKK downregulation substantially affects secretory peroxidases in nodules. Further investigation is necessary to explain this downregulation.

SIMKKi possesses elevated abundance of CYTOSOLIC GLUTAMINE SYNTHETASE, a master enzyme involved in nitrogen assimilation (Kaur et al., 2019), indicating possible increased efficiency of N assimilation. The concept of elevated N assimilation may be also substantiated by increased cysteine biosynthesis in the SIMKKi line. This increased amino acid production requires an elevated supply of carbon assimilates. PHOSPHOENOLPYRUVATE CARBOXYLASE, which provides a substantial portion of carbon required for nitrogenase activity and ammonia assimilation (Pathirana et al., 1992) is downregulated in the transgenic line. Moreover, energy-providing glycolysis shows also disturbances, since glycolytic enzymes such as FRUCTOSE-BISPHOSPHATE ALDOLASE, PHOSPHOGLYCERATE KINASE, both cytosolic, show altered abundances. Taken together, except for reduced nodule formation, SIMKKi nodules exhibit apparent disturbances in N assimilation and carbon supply.

5 PART III – 3 FSD1 is a plastidial, cytosolic and nuclear enzyme and plays a role in *Arabidopsis* root development and stress tolerance

5.1 Materials and methods

Herein, the plant material and methods used are summarized. All details are described in the Ph.D. thesis.

Seeds of *Arabidopsis thaliana* (L.) Heynh of the wild-type Columbia (Col-0) and *fsd1-1*, *fsd1-2* and *A. thaliana* transgenic line carrying *35S::sGFP* construct cloned using pMAT037 plasmid were used for the following experiments.

For cloning of GFP-tagged FSD1 gene both C- and N-terminal fusion constructs of eGFP with genomic DNA of FSD1 (pFSD1-gFSD1::GFP:3ˈUTR-FSD1 (GFP-FSD1) and pFSD1::GFP:gFSD1-3ˈUTR-FSD1 (FSD1-GFP)) were cloned under its native promoter from *Arabidopsis* wild type (Col-0). MultiSite Gateway® Three-Fragment Vector Construction (Thermo Fisher Scientific) was used as the cloning method for the preparation of these constructs. Sequencing-validated cloning products were transformed into *Agrobacterium tumefaciens* GW3101, and used further for floral dip stable transformation of *fsd1-1* and *fsd1-2* mutants. Selected lines with one insertion were propagated into T3 homozygous generation and used in further experiments.

Immunoblotting and SOD isoenzymatic activities on native PAGE were performed as described in section 4.1 with slight modifications. For immunoblotting, seedlings of each line were homogenized into fine powder in a mortar with liquid nitrogen. Membranes were blocked by overnight incubation of the membrane either in 5% low-fat dry milk (for the detection of FSD1) or in 4% low-fat dry milk and 4% BSA (for detection of GFP), in TBS-T. The membranes were incubated with anti-FSD primary antibodies (both Agrisera, dilution 1:3000 in TBS-T with 3% low-fat dry milk) primary antibody at 4°C overnight. Membranes were incubated with a secondary antibody diluted in TBS-T containing 1% BSA for 1.5 h. Horseradish peroxidase-conjugated goat anti-rabbit IgG secondary antibody (Thermo Scientific, both diluted 1:5000) was used for the detection of FSD1.

For the detailed root phenotyping, seedlings were recorded daily and documented using a scanner (ImageScanner TM III, Little Chalfont, UK) and ZOOM microscope (Leica MZ FLIII 165FC, Mannheim, Germany) for two weeks. The primary root lengths of 7- and 10- day-old seedlings were measured from the individual scans using ImageJ. Lateral root number was counted on the 7^{th} and 10^{th} day after germination and it was standardized to the primary root length. Fresh weight of 14-day-old seedlings was measured from 30 plants in three independent repetitions for each plant line.

For co-immunoprecipitation, 3g from 14-day-old *fsd1-1* lines complemented by either FSD1-GFP or GFP-FSD1 constructs (both in four repetitions) were used. Proteins were extracted using extraction buffer (50 mM Tris-HCl (pH 7.5), 150 mM NaCl, 1% Nonidet P-40 (NP40), protease inhibitors mix cocktail) for 30 min. Subsequently, supernatant was collected after centrifugation. The co-immunoprecipitation (by using anti-GDF beads; Miltenyi Biotec) and the preparation of protein digest was performed according to Hunter et al. (2019). The mass spectrometry analysis and the protein identification from eluted fractions was performed as a commercial service at University of Turku.

For immunofluorescence labelling of the root tips according to the protocol established by Šamajová et al. (2014) with minor modifications. Samples were incubated with rat anti-FSD (Agrisera) primary antibody diluted at 1:250, in phosphate-buffered saline (PBS) containing 3% BSA at 4°C overnight. In the next step, samples were incubated with Alexa-Fluor 488 conjugated goat anti-rat secondary antibody diluted at 1:500 in PBS with 3% BSA at room temperature for 3 h. DNA was counterstained with 250 $\mu g \cdot ml^{-1}$ 4,6-diamidino-2-phenylindole (DAPI, Sigma-Aldrich) in PBS for 10 min. After a final wash in PBS, the specimens were mounted in an antifade solution (0.5% (w/v) p-phenylenediamine in 90% (v/v) glycerol in PBS or 1 M Tris-HCl, pH 8.0) or in the commercial antifade VectashieldTM (Vector Laboratories).

Germination analysis of Col-0, both *fsd1* mutants and *fsd1-1* complemented lines (GFP-FSD1 and FSD1-GFP) was performed on 1/2 MS medium with and without 150 mM NaCl. Plates with seeds were kept at 4°C for 2 days and incubated as mentioned above. Percentage of

germinated seeds (with visible radicle) was counted under stereomicroscope after 24, 48, and 78 h.

For salt stress sensitivity determination, 4-day-old seedlings of Col-0, *fsd1* mutants and *fsd1-1* complemented lines (GFP-FSD1 and FSD1-GFP) growing on 1/2 MS medium were transferred to 1/2 MS medium containing 150 mM NaCl. The ratio of bleached seedlings was counted at the 5th day after transfer. Both Measurements were performed in four repetitions and statistical significance was tested by one-way ANOVA test.

For plasmolysis induction, 4-day-old seedlings of *fsd1-1* complemented lines (FSD1-GFP and GFP-FSD1) and *Arabidopsis* transgenic line expressing *35S::eGFP* were mounted between glass slide and coverslip in liquid 1/2 MS media. Plasmolysis was induced with 500 mM NaCl (hypocotyls) or 250 mM NaCl (roots) in liquid 1/2 MS media applied by perfusion. Plasmolysed cells were observed 5–30 min after the perfusion by confocal laser scanning microscopy (CLSM) 880 equipped with an Airyscan detector (ACLSM, Carl Zeiss, Germany).

For oxidative stress analysis, all lines were grown on 1/2 MS medium and 4-day-old seedlings were transferred to 1/2 MS medium containing 2 μM MV. The ratio of seedlings with fully green cotyledons was counted at the 5th day after transfer. Measurements were performed in four repetitions. Measurements were performed in four repetitions.

The relative amount of chlorophyll a and b was measured from 30 seedlings of each line according to Barnes et al. (1992). The measurement correlated to the weight of examined seedlings was performed in three repetitions and both oxidative stress analysis were evaluated by one-way ANOVA test.

Three-day-old seedlings of *fsd1-1* mutants carrying recombinant GFP-fused FSD1 were used for microscopy. Imaging of living or fixed samples was performed using a confocal laser scanning microscope LSM710 (Carl Zeiss, Germany) and ACLSM (Carl Zeiss, Germany). Image acquisition was done with 20× (0.8 numerical aperture (NA)) dry Plan-Apochromat, 40× (1.4 NA) and 63× (1.4 NA) Plan-Apochromat oil-immersion objectives. Samples were imaged with a 488 nm excitation laser using emission filters BP420–480+BP495–550 for eGFP detection and BP 420–480 + LP 605 for chlorophyll a detection. Laser excitation intensity did not exceed 2% of the available laser intensity range. Immunolabelled samples were imaged using the excitation laser line 488 nm and emission spectrum 493–630 nm for Alexa-Fluor 488 fluorescence detection, and excitation laser line 405 nm and emission spectrum 410–495 nm for DAPI. Images were processed as single plane maximum intensity projections of Z-stacks in Zen Blue 2012 software (Carl Zeiss, Jena, Germany), assembled and finalized in Microsoft PowerPoint to final figures.

For light-sheet fluorescence microscopy seedlings were inserted into fluorinated ethylene propylene (FEP) tubes with an inner diameter of 2.8 mm and wall thickness of 0.2 mm (Wolf-Technik, Germany), in which roots grew in the block of the culture medium inside the FEP tube, while the upper green part of the seedling developed in an open space of the FEP tube with access to the air (Ovečka et al., 2015). Sample was inserted into a sample holder and placed into the observation chamber of the light-sheet Z.1 fluorescence microscope (Carl Zeiss, Germany). The sample chamber of the microscope was filled with sterile 1/2 MS medium and tempered to 21°C using the peltier heating/cooling system. Developmental live cell imaging was done with dual-side light-sheet illumination using two light sheet fluorescence microscopy 10× (0.2 NA) illumination objectives (Carl Zeiss, Germany) with excitation laser line 488 nm,

beam splitter LP 560 and with emission filter BP505–545. Image acquisition was done with a W Plan-Apochromat 20× (1.0 NA) objective (Carl Zeiss, Germany) and images were recorded with the PCO. Edge sCMOS camera (PCO AG, Germany) with an exposure time of 100 ms and imaging frequency of every 2 min in the Z-stack mode for 2–20 h.

The post-processing, default deconvolution and profile measurement of all fluorescence images in this study, including 3D reconstruction or maximum intensity projection from individual Z-stacks and creating subsets was done using ZEN 2010 software.

For Bioinformatics predictions AthaMap (Hehl et al., 2016) was used to predict possible TFs binding to cis-elements present in promoter sequence of FSD1. Identified putative TFs were analyzed with GPS 3.0 (Species Specific, All kinases; Xue et al., 2005) and annotated by PhosPhAt 4.0 (Zulawski et al., 2013) to obtain information about possible and experimentally confirmed phosphorylation and presence of phosphopeptides. The presence of MAPK-specific docking sequence in TFs protein sequences (retrieved from Araport11; Cheng et al., 2017) was evaluated by ELM (Cell compartment: not specified, Taxonomic Context: *Arabidopsis thaliana*; Kumar et al., 2020). Coexpression of identified TFs with FSD1 and MPK3, MPK4, and/or MPK6 was inspected by ATTED-II (CoExSearch; Obayashi et al., 2018).

Constructs for GST-SPL1 (Glutathione S-transferase tag), MBP-SPL1 (Maltose-binding protein tag), MBP-SPL7 and MBP-FSD1 recombinant proteins were generated using double restriction and ligation into pGEX-6P-1 (Sigma-Aldrich) and pMAL-p2 (NEB) vectors, respectively. Final product was transformed into *E. coli* BL21 Star (DE3). Constructs of GST-MPK3 and GST-MPK6 were kindly provided by Michael Wrzaczek (Helsinki University). The protein expression, purification and *in vitro* kinase assay were performed according to Hunter et al., (2019). Myelin basic protein (MyBP; Sigma-Aldrich) was used as an artificial substrate for *in vitro* kinase assay.

5.2 Results

5.2.1 Verification of rescued *fsd1* mutants by prepared constructs

For the elucidation of *FSD1* expression and localization *in vivo*, we generated stably transformed *fsd1* mutants carrying *FSD1* under its own native promoter and fused with GFP to both N- and C-terminus. All lines with one insertion were propagated into the T3 homozygous generation.

The presence of FSD1 protein and its GFP-fused variants were examined in wild type and transgenic lines by immunoblotting with anti-FSD (Figure 11A, B) antibody and by analysis of SOD isoforms activities on the native PAGE gel (Figure 11C, D). Immunoblotting analysis showed the presence of FSD1-GFP and GFP-FSD1 proteins in transgenic lines. While FSD1 protein levels were comparable in wild type and FSD1-GFP line, GFP-FSD1 line showed significantly lower FSD1 abundance (Figure 11A, B). This trend was also observed at the level of FSD1 activity as examined by specific activity staining on native gels (Figure 11C, D).

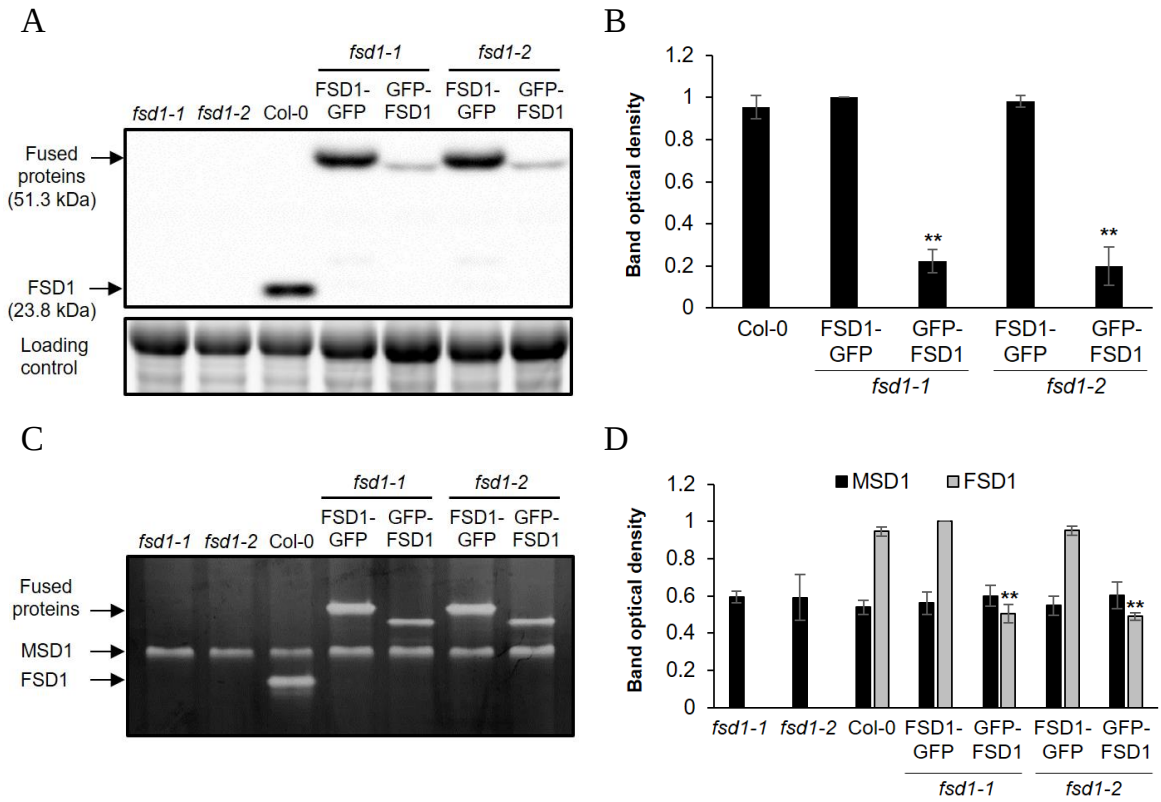

Figure 11 Verification of stably transformed *fsd1* mutant lines by GFP-FSD1 and FSD1-GFP using immunoblotting and SODs activity analysis. (A) Immunoblotting analysis of FSD1, FSD1-GFP and GFP-FSD1 abundance in 14-day-old *fsd1* mutants, Col-0 and complemented *fsd1* mutants using anti-FSD antibody. (B) Quantification of band optical densities in (A). (C) Visualization of SODs isoforms activities on native polyacrylamide gels in indicated plant lines by specific staining. (D) Quantification of optical densities of bands in (C). The optical densities are displayed as relative to the highest value. Error bars represent standard deviation. Stars indicate statistically significant difference as compared to Col-0 (one-way ANOVA, *p < 0.05, **p < 0.01). Adopted from Dvořák et al. (2021).

5.2.2 Early developmental and phenotypic analysis *fsd1* mutants and rescued lines

According to the public expression data deposited in the Genevestigator database (presented also in Pilon et al., 2011), *FSD1* is developmentally regulated and is abundantly expressed at early developmental stages. Analysis of FSD1 abundance and activity during *Arabidopsis* early seedling growth revealed that both parameters gradually increased from the 3rd to 13th DAG, but significantly decreased in following days (Figure 12A-D). Possible phenotypic consequences of FSD1 deficiency at early developmental stages were addressed in two independent homozygous T-DNA insertion *fsd1* mutants. It was found that both mutants exhibited reduced lateral root density, while no significant difference was found in the primary root length and seedling fresh weight compared to the wild type (Figure 13A-D). In summary, our data suggest, that FSD1 activity and abundance in *Arabidopsis* depends on the growth phase and its deficiency leads to reduced lateral root numbers.

The complementation of *fsd1-1* via both FSD1-GFP and GFP-FSD1 constructs leads to the reversion of the lateral root phenotypes of *fsd1* mutants (Figure 14A, C). In addition, primary root length (Figure 14B), lateral root density (Figure 14C), and seedling fresh weight (Figure 14D) in complemented lines slightly exceeded the respective values in wild type plants.

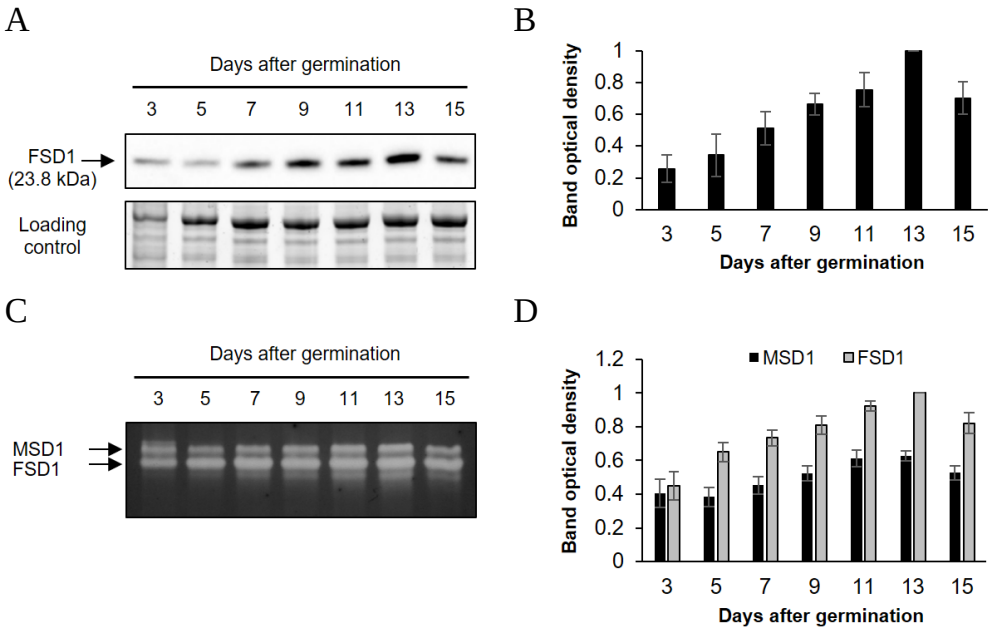

Figure 12 Early developmental analysis of *Arabidopsis* FSD1 using immunoblotting and SODs activity visualization. (A) Measurement of abundance using anti-FSD antibody during early development of wild type seedlings. (B) Quantification of optical densities of bands in (A). (C) Visualization of SOD isoform activities on native polyacrylamide gels during early development of wild type seedlings. (D) Quantification of optical densities of bands in (C). All densities are expressed as relative to the highest value. Error bars represent standard deviation. Adopted from Dvořák et al. (2021).

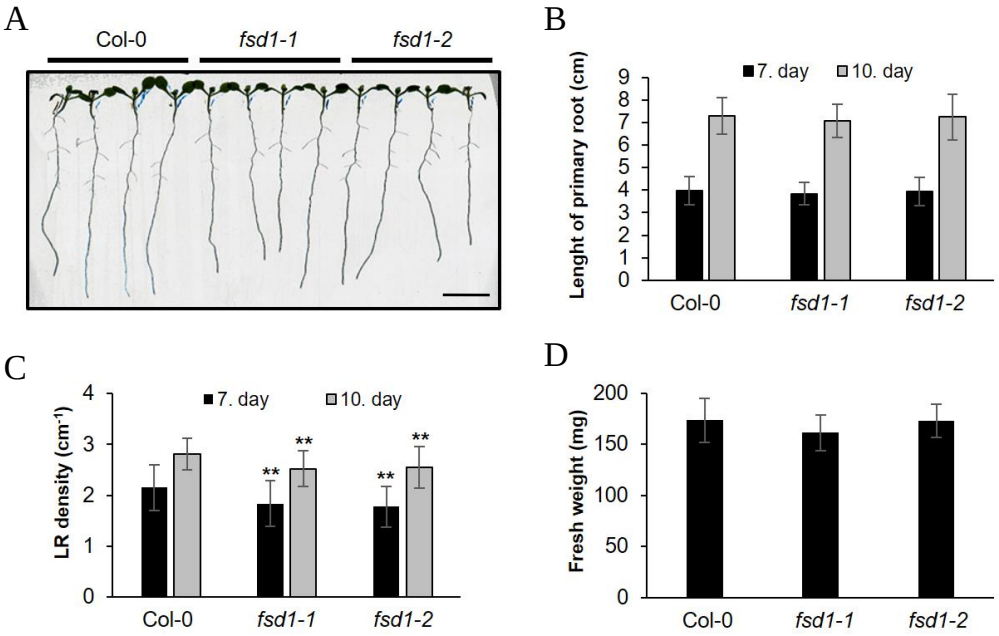

Figure 13 Phenotypical analysis of *fsd1* mutant lines. (A) Representative picture of Col-0 and *fsd1* mutants seedlings on seventh day after germination. (B-D) Quantification of primary root length (B), the lateral root density (C) of indicated 7- or 10-day-old seedlings and fresh weight of 14-day-old seedlings (D). Phenotypic analysis was performed in three repetitions (n = 90). Error bars represent standard deviation. Stars indicate statistically significant difference as compared to Col-0 (one-way ANOVA, **p < 0.01). Scale bar: 1 cm. Adopted from Dvořák et al. (2021).

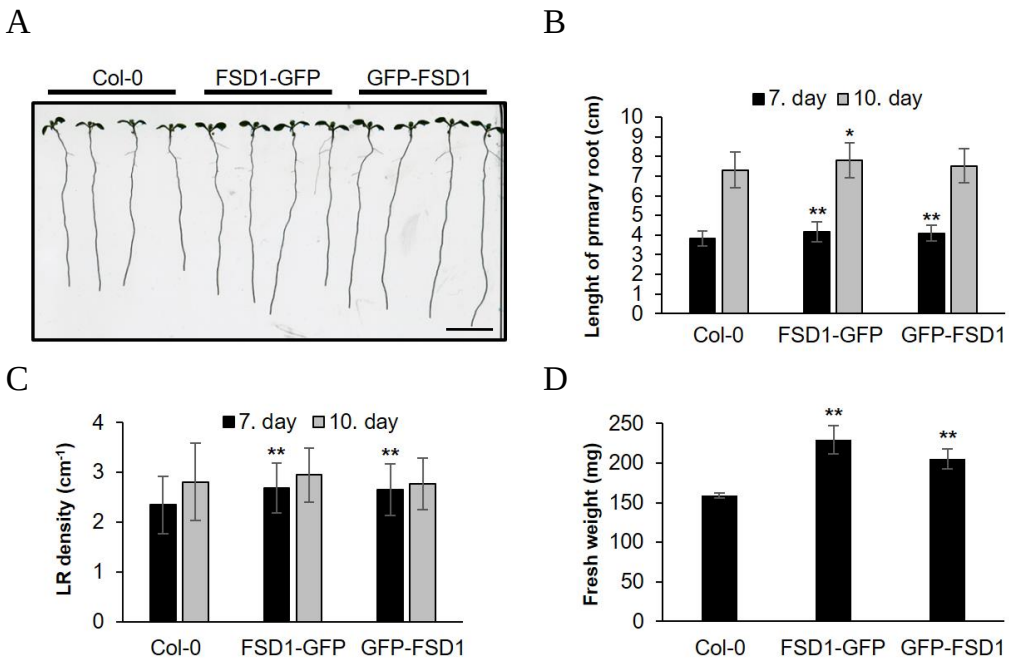

Figure 14 Phenotypical analysis of complemented line of *fsd1* mutant. (A) Representative picture of Col-0 and *fsd1* mutants seedlings by FSD1-GFP and GFP-FSD1 on seventh day after germination. (B-D) Quantification of primary root length (B), lateral root density (C) of indicated 7- or 10-day-old seedlings and fresh weight of 14-day-old seedlings (D). Phenotypic analysis was performed in three repetitions (n = 90). Error bars represent standard deviation. Stars indicatestatistically significant difference as compared to Col-0 (one-way ANOVA, *p < 0.05, **p < 0.01). Scale bar: 1 cm. Adopted from Dvořák et al. (2021).

5.2.3 FSD1-GFP expression during germination and early seedling development

Spatial and temporal patterns of FSD1-GFP expression in the early stages of development were monitored *in vivo* using light-sheet fluorescence microscopy. This allowed the time-lapse monitoring of FSD1-GFP distribution during the whole process of seed germination at nearly environmental conditions (Figure 15). Within the first 6 h of seed germination, still before radicle emergence, we observed an increase of FSD1-GFP signal in the micropylar endosperm with a maximum at the future site of radicle protrusion (Figure 15A-G). With the endosperm rupture and emergence of the primary root, FSD1-GFP signal gradually decreased in the micropylar endosperm (Figure 15H-J), while a strong FSD1-GFP signal appeared in the fast-growing primary root (Figure 15K, L). Strong expression of FSD1-GFP was visualized in the transition and elongation zones of the primary root (Figure 15L, M), which was, however, gradually decreasing in the differentiation zone, particularly after the emergence of the root hairs in the collar region (Figure 15M-O). During seed germination, FSD1-GFP-labelled plastids in endosperm cells showed a high degree of motility. Thus, FSD1 may be involved in the process of endosperm rupture during seed germination.

After germination, which occurred during the first DAG, growth of the primary root continued and cotyledons were released from the seed coat during the second DAG. Expression levels of FSD1-GFP in emerging cotyledons were high. Hypocotyl and fully opened cotyledons in developing seedlings at fifth DAG contained moderate amount of FSD1-GFP, while the strongest signal was detectable in the shoot apex and emerging first true leaves. FSD1-GFP signal considerably increased in the lateral root primordia. Accumulation of FSD1-GFP was still visible in the apices of the lateral roots as well as in the basal parts, at the connection of the lateral roots to the primary root. In growing apex of the primary root, the strongest FSD1-GFP signal was located in the transition zone (data not shown; available in Ph.D. thesis).

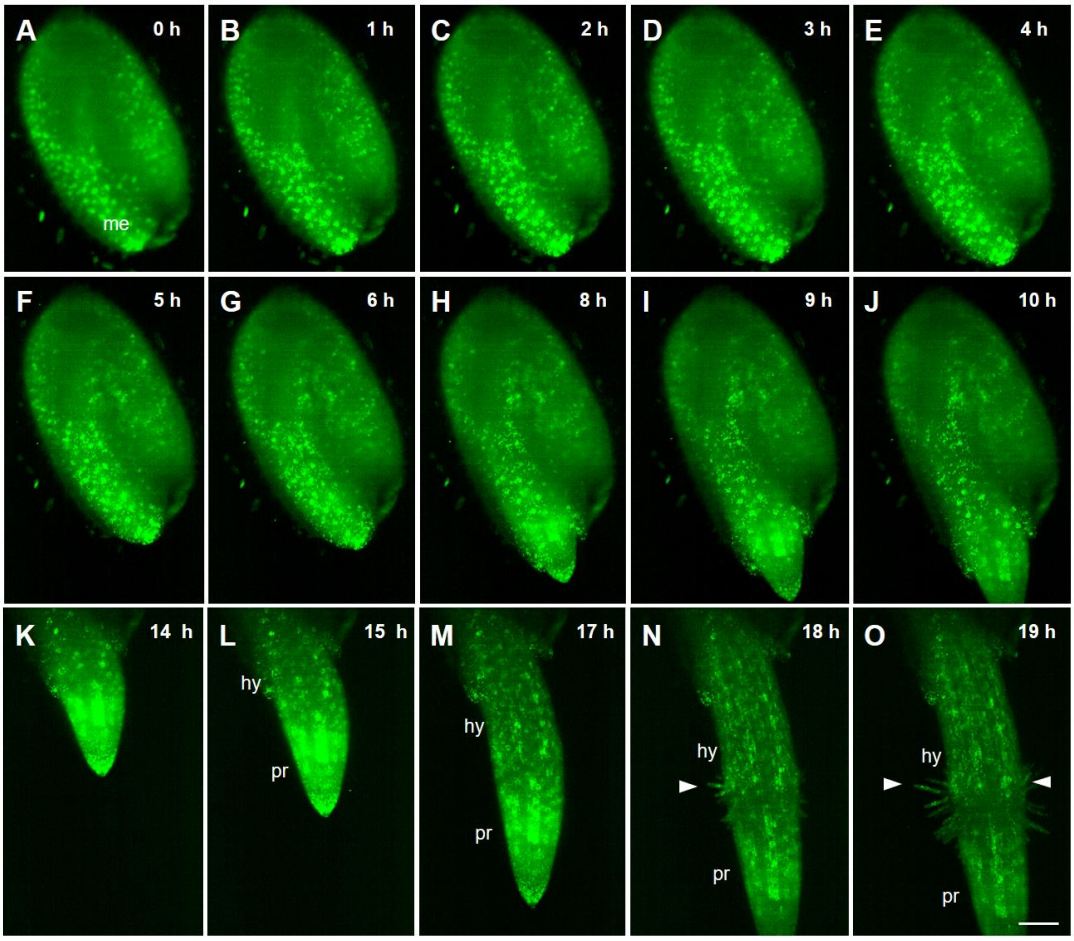

Figure 15 Time-lapse observing of FSD1-GFP expression during seed germination captured by using light-sheet fluorescence microscopy. (A-F) Gradual accumulation and relocation of the signal expression in micropylar endosperm (me) to the site of radicula protrusion. (G-H) endosperm ruptureand radicula protrusion. (I-O) Primary root elongation, (N, O) root hair emergence and elongation. Arrowheads point to the site of root hairs in thecollar region on the border between the elongating primary root (pr) and hypocotyl (hy). Scale bar: 100 μm. Adopted from Dvořák et al. (2021). Miroslav Ovečka and Jasim Basheer performed image acquisition.

In the cells of both above- and underground organs of light-exposed seedlings of *fsd1-1* mutants harboring *proFSD1::FSD1:GFP* construct, FSD1-GFP fusion protein was localized in plastids, nuclei, and cytosol, especially in the cortical cytosolic layer in close proximity to the plasma membrane. Such localization of FSD1-GFP was consistent in cells of all aboveground organs in light exposed seedlings, such as cotyledon epidermis (mature pavement cells, stomata and their precursors, Figure 16A, B, D-F), leaf mesophyll cells (Figure 16G-I), hypocotyl epidermis (Figure 16J), and first true leaf epidermis with branched trichomes (Figure 16C). In epidermal cells, FSD1-GFP-labelled plastids were located around the nucleus and in the cytosolic strains traversing the vacuole (Figure 16A, B, D, G).

Plastidic, nuclear and cytosolic localization of FSD1-GFP was detected also in cells of the root apex (Figure 17A). This localization pattern was visible in cells of the lateral root cap (Figure 17A, B), in meristematic cells (Figure 17A, C), epidermal cells of elongation zone (Figure 17D, E) as well as in trichoblasts within the differentiation zone (Figure 17F) of primary root. It showed lower FSD1-GFP signal intensity in central columella cells (Figure 17A).

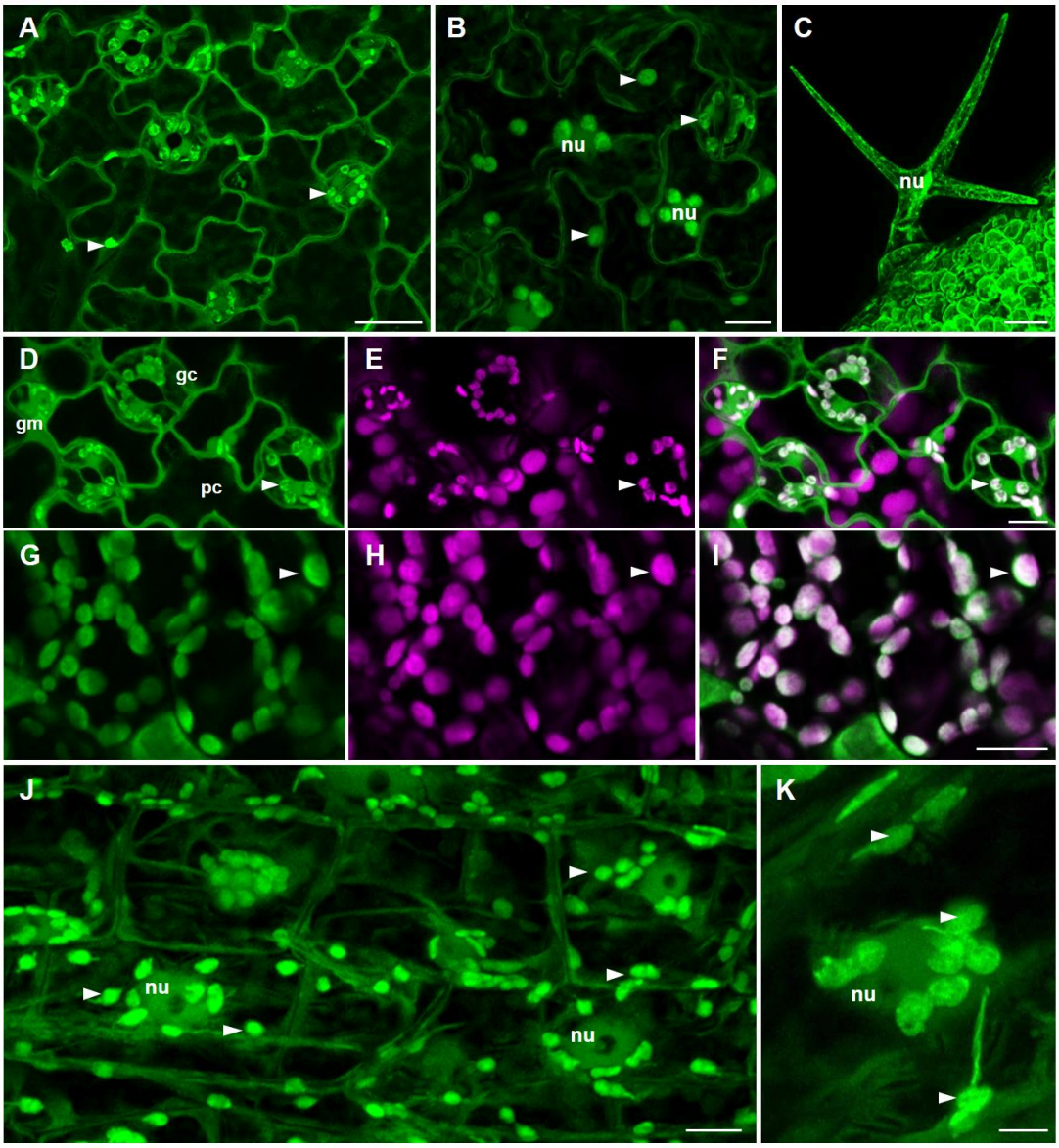

Figure 16 The localization of FSD1-GFP protein in cells of *Arabidopsis* aboveground organs observed using Airyscan confocal laser scanning microscopy. (A-B) FSD1 localization in cotyledon epidermal cells, stomata and leaf epidermal pavement cells and stomata guard cells. (C) Triple-branched leaf trichome. (D-F) Adaxial surface of cotyledons with pavement (pc), guard (gc) and guard mother (gm) cells. (G-I) Leaf mesophyll cells. (J) Hypocotyl cells of epidermis. (K) Magnification of area hypocotyl cells with visible chloroplast stromules. Indications: (nu) nucleus. Arrowheads point on accumulation of FSD1-GFP in plastids. Channels: green – FSD1-GFP; magenta – chlorophyll a autofluorescence. Scale bars: A, C, 20 μm; B, D-J, 10 μm; K, 5 μm. Adopted and modify from Dvořák et al. (2021) and modified.

Furthermore, accumulation of FSD1-GFP was observed in the LRP emerging from the pericycle (Figure 17K-N). FSD1-GFP signal increased first in cells of forming lateral root primordium still enclosed by tissues of the primary root (Figure 17K). Strong signal of FSD1-GFP was found in cells of the central region, where the apical meristem of the emerging lateral root was established (Figure 17L, M). Considerably high levels of FSD1-GFP also persisted during the release of the lateral root from the primary root tissue (Figure 17N).

The process of root hair formation from trichoblasts was connected with the accumulation of FSD1-GFP in the cortical cytosol of the emerging bulge (Figure 17G). In tip-growing root hairs, FSD1-GFP accumulated in the apical and subapical zone (Figure 17H, I). It is noteworthy

that after the termination of root hair elongation, FSD1-GFP signal dropped at the tip, while typical strong plastidic signal appeared in the cortical cytosol (Figure 17J).

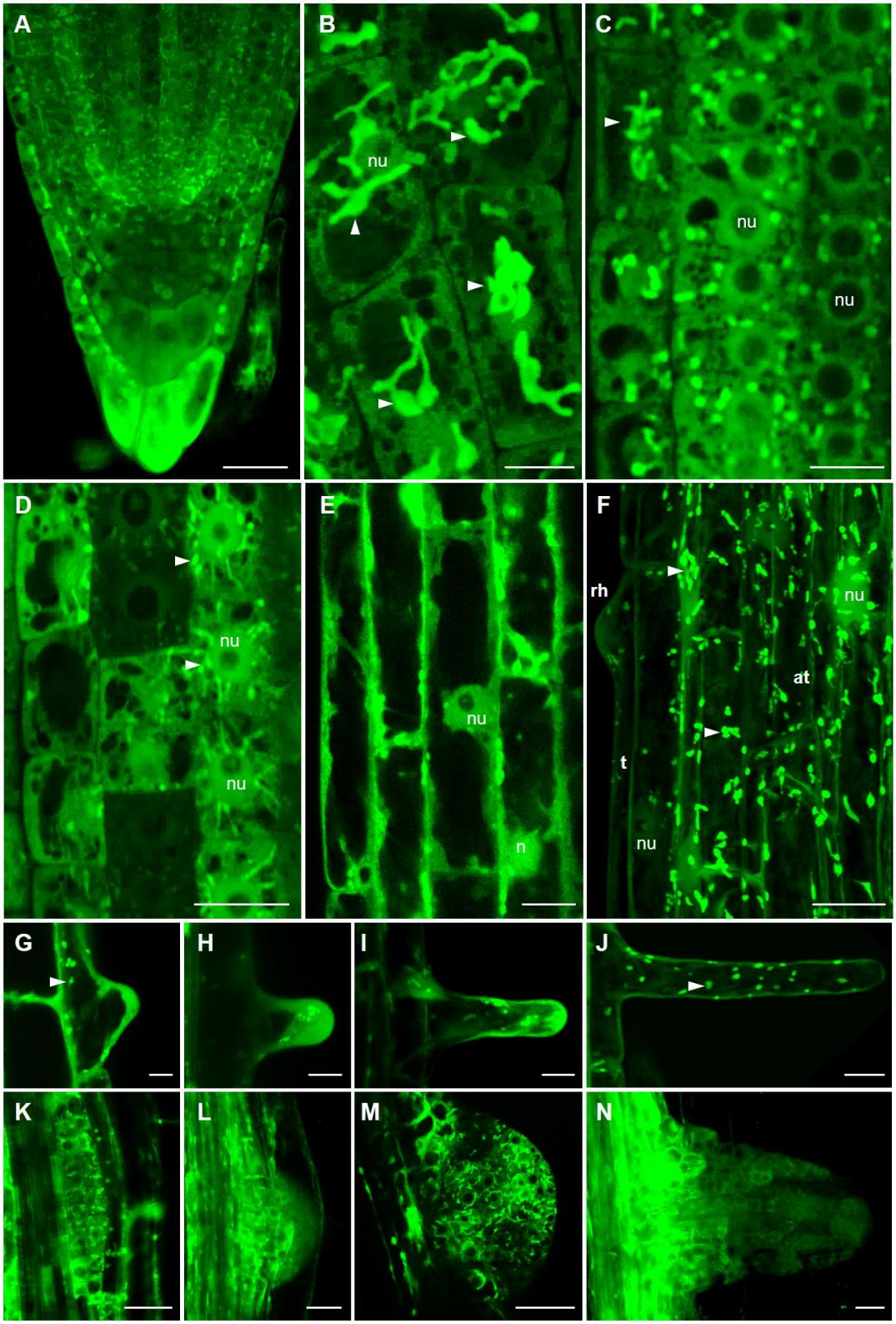

Figure 17 Tissue- and organ-specific subcellular FSD1-GFP presence in *Arabidopsis* roots. (A) Primary root apex (B), root cap cells with GFP-signal in plastids (arrowheads) and nuclei (nu). (C) Epidermal and cortical meristem cells, (D) cortical cells of distal elongation zone, (E) cortical cells of elongation zone. (F) Trichoblasts (t) with an emerging root hair (rh) and atrichoblasts (at) of differentiation zone. (G-J) Mid-plane sections of root hairs, (G) root hair bulge, (H, I) elongating root hair, (J) mature root hair. (K-M) Mid-plane sections of forming lateral root primordia at diverse developmental stages. (N) Emerged lateral root. Scale bars: A, E, F, K-N, 20 μm; B, C, D, G-J, 10 μm. Adopted from Dvořák et al. (2021).

Plastids were the organelles most strongly accumulating FSD1-GFP and located either around the nuclei or distributed throughout the cytosol (Figures 16, 17). Typically, plastids in cells of different tissues formed polymorphic stromules, which displayed different tissue-specific shape, length, branching (Figures 16 J, K, 17B-D) and dynamicity. Since stromules are tubular plastid extensions filled with stroma (Köhler and Hanson, 2000), FSD1 might be considered as stromal protein. In contrast to FSD2 and FSD3 (Myouga et al., 2008), FSD1 was not detected in the chloroplast nucleoids.

Subcellular localization pattern of FSD1 was confirmed by the whole mount immunofluorescence localization method in fixed samples using anti-FSD antibody. This technique showed prominent strong immunolocalization of FSD1 to plastids distributed around nuclei and in the cytosol, as well as nuclear and cytosolic localization in meristematic cells of the primary root (Figure 18A-C).

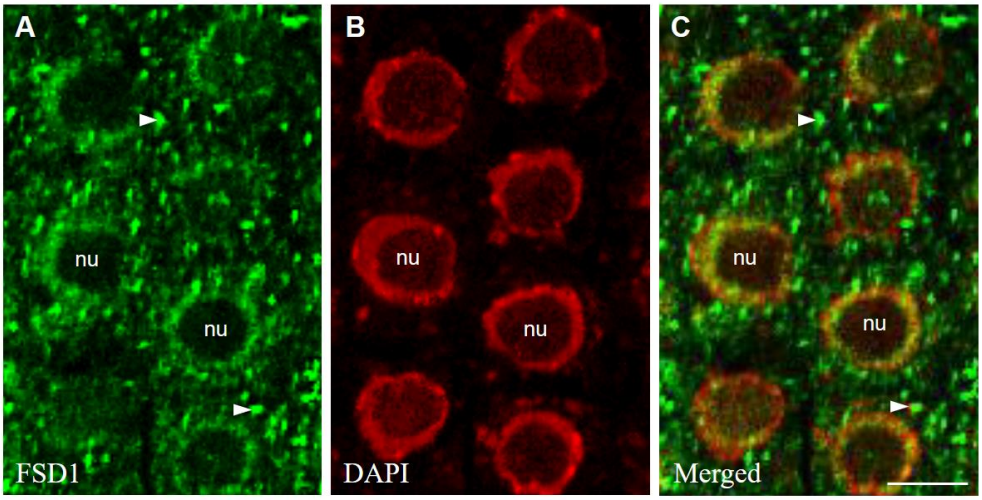

Figure 18 Whole-mount immunofluorescence staining of FSD1 protein by using specific anti-FSD antibody in *Arabidopsis* wild-type seedling. A-C The images of root meristem cells specifically labled agaist FSD1 protein. Green immunolabelling with anti-FSD – Alexa Fluor 488; red pseudocolour – DAPI staining. Arrowheads indicate plastids and (nu) stands for nuclei. Whole-mount immunofluorescence staining and preparation of samples were performed by Yuliya Krasylenko. Adopted from Dvořák et al. (2021) and modified

5.2.4 Role of FSD1 during salt and induced oxidative stress tolerance in *Arabidopsis*

Protective role of FSD1 during the early stages of post-embryonic plant development was tested in *fsd1* mutants and complemented lines on seed germination under salt stress conditions. Seed germination of *fsd1* mutants was strongly reduced by the presence of 150 mM NaCl in the 1/2 MS medium, while FSD1-GFP lines exhibited germination rates comparable to that of wild type (Figure 19A). GFP-FSD1 line showed an insignificantly reduced germination rate on the first day, but germination efficiency was synchronized with wild type and FSD1-GFP line from the second day onwards (Figure 19A). The results indicated that *FSD1* expressed under its own native promoter functionally complemented the salt stress-related deficiency of *fsd1* mutants.

To further test the new role of FSD1 in salt stress sensitivity, we characterized the response of developing seedlings to the high salt concentration in the culture medium. We found that both *fsd1* mutants showed hypersensitivity to NaCl and exhibited increased cotyledon bleaching. Both FSD1-GFP and GFP-FSD1 fusion proteins efficiently reverted the salt hypersensitivity of *fsd1* mutants (Figure 19B, C). These results supported the new functional role of FSD1 in *Arabidopsis* salt stress tolerance.

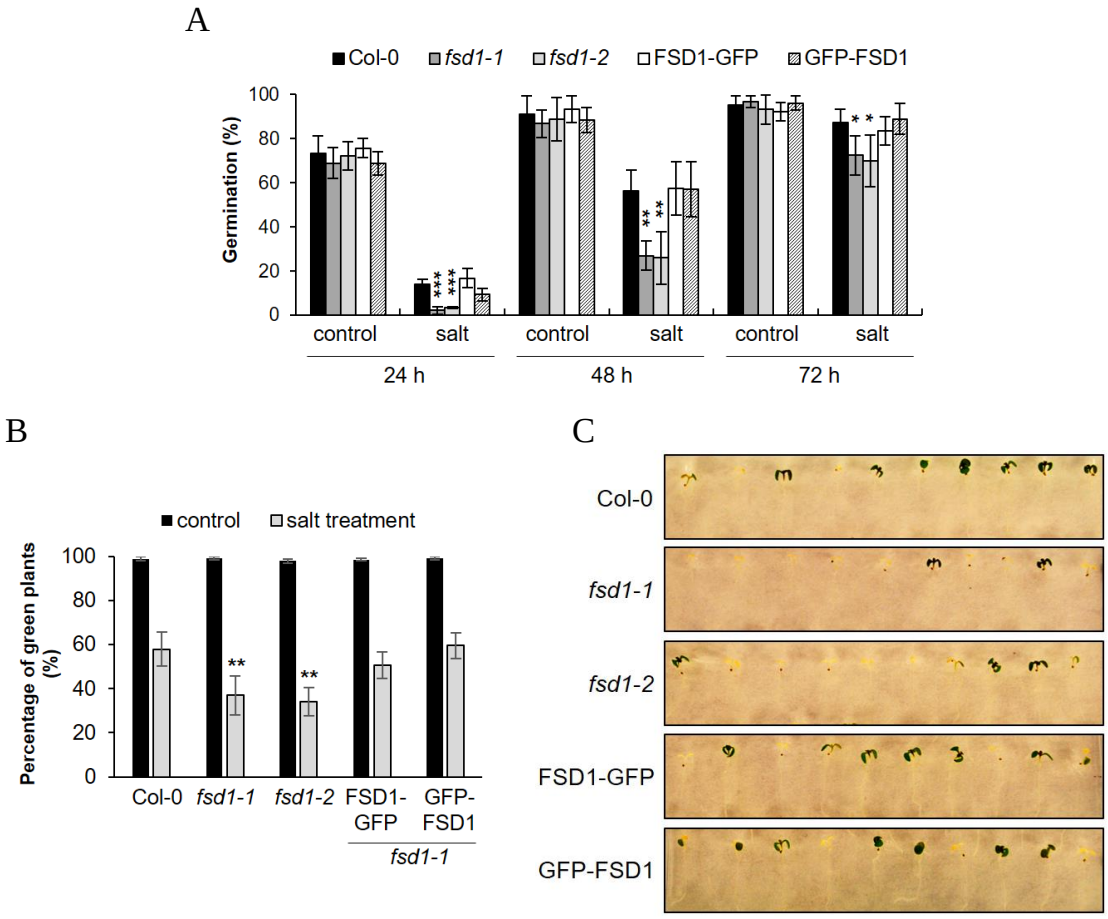

Figure 19 Salt stress response of *fsd1* mutants and complemented mutant lines during germination and aplication stress on young seedlings. (A) Efficiency of seed germination in control and stress conditons induced 150 mM NaCl. Germination is evaluated as a percentage of germinated seeds relative to the total number of examined seeds (n = 120). (B) Viability (fully green cotyledons) of plants on fifth day after the transplantation to the medium with and without 150 mM NaCl. Viability was evaluated as a percentage of seedlings with green cotyledons (n = 120). (C) Representative pictures transplantated seedling growing on 1/2 MS media containing 150 mM NaCl. Error bars in (A) and (B) represent standard deviations. Stars indicate statistically significant difference as compared to Col-0 (one-way ANOVA, *p < 0.05, **p < 0.01, ***p < 0.001). Adopted from Dvořák et al. (2021) and modified.

To gain deeper insight into FSD1 function during plant response to the salt stress, we performed subcellular localization of FSD1-GFP in hypocotyl epidermal cells plasmolysed by 500 mM NaCl (Figure 20A-G). In addition to plastidic, nuclear, and cytosolic localization in untreated cells (Figure 20A), FSD1-GFP was detected in Hechtian strands and Hechtian reticulum, interconnecting retracted protoplast with the cell wall of plasmolysed cells (Figure 20B-G). Hechtian reticulum located in close proximity to the cell wall (Figure 20D), and thin attachments of Hechtian strands to the cell wall in the form of bright adhesion spots were enriched with FSD1-GFP (Figure 20C, E-G;). Plasmolysed cells showed strong GFP signal at plasma membrane and also contained vesicle-like structures decorated by FSD1-GFP, in their cytosol and also within the Hechtian strands (Figure 20F, G).

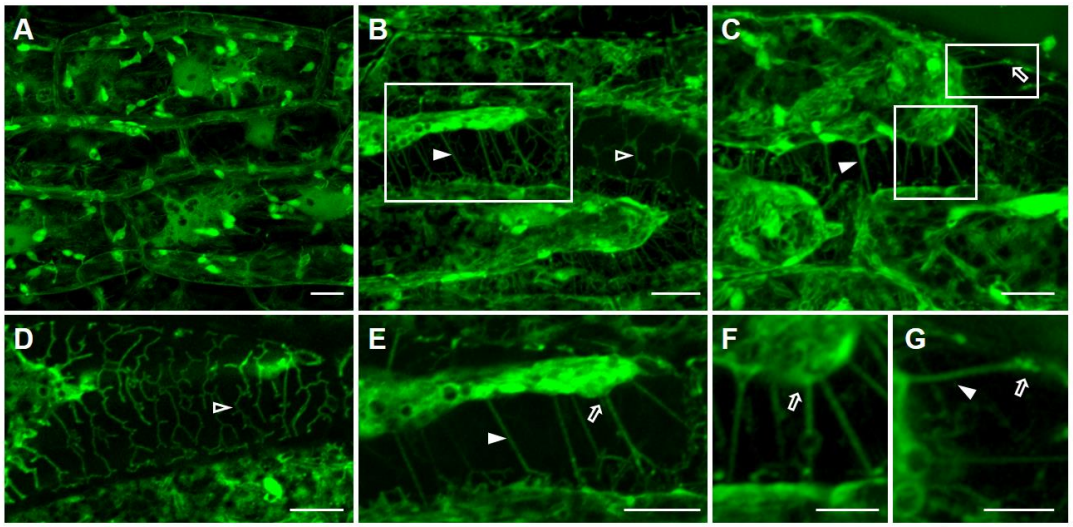

Figure 20 FSD1 localization in plasmolysed hypocotyl epidermal cells treated by salt. (A-G) FSD1-GFP signal in seedlings treated with liquid 1/2 MS media (A) or 1/2 MS media containing 500 mM NaCl (B-G) for 30 min. (B, C) Representative images of plasmolysed cells. (D) Hechtian reticulum. (E-G) Hechtian strands with connections to cell wall, close-ups from pictures (B, C). Filled arrowheads indicate Hechtian strands; blank arrowheads Hechtian reticulum; blank arrows – showing Hechtian strands connected to cell wall. Scale bars: A-E, H-Q, 10 μm; F, G, 5 μm. Adopted from Dvořák et al. (2021).

In order to reveal the role of FSD1 in scavenging of ROS generated in the chloroplast, we exposed mutant and transgenic lines to MV. Both mutant lines exhibited a hypersensitivity to this agent as estimated by lowest number of fully green cotyledons (Figure 21A, B). The GFP-FSD1 line was hypersensitive as well, but showed slightly elevated number of seedlings with fully green cotyledons when compared to mutants (Figure 21A, B). On the other hand, FSD1-GFP line showed a response resembling the wild type (Figure 21A, B). These results show that plastidic FSD1 pool is decisive for acquiring oxidative stress tolerance in *Arabidopsis*.

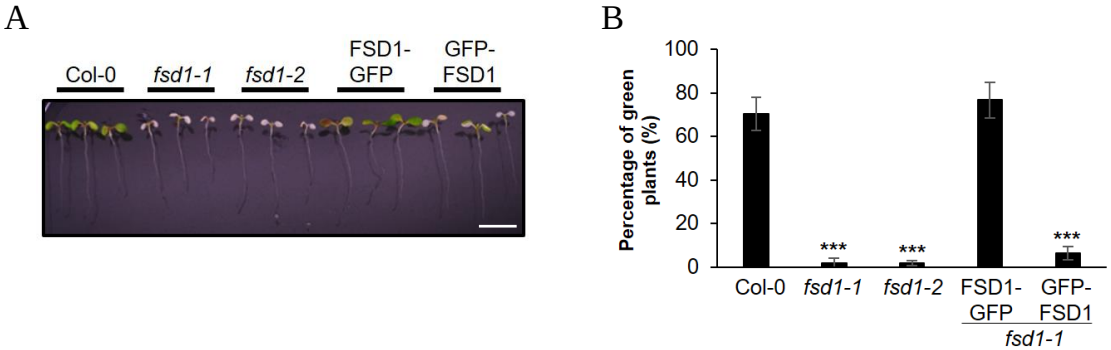

Figure 21 Impact of methyl viologen (MV)-induced oxidative stress on *fsd1* mutant and complemented lines. (A) Representative image of seedlings on fifth day after the transfer to 2 μM MV-containing medium (B) Quantification of seedling with not affected leaves (fully green cotyledons). Measurement was performed in four repetitions (n = 160). Error bars represent standard deviation. Stars indicate statistically significant difference as compared to Col-0 (one-way ANOVA, ***$p < 0.001$). Scale bar: 1 cm. Adopted from Dvořák et al. (2021).

5.2.5 Proteomic analysis of FSD1 interactome

The stable expression of FSD1 fused to GFP in *Arabidopsis* offers an opportunity to identify putative interacting partners of FSD1 using co-immunoprecipitation combined with proteomic analysis. Moreover, proteins, found only in one repetition were eliminated as well. We selected 44 putative interaction partners including their function and localization (listed in Ph.D. thesis). These commonly identified proteins included cytosolic proteins (e.g. PLDα1 and 2, HEAT SHOCK 70 KDA PROTEIN 18), several proteins localized to endoplasmic reticulum

bodies (e.g. beta glucosidases) and nucleus (e.g. splicing factors, ETHYLENE-RESPONSIVE TRANSCRIPTION FACTOR TINY). Ribosomal (e.g. UBIQUITIN-40S RIBOSOMAL PROTEIN S27A-3, ELONGATION FACTOR 1-ALPHA 1) and one chloroplastic protein (GLYCERALDEHYDE-3-PHOSPHATE DEHYDROGENASE GAPA1, CHLOROPLASTIC) were also identified in both lines. Interactors uniquely found in the FSD1-GFP line (together fifteen proteins) included mainly chloroplastic proteins such as CPN20, which is a known FSD1 interactor (Kuo et al., 2013).

Several interesting proteins were identified which were previously described to be involved in stress responses, such as PLDα1 and 2, DEHYDRIN HIRD11, CALMODULIN-1, GLYCINE-RICH PROTEIN 3, LACTOYLGLUTATHIONE LYASE GLX1, ETHYLENE-RESPONSIVE TRANSCRIPTION FACTOR TINY, Pre-mRNA-PROCESSING PROTEIN 40A. Interestingly, several proteins involved in pre-mRNA splicing were identified such as pre-mRNA-PROCESSING PROTEIN 40A, SPLICING FACTOR U2AF LARGE SUBUNIT A and B, SERINE/ARGININE-RICH SPLICING FACTOR SC35, CACTIN, DEAD-BOX ATP-DEPENDENT RNA HELICASE 42.

Taken together, the identification of FSD1 interactome changes the view on FSD1 as a conservative antioxidant enzyme.

5.2.6 Bioinformatics analysis of potential regulatory mechanisms of FSD1

Proteomic and transcriptomic analyses of MAPKs mutant indicated the MAPK mediated regulation of *FSD1* expression (Frei dit Frey et al., 2014; Takáč et al., 2014; Takáč et al., unpublished results). It is expected that *FSD1* might be controlled by MAPKs transcriptionally by TFs. Based on above mentioned data, we performed the bioinformatics analysis by integrating four different parameters to found potential TFs regulating *FSD1* expression under MPKs control: 1) the presence of *cis*-element(s) in the promoter sequence of *FSD1* gene (predicted by AthaMap; Hehl et al., 2016), (2) TFs co-expressed with *FSD1* and MAPKs (determined by ATTED-II; Obayashi et al., 2018), (3) TFs containing a MAPK-specific phosphorylation site (S(p)P or S(p)T; evaluated by PhosPhat 4.0 and GPS 3.0; Xue et al., 2005; Zulawski et al., 2013), and (4) the presence of a MAPK-specific docking site in the amino acid sequence of the TFs (evaluated by ELM; Kumar et al., 2020). Overall 31 potential TFs have been predicted for the control of *FSD1* expression by MAPKs.

Three candidates belonging to the SPL protein family, namely SPL1, SPL7 and SPL8, were identified as well. SPL7 was described as a TF with direct influence on *FSD1* expression (Yamasaki et al., 2009; Andrés-Colás et al., 2013; Garcia-Molina et al., 2014). We selected SPL1 and SPL7 as the most promising MAPK-phosphorylated TFs regulating *FSD1* expression.

As noted in the introduction, FSD1 activity may be regulated also by phosphorylation. We performed a bioinformatic prediction of phosphorylation sites in the amino acid sequence of FSD1 protein. We found that MAPK is the kinase predicted with the highest probability to phosphorylate FSD1, most likely on EKLKVVKTPNAVNPL peptide. This sequence partially overlapped with the predicted MAPK docking site (KTPNAVNPLVL).

5.2.6 Validation of predicted regulatory mechanisms of FSD1

In order to confirm the hypothesis about MAPK mediated FSD1 regulation, we decided to employ *in vitro* kinase assay, to examine FSD1, SPL1 and SPL7 phosphorylation by MPK3 and MPK6. We prepared constructs for heterologous recombinant protein expression by using

pMAL-p2 or pGEX-6P-1 vectors. *In vitro* kinase assay reactions were performed for testing the phosphorylation of SPL1, SPL7, FSD1 by MPK3 (Figure 22A, B) and MPK6 (Figure 22C, D) in two repetitions. However, no radioactive signal was obtained from the area where the recombinant GST-SPL1, MBP-SPL1, MBP-SPL7 and even MBP-FSD1 were separated (Figure 22A-D). MPK3 (Figure 22A, B) and MPK6 (Figure 22C, D) showed pronounced autophosphorylation. Together, we did not prove the phosphorylation of SPL1, SPL7 and FSD1 by MAPKs in our experiment.

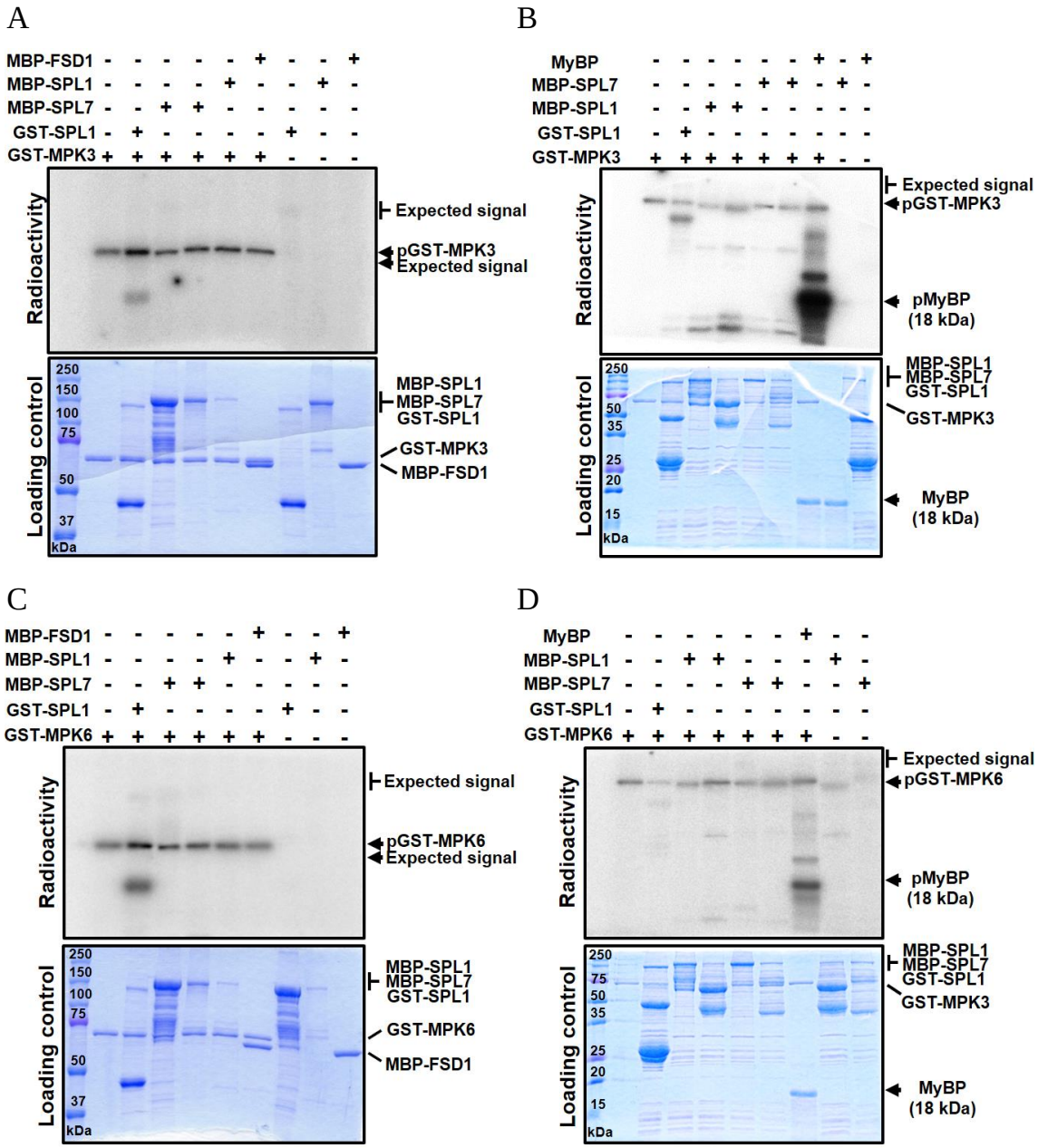

Figure 22 *In vitro* kinase assay of recombinant MPK3 (A, B) and MPK6 (C, D) using predicted recombinant substrates SPL1, SPL7 (both tested in all gels) and FSD1 (A, C). The testing of SPL1 and SPL7 phosphorylation is shown in two repetitions (A, B and C, D, respectively). Gels in (C and D) shows phosphorylation of Myelin basic protein (MyBP) at 18 kDa as a positive control. Arrows mark the area with detected radioactivity and the presence of recombinant protein. The expected Mr of SPL1, SPL7 and FSD1 phosphorylation is indicated by ⊢ and arrows. Gels below the autoradiographs represent the same gels stained by coomassie blue staining.

5.3 Discussion

FSDs were long believed to be chloroplast proteins involved in $O_2^{\cdot-}$ scavenging during photosynthesis. However, the scavenging capacity of *Arabidopsis* FSD1 was challenged, because its transcript levels remained unchanged in response to many environmental conditions (Kliebenstein et al., 1998; Myouga et al., 2008; Xing et al., 2015; Gallie and Chen, 2019). This work shows for the first time that FSD1 is localized not only in plastids, but simultaneously also in the nuclei and cytosol of *Arabidopsis* cells. Moreover, FSD1 accumulates in Hechtian strands and Hechtian reticulum interconnecting retracted protoplast with the cell wall under salt stress conditions.

Using translational fusion constructs with native promoter, GFP-tagged FSD1 exhibited a tissue-specific expression pattern in *Arabidopsis* root tip. This indicates that FSD1 may also have developmental roles that are conditionally determined. Hence, FSD1 might be involved in the regulation of the redox status in dividing cells, like root initials. It is known that the root meristematic activity as well as the quiescent centre organization is maintained by redox homeostasis which acts downstream of the auxin transport (Jiang, 2003; Barlow, 2016; Gallie and Chen, 2019; Horváth et al., 2019). Intriguingly, *FSD1* tissue-dependent expression pattern largely correlates with auxin maxima in the root tip (Petersson et al., 2009; Hayashi et al., 2014), as well as with $O_2^{\cdot-}$ maxima (Dunand et al., 2007). Furthermore, endodermis formation requires SCARECROW (SCR) and SHORTROOT (SHR), two GRAS-type TFs, expressed in the endodermis/cortex initials and quiescent centre (Helariutta et al., 2000; Carlsbecker et al., 2010). FSD1 might also contribute to the regulation of SCR and SHR, which is supported by the high expression of *FSD1* in fluorescence-activated cell sorting-isolated protoplasts expressing endoplasmic reticulum-targeted GFP under the control of the SCR promoter (Geng et al., 2013). This expression was elevated in salt-stressed protoplasts.

According to our study, FSD1 is required for proper establishment of lateral roots in *Arabidopsis*. Considering that both N- and C-terminal GFP fusions with FSD1 complemented defective lateral root formation in *fsd1* mutants, one can assume that these fusion proteins are functional and sufficient for full acquisition of lateral root formation capacity in *Arabidopsis*, but further investigation is necessary to verify this hypothesis. Lateral root formation is dependent on complementary action of multiple regulatory systems governed by auxin (Banda et al., 2019). RBOH-generated ROS are major modulators of this process via cell wall remodeling of overlying parental root tissues (Orman-Ligeza et al., 2016). RBOH activity is controlled by multiple factors including phosphorylation, Ca^{2+}, PA and protein-protein interactions (Ogasawara et al., 2008; Zhang et al., 2009), while ROS accumulation must be controlled in order to ensure proper lateral root formation. As a proof of this concept, we provided experimental evidence showing strong accumulation of FSD1 in LRP, and reduced lateral root number in *fsd1* mutants. Hence, FSD1 appears as an enzyme participating in maintenance of proper redox homeostasis during lateral root formation.

The localization of FSD1 to chloroplasts is determined by an N-terminal transit peptide identified previously (Kuo et al., 2013). According to comparative studies of three *Arabidopsis* isoforms, FSD1 is crucial neither for chloroplast integrity (Myouga et al., 2008), nor for cell protection under photooxidative stress (Gallie and Chen, 2019). It has 3–10 times higher expression compared to *FSD2* and *FSD3* (Pilon et al., 2011) in *Arabidopsis*, depending on developmental stage, and unlike *FSD2* and *FSD3*, it remains insensitive to MV and high light irradiation (Myouga et al., 2008). Evidence was provided for cooperative roles of FSD2 and FSD3 to ensure defense against high light and MV-generated ROS (Myouga et al., 2008; Gallie

and Chen, 2019). We show that plastidic pool of FSD1 is important for *Arabidopsis* tolerance against MV-induced oxidative stress, while cytosolic and nuclear pools are inefficient.

FSD1 is also important for *Arabidopsis* germination under salt stress and for salt stress tolerance in general. As indicated by the FSD1 localization and salt stress response in the complemented lines, cytosolic FSD1, FSD1 in the Hechtian strands and Hechtian reticulum (as discussed below) and likely also nuclear FSD1 pool are crucial for the acquisition of tolerance to salinity during germination. Altogether, our results emphasize the importance of FSD1 in the regulation of cytosolic and also possibly nuclear redox homeostasis in response to salinity stress.

Seed germination is a complex process encompassing multiple events governed by tight phytohormonal regulation. Micropylar endosperm represents the last mechanical barrier constraining the radicle emergence. Endosperm rupture is preceded by its weakening, controlled by the inhibitory effect of ABA and promoting effect of ethylene (Linkies et al., 2009). Furthermore, ROS contribute to this process by oxidizing the cell wall polysaccharides and subsequent cell wall loosening (Müller et al., 2009). Here, we provide data showing FSD1 upregulation and local accumulation in the micropylar endosperm during endosperm weakening and rupture, which is subsequently decreased after primary root emergence.

Our localization data suggest that FSD1 functions are not only restricted to the cytosol and plastids, because we provide here the first evidence on the nuclear localization of SOD in plants. It was previously found that mammalian SOD1 is rapidly relocated to the nucleus upon H_2O_2-triggered oxidative stress (Volkening et al., 2009). In this case, SOD1 binds to specific DNA nucleotide sequences and triggers the expression of genes involved in oxidative resistance and DNA repair. It may also bind to and regulate the stability of specific mRNAs (Volkening et al., 2009). SOD1 nuclear functions are unrelated to its catalyzing of $O_2^{\cdot -}$ removal (Tsang et al., 2014).

Our FSD1 interactome analysis showed that FSD1 may participate in the regulation and proper function of spliceosome. The interactome included SPLICING FACTOR U2AF LARGE SUBUNIT B, which is involved in ABA-mediated flowering via pre-mRNA splicing of *ABSCISIC ACID-INSENSITIVE 5* and *FLOWERING LOCUS C*, which are both involved in ABA-mediated floral transition (Shu et al., 2016; Xiong et al., 2019). Another component of the spliceosome, SERINE/ARGININE-RICH SPLICING FACTOR SC35 identified in our analysis, has been previously described as regulator of FLOWERING LOCUS C splicing and flowering time (Yan et al., 2017). Additionally, DEAD-BOX ATP-DEPENDENT RNA HELICASE 42 (Guan et al., 2013; Lu et al., 2020), SPLICING FACTOR U2AF LARGE SUBUNIT A (Wang and Brendel, 2006; Jang et al., 2014), pre-mRNA-PROCESSING PROTEIN 40A (Kang et al., 2009; Hernando et al., 2019) and CACTIN (Baldwin et al., 2013) have been associated with pre-mRNA splicing. Thus FSD1 may likely link ROS signaling to alternative splicing by interacting with the spliceosome complex. This interaction is most probably connected to the control of flowering time, which is also suggested by phenotypes of *fsd1-1* and *fsd1-2* mutants, having delayed flowering (Samakovli et al., unpublished data). FSD1 may also bind STYLE CELL-CYCLE INHIBITOR 1 (DePaoli et al., 2014) and ETHYLENE-RESPONSIVE TRANSCRIPTION FACTOR TINY (Xie et al., 2019), two TFs in our screen.

Our phenotypic and microscopic analyses assigned osmoprotective roles to FSD1. In this sense, putative FSD1 interaction with a protein involved in ABA signaling, PLDα1 (found in all of the examined replicates), appears as a very interesting finding. PLDα1 is implicated in plant response to salt stress (Vadovič et al., 2019). Its phospholipid hydrolyzing activity results in the

production of PA, an important signaling molecule. It activates MAPKs in response to salt stress (Yu et al., 2010). PLDα1-mediated changes in membrane properties lead to activation of CYSTEINE-RICH RECEPTOR-LIKE KINASE 2, which relocalizes to plasmodesmata and promotes callose deposition under salt stress (Hunter et al., 2019). Interestingly, FSD1 showed localization very similar to PLDα1 after salt stress and fluorescent signals of both FSD1 and PLDα1 were increased close to the plasma membrane and on Hechtian strands (Novák et al., 2018). The similarity of FSD1 and PLDα1 is apparent also considering the tissue specific expression pattern in the root tip (Novák et al., 2018). These data, together with the ABA responsivity of FSD1 (Müller et al., 2009), support possible interaction between PLDα1 and FSD1 during salt stress. FSD1 may link the ROS signaling (by controlling $O_2^{\cdot -}$ conversion to H_2O_2) with functions of PLDα1 in membrane biophysical properties in order to contribute to osmoprotection.

We also address the question of possible mechanisms of FSD1 regulation. Our bioinformatics pipeline resulted in the identification of 31 putative MAPK-phosphorylated TFs with high potential to bind to *cis*-elements in FSD1 promoter sequence. SPL7 and SPL1 were selected for further studies. The promoter sequences of several *SODs* (*FSD1*, *CSD1*, *CSD3*, *MSD1*) contain the core motif GTAC (Perea-García et al., 2016), specific for SPL binding. More specifically, *FSD1* promoter sequence contains six independent GTAC motifs and three motifs in first intron. Previously, the presence of GTAC motif in the first intron was suggested as a possible binding site for SPL proteins (Yamaguchi et al., 2009). Additionally, the *FSD1* expression is strongly suppressed in *Arabidopsis spl7* mutant (Yamasaki et al., 2009) and mutation of four GTAC motifs in *FSD1* promoter led to significant downregulation of *FSD1* expression (Andrés-Colás et al., 2013). In this sense, the presence of multiple binding motifs may suggest the binding of other SPL isoforms, dependent on developmental stage and stress conditions. As a proof of concept, *spl1/spl12* showed downregulated SOD activity in response to heat stress (Chao et al., 2017). In addition to the transcriptional control of FSD1, the regulation of FSD1 via phosphorylation by MAPKs cannot be excluded, as indicated by our bioinformatics analysis. Previously yeast (Leitch et al., 2012) and human SOD1 (Tsang et al., 2018) has been found phosphorylated and with direct impact on activity and leads to the translocation of this SOD1 to the nucleus.

The possible phosphorylation of SPL1, SPL7 and FSD1 by MPK3 and MPK6 was tested by *in vitro* kinase assay by using recombinant proteins. Unfortunately, we failed to prove any of the analyzed phosphorylations. The bacterial cytoplasm provides a reducing environment, which is not suitable for formation of disulfide bonds. Proteins, which require the formation of disulfide bonds, might be misfolded leading to aggregation and formation of insoluble inclusion bodies (Gąciarz et al., 2017). Indeed, both SPL7 and SPL1 contain in their structure relatively high amount of cysteine and it is possible, that the protein folding was incorrect in *E.coli*. This may affect the access of MPKs to the putatively phosphorylated residues. For this reason, the possible phosphorylation of SPLs by MAPKs cannot be excluded.

On the other hand, results of FSD1 phosphorylation by MPK3 and MPK6 showed negative results. In this case, MBP-FSD1 protein purification was working with enormous efficiency. Based on these results, it is highly possible, that FSD1 is not phosphorylated by MPK3 and MPK6 *in planta*.

7 General conclusions

This Ph.D. thesis is focused on the crosstalk of plant MAPKs with ROS signaling. First, we used proteomic, phenotypic and biochemical analyses to examine the impact of MAPKs on the establishment of symbiotic interaction of alfalfa with *S. meliloti*, with accent on antioxidant defense. Secondly, we studied the developmental and protective roles of *Arabidopsis* FSD1 a protein potentially regulated by MAPKs.

Within the theoretical part, a current knowledge about plant MAPK signaling with a focus on abiotic and biotic stresses is summarized. A separate chapter is devoted to MAPK cascades in legumes (mainly alfalfa) and their function during the alfalfa – rhizobia interaction. Next, recent findings connected to ROS signaling and their crosstalk with MAPKs during plant stress response are discussed. The last chapter of the theoretical part addresses antioxidant enzymes, including SODs and mechanisms of their regulation.

In the frame of the experimental part a series of phenotypical, biochemical and proteomic analyses were carried out on alfalfa wild type and transgenic *SIMKK RNAi* line (SIMKKi). The most important results showed that SIMKKi displays significantly decreased number of nodules in comparison with wild type. Combined proteomic and biochemical analyses indicated that SIMKKi may have significant impact on regulation of SODs, bacteria attachment and sterol rearrangements in plasma membrane, all being important for establishment of symbiotic interaction. Together, SIMKK positively regulates the establishment of alfalfa-rhizobia interaction likely through multiple mechanisms.

Since FSD1 was selected as a protein potentially regulated by MAPKs, the second part of experiments was focused on its developmental and protective roles in *Arabidopsis*. FSD1-GFP temporarily accumulated at the site of endosperm rupture during seed germination. In emerged roots, it showed the highest abundance in cells of the lateral root cap, columella, and endodermis/cortex initials. The largest subcellular pool of FSD1-GFP was localized in the plastid stroma, while it was also located in the nuclei and cytosol. We found that *fsd1* knockout mutants exhibit reduced lateral root number and this phenotype was reverted by genetic complementation. Mutant analysis also revealed a requirement for FSD1 in seed germination during salt stress. Salt stress tolerance was coupled with the accumulation of FSD1-GFP in Hechtian strands and $O_2^{\cdot -}$ removal. It is likely that the plastidic pool is required for acquiring oxidative stress tolerance in *Arabidopsis*.

The FSD1 interactome identification by using co-immunoprecipitation coupled to proteomic analyses suggested several putative interaction partners of FSD1 and its possible role in pre-mRNA splicing. Finally, we predicted putative TFs controlling FSD1 expression under the control of MAPKs. Among them, putative phosphorylation of two SPL7 and SPL1 TFs by MPK3 and MPK6 was validated by using *in vitro* kinase assay. However, the predicted MAPK-mediated phosphorylation of SPLs was not confirmed. These results suggest a new nuclear, developmental and osmoprotective functions of SODs in plants.

8 References

Abdel-Ghany, S. E., Burkhead, J. L., Gogolin, K. A., Andrés-Colás, N., Bodecker, J. R., Puig, S., et al. (2005). AtCCS is a functional homolog of the yeast copper chaperone Ccs1/Lys7. *FEBS Lett.*, *579*, 2307–2312.

Abercrombie, J. M., Halfhill, M. D., Ranjan, P., Rao, M. R., Saxton, A. M., Yuan, J. S., and Stewart, C. N., Jr. (2008). Transcriptional responses of *Arabidopsis thaliana* plants to As (V) stress. *BMC Plant Biol.*, *8*, 87.

Almagro, L., Gómez Ros, L. V., Belchi-Navarro, S., Bru, R., Ros Barceló, A., and Pedreño, M. A. (2009). Class III peroxidases in plant defence reactions. *J. Exp. Bot.*, *60*, 377–390.

Andrási, N., Rigó, G., Zsigmond, L., Pérez-Salamó, I., Papdi, C., Klement, E., et al. (2019). The mitogen-activated protein kinase 4-phosphorylated heat shock factor A4A regulates responses to combined salt and heat stresses. *J. Exp. Bot.*, *70*, 4903–4918.

Andreasson, E., Jenkins, T., Brodersen, P., Thorgrimsen, S., Petersen, N. H., Zhu, S., et al. (2005). The MAP kinase substrate MKS1 is a regulator of plant defense responses. *EMBO J.*, *24*, 2579–2589.

Andrés-Colás, N., Perea-García, A., Mayo de Andrés, S., Garcia-Molina, A., Dorcey, E., Rodríguez-Navarro, S., et al. (2013). Comparison of global responses to mild deficiency and excess copper levels in Arabidopsis seedlings. *Metallomics*, *5*, 1234–1246.

Apel, K., and Hirt, H. (2004). REACTIVE OXYGEN SPECIES: metabolism, oxidative stress, and signal transduction. *Annu. Rev. Plant Biol.*, *55*, 373–399.

Araki, R., Mermod, M., Yamasaki, H., Kamiya, T., Fujiwara, T., and Shikanai, T. (2018). SPL7 locally regulates copper-homeostasis-related genes in *Arabidopsis*. *J. Plant Physiol.*, *224–225*, 137–143.

Asai, T., Tena, G., Plotnikova, J., Willmann, M. R., Chiu, W. L., Gomez-Gomez, L., et al. (2002). MAP kinase signalling cascade in Arabidopsis innate immunity. *Nature*, *415*, 977–983.

Bailly, C., El-Maarouf-Bouteau, H., and Corbineau, F. (2008). From intracellular signaling networks to cell death: the dual role of reactive oxygen species in seed physiology. *C. R. Biol.*, *331*, 806–814.

Baldwin, K. L., Dinh, E. M., Hart, B. M., and Masson, P. H. (2013). CACTIN is an essential nuclear protein in Arabidopsis and may be associated with the eukaryotic spliceosome. *FEBS Lett.*, *587*, 873–879.

Banda, J., Bellande, K., von Wangenheim, D., Goh, T., Guyomarc'h, S., Laplaze, L., and Bennett, M. J. (2019). Lateral root formation in *Arabidopsis*: A well-ordered LRexit. *Trends Plant Sci.*, *24*, 826–839.

Barlow, P. W. (2016). Origin of the concept of the quiescent centre of plant roots. *Protoplasma*, *253*, 1283–1297.

Barnes, J. D., Balaguer, L., Manrique, E., Elvira, S., and Davison, A. W. (1992). A reappraisal of the use of DMSO for the extraction and determination of chlorophylls a and b in lichens and higher plants. *Environ. Exp. Bot.*, *32*, 83–100.

Becana, M., Matamoros, M. A., Udvardi, M., and Dalton, D. A. (2010). Recent insights into antioxidant defenses of legume root nodules: Tansley review. *New Phytol.*, *188*, 960–976.

Bekešová, S., Komis, G., Křenek, P., Vyplelová, P., Ovečka, M., Luptovčiak, I., et al. (2015). Monitoring protein phosphorylation by acrylamide pendant Phos-Tag™ in various plants. *Front. Plant Sci.*, *6*, 336.

Bethke, G., Unthan, T., Uhrig, J. F., Poschl, Y., Gust, A. A., and Lee, J. (2009). Flg22 regulates the release of an ethylene response factor substrate from MAP kinase 6 in *Arabidopsis thaliana* via ethylene signaling. *Proc. Natl. Acad. Sci. U. S. A.*, *106*, 8067–8072.

Bheri, M., Mahiwal, S., Sanyal, S. K., and Pandey, G. K. (2020). Plant protein phosphatases: What do we know about their mechanism of action?. *FEBS J.*, 10.1111/febs.15454. Advance online publication.

Bi, G., Zhou, Z., Wang, W., Li, L., Rao, S., Wu, Y., et al. (2018). Receptor-Like Cytoplasmic Kinases Directly Link Diverse Pattern Recognition Receptors to the Activation of Mitogen-Activated Protein Kinase Cascades in Arabidopsis. *Plant Cell*, *30*, 1543–1561.

Birkenbihl, R. P., Jach, G., Saedler, H., and Huijser, P. (2005). Functional dissection of the plant-specific SBP-domain: overlap of the DNA-binding and nuclear localization domains. *J. Mol. Biol.*, *352*, 585–596.

Bögre, L., Calderini, O., Binarova, P., Mattauch, M., Till, S., Kiegerl, S., et al. (1999). A MAP kinase is activated late in plant mitosis and becomes localized to the plane of cell division. *Plant Cell*, *11*, 101–113.

Burkhead, J. L., Reynolds, K. A., Abdel-Ghany, S. E., Cohu, C. M., and Pilon, M. (2009). Copper homeostasis. *New Phytol.*, *182*, 799–816.

Cai, C., Guo, W., and Zhang, B. (2018). Genome-wide identification and characterization of SPL transcription factor family and their evolution and expression profiling analysis in cotton. *Sci. Rep.*, *8*, 762.

Cardinale, F., Jonak, C., Ligterink, W., Niehaus, K., Boller, T., and Hirt, H. (2000). Differential activation of four specific MAPK pathways by distinct elicitors. *J. Biol. Chem.*, *275*, 36734–36740.

Cardinale, F., Meskiene, I., Ouaked, F., and Hirt, H. (2002). Convergence and divergence of stress-induced mitogen-activated protein kinase signaling pathways at the level of two distinct mitogen-activated protein kinase kinases. *Plant Cell*, *14*, 703–711.

Cardon, G., Höhmann, S., Klein, J., Nettesheim, K., Saedler, H., and Huijser, P. (1999). Molecular characterisation of the Arabidopsis SBP-box genes. *Gene, 237*, 91–104.

Carlsbecker, A., Lee, J. Y., Roberts, C. J., Dettmer, J., Lehesranta, S., Zhou, J., et al. (2010). Cell signalling by microRNA165/6 directs gene dose-dependent root cell fate. *Nature, 465*, 316–321.

Chan, K. X., Phua, S. Y., Crisp, P., McQuinn, R., and Pogson, B. J. (2016). Learning the languages of the chloroplast: retrograde signaling and beyond. *Annu. Rev. Plant Biol*., *67*, 25–53.

Chang, R., Jang, C. J., Branco-Price, C., Nghiem, P., and Bailey-Serres, J. (2012). Transient MPK6 activation in response to oxygen deprivation and reoxygenation is mediated by mitochondria and aids seedling survival in *Arabidopsis*. *Plant Mol. Biol*., *78*, 109–122.

Chao, L. M., Liu, Y. Q., Chen, D. Y., Xue, X. Y., Mao, Y. B., and Chen, X. Y. (2017): *Arabidopsis* Transcription Factors SPL1 and SPL12 Confer Plant Thermotolerance at Reproductive Stage. *Mol. Plant*, *10*, 735–748.

Chaouch, S., Queval, G., and Noctor, G. (2012). AtRbohF is a crucial modulator of defence-associated metabolism and a key actor in the interplay between intracellular oxidative stress and pathogenesis responses in Arabidopsis. *Plant J.*, *69*, 613–627.

Chen, T., Zhou, B., Duan, L., Zhu, H., and Zhang, Z. (2017). MtMAPKK4 is an essential gene for growth and reproduction of *Medicago truncatula*. *Physiol. Plant.*, *159*, 492–503.

Chen, T., Zhu, H., Ke, D., Cai, K., Wang, C., Gou, H., et al. (2012). A MAP kinase kinase interacts with SymRK and regulates nodule organogenesis in *Lotus japonicus*. *Plant Cell*, *24*, 823–838.

Cheng, C. Y., Krishnakumar, V., Chan, A. P., Thibaud-Nissen, F., Schobel, S., and Town, C. D. (2017). Araport11: a complete reannotation of the *Arabidopsis thaliana* reference genome. *Plant J.*, 89, 789–804.

Cheng, Z., Li, J. F., Niu, Y., Zhang, X. C., Woody, O. Z., Xiong, Y., et al. (2015). Pathogen-secreted proteases activate a novel plant immune pathway. *Nature*, *521*, 213–216.

Choudhary, A., Kumar, A., and Kaur, N. (2019). ROS and oxidative burst: Roots in plant development. *Plant Divers.*, *42*, 33–43.

Cohu, C. M., Abdel-Ghany, S. E., Gogolin Reynolds, K. A., Onofrio, A. M., Bodecker, J. R., Kimbrel, J. A., et al. (2009). Copper delivery by the copper chaperone for chloroplast and cytosolic copper/zinc-superoxide dismutases: regulation and unexpected phenotypes in an *Arabidopsis* mutant. *Mol. Plant*, *2*, 1336–1350.

Considine, M. J., and Foyer, C. H. (2020) Oxygen and reactive oxygen species-dependent regulation of plant growth and development. *Plant Physiol*., kiaa077.

Cui, F., Brosché, M., Shapiguzov, A., He, X. Q., Vainonen, J. P., Leppälä, J., et al. (2019). Interaction of methyl viologen-induced chloroplast and mitochondrial signalling in *Arabidopsis*. *Free Radic. Biol. Med.*, *134*, 555–566.

Daneva, A., Gao, Z., Van Durme, M., and Nowack, M. K. (2016). Functions and Regulation of Programmed Cell Death in Plant Development. *Annu. Rev. Cell Dev. Biol.*, *32*, 441–468.

De Pinto, M. C., Locato, V., and De Gara, L. (2012). Redox regulation in plant programmed cell death: redox regulation in plant PCD. *Plant Cell Environ.*, *35*, 234–244.

De Simone, A., Hubbard, R., de la Torre, N. V., Velappan, Y., Wilson, M., Considine, M. J., et al. (2017). Redox changes during the cell cycle in the embryonic meristem of *Arabidopsis thaliana*. *Antioxid. Redox Signal*, 27, 1505–1519.

DePaoli, H. C., Dornelas, M. C., and Goldman, M. (2014). SCI1 is a component of the auxin-dependent control of cell proliferation in Arabidopsis upper pistil. *Plant Sci.*, *229*, 122–130.

Dhanasekaran, D. N., Kashef, K., Lee, C. M., Xu H., and Reddy, E. P. (2007). Scaffold proteins of MAP-kinase modules. *Oncogene*, *26*, 3185–3202.

Diaz-Vivancos, P., De Simone, A., Kiddle, G. and Foyer, C. H. (2015). Glutathione- linking cell proliferation to oxidative stress. *Free Radic. Biol. Med*., *89*, 1154–1104.

Dietz, K. J. (2011). Peroxiredoxins in plants and cyanobacteria. *Antioxid. Redox Signal*., *15*, 1129–1159.

Dóczi, R., and Bögre, L. (2018). The Quest for MAP Kinase Substrates: Gaining Momentum. *Trends Plant Sci*., *23*, 918–932.

Dóczi, R., Brader, G., Pettkó-Szandtner, A., Rajh, I., Djamei, A., Pitzschke, A., et al. (2007). The Arabidopsis mitogen-activated protein kinase kinase MKK3 is upstream of group C mitogen-activated protein kinases and participates in pathogen signaling. *Plant Cell*, *19*, 3266–3279.

Downie, J. A. (2010). The roles of extracellular proteins, polysaccharides and signals in the interactions of rhizobia with legume roots. *FEMS Microbiol. Rev*., *34*, 150–170.

Dugas, D. V., and Bartel, B. (2008). Sucrose induction of *Arabidopsis* miR398 represses two Cu/Zn superoxide dismutases. *Plant Mol. Biol.*, *67*, 403–417.

Dunand, C., Crèvecoeur, M., and Penel, C. (2007). Distribution of superoxide and hydrogen peroxide in *Arabidopsis* root and their influence on root development: Possible interaction with peroxidases. *New Phytol.*, *174*, 332–341.

Dvořák, P., Krasylenko, Y., Ovečka, M., Basheer, J., Zapletalová, V., Šamaj, J., and Takáč, T. (2021). *In vivo* light-sheet microscopy resolves localisation patterns of FSD1, a superoxide dismutase with function in root development and osmoprotection. *Plant Cell Environ.*, *44*, 68–87.

Erickson, J. L., Kantek, M., and Schattat, M. H. (2017). Plastid-nucleus distance alters the behavior of stromules. *Front. Plant Sci.*, *8*, 1135.

Evrard, A., Kumar, M., Lecourieux, D., Lucks, J., von Koskull-Döring, P., and Hirt, H. (2013). Regulation of the heat stress response in Arabidopsis by MPK6-targeted phosphorylation of the heat stress factor HsfA2. *PeerJ*, *1*, e59.

Fernández-Pérez, F., Pomar, F., Pedreño, M. A., and Novo-Uzal, E. (2015). Suppression of Arabidopsis peroxidase 72 alters cell wall and phenylpropanoid metabolism. *Plant Sci.*, *239*, 192–199.

Fichman, Y., and Mittler, R. (2020). Rapid systemic signaling during abiotic and biotic stresses: is the ROS wave master of all trades?. *Plant J.*, *102*, 887–896.

Fischer, B. B., Hideg, É., and Krieger-Liszkay, A. (2013). Production, detection, and signaling of singlet oxygen in photosynthetic organisms. *Antioxid. Redox Signal.*, *18*, 2145–2162.

Foreman, J., Demidchik, V., Bothwell, J. H., Mylona, P., Miedema, H., Torres, M. A., et al. (2003). Reactive oxygen species produced by NADPH oxidase regulate plant cell growth. *Nature*, *422*, 442–446.

Foyer, C. H., and Noctor, G. (2005). Oxidant and antioxidant signalling in plants: a re-evaluation of the concept of oxidative stress in a physiological context. *Plant Cell Environ.*, *28*, 1056–1071.

Foyer, C. H., and Noctor, G. (2020). Redox homeostasis and signaling in a higher-CO_2 world. *Annu. Rev. Plant Biol.*, *71*, 157–182.

Frei dit Frey, N., Garcia, A. V., Bigeard, J., Zaag, R., Bueso, E., Garmier, M., et al. (2014). Functional analysis of Arabidopsis immune-related MAPKs uncovers a role for MPK3 as negative regulator of inducible defences. *Genome Biol.*, *15*, R87.

Fridovich, I. (1978). Superoxide radicals, superoxide dismutases and the aerobic lifestyle. *Photochem. Photobiol.*, *28*, 733–741.

Gąciarz, A., Khatri, N. K., Velez-Suberbie, M. L., Saaranen, M. J., Uchida, Y., Keshavarz-Moore, E., and Ruddock, L. W. (2017). Efficient soluble expression of disulfide bonded proteins in the cytoplasm of *Escherichia coli* in fed-batch fermentations on chemically defined minimal media. *Microb. Cell Fact.*, *16*, 108.

Gallie, D. R., and Chen, Z. (2019). Chloroplast-localized iron superoxide dismutases FSD2 and FSD3 are functionally distinct in Arabidopsis. *PLOS ONE*, *14*, e0220078.

Gao, M., Liu, J., Bi, D., Zhang, Z., Cheng, F., Chen, S., and Zhang, Y. (2008). MEKK1, MKK1/MKK2 and MPK4 function together in a mitogen-activated protein kinase cascade to regulate innate immunity in plants. *Cell Res.*, *18*, 1190–1198.

Gao, J., Wang, Y., Cai, M., Pan, Y., Xu, H., Jiang, J., et al. (2015). Mechanistic insights into EGFR membrane clustering revealed by super-resolution imaging. *Nanoscale*, *7*, 2511–2519.

Garcia-Molina, A., Xing, S., and Huijser, P. (2014). Functional characterisation of *Arabidopsis* SPL7 conserved protein domains suggests novel regulatory mechanisms in the Cu deficiency response. *BMC Plant Biol.*, *14*, 231.

Gayomba, S. R., Jung, H. I., Yan, J., Danku, J., Rutzke, M. A., Bernal, M., et al. (2013). The CTR/COPT-dependent copper uptake and SPL7-dependent copper deficiency responses are required for basal cadmium tolerance in *A. thaliana*. *Metallomics*, *5*, 1262–1275.

Geng, Y., Wu, R., Wee, C. W., Xie, F., Wei, X., Chan, P. M. Y., et al. (2013). A spatio-temporal understanding of growth regulation during the salt stress response in Arabidopsis. *Plant Cell*, *25*, 2132–2154.

Gilroy, S., Białasek, M., Suzuki, N., Górecka, M., Devireddy, A. R., Karpiński, S., and Mittler, R. (2016). ROS, Calcium, and Electric Signals: Key Mediators of Rapid Systemic Signaling in Plants. *Plant Physiol.*, *171*, 1606–1615.

Good, M. C., Zalatan, J. G., and Lim, W. A. (2011). Scaffold proteins: hubs for controlling the flow of cellular information. *Science*, *332*, 680–686.

Guan, Q., Wu, J., Zhang, Y., Jiang, C., Liu, R., Chai, C., and Zhu, J. (2013). A DEAD box RNA helicase is critical for pre-mRNA splicing, cold-responsive gene regulation, and cold tolerance in *Arabidopsis*. *Plant Cell*, *25*, 342–356.

Gudesblat, G. E., Iusem, N. D., and Morris, P. C. (2007). Guard cell-specific inhibition of *Arabidopsis MPK3* expression causes abnormal stomatal responses to abscisic acid and hydrogen peroxide. *New Phytol.*, *173*, 713–721.

Guo, A. Y., Zhu, Q. H., Gu, X., Ge, S., Yang, J., and Luo, J. (2008). Genome-wide identification and evolutionary analysis of the plant specific SBP-box transcription factor family. *Gene*, *418*, 1–8.

Han, S., Fang, L., Ren, X., Wang, W., and Jiang, J. (2015). MPK6 controls H_2O_2-induced root elongation by mediating Ca^{2+} influx across the plasma membrane of root cells in *Arabidopsis* seedlings. *New Phytol.*, *205*, 695–706.

Haney, C. H., Riely, B. K., Tricoli, D. M., Cook, D. R., Ehrhardt, D. W., and Long, S. R. (2011). Symbiotic rhizobia bacteria trigger a change in localization and dynamics of the *Medicago truncatula* receptor kinase LYK3. *Plant Cell*, *23*, 2774–2787.

Hanson, M. R., and Conklin, P. L. (2020). Stromules, functional extensions of plastids within the plant cell. *Curr. Opin. Plant Biol.*, *58*, 25–32.

Hayashi, K., Nakamura, S., Fukunaga, S., Nishimura, T., Jenness, M. K., Murphy, A. S., et al. (2014). Auxin transport sites are visualized in planta using fluorescent auxin analogs. *Proc. Natl. Acad. Sci. U. S. A.*, *111*, 11557–11562.

Hehl, R., Norval, L., Romanov, A., and Bülow, L. (2016). Boosting AthaMapdatabase content with data from protein binding microarrays. *Plant Cell Physiol.*, 57, e4.

Helariutta, Y., Fukaki, H., Wysocka-Diller, J., Nakajima, K., Jung, J., Sena, G., et al. (2000). The *SHORT-ROOT* gene controls radial patterning of the *Arabidopsis* root through radial signaling. *Cell*, *101*, 555–567.

Hernando, C. E., García Hourquet, M., de Leone, M. J., Careno, D., Iserte, J., Mora Garcia, S., and Yanovsky, M. J. (2019). A role for pre-mRNA-PROCESSING PROTEIN 40C in the control of growth, development, and stress tolerance in *Arabidopsis thaliana*. *Front. Plant Sci.*, *10*, 1019.

Horváth, E., Bela, K., Holinka, B., Riyazuddin, R., Gallé, Á., Hajnal, Á., et al. (2019). The *Arabidopsis* glutathione transferases, AtGSTF8 and AtGSTU19 are involved in the maintenance of root redox homeostasis affecting meristem size and salt stress sensitivity. *Plant Sci.*, *283*, 366–374.

Hrbáčková, M., Luptovčiak, I., Hlaváčková, K., Dvořák, P., Tichá, M., Šamajová, O., et al. (2020). Overexpression of alfalfa SIMK promotes root hair growth, nodule clustering and shoot biomass production. *Plant Biotechnol J.*, 1–18. doi: 10.1111/pbi.13503.

Hsu, S. F., Lai, H. C., and Jinn, T. L. (2010). Cytosol-Localized Heat Shock Factor-Binding Protein, AtHSBP, Functions as a Negative Regulator of Heat Shock Response by Translocation to the Nucleus and Is Required for Seed Development in Arabidopsis. *Plant Physiol.*, *153*, 773–784.

Huang, Y., Yin, C., Liu, J., Feng, B., Ge, D., Kong, L., et al. (2020). A trimeric CrRLK1L-LLG1 complex genetically modulates SUMM2-mediated autoimmunity. *Nat. Commun.*, *11*, 4859.

Huber, S. C. (2007). Exploring the role of protein phosphorylation in plants: from signalling to metabolism. *Biochem. Soc. Trans.*, *35*, 28–32.

Hunter, K., Kimura, S., Rokka, A., Tran, H. C., Toyota, M., Kukkonen, J. P., and Wrzaczek, M. (2019). CRK2 Enhances Salt Tolerance by Regulating Callose Deposition in Connection with PLDα1. *Plant Physiol.*, *180*, 2004–2021.

Ichimura, K., Mizoguchi, T., Yoshida, R., Yuasa, T., and Shinozaki, K. (2000) Protein phosphorylation and dephosphorylation in environmental stress responses in plants. *Adv. Bot. Res.*, *32*, 355–377.

Jain, A., Wilson, G. T., and Connolly, E. L. (2014). The diverse roles of FRO family metalloreductases in iron and copper homeostasis. *Front. Plant Sci.*, *5*, 100

Jammes, F., Song, C., Shin, D., Munemasa, S., Takeda, K., Gu, D., et al. (2009). MAP kinases MPK9 and MPK12 are preferentially expressed in guard cells and positively regulate ROS-mediated ABA signaling. *Proc. Natl. Acad. Sci. U. S. A.*, *106*, 20520–20525.

Janczarek, M., Rachwał, K., Marzec, A., Grządziel, J., and Palusińska-Szysz, M. (2015). Signal molecules and cell-surface components involved in early stages of the legume–rhizobium interactions. *Appl. Soil Ecol.*, *85*, 94–113.

Jang, Y. H., Park, H. Y., Lee, K. C., Thu, M. P., Kim, S. K., Suh, M. C., et al. (2014). A homolog of splicing factor SF1 is essential for development and is involved in the alternative splicing of pre-mRNA in *Arabidopsis thaliana*. *Plant J.*, *78*, 591–603.

Jiang, K. (2003). Quiescent center formation in maize roots is associated with an auxin-regulated oxidizing environment. *Development*, *130*, 1429–1438.

Jonak, C., Kiegerl, S., Ligterink, W., Barker, P. J., Huskisson, N. S., and Hirt, H. (1996). Stress signaling in plants: a mitogen-activated protein kinase pathway is activated by cold and drought. *Proc. Natl. Acad. Sci. U. S. A.*, *93*, 11274–11279.

Jonak, C., Ligterink, W., and Hirt, H. (1999). MAP kinases in plant signal transduction. *Cell. Mol. Life Sci.*, *55*, 204–213.

Jonak, C., Nakagami, H., and Hirt, H. (2004). Heavy metal stress. Activation of distinct mitogen-activated protein kinase pathways by copper and cadmium. *Plant Physiol.*, *136*, 3276–3283.

Jorgensen, S. A., and Preston, J. C. (2014). Differential *SPL* gene expression patterns reveal candidate genes underlying flowering time and architectural differences in *Mimulus* and *Arabidopsis*. *Mol. Phylogenet. Evol.*, *73*, 129–139.

Jung, H. I., Gayomba, S. R., Rutzke, M. A., Craft, E., Kochian, L. V., and Vatamaniuk, O. K. (2012). COPT6 is a plasma membrane transporter that functions in copper homeostasis in *Arabidopsis* and is a novel target of *SQUAMOSA* promoter-binding protein-like 7. *J. Biol. Chem.*, *287*, 33252–33267.

Kang, C. H., Feng, Y., Vikram, M., Jeong, I. S., Lee, J. R., Bahk, J. D., et al. (2009). *Arabidopsis thaliana* PRP40s are RNA polymerase II C-terminal domain-associating proteins. *Arch. Biochem. Biophys.*, *484*, 30–38.

Kang, Z., Qin, T., and Zhao, Z. (2019). Thioredoxins and thioredoxin reductase in chloroplasts: A review. *Gene*, *706*, 32–42.

Kang, S., Yang, F., Li, L., Chen, H., Chen, S., and Zhang, J. (2015). The Arabidopsis transcription factor BRASSINOSTEROID INSENSITIVE1-ETHYL METHANESULFONATE-SUPPRESSOR1 is a direct substrate of MITOGEN-ACTIVATED PROTEIN KINASE6 and regulates immunity. *Plant Physiol.*, *167*, 1076–1086.

Kaur, H., Peel, A., Acosta, K., Gebril, S., Ortega, J. L., and Sengupta-Gopalan, C. (2019). Comparison of alfalfa plants overexpressing glutamine synthetase with those overexpressing sucrose phosphate synthase demonstrates a signaling mechanism integrating carbon and nitrogen metabolism between the leaves and nodules. *Plant Direct*, *3*, e00115.

Kiegerl, S., Cardinale, F., Siligan, C., Gross, A., Baudouin, E., Liwosz, A., et al. (2000). SIMKK, a mitogen-activated protein kinase (MAPK) kinase, is a specific activator of the salt stress-induced MAPK, SIMK. *Plant Cell*, *12*, 2247–2258.

Kim, S. H., Oikawa, T., Kyozuka, J., Wong, H. L., Umemura, K., Kishi-Kaboshi, M., et al. (2012a). The bHLH Rac Immunity1 (RAI1) Is Activated by OsRac1 via OsMAPK3 and OsMAPK6 in Rice Immunity. *Plant Cell Physiol.*, *53*, 740–754.

Kim, J. M., Woo, D. H., Kim, S. H., Lee, S. Y., Park, H. Y., Seok, H. Y., et al. (2012b). Arabidopsis MKKK20 is involved in osmotic stress response via regulation of MPK6 activity. *Plant Cell Rep.*, *31*, 217–224.

Kimura, S., Waszczak, C., Hunter, K., and Wrzaczek, M. (2017). Bound by Fate: The Role of Reactive Oxygen Species in Receptor-Like Kinase Signaling. *Plant Cell*, *29*, 638–654.

Kliebenstein, D. J., Monde, R. A., and Last, R. L. (1998). Superoxide dismutase in Arabidopsis: an eclectic enzyme family with disparate regulation and protein localization. *Plant Physiol.*, *118*, 637–650.

Köhler, R. H., and Hanson, M. R. (2000). Plastid tubules of higher plants are tissue-specific and developmentally regulated. *J. Cell Sci.*, *113*, 81–89.

Komis, G., Šamajová, O., Ovečka, M., and Šamaj, J. (2018). Cell and Developmental Biology of Plant Mitogen-Activated Protein Kinases. *Annu. Rev. Plant Biol.*, *69*, 237–265.

Kong, Q., Qu, N., Gao, M., Zhang, Z., Ding, X., Yang, F., et al. (2012). The MEKK1-MKK1/MKK2-MPK4 kinase cascade negatively regulates immunity mediated by a mitogen-activated protein kinase kinase kinase in *Arabidopsis*. *Plant Cell*, *24*, 2225–2236.

Kovtun, Y., Chiu, W. L., Tena, G., and Sheen, J. (2000). Functional analysis of oxidative stress-activated mitogen-activated protein kinase cascade in plants. *Proc. Natl. Acad. Sci. U. S. A.*, *97*, 2940–2945.

Kropat, J., Tottey, S., Birkenbihl, R. P., Depège, N., Huijser, P., and Merchant, S. (2005). A regulator of nutritional copper signaling in *Chlamydomonas* is an SBP domain protein that recognizes the GTAC core of copper response element. *Proc. Natl. Acad. Sci. U. S. A.*, *102*, 18730–18735.

Kumar, M., Gouw, M., Michael, S., Sámano-Sánchez, H., Pancsa, R., Glavina, J., et al. (2020). ELM-the eukaryotic linear motif resource in 2020. *Nucleic Acids Res.*, 48, D296–D306.

Kuo, W. Y., Huang, C. H., Liu, A. C., Cheng, C. P., Li, S. H., Chang, W. C., et al. (2013). CHAPERONIN 20 mediates iron superoxide dismutase (FeSOD) activity independent of its co-chaperonin role in Arabidopsis chloroplasts. *New Phytol.*, *197*, 99–110.

Lagarda-Diaz, I., Guzman-Partida, A., and Vazquez-Moreno, L. (2017). Legume Lectins: Proteins with Diverse Applications. *Int. J. Mol. Sci.*, *18*, 1242.

Larrainzar, E., Wienkoop, S., Weckwerth, W., Ladrera, R., Arrese-Igor, C., and González, E. M. (2007). *Medicago truncatula* Root Nodule Proteome Analysis Reveals Differential Plant and Bacteroid Responses to Drought Stress. *Plant Physiol.*, *144*, 1495–1507.

Lee, H., Kim, J., Im, J. H., Kim, H. B, Oh, C. J., and An, C. S. (2008). Mitogen-activated protein kinase is involved in the symbiotic interaction between *Bradyrhizobium japonicum* USDA110 and soybean. *J. Plant Biol.*, *51*, 291–296.

Leitch, J. M., Li, C. X., Baron, J. A., Matthews, L. M., Cao, X., Hart, P. J., et al. (2012). Post-translational modification of Cu/Zn superoxide dismutase under anaerobic conditions. *Biochemistry*, *51*, 677–685.

Li, H., Ding, Y., Shi, Y., Zhang, X., Zhang, S., Gong, Z., and Yang, S. (2017a). MPK3- and MPK6-Mediated ICE1 Phosphorylation Negatively Regulates ICE1 Stability and Freezing Tolerance in *Arabidopsis*. *Dev. Cell*, *43*, 630–642.

Li, F., Li, M., Wang, P., Cox, K. L., Jr., Duan, L., Dever, J. K., et al. (2017b). Regulation of cotton (*Gossypium hirsutum*) drought responses by mitogen-activated protein (MAP) kinase cascade-mediated phosphorylation of GhWRKY59. *New Phytol.*, *215*, 1462–1475.

Li, G., Meng, X., Wang, R., Mao, G., Han, L., Liu, Y., and Zhang, S. (2012). Dual-level regulation of ACC synthase activity by MPK3/MPK6 cascade and its downstream WRKY transcription factor during ethylene induction in Arabidopsis. *PLOS Genet.*, *8*, e1002767.

Li, N., Sun, L., Zhang, L., Song, Y., Hu, P., Li, C., and Hao, F. S. (2015). AtrbohD and AtrbohF negatively regulate lateral root development by changing the localized accumulation of superoxide in primary roots of Arabidopsis. *Planta*, *241*, 591–602.

Li, C. H., Wang, G., Zhao, J. L., Zhang, L. Q., Ai, L. F., Han, Y. F., et al. (2014). The Receptor-Like Kinase SIT1 Mediates Salt Sensitivity by Activating MAPK3/6 and Regulating Ethylene Homeostasis in Rice. *Plant Cell*, *26*, 2538–2553.

Linkies, A., Müller, K., Morris, K., Turečková, V., Wenk, M., Cadman, C. S. C., et al. (2009). Ethylene interacts with abscisic acid to regulate endosperm rupture during germination: A comparative approach using *Lepidium sativum* and *Arabidopsis thaliana*. *Plant Cell*, *21*, 3803–3822.

Liu, J., Huang, Y., Kong, L., Yu, X., Feng, B., Liu, D., et al. (2020). The malectin-like receptor-like kinase LETUM1 modulates NLR protein SUMM2 activation via MEKK2 scaffolding. *Nat. Plants*, *6*, 1106–1115.

Livanos, P., Galatis, B., Quader, H., and Apostolakos, P. (2012). Disturbance of reactive oxygen species homeostasis induces atypical tubulin polymer formation and affects mitosis in root-tip cells of *Triticum turgidum* and *Arabidopsis thaliana*. *Cytoskeleton*, *69*, 1–21.

Locato, V., Cimini, S., and De Gara, L. (2017). "Glutathione as a key player in plant abiotic stress responses and tolerance," in Glutathione in Plant Growth, Development, and Stress Tolerance, eds M. A. Hossain, M. G. Mostofa, P. Diaz-Vivancos, D. J. Burritt, M. Fujita, and L. S. P. Tran (Cham: Springer International Publishing), 127–145.

Lopez-Gomez, M., Sandal, N., Stougaard, J., and Boller, T. (2012). Interplay of flg22-induced defence responses and nodulation in *Lotus japonicus*. *J. Exp. Bot.*, *63*, 393–401.

Lu, C. A., Huang, C. K., Huang, W. S., Huang, T. S., Liu, H. Y., and Chen, Y. F. (2020). DEAD-Box RNA Helicase 42 Plays a Critical Role in Pre-mRNA Splicing under Cold Stress. *Plant Physiol.*, *182*, 255–271.

Mao, G., Meng, X., Liu, Y., Zheng, Z., Chen, Z., and Zhang, S. (2011). Phosphorylation of a WRKY transcription factor by two pathogen-responsive MAPKs drives phytoalexin biosynthesis in Arabidopsis. *Plant Cell*, *23*, 1639–1653.

Matamoros, M. A., Kim, A., Peñuelas, M., Ihling, C., Griesser, E., Hoffmann, R., et al. (2018). Protein Carbonylation and Glycation in Legume Nodules. *Plant Physiol.*, *177*, 1510–1528.

McCord, J. M., Keele, B. B., Jr., and Fridovich, I. (1971). An enzyme-based theory of obligate anaerobiosis: the physiological function of superoxide dismutase. *Proc. Natl. Acad. Sci. U. S. A.*, *68*, 1024–1027.

Meng, X., Xu, J., He, Y., Yang, K. Y., Mordorski, B., Liu, Y., and Zhang, S. (2013). Phosphorylation of an ERF transcription factor by *Arabidopsis* MPK3/MPK6 regulates plant defense gene induction and fungal resistance. *Plant Cell*, *25*, 1126–1142.

Meng, X., and Zhang, S. (2013). MAPK cascades in plant disease resistance signaling. *Annu. Rev. Phytopathol.*, *51*, 245–266.

Mermod, M., Takusagawa, M., Kurata, T., Kamiya, T., Fujiwara, T., and Shikanai, T. (2019). SQUAMOSA promoter-binding protein-like 7 mediates copper deficiency response in the presence of high nitrogen in *Arabidopsis thaliana*. *Plant Cell Rep.*, *38*, 835–846.

Mhamdi, A., and Van Breusegem, F. (2018). Reactive oxygen species in plant development. *Development*, *145*, dev164376.

Mignolet-Spruyt, L., Xu, E., Idänheimo, N., Hoeberichts, F. A., Mühlenbock, P., Brosché, M., et al. (2016). Spreading the news: subcellular and organellar reactive oxygen species production and signalling. *J. Exp. Bot.*, *67*, 3831–3844.

Miller, E. W., Dickinson, B. C., and Chang, C. J. (2010). Aquaporin-3 mediates hydrogen peroxide uptake to regulate downstream intracellular signaling. *Proc. Natl. Acad. Sci. U. S. A.*, *107*, 15681–15686.

Mittler, R. (2017). ROS are good. *Trends Plant Sci.*, *22*, 11–19.

Morgan, M. J., Lehmann, M., Schwarzländer, M., Baxter, C. J., Sienkiewicz-Porzucek, A., Williams, T. C., et al. (2008). Decrease in manganese superoxide dismutase leads to reduced root growth and affects tricarboxylic acid cycle flux and mitochondrial redox homeostasis. *Plant Physiol.*, *147*, 101–114.

Müller, K., Linkies, A., Vreeburg, R. A. M., Fry, S. C., Krieger-Liszkay, A., and Leubner-Metzger, G. (2009). *In vivo* cell wall loosening by hydroxyl radicals during cress seed germination and elongation growth. *Plant Physiol.*, *150*, 1855–1865.

Muñoz, P., and Munné-Bosch, S. (2019). Vitamin E in plants: biosynthesis, transport, and function. *Trends Plant Sci.*, *24*, 1040–1051.

Murphy, M. P. (2009). How mitochondria produce reactive oxygen species. *Biochem. J.*, *417*, 1–13.

Myouga, F., Hosoda, C., Umezawa, T., Iizumi, H., Kuromori, T., Motohashi, R., et al. (2008). A heterocomplex of iron superoxide dismutases defends chloroplast nucleoids against oxidative stress and is essential for chloroplast development in Arabidopsis. *Plant Cell*, *20*, 3148–3162.

Nakagami, H., Soukupová, H., Schikora, A., Zárský, V., and Hirt, H. (2006). A Mitogen-activated protein kinase kinase kinase mediates reactive oxygen species homeostasis in Arabidopsis. *J. Biol. Chem.*, *281*, 38697–38704.

Noctor, G., Reichheld, J. P., and Foyer, C. H. (2017). ROS-related redox regulation and signaling in plants. *Cell Dev. Biol.*, *80*, 3–12.

Nodine, M. D., and Bartel, D. P. (2010). MicroRNAs prevent precocious gene expression and enable pattern formation during plant embryogenesis. *Genes Dev.*, *24*, 2678–2692.

Novák, D., Vadovič, P., Ovečka, M., Šamajová, O., Komis, G., Colcombet, J., and Šamaj, J. (2018). Gene Expression Pattern and Protein Localization of Arabidopsis Phospholipase D Alpha 1 Revealed by Advanced Light-Sheet and Super-Resolution Microscopy. *Front. Plant Sci.*, *9*, 371.

Obayashi, T., Aoki, Y., Tadaka, S., Kagaya, Y., and Kinoshita, K. (2018). ATTED-II in 2018: a plant coexpression database based on investigationof thestatistical property of the mutual rank index. *Plant Cell Physiol.*, *59*, e3.

Ogasawara, Y., Kaya, H., Hiraoka, G., Yumoto, F., Kimura, S., Kadota, Y., et al. (2008). Synergistic activation of the Arabidopsis NADPH oxidase AtrbohD by Ca^{2+} and phosphorylation. *J. Biol. Chem.*, *283*, 8885–8892.

Oldroyd, G. E. (2013). Speak, friend, and enter: signalling systems that promote beneficial symbiotic associations in plants. *Nat. Rev. Microbiol.*, *11*, 252–263.

Orman-Ligeza, B., Parizot, B., de Rycke, R., Fernandez, A., Himschoot, E., Van Breusegem, F., et al. (2016). RBOH-mediated ROS production facilitates lateral root emergence in Arabidopsis. *Development*, *143*, 3328–3339.

Ortiz-Masia, D., Perez-Amador, M. A., Carbonell, J., and Marcote, M. J. (2007). Diverse stress signals activate the C1 subgroup MAP kinases of *Arabidopsis*. *FEBS Lett.*, *581*, 1834–1840.

Ott, T. (2017). Membrane nanodomains and microdomains in plant–microbe interactions. *Curr. Opin. Plant Biol.*, *40*, 82–88.

Ovečka, M., Berson, T., Beck, M., Derksen, J., Šamaj, J., Baluška, F., et al. (2010). Structural sterols are involved in both the initiation and tip growth of root hairs in *Arabidopsis thaliana*. *Plant Cell.*, *22*, 2999–3019.

Ovečka, M., Takáč, T., Komis, G., Vadovič, P., Bekešová, S., Doskočilová, A., et al. (2014). Salt-induced subcellular kinase relocation and seedling susceptibility caused by overexpression of *Medicago* SIMKK in *Arabidopsis*. *J. Exp. Bot.*, *65*, 2335–2350.

Ovečka, M., Vaškebová, L., Komis, G., Luptovčiak, I., Smertenko, A., and Šamaj, J. (2015). Preparation of plants for developmental and cellular imaging by light-sheet microscopy. *Nat. Protoc.*, *10*, 1234–1247.

Passardi, F., Tognolli, M., De Meyer, M., Penel, C., and Dunand, C. (2006). Two cell wall associated peroxidases from Arabidopsis influence root elongation. *Planta*, *223*, 965–974.

Pathirana, S. M., Vance, C. P., Miller, S. S., and Gantt, J. S. (1992). Alfalfa root nodule phosphoenolpyruvate carboxylase: characterization of the cDNA and expression in effective and plant-controlled ineffective nodules. *Plant Mol. Biol.*, *20*, 437–450.

Perea-García, A., Andrés-Bordería, A., Mayo de Andrés, S., Sanz, A., Davis, A. M., Davis, S. J., et al. (2016). Modulation of copper deficiency responses by diurnal and circadian rhythms in *Arabidopsis thaliana*. *J. Exp. Bot.*, *67*, 391–403.

Petersen, M., Brodersen, P., Naested, H., Andreasson, E., Lindhart, U., Johansen, B., et al. (2000). Arabidopsis map kinase 4 negatively regulates systemic acquired resistance. *Cell*, *103*, 1111–1120.

Petersson, S. V., Johansson, A. I., Kowalczyk, M., Makoveychuk, A., Wang, J. Y., Moritz, T., et al. (2009). An auxin gradient and maximum in the Arabidopsis root apex shown by high-resolution cellspecific analysis of IAA distribution and synthesis. *Plant Cell*, *21*, 1659–1668.

Pilon, M. (2017). The copper microRNAs. *New Phytol*., *213*, 1030–1035.

Pilon, M., Ravet, K., and Tapken, W. (2011). The biogenesis and physiological function of chloroplast superoxide dismutases. *Biochim. Biophys. Acta*, *1807*, 989–998.

Pitzschke, A., Djamei, A., Bitton, F., and Hirt, H. (2009). A major role of the MEKK1-MKK1/2-MPK4 pathway in ROS signalling. *Mol. Plant*, *2*, 120–137.

Preston, J. C., and Hileman, L. C. (2013). Functional Evolution in the Plant *SQUAMOSA-PROMOTER BINDING PROTEIN-LIKE* (*SPL*) Gene Family. *Front. Plant Sci.*, *4*, 80.

Qi, J., Wang, J., Gong, Z., and Zhou, J. M. (2017). Apoplastic ROS signaling in plant immunity. *Curr. Opin. Plant Biol.*, *38*, 92–100.

Radović, J., Sokolović, D., and Marković, J. (2009). Alfalfa-most important perennial forage legume in animal husbandry. *Biotechnol. Anim. Husb*., *25*, 465–475.

Rayapuram, N., Bigeard, J., Alhoraibi, H., Bonhomme, L., Hesse, A. M., Vinh, J., et al. (2018). Quantitative phosphoproteomic analysis reveals shared and specific targets of *Arabidopsis* mitogen-activated protein kinases (MAPKs) MPK3, MPK4, and MPK6. *Mol. Cell. Proteom*., *17*, 61–80.

Rodriguez, M. C., Petersen, M., and Mundy, J. (2010). Mitogen-activated protein kinase signaling in plants. *Annu. Rev. Plant Biol.*, *61*, 621–649.

Roy, S., Liu, W., Nandety, R. S., Crook, A., Mysore, K. S., Pislariu, C. I., et al. (2020). Celebrating 20 Years of Genetic Discoveries in Legume Nodulation and Symbiotic Nitrogen Fixation. *Plant Cell*, *32*, 15–41.

Ryu, H., Laffont, C., Frugier, F., and Hwang, I. (2017). MAP Kinase-Mediated Negative Regulation of Symbiotic Nodule Formation in *Medicago truncatula*. *Mol. Cells*, *40*, 17–23.

Salinas, M., Xing, S., Höhmann, S., Berndtgen, R., and Huijser, P. (2012). Genomic organization, phylogenetic comparison and differential expression of the SBP-box family of transcription factors in tomato. *Planta*, *235*, 1171–1184.

Šamaj, J., Ovečka, M., Hlavačka, A., Lecourieux, F., Meskiene, I., Lichtscheidl, I., et al. (2002). Involvement of the mitogen-activated protein kinase SIMK in regulation of root hair tip growth. *EMBO J.*, *21*, 3296–3306.

Šamajová, O., Komis, G., and Šamaj, J. (2014). Immunofluorescent localization of MAPKs and colocalization with microtubules in Arabidopsis seedling whole-mount probes. In G. Komis and J. Šamaj (Eds.), Plant MAP kinases (pp. 107–115). New York, NY: Humana Press.

Šamajová, O., Plíhal, O., Al-Yousif, M., Hirt, H., and Šamaj, J. (2013). Improvement of stress tolerance in plants by genetic manipulation of mitogen-activated protein kinases. *Biotechnol. Adv.*, *31*, 118–128.

Samakovli, D., Tichá, T., Vavrdová, T., Ovečka, M., Luptovčiak, I., Zapletalová, V., et al. (2020). YODA-HSP90 module regulates phosphorylation-dependent inactivation of SPEECHLESS to control stomatal development under acute heat stress in *Arabidopsis*. *Mol. Plant*, *13*, 612–633.

Savatin, D. V., Bisceglia, N. G., Marti, L., Fabbri, C., Cervone, F., and De Lorenzo, G. (2014). The Arabidopsis NUCLEUS- AND PHRAGMOPLASTLOCALIZED KINASE1-related protein kinases are required for elicitorinduced oxidative burst and immunity. *Plant Physiol*., *165*, 1188–1202.

Schmid, M., Uhlenhaut, N. H., Godard, F., Demar, M., Bressan, R., Weigel, D., and Lohmann, J. U. (2003). Dissection of floral induction pathways using global expression analysis. *Development*, *130*, 6001–6012.

Schulten, A., Bytomski, L., Quintana, J., Bernal, M., and Krämer, U. (2019). Do Arabidopsis *Squamosa promoter binding Protein-Like* genes act together in plant acclimation to copper or zinc deficiency? *Plant Direct*, *3*, e00150.

Sheng, Y., Abreu, I. A., Cabelli, D. E., Maroney, M. J., Miller, A. F., Teixeira, M., and Valentine, J. S. (2014). Superoxide dismutases and superoxide reductases. *Chem. Rev.*, *114*, 3854–3918.

Shu, K., Chen, Q., Wu, Y., Liu, R., Zhang, H., Wang, S., et al. (2016). ABSCISIC ACID-INSENSITIVE 4 negatively regulates flowering through directly promoting Arabidopsis FLOWERING LOCUS C transcription. *J. Exp. Bot.*, *67*, 195–205.

Singh, R., Singh, S., Parihar, P., Mishra, R. K., Tripathi, D. K., Singh, V. P., et al. (2016). Reactive Oxygen Species (ROS): Beneficial Companions of Plants' Developmental Processes. *Front. Plant Sci.*, *7*, 1299.

Smékalová, V., Doskočilová, A., Komis, G., and Šamaj, J. (2014). Crosstalk between secondary messengers, hormones and MAPK modules during abiotic stress signalling in plants. *Biotechnol. Adv.*, *32*, 2–11.

Smit, P., Limpens, E., Geurts, R., Fedorova, E., Dolgikh, E., Gough, C., et al. (2007). Medicago LYK3, an Entry Receptor in Rhizobial Nodulation Factor Signaling. *Plant Physiol*., *145*, 183–191.

Smit, G., Tubbing, D. M. J., Kijne, J. W., and Lugtenberg, B, J. J. (1991). Role of Ca^{2+} in the activity of rhicadhesin from *Rhizobium leguminosarum* biovar *viciae*, which mediates the first step in attachment of *Rhizobiaceae* cells to plant root hair tips. *Arch. Microbiol.*, *155*, 278–283.

Soitamo, A. J., Piippo, M., Allahverdiyeva, Y., Battchikova, N., and Aro, E. M. (2008). Light has a specific role in modulating Arabidopsis gene expression at low temperature. *BMC Plant Biol.*, *8*, 13.

Stief, A., Altmann, S., Hoffmann, K., Pant, B. D., Scheible, W. R., and Bäurle, I. (2014). *Arabidopsis* miR156 Regulates Tolerance to Recurring Environmental Stress through SPL Transcription Factors. *Plant Cell*, *26*, 1792–1807.

Su, S. H., Suarez-Rodriguez, M. C., and Krysan, P. (2007). Genetic interaction and phenotypic analysis of the Arabidopsis MAP kinase pathway mutations mekk1 and mpk4 suggests signaling pathway complexity. *FEBS Lett.*, 581, 3171–3177.

Su, J., Zhang, M., Zhang, L., Sun, T., Liu, Y., Lukowitz, W., et al. (2017). Regulation of Stomatal Immunity by Interdependent Functions of a Pathogen-Responsive MPK3/MPK6 Cascade and Abscisic Acid. *Plant Cell*, *29*, 526–542.

Suarez-Rodriguez, M. C., Adams-Phillips, L., Liu, Y., Wang, H., Su, S. H., Jester, P. J., et al. (2007). MEKK1 is required for flg22-induced MPK4 activation in Arabidopsis plants. *Plant Physiol.*, *143*, 661–669.

Suzaki, T., Yoro, E., and Kawaguchi, M. (2015). Leguminous plants: Inventors of root nodules to accommodate symbiotic bacteria. *Int. Rev. Cell Mol. Biol.*, *316*, 111–158.

Swart, S., Logman, T. J., Smit, G., Lugtenberg, B. J., and Kijne, J. W. (1994). Purification and partial characterization of a glycoprotein from pea (*Pisum sativum*) with receptor activity for rhicadhesin, an attachment protein of Rhizobiaceae. *Plant Mol. Biol.*, *24*, 171–183.

Takáč, T., and Šamaj, J. (2015). Advantages and limitations of shot-gun proteomic analyses on Arabidopsis plants with altered MAPK signaling. *Front. Plant. Sci.*, *6*, 107.

Takáč, T., Šamajová, O., Pechan, T., Luptovčiak, I., and Šamaj, J. (2017). Feedback Microtubule Control and Microtubule-Actin Cross-talk in *Arabidopsis* Revealed by Integrative Proteomic and Cell Biology Analysis of *KATANIN 1* Mutants. *Mol. Cell Proteomics*, *16*, 1591–1609.

Takáč, T., Šamajová, O., Vadovič, P., Pechan, T., Košútová, P., Ovečka, M., et al. (2014). Proteomic and biochemical analyses show a functional network of proteins involved in antioxidant defense of the *Arabidopsis anp2anp3* double mutant. *J. Proteome Res.*, *13*, 5347–5361.

Tanoue, T., and Nishida, E. (2003). Molecular recognitions in the MAP kinase cascades. *Cell Signal.*, *15*, 455–462.

Tavormina, P., De Coninck, B., Nikonorova, N., De Smet, I., and Cammue, B. P. (2015). The Plant Peptidome: An Expanding Repertoire of Structural Features and Biological Functions. *Plant Cell*, *27*, 2095–2118.

Teige, M., Scheikl, E., Eulgem, T., Dóczi, R., Ichimura, K., Shinozaki, K., et al. (2004). The MKK2 pathway mediates cold and salt stress signaling in *Arabidopsis*. *Mol. Cell*, *15*, 141–152.

Thulasi Devendrakumar, K., Li, X., and Zhang, Y. (2018). MAP kinase signalling: interplays between plant PAMP- and effector-triggered immunity. *Cell. Mol. Life Sci.*, *75*, 2981–2989.

Tian, C. F., Garnerone, A. M., Mathieu-Demazière, C., Masson-Boivin, C., and Batut, J. (2012). Plant-activated bacterial receptor adenylate cyclases modulate epidermal infection in the *Sinorhizobium meliloti–Medicago* symbiosis. *Proc. Natl. Acad. Sci. U. S. A.*, *109*, 6751–6756.

Tsang, C. K., Chen, M., Cheng, X., Qi, Y., Chen, Y., Das, I., et al. (2018). SOD1 phosphorylation by mTORC1 couples nutrient sensing and redox regulation. *Mol. Cell*, *70*, 502–515.e8.

Tsang, C. K., Liu, Y., Thomas, J., Zhang, Y., and Zheng, X. F. (2014). Superoxide dismutase 1 acts as a nuclear transcription factor to regulate oxidative stress resistance. *Nat. Commun.*, *5*, 3446.

Tsukagoshi, H. (2012). Defective root growth triggered by oxidative stress is controlled through the expression of cell cycle-related genes. *Plant Sci.*, *197*, 30–39.

Tsukagoshi, H. (2016). Control of root growth and development by reactive oxygen species. *Curr. Opin. Plant Biol.*, *29*, 57–63.

Usami, T., Horiguchi, G., Yano, S., and Tsukaya, H. (2009). The *more and smaller cells* mutants of *Arabidopsis thaliana* identify novel roles for *SQUAMOSA PROMOTER BINDING PROTEIN-LIKE* genes in the control of heteroblasty. *Development*, *136*, 955–964.

Vadovič, P., Šamajová, O., Takáč, T., Novák, D., Zapletalová, V., Colcombet, J., and Šamaj, J. (2019). Biochemical and Genetic Interactions of Phospholipase D Alpha 1 and Mitogen-Activated Protein Kinase 3 Affect Arabidopsis Stress Response. *Front. Plant Sci.*, *10*, 275.

Van Breusegem, F., and Dat, J. F. (2006). Reactive oxygen species in plant cell death. *Plant Physiol.*, *141*, 384–390.

Van Breusegem, F., Slooten, L., Stassart, J. M., Moens, T., Botterman, J., Van Montagu, M., and Inzé, D. (1999). Overproduction of *Arabidopsis thaliana* FeSOD confers oxidative stress tolerance to transgenic maize. *Plant Cell Physiol.*, *40*, 515–523.

Van Camp, W., Capiau, K., Van Montagu, M., Inzé, D., and Slooten, L. (1996). Enhancement of oxidative stress tolerance in transgenic tobacco plants overproducing Fe-superoxide dismutase in chloroplasts. *Plant Physiol.*, *112*, 1703–1714.

Volkening, K., Leystra-Lantz, C., Yang, W., Jaffee, H., and Strong, M. J. (2009). Tar DNA binding protein of 43 kDa (TDP-43), 14-3-3 proteins and copper/zinc superoxide dismutase (SOD1) interact to modulate NFL mRNA stability. Implications for altered RNA processing in amyotrophic lateral sclerosis (ALS). *Brain Res.*, *1305*, 168–182.

Vu, L. D., Gevaert, K., and De Smet, I. (2018). Protein language: post-translationalmodifications talking to each other. *Trends Plant Sci.*, *23*, 1068–1080.

Wang, B. B., and Brendel, V. (2006). Molecular characterization and phylogeny of U2AF35 homologs in plants. *Plant Physiol.*, *140*, 624–636.

Wang, X. L., Cui, W. J., Feng, X. Y., Zhong, Z. M., Li, Y., Chen, W. X., et al. (2018). Rhizobia inhabiting nodules and rhizosphere soils of alfalfa: A strong selection of facultative microsymbionts. *Soil Biol. Biochem.*, *116*, 340-350.

Wang, P., Du, Y., Li, Y., Ren, D., and Song, C. P. (2010). Hydrogen peroxide-mediated activation of MAP kinase 6 modulates nitric oxide biosynthesis and signal transduction in *Arabidopsis*. *Plant Cell*, *22*, 2981–2998.

Wang, Z., and Gou, X. (2020). Receptor-Like Protein Kinases Function Upstream of MAPKs in Regulating Plant Development. *Int. J. Mol. Sci.*, *21*, 7638.

Wang, P., Hawkins, T. J., and Hussey, P. J. (2017). Connecting membranes to the actin cytoskeleton. *Curr. Opin. Plant Biol.*, *40*, 71–76.

Waszczak, C., Akter, S., Eeckhout, D., Persiau, G., Wahni, K., Bodra, N., et al. (2014). Sulfenome mining in *Arabidopsis thaliana*. *Proc. Natl. Acad. Sci. U. S. A.*, *111*, 11545–11550.

Waszczak, C., Akter, S., Jacques, S., Huang, J., Messens, J., and Van Breusegem, F. (2015). Oxidative post-translational modifications of cysteine residues in plant signal transduction. *J. Exp. Bot.*, *66*, 2923–2934.

Waszczak, C., Carmody, M., and Kangasjärvi, J. (2018). Reactive Oxygen Species in Plant Signaling. *Annu. Rev. Plant Biol.*, *69*, 209–236.

Waters, B. M., McInturf, S. A., and Stein, R. J. (2012). Rosette iron deficiency transcript and microRNA profiling reveals links between copper and iron homeostasis in *Arabidopsis thaliana*. *J. Exp. Bot.*, *63*, 5903–5918.

Wu, F., Chi, Y., Jiang, Z., Xu, Y., Xie, L., Huang, F., et al. (2020). Hydrogen peroxide sensor HPCA1 is an LRR receptor kinase in *Arabidopsis*. *Nature*, *578*, 577–581.

Xia, X. J., Zhou, Y. H., Shi, K., Zhou, J., Foyer, C. H., and Yu, J. Q. (2015). Interplay between reactive oxygen species and hormones in the control of plant development and stress tolerance. *J. Exp. Bot.*, *66*, 2839–2856.

Xie, Z., Nolan, T., Jiang, H., Tang, B., Zhang, M., Li, Z., and Yin, Y. (2019). The AP2/ERF Transcription Factor TINY Modulates Brassinosteroid-Regulated Plant Growth and Drought Responses in Arabidopsis. *Plant Cell*, *31*, 1788–1806.

Xing, Y., Cao, Q., Zhang, Q., Qin, L., Jia, W., and Zhang, J. (2013). MKK5 regulates high light-induced gene expression of Cu/Zn superoxide dismutase 1 and 2 in Arabidopsis. *Plant Cell Physiol.*, *54*, 1217–1227.

Xing, Y., Chen, W. H., Jia, W., and Zhang, J. (2015). Mitogen-activated protein kinase kinase 5 (MKK5)-mediated signalling cascade regulates expression of iron superoxide dismutase gene in *Arabidopsis* under salinity stress. *J. Exp. Bot.*, *66*, 5971–5981.

Xiong, F., Ren, J. J., Yu, Q., Wang, Y. Y., Lu, C. C., Kong, L. J., et al. (2019). AtU2AF65b functions in abscisic acid mediated flowering via regulating the precursor messenger RNA splicing of *ABI5* and *FLC* in *Arabidopsis*. *New Phytol.*, *223*, 277–292.

Xue, Y., Zhou, F., Zhu, M., Ahmed, K., Chen, G., and Yao, X. (2005). GPS: acomprehensive www server for phosphorylation sites prediction. *Nucleic Acids Res.*, 33, W184–W187.

Yamaguchi, A., Wu, M. F., Yang, L., Wu, G., Poethig, R. S., and Wagner, D. (2009). The microRNA-regulated SBP-Box transcription factor SPL3 is a direct upstream activator of LEAFY, FRUITFULL, and APETALA1. *Dev. Cell.*, *17*, 268–278.

Yamasaki, H., Abdel-Ghany, S. E., Cohu, C. M., Kobayashi, Y., Shikanai, T., and Pilon, M. (2007). Regulation of copper homeostasis by micro-RNA in Arabidopsis. *J. Biol. Chem.*, *282*, 16369–16378.

Yamasaki, H., Hayashi, M., Fukazawa, M., Kobayashi, Y., and Shikanai, T. (2009). SQUAMOSA promoter binding protein-like7 is a central regulator for copper homeostasis in Arabidopsis. *Plant Cell*, *21*, 347–361.

Yamasaki, K., Kigawa, T., Inoue, M., Tateno, M., Yamasaki, T., Yabuki, T., et al. (2004). A novel zinc-binding motif revealed by solution structures of DNA-binding domains of Arabidopsis SBP-family transcription factors. *J. Mol. Biol.*, *337*, 49–63.

Yan, J., Chia, J. C., Sheng, H., Jung, H. I., Zavodna, T. O., Zhang, L., et al. (2017a). Arabidopsis Pollen Fertility Requires the Transcription Factors CITF1 and SPL7 That Regulate Copper Delivery to Anthers and Jasmonic Acid Synthesis. *Plant Cell*, *29*, 3012–3029.

Yan, Q., Xia, X., Sun, Z., and Fang, Y. (2017b). Depletion of *Arabidopsis* SC35 and SC35-like serine/arginine-rich proteins affects the transcription and splicing of a subset of genes. *PLOS Genet.*, *13*, e1006663.

Yang, Z., Wang, X., Gu, S., Hu, Z., Xu, H., and Xu, C. (2008). Comparative study of SBP-box gene family in Arabidopsis and rice. *Gene*, *407*, 1–11.

Yin, J., Guan, X., Zhang, H., Wang, L., Li, H., Zhang, Q., et al. (2019) An MAP kinase interacts with LHK1 and regulates nodule organogenesis in Lotus japonicus. *Sci. China Life Sci.*, *62*, 1–15.

Yoo, S. D., Cho, Y. H., Tena, G., Xiong, Y., and Sheen, J. (2008). Dual control of nuclear EIN3 by bifurcate MAPK cascades in C_2H_4 signalling. *Nature*, *451*, 789–795.

Yu, L., Nie, J., Cao, C., Jin, Y., Yan, M., Wang, F., et al. (2010). Phosphatidic acid mediates salt stress response by regulation of MPK6 in *Arabidopsis thaliana*. *New Phytol.*, *188*, 762–773.

Zechmann, B. (2018). Compartment-specific importance of ascorbate during environmental stress in plants. Antioxid. *Redox Signal.*, *29*, 1488–1501.

Zhang, Z., Liu, Y., Huang, H., Gao, M., Wu, D., Kong, Q., and Zhang, Y. (2017). The NLR protein SUMM2 senses the disruption of an immune signaling MAP kinase cascade via CRCK3. *EMBO Rep.*, *18*, 292–302.

Zhang, Z., Wu, Y., Gao, M., Zhang, J., Kong, Q., Liu, Y., et al. (2012). Disruption of PAMP-induced MAP kinase cascade by a *Pseudomonas syringae* effector activates plant immunity mediated by the NB-LRR protein SUMM2. *Cell Host Microbe*, *11*, 253–263.

Zhang, Y., Xiao, Y., Du, F., Cao, L., Dong, H., and Ren, H. (2011). Arabidopsis VILLIN4 is involved in root hair growth through regulating actin organization in a Ca^{2+}-dependent manner. *New Phytol*., *190*, 667–682.

Zhang, T., Zhu, M., Song, W. Y., Harmon, A. C., and Chen, S. (2015). Oxidation and phosphorylation of MAP kinase 4 cause protein aggregation. *Biochim. Biophys. Acta*, *1854*, 156–165.

Zhang, Y., Zhu, H., Zhang, Q., Li, M., Yan, M., Wang, R., et al. (2009). Phospholipase Dα1 and Phosphatidic Acid Regulate NADPH Oxidase Activity and Production of Reactive Oxygen Species in ABA-Mediated Stomatal Closure in Arabidopsis. *Plant Cell*, *21*, 2357–2377.

Zhao, Q., and Guo, H. W. (2011). Paradigms and paradox in the ethylene signaling pathway and interaction network. *Mol Plant.*, *4*, 626–634.

Zhao, C., Wang, P., Si, T., Hsu, C. C., Wang, L., Zayed, O., et al. (2017). MAP Kinase Cascades Regulate the Cold Response by Modulating ICE1 Protein Stability. *Dev. Cell*, *43*, 618–629.e5.

Zou, M., Ren, H., and Li, J. (2019). An Auxin Transport Inhibitor Targets Villin-Mediated Actin Dynamics to Regulate Polar Auxin Transport. *Plant Physiol*., *181*, 161–178.

Zulawski, M., Braginets, R., and Schulze, W. X. (2013). PhosPhAtgoeskinases-searchable protein kinase target information in the plantphosphorylation site database PhosPhAt. *Nucleic Acids Res*., *41*, D1176–D1184.

Zulawski, M., Schulze, G., Braginets, R., Hartmann, S., and Schulze, W. X. (2014). The Arabidopsis Kinome: phylogeny and evolutionary insights into functional diversification. *BMC Genomics*, *15*, 548.

9 List of publications

Published manuscripts:

1. **Dvořák, P.**, Krasylenko, Y., Ovečka, M., Basheer, J., Zapletalová, V., Šamaj, J., Takáč, T. *In vivo* light-sheet microscopy resolves localisation patterns of FSD1, a superoxide dismutase with function in root development and osmoprotection. (2021). *Plant, cell & environment,* 44, 68–87. doi: 10.1111/pce.13894.

2. **Dvořák, P**., Krasylenko, Y., Zeiner, A., Šamaj, J., Takáč, T. (2021). Signaling Toward Reactive Oxygen Species-Scavenging Enzymes in Plants. *Frontiers in Plant Science*, 11, 618835. doi: 10.3389/fpls.2020.618835.

3. Hrbáčková, M.*, **Dvořák, P**.*, Takáč, T., Tichá, M., Luptovčiak, I., Šamajová, O., Ovečka, M., Šamaj, J. (2020). Biotechnological perspectives of omics and genetic engineering methods in alfalfa. *Frontiers in Plant Science* 11, 592. doi: 10.3389/fpls.2020.00592. * joined first authors.

4. Tichá, M., Richter, H., Ovečka, M., Maghelli, N., Hrbáčková, M., **Dvořák, P**., Šamaj, J., Šamajová, O. (2020). Advanced microscopy reveals complex developmental and subcellular localization patterns of ANNEXIN 1 in Arabidopsis. *Frontiers in Plant Science* 11, 1153. doi: 1153.10.3389/fpls.2020.01153.

5. Hrbáčková, M.*, Luptovčiak, I.*, Hlaváčková, K.*, **Dvořák, P**., Tichá, M., Šamajová, O., Novák, D., Bednarz, H., Niehaus, K., Ovečka, M., Šamaj, J. (2020). Overexpression of alfalfa SIMK promotes root hair growth, nodule clustering and shoot biomass production. *Plant biotechnology journal,* 1–18. doi: 10.1111/pbi.13503. Advance online publication. * joined first authors.

11 Abstrakt

Mitogen-aktivované protein kinasové (MAPK) kaskády řadíme mezi evolučně vysoce konzervované signalizační dráhy, které hrají důležitou úlohu v řadě buněčných procesů. Jednou z jejich hlavních úloh je přenos signálu přijatého z vnějšího prostředí skrze receptory s nitro- a mezibuněčnou signalizací. Taktéž hrají nezastupitelnou signalizační roli během navazování patogenních nebo symbiotických vztahů mezi rostlinou a mikroorganizmy. V rostlinách vystavených podmínkám působení biotického a abiotického stresu dochází ke značné akumulaci reaktivních forem kyslíku (ROS) způsobujících v buňkách oxidační stres, který v krajních případech může vést až k buněčné smrti. ROS hrají nezastupitelnou roli v buněčné signalizaci a během vývojových procesů rostlin. Zvýšená akumulace ROS aktivuje některé MAPK, které následně regulují řadu buněčných pochodů včetně modulace antioxidační obrany zahrnující superoxiddismutasy (SOD). Předchozí studie naznačují, že enzymatická aktivita a abundance některých SOD je regulována pomocí MAPK v odpovědi na různé stresové podmínky vedoucí k akumulaci ROS.

První část této práce se zabývá studiem MAPK při působení oxidačního stresu a jejich zapojením do procesu iniciace symbiotických vztahů s beneficiálními bakteriemi *Sinorhizobium meliloti* a následné nodulace u rostliny *Medicago sativa*. Biochemická, fenotypová a proteomická analýza linie *M. sativa* s cíleně sníženou abundancí MAPK kinasy (*SIMKK RNAi* linie) odkryly možné zapojení MAPK kaskád do těchto procesů. *SIMKK RNAi* linie vykazovala snížený počet nodulů v porovnání s divokým typem. Následná biochemická a proteomická analýza ukázala, že tento fenotyp může být způsoben poruchami adheze bakterií na povrch kořenů, remodelace plazmatické membrány a poruchami redox regulace včetně antioxidačních proteinů. Noduly transgenní linie vykazují postižený metabolismus dusíku a uhlíku, jak naznačuje proteomická analýza.

Cílem druhé části práce bylo popsat vývojové a lokalizační role SOD isoenzymu (FSD1) v rostlině *Arabidopsis thaliana* a navrhnout možné mechanismy jeho regulace pomocí MAPK. Zjistili jsme, že FSD1 je zapojena do vývoje laterálních kořenů a má ochrannou roli během indukovaného oxidačního a solného stresu. Pomocí mikroskopické analýzy byla definována subcelulární lokalizace FSD1 v cytoplasmě, chloroplastech a překvapivě i v buněčném jádře. FSD1 má specifickou roli při narušení epidermis během prorůstání radikuly ze semena při klíčení. FSD1 protein byl taktéž akumulován ve vyvíjející se špičce kořenového vlásku. Pomocí ko-imunoprecipitační metody v kombinaci s hmotnostní spektrometrií byli identifikováni potenciální interakční partneři FSD1 a navrženy možné úlohy FSD1. Závěr této části je věnován možnému zapojení MPK3 a MPK6 v regulaci exprese *FSD1* skrze SPL transkripční faktory.

Se zvyšujícími se potřebami lidstva a současně velmi dynamicky se měnícími environmetálními podmínkami je již v současné době konvenční zemědělství na hranici svých limitů. Pochopení mechanizmů symbiotických vztahů, a to především jeho úvodních signalizačních drah, může vést k novým biotechnologickým aplikacím spojených s možností zvýšení výnosů pícnin, jako je *Medicago sativa*. Velmi vhodnou variantou je taktéž cílená modifikace antioxidačních enzymů, která by vedla k vyšší rezistenci rostlin jak na biotický, tak především abiotický stres. Pro jejich cílenou modifikaci je však nejprve důležité pochopit veškeré jejich funkční úlohy v rostlinách. Tato práce částečně přispívá k pochopení úlohy MAPK kaskád a FSD1 proteinu v rostlinách a podporuje jejich možné zapojení do biotechnologických aplikací v zemědělství.